

PROCEEDINGS OF THE THIRD INTERNATIONAL SYMPOSIUM ON ARTIFICIAL LIFE AND ROBOTICS

(AROB 3rd '98)

Vol.2

Jan. 19-Jan. 21, 1998
B-Con Plaza, Beppu, Oita, JAPAN

Editor : Masanori Sugisaka
ISBN4-9900462-8-5

Proceeding of The Third International Symposium on

ARTIFICIAL LIFE AND ROBOTICS

(AROB 3rd '98)

January 19-21, 1998
B-Con Plaza, Beppu, Oita, JAPAN

Editor: Masanori Sugisaka

ISBN4-9900462-8-5, 1998

THE THIRD INTERNATIONAL SYMPOSIUM ON ARTIFICIAL LIFE AND ROBOTICS (AROB 3rd '98)

ORGANIZED BY

Oita University
Under The Sponsorship of Ministry of Education,
Science, Sports, and Culture, Japanese Government

CO-SPONSORED BY

Robotics Society of Japan(RSJ, Japan)
Santa Fe Institute(SFI, USA)
The Institute of Electrical Engineers of Japan(IEEJ, Japan)
The Society of Instrument and Control Engineers(SICE, Japan)

CO-OPERATED BY

Japan Robot Association(JARA, Japan)
The Institute of Electrical and Electronics Engineers,
Tokyo Section(IEEE, USA)
The Institute of Electronics, Information and
Communication Engineers(IEICE, Japan)
The Institute of System, Control and Information
Engineers(ISCIE, Japan)

SUPPORTED BY

Asahi Shimbun
Beppu Municipal Government
Kyushu Bureau of International Trade and Industry, MITI
NHK Oita Station
Nihonkeizai Shimbun
Nikkan Kogyo Shimbun
Oita Asahi Broadcasting
OBS Broadcast Company
Oita Chamber of Commerce and Industry
Oitagodo Shinbunsya
Oita Industrial Group Society
Oita Municipal Government
Oita Prefectural Government
Oita System Control Society
Science and Technology Agency
TOS Broadcast Company

HONORARY PRESIDENT

M.Hiramatsu (Governor, Oita Prefecture)

ORGANIZING COMMITTEE

K.Abe (Tohoku University, Japan)
K.Akizuki (Waseda University, Japan)
S.Arimoto (Ritsumeikan University, Japan)
W.B.Arthur (Santa Fe Institute, USA)
C.Barrett (Los Alamos National Laboratory, USA)
Z.Bubunicki (Wroclaw University of Technology, Poland)
J.L.Casti (Santa Fe Institute, USA) (Vice Chairman)
T.Christaller (GMD-German National Research Center for Information Technology, Germany)
J.M.Epstein (Brookings Institution, USA)
T.Fujii (RIKEN, Japan)
S.Fujimura (The University of Tokyo, Japan)
Y.Fujita (The Japan Academy, Japan)
T.Fukuda (Nagoya University, Japan)
M.Gen (Ashikaga Institute of Technology, Japan)
T.Gomi (AAI, Canada)
H.Hagiwara (Kyoto School of Computer Science, Japan)
I.Harvey (University of Sussex, UK)
P.Husbands (University of Sussex, UK)
M.Ito (RIKEN, Japan)
D.J.G.James (Coventry University, UK)
T.Jinzenji (Sanyodenki Co. Ltd., Japan)
J.Johnson (The Open University, UK)
R.E.Kalaba (University of Southern California, USA)
H.Kashiwagi (Kumamoto University, Japan)
O.Katai (Kyoto University, Japan)
S.Kauffman (Santa Fe Institute, USA)
J.H.Kim (KAIST, Korea)
H.Kimura (The University of Tokyo, Japan)
S.Kitamura (Kobe University, Japan)
H.Kitano (Sony Computer Science Laboratory Inc., Japan)
K.Kyuma (Mitsubishi Electric Co., Japan)
C.G.Langton (Santa Fe Institute, USA)
J.J.Lee (KAIST, Korea)
C.Looney (University of Nevada-Reno, USA)
G.I.Marchuk (Russian Academy of Sciences, Russia)
G.Matsumoto (RIKEN, Japan)
K.Mastuno (MITI, AIST, Japan)
H.Miura (The University of Tokyo, Japan)
T.Mushya (Brain Function Laboratory, Inc., Japan)
T.Nagata (Inst. of Sys. and Inf. Tech. / Kyushu, Japan)
M.Nakamura (Saga University, Japan)

H.H.Natsuyama (Advanced Industrial Materials, USA)
Y.Nishikawa (Osaka Institute of Technology, Japan)
R.G.Palmer (Santa Fe Institute, USA)
R.Pfeifer (University of Zurich-Irchel, Switzerland)
M.Raibert (MIT, USA)
S.Rasmussen (Santa Fe Institute, USA)
T.S.Ray (ATR, Japan)
P.Schuster (Santa Fe Institute, USA)
T.Shibata (MITI, MEL, Japan)
K.Shimohara (ATR, Japan)
C.Sommerer (ATR, Japan)
L.Steels (VUB AI Laboratory, Belgium)
M.Sugisaka (Oita University, JAPAN) (Chairman)
K.Tamura (MITI, AIST, Japan)
H.Tanaka (Tokyo Medical & Dental University, Japan)
Y.Tokura (ATR, Japan)
N.Tosa (ATR, Japan)
K.Tsuchiya (Kyoto University, Japan)
S.Ueno (Kyoto School of Computer Science, Japan)
Y.Ueno (Professor emeritus of Kyoto University, Japan)
A.P.Wang (Arizona State University, USA)
W.R.Wells (University of Nevada-Las Vegas, USA)
T.Yamakawa (Kyushu Institute of Technology, Japan)
Y.G.Zhang (Academia Sinica, China)

STEERING COMMITTEE

M.Asada (Osaka University, Japan)
H.Asama (RIKEN, Japan)
J.L.Casti (Santa Fe Institute, USA)
S.Fujimura (The University of Tokyo, Japan)
T.Fukuda (Nagoya University, Japan)
H.Kashiwagi (Kumamoto University, Japan)
J.J.Lee (KAIST, Korea)
M.Nakamura (Saga University, Japan)
T.S.Ray (ATR, Japan)
K.Shimohara (ATR, Japan)
M.Sugisaka (Oita University, Japan) (Chairman)
H.Tanaka (Tokyo Medical & Dental University, Japan)
K.Ueda (Kobe University, Japan)
S.Ueno (Kyoto School of Computer Science, Japan)
Y.G.Zhang (Academia Sinica, China)

PROGRAM COMMITTEE

K.Aihara (The University of Tokyo, Japan)
S.Arimoto (Ritsumeikan University, Japan)
J.L.Casti (Santa Fe Institute, USA)

T.Fujii (RIKEN, Japan)
S.Fujimura (The University of Tokyo, Japan) (Chairman)
T.Fukuda (Nagoya University, Japan)
M.Gen (Ashikaga Institute of Technology, Japan)
I.Harvey (University of Sussex, UK)
T.Hasegawa (Kyushu University, Japan)
Y.Hori (The University of Tokyo, Japan)
P.Husbands (University of Sussex, UK)
H.Inooka (Tohoku University, Japan)
Y.Kakazu (Hokkaido University, Japan)
J.H.Kim (KAIST, Korea)
S.Kitamura (Kobe University, Japan)
H.Kitano (Sony Computer Science Laboratory Inc., Japan)
H.Kobatake (Tokyo University of Agriculture & Technology, Japan)
K.Kumamaru (Kyushu Institute of Technology, Japan)
J.J.Lee (KAIST, Korea)
T.Nagata (Inst. of Sys. and Inf. Tech. / Kyushu, Japan)
M.Nakamura (Saga University, Japan)
Y.Nishikawa (Osaka Institute of Technology, Japan)
T.Omori (Tokyo University of Agriculture & Technology, Japan)
K.Okazaki (Fukui University, Japan)
R.Pfeifer (University of Zurich-Irchel, Switzerland)
T.S.Ray (ATR, Japan)
T.Sawaragi (Kyoto University, Japan)
T.Shibata (MITI, MEL, Japan)
K.Shimohara (ATR, Japan)
S.Shin (The University of Tokyo, Japan)
M.Sugisaka (Oita Unuversity, Japan)
H.Tamaki (Kobe University, Japan)
H.Tanaka (Tokyo Medical & Dental University, Japan)
N.Tosa (ATR, Japan)
K.Tsuchiya (Kyoto University, Japan)
K.Ueda (Kobe University, Japan)
S.Ueno (Kyoto School of Computer Science, Japan)
X.Wang (Oita Unuversity, Japan)
K.Watanabe (Saga University, Japan)
T.Yamakawa (Kyushu Institute of Technology, Japan)
X.Yao (The University of New South Wales, Australia)

LOCAL ARRANGEMENT COMMITTEE

T.Endo (Oita University, Japan)
T.Ezaki (Research and Development Center, Oita University, Japan)
T.Hano (Oita University, Japan)
H.Hikawa (Oita University, Japan)
H.Ikeuchi (Oita University, Japan)
K.Kinoshita (Oita University, Japan)
A.Kuriyakawa (Oita University, Japan)

E.Kusayanagi (Oita University, Japan)
T.Matsuo (Oita University, Japan)
Y.Morita (Oita University, Japan)
T.Nabeshima (Oita University, Japan)
T.Nakano (Oita University, Japan) (Chairman)
K.Ohta (Oita-Aist Joint Research Center, Japan)
M.Sugisaka (Oita University, Japan)
A.Tominaga (Oita University, Japan)
K.Yoshida (Oita University, Japan)

TOPICS

Hardware Oriented Topics are welcome
in the fields given by

Artificial Brain
Artificial Intelligence
Artificial Life
Artificial Livings
Artificial Mind
Brain Science
Chaos
Cognitive Science
Complexities
Computer Graphics
Evolutionary Computations
Fuzzy Control
Genetic Algorithms
Human Care Robotics
Innovative Computations
Intelligent Control and Modeling
Micro Machine
Micro-Robot World Cup Soccer Tournament
Neural Networks
Neurocomputers
Neuro Computing Technologies
and Its Application for Hardware
Robotics
Robust Virtual Engineering
Virtual Reality
Related Fields

COPYRIGHT

Accepted papers will be published in the proceeding of AROB and some of high quality papers in the proceeding will be requested to re-submit for the consideration of publication in an international journal ARTIFICIAL LIFE AND ROBOTICS (Springer-Verlag) and APPLIED

MATHEMATICS AND COMPUTATION (North-Holland).

All correspondence relating to the symposium should be addressed to:

Prof. Masanori Sugisaka
Chairman of International Symposium on Artificial Life and Robotics (AROB)
AROB Secretariat
Dept. of Electrical and Electronic Engineering
Oita University
700 Dannoharu, Oita 870-11
JAPAN
TEL 001-81-975-54-7831
FAX 001-81-975-54-7841
E-MAIL msugi@cc.oita-u.ac.jp

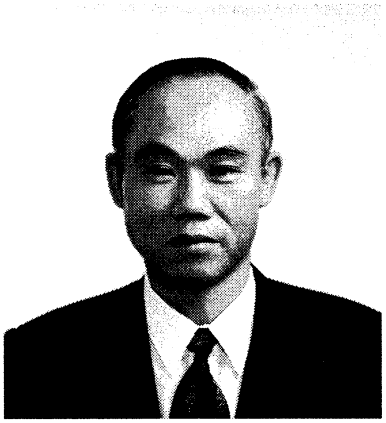
WWW Home Page http://AROB.cc.oita-u.ac.jp/

AROB 3rd '98 is supported financially by the following companies

All Nippon Airways Co., Ltd.
Japan Air System
Mitsubishi Heavy Industries, Ltd.
NEC Corporation
Nishi Nippon Electric Wire Cable Co., Ltd.
Oita Gas Co., Ltd.
Sanwa Shurui Co., Ltd.
Shintsurukai Kosan Co., Ltd.
Sony Oita Corporation
Sugahara Industry Co., Ltd.
Yanai Denki Kogyo Co, Ltd.
Yasukawa Electric Co., Ltd.
Yatsushika Sake-Brewing Co., Ltd.

PREFACE

Masanori Sugisaka
Chairman of AROB
(Professor, Oita University)



It is our great pleasure to invite you all to The Third International Symposium on Artificial Life and Robotics(AROB 3rd '98), organized by Oita University under the sponsorship of Ministry of Education, Science, Sports, and Culture(Monbusho), Japanese Government and co-sponsored by Santa Fe Institute(SFI), USA, SICE, RSJ, and IEEJ, Japan. This symposium invites you all to discuss development of new technologies concerning Artificial Life and Robotics based on simulation and hardware in 21st century. It is also our great honor to welcome several famous scientists and engineers as members of the International Organizing, Steering, Program Committees from this year.

This symposium is also financially supported by not only Monbusho but also other private companies. On behalf of the International Steering Committee we would like to express our gratitude to Honorary President Mr. Hiramastu(Governer, Oita Prefecture), members of the International Organizing Committee, the International Program Committee, the Local Arrangement Committee, Session Chairmans and Co-Chairmans and all the presenters. We acknowledge also the strong support of Monbusho and the sponsoring organizations in promoting the event. Finally we thank all who have contributed towards the sucess of this symposium.

We hope that AROB 3rd '98 will become a celebration to the establishment of our international joint research institute on artificial life, complexity, and robotics for twenty first century by the support of Monbusho's program of center of excellence. we hope that you will obtain fruitful results by exchanging ideas through discussions during the symposium and also will enjoy your stay in Beppu, Oita.

Masanori Sugisaka
M. Sugisaka

January 12, 1998

TECHNICAL PAPER INDEX

Special lecture(Invited Talk)

Neuroscience of the brain mechanisms of mind and behavior I-1
M. Ito(RIKEN, Japan)

Design of an artificial brain for robots I-2
M. Sugisaka(Oita Univ., Japan)

Risk, simulation, and the insurance industry I-12
J. L. Casti(Tech. Univ. of Vienna, Austria / Santa Fe Inst., USA)

Molecular insights into evolution I-18
P. Schuster(Univ Wien, Austria / Santa Fe Inst., USA)

Brain computing I-24
G. Matsumoto(RIKEN, Japan)

Some theoretical issues on computer simulations I-28
C. L. Barrett, C. M. Reidys(Los Alamos National Labs., USA)

An artificial stock market I-34
R. G. Palmer, W. B. Arthur, J. H. Holland, B. LeBaron
(Santa Fe Inst., USA)

Virtual engineering and complex system I-40
J. Doyle(California Inst. of Tech., USA)

Intelligent robotic system-adaptation, learning and evolution I-41
T. Fukuda(Nagoya University, Japan)
N. Kubota(Osaka Institute of Technology, Japan)

Future of the observable universe I-47
Y. Fujita(The Japan Academy, Japan)

Origins of order in biology, economics, and technology I-48
S. Kauffman(Santa Fe Institute, USA)

Development of micro robot system for playing soccer games I-49
J. J. Lee(KAIST, Korea)

S-B1:Bio-Informatics(Invited Session)

B1-1 Bio-informatic activity modelling for human-artifacts symbiosisunder resource-boundedness 1
T. Sawaragi, O. Katai(Kyoto Univ., Japan)

B1-2 Development of eye-sensing HMD and its application experiments for observing human ocular information processing characteristics 7
H. Yoshikawa, H. Shimoda, S. Fukushima, D. Morikawa,
H. Fujiyama(Kyoto Univ., Japan)

B1-3 A study on optimal motion of a biped locomotion machine 11
K. Tsujita, K. Tsuchiya, H. Kawano (Kyoto Univ., Japan)

B1-4 A simulation study on cooperative behavior in a fish school 17
N. Sannomiya(Kyoto Inst. of Tech., Japan)
H. Nakamine(Kyoto Univ. of Education, Japan)

B1-5 Developing artificial retina by evolutionary cellular automata and self-organizing neural networks 23
X. Wu, Y. Zhang(Academia Sinica, China)
M. Sugisaka(Oita Univ., Japan)

S-B2:Evolutionary Computations and Applications (Invited Session)

B2-1 Effectiveness of matrix-based encoding for spanning tree problem on sparse graph 27
G. Zhou, M. Gen, M. Takayama (Ashikaga Inst. of Tech., Japan)

B2-2 Spanning tree-based genetic algorithm for bicriteria transportation problem with fuzzy coefficients 31
Y. Z. Li, M. Gen, K. Ida (Ashikaga Inst. of Tech., Japan)

B2-3 Bicriteria machine scheduling problem using genetic algorithms 35
D. Zheng, M. Gen (Ashikaga Inst. of Tech., Japan)

B2-4 Evolutionary feature recognition of CAD data employing boundary representation method. 39
Y. Tsujimura, M. Gen, M. Hiji (Ashikaga Inst. of Tech., Japan)

B2-5 Bicriteria network design using spanning tree-based genetic algorithm 43
M. Gen, K. Ida, J. Kim(Ashikaga Inst. of Tech., Japan)
J. Lee(Dongseo Univ., Korea)

B2-6 An evolutionary computation-based model for process plan selection considering AGV guidepath and operation flexibility 47
C. Moon, J. Kim, K. An(Cheju National Univ., Korea)
M. Gen(Ashikaga Inst. of Tech., Japan)

S-C1:Robot Motions(Invited Session)

C1-1 Hitting robot with a flexible link hammer 51
T. Izumi, H. Zhou(Shimane Univ., Japan)
Y. Hitaka(Ube National College of Tech., Japan)

C1-2 Stability analysis of 3-D grasps considering rolling contact 55
S. K. Saha, T. Yamada, T. Sakurayama (Nagoya Inst. of Tech., Japan)
N. Mimura(Niigata Univ., Japan)
Y. Funahashi(Nagoya Inst. of Tech., Japan)

C1-3 An algorithm for identification of contact condition from contaminated data of contact moment 59

T. Mouri, T. Yamada(Nagoya Inst. of Tech., Japan)
N. Mimura(Niigata Univ., Japan)
Y. Funahashi(Nagoya Inst. of Tech., Japan)

C1-4 Stiffness condition for stabilization of grasps with interference between translational and rotational displacements 63
Y. Funahashi, T. Yamada, Y. Suzuki(Nagoya Inst. of Tech., Japan)
N. Mimura(Niigata Univ., Japan)

C1-5 Dynamic control of redundant manipulators using artificial potential field approach with time scaling 67
Y. Tanaka, T. Tsuji, M. Kaneko(Hiroshima Univ., Japan)

C1-6 Force display for inter-atomic bonds 73
M. Hashimoto(Kagoshima Univ., Japan)
S. Morioka(Dai Nippon Printing Co., Ltd., Japan)
R. Yamamoto(The Univ. of Tokyo, Japan)

S-C2:Design of Emergence(Invited Session)

C2-1 An approach to the emergent design theory and applications 77
S. Kitamura, Y. Kakuda, H. Tamaki (Kobe Univ., Japan)

C2-2 Evolutionary design of lens System 81
I. Ono, Y. Tatsuzawa, S. Kobayashi (Tokyo Inst. of Tech., Japan)

C2-3 An adaptive state space design for reinforcement learning 85
H. Murao, S. Kitamura(Kobe Univ., Japan)

C2-4 Learning control of autonomous robots using instance-based classifier generator in the continuous state space 89
K. Kuroyama, M. M. Svinin, Y. Nakamura, K. Ueda (Kobe Univ., Japan)

C2-5 Intelligent manufacturing by simple Robots 93
J. Vaario(NTT, Japan)
K. Ueda(Kobe Univ., Japan)

S-D1:Locomotion Robots(Invited Session)

D1-1 Involvement of cerebellar synaptic plasticity in adaptive control of locomotion of cat 97
D. Yanagihara(RIKEN, Japan)

D1-2 Adaptive locomotion to periodic perturbation: Adaptation mechanism with coupling of oscillator and link dynamics 101
S. Ito(RIKEN, Japan)
H. Yuasa(Nagoya Univ., Japan)
Z. W. Luo, M. Ito, D. Yanagihara(RIKEN, Japan)

D1-3 The optimal gait pattern in hexapods based on energetic efficiency 106
J. Nishii(RIKEN, Japan)
K. Ogawa(Nissan-motor co., ltd., Japan)
R. Suzuki(Kanazawa Inst. of Tech., Japan)

D1-4 An insect robot controlled by emergence of gait patterns 110
K. Akimoto, S. Watanabe, M. Yano (Tohoku Univ., Japan)

D1-5 The application of autonomous decentralized system to myriapod locomotion robot 114
T. Odashima, H. Yuasa(Nagoya Univ., Japan)
M. Ito(RIKEN, Japan)
M. Yasubayashi(Chubu Univ., Japan)

D1-6 Evolving neural controllers that elicit non-trivial behaviors using developmental process 119
A. Ishiguro, H. Iwaki, A. Fujii, Y. Uchikawa (Nagoya Univ., Japan)

S-D2:Why is Intelligent Control?(Invited Session)

D2-1 Toward a paradigm for information integrated control system 125
S. Kawaji(Kumamoto Univ., Japan)
N. Matsunaga(OMRON Corp., Japan)

D2-2 Intelligence based on the adaptive control 129
S. Shin(The Univ. of Tokyo, Japan)

D2-3 Intelligence based on fuzzy control 133
K. Tanaka(Kanazawa Univ., Japan)

D2-4 Intelligence based on neuro-control 137
S. Omatu(Osaka Prefecture Univ., Japan)

D2-5 Evolutionary algorithm for intelligent control 141
T. Furuhashi(Nagoya Univ., Japan)

S-E1:Robotics I(General Session)

E1-1 A scaling law between number of multi-robots and their task performance 145
K. Sugawara, I. Yoshihara, K. Abe (Tohoku Univ., Japan)

E1-2 Learning cooperative action rules for mobile robots from uncertain human instruction 149
H. Hiraishi, F. Mizoguchi(Science Univ. of Tokyo, Japan)

E1-3 Task level instructions for an arc welding robot 153
T. Yoshitomi(Kyushu Kyoritsu Univ., Japan)

S-E2:Evolutionary Computations(General Session)

E2-1 Evolving computing theory brings hopes to automatic programming 157
Q. Wang(Wuhan Inst. of Chemical Tech., China)

E2-2 Evolution on folding landscapes in combinatorial structures 161
S. M. Fraser(Santa Fe Inst., USA)

C. M. Reidys(Los Alamos National Labs., USA)

E2-3 Evolution of herding behavior of multiple autonomous mobile robots 166
B. T. Zhang(Seoul National Univ., Korea)
Y. J. Hong(Konkuk Univ., Korea)

E2-4 The species fitness method for the evolution of cooperative behavior in a group task 170
M. Kitahashi, T. Yamaguchi, M. Yachida (Osaka Univ., Japan)

E2-5 Computational evolution of human bipedal walking by a neuro-musculo-skeletal model 174
K. Hase(National Inst. of Bioscience and Human Tech., Japan)
N. Yamazaki(Keio Univ., Japan)

E2-6 The genetic algorithms(GAs) to evolve multiple agent cooperative system 178
M. Sugisaka, X. Wang(Oita Univ., Japan)
J. J. Lee(KAIST, Korea)

S-A1:Hardware Evolution(Invited Session)

A1-1 The gesture-controlled interactive games by artificial retina chips 182
K. Kyuma, H. Kage, Y. Miyake(Mitsubishi Electric Corporation, Japan)

A1-2 Building a machine for evolution in silico 186
E. A. Rietman(Bell Labs., USA)
R. Slous(Xilinx, USA)
H. Hemmi(NTT, Japan)
H. D. Garis, K. Shimohara(ATR, Japan)

A1-3 H^3:high-speed hardware for human-like genetic algorithm 190
H. Asada, H. Sugiura, T. Kawai, H. Ando, T. Shimada
(Nagoya Univ., Japan)

A1-4 On mixed-level real-time hardware evolutionary system 196
H. Hemmi, T. Hikage, K. Shimohara(NTT, Japan)

A1-5 A new structure of EHW 200
W.He, L. Kang, B. Wang(Wuhan Univ., China)

A1-6 Adaptive gait generation as an analogy to magnetising process 204
S. Mikami, M. Kubo, M. Wada (Hokkaido Univ., Japan)

S-A2:Brain Computing and Brainware(Invited Session)

A2-1 Realization model for brain computing 205
M. Ichikawa, H. Yamada, G. Matsumoto(RIKEN, Japan)

A2-2 Large-scale neural network method for brain computing 207
N. Miyakawa(Fuji Xerox, Japan)
M. Ichikawa, G. Matsumoto(RIKEN, Japan)

A2-3 Temporal learning rule and dynamic neural network model 210
Y. Shigematsu(Electrotechnical Laboratory, Japan)

A2-4 Robust segmentation of behaviorally relevant events in sensory recognition 214
by synergy of thalamo-cortical and cortico-cortical control
E. Koerner, U. Koerner(HONDA R and D Europe GmbH, Germany)

A2-5 Hypothetical reasoning and brainware 220
H. Tsujino(HONDA R and D Co., Ltd., Japan)
E. Koerner(HONDA R and D Europe GmbH, Germany)
H. Kondo(HONDA R and D Co., Ltd., Japan)

S-A3:Neuro Computing Technology(General Session)

A3-1 Identification of nonlinear dynamic systems based 224
on universal learning network
M. Han, K. Hirasawa, M. Ohbayashi, J. Murata, J. Hu, M. Hashimoto
(Kyushu Univ., Japan)

A3-2 Recognition of shapes and shape-changes in 3D objects by GRBF 228
(Generalized Radial Basis Function)network
N. Kinoshita, T. Katsuki, T. Miyazaki, M. Hirakawa, M. Okamoto
(Kyushu Institute of Technology, Japan)

S-B3:Agricultural Robot(Invited Session)

B3-1 Adaptive control for autonomous tractor using gyroscope and DGPS 234
K. Inoue, K. Otuka, M. Sugimoto, N. Murakami
(Japan National Agriculture Research Center, Japan)

B3-2 Development of an autonomous tractor for forage production 238
A. Okado, N. Itokawa (National Grassland Research Institute, Japan)
M. Ishida, H. Takenaga (Utsunomiya Univ., Japan)
K. Imou(The Univ. of Tokyo, Japan)

B3-3 Development of watermelon harvesting robot 'STORK' 242
M. Umeda, S. Kubota, M. Iida(Kyoto Univ., Japan)

B3-4 An image processing technique for automatic steering vehicle 246
in Japanese pear orchard
Y. Misao(Tottori Univ., Japan)

B3-5 Autonomous vehicle guidance system in paddy field 250
Y. Nagasaka, R. Otani, K. Shigeta, K. Taniwaki
(Japan National Agriculture Research Center, Japan)

B3-6 Measurement of the vibration characteristic with image processing 254
-Measurement of natural frequency with HSI color space-
H. Takeda(Tottori Univ., Japan)
K. Namikawa, M. Umeda(Kyoto Univ., Japan)
M. Iwasaki(Tottori Univ., Japan)

S-B4:Artificial Brain(Invited Session)

B4-1 Building an artificial brain using an FPGA based "CAM-brain machine" 258
H. D. Garis, N. E. Nawa (ATR, Japan)
F. Gers(I D SIA, Switzerland)
M. Korkin(Genobyte Inc., USA)
A. Agah(Univ. of Kansas, USA)

B4-2 "CoDi-1Bit": a cellular automata based neural net model simple enough to be implemented in evolvable hardware 263
F. Gers(IDSIA, Switzerland)
H. D. Garis(ATR, Japan)
M. Korkin(Genobyte Inc., USA)

B4-3 Learning and relocation capabilities of CAM-brain machine 267
H. Hemmi, K. Shinozawa, T.Hikage, K. Shimohara(NTT, Japan)

B4-4 Evolving CAM-brain to control a mobile robot 271
S. B. Cho, G. B. Song, J. H. Lee, S. I. Lee(Yonsei Univ., Korea)

B4-5 Artificial brain for a mobile vehicle 275
M. Sugisaka, X. Wang(Oita Univ., Japan)

S-B5:Genetic Algorithms and Genetic Programming(General Session)

B5-1 Genetic programming with loops 279
Y. Qi, B. Wang, L. Kang(Wuhan Univ., China)

B5-2 A fast TSP solver using GA on JAVA 283
H. Sengoku(Hitachi, Ltd., Japan)
I. Yoshihara(Tohoku Univ., Japan)

B5-3 Automatic programming of autonomous robots using a genetic algorithm 289
K. Tagawa, S. Kawaguchi, H. Iwamoto, K. Inoue, H. Haneda
(Kobe Univ., Japan)

B5-4 A novel genetic algorithm based on the theory of virus evolution 293
N. Nakaya, A. Kanasugi, K. Kondo(Saitama Univ., Japan)

B5-5 Learning of static evaluation function in tsume-shogi with genetic programming 297
T. Sawada, K. Suzuki, A. Ohuchi (Hokkaido Univ., Japan)

S-C3:Modeling and Complexity I(Invited Session)

C3-1 Modeling and complexity: control engineering point of view 301
H. Kimura(The Univ. of Tokyo, Japan)

C3-2 Deterministic and probabilistic approaches to model set validation 306
T. Zhou, S. Hara(Tokyo Institute of Technology, Japan)

C3-3 Statistical mechanics of learning and generalization 310
Y. Kabashima(Tokyo Institute of Technology, Japan)

S-C4:Sensor and Vision(General Session)

C4-1 A canceling method against equi-status noises for rotary optical sensor 314
K. Mine, N. Kubota, F. Morimoto, K. Fujii, S. Yamaguchi
(Kyushu Kyoritsu Univ., Japan)

C4-2 Sequential stereo vision and phase transition 318
Y. Yoshitomi, T. Kitazoe, J. Tomiyama, Y. Tatebe(Miyazaki Univ., Japan)

C4-3 A new sensorless AC survo motor and variable-speed control system driven by VSI 324
K. Fujii, K. Mine, N. Kubota, S. Yamaguchi(Kyushu Kyoritsu Univ., Japan)
S. Nonaka(Kinki Univ., Japan)

S-C5:Modeling and Complexity II (Invited Session)

C5-1 Modeling and complexity in neural networks 328
K. Aihara, N. Ichinose(The Univ. of Tokyo, Japan)

C5-2 Complex dynamics of chaotic neural networks with an asynchronous updating..... 332
M. Adachi(RIKEN, Japan)
K. Aihara(The Univ. of Tokyo, Japan)

C5-3 An asynchronous pulse neural network model and its analog circuit implementation 336
Y. Horio, M. Hanagata, H. Yasuda (Tokyo Denki Univ., Japan)

C5-4 Local and global modeling for complex time series 342
T. Ikeguchi(Science Univ. of Tokyo, Japan)
K. Aihara(The Univ. of Tokyo, Japan)

C5-5 Mixing invariant densities 346
G. Froyland(The Univ. of Tokyo, Japan)

C5-6 Nonlinear dynamical analysis of Japanese vowels 350
T. Miyano, A. Nagami(Sumitomo Metal Industries, Ltd., Japan)
I. Tokuda(Muroran Institute of Technology, Japan)
K. Aihara(The Univ. of Tokyo, Japan)

S-C6:Neural Network(General Session)

C6-1 A pruning algorithm for higher order neural networks 354
L. Ma, B. Xu, H. Miyajima(Kagoshima Univ., Japan)

C6-2 A learning method for large-scale recurrent neural networks 358
N. Honma, K. Abe(Tohoku Univ., Japan)
H. Takeda(Tohoku Gakuin Univ., Japan)

C6-3 Behavior planning of autonomous mobile robots based on cooperative neural networks 362
M. Murata, M. Nakamura, T. Ono, K. Onaga (Univ. of The Ryukyus, Japan)

C6-4 Food search behavior and neural networks 366
T. Kitazoe, Y. Yoshitomi, J. Tomiyama (Miyazaki Univ., Japan)

S-D3:Intelligent Control and Modeling (General Session)

D3-1 Reinforcement learning of airship control with adaptive state space segmentation 372
Y. Akisato, K. Suzuki, A. Ohuchi(Hokkaido Univ., Japan)

D3-2 An application of genetic algorithm on designing nonlinear model following control systems 376
W. Liu, S. Okubo, T. Li(Yamagata Univ., Japan)

D3-3 Application of a model independent control strategy 380
R. Chatterjee, F. Matsuno (Tokyo Institute of Technology, Japan)

D3-4 A probabilistic hilbert space approach towards understanding nonlinear dynamical systems in an observer's endo-and exo-variables 384
T. E. Schilhabel, C. J. Harris (Univ. of Southampton, UK)

D3-5 An experiment dynamic modelling scheme for flexible systems 388
Q. Guo, Y. Wu, J. L. Lu(Beijing Institute of Technology, China)

S-D4:Robotics II(General Session)

D4-1 Reinforcement learning for multiple robots with organizational learning 392
K. Takadama, K. Hajiri, T. Nomura(ATR, Japan)
S. Nakasuka(The Univ. of Tokyo, Japan)
K. Shimohara(ATR, Japan)

D4-2 Organizational knowledge on formation in multiple robots learning 397
K. Takadama, K. Hajiri, T. Nomura(ATR, Japan)
S. Nakasuka(The Univ. of Tokyo, Japan)
K. Shimohara(ATR, Japan)

D4-3 A study for construction of a 'biologically' autonomous robot 402
M. Migita, K. Ueda(Kobe Univ., Japan)

D4-4 Robust control of a robot manipulator by PID+Q controller 406
T. Matsuo, H. Suemitsu, S. Fujiwara(Oita Uiversity, Japan)

S-D5:Micro Machine and Micro Soccer Robot (General Session)

D5-1 Measuring dynamic viscoelasticity of a microscopic organism 410
K. Shigeta, R. Otani, Y. Nagasaka, K. Taniwaki
(Japan National Agriculture Research Center, Japan)

D5-2 Behaviors of a micro-robot imitating bacteria with flagella 414
T. Goto, M. Itou, Y. Takano (Tottori Univ., Japan)

D5-3 Dynamic position arrangements of soccer agents with genetic algorithms 418

T. Murata, K. Suzuki, A. Ohuchi (Hokkaido Univ., Japan)

D5-4 Robot soccer: sensing, planning, strategy and control, a distributed real time intelligent system approach 422
C. Messom(Singapore Polytechnic, Singapore)

S-E3:Artificial Life, Brain, and Organs(General Session)

E3-1 An application of a new model of cam-brain 427
B. Wang, L. Kang, W. He(Wuhan Univ., China)

E3-2 Distributed optimization by using artificial life system 431
T. Satoh(Yamaguchi Univ., Japan)
T. Okita(Hiroshima City Univ., Japan)

E3-3 Artificial Life and natural stories 435
K. Dautenhahn(Univ. of Reading, UK)
C. Nehaniv(Univ. of Aizu, Japan)

E3-4 Artificial visual system evolution for stereo perception by GA 440
W. Nian, K. Okazaki(Fukui Univ., Japan)
S. Tamura(Osaka Univ., Japan)

E3-5 The application of neurocomputer for a control problem 444
M. Sugisaka, Z. J. Liu(Oita Univ., Japan)

S-E4:Genetic Algorithms and Neural Network(General Session)

E4-1 Automatic path planning of spray robot for a die casting process by using genetic algorithm 448
T. Sakamoto(Ube Industries Co., Ltd., Japan)
K. Kuribayashi, S. Matsumoto, M. G. Franco, J. Tang
(Yamaguchi Univ., Japan)
K. Murakami, H. Komeya(Ube Industries Co., Ltd., Japan)

E4-2 Cooperative behavior and contol of collective autonomous mobile robots using reinforcement genetic programming 454
H. B. Jun, D. J. Kim, K. B. Sim(Chung-Ang Univ., Korea)

E4-3 A genetic algorithm for design of boundary filter in subband coding by using wavelet transform 458
J. Tang(Beijing Univ. of Posts and Telecommunications, China)
Y. Zhang(Academia Sinica, China)

E4-4 Structure optimization and learning of neural networks by co-evolution 462
D. W. Lee, S. H. Lee, K. B. Sim(Chung-Ang Univ., Korea)

E4-5 Discovery of intelligence -beyond discrimination between artificial and natural- 466
T. Moriyama(Kobe Univ., Japan)

E4-6 Variation of activation functions for accelerating the back-propagation algorithm 470
B. Lee, M. Lee(Korea Maritime Univ., Korea)

S-E5:Artificial Mind, Chaos, and Complexties(General Session)

E5-1 An architecture of an artificial mind for collaborating and communicating robots 474
A. Ito, H. Kozima(Communications Research Laboratory, Japan)

E5-2 Towards mindreading by an attention-sharing robot 478
H. Kozima, A. Ito(Communications Research Laboratory, Japan)

E5-3 The effect of self organization in the trade cycle 482
M. Tabuse, M. Tanaka-Yamawaki(Miyazaki Univ., Japan)

E5-4 Introduction of functional boundary model for emergent organization 486
K. Shono, K. Suzuki, A. Ohuchi (Hokkaido Univ., Japan)

S-A4:Complex Adaptive System I(Special Session)

A4-1 Uncertain variables and learning algorithms in knowledge-based control systems 490
Z. Bubnicki(Wroclaw Univ. of Tech., Poland)

A4-2 Cognitive robotics : A new approach to artificial intelligence 495
T. Christaller(GMD-German National Research Center for Information Tech., Germany)

A4-3 A modification of (M-R) systems and its simulation 499
Y. G. Zhang, C. M. Xu (Academia Sinica, China)
M. Sugisaka(Oita Univ., Japan)

A4-4 Robot football, artificial life, and complexity 503
J. Johnson(The Open Univ., UK)

A4-5 Robocup challenge 509
H. Kitano(Sony Computer Science Laboratory, Japan)

S-A5:Robot and Mechatronics Control via Softcomputing (Invited Session)

A5-1 Initial configuration dependence in a self-organizing robot 510
K. Izumi, H. Tamura, K. Watanabe (Saga Univ., Japan)
Y. Ikeda(Mitsubishi Electric Corp., Japan)

A5-2 An incest prevented evolution strategy and its application in optimal gain tuning for a mobile robot contorl system 514
M. M. A. Hashem, K. Watanabe, K. Izumi, T. Miyazaki
(Saga Univ., Japan)

A5-3 Construction of fuzzy behavior-based control systems for a mobile robot 518
K. Watanabe, K. Izumi(Saga Univ., Japan)

A5-4 Fuzzy behavior-based tracking control for an omnidirectional mobile robot 524

K. Izumi, K. Watanabe(Saga Univ., Japan)

A5-5 Neuro-approach to motion control 528
S. Omatu(Osaka Prefecture Univ., Japan)

A5-6 A proposal of human-machine interactive system through linguistic instructions using fuzzy classifier system 532
M. Fujii, T. Furuhashi(Nagoya Univ., Japan)

A5-7 Trajectory prediction and catching system of moving target under fuzzy reasoning method 537
T. Yasuno, T. Kamano, T. Suzuki, K. Kumabe
(The Univ. of Tokushima, Japan)
Y. Kataoka(Kataoka Machine Co., Ltd., Japan)

S-B6:Complex Adaptive System II (Special Session)

B6-1 Improving vehicle performance using adaptive control techniques 541
D. J. G. James, K. J. Burnham(Coventry Univ., UK)
M. J. Richardson, R. A. Williams(Jaguar Cars Ltd., UK)

B6-2 Sliding mode cooperative motion control of dual arm manipulators 546
W. Yim, M. Selvarajan, W. R. Wells (Univ. of Nevada-Las Vegas, USA)

B6-3 Real-time control schemes for mirosot 550
J. H. Kim, K. C. Kim, D. H. Kim, Y. J. Kim, P. Vadakkepat (KAIST, Korea)

B6-4 Estimation problems in artificial intelligence 556
F. S. Mistiri(Univ. of Garyounis, Libya)
A. P. Wang(Arizona State Univ., USA)
S. Ueno(Kyoto School of Computer Science, Japan)

S-B7:Control in Robotics(Invited Session)

B7-1 An area filling algorithm for autonomous sweeping robot 564
W. K. Hyun, J. Cho, C. S. Park (Honam Univ., Korea)
T. K. Park(KIMM, Korea)

B7-2 An appropriate parameter selection for designing motor and servo controller of robot manipulator to achieve precise contour control 568
N. Egashira(Kurume National College of Tech., Japan)
M. Nakamura, S. Goto(Saga Univ., Japan)
N. Kyura(Kinki Univ., Japan)

B7-3 Real-time control of a SCARA robot by visual servoing with the stereo vision 572
S. H. Han(Kyungnam Univ., Korea)
M. H. Lee(Pusan National Univ., Korea)
J. I. Bae(Pukyung National Univ., Korea)
K. S. Yoon(The Univ. of Tokyo, Japan)

B7-4 Detection of human's confusion from their unconscious action with neural networks 578

K. Nakatsukasa, H. Hashimoto, F. Harashima (The Univ. of Tokyo, Japan)

B7-5 Robust robot controller through feedback sliding mode observer 582
K. B. Park, J. J. Lee(KAIST, Korea)
T. Tsuji(Kyushu Inst. of Tech., Japan)

B7-6 Implementation of multilayer neural network with threshold neurons 586
K. Sato, H. Hikawa(Oita Univ., Japan)

B7-7 Motion planning in dynamic environments -a parallel online approach 590
H. Worn, D. Henrich, C. Wurll (Univ. of Karlsruhe, Germany)

S-C7:Artistic Communication for Artificial Life and Robotics (Invited Session)

C7-1 The consciousness of artificial life 594
R. Ascott(Univ. of Wales College, UK)

C7-2 Artistic communication for a-life and robotics 598
N. Tosa(ATR, Japan)

C7-3 Evolution as artist 604
T. Ray(ATR, Japan)

C7-4 Communications, artificial life, and art 605
R. Nakatsu(ATR, Japan)

S-C8:Communication(General Session)

C8-1 HMM analyses of human random number generators 610
M. Tanaka-Yamawaki, H. Masuda, M. Kawagoe (Miyazaki Univ., Japan)

C8-2 Cooperative task processing with adaptive communication 614
in baggage carrying problem
M. Katsura, K. Suzuki, A. Ohuchi (Hokkaido Univ., Japan)

C8-3 Learning of pheromone communication for adaptive organizations 618
in multiple monkey banana problem
K. Suzuki, A. Ohuchi(Hokkaido Univ., Japan)

S-C9:Vision Application(Invited Session)

C9-1 Hovering control of model-helicopter by vision 622
T. Ishimatsu, K. C. Ung, T. Fujito (Nagasaki Univ., Japan)
S. Nagata(Tech. Center of Nagasaki, Japan)

C9-2 A morphological approach to feature extraction for fish discrimination robot 626
Y. Nagashima, T. Nakazono (Sasebo National College of Tech., Japan)
T. Ishimatsu(Nagasaki Univ., Japan)

C9-3 Three-dimensional measurement of object surface and moving particles 630
using circular bias

K. Kawasue, I. Iwamoto (Sasebo National College of Tech., Japan)
T. Ishimatsu(Nagasaki Univ., Japan)

C9-4 Computer input device for handicapped using vision sensor 634
T. Ochiai, R. Matsui (Ube National College of Tech., Japan)
T. Ishimatsu(Nagasaki Univ., Japan)
O. Takami(Tech. Center of Nagasaki Prefecture, Japan)

C9-5 A technique of three-dimensional measurement of huge object 638
K. Fujimoto, S. Nagata (Tech. Center of Nagasaki Prefecture, Japan)
T. Ishimatsu(Nagasaki Univ., Japan)

C9-6 Recognition of both pattern and position of color objects using a visual system with two cameras 642
M. Sugisaka, H. Okuzono, K. Yamada (Oita Univ., Japan)

S-D6:Life and Complexity(Invited Session)

D6-1 Towards the theory of bio-complexity 646
H. Tanaka(Tokyo Medical and Dental Univ., Japan)

D6-2 Evolvability of machines and tapes 650
T. Ikegami(The Univ. of Tokyo, Japan)

D6-3 Evolution of fitness landscapes 654
Y. Toquenaga(Univ. of Tsukuba, Japan)
M. J. Wade(Univ. of Chicago, USA)

D6-4 A description of quasi-autopoietic systems based on the framework of (M,R) systems 658
T. Nomura, K. Shimohara(ATR, Japan)

D6-5 Development of meaning structure by usage-based word relationships 662
T. Hashimoto(RIKEN, Japan)

D6-6 Nonlinear oscillations on an abstract rewriting system on multisets 666
Y. Suzuki, H. Tanaka(Tokyo Medical and Dental Univ., Japan)

S-D7:Robotics(Invited Session)

D7-1 A method of a mobile robot navigation by a task-level feedback control 670
Y. Hada, K. Takase(Univ. of Electro-Communications, Japan)

D7-2 Strategies for changing configurations of autonomous arms in a complex pushing task 674
H. Zha, H. Nagahama, T. Hasegawa(Kyushu Univ., Japan)

D7-3 On why should a robot recognize itself? 678
L. Berthouze(Electrotechnical Laboratory, Japan)
S. Itakura(Emory Univ., USA)

D7-4 Interactive 3D walk-through system using dynamic gestures 682

D. Nariman, H. Nishino, K. Utsumiya(Oita Univ., Japan)

D7-5 Multi-functional robot-hand tactile sensor for material recognition 686
K. Shida, J. Yuji(Saga Univ., Japan)

D7-6 Development of a multi-freedoms controller using FPGA 690
S. Kurono, T. Toyofuku(Kyushu Sangyo Univ., Japan)
S. Aramaki(Fukuoka Univ., Japan)

D7-7 Analysis of human transient walking by wavelet trasform 695
H. Ikeuchi(Oita Univ., Japan)
K. Shinkoda(Univ. Hospital of Occupational and Environmental Health, Japan)
R. Katoh(Kyushu Inst. of Tech., Japan)
M. Sato(Kitakyushu National College of Tech., Japan)
T. Yamashita(Kyushu Inst. of Tech., Japan)

S-E6:Fuzzy Control and Virtual Reality (General Session)

E6-1 On fuzzy stochastic control process and its application 699
T. Odanaka(Hokkaido Information Univ., Japan)
T. Shohdohji, S. Kitakubo (Nippon Inst. of Tech., Japan)

E6-2 Holonic control system using fuzzy criterion 703
N. Kusumi, K. Hirasawa, M. Ohbayashi, J. Hu (Kyushu Univ., Japan)

E6-3 Autonomous navigation for mobile robot using hierarchical fuzzy inference and genetic algorithm 707
D. Y. Ju, M. Nemoto, T. Iwata(Saitama Inst. of Tech., Japan)
K. Toyoda(Ebara Corporation, Japan)

E6-4 Kinetic characteristics of human binocular vision for wide view head mounted display in virtual reality 711
J. L. Wu, L. Wang, K. Kuribayashi (Yamaguchi Univ., Japan)

E6-5 Measurement of human visual and auditory characteristics for a virtual driving system 715
J. L. Wu, H. Mizuhara(Yamaguchi Univ., Japan)
Y. Nishikawa(Osaka Inst. of Tech., Japan)

E6-6 Human visual and haptic characteristics on distance perception for virtual teleoperation systems 719
J. L. Wu, T. Miyake(Yamaguchi Univ., Japan)

S-E7:Evolutionary Computation and Neural Network (Invited Session)

E7-1 Competitive associative networks for control of linear and nonlinear plants 723
S. Ren, S. Kurogi(Kyushu Inst. of Tech., Japan)

E7-2 A general class of neural nets for principal and minor component analysis 727
K. Matsuoka(Kyushu Inst. of Tech., Japan)

E7-3 Blind signal separation of convolved non-stationary signals 731
M. Kawamoto(RIKEN, Japan)

K. Matsuoka(Kyushu Inst. of Tech., Japan)
N. Ohnishi(Nagoya Univ., Japan)

E7-4 Negatively correlated neural networks for classification 736
Y. Liu, X. Yao(The Univ. of New South Wales, Australia)

E7-5 On-line evolutionary learning of NN-MLP 740
T. Suzuki, Q. Zhao(The Univ. of Aizu, Japan)

E7-6 Autonomous mobile robot rendezuous 744
P. Pawicz, P. Kalata, M. Kam(Drexel University, USA)

Proc. of Third Int. Symp. on Artificial Life, and Robotics (AROB III' 98),
Oita, Japan, 19-21, January, 1998,

Organizational Knowledge on Formation in Multiple Robots Learning *

○ Keiki Takadama
ATR Human Information Processing Research Labs. / The University of Tokyo

Koichiro Hajiri
ATR Media Integration & Communications Research Labs. / Ritsumeikan University

Tatsuya Nomura
ATR Human Information Processing Research Labs.

Shinichi Nakasuka
The University of Tokyo

Katsunori Shimohara
ATR Human Information Processing Research Labs.

2-2 Hikaridai, Seika-cho, Soraku-gun, Kyoto 619-02 Japan, Tel:+81-774-95-1093 Fax:+81-774-95-1008
Email: takadama@hip.atr.co.jp/keiki@ai.rcast.u-tokyo.ac.jp

Abstract

This paper extends our organizational learning model by adding the utilization of the organizational knowledge on formation to improve the collective performance, and focuses on how this organizational knowledge works for supporting new robots in the process of their adaptation to the organization. Through intensive simulations of truss construction by multiple robots, the following experimental results have suggested: (1) Robots with the organizational knowledge on formation complete given tasks in fewer iterations than those without the organizational knowledge; (2) the steps with the organizational knowledge become fewer as the number of robots increases; (3) The organizational knowledge on formation enables robots to complete tasks which cannot be completed without the organizational knowledge.

Keywords: organizational learning, organizational structure, formation, multiple robots, emergence, adaptive behavior

1 Introduction

When some robots are defective or inoperative in space, it is difficult to repair those robots. Therefore, robots continue to complete given tasks by adding new robots to robot organization, instead of repairing the broken ones. In this case, it is important for new robots to acquire their own appropriate functions to maintain or even increase the collective performance. In order to acquire appropriate functions through interaction among multiple robots, we have already proposed a novel organizational learning model [6, 7, 9]. However, this model only focuses on the emergent processes that robots dynamically form an organizational structure to complete given tasks effectively, and does not focus on the effect of the knowledge acquired in the cycle of completing tasks. Although the former bottom-up approaches improve the collective performance, the latter top-down approaches also contributes to supporting new robots to adapt to the organization. In order to combine both these bottom-up and top-down approaches, we extend our organizational learning model [6, 7, 9] by adding the utilization of the organizational knowledge on formation.

This paper is organized as follows. Next section starts to explain the concept of the organizational learning, and section 3 gives the details of the organizational learning model with learning classifier systems. In section 4, new utilization method for the organizational knowledge is proposed. An example of multiple robots for truss construction task is given in section 5, and section 6 discusses the experimental results. Finally, the conclusion is given in section 7.

2 Organizational Learning

2.1 Multiple Robots and Organizational Learning

In the multiple robots learning, it is important for robots to have some mechanisms for self-evaluating their adaptive behaviors to improve the collective performance. The easiest way of evaluating behaviors is to employ a global evaluation function as an explicit control. However, robots must communicate with the central control system or must broadcast information to get the results of a global evaluation function. This approach makes communication cost high. Especially in space, since an amount of communication is limited by the weight or electrical power of robots, it is quite importance to reduce the communication cost. Furthermore, since communication traffic increases as the number of robots increases, it is difficult for robots to perform the tasks with cooperating in real time. Moreover, it is generally difficult to define an appropriate global evaluation function which assigns an optimal and rational behavior to all robots. Therefore, we employ only local evaluation functions instead of a global one, and aim to make robots perform inter-

* Paper submitted to the Third International Symposium on ARTIFICIAL LIFE AND ROBOTICS (AROB'98)

actions among their neighborhoods and acquire their own functions for adaptive collective behaviors only with local evaluation functions.

This kind of bottom-up approach is studied in the context of management organizational sciences as organizational learning, and a lot of researches focus on economical market systems or human organizations [1, 2, 3, 5]. In management organizational sciences, organizational learning is generally defined as follows: "*Organizational Learning* is the creating, acquiring and transferring of *distinctions* and *practices* in the organizations. It is effective if it increases the organization's fit to its environment. Organizational learning implies behavior modification, including changes in relationships, in order to create the conditions for creating, acquiring and transferring distinctions and practices [3]". Since this concept enables robots to autonomously form an organizational structure which completes given tasks effectively, we have already proposed Organizational-learning oriented Classifier System which introduces the properties of organizational learning [7, 9].

2.2 Organizational Structure and Functions

Before we explain our organizational learning model, two technical terms are defined as follows.

- **Organizational Structure:** A structure in which robots acquire their own functions.
- **Function:** A sequence of behaviors determined by rules.

Since the organizational structure dynamically changes, robots must adapt to a new organization to maintain or improve the organizational performance. For effective adaptation to the new organization, robots learn adaptive strategies as the order of using the rules, and acquire the effective long sequence of behaviors. Since the long sequence of behaviors produces a lot of variety of behaviors, this variety provides a chance to improve the total organizational performance.

3 Organizational-Learning Oriented Classifier System

In this section, we explain Organizational-learning oriented Classifier System (OCS) [7, 9] which is an extended multiagent version of Learning Classifier System (LCS) with the concept of organizational learning. OCS enables robots to acquire their own appropriate functions through the local interaction among them and form organizational structure which improves organizational performance. In OCS, robots behave only according to their own local evaluation functions, instead of a global evaluation function as an explicit control. Although Michigan approach and Pittsburgh approach for the LCS are proposed, we modify both approaches with introducing the concept of the organizational learning as follows.

- As shown in Fig. 1, each robot does not employ the explicit global evaluation function, but employs the local evaluation function which is composed of the following four parts: (1) Rule base composed of a lot of rules (CFs: Classifiers) in LCS, (2) Working Memory (WM) for storing information on the environment state, (3) Memory for storing the behavior rule sequence which is cleared after rewards are distributed to robots, and (4) Evaluation Mechanism to evaluate the sequence of behavior rules.

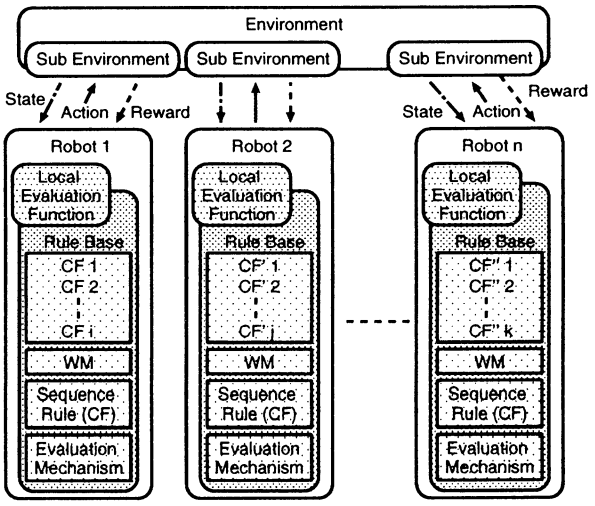


Figure 1: **Architecture of OCS**

- Robots can obtain their own environmental states, however the total environment states around robots cannot be obtained. Robots determine the behavior according to the state.
- The crossover operation used in Michigan approach is not performed between the rules, and a global evaluation function for selecting elite LCS used in Pittsburgh approach is not also employed.
- All robots have a set of the same simple and rational rules except for the strength of their own rules, and modify or acquire their own functions by self-organizing the strength when rewards are distributed to robots.

In OCS, the following mechanisms and assumptions are also employed.

- A robot performs one behavior by selecting one rule.
- A rule is selected according to a roulette selection used in usual LCS.
- At the beginning, all strength are set to the same value.

4 Organizational Knowledge on Formation

In order to enhance our organizational learning model by adding the top-down approaches, this section proposes the utilization formation method. As a definition, "formation" is the organizational structure which completes given tasks with minimum steps, and is stored as organizational knowledge after robots complete tasks. Although different formations are formed according to the number of robots, the organizational knowledge on formation for a certain number of robots can be transferred to different numbers of robots. In order to utilize these formations, we propose the following four types of methods:

1. **Gathering Formation Method:**
   This method as shown in Fig. 2 (a) adds the units of formation to the robot organization up to the present total number of robots. For example, when 6 new robots are added to 3 robots, Robot(n+3) and Robot(n+6) where n=1,2,3 utilize the same formation for 3 robots. In the above variables, Robot(n) indicates the nth robots. Especially when the present number of robots is not multiple of the number of robots in the stored organizational knowledge, some robots utilize a part of the knowledge.
2. **Gathering Random Method:**
   This method as shown in Fig. 2 (b) adds some robots in formation to the organization up to the present total number of robots. In this figure, robots with function A, B, B, B, C, C are selected at random and are added to the organization.
3. **Progressive Additional Formation Method:**
   This method as shown in Fig. 2 (c) adds one unit of formation to the robot organization when the performing robots form effective organization structure. For example, when 6 new robots are added to 3 robots, 3 new robots are added at first with utilizing the stored organizational knowledge for 3 robots. After effective organizational structure is formed by the performing 6 robots, the remaining 3 new robots are added to the organization. In this case, new function D and E are produced through the interaction between two formations for 3 robots, and a new formation for 4 robots is formed by composing of the function A, A, C and D.
4. **Progressive Additional Random Method:**
   This method as shown in Fig. 2 (d) adds some robots in formation to the robot organization when the performing robots form effective organization structure. In this figure, robots with function A, A, C are selected at random and are added to the organization at first. After effective organizational structure is formed by the performing 6 robots, the remaining 3 new robots are selected at random and added to the organization. In this case, a new function D is produced through the interaction among robots, and a new formation for 4 robots is formed by composing of the function A, C, C and D.

After adding robots to the robot organization, robots start to modify their own functions to improve the collective performance according to the reinforcement learning proposed in [8]. Since functions are assigned according to the the organizational knowledge, robots do not have to acquire their own new appropriate functions, but just modify the assigned functions. As a result of the function modification, robots form 3 new types of formations as shown in Fig. 2 .

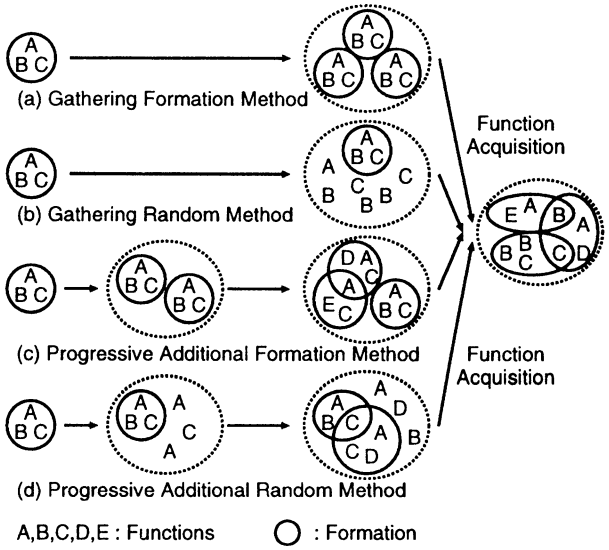


Figure 2: **Utilization Formation Method**

5 Multiple Robots in Space

5.1 Example

To verify the effect of the utilization formation method with OCS, we perform experiments of truss construction combined by beams in space as quickly as possible. In order to complete this task, robots must perform the following matters.

- **Cooperation: Behavior order**
  Robots must learn the behavior order to cooperate. For example, two robots hold beams respectively with setting a desired location in a desired angle between the two beams, and the third robot welds the two beams.
- **Acquisition of Different Functions**
  Robots must acquire different functions even if the situation is the same. For example, robots acquire the following functions to cooperate with

each other: "hold a beam", "weld beams", or "the combination of them".

5.2 Robots

In order to reduce the weigh of robots, each robot has one arm and holds either a beam or a welding tool. Robots hold their own beams at the station and wait for welding beams at the beam constructing location. The other robots go to the welding location to weld beams or return to the station to get another beams. As other assumptions or limitations, the following matters are taken into consideration.

- Robots can move or rotate for setting a beam at the desired location and angle.
- Robots which wait at the beam constructing location cannot release beams until beams are welded by welding robots.
- Robots cannot pass a beam to other robots.
- Robots cannot weld beams at the welding location until the beams are set at the desired location with the desired angle.
- Robots do not know their appropriate functions beforehand.

In this task, robots get into deadlock situations when all robots hold their own beams or hold the welding tools, or when some robots cannot go to the beam constructing or welding location in the case that other robots wait in the course of the beam constructing or welding location.

6 Simulation

6.1 Experiments

We perform the following five experiments: Non utilization formation method and New four methods in Fig. 2 (a) ~ (d), and compare the results of the above five experiments in term of both the steps and the iteration counts. In the experiments, we count one step when all robots perform one behavior, and count one iteration when robots complete a task or get into deadlock situations. In each case, 8, 12 and 16 robots perform to construct the truss with combining 13 beams, and continue to complete the same task with utilizing the organizational knowledge on formation for 4 robots.. In this function acquisition, behaviors are reinforced according to the method [8].

6.2 Results

Table 1, 2 and 3 show three results: "Final steps for completing tasks", "Iteration counts" and "Final steps × Iteration counts". The first result indicates the steps after robots acquire their own appropriate functions, the second indicates the iteration counts from the beginning to the convergence of acquiring functions, and the third indicates the multiplication values between the final steps and the iteration counts.

As shown in table 1, robots with the method in Fig.2 (a) ~ (d) cannot complete given tasks with fewer steps than those without the organizational knowledge on formation when the number of robots is small. However, the steps with these utilization formation methods become fewer than those without the organizational knowledge as the number of robots increases. Furthermore, robots with this method can complete tasks which cannot be completed without the organizational knowledge. Especially in the utilization formation methods, the progressive additional formation method as shown in Fig.2 (c) contributes to finding fewer steps than those with other methods.

From table 2, we have found that robots with the gathering formation method as shown in Fig.2 (a) complete tasks with fewer iterations than those with other methods. Since a certain number of robots in the progressive method as shown in Fig.2 (c) and (d) are added to the robot organization little by little, the iterations are larger than those with other methods.

Finally, as shown in table 3, the steps with the gathering formation method in Fig.2 (a) are fewer than those with other methods in term of the multiplication values between the final steps and the iterations.

Table 1: **Final Steps for Completing Task**

Robots	Without Organizational Knowledge	Utilization Formation Fig.2			
		(a)	(b)	(c)	(d)
8	128	143	154	143	154
12	143	127	126	116	124
16	—	115	109	109	111

Table 2: **Iteration Counts**

Robots	Without Organizational Knowledge	Utilization Formation Fig.2			
		(a)	(b)	(c)	(d)
8	56	41	53	41	53
12	11	1	43	58	64
16	—	10	22	59	174

Table 3: **Final Steps × Iteration Counts**

Robots	Without Organizational Knowledge	Utilization Formation Fig.2			
		(a)	(b)	(c)	(d)
8	7168	5863	8162	5863	8162
12	1573	127	5418	6728	7936
16	—	1150	2398	6104	19314

6.3 Findings and Discussions

From the experimental results in the above simulations of truss construction with multiple robots, the following findings are obtained.

- **Effectiveness of Organizational Knowledge on Formation :**
  Although 16 robots without the organizational

knowledge on formation cannot complete given tasks, the utilization of the organizational knowledge enables robots to complete them. Furthermore, the steps for completing tasks become fewer than those without the organizational knowledge as the number of robots increases. From these results, this organizational knowledge contributes to completing tasks which cannot be completed without organizational knowledge, and also contributes to reducing the steps.

- **Effectiveness of Progressive Additional Formation Method :**
  The progressive additional formation method extends the search space by adding one unit of formation to the robot organization. Since this search space is bigger than the space with the gathering formation method and is smaller than the space without the organizational knowledge on formation, this method enables robots to find the effective solution in a certain search range. Therefore, robots with this method complete given tasks with fewer steps than those with other methods. However, this method takes more time than the gathering formation/random methods to complete tasks. From these factors, the progressive additional formation method is effective for the tasks which do not care the time for completion but must be completed in fewer steps.

  Although the similar research is studied by Hikage et al., this research focuses on the single agent learning with the concept of progressive evolution [4]. This paper, on the other hand, proposes the method for multiple robots with focusing on the advantages of formation.

- **Effectiveness of Gathering Formation Method :**
  Since the search space for the gathering formation method is smaller than the space with other methods, this method concentrates on finding the solution in the limited search space. Therefore, robots with this method complete given tasks with fewer iteration counts than those with other methods. Furthermore, since the multiplication values between the final steps and the iterations with this method are the smallest in the utilization formation methods, this method is effective for the practical and engineering use.

- **Effectiveness of Random Addition :**
  The steps with the gathering random method is fewer than those with the gathering formation method as the number of robots increases. This is because the former search space is larger than the latter one. This result indicates that a certain amount of randomness is needed to extend the search space and to reduce the steps.

7 Conclusion

This paper has extended our organizational learning model by adding the utilization of the organizational knowledge on formation, and has shown its effectiveness in the task construction problems. By addressing the bottom-up and top-down approaches in the multiple robots environment, the organizational knowledge on formation contributes to completing given tasks which cannot be completed without the organizational knowledge. Furthermore, we have found that the progressive additional formation method is effective for the tasks which must be completed in fewer steps, and also found that the gathering formation method enables robots to complete given tasks with fewer iteration counts than those with other methods. Future researches include:

- Theoretical analysis of the effectiveness of the organizational knowledge on formation.
- Investigation of the effectiveness of our method with real robots.

References

[1] C. Argyris and D. A. Schon: "*Organizational Learning*", Addison-Wesley, 1978.

[2] R. Duncan and A. Weiss: "*Organizational Learning: Implications for organizational design*", in B. M. Staw (Ed.), Research in organizational behavior, Vol. 1, JAI Press, pp. 75-123, 1979.

[3] R. Espejo, W. Schuhmann, M. Schwaninger and U. Bilello: "*Organizational Transformation and Learning*", John Wiley & Sons, 1996.

[4] T. Hikage, H. Hemmi and K. Shimohara: "*Progressive Evolution Model Using A Hardware Evolution System*", The Second International Symposium on ARTIFICIAL LIFE AND ROBOTICS (AROB'97), pp. 18-21, 1997.

[5] J. G. March:, "*Exploration and Exploitation in Organizational Learning*", Organizational Science, Vol. 2, No. 1, pp. 71-87, 1991.

[6] K. Takadama, K. Hajiri, T. Nomura, M. Okada and K. Shimohara: "*Learning Model for Adaptive Behaviors as an Organized Group of Swarm Robots*", The 2nd International Symposium on Artificial Life and Robotics (AROB'97), pp. 103-106, 1997.

[7] K. Takadama and T. Terano: "*Good Solutions will Emerge without a Global Objective Function: Applying Organizational Classifier System to Printed Circuit Board Design*", The IEEE International Conference on Systems, Man, and Cybernetics (SMC'97), pp. 3355-3360, 1997.

[8] K. Takadama, K. Hajiri, T. Nomura, S. Nakasuka and K. Shimohara: "*Reinforcement Learning for Multiple Robots with Organizational Learning*", The 3nd International Symposium on Artificial Life and Robotics (AROB'98), 1998, to appear.

[9] K. Takadama, S. Nakasuka and T. Terano: "*Printed Circuit Board Design via Organizational-Learning Agents*", Applied Intelligence: Special Issue on Intelligent Adaptive Agents, 1998, to appear.

Proc. of Third Int. Symp. on Artificial Life, and Robotics (AROB III' 98),
Oita, Japan, 19-21, January, 1998,

A study for construction of a 'biologically' autonomous robot

Masao Migita and Kanji Ueda
Department of Mechanical Engineering, Kobe University,
Nada, Kobe 657, Japan
migita@mi-2.mech.kobe-u.ac.jp
ueda@mech.kobe-u.ac.jp

Abstract

Autonomy in animal behavior was investigated with the ultimate goal to construct an autonomous robot in the biological sense of the word. It is discussed that no specific mechanism is needed for describing the autonomy of the agent: "autonomy" is captured as a parameter change by the agent, originated from an assumption that the agent follows a specific rule.

1 Introduction

An autonomous robot is expected to work well in a field where a man cannot control directly. Usually, therefore, the term "autonomous robot" means that it is not connected to the user with an interface, however, its decision making is programmed by the user. This entails the so-called frame problem: the robot cannot determine the relevant frame of reference in executing its task [1]. In contrast with this, we do not think that an animal worries about the frame problem, though it is often said to act following to some 'programmed' behavior [2,3]. In the present paper the authors suggest that if we persist in defining the task of an autonomous robot explicitly, the frame problem cannot be avoided. Therefore, we should not think that the frame of reference is explicit, not even in our mind before the robot starts to work, if we want the robot to behave autonomously, i.e. without being exposed to the frame problem. Rather, we should consider of an interface between man and robot through which we describe the robot's own frame of reference.

In order to construct such an interface, we investigated the homing behavior, which means repetitive use of a certain sheltering place in our study, of a fish and tried to simulate the behavior in a computer. However, the modes of behavior are not clearly separated in the homing of the real fish. Therefore, the real homing behavior is not expressed as a sequence of choices from a 'predefined' set of behavioral acts but from a 'redefined' set of those.

We present a method of expressing such an aspect of animal behavior formally and will discuss the interface through which we can find a meaningful frame of reference of the simulated agent.

2 Autonomy in animal behavior

In the discourse of Neo-Darwinism, various behavioral patterns of animals are considered to have some advantages in their habitat: in this sense every behavior should be recognized as a response following to a specific rule of stimulus-response. However, every information processing by an organism includes slow processes such as chemical reactions in the receptor of the stimulus. This implies that stimulus-response cannot be described as a unique rule [4]. In the realm of biology, where one cannot claim an infinite velocity of observation propagation, i.e., an individual never identifies its surroundings completely before its decision making, one-to-many types of mappings between stimuli and responses are certainly observed. We may call

this biological autonomy, since the individual appears to determine the boundary conditions of its dynamics, the frame of reference in our case, by itself. Thus, the 'task' in an animal's behavior is retrospectively and implicitly found, while that of an autonomous robot must be defined beforehand and explicitly[5, 6, 7].

3 Observation of behavior of a fish

3-1 The fish and experimental settings

The fish used for the observation is a blenny fish *Meiacanthus kamoharai,* distributed in the southern waters of Japan. This fish appears to have spatial knowledge of its habitat, for instance, a nest site, feeding sites and so on. It was also observed that the fish often used unusual sheltering places when an observer approached to it, and the sheltering place appeared to be selected temporally. It is obvious that this fish carries the ability of homing, which implies that the fish is able to make a structured map of its habitat, and to do so even in a short time.

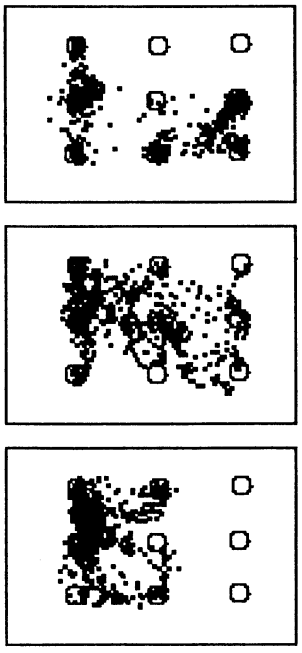


Fig.1. The transition of movement pattern of the fish. Open circles are represent the shelters. They were obtained from the 1 st, the 6 th and the 11 th data window on the experiment on individual 1.

Young individuals of *M. kamoharai* were captured and kept in laboratory. The individuals were placed in an experimental tank ($60 \times 40 \times 40 cm^3$) one by one, and their behaviors were recorded for two hours with a video set. Nine identical shelters were arranged in the aquarium. The position of the individuals, projected on a 2-D space of the floor of experimental tank, was recorded at every second.

3-2 Results

In the experimental tank, the fish spent most of the time in the shelters, moving from one to the others frequently (Fig. 1). In order to investigate whether the fish constructs any pattern of movement among the shelters, the information value of sequence was calculated with each data set. Frequency of use of each shelter was investigated with χ^2–test. The correlation between the probability of a certain sequence of shelter i to j and the distance between shelters i and j was also tested.

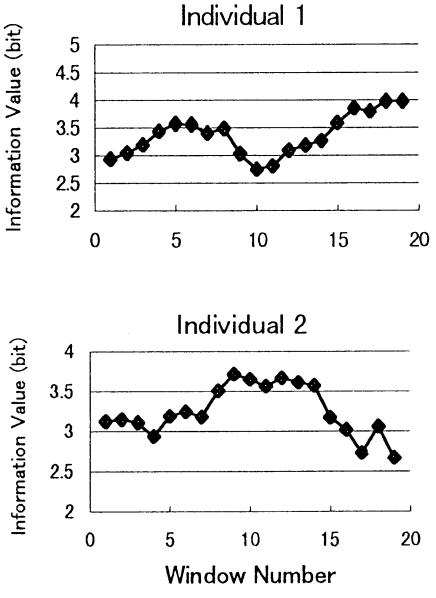


Fig. 2. The transition of the information values. Note differing axes.

lengths of durations called data windows: one is the two hours (7200s) window, that is, the whole data, and the other is 30 minutes (1800s) window, which was employed to investigate the transitions of behavioral patterns. Nineteen data sets of 30 minutes were obtained from the two hours data by setting off the starting time by five minutes.

During the two hours observation, the fish sometimes formed certain patterns of movement in which the individuals came to use certain shelters and to pass over the others. It was also observed that such patterns disappeared if the fish came to every shelter evenly. We found these both in several two hours data sets at the same time (Fig. 2). This suggests that pattern formation, or learning of the environment, occurred in two ways; the balanced use of the shelters can be considered as an evidence that the fish has learned that one shelter could be used as well as the one which had been more frequently used earlier.

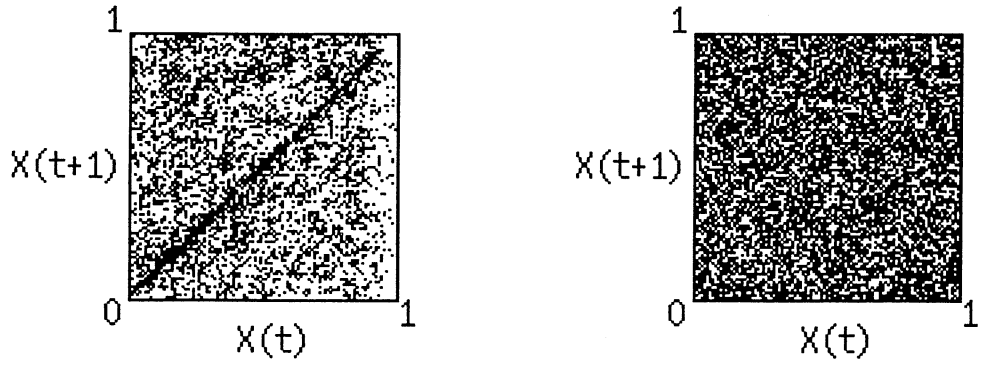
4 Simulation with contraction map

4-1 The incomplete identification model

We conducted computer simulations to investigate how can we describe transitions of the movement pattern. We employed the incomplete identification model proposed by Gunji and Kusunoki [8,9]. The incomplete identification model illustrates a process through which a rule is made up from finite data set, as if it is valid for infinite numbers of input.

The environment has nine shelters as the experimental. The simulated fish contains a value which describe sheltering behavior as the following way. In the experiment, *M. kamoharai* exhibited negative correlation between the probability of movement between two shelters and their distance. In order to express this character of movement, we employed a value which is a real number distributed in the interval from 0 to 1. The value determines the new sheltering place according to the distance between current shelter and the other shelters, so that the probability and the distance are negatively correlated if the next value is chosen at random. A pattern of movements among the shelters is represented by a sequences of this value.

The simulated fish memorizes twenty successive pairs of values which consist of the values representing previous and current shelters, then makes a map by the following procedure. First, the data represented as $(X_i(t), X_i(t+1))$, $(i=1,\cdots,20)$, and $0<X_i(t)<1$, are plotted on a $X(t)$-$X(t+1)$ space. The suffix i is assigned to each data so as to be $X_i<X_j$ if $i<j$. Then, each value are coarse grained as intervals $I_i(t)$, where $I_i(t) \cap I_j(t)=\phi$, so as to cover the whole interval of (0, 1). Thus, we obtain a coarse grained map consisting of set of rectangles, which is a set of 'coarse grained points', denoted by $I_i(t)$ and corresponding $I_j(t+1)$. And then, contract the structure of this coarse grained map into each coarse grained point. By iterating these procedures, we obtain a map from $X(t)$ to $X(t+1)$. The simulated fish calculates the value for its next step with this map. Thus, the rule which determines the behavior of the simulated fish is altered at every time step.



(a) (b)

Fig. 3. Return maps obtained (a) by our model and (b) by a random walk model.

4-2 Results

The return map (Fig.3) shows that the simulated fish often revisits one shelter in successive time steps, but it does not persist in visiting that shelter; successively visited shelters are soon altered.

The graph of the information value (Fig.4) shows a transition of movement pattern. It is obvious that the simulated fish formed some movement patterns, i.e., frequent use of a certain shelter and less use some others, and that these patterns are altered to that of even use of each shelter, as time elapsed, which is indicated by large amount of the information value. Our model, thus, describes the temporality of the behavior of homing, without any external parameter change.

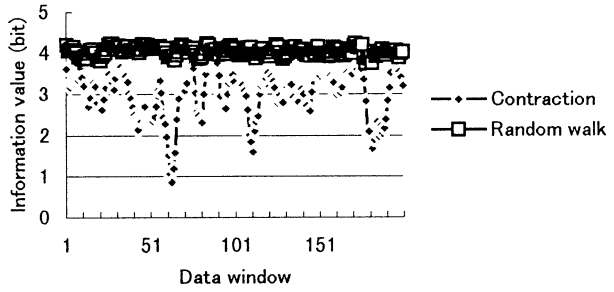


Fig. 4. The information values of our model and a random walk model. Each data window contains 60 data of choice of the shelter.

5 Concluding remarks

As Rosen discussed, organisms appear as if they often alter the parameters of their behavior internally [10]. The difference between Rosen's 'feedforward model' and the incomplete identification is that feedforward model assumes that the organism can be described as a specific dynamical system. On the other hand, the incomplete identification model sketches the process so that the motion of an observed agent comes to be seen as a dynamical system, thus no parameters can be recognized *a priori*. We would like to construct autonomy not as a real entity with a certain mechanism but as a complementary concept which lies between the observer (user) and the object.

Acknowledgements

The study has been supported in part by the grant of "Methodology for Emergent Synthesis" Project (project number 96P00702), "Research for the Future" Program of the Japan Society for the Promotion of Science (JSPS). We gratefully appreciate the improvement of the English text given by A. Markus.

References

[1] D. Dennett, "Cognitive wheels: The frame problem of AI", In: The robots dilemma: The frame problem in artificial intelligence. (ed. Z.W.Pylyshyn), ABLEX.

[2] J.R. Krebs and N.B. Davies, "An introduction to behavioural ecology 2nd ed." Blackwell Scientific, Oxford.

[3] R. A. Brooks, "Elephants don't play chess", Robotics and autonomous systems pp. 3-16, 1990.

[4] K. Matsuno, "Protobiology: Physical basis of biology" CRC Press, Boca Raton, 1989.

[5] T. Moriyama and Y.-P. Gunji, "Autonomous learning in maze solution by *Octopus*", Ethology 103, pp.499-513, 1997.

[6] Y.-P. Gunji, "Behavioural plasticity of hermit crab, Riv. Biol. 89, pp. 69-78.

[7] M. Migita and Y.-P. Gunji, "Plasticity in symbiotic behavior", Riv. Biol. 89, pp.389-406, 1996.

[8] Y.-P. Gunji and Y. Kusunoki, "A model of incomplete identification illustrating schooling behavior", Chaos, Solitons & Fractals 8(10), pp.1623-1630, 1997.

[9] Y. Kusunoki, N. Kitabayashi and Y.-P. Gunji, "A model of incomplete identification for pattern formation of foraging ants" (in Japanese), Biophysics 37 supp. 2, pp. 63, 1997.

[10] R. Rosen, "Feedforwards and global system failure" , J. Theor. Biol. 74, pp.579-590.

Proc. of Third Int. Symp. on Artificial Life, and Robotics (AROB III' 98),
Oita, Japan, 19-21, January, 1998,

Robust Control of a Robot Manipulator by PID+Q Controller

Takami Matsuo, Haruo Suemitsu
Department of Human Welfare Engineering
Oita University
700 Dannoharu, Oita, JAPAN 870-11
Email : {matsuo, suemitu}@cc.oita-u.ac.jp

Shuichi Fujiwara
Graduate School of Production Systems Engineering
Oita University
700 Dannoharu, Oita, JAPAN 870-11
Email : fuji@engy.en.oita-u.ac.jp

Abstract

The Youla parametrization of all stabilizing compensators consists of a full-order observer-based controller and free parameters in RH_∞. Recently, we derived a parametrization of all stabilizing compensators, which has a static output feedback term in the central part, by state-space methods instead of coprime factorization methods. Using the parametrization obtained here, we propose the PID+Q controller which consists of a PID controller with an internal model and a free parameter. Moreover, we design a robust stabilizer for a parallel link robot manipulator using the PID+Q controller.

1. Introduction

The parametrization of all stabilizing compensators, so-called the Youla parametrization, can be expressed as a coprime factorization from with any free parameter in RH_∞. Moreover, Doyle rewrote the Youla parametrization in terms of the full-order observer and a free parameter in RH_∞ [1]. Mita proved that the Youla parametrization can be derived by the linear fractional transformation (LFT) in the state-space setting [2]. Recently, we showed that a stabilizing compensator, with the order greater than the system's order, consists of a full-order observer-based compensator, a static output feedback and any free parameter in RH_∞, and pointed out that any linear time-invariant finite-dimensional stabilizing compensator can be expressed as the linear-fractional-transformation-type controller for appropriate choice of the free parameter when the others are fixed [3].

Moreover, we derived the parametrization of all stabilizing compensators based on a static output feedback and obtain the PID controller-based compensator with a free parameter for multivariable systems [5]. We call this compensator the PID+Q controller. It is an important problem in designing a PID controller to achieve a specified robust performance, since PID controllers are widely used in industrial processes with time delay or other uncertainties. Many researchers have attracted the attention of PID-parameter tuning to design a robust PID controller [4]. We show the free parameter in the PID+Q controller can be used to improve the performance or the stability of the control systems using the H_∞ technique. The PID+Q controller has the following characteristics:

- The nominal performance of the PID+Q controller coincides with that of PID controller. It is not dependent on the free parameter Q in the PID+Q controller. Therefore, three PID parameters should be used to achieve good nominal performance.
- The PID+Q controller represents all stabilizing controllers which guarantee Type-I closed-loop response.
- The free parameter Q can be designed to achieve good robust performance and robust stability of the system.

Most commercial robots use simple PD or PID controllers. Although these controllers install independently and locally at each joint actuator, these control schemes guarantee local asymptotic stability for setpoint position control and satisfactory performance may also be accomplished for low-speed motion [6]. However, robot manipulators have dynamic couplings and gravity forces which can be treated as structures uncertainties. Therefore, for high-speed motion the

coupling effects become active and PD or PID controllers can not stabilize the systems. Namerikawa et al. designed the H_∞ controller for a parallel link robot manipulators and showed the effectiveness of the proposed controller with experimental results [7].

The purpose of this paper is to show that we can improve the performance and the stability of a parallel link robot manipulators with structured uncertainties such as dynamic couplings and gravity forces, using the PID+Q controller. In this paper, the following notation is used:

$\mathcal{F}_l(G,Q)$: lower LFT

$\left[\begin{array}{c|c} A & B \\ \hline C & D \end{array}\right] := C(sI-A)^{-1}B+D$

2. Design of PID+Q Controller

In this section, we give the PID+Q controller by using the static output-feedback-based parametrization, which consists of a PID controller, an internal model and free parameter Q. The free parameter in the PID+Q controller can be used to improve the robust performance or the robust stability of the control systems. In the following subsection, we discuss the characteristics of the PID+Q controller.

2.1. Definition of PID+Q Controller

Consider the following MIMO plant

$$y(s) = G_s(s)u(s) \tag{1}$$

where $y \in R^m$, $u \in R^r$ and

$$G_s(s) = \left[\begin{array}{c|c} A & B \\ \hline C & 0 \end{array}\right]. \tag{2}$$

We derive the parametrization of all stabilizing compensators based on the following PID controller

$$\begin{aligned} u(s) &= -(K_P + K_I\frac{1}{s} + \frac{K_D s}{\tau s+1})(y(s)-r(s)) && (3)\\ &= -\{(K_P+\frac{1}{\tau}K_D) + K_I\frac{1}{s} - \frac{1}{\tau}K_D\frac{1}{\tau s+1}\} \\ &\quad (y(s)-r(s)) && (4)\end{aligned}$$

where $r(s)$ is a set point, K_P, K_I and K_D are matrices in $R^{r\times m}$.

To convert the PID controller into a static output feedback controller, we augment the outputs of the plant as follows:

$$y_a(s) = \left[\begin{array}{c} y_1(s) \\ y_2(s) \\ y_3(s) \end{array}\right] = G_p(s)y(s) \tag{5}$$

$$G_p(s) = \left[\begin{array}{c} I_m \\ \frac{1}{s}I_m \\ \frac{1}{\tau s+1}I_m \end{array}\right] \tag{6}$$

Note that the closed-loop system of the above augmented plant is type-I although the system type of the closed-loop system with a so-called two-stage compensator may not be type-I. From straightforward computations, the PID controller is interpreted as the static output feedback controller for the augmented plant $G_a(s)$,

$$\begin{aligned} y_a(s) &= G_a(s)u(s) && (7)\\ G_a(s) &= G_p(s)G_s(s) && (8)\end{aligned}$$

Moreover, we can rewrite the augmented plant with disturbances as the following generalized plant :

$$G_a(s) = \left[\begin{array}{c|cc} A_a & B_1 & B_2 \\ \hline C_1 & D_{11} & D_{12} \\ C_2 & D_{21} & 0 \end{array}\right]. \tag{9}$$

We assume that the generalized plant can be stabilized by a static output feedback, i.e. there exists a output feedback gain K_0 such that $A_a + B_2K_0C_2$ is stable. In this case, $u(s) = K_0y_a(s)$ is a PID controller which stabilizes the MIMO plant $G(s)$. We note that K_0 cannot be selected as zero vector, because the A-matrix of the generalized plant include the poles of the integrators. The use of the augmented output y_a allows us to stabilize the plants with its relative degree 2, *i.e.* $G_s(s) = \frac{1}{s^2}$, by static output feedback.

Using our parametrization of all stabilizing compensators with the static output feedback, we can obtain the following parametrization of all stabilizing compensators for the augmented plant, which has the PID controller in the central part, the internal model of the augmented plant and a free parameter $Q(s)$. We obtained the parametrization of all stabilizing LTI compensators, $K(s)$, for the augmented plant $G_a(s)$ as follows [3]:

$$\begin{aligned} K(s) &= \mathcal{F}_l(\tilde{K}(s), Q(s)) && (10)\\ \tilde{K}(s) &= \left[\begin{array}{c|cc} A_K & 0 & B_2 \\ \hline 0 & K_0 & I \\ -C_2 & I & 0 \end{array}\right] \\ A_K &= A_a + B_2K_0C_2 \end{aligned}$$

where $Q(s) \in RH_\infty$.

Although the controller $K(s)$ can be interpreted as a two stage compensator, it gives us all stabilizing compensators of the augmented plant $G_a(s)$ by making choice of $Q(s)$ in RH_∞. The overall controller $K_a(s)$ for the plant $G_s(s)$ is given as follows:

$$K_a(s) = K(s)G_p(s) \tag{11}$$

We will call this the PID+Q controller. The closed-loop response with the PID+Q controller has the type-I characteristics, because the augmented plant has an integrator. The design parameters can be considered as K_0 and $Q(s)$. We will discuss how to design controller parameters K_0 and $Q(s)$.

2.2. Nominal Performance of Closed-Loop Systems with PID+Q Controller

Consider the nominal plant model case where the internal model is set to be equal to the nominal plant

model and the setpoint signal r_s is added to the internal model as well as the central PID controller as in Figure 1. Defining the signals p_s, r_s, z_s and q_s as in Figure 1, we get the following equations:

$$(I - K_0 G_p(s) G_s(s))(z_s - q_s) = 0$$
$$z_s = K_0 G_p(s) p_s + Q(s) G_p(s) G_s(s)(z_s - q_s)$$
$$p_s = -r_s + G_s(s) z_s$$

We can set $z_s = q_s$ when the initial value of the plant equals that of the internal model. In this case, we get the following sensitivity transfer function:

$$p_s = -(I - G_s(s) K_0 G_p(s))^{-1} r_s \qquad (12)$$

Thus, the sensitivity transfer function of the nominal plant with the PID+Q controller is equal to that with the normal PID controller. The nominal performance is only depend on the PID parameters K_0 but not on the free parameter $Q(s)$. Therefore, the free parameter $Q(s)$ as a robust stabilizer does not worsen the nominal performance.

2.3. Robust Stability of Closed-Loop System with PID+Q Controller

In this subsection, we show that the robust stability of a plant operated by a PID controller can be improved by implementing the free parameter and its internal model. We will design the robustly stable system with the PID+Q controller for multiplicative uncertainties by selecting Q-parameter appropriately. Consider the following plant $\tilde{G}_s(s)$ with the multiplicative uncertainty:

$$\tilde{G}_s(s) = G_s(s)(1 + \Delta(s)) \qquad (13)$$

where $G_s(s)$ is given by (2) and $\Delta(s)$ is a stable multiplicative uncertainty. The augmented plant $\tilde{G}_a(s)$ is as follows:

$$\tilde{G}_a(s) = G_a(s) + G_a(s)\Delta(s) \qquad (14)$$

We assume that the uncertainty satisfies

$$|\Delta(j\omega)| \le |W(j\omega)|, \quad 0 \le \omega \le \infty.$$

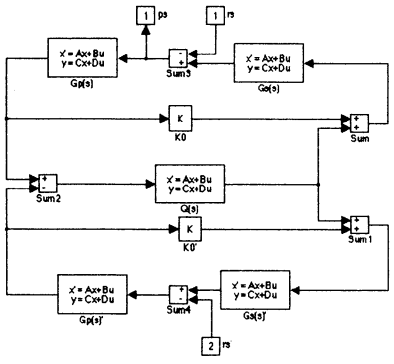


Figure 1: Closed-loop system with PID+Q controller.

In [5], we showed if the model matching condition:

$$\|(T_1(s) - T_2(s)Q(s)T_3(s))W(s)\|_\infty < 1 \qquad (15)$$

is satisfied for $Q(s) \in RH_\infty$, then the closed-loop system is stable for any $\Delta(s)$, where

$$T_1(s) = (I - K_0 G_a(s))^{-1} K_0 G_a(s)$$
$$T_2(s) = (I - K_0 G_a(s))^{-1}$$
$$T_3(s) = G_a (I - K_0 G_a(s))^{-1}.$$

3. Application to Robot Manipulators

We design the PID+Q controller to stabilization of a parallel link robot manipulator as an example of MIMO nonlinear mechanical systems. We adopt the model of the two-parallel-link manipulator given by Namerikawa et al. [7]. The dynamic model of the manipulator-plus-actuator is obtained as follows:

$$M(q)\ddot{q} + D(q,\dot{q})\dot{q} + g(q) = \alpha f(v) \qquad (16)$$
$$M(q) = \begin{bmatrix} m_{11} & m_{12} \\ m_{21} & m_{22} \end{bmatrix}, D(q) = \begin{bmatrix} d_{11} & d_{12} \\ d_{21} & d_{22} \end{bmatrix}$$
$$f(v) = \begin{bmatrix} f_1(v_1) \\ f_2(v_2) \end{bmatrix}, g(q) = \begin{bmatrix} g_1 \\ g_2 \end{bmatrix}$$
$$q = \begin{bmatrix} q_1 \\ q_2 \end{bmatrix}, v = \begin{bmatrix} v_1 \\ v_2 \end{bmatrix}$$

where q_i is the i-th link angle, v_i is the control voltage of the i-th actuator and $f(v)$ represents the actuator nonlinearities. The phisical parameters of the two-parallel-link manipulator given by Namerikawa et al. are as follows [7]:

$$m_{11} = \eta^2 J_m + M_{11}, m_{22} = \eta^2 J_m + M_{22}$$
$$m_{12} = M_{12}\cos(q_2 - q_1) = m_{21}$$
$$d_{11} = \eta^2 (D_m + \frac{K_t K_b}{R}) + F_{v1}$$
$$d_{22} = \eta^2 (D_m + \frac{K_t K_b}{R}) + F_{v2}$$
$$d_{12} = -M_{12}\dot{q}_2 \sin(q_2 - q_1)$$
$$d_{21} = M_{12}\dot{q}_1 \sin(q_2 - q_1)$$
$$g_1 = V_1 \cos q_1, g_2 = V_2 \cos q_2$$
$$\alpha = \frac{\eta K_a K_t}{R}$$
$$M_{11} = m_1 l_{c1}^2 + m_3 l_{c3}^2 + m_4 l_1^2 + I_1 + I_3$$
$$M_{12} = m_3 l_2 l_{c3} - m_4 l_1 l_{c4}$$
$$M_{22} = m_2 l_{c2}^2 + m_3 l_2^2 + m_4 l_{c4}^2 + I_2 + I_4$$
$$V_1 = (m_1 l_{c1} + m_3 l_{c3} + m_4 l_1) g$$
$$V_2 = (m_2 l_{c2} + m_3 l_2 - m_4 l_{c4}) g$$

and the nominal plant model is selected as follows:

$$M_0\ddot{q} + D_0\dot{q} = \alpha v \qquad (17)$$
$$M_0 = \begin{bmatrix} m_{11} & 0 \\ 0 & m_{22} \end{bmatrix}$$

$$D_0 = \begin{bmatrix} d_{11} & 0 \\ 0 & d_{22} \end{bmatrix}.$$

We take an internal model as in Figure 2 where the signals are defined as follows:

q_{d1}, q_{d2}	: set point values
e_1, e_2	: controlled signals
q_1, q_2, q_1', q_2'	: augmented outputs
v_1, v_2	: control input.

We suppose that the target position q_d is given and consider a setpoint control problem in which the posture of the robot manipulator is allowed to approach asymptotically the target state $(q, \dot{q}) = (q_d, 0)$ from any initial state [8]. We use the central controller as the PD controller without the nonlinear compensation as follows:

$$v = \frac{1}{\alpha}\{-K_v\dot{q} + K_p(q_d - q)\} \quad (18)$$

$$K_v = \begin{bmatrix} 300 & 0 \\ 0 & 300 \end{bmatrix}, \; K_p = \begin{bmatrix} 10000 & 0 \\ 0 & 10000 \end{bmatrix}$$

We consider the plant perturbation as the following two cases:

- Case 1 : uncertainties such as link-parameters
- Case 2 : actuator nonlinearities such as saturation, backlash

The high gain PD feedback is robust for the parameter uncertainties such as $\delta M, \delta D$ and δg, but not for the input nonlinearities. Therefore, we design the free parameter $Q(s)$ to stabilize the closed-loop system with the input nonlinearities. We can get the solution $Q(s)$ using MATLAB LMI toolbox after converting Equation (15) to the generalized plant and checking whether the free parameter $Q(s)$ is stable or not. Figure 3 shows the feedback configuration of the manipulator with PID+Q controller via SIMULINK.

4. Conclusion

In this paper, we proposed the PID+Q controller which can be interpreted as the PID controller with an internal model and a free parameter. Moreover, we designed a robust stabilizer for a parallel link robot manipulator with the PID+Q controller.

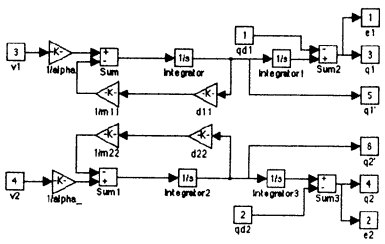


Figure 2: The internal model via SIMULINK.

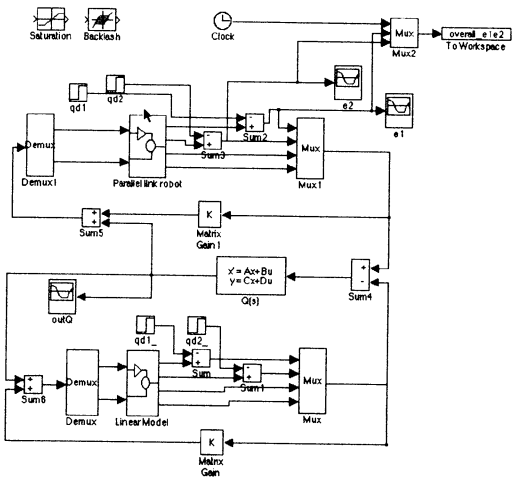


Figure 3: Feedback configuration of the parallel link robot manipulator with PID+Q controller.

References

[1] Doyle, J. C., K. Glover , P. P. Khargonekar and B. A. Francis, "State-Space Solutions to Standard H_2 and H_∞ Control Problems", *IEEE Trans. on Automatic Control*, **AC-34-8**, 831-846 (1989).

[2] Mita, T. and Z.Hui, "Youla Parametrization without Using Coprime Factorization", *Trans. of the Instrument and Control Engineers*, **31-4**, 540-541 (1995). (*in Japanese*)

[3] Matsuo T. and K. Nakano, "A Parametrization of All Stabilizing Compensators with a Static Output Feedback in the Central Part and Its Application to PID controller", *Preprints of 13th IFAC World Congress*, **vol.C**, 229-234 (1996).

[4] Musch,H. E. and M. Steiner, "Robust PID Control for an Industrial Distillation Column", *IEEE Control Systems Magazine*, **August 1995**, 46-55 (1995).

[5] Matsuo T. and K. Nakano, "Robust Control of Multivariable Systems by PID+Q Controller", *Proceedings of American Control Conference*, 3674-3678 (1997).

[6] Lee G.-W. and Cheng F.-T., "Robust control of manipulators using the computed torque plus H_∞ compensation method", *IEE Proc.-Control Theory Appl.*, **vol.143**, **no.1**, 64-72 (1996).

[7] Namerikawa T., M. Fujita and F. Matsumura, "Robust H_∞ Control of a Parallel Link Robot Manipulator", *Transaction of IEEJ-D*, **vol.116**, **no.2**, 207-215 (1996). (*in Japanese*)

[8] Arimoto, S. : *Control Theory of Non-Linear Mechanical Systems, A Passive-Based and Circuit-Theoretic Approach.* Oxford University Press (1996).

Proc. of Third Int. Symp. on Artificial Life, and Robotics (AROB III' 98),
Oita, Japan, 19-21, January, 1998,

Measuring Dynamic Viscoelasticity of a Microscopic Organism

K. Shigeta, R. Otani, Y. Nagasaka, K. Taniwaki
Dept. of Farm Mechanization
National Agriculture Research Center
Tsukuba 305, Japan

Abstract

Dynamic viscoelasticity measuring system for small sized bio-materials like small organs or cells was developed. Control program of Atomic Force Microscope (AFM) was modified in order to apply sine wave on material through the piezoelectric device of AFM. The material under test is vibrated an up-and-down motion and makes the cantilever bent which has been come in contact with the upper part of the material. The tip of micro cantilever was also remodeled in order to make contact to the material by flat surface. A linearity of deformation of vibrating device and spring constant of micro cantilever were measured in order to perform quantitative analysis.

A dry yeast was used as test sample to investigate the properties of the measuring device, and measurement results showed that it was possible to detect internal losses caused by viscoelasticity of the yeast.

Keywords: dynamic viscoelasticity, AFM, bio-material, micro-cantilever

1. Introduction

This paper describe about dynamic viscoelasticity measuring system for micro bio-materials like small organs or cells. Measurement of relationship between the displacement of piezo electric device and applied electric voltage and spring constant of micro-cantilever were conducted.

In order to develop a micro machine by material of microscopic organism like protein or cellulose, it is necessary to measure mechanical characteristics or electrical properties of these microscopic organisms. With regard to mechanical characteristics of organism, measurement of dynamic viscoelasticity is more important than that of static stress and distortion since the viscoelasticity has an effect on transfer characteristics of kinetic energy or an absorption of forces applied. There are studies about viscoelastic characteristics of material's surface[1], or metal bar[2], however studies about dynamic viscoelasticity of micro bio-material are rare.

Looking at a present measuring apparatus, a displacement of stress sensor used in the apparatus and the size of a microscopic organism such as a plant cell makes little difference. However the displacement of the stress sensor itself is disregarded in the present apparatus. Therefore it is difficult to use the present measuring apparatus for microscopic organism. There are no known methods for measuring dynamic viscoelasticity of a microscopic bodies.

In order to measure dynamic viscoelasticity of material, a frequency response of a distortion should be detected with a very few stress in sinusoidal wave applied to the material under test. A piezoelectric device of AFM have minute vibrating mechanism. Also it is able to measure a deflection of a micro cantilever which is in contact to the object, by laser and a photo detector. In this study, AFM was remodeled to make dynamic viscoelasticity measurement of a microscopic organism.

2. Dynamic viscoelasticity measuring system

Fig. 1 shows the schematic diagram of dynamic viscoelasticity measuring system in this study. With AFM standard, since it was not fit for measurement, remodeling was given. A possible amplitude of piezoelectric device of AFM was about 100 nm and this value was too small to make enough deformation to test sample. Therefore by means of making some modification to internal hardware of AFM, the maximum amplitude was expanded to about 2 micrometer. A feedback loop makes the output from photodetector constant in normal use of AFM and it is impossible to detect deformation of test object. Therefore control program was modified in order to follow the deformation of test object precisely by the micro cantilever. Usually the AFM tip which is sharpened to get higher resolution will make damage to test object in this study. Fig. 2 shows the tip processed to give flat contact to the test

object by Fixed Ion Beam method (FIB). By these remodeling and modifications of original AFM, an enough vibration amplitude was able to be applied to the object, also the micro cantilever which is in contact with the top of object came to be bent to measure the stress which is added to the object.

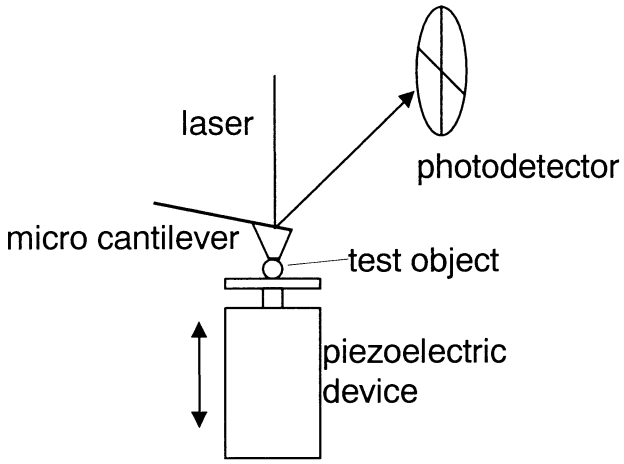


Fig.1 Schematic diagram of dynamic viscoelasticity measuring system

Test object, such as a plant cell, is set on a stage which is connected to the upper part of the piezoelectric device. As sine wave is input on piezoelectric device of AFM, test object is vibrated an up-and-down motion and makes the cantilever bent which has been come in contact with the upper part of the object. The force added to sample is able to be found from a deflection of cantilever. The distortion of sample is found by the difference of piezoelectric device amplitude and a cantilever deflection.

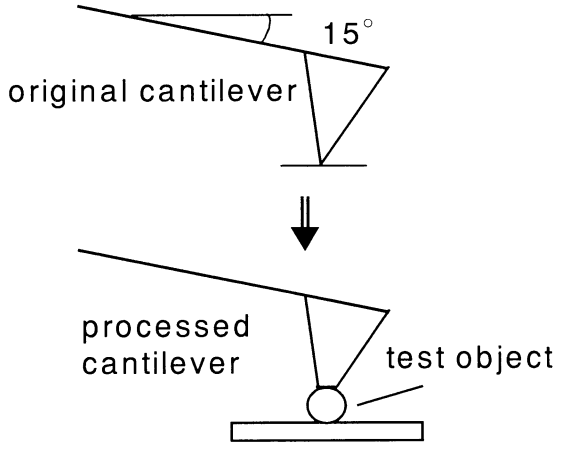


Fig. 2 AFM tip processed to make flat contact by FIB

3. Strain linearity of vibrating device and spring constant of micro cantilever

In order to measure dynamic viscoelasticity of micro bio-material quantitatively, it is necessary to calibrate the sensitivities of sensors and the linearity of vibrating devices. In this study, micro-laser interferometer was applied to measure the linearity of piezoelectric device. Fig. 3 shows schematic diagram of piezoelectric device deformation measuring system. The beam emitted by the laser diodes is split into two parts in order to constitutes the reference and the measurement beams. After being reflected back by the mirror on the moving object the measurement beam interferes with the reference beam. Fig. 4 shows the deformation of piezo electric device was almost linear.

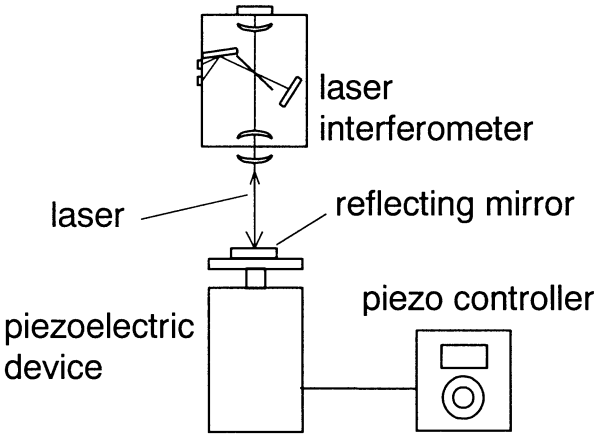


Fig. 3 A laser interferometer to measure deformation of piezoelectric device

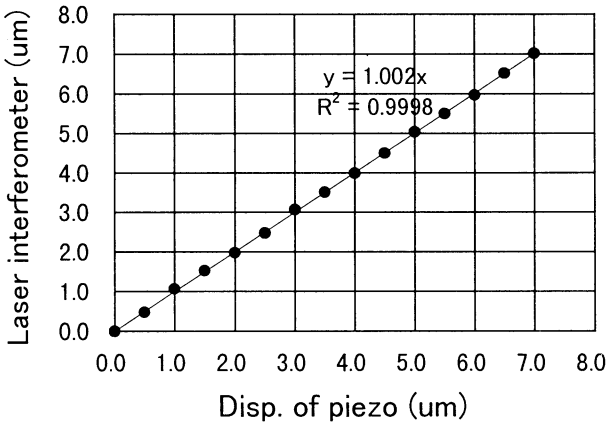


Fig. 4 The linearity of piezo electric device deformation

The stress applied to test objects are detected by means of converting bend of micro cantilever into force. Fig. 5 shows schematic diagram of spring constant measuring system.

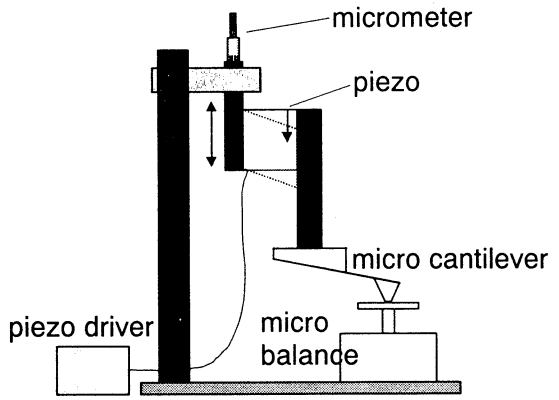


Fig. 5 Precision micro balance and piezoelectric device were applied for measuring spring constant of micro cantilever

From the position where the micro cantilever make a little contact with the top of the table of micro balance, the piezo started to deform by 0.5 micrometer step. Fig. 6 shows the spring constant measurement result. This result shows that the spring constant of micro cantilever used for the dynamic viscoelasticity measuring system was 0.17 N/m.

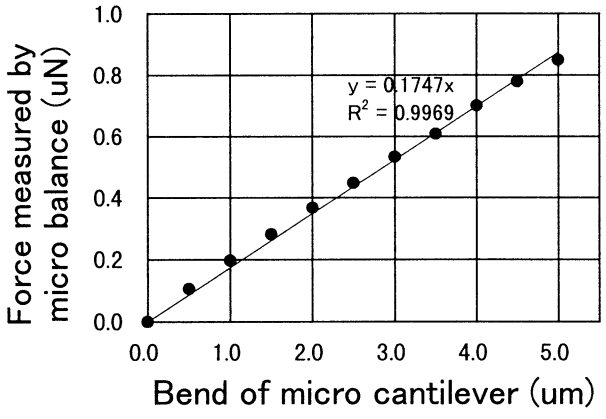


Fig. 6 Spring constant of micro cantilever

4. Dynamic viscoelasticity measurement result

Dry bread yeast of diameter about 3 micrometer was used as a bio-material under test. Silicon wafer was also measured for comparison. In order to measure one piece of yeast, it is necessary to locate the yeast just under the tip of the micro cantilever. A rough image of the yeast was measured by contact AFM in advance, then the top of the image was moved right under the tip of micro cantilever. The piezoelectric device was vibrated in a frequency range from 10Hz to 100Hz and a frequency response of micro cantilever was measured. It was possible to detect phase lag of about 55 degree in frequency range from 20Hz to 100Hz, which is a time-lag of a response according to an inside loss of one piece of yeast(Fig. 7). It is expected to come into use for many kind of microscopic organism. However, in order to apply this measuring system to irregular shaped materials, at this point it is necessary to consider the influence of shape which will affect on deformation of test objects.

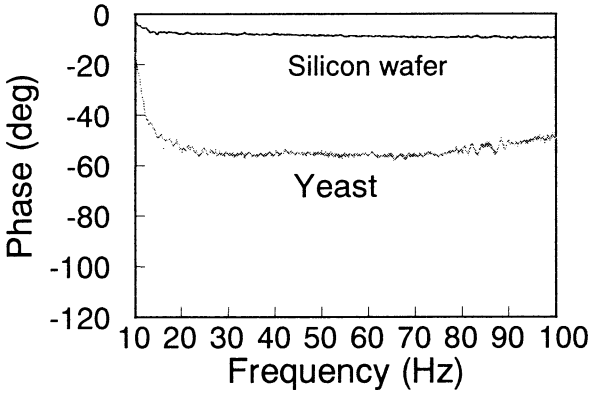


Fig. 7 Phase shift of deformation of dry yeast and silicon wafer detected by the dynamic viscoelasticity measurement system

5. Conclusion

In order to measure dynamic viscoelasticity of small sized bio-materials like small organs or cells, AFM was remodeled to develop measurement system. Test object is vibrated an up-and-down motion and makes the cantilever bent which has been come in contact with the upper part of the specimen. Linearity of piezoelectric device deformation was verified and the spring constant of micro cantilever was measured in order to perform quantitative analysis. A dry yeast was used as test specimen to investigate the properties of the measuring device, and measurement results

showed that it was possible to detect internal losses caused by viscoelasticity of the dry yeast.

References

[1] T. Kajiyama, "Analyses of Aggregation Structure and Viscoelastic Characteristics of Polymeric Surface(in Japanese)" J. Adhesion, Vol.31, No. 9,pp363-368, 1995

[2] A. Umeda, et al, "Measurement of Dynamic Mechanical Properties in Microstructures by Impact", Proc. Int. Sym. on Microsystems, pp169-172, 1995

Proc. of Third Int. Symp. on Artificial Life, and Robotics (AROB III' 98),
Oita, Japan, 19-21, January, 1998,

Behaviors of a Micro-Robot Imitating Bacteria with Flagella

Tomonobu GOTO, Makoto ITOU, and Yasunari TAKANO
Department of Mechanical Engineering
Tottori University, Tottori 680, Japan

Abstract

A micro-robot imitating mobile bacteria with helical flagella learns a strategy to approach a destination. The robot is assumed to consist of a spherical body and two helical screws. While one of the screws rotates steadily, the other screw alternates two modes, rotation and standstill. Numerical simulations are performed to analyze the motion of the robot. The resistive force theory derived from the fluid dynamics of Stokes flow is employed to evaluate fluid force exerted on the robot. After adequate learning, the robot can approach the destination moving zigzag as bacteria do. If the robot is coming up to the destination, it moves straight utilizing two screws, or else, the robot changes its direction rotating only one screw.

Key Words: Bacterium, Micro-Robot, Helical Screw, Learning, Resistive Force Theory

1 Introduction

Typical mobile bacteria such as *Escherichia coli* and *Salmonella* consist of a cell body of the size of $1 \sim 2\mu m$ and several flagella in helical shape. They swim in water at the speed of $10 \sim 100\mu m/s$ by use of rotating flagella in a bundle at the rate of $100 \sim 1000rps$ driven by flagellar motors on their cell body. Such microorganisms alternate between straight swimming and random tumbling. During tumbling, the bundled flagella are released by inverse rotation of the flagellar motors and the cell body turns to a random direction. Swimming zigzag, the bacteria can gather round attractants and escape from repellents [1].

In the present investigation, we propose a concept of a micro-robot imitating bacteria with several flagella. The robot consists of a spherical body and two helical screws. It swims straight rotating two screws, and turns to other directions stopping one of the screws while keeping the other rotating. We derive the equations for analyses of robot motion employing the resistive force theory of Stokes flow to evaluate fluid force exerted on the robot [2]-[4]. The velocity and angular velocity are calculated as functions of rotation rate of the screws. The result of numerical simulations shows that the robot can approach a destination changing its direction as bacteria do. Moreover, it reveals that the robot learns the strategy for approach if it can detect whether it is getting close to the destination.

2 Motion Analysis of Micro-Robot

2.1 Model

Figure 1 illustrates a schematic of the micro-robot. The two screws in the shape of left-handed helix are joined to motors fixed on the body. The motors drive the screws clockwise (if it is seen from the root to the tip). The axis of motor rotation passes through the center of the body.

2.2 Determination of Velocity and Angular Velocity

We assume that the micro-robot is so small that the Reynolds number of the flow induced by the motion of the robot is less than one. Therefore, the robot is propelled by resistant force generated by the screw motion in viscous fluid, and the net force and torque exerted on the robot must be zero:

$$\sum_{k=1}^{2} \boldsymbol{F}_k + \boldsymbol{F}_b = 0 \ , \tag{1}$$

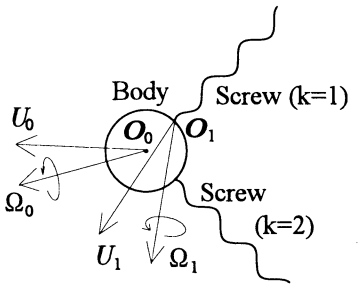


Figure 1 Micro-robot imitating bacteria. The two screws rotate and propel the body. The radius of the body is r_b.

$$\sum_{k=1}^{2}(\boldsymbol{M}_k + \boldsymbol{r}_k \times \boldsymbol{F}_k) + \boldsymbol{M}_b = 0 \ . \tag{2}$$

Here $\boldsymbol{F}$ and $\boldsymbol{M}$ are force and torque, respectively, where the subscript b means the body, k means the screw (k=1,2). Also $\boldsymbol{r}_k$ denotes the vector of $\overrightarrow{O_0O_k}$.

The force $\boldsymbol{F}_b$ and torque $\boldsymbol{M}_b$ are expressed by the Stokes's law [5] as

$$\boldsymbol{F}_b = -6\pi\mu r_b \boldsymbol{U}_0 \tag{3}$$

$$\boldsymbol{M}_b = -8\pi\mu r_b^3 \boldsymbol{\Omega}_0 \ , \tag{4}$$

where $\boldsymbol{U}_0$ and $\boldsymbol{\Omega}_0$ are the velocity vector and angular velocity vector of the body, respectively, as shown in Fig.1.

In the resistive force theory, the force $\boldsymbol{F}_b$ and torque $\boldsymbol{M}_k$ exerted on the screws can be written as

$$\boldsymbol{F}_k^{\xi_k} = A\boldsymbol{U}_k^{\xi_k} + B(\boldsymbol{\Omega}_k^{\xi_k} + \boldsymbol{\omega}_k^{\xi_k}) \tag{5}$$

$$\boldsymbol{M}_k^{\xi_k} = C\boldsymbol{U}_k^{\xi_k} + D(\boldsymbol{\Omega}_k^{\xi_k} + \boldsymbol{\omega}_k^{\xi_k}) \ , \tag{6}$$

where $\boldsymbol{\omega}_k$ is the angular velocity vector of the k-th motor. Eqs.(5) and (6) hold in the ξ_k-coordinate fixed to the k-th screw. The superscript on the vector means which coordinate the vector is expressed in. Since the dimensions of the screws are same, the matrices A, B, C and D are in common with them and become constant in the ξ_k-coordinate [4].

Through an appropriate transformation between coordinates employing a transformation matrix T_k and a rotation matrix R_k [4], we can rewrite the equations of balance for forces and torques, Eqs.(1) and (2), as follows,

$$\left[\sum_{k=1}^{2} T_k^{-1}AT_k - 6\pi\mu r_b I\right]\boldsymbol{U}_0^{\eta} + \left[\sum_{k=1}^{2}(T_k^{-1}BT_k + T_k^{-1}AT_kR_k)\right]\boldsymbol{\Omega}_0^{\eta} = -\sum_{k=1}^{2} T_k^{-1}B\boldsymbol{\omega}_k^{\xi_k} \tag{7}$$

$$\left[\sum_{k=1}^{2}(T_k^{-1}CT_k + R_kT_k^{-1}AT_k)\right]\boldsymbol{U}_0^{\eta} + \left[\sum_{k=1}^{2}(T_k^{-1}DT_k - T_k^{-1}CT_kR_k) + \sum_{k=1}^{2}(R_kT_k^{-1}BT_k - R_kT_k^{-1}AT_kR_k) - 8\pi\mu r_b I\right]\boldsymbol{\Omega}_0^{\eta} = -\sum_{k=1}^{2}(T_k^{-1}D + RT_k^{-1}B)\boldsymbol{\omega}_k^{\xi_k} \ . \tag{8}$$

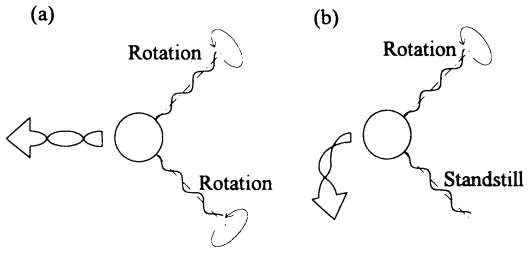


Figure 2 Moving modes of the robot. (a) Mode 1, screws are rotating in the same direction and the robot moves almost straight, (b) Mode 2, one screw stops while the other keeps rotating, and the robot turns.

The velocity and angular velocity of the robot can be determined by Eqs.(7) and (8) when the rotation rate of the motors are known. The position is calculated by integrating the velocities.

2.3 Moving Modes and Motions

We presume that the robot swims in two modes, as shown in Fig.2. In the mode 1, two screws are rotating and the robot moves straight. In the mode 2, one of the screws is at standstill while the other continues rotation, and the robot turns to other directions. The body of the robot rotates in either mode to cancel out the torque generated by the screws.

Figure 3 shows an example of tracks of the robot alternating the modes. The angle between the axes of motor rotation is assumed to be 90°. The robot starts from the origin of the coordinate and proceeds straight for a while in the mode 1. Then, it changes the direction of motion abruptly when the mode is switched from 1 to 2. Before the mode is switched again from 2 to 1, the robot moves along a helix for a certain time in the mode 2. Iterating direction changes, the robot can reach the goal.

3 Learning for Approach to Attractant

3.1 States and Actions

As mentioned previously, bacteria can approach attractant moving randomly. Probably they recognize whether they come nearer to it detecting the density variation of the material diluted in water.

We assume that the robot detects the density of attractive material at regular intervals, compares the value with that previously detected, and judges the current state. The density ρ is assumed to be inversely proportional to the distance from the material that diffuses in water. Therefore, two states can be sensed;

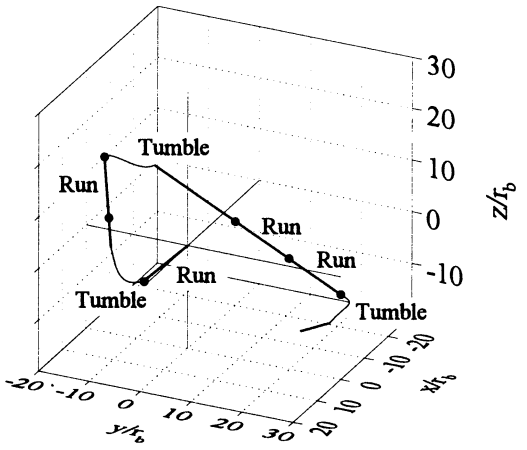


Figure 3 Direction changes by mode alternations. The robot is initially at the origin. ——, mode 1; ——, mode 2. *Run*, the robot moves in the mode 1; *Tumble*, the robot moves in the mode 2 accompanied by the mode 1.

Table 1 Rules for motion of the robot.

		State	
		$\Delta\rho > 0$	$\Delta\rho \leq 0$
Action	Run	1	3
	Tumble	2	4

the density is increasing ($\Delta\rho > 0$) or the density is decreasing ($\Delta\rho \leq 0$).

We define two actions, *run* and *tumble*, referring to the motion patterns of bacteria. The former is straight transportation in which the robot moves in the mode 1, and the latter is changing the direction in which the robot moves in the mode 2 accompanied by the mode 1. (See Fig.3)

The states and actions are summarized in Table 1. The rule 1 and 3 compete with the rule 2 and 4, respectively.

3.2 Learning Algorithm

The Q-learning algorithm [6] is used to weight these four rules. An optimal strategy is determined by the function $Q(x, a)$, where x is a current state and a is an available action. The probability of an action in a state x is expressed by the Bolzmann distribution:

$$P(a|x) = \frac{\exp(Q(x,a)/T)}{\sum_b \exp(Q(x,b)/T)}, \quad (9)$$

where $\sum_b$ means the sum of all possible actions, *run* and *tumble*, and T is the temperature parameter that

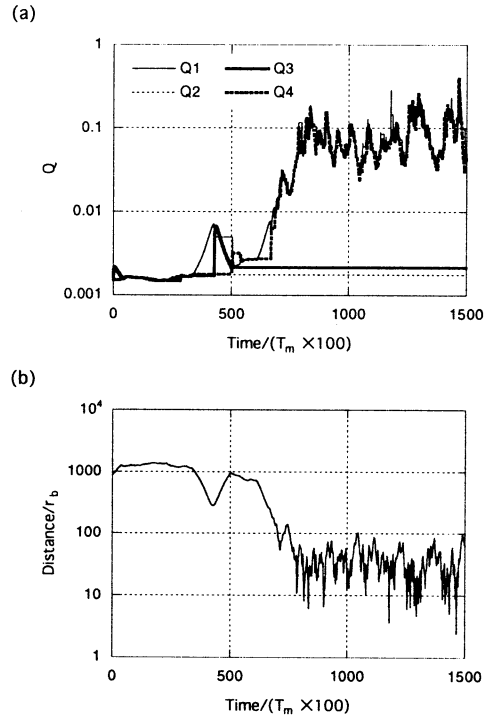


Figure 4 Learning for approaching the attractant. T_m is the period of motor rotation. (a) Q-functions. The number after Q in the legend correspond to the rule number in Table 1, (b) Distance between the robot and the attractive material.

adjusts the randomness of decisions.

The function $Q(x, a)$ is updated using discounting future value and a positive learning rate α:

$$Q(x_t, a_t) \leftarrow (1-\alpha)\, Q(x_t, a_t) + \alpha(\rho_t + \gamma \max_b Q(x_{t+1}, b)), \quad (10)$$

where γ is a discount parameter, x_t is the current state and it will be changed to x_{t+1} by the current action a_t.

3.3 Simulations of Approach to Attractant

The interval of state judgment is $T_m \times 100$, where T_m is the period of motor rotation. The periods of the mode 1 in a *run* and the mode 2 in a *tumble* are $T_m \times 100$ and $T_m \times 105$, respectively. The period of the mode 1 in a *tumble* randomly changes in the range of 0 to $T_m \times 263$. The learning parameters are set as $T = \max_b Q(x, b) \times 0.05$, $\alpha = 0.8$, and $\gamma = 0.5$.

Figure 4(a) shows an example of the time histories of the Q-function of each rule. Fig.4(b) shows the dis-

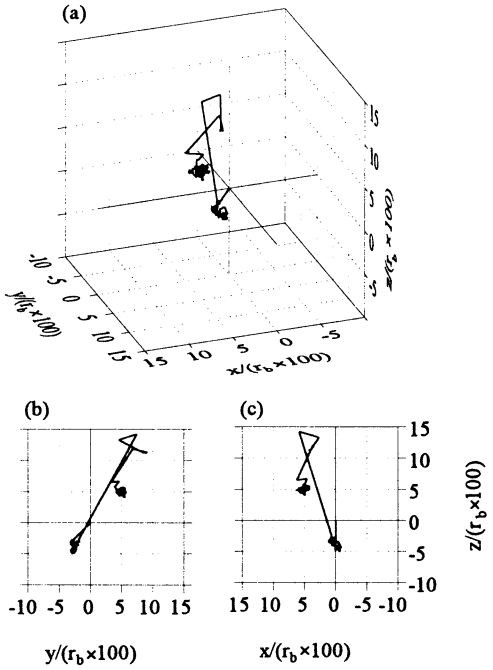


Figure 5 Trajectory of the robot approaching the attractant at (500, 500, 500). The robot starts from the origin. (a) Bird's-eye view, (b) Cross-sectional view; y-z plane, (c) Cross-sectional view; x-z plane.

tance from the attractive material. The robot learns an optimal strategy while it is approaching the destination occasionally. When the nondimensional time is around 400, the robot is coming up to the destination selecting the rule 1 continuously. At a moment that the state changes from $\Delta\rho > 0$ to $\Delta\rho \leq 0$ (the nondimensional time $\simeq$ 428), the robot takes the rule 3 , the Q-function of which becomes superior to that of the rule 4. After a while, however, the robot learns that this strategy is not appropriate to get close to the destination. At last, the rule 1 and 4 defeat the rule 2 and 3, respectively. Once the optimal strategy is acquired, the robot comes to close the goal very rapidly. This is because T is so small that the robot selects its action almost greedily.

Figure 5 shows the path of the robot in the case shown in Fig.4. At the beginning, the robot prowls and tumbles very often. After the robot obtain the strategy, it moves straight until the state changes from $\Delta\rho > 0$ to $\Delta\rho \leq 0$. Moving zigzag, the robot approaches the destination. When the robot comes close to the destination, the robot is hanging around it since the robot does not have an action to stop its motion. The radius of the area is about 50 times of the radius of the body, as shown in Fig.4(b)

The strategy acquired here is probably the same as that bacteria adopt. Bacteria usually alternate run and tumble. In a comfortable circumstance, the frequency of the tumbles are reduced and they swim straight than usual.

4 Summary

We propose a concept of a micro-robot imitating bacteria that possesses two helical screws. The motion of the robot is numerically simulated using the resistive force theory. When the robot senses whether it is approaching to a destination or not, it can go to the place randomly changing directions many times. The robot acquires the same strategy as bacteria take; if the robot is coming up to the place, it moves straight, otherwise, it changes direction.

Acknowledgment

This study was partly supported by Grant-in-Aid for Scientific Research (No. 09450077 and No. 09750194) from the Ministry of Education, Science and Culture of Japan.

References

[1] Macnab, R. M. and Ornston, M. K., "Normal-to-curly flagellar transitions and their role in bacterial tumbling: Stabilization of an alternative quaternary structure by mechanical force, *J. Mol. Biol.*, 112 (1977), 1-30.

[2] Takano, Y., Goto, T. & Usui, Y., "Analyses on Propulsion Mechanism of Micro-Organism with a Helical Flagellum" (in Japanese), *Trans. JSME*, B 62-593 (1996), 211-217.

[3] Goto, T., Itou, M. & Takano, Y., "An Application of the Resistive Force Theory to Helical Flagellar Motions", *Proc. of JSME International Conference in Fluid Engineering, Tokyo*, (1997), 1819-1824.

[4] Goto, T., Itou, M. & Takano, Y., "Analysis of Motion of Bacteria with Rotating Flagella" (in Japanese), *Trans. JSME* B 63-606 (1997), 410-416.

[5] Happel, J. & Brenner, H., *Low Reynolds number hydrodynamics*, Martinus Nijhoff Pub. (1983) p.169, p.173.

[6] Watkins, C. J. C. H. & Dayan, P., "Technical Note: Q-Learning", *Reinforcement Learning* (Sutton, R. S. (ed.)), Kluwer Academic (1993) 55-68.

Proc. of Third Int. Symp. on Artificial Life, and Robotics (AROB III'98),
Oita, Japan, 19-21, January, 1998,

Dynamic Position Arrangements of Soccer Agents with Genetic Algorithms

Tetsuya MURATA † Keiji SUZUKI † Azuma OHUCHI †

† Research Group of Complex Systems Engineering,
Graduated School of Engineering, Hokkaido University,
Kita 13 Nishi 8, Sapporo, Japan
{tetuya, suzuki, ohuchi}@complex.eng.hokudai.ac.jp

Abstract

In this paper, we propose the dynamic position arrangements of the soccer agents for realizing the autonomous team play. In addition, we adopt the genetic algorithms for obtaining the adaptive position arrangements to defeat the opponent teams.

Recently, as a test-bed for multi-agent systems, Soccer Server is served for the research of realizing the cooperative team behavior to defeat opponent teams in complex game environments. In real soccer game, the formations of the players are important factor to defeat the opponent team. The formations can be thought as the arrangements of the positions assigned to the players as home positions to proceed the specific roles in the team plays. Thus, each player basically moves around the neighbor of the assigned home positions and plays to realize the effective team play.

To search the appropriate home positions in the Soccer Server domain, we adopt the genetic algorithms as robust optimization methods. However, it is very difficult problem to judge the effectiveness of the position arrangements. Because even if the team succeeds to make the effective position arrangement, the team can't always win the games. Namely, the result of the games includes many noises in every time.

So, in order to evaluate the position arrangements, we suggest the behavior based evaluation function which consists of the frequency of each agent's behavior, i.e., shoot, pass, search ball and etc.

We will show the experimental results applied the proposed methods on the soccer server.

1 Introduction

Recently, as a test-bed for multi-agent systems, Soccer Server is served for the research of realizing the cooperative team behavior to defeat opponent teams in complex game environments. In the soccer game problem, it is very difficult to connect the behavior selection problem in each agent with the problem of realizing the effective autonomous team play. In this paper, the important factor for realizing the autonomous team play, we assume, is to make the appropriate formation of the players. In addition, the formation should dynamically change in accordance with the situation in the game. Here, the formations can be thought as the arrangements of player's home positions in the soccer field. Therefore, we prepare the agents embedded with the behavior selection based on a given home position. Then we try to search the adaptive position arrangements of the agents, which will be dynamically changed, for realizing the autonomous team play.

While, the result of the games includes many noises in every time. Namely even if the team having the effective position arrangement, the team can't always win the games. So, it is required that the robust search method and the evaluation method to make the appropriate formations in the noisy environment.

As robust search method, we adopt the genetic algorithms with the improved genetic operations. As evaluation method that doesn't only depend the score of the games, we introduce the behavior based evaluation function. The behavior based evaluation function consists of the frequency of each agent's behavior in the given position, e.g., shoot, pass, search ball, and etc. Because if an effective team play can be realized, the agents in the team will become to play that the effective behavior related to win the team, such as, shoot, kick and pass, will be increased against to the time consuming behaviors and the ineffective behaviors like as searching the loose boll.

We will show the experimental results applied the proposed methods on the soccer server.

2 Dynamic Position Arrangements Problem

We use the analogy of the adaptive formation in real soccer games for constructing the autonomous team play with soccer agents. In real soccer games, players adaptively change the home positions according to the current situations. Thus, to realize the adaptability concerning the formations, the dynamic position arrangement problem is proposed.

In this chapter, the proposed method will be explained.

2.1 Agents

To implement the dynamic position arrangements problem, each agent is required the fundamental activity such as catching a ball. So we construct the action-selection architecture of the agents based on the winner's architecture of Pre-RoboCup 96[Ogawara 96].

In the architecture, the agents can perform the several behaviors around one fixed home position. These behaviors are pass, shoot, search the ball, approach the ball, and go back own home position.

The selection of the behavior is done according to the distances between own home positions, the ball, and other agents. For instance, each agent approaches the ball if the ball is closed to itself, but it goes back own home position if the ball is far from itself.

2.2 Dynamic Position Arrangements

To adopt the proposed method, we improve the above architecture as the agents can take the several home positions in each game and can dynamically change current home position in accordance with the situation in the game. We describe the method as follow:

- We prepare the candidates for the home positions. That is, the field is divided into $m \times n$ square areas(Fig.1). Then the centers of each square area apply to the candidates assigned to the agents as own home positions. Each candidate is indexed from 0 to $m \times n - 1$.
- Each player can use H home positions. These are assigned from $m \times n$ candidates. In this case, it is allowed to assign the same home position in H positions.
- To introduce the condition of changing current home position, the agent architecture is improved. That is, the agents should select the current home position with the minimal distance to the ball from the assigned home positions.

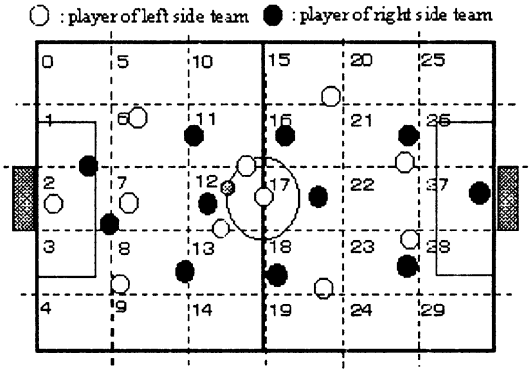


Figure 1: The divided field

The agents with the improved architecture can move around the home positions. Therefore the agents will be expected to perform the suitable behavior according to the current situations if they are assigned the appropriate home positions.

2.2.1 Evaluate the Formation

To search the appropriate home positions, the evaluation function for the arrangements has to be constructed. However, it is very difficult problem to judge the effectiveness of the position arrangements. For example, the evaluation function can't be constructed with only the score of games since the score includes several noises. Therefore, we propose the behavior based evaluation function as follows;

In the team level, we assume if the total occurrence of the pass behavior and the shoot behavior in the game are increased than other behavior, the position arrangements may be effective even if these behaviors didn't succeed.(It requires the notice that the commands of behaviors are often failed with the noise in the Soccer Server.)

In the individual level, each agent should dash to catch the ball immediately when the ball is closed to the agent. While, the agent should go back own home position when the ball is far from the agent. In addition, each agent shouldn't lose the ball position because the search of the lost ball requires the time consuming behavior and the activities of the agents quietly decreased.

Thus, the number of the occurrence concerning with these behaviors is considered to evaluate the position

arrangements. Of course, the number of the team getting the goal is added to evaluate the arrange of positions. Thus, we suggest the behavior based evaluation function which consists of the frequency of each agent's behavior and the score. The constructed evaluation function is described as follow:

$$fitness = (\sum pass/5) \times (\sum shoot)$$

$$\times \frac{(\overline{predict}/6) \times (go_home/15)}{\overline{search}/50} \times (\frac{Goals}{10} + 1) \quad (1)$$

where

$\sum pass$: the total of the frequency of pass in the team

$\sum shoot$: the total of the frequency of shoot in the team

$\overline{predict}$: the average of the frequency each player approached the ball

$\overline{go_home}$: the average of the frequency each player went back own home position

$\overline{search}$: the average of the frequency each player searched the ball

Goals : the frequency of goals the team got

2.3 Searching Positions with GA

To search the adaptive home position arrangements against to an opponent team, a robust optimization method is required in this domain. Therefore, we use the Genetic Algorithm (GA) with inheritance of the fitness for increasing the robustness in noisy optimization space.

2.3.1 Coding

One chromosome express one formation in the game. Genotype consists of the indices of home position candidates. In case of N players and H home positions assigned to one player, the length of a chromosome is $N \times H$.

2.3.2 Inheritance of Fitness

As the improvements of GA, it is introduced the inheritance of the fitness. The fitness values of the parents are inherited to the fitness of offspring according to the resemble between the parent and the offspring. The inheritance of the fitness will be expected to decrease the effect of noisy search space. The fitness of the offspring is calculated by fit_{cal}, which is evaluation value of the above function according to the formation assigned by the offspring, adding the value, (fit_{old}), which is calculated based on the resemblance between the offspring and their parents. The resemblance is defined based on the ratio of inherited genes from the parent in the crossover operation.

3 Experiment

To confirm the effectiveness of the proposed method, we carry out the experiment. In each game for evaluating the formation of the chromosome, the winner's team of Pre-RoboCup 96 ([Ogawara 96]) is used as the opponent team. The opponent team already has the hand-coded fixed home positions. The arrangement of the opponent's positions can be thought as enough to perform the autonomous team play. Basically, the ability of the agents in both teams is same except for our agents being available the multiple home positions. Thus, we expect that the GA will find the dynamic position arrangements of the agents to perform the flexibility and the adaptability against the fixed position arrangement of the opponent team.

The detailed settings of the experiment are represented as follow:

- The number of players in the game : 11 vs 11
- The field is divided in 5 x 6 square area (Fig.1).
- 3 home positions are assigned to each player.
- The number of individuals : 36
- The number of generations : 50
- The crossover rate: 1.0
- The mutation rate: 0.1

3.1 Result

We show the progress of the maximum fitness and the average fitness in each generation in Fig.2, and the formation with maximum fitness in Fig.3. The results of games between the team with this formation and the winner's team ([Ogawara 96]) are in Table 1. Fig.4 show the frequencies of the averaged agent's behavior. In this Figure, the histgrams present the behaviors with maximum and minimum fitness in the formations.

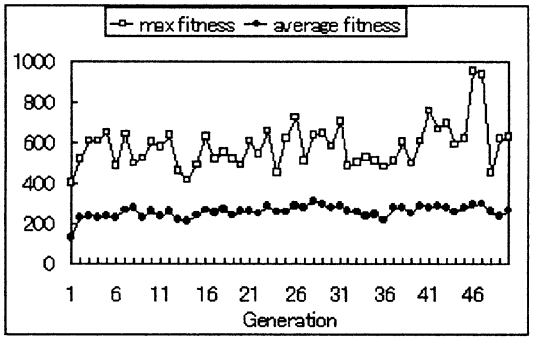


Figure 2: The Progress of the fitness in each generation

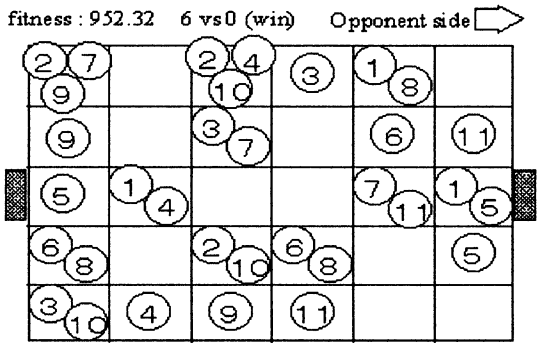


Figure 3: The formation of the maximum fitness

3.2 Discussion

As the Figure 2 indicates, the fitness values both of the maximum and the average are fluctuated widely in search process. Because even if the formation assigned by the chromosome and the opponent team are same, the evaluation value of the chromosome is varied in every game. That is, the search process can't avoid the noisy environment.

The formation obtained from the experiment, however, seems to realize the allotment of each role in the field. For instance, the players with the assignment of the number 5 and 11 seem to behave like forward, and the player with the assignment of the number 4 seems to behave defensive half. In the games, the team with this formation can fight enough against the winner's team. The results of score show the ability of both teams is almost equal and the proposed team slightly exceed the opponent team (Table 1). Comparing with the formation of minimum fitness, the effective behaviors(pass,predict) are selected more in the match.(Fig.4) So, it is consider that searching the adaptive formation was successful.

game	1	2	3	4	5
result	○	×	△	○	○
score	11 vs 9	7 vs 9	13 vs 13	14 vs 9	7 vs 6

Table 1: The result of the games with the formation of the maximum fitness

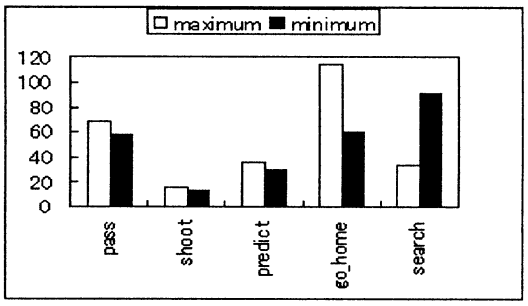


Figure 4: The frequency of each agent's behavior

4 Conclusion

In this paper, we proposed the dynamic position arrangements of the soccer agents for realizing the autonomous team play. So we adopted the genetic algorithms for obtaining the adaptive position arrangements to defeat the opponent teams, and showed about the result of our experiment.

In our experiment, we found the adoptive position arrangements to defeat the winner's team of Pre-RoboCup 96 with changing current formation according to the situation in the game dynamically.

References

[Stone 96] Peter Stone and Manuela Veloso : Towards Collaborative and Adversarial Learning : A Case Study in Robotic Soccer. *Proc.SS-96-01,1996 AAAI Symp.* pp.88–92 (March 1996)

[Ogawara 96] Koichi Ogawara's program : University of Tokyo, Japan.(Winner of preRoboCup96) ftp://ci.etl.go.jp/pub/soccer/client/ogalets.tar.gz

Proc. of Third Int. Symp. on Artificial Life, and Robotics (AROB III' 98),
Oita, Japan, 19-21, January, 1998,

Robot Soccer:- Sensing, Planning, Strategy and Control, a distributed real time intelligent system approach

Christopher Messom,
Electronics and Communication Engineering,
Singapore Polytechnic,
500 Dover Rd,
Singapore 139651
CHMessom@sp.ac.sg

Abstract:

This paper presents an analysis of the different components, sensing, path planning, strategy and control for a distributed real time intelligent system, namely a robot soccer system. The robot soccer system (as described by Kim[1], Shim[2]) consists of two teams of wheel based micro robots with an external vision system and host processing unit as well as local on board intelligence. Communication between robots and host computer is via wireless communication. The system is inherently real time with many hard and soft real time constraints. On board motor control has to meet hard real time constraints (in the order of ms), while higher level control such as set point selection (10 ms), path planning (1 s) and strategy (10 s) have softer real time constraints.

Keywords: intelligent control, multi-agent systems, distributed systems, real-time systems.

1.0 Introduction

Robot soccer has been proposed as a test-bed for real-time distributed intelligent control systems (Kim[1]). The test-bed has the advantage that it is a real physical system with sufficient complexity (21 degrees of freedom) that it can not be trivially solved. Some of the real world problems include vision, motor control and wireless communication. Intelligent systems problems include learning, sensor fusion, multi-agent systems, cooperation and collaboration (Kitano[3]).

Various techniques have been proposed for controlling the robot soccer system. Shim[2] proposed two techniques. The first a vision based system where the global positions are identified by a central system and the robot movements decided by hard coded strategies. The second involves a multi-agent approach where each robot cooperates with its teammates based on information about the robot positions. Oller[4] adopts another multi-agent approach (under Matlab-Simulink). The system allows agents to communicate in a cooperative and collaborative manner so that the robots do not adopt conflicting behaviours (such as one robot adopting a defensive behaviour while another adopts an offensive behaviour).

Stone[5] adopts a hierarchical multi-agent approach. This approach structures the system so that learning of behaviours at the strategic layer can occur.

The systems introduced above show that techniques originally developed in simulation environments can be applied to real systems. Once applied to the real system the performance of each system can be compared. Invariably the more intelligent the system (in terms of communication, distributed processing and learning) the worse the system's performance. In fact hard coded behaviours such as Shim[2], Sargent[6] have proved to be the most successful.

Hard coding all behaviours is not a solution (Brooks[7]). We need some techniques to reduce the combinatorial problem of the 21 degrees of freedom on a field that is not easily partitioned in to discrete regions. It is proposed in this paper that low level behaviours are hard coded while higher level strategies are specified with soft constraints. These soft constraints are both in time and position. As high level behaviours are executed, performance may degrade leading to alternative strategies being selected. This approach has parallels to Maes[8], whose action selection scheme has been implemented in simulation.

This soft alternative action selection scheme is preferable to that of a system with high precision. In a high precision system, the behaviour can be brittle, if things are going well, the performance fits the low tolerance constraints. If the low tolerance constraints are

not met then the system may fail catastrophically. In a system such as robotic soccer where several components are inherently distributed the sample times of the different components are different. Small variations in the sample times should not effect the overall performance of the system. The system is designed to be robust relative to this inter-component variable latency. The distributed approach naturally allows for multi process parallel execution. The system is designed so that the different components of the system are not forced to act in a lock step fashion.

Section 2 includes an analysis of the kinematic and dynamic models of the robots and how these are used for developing the strategy and control. Section 3 discusses the sensing system including the types of real-time constraints they must meet. Section 4 describes the strategy layer while Section 5 and 6 discusses the path planning and control layers that are required to implement the distributed control.

2.0 System modeling

The most popular wheeled robot used in robot soccer is the wheel chair model (Kim[1], Shim[2], Sargent[6]). Oller[4] used a modified wheel chair design, while Michel[9] introduced an omnidirection design (see fig 1). The model adopted for the analysis in this paper is the wheel chair design.

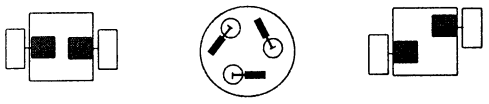


Figure 1. Robot designs: wheel chair, omnidirectional and modified wheel chair

2.1 Kinematic model

In the kinematic model for the wheel chair robot, we consider velocity of the robot wheel as the primitive. The system variables are the robot position and orientation (x, y, θ). If the wheel velocities are V_L and V_R (and the distance between the wheels d), then the kinematic equations are given in equation 1.

$$\begin{bmatrix} 1 & 0 & 0 \\ 0 & 1 & 0 \\ 0 & 0 & d/2\pi \end{bmatrix} \begin{bmatrix} dx/dt \\ dy/dt \\ d\theta/dt \end{bmatrix} = \begin{bmatrix} \tfrac{1}{2}\cos(\theta) & \tfrac{1}{2}\cos(\theta) \\ \tfrac{1}{2}\sin(\theta) & \tfrac{1}{2}\sin(\theta) \\ -1/2 & 1/2 \end{bmatrix} \begin{bmatrix} Vl \\ Vr \end{bmatrix}$$

2.2 Dynamic model

For the dynamic model the acceleration of the robot wheel is considered the primitive. The system variables are the robot position and orientation and their time derivatives (x, y, θ, dx/dt, dy/dt, dθ/dt). If the wheel forces are F_L and F_R then the dynamic equations of the system are given in equation 2. (C = cos(θ), S=sin(θ))

$$\begin{bmatrix} M & 0 & 0 & S \\ 0 & M & 0 & -C \\ 0 & 0 & Jd/2\pi & 0 \\ S & -C & 0 & 0 \end{bmatrix} \begin{bmatrix} d^2x/dt^2 \\ d^2y/dt^2 \\ d^2\theta/dt^2 \\ \lambda \end{bmatrix} = \begin{bmatrix} (Fl + Fr)C/2 \\ (Fl + Fr)S/2 \\ (-Fl + Fr)/2 \\ -(Cdx/dt + Sdy/dt)d\theta/dt \end{bmatrix}$$

M is the robot mass, J its angular moment of inertia and λ the Lagrangian constraint force.

2.3 Kinematic and dynamic models compared

For a kinematic model we can only specify wheel velocities, while accelerations can be specified in the dynamic model. Examining fig 2 and fig 3 we see that considering the real system as a kinematic model or a dynamical model results in not only position differences but more importantly time differences.

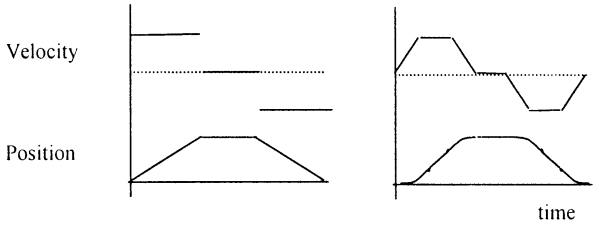


Figure 2. Position and velocity profiles for kinematic and dynamic systems

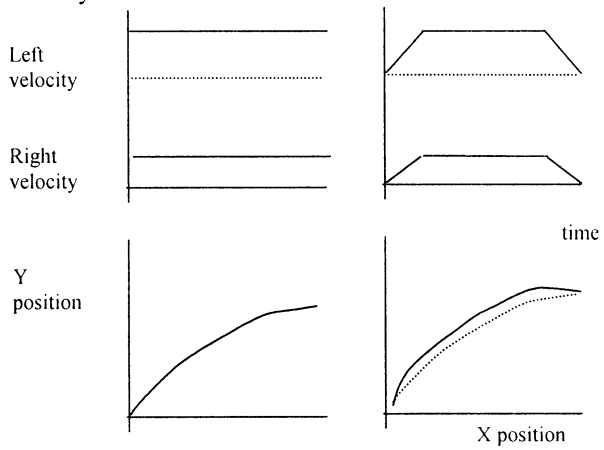


Figure 3. Left and right wheel velocity profile and curved path for kinematic and dynamic models

Synchronising events precisely under both kinematic and dynamic models are difficult, but especially difficult

for dynamic models. Due to these computational load factors real-time path planning is done using kinematic models. With suitable velocity control algorithms (see section 6) the kinematic model can accurately model a real physical system. Errors, especially in the time variable are inevitable, so the strategy layer should be designed to be robust to these variations.

The dynamic model is only used for evaluating performance of the overall system and is not used as part of the planning. It is used as an alternative to evaluating the algorithms on a physical system.

3.0 Sensing

The sensing system includes external vision, on board encoders, current measurement, IR sensors for obstacle avoidance and landmark detection and recognition. As seen from fig 4, the sensor system provides information for the strategy, planning and control layers. A sensor fusion approach is used where sensor data is tagged with a time at which it is collected. This time will give a real-time event horizon for each item of data. Based on this data value, information such as robot position and speed can be derived. Tagging time information to sensor values allows data to be discarded once it is out of date. It also allows the reliability of predicted values to be evaluated.

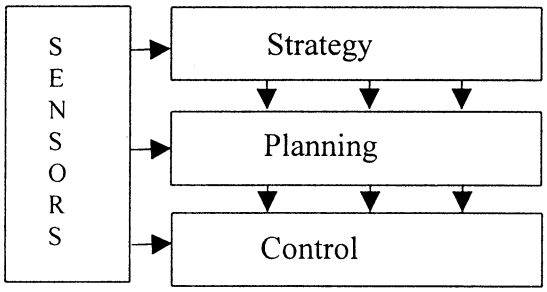


Figure 4. Layered structure of system

This is best illustrated by the vision component of the robot soccer system. The vision is a global system that has a frame rate of 30 to 60 Hz (Sargent[6]). Vision processing often takes up to one frame and adding strategy, planning and control processing results in information latency of 2.5 to 3 frames. Adding a time tag to the vision data allows us to predict system variables more than 2 frames ahead, resulting in a system that is more accurate and reliable.

A problem with tagged times is the different distributed system clocks. Synchronising the clocks in an environment where there is variable latency in the communication channels is a difficult task. We approximately synchronise the system clocks by passing messages between the distributed components or use an external signal to calibrate the system. The system itself is then designed to be robust to the small synchronising errors.

On board the robots, the variable sample times are a major issue. The accuracy of the different sensors may vary such that a sensor with a large sample time (such as vision) may have good reliability and low accuracy, while a system with a small time constant (such as IR sensors) may have low reliability though they are highly accurate. Solving this sensor fusion problem represents a major goal of developing fully autonomous robots.

4.0 Strategy

The strategy layer has the largest sample time and the softest real time constraint of the whole system. This layer generates and maintains the behaviour of the robots depending on the state of the system. Issues related to the strategy include state recognition, generation of behaviours, and persistence of behaviours.

4.1 State recognition

For an intelligent system with many behaviours it is important to recognise the current state of the system so that the appropriate behaviour is selected. In a robotic soccer system the fundamental decision is between that of offensive and defensive behaviours. Lee[10] and Messom[11] discuss several metrics including Euclidean distance, region of control and time restricted region of control for deciding which team has possession of the ball. In cases where possession is ambiguous a more sophisticated state recognition system is required. In such a system the current behaviour may influence the selected behaviour. E.g. the offensive behaviour persists even though the ball is not under any players control in the anticipation that the ball will return to the possession of the offensive robot.

4.2 Behaviour generation

4.21 Fundamental moves

The fundamental motion of the soccer robot as described by fixed wheel velocities are straight lines (V_L=V_R), rotations (V_L= -V_R) and curved arcs of circles ($|V_L|$!=$|V_R|$). By supplying a sequence of wheel velocities more general paths can be specified.

A useful path is the S-curve. This is the path required to reach a given final position and orientation from a given start point and orientation. The path can be formed by two arcs of a circle with a straight path between them. The path can be classified based on the direction the

robot moves around the two circles, left or right. This is illustrated in fig 5.

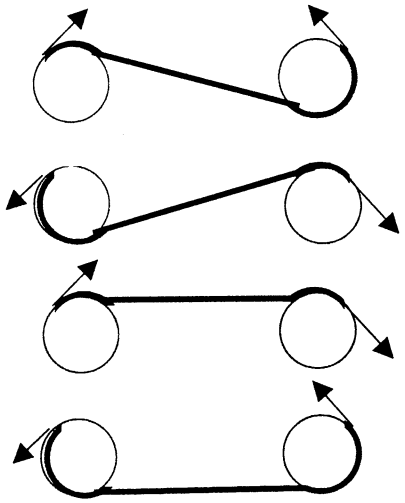


Figure 5. S-curves, Right-Left, Left-Right, Right-Right and Left-Left

The S-curve is considered a fundamental atomic action. The higher level strategies and path planning relies on the S-curve to fill in the paths between successive specified positions.

4.22 Prescribed plays

Given the fundamental moves and atomic actions available the strategy layer of the system needs only supply the positions and orientation of the robots required at successive time points. The order of these time points are in the range 2-10 seconds, so that the actual details of the motion are handled by the lower levels of the system.

An example of an offensive play is illustrated in fig 6. In this example only 3 sets of positions are specified, the lower levels handle the implementation details of the movement.

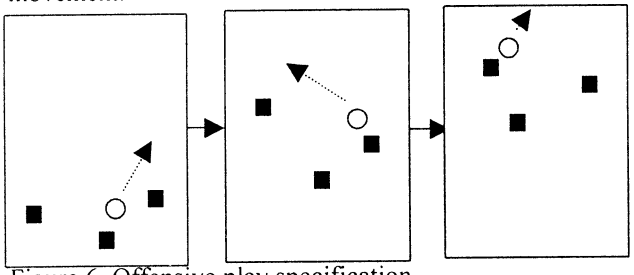


Figure 6. Offensive play specification

The robots move to their start position and then execute the play. Obstacle avoidance is handled at the next level down, if necessary breaking down a single S-curve into two or more S-curves so that the obstacle (the opposition) is avoided. This is illustrated in fig 7. For the system to meet the soft real time constraints while avoiding obstacles requires overall speed of movement to be adjusted based on path lengths. The longer the path of the robot the faster it needs to move to maintain its position in the play.

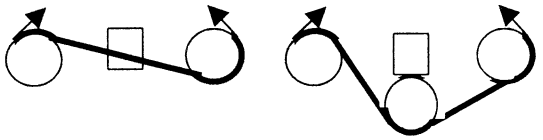


Figure 7. Obstacle avoidance: Path adjusted to avoid opposition robot

4.3 Behaviour persistence

Given a system with multiple behaviours, both offensive and defensive, it becomes necessary to make the robots actions persistent. This means that the robots don't stop acting or act in a contradictory manner for slightly varying conditions. An illustration is when two robots have a shot at the ball. If the decision to have robot A shoot the ball and robot B shoot the ball act alternately one after each other, then no one will actually take the shot. Allowing an initiated action to persist will allow a single robot to shoot the ball unless the state of play changes so fundamentally that the current behaviour is abandoned and an alternate action is executed.

The intelligence of the system resides at the strategy layer of the system. The other layers of the system, the path planning and control layers, aim to provide a level of performance that allows the behaviours generated by the strategy layer to be reliably executed.

5.0 Path Planning

Given the behaviours generated by the strategy layer, the path-planning layer generates a plan of the robot positions and velocities that will produce the required behaviour. These behaviours are specified as isolated robot positions and orientations at specified times in the future. The planning layer provides the velocity setpoints that will achieve the required result. This path plan is implemented at the kinematic level (using the kinematic equations given in section 2, equation 1). The kinematic model allows large step jumps in the specified wheel velocities, which are unrealistic. This is due to the acceleration constraints of the robot. Since an infinite torque is not possible the path planning level should generate a continuous set of wheel velocities.

For example moving from a circular path to a straight path would result in a step change in wheel velocities. Instead of giving these discontinuous velocity set points, a continuous one is given. (See figure 8)

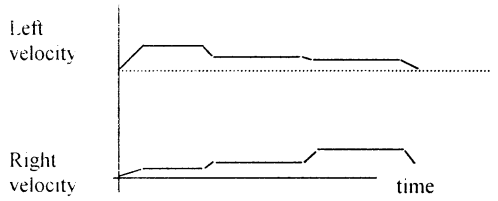


Figure 8. Wheel velocity profiles for a Right-Left S-curve

6.0 Control

At the control level of the system, the paths planned at the higher level are implemented. The control layer aims to meet the requirements of the plans. The control layer should be able to offer a level of performance that is robust to sensor noise, power degradation, load variation and variable latency in the higher level of the system

The system presented here uses a position or velocity control system (depending on whether the robot is stationary or moving). For high performance systems, the inner loop of the controller is a current feedback system. This is so that the system performance does not degrade significantly with power degradation and load variation (motor temperature).

The set points of the controller are either constant acceleration, constant velocity or constant position. These fixed set points persist for a significant finite length of time and vary continuously (no step change). This lends itself to be solved by a PID controller with a fixed set of gains. The only point of concern is that the set points don't exceed the maximum accelerations and velocities. Exceeding the maximum acceleration will result in wheel slippage while exceeding the maximum velocity setpoint will result in poor acceleration characteristics. In robot soccer, beating an opponent relies on good acceleration control, so the velocity range must not be exceeded so that the full acceleration is available during robot maneuvers.

7.0 Conclusions

The system described in this paper is currently being implemented in hardware. The hardware used is similar to that described by Shim[2]. The three layer, strategy, planning and control scheme allows us to separate the intelligence from the details of the implementation.

The experience gained with this system will allow us to examine further real-time issues of distributed intelligent systems. This work will allow us to develop a strategy programming language that will remove some of the tedious coding required to implement the strategy layer.

8.0 References

1. S.H Kim, J.K Kim, J.S Choi, B.K Kim, Development of Cooperation for a Robot Soccer Team, MIROSOT workshop proceedings, 1996, pp 90-94.
2. H.S Shim, M.J. Jung, H.S Kim, I.H Choi, W.S Han. & J.H Kim, Designing Distributed Control Architecture for Cooperative Multi-agent Systems, MIROSOT workshop proceedings, 1996, pp 19-25.
3. Hiroaki Kitano, Minoru Asada, Yasuo Kuniyoshi, Itsuki Noda, Eichi Osawa, RoboCup: The Robot World Cup Initiative, Proceedings of IJCAI, 1997.
4. Oller A., Esteva S., Humet L., Fernandez A., de la Rosa J. & Puyol J., Soccer Team Based on Agent-Oriented Programming, MIROSOT workshop proceedings, 1996, pp 110-116
5. Stone P, Achim S. & Veleso M., Collaborating and Learning in Robotic Soccer, MIROSOT workshop proceedings, 1996, pp 26-37.
6. Sargent R., Bailey B., Witty C. & Wright A., Using Fast Vision Tracking for Cooperating Robots in MIROSOT, MIROSOT workshop proceedings, 1996, pp 155-157.
7. Brooks R., A Robust Layered Control System for a Mobile Robot, IEEE Journal of Robotics and Automation. Vol RA-2 No. 1.
8. Maes, The Dynamics of Action Selection, Proceedings IJCAI, 1989.
9. Michel, An Omnidirectional Robot for Robot Soccer, MIROSOT Workshop proceedings, 1997.
10. Lee S.H., Wang J.H & Lee H., Coordination of a Team of Micro Robots Playing Soccer Game, MIROSOT workshop proceedings, 1996, pp 133.
11. Messom C.H., Determining Offensive and Defensive Possession in Multi-agent Team Based Competitive Games, MIROSOT Workshop proceedings, 1997.

Proc. of Third Int. Symp. on Artificial Life, and Robotics (AROB III' 98),
Oita, Japan, 19-21, January, 1998,

AN APPLICATION OF A NEW MODEL OF CAM-BRAIN *

Wang Baozhong Kang Lishang Hewei
The State Key Laboratory of Software Engineering
Wuhan University
Wuhan, HuBei 430072
P. R. China

Abstract

A model of artificial brain based on Cellular Automata Machine, e.g., CAM-Brain model was introduced by Felix Gers and de Garis Hugo on the First International Conference of Evolvable Hardware. Till now ,they have built up artificial brains with millions of neuron cells. But it is pity that in their paper they did not present much application of it except a statement saying that any application of it can be made by using Genetic Algorithm(GA) . In this paper, aiming to make up the deficiency of lacking of applications of the CAM-Brain model, the authors tries to find out whether the CAM-Brain could solve the XOR problem efficiently. This is a crucial problem because whether the CAM-Brain model is useful completely depends on whether the model is efficient in its possible applications. This paper first presents the conclusion that CAM-Brain is equivalent to EQUnn model, which is one kind of traditional neural network and can be evolved more easily than CAM-Brain model. With the use of EQUnn model an positive result is obtained finally.

Key Words:

artificial brains, evolvable hardware, cellular automata, neural network, genetic algorithm

1. Introduce

Since a new kind of CAM-Brain model was invented in 1996[1], Doctor Hugo de Garis, who is leading a world wide group to build a CAM-Brain Machine(CBM), hopes to use the CBM to build/grow/evolve an artificial brain module with one million neuron cells by the end of 1997,and one billion artificial neuron cells by the year of 2001[2].Indeed, This Artificial Brain Project is ambitious. But pitifully, the group has not yet done much research in the application ability of the CAM-Brain model. So a crucial problem is left that what can the artificial brain can or can not do? the XOR problem [3]is a good start point. It was because Marvin Minsky and Symour Paper had proved that Perceptron model could not be used to solve the XOR problem in 1969 that XOR problem became a good testing problem for one neural network model. If the artificial could not do even this simple basic problem, what else could be done by the CAM-Brain?

The remainder of this paper consists of the following: Section 2 simply describes the CAM-Brain model. Section 3 presents the experiment used to test the efficiency of the CAM-Brain model. Section 4 reports some results. Section 5 the conclusion.

2. Brief description of the CAM-Brain model

It has been mentioned above that CAM-Brain model

*This paper is supported by the National Natural Science Foundation of China.
The author's email address wbz@rigc.whu.edu.cn

can be viewed as a new kind of NN model. It is based on CA and includes two phases: growth phase and signaling phase.

In the signaling phase the states of CAs have two parts which are treated in different way. The first part of the cell state contains the cell's type and activity level, and the second part serves as an interface to the cell's neighborhood by contained the input signals from the neighbors. The characteristic of this CA is that the state is partitioned into two parts, the first is fixed and the second is variable for each cell(see fig.1). So this CAs called partitioned CA. The advantage of this partitioned CA is that only the second part of a cell is passed to its neighbors. In the growth phase the mechanism is the same as in the signaling phase. Next we will explain the meaning of the each bit of the state of each cell and the two phases.

2 bits	2 bits	3 bits	2 bits	2 bits	2 bits	2 bits
Cell Type	Gate	Activity/ Chromo-some	signals from/to Left neighbor	signals from/to bottom neighbor	signals from/to Right neighbor	signals from/to Top neighbor

Fig. 1 State representation in the CAM-Brain model
The bits from the 1^{st} to 7^{th} bit are the fixed part of cell state
The bits from the 8^{th} to 15^{th} bit ate the variable part of the cell state

2.1 the meaning of each bit and the growth phase

The 1^{st}, 2^{nd} bits specify the types of the cells. According to the CAM-Brain model there are four types of cell: Neuron cell, Dendrite cell ,Axon cell and Blank cell. During the growth phase, A blank cell can change to Axon cell or Dendrite cell according to the instructions stored in state of one cell. Different type of cells imply these cells will behave differently in the signaling phase.

The 3^{rd},4^{th} bits of the state of a cell specify the gate of a cell. The gate indicates the signal transferred to one cell is from which neighbor, or the signal of one cell will be transferred to which neighbor. The neighborhood we use is von Neumann neighborhood[4]. During the growth phase , the gate of an axon cell points the to the neighbor from which the signals are received. An axon cell accepts input only from this neighbor and makes its own output available to the other three neighbors; The gate of a dendrite cell points to the neighbor to which the output signal of this dendrite cell should give, and the dendrite cell collects the signal from all the rest three neighbors. In addition, the gate of a neuron cell, during the growth phase indicates the directions in which the two neighbors axon cells of the neuron cell should grow.

The 5^{th},6^{th} and 7^{th} bits indicate the growth instruction. The three-bit string represents seven different growth styles whose underlying meaning is one cell should transfer its signal to which neighbors of it, and those cells which receive the signal will store it in one of the two-bit strings from 8^{th} to 15^{th} bits.

It is obvious that during the signaling phase the growth instruction is no longer used due to the over of the growth phase. So this three-bit string can be used to store the activity of the cell.

The bits from 8^{th} to 15^{th} are used to store the message transferred to the cell. The 8^{th} , 9^{th} ; 12^{th} , 13^{th} ; 14^{th} , 15^{th} of one cell are assigned to store the signal transferred to this cell. If there is one neighbor which do not transfer any signal, then the value of zero is assumed to be transferred.

According to the signal stored in the bit string from the 8^{th} to 15^{th} bit, by using the LUT(look up table), a blank cell can be decided to which type of cell it should change. Surely the LUT should be designed to assure that axon cell connects to axon cell while dendrite cell connects to dendrite cell. Step by step, for each neuron cell, are forming 2 axon trails and 2 dendrite trails which belong to the neuron cell.

2.2 The signaling phase

After the growth phase, the signaling phase can begin. The signaling process is carried out by the neuron cells through their axon and dendrite trails. An axon cell receives signal from the neighbor specified by its gate and then distributes the signal to all the three other neighbors; a dendrite collects signals from the three neighbors, adds the signals and then passes the sum to the neighbor specified by its gate. It is worth noting that one axon trail of a neuron cell multiplies -1 by the output signal of the neuron cell and then distributes signal while the other trail distributes the signal without changing the output of the neuron cell.

All in one word, the function of axon cell is to "distribute" signal and the function of dendrite cell is to "collect" signal. Step by step, input signals are transferred and changed through the neuron cells and their trails, finally the output signals can be obtained from the output layer neuron cells.

3. Experiment

From the simple description above, one can easily comes the following conclusion:

If the range of the output value of the dendrite cells is not constrained, the 3D CAM-Brain model is equivalent to the neural network(EQUnn) model which is fully connected and fits to the following conditions:

(1) the weights between neurons are integral

(2) the changes of the neurons' state are carried out non-synchronously

(3) suppose the output value of ith neuron isO_i ,the weight from jth neuron to ith neuron is $W_{j,i}$, the output from jth neuron to ith neuron is $O_{j,i}$, the relation between them is that

$$O_i=1 \text{ if} \sum_{j=1}^{N_i} W_{j,i} \cdot O_{j,i} > 0$$

or

$$O_i=0 \text{ if} \sum_{j=1}^{N_i} W_{j,i} \cdot O_{j,i} \leqslant 0$$

XOR problem is in fact a mapping problem. When the input signals (0,0),(1,0),(0,1),(1,1) are given, output value 0,1,1,0 should be obtained. In this paper, to solve the XOR problem we used EQUnn model with 2 input neurons ,1 hide layer neuron and 1 output neuron.

GA was engaged to evaluate the weights between these 4 neurons. Because one neuron is connected to itself and all others, the weights of the above EQUnn can be stored in a 4 by 4 matrix. Each element of the matrix represents the weight of one connection. If we use 4 bits to represent each weight—each weight ranges from -8 to 7—one individual of the GA's populations is 16*4=64 bits long. But if we evolve a 2 dimensions CAM-Brain with 11*11 cells ,each cell needs 3 bits to code its growth instruction, the length of the chromosome of an individual will be 11*11*3=363 bits , which is much longer than the chromosome of an individual if EQUnn model is engaged. So in this paper we use EQUnn model first, then interpret it in CAM-Brain model according to the equivalence of CAM-Brain model and EQUnn model.

The fitness function is defined as follow:

Suppose input signal (0,0),(1,0),(0,1),(1,1) are fed to the input neurons n_{total} times respectively, $n_{correct}$ is the times of the obtained output hits the correct output, then the fitness function is defined as $f = n_{correct}/(4*n_{total})$. It is obvious that the value of f is between 0 and 1,and the closer to 1 the fitness is ,the better the individual is. In this paper 100 is assigned to n_{total}.

Crossover operator and mutation operation in this

paper is the uniform crossover and mutation operator described in [5].In this paper the probability of crossover P_c=0.8,the probability of the mutation P_r=0.01.

4. Result

When we use a population of 50 individual, generally on the 50th generation one best individual can be obtained. for example, one of the best EQUnn models structure and weight is figured as figure 2.

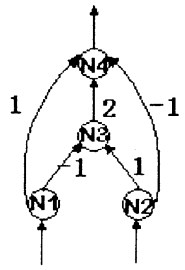


Fig 2 The structure and weight of EQUnn model which can be used to solve the XOR problem.N1,N2 represent the input neurons, N3 the hidden layer neuron and N4 the output neuron.

This EQUnn's model can be easy translated into CAM-Brain model as figure 3

5. Conclusion

In order to investigate the application ability of the CAM-Brain model , the XOR problem was solved by using the EQUnn model which is equivalent to the CAM-Brain model. The fact that the XOR problem can be solved by the CAM-Brain model implies that this artificial brain model can also be used to solve other more complex problems. For the more, it is worth mentioning that if one do not intend to implement the CAM-Brain model on FPGA he could evolve the EQUnn model instead of the CAM-Brain model due to the much shorter chromosome of an individual.

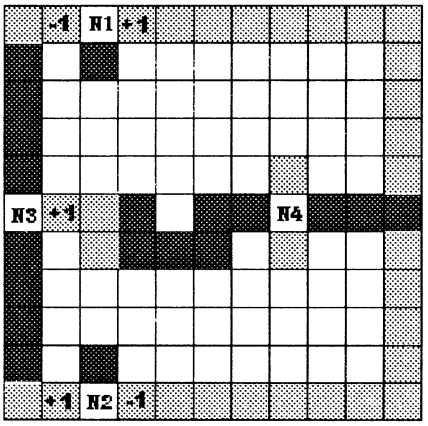


Fig 3 The structure which can be used to solve the XOR problem. The gray grids represent the axon cells and the dark cells the dendrite cells. -1 means that the axon trail the signal by -1 while +1 means the axon pass down the signal without change.

References:

[1]Felix Gers, H. de Garis(1996)CAM-Brain:A new model for ATR's cellular automata based artificial brain project,

The First Int. Conf. on Evolvabe Systems, Tskuba, Japan

[2]Michael Korkin, Hugo de Garis, Felix Gers, Hitoshi Hemmi (1997) "CBM (CAM-BRAIN MACHINE) " A Hardware Tool which Evolves a Neural Net Module in a Fraction of a Second and Runs a Million Neuron Artificial Brain in Real Time, Genetic Programming Conference, Stanford, USA

[3]Minsky M., Pal S. K.(1969)Perceptrons, MIT Press

[4]von Neumann J.(1966)Theory of Self-Reproducing Automata, ed. Burks A. W. University of Illinois Press, Urbana

[5]bigniew Michalewicz (1992) Genetic Alogrithms +Data Structures = Evolution Programs, Springer-Varlag Berlin Heidelberg, New York.

Proc. of Third Int. Symp. on Artificial Life, and Robotics (AROB III'98),
Oita, Japan, 19-21, January, 1998,

Distributed Optimization by Using Artificial Life System

Taiji Satoh
Dept. of Electrical and Electronic Engineering
Yamaguchi University
Ube, 755 Japan

Tsuyoshi Okita
Dept. of Information Machines and Interfaces
Hiroshima City University
Hiroshima, 731-31 Japan

Abstract

This paper presents a distributed algorithm for minimizing a nonconvex multimodal function. In recent years, new distributed algorithms based on Artificial Life (ALife) system has been studied and its potential power was demonstrated. In this paper, therefore, the frame work of ALife system is employed into a function minimization. This paper also proposes a hybrid algorithm in which Alife system is incorporated with the local search method for finding good start points for the local search. Since the proposed method utilizes no gradient information, it can be applied to very wide class of optimization problems. The effectiveness of the proposed method is demonstrated through some numerical tests.

Key Words : Artificial Life, Global Optimization, Distributed Optimization, Emergent Colonization

1 Introduction

This paper presents a distributed algorithm for minimizing a nonconvex multimodal function. The local search methods based on the gradient information have efficient convergence property, but these methods have a tendency to get stuck at local minima[1]. Therefore a global optimization method with good convergence property is desired.

Although many global optimization methods such as the Simulated Annealing method[2] for discrete optimization problems and the Tree Annealing method[3] for continuous optimization problems have been proposed, these methods require much computational cost.

In recent years, new distributed algorithms based on the Multi-Agent system[4] and the Artificial Life (ALife) system[5] has been studied and its potential power was reported. The underlying idea is that some complex tasks may be performed by distributed activities over massively parallel systems composed of computationally simple elements. Colorni et al.[4] proposed so-called *ant algorithm* for solving the Travelling Salesman Problem. In the ant algorithm, each agent (ant) interacts through *pheromone trails*. However, the ant algorithm is a problem-oriented one, i.e., it can be applied to the TSP only.

On the other hand, Assad and Packard[5] studied an general emergent phenomenon (colonization) of distributed agents called *artificial organisms*. The main purpose of this paper is to construct a distributed algorithm for a function minimization by using the emergent colonization of artificial organisms.

In this paper, firstly, ALife system in the two-dimensional discrete system presented in Ref.[5] is extended to the multi-dimensional continuous system. Next, ALife system is applied to an optimization problem of function minimization[6]. Then the hybrid algorithm of Alife system and the local search method[8] is proposed. In the proposed algorithm, Alife system is incorporated into the local search method for finding good start points for the local search.

Since the proposed method utilizes no gradient information, it can be applied to very wide class of optimization problems. The effectiveness of the proposed method is demonstrated through some numerical tests on multimodal test functions. The numerical tests also show that the proposed algorithm is superior to the Tree Annealing method.

2 Optimization Problem

The optimization problem to be solved is to minimize a multimodal nonlinear function over hyper-rectangular domain. Such a problem is mathematically formulated by

$$\underset{\boldsymbol{x}_{min} \leq \boldsymbol{x} \leq \boldsymbol{x}_{max}}{Minimize} \; f(\boldsymbol{x}) \tag{1}$$

where $f : R^n \rightarrow R$. $\boldsymbol{x}_{min}$ and $\boldsymbol{x}_{max}$ are lower and upper limits on $\boldsymbol{x}$, respectively.

3 Artificial Life System

3.1 Emergent Colonization

The colonization appears to be an important and widespread phenomenon in living systems. The colony is considered to be a group of organisms which is spatially clustered, relatively stable in size over time, and exhibiting high levels of interaction amongst its members[5]. The motivation for choosing emergent colonization of artificial organisms as an optimization mechanism for minimizing eqn.(1) is that the colonization may occur in the promising area with lower function values if the ability of artificial organisms in the ALife system is properly selected[6].

3.2 Artificial World

The Artificial World (AWorld) implemented in Ref.[5] is square Cartesian plane containing N by N discrete points. In their approach, each point in the AWorld can contain energy resources (food), and can also be inhabited by members of the four different species of Artificial Organisms (Artorgs).

In our implementation[6], for the purpose of function minimization shown in eqn.(1), the AWorld is defined as n–dimensional continuous Euclidean space with lower and upper limits, i.e.,

$$\{\boldsymbol{x} \in R^n \mid \boldsymbol{x}_{min} \leq \boldsymbol{x} \leq \boldsymbol{x}_{max}\}. \qquad (2)$$

3.3 Artificial Organisms

Artorgs can move about in the AWorld consuming energy resources and metabolize it producing waste. The four species of Artorgs (white, red, green, and blue) compose a circular food chain where one species' waste is another's food. An Artorg must maintain a minimum internal energy level by consuming enough food in order to exist, otherwise it will die and is removed from the AWorld.

The neighbourhood of the point $\hat{\boldsymbol{x}}$ at which an Artorg is inhabited is defined by

$$C = \{\boldsymbol{x} \in R^n \mid ||\boldsymbol{x} - \hat{\boldsymbol{x}}|| \leq D\}, \qquad (3)$$

where $||\cdot||$ denotes the Euclidean norm and D is a distance each Artorg can move in one step.

3.4 Sensor System

Artorgs have a sensory system which enables them to see resource as well as other Artorgs in the AWorld. Moreover, in order to apply the ALife system to the function minimization, the authors introduced the following objective function[6] :

$$F(\tilde{\boldsymbol{x}}, \hat{\boldsymbol{x}}) = ||\tilde{\boldsymbol{x}} - \hat{\boldsymbol{x}}|| + W \cdot \{f(\tilde{\boldsymbol{x}}) - f(\hat{\boldsymbol{x}})\} \qquad (4)$$

where $\hat{\boldsymbol{x}}$ is the present location of an Artorg and $\tilde{\boldsymbol{x}}$ is that of the nearest resource. The constant $W > 0$ is a weight for balancing the distance and function value.

The location which minimizes this weighted objective function becomes the goal which drives an Artorg's movement strategy. The first term of eqn.(4) implies that an Artorg tends to move toward the nearest food, and the second term will drive an Artorg to the point with lower function value of $f(\boldsymbol{x})$. In consequence, it is expected that emergent colonization will occur in the promising area.

3.5 Resource Trading

Artorgs can also carry and exchange food which they cannot be able to metabolize. Whether an Artorg will trade the food or not depends upon its simple trading strategy. The trading strategy is essentially a sixteen bit table as shown in Table 1. In this table, "1" ("0") indicates that an Artorg makes (refuses) the corresponding trade. The trade actually occurs if the both parties of the exchange agree.

Table 1: An Example of Trading Strategy

	White	Red	Green	Blue
White	0	1	1	0
Red	1	0	0	1
Green	0	1	1	1
Blue	1	0	0	1

3.6 Reproduction

The trading strategy of an Artorg is fixed over its lifetime. But reproduction using the genetic operators of the simple Genetic Algorithm[7] provides the mechanism for the evolution of better trading strategies in future generations[5].

If the age of sexual maturity is reached, two Artorgs with the same color can mate and produce an offspring. The offspring inherits its trading strategy from both parents. Trading strategies are represented as sixteen bit strings equivalent to sequentially listing the bits of the strategy shown in Table 1. Single point crossover[7] combines part of one parent's strategy to create the offspring's strategy.

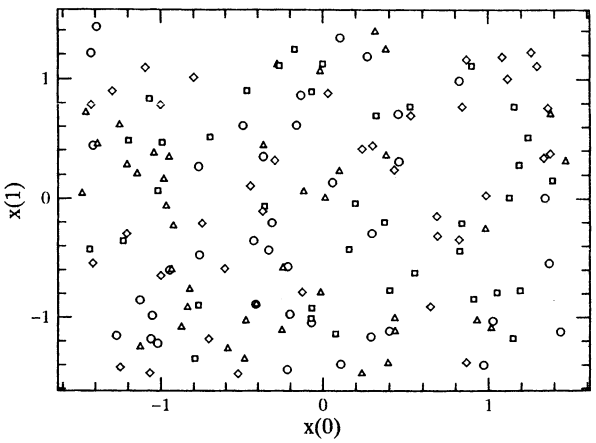


Figure 1: Initial Distribution (160 Artorgs)

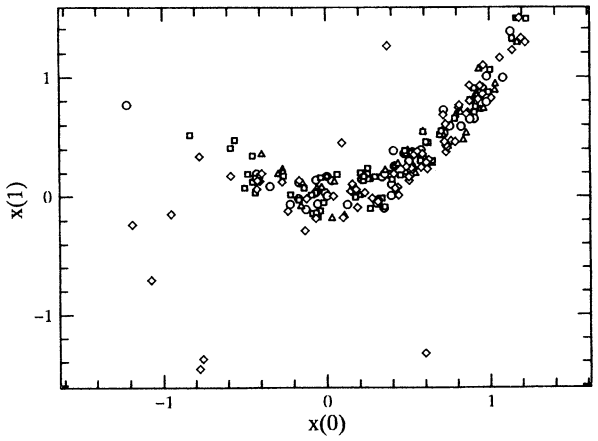


Figure 2: Emergent Colonization (232 Artorgs)

4 Algorithm

4.1 Simple ALife Algorithm

The AWorld is initialized by randomly putting equal numbers of each of the four species of Artorgs and resources, and by randomly generating sixteen bit string as trading strategies of the initial population. Then the Artorgs enter their life cycles, moving about in the AWorld, consuming and trading energy resources, mating, reproducing and dying.

4.2 Hybrid Algorithm

As shown in the numerical example of the next section, although some promising area can be found by the ALife system, only a quasi-optimal solution may be obtained. So a hybrid algorithm composed of two phase is proposed in this paper; the first phase is a distributed global search by the simple ALife system, and the second phase is a local search by the Simplex method[8]. This hybrid algorithm enables us to find the global optimal solution efficiently.

Phase I : Simple ALife Algorithm

Execute the simple ALife algorithm in section 4.1 until colonies of Artorgs are formed.

Phase II : Local Search Method

Step 1 : Select an Artorg randomly from colonies.

Step 2 : Execute the Simplex method[8] from the initial point selected in Step 1.

Step 3 : Repeat Step 1 and 2 for prespecified number of iterations, then output the best solution found so far.

5 Numerical Examples

5.1 Test Functions

In order to demonstrate the effectiveness of the proposed method, two test functions (Banana Function and Camel Function) are used. *Banana Function* is defined by

$$f_B(\boldsymbol{x}) = 100.0 \times (x_2 - x_1^2)^2 + (1.0 - x_1)^2. \quad (5)$$

This function has one global minimum at $(1.0, 1.0)$ and its optimal value is $f_B(1.0, 1.0) = 0.0$.

Camel Function is defined by

$$\begin{aligned} f_C(\boldsymbol{x}) &= (4.0 - 2.1 \cdot x_1^2 + \frac{x_1^4}{3}) \cdot x_1^2 \quad (6) \\ &\quad + x_1 \cdot x_2 + (-4.0 + 4.0 \cdot x_2^2) \cdot x_2^2. \end{aligned}$$

This function has six local minima and two of them are global optimum. The optimal solutions are $(\pm 0.0898, \mp 0.7126)$ and $f_C(\pm 0.0898, \mp 0.7126) = -1.0316$.

5.2 Simulation Results

In this simulation, values of parameters are $D = 1.0$, $W = 0.2$ and number of Artorgs in the initial configuration are $160 = 40 \times 4$. The search space is $\boldsymbol{x}_{min} = (-1.5, -1.5)$, $\boldsymbol{x}_{max} = (1.5, 1.5)$.

To demonstrate the fact that the emergent colonization occurs at promising area, the result for the Banana function is presented. The initial distribution of Artorgs and the final configuration are shown in Fig. 1 and 2, respectively. The configuration in Fig. 2 is obtained after 2000 cycles and 232 Artorgs are inhabited in this AWorld. As shown in this figure, the colony is banana-shaped; this is the reason why it is called as *banana*.

Table 2 shows the best function value of Artorgs in the final configuration.

Table 2: Simulation Results

	Best Sol.	Optimal
Banana	0.0009	0.0000
Camel	-1.0312	-1.0316

To show the effectiveness of the ALife technique, the proposed method is compared with the Simplex method[8] and the Tree Annealing method[3]. Table 3 shows the CPU time of three methods for Camel function. In this table, CPU times are normalized by using that for the Simplex method. Table 3 indicates that the proposed ALife algorithm is superior to the Tree Annealing method.

Table 3: Comparison of CPU Time

Method	CPU Time
Simplex	1.00
ALife	21.76
Tree Annealing	43.53

In order to improve the accuracy of the solution obtained by the ALife algorithm, the Simplex method is executed after the distributed global search of the ALife algorithm. Table 4 shows the comparison of simple ALife algorithm and the hybrid algorithm. As shown in this table, the accuracy of the solution obtained by the Alife algorithm is improved by Phase II of the Hybrid algorithm. Since the local search by using the Simplex method is very efficient (see table 3), increase of computation time is negligible small as compared with that for the Alife algorithm.

Table 4: Hybrid Algorithm

	ALife	Hybrid	Optimal
Banana	0.0008	0.0000	0.0000
Camel	-1.0291	-1.0316	-1.0316

6 Conclusions

In this paper, an optimization algorithm based on the ALife system is proposed and its effectiveness is demonstrated through some numerical tests. Since the proposed algorithm requires additional assumptions such as continuity and differentiability, it can be applied to very wide class of optimization problems.

References

[1] A. L. Peressini, F. E. Sullivan and J. J. Uhl, Jr., *The Mathematics of Nonlinear Programming*, Springer-Verlag, 1993.

[2] P. J. M. van Laarhoven and E. H. L. Aarts, *Simulated Annealing : Theory and Applications*, Kluwer Academic Publishers, 1987.

[3] G. L. Bilbro and W. E. Snyder, "Optimization of Function with Many Minima", *IEEE Trans. Syst., Man & Cybern.*, Vol. 21, No. 4, pp. 840–849, 1991.

[4] A. Colorni, M. Dorigo and V. Maniezzo, "Distributed Optimization by Ant Colonies", in *Toward A Practice of Autonomous Systems*, MIT Press, pp.134-452, 1992.

[5] A. M. Assad and N. H. Packard, "Emergent Colonization in an Artificial Ecology", in *Toward A Practice of Autonomous Systems*, MIT Press, pp.143-152, 1992.

[6] D. Hayashi, T. Satoh and T. Okita, "Distributed Optimization by Using Artificial Life (in Japanese) ", *Trans. IEE Japan*, Vol. 116-C, No. 5, pp. 584–590, 1996.

[7] D. E. Goldberg, *Genetic Algorithms in Search, Optimization, and Machine Learning*, Addison-Wesley, 1989.

[8] J. A. Nelder and R. Mead, "A Simplex Method for Function Minimization", *Computer J.*, Vol. 7, pp. 308–313, 1965.

Proc. of Third Int. Symp. on Artificial Life, and Robotics (AROB III' 98),
Oita, Japan, 19-21, January, 1998,

Artificial Life and Natural Stories

Kerstin Dautenhahn
Department of Cybernetics
University of Reading
U.K.
kd@cyber.reading.ac.uk

Chrystopher Nehaniv
Cybernetics & Software Systems Group
University of Aizu
Japan
nehaniv@u-aizu.ac.jp

Abstract

This paper speculates about 'stories' as potentially useful units to construct historically grounded artificial life forms. We draw our motivation from the structure and organisation of biological life forms and the organisation of human memory and sociality. A fresh approach towards historical artificial life creatures is to develop story-telling systems supported on situationally grounded, discrete dynamical systems. This involves creating *autobiographic agents* which, by telling through remembering, by constructing stories, might 'understand' the world. We address these issues using methods from the area of Algebraic Engineering, growing out of the algebraic theory of automata developed by Krohn and Rhodes. Our approach affords mathematical methods for expressing events during the existence of an agent in an associative multiplicative structure that adequately captures the notion of irreversibility of events in life histories. Furthermore, story-telling and autobiographic re-construction are supported within this framework by appropriate historical expansions (which are themselves amenable to algebraic manipulation). Upcoming implementations of this framework in simulation and robotic agents have to demonstrate the validity of this approach.

1 Historical Life

The basic Artificial Life (AL) endeavour concerns the study of life-as-it-could-be in physical and other media rather than life-as-it-is just on the single example of planet Earth. AL's methods typically involve the study of emergence of complexity, defining primitive units, e.g. cellular automata, and defining (often non-linear) local interactions between these units [10]. Putting the system in the appropriate context, e.g. executing these rules, can lead to a phenotype with properties (behaviour or appearance) which might not be predictable in advance from knowing the set of transformation rules and the initial state. Thus, emergence of something "new" which requires a new level of description depends crucially on the choice and the representation of the units and the transformations. So, what are the appropriate units for designing or evolving physical artifacts, robots, supposed to behave in a life-like way, animal-like, or humanoid, i.e., a bit like us? Each natural living system can only be understood and its phenotype can only be interpreted by taking into account its historical context, its evolutionary context, phylogeny, and individual developmental context, ontogeny. Each creature has its own history. Such an 'history' encompasses its morphology, behaviour, and cognition over time. In this paper we will present a particular approach and philosophy of thinking about historical creatures, story-telling, and socially embedded creatures.

2 Life-like Stories

The past decade has shown a number of successful a-historical artificial life implementations, Brooks's insectoid walking machines [7], Mataric's flocking robots [11, 12], etc. However, were these basically reactive machines "living"? Being alive means having a lifetime, without a reset button. Reactive robots do have a certain history encoded in their bodies, chassis and control architecture, reflecting the (human) designer's history of understanding and gaining insight. But beyond that, the experiences of these robots did not irreversibly influence their future behaviour. What about cognitive robotics, like the MIT COG project [1]? Again, the body of the humanoid robot reflects a process and progress of science, but not a "lifetime". So, how can we make robots "historical" without reproducing the pitfalls of GOFAI research focusing on modelling the world by re-building its representations inside the "mind" of the artifact? A fresh approach is

to introduce story-telling systems supported on situationally grounded, discrete dynamical systems. This involves the creation of *autobiographic agents* [3, 5]. Such agents can dynamically reconstruct their individual 'history' (the autobiography) during their lifetimes. Such stories are not stored away as database entries, they are rather constructed during a process of telling through remembering, and taking into account the current state of the agent situated in the world.

Evidence from psychology suggests that stories might be fundamental units [20, 8] in human cognition, or at least that they might have a privileged status. Stories can serve to record one's own experience and to communicate experience to others. According to Read and Miller [19] the evolution of stories could have been favoured by the fact that they seem to be efficient means for managing social interactions. However, communication and interaction processes in human society are concepts on a very high level of (cognitive) complexity and it might not seem straightforward to find analogues in unicellular organisms or simple artificial systems like autonomous robots. Nevertheless, we can abstract from the specific discussion of stories as constructs in human cognition, and rather consider stories as primitive units for life-like systems as such. We can then formulate three arguments for life-like story-telling systems, as a response to Schank and Abelson's main arguments on human knowledge and memory (see [20]):

(1) Life and living, biological or artificial, is based on lifetime experiences with the embodied system as the point of reference. Experiences are based on stories constructed around past experiences.

(2) New experiences are interpreted in terms of old stories.

(3) The content of story memories depends on whether and how they are expressed to the environment and told to others, and how the world in return responds to the stories, i.e. gives feedback on whether the story is 'good'. These reconstituted memories form the basis of the individual's remembered autobiography.

Thus, an objective of our research is to study what kind of narrative complexity might emerge from a story-telling system acting and interacting in its environment. Such systems would be situated not only in space, but also in time. Their autobiographies and story-telling skills could make their behaviour more 'consistent', consistent with what has happened before and what might happen later. Such spatio-temporally situated consistency would support the appropriateness of the system's actions when interacting with its environment. Additionally, story-telling could improve social and cooperative capabilities, which in primate evolution were milestones in the evolution of intelligence.

3 Algebras for Grounded Histories

We address these issues using methods from the area of Algebraic Engineering, growing out of the algebraic theory of automata developed by Krohn and Rhodes. This provides a rigorous mathematical viewpoint on life-events in biological/artificial systems and formalizes the previously somewhat mysterious intuition of 'complexity' as the number of essential levels of dependency within the system [17].

Embodied agents and robots have discrete sets of states which are transformed by (noisy) inputs from sensors to new states, while at the same time inducing action in the environment with effectors. Thus, the theory of automata provides a natural mathematical framework for their treatment. Since real biological systems are subject to irreversibility [16] via, for example, development, damage, adaptation and death, automata theory is more appropriate than, say, the theory of differential equations, which due to uniqueness theorems, seals its fate as incapable of capturing the irreversibility inherent in life. Algebraically, this means that event sequences acting on the state-space are given as elements of semigroup structures, rather than groups (which are time-symmetric) [9]. Semigroups are thus appropriate models-of-time for systems exhibiting irreversibility [15]. Thus, our approach affords mathematical methods for expressing events during the existence of an agent via an associative multiplicative structure[1] that adequately captures the notion of irreversibility of events in life histories.

Semigroup theory also affords us with the notion of *expansions*, which intuitively are larger models of time in which sequences of events are encoded or condensed systematically. Thus, the elements of an expansion for the temporal event-structure acting on the state-space of an agent are fragments of possible histories for that agent. So story-telling and autobiographic re-construction are supported within this framework

[1] *Associativity* means just that the event sequence α then β then γ has the property: β followed by γ and prior to both α is the same as α followed by β and after both γ, i.e.

$$\alpha(\beta\gamma) = (\alpha\beta)\gamma,$$

a property of time known probably since Aristotle.

by appropriate historical expansions (which are themselves amenable to algebraic manipulation). Various expanisons — different systematic historizations of event sequences — are possible. Thus situated agents that use algebraic methods to manipulate, combine and re-construct sequences of events relevant to them in their environments might become empowered as autobiographic agents, telling and exchanging stories about themselves and events in their worlds.

4 Key Concepts for an Historical Approach to Artificial Life Systems

The Artificial in Natural Design. Artificial designs are those that have a given form and behaviour only because they adapt or are adapted in reference to 'goals' or 'purposes' in their environment. They have interfaces to the world that are contingent on possibly teleological circumstances (choice or design). Populations of biological systems are adapted to their environments in what may appear to be conscious design, but is now generally accepted to be a result of a contingent historical constraints and potentialities under the action of evolution. Thus, as one of us has argued [13], the concept of 'artificial' has a natural extension to the biological (and even cognitive) realm.

Life on Earth has emerged from non-living matter, a particular interrelationship between two classes of macromolecules (proteins and ribonucleic acids) seems to have played a major role. But we know very little about the details of this process, it is still unclear where life emerged (far deep in the ocean or close to the surface), whether it happened only once, and whether it happened on this planet at all. No matter what happened exactly, the process led to creatures which we consider today as 'natural', plants and animals, which can be distinguished by an (open) list of features (e.g. reproduction, metabolism, homeostasis, irritability) from non-living matter.

However, if we use the term 'natural' (like "This keyboard can be used in a very natural way."), we usually refer to an unconstrained process (e.g. we can use the keyboard by movements of our fingers and and hands which are similar to the movements we do when not working with the keyboard.). However, the processes of origin of life and evolution were highly constrained, and still are. Life emerged from constraints, there is no 'natural spirit' called life which developed despite the constraints which the environment imposed on it. Constraints are advantageous, not disadvantageous. It is very difficult to *observe* the evolution of animals and plants, but human culture evolves at a much higher speed, so it might exemplify the necessity of constraints much more clearly. Producing tools means making life easier (e.g. freeing us from laborious work), but also putting lots of constraints on our life, e.g. in terms of time management. Tools themselves are designed according to constraints, e.g. how humans like to use these tools. The design and the tools themselves should therefore be similarly 'natural' to their biological users. Biological systems like animals, plants and designed tools like computers, cars, and houses are thus both 'natural' and 'artificial'. Some of these things appear more life-like then others. The study of properties and mechanisms which make a system life-like seems to be more promising than discussion about distinctions between biology and other sciences of the artificial.

Historical Expansions. The fundamentality of irreversibility for biological systems mentioned above implies that the same state of a living system may be reached from various paths (various histories of events), just as when multiplying numbers two products may be zero even though they involve quite different factors. The history of how a state arose is not recoverable from a current state, but a 'story' of how the state was attained is in general necessary to understand how the living system (even the self) came to be as it is. There are many ways to provide systematic historical expansions, each which corresponds to a different notion of history [16, 14].

In order to understand another social being, an empathic recognition of the being as a system experiencing through a body like our own is necessary, but futhermore one may imagine or receive stories about that social being which provide a second level of awareness that reveals its individual nature, its historical relationship to its environment, including social relatedness [4, 6].

These two levels of awareness have analogues in algebra: Realizing that another system undergoes changes given by an event-structure is the realization that a semigroup of transformations describes it, and further knowledge of that structure reveals how its state may change. An historical expansion of the semigroup provides an analogue of the second level, as a mathematical expression of possible histories which may be communicated, exchanged, and combined. Spatio-temporal grounding of such expressions based on the body of the agent interacting with its environment provides meaning for expresssions of the agent's sensory perception and actions in histories.

The Truth is Not Out There. Life appears to us in various forms and variations. Scientific inquiry results in formulas, theories, and models, generally focusing on one particular aspect of life and living, and shaped by historical and social conditions which science is embedded in. Ambitious contemporary scientific endeavours are the search for a theory of everything (explaining the universe), and the 'decoding' of the human genome. To an external observer this might appear as if the success in both areas (the latter more likely than the former) will be major milestones, showing that we only have to work and think hard enough to reveal nature's mysteries, to be able to look 'behind' all things. Unfortunately, we still do not know if life as we know it has evolved on this planet, why viruses are so incredibly successful, and we are far from being able to build an artificial lifeform which is as 'complete' and 'life-like' as the protist *Paramecium caudatum*. All what we know is socially constructed scientific knowledge, based on single human beings and their subjective, personal interpretation of life and living. By communication and scientific discourse this knowledge is made more acceptable, and more grounded in observations and evidence. Some ideas might then be considered to represent the objective truth, the ideal, universal truth which has been revealed. Truth in an objective external world remains for the scientist only an operational assumption. However beautiful this truth might be, we find it within us, interacting with the world, and not out there.

The Social World is Its Own Best Model. Stephen John Read and Lynn Carol Miller [19] propose that social context may have provided the primary constraints for why human cognition developed towards story-telling, since stories are simply very effective re-presentations to code complex experience. Thus, it does not make sense to investigate story-telling systems in isolation, they have to put into a social context. In [4] one of us argues for socially situated agents where internal dynamics are linked to the social environment. This provides a way of grounding social understanding in the real world. Instead of (for example, symbolically) modelling social understanding, and wants, beliefs, desires, and intentions of both oneself and others, being immersed in a social situation can directly provide the context, meaning, sensory feedback, and the 'right' perspective in which social interactions and understanding can emerge. 'The social world is its own best model' summarizes this bottom-up approach towards social understanding for artificial agents [6].

Emotional Grounding: Life Matters! Natural life demonstrates that emotions seem to ground intelligence. Brain scientists give evidence that people who are no longer able to experience and express emotions are no longer behaving 'intelligently' [2]. Thus, story-telling has to be emotionally grounded. Stories are experienced, so cannot be separated from the experiential, embodied context where they 'happened'. Emotions can refer to a single agent's experiences, and to the agent's relationship to others [18]. Although emotions have a physiological, phenomenological dimension, they are complex processes produced by interactions between motives, beliefs, percepts etc. How could we make artificial system 'emotional'? In contrast to GOFAI models of emotions, biological forms of emotions are definitely dynamic in nature, and emotions are *expressed* rather than represented. Expression involves reactions and actions of an organism. In robotics research the designer is generally putting 'meaning' into the system, by defining emotional quantities, motivations, and drives. Artificial, story-telling systems should ground action and cognition in an experiential, 'meaningful' context which is naturally provided in biological systems by the fact of possessing a living body. It is still an open question how to incorporate the emotional dimension in artificial systems in an appropriate 'non-symbolic' way. However, if our story-telling approach should be grounded in a complete system then we have to tackle issues of motivations and emotions as central parts of autobiographical remembering and construction of memories [14].

In order for historical expressions to have real meaning for agents, situatedness and social grounding of the agent in its environment mean that consequences of actions must have an effect on emotional/motivational states of the agent, who would 'enjoy' the rewards or 'suffer' the consequences, acting in the world based on stories about itself or others, just as we humans use as tools stories about ourselves, about others, dynamically changing, emerging, and organizing life.

5 Summary

In this paper we have argued that a natural lifeform can be considered as a complex story, embodied in biological matter. We proposed a particular formal approach toward story-telling mechanisms which should be able to account for a variety of aspects of natural stories, and which should provide a basis for implementing artificial, but nevertheless 'natural', story-telling systems. Upcoming implementations of this framework in simulation and robotic agents have to demonstrate the validity of this approach.

References

[1] Rodney Brooks. Behavior-based humanoid robotics. In *Proc. 1996 IEEE/RSJ International Conference on Intelligent Robots and Systems, IROS 96*, pages 1–8, 1996.

[2] Antonio R. Damasio. *Descartes' Error. Emotion, Reason and the human brain.* G.P. Putnam's Sons, New York, 1994.

[3] Kerstin Dautenhahn. Embodiment in animals and artifacts. In *Working Notes AAAI 96 Symposium on Embodied Action and Cognition, Boston, November 1996.* American Association for Artificial Intelligence, 1996.

[4] Kerstin Dautenhahn. I could be you — the phenomenological dimension of social understanding. *Cybernetics and Systems*, 25(8):417–453, 1997.

[5] Kerstin Dautenhahn. The role of interactive conceptions of intelligence and life in cognitive technology. In Jonathon P. Marsh, Chrystopher L. Nehaniv, and Barbara Gorayska, editors, *Proceedings of the Second International Conference on Cognitive Technology*, pages 33–43. IEEE Computer Society, 1997.

[6] Kerstin Dautenhahn. Grounding agent sociality: The social world is its own best model. Submitted to *14th European Meeting on Cybernetics and Systems Research, EMCSR'98.*

[7] Cynthia Ferrell. A comparison of three insect-inspired locomotion controllers. *Robotics and Autonomous Systems*, 16:135–159, 1995.

[8] Arthur C. Grässer and Victor Ottati. Why stories? some evidence, questions, and challenges. In Robert S. Wyer, editor, *Knowledge and memory: the real story*, pages 121–132, Hillsdale, New Jersey, 1995. Lawrence Erlbaum Associates.

[9] K. Krohn, J. Rhodes, and B. Tilson. Chapters 1,5,7-8. In M. Arbib, editor, *Algebraic Theory of Machines, Languages, and Semigroups.* Academic Press, 1968.

[10] Christopher G. Langton. Artificial life. In *Artificial Life: The Proceedings of an Interdisciplinary Workshop on The Synthesis and Simulation of Living Systems Held September 1987 in Los Alamos Mexico*, pages 1–47. Addison-Wesley Publishing Company, 1989.

[11] M. J. Mataric. Learning to behave socially. In *From animals to animats, Proc. of the Third International Conference on Simulation of Adaptive Behavior*, 1994.

[12] Maja J. Mataric. Issues and approaches in design of collective autonomous agents. *Robotics and Autonomous Systems*, 16:321–331, 1995.

[13] C. L. Nehaniv. Formal models for understanding: Coordinate systems and cognitive empowerment. In *Proceedings of the Second International Conference on Cognitive Technology*, pages 147–162. IEEE Computer Society, 1997.

[14] Chrystopher Nehaniv and Kerstin Dautenhahn. Embodiment and memories - algebras of time and history for autobiographic agents. Submitted to *14th European Meeting on Cybernetics and Systems Research, EMCSR'98.*

[15] Chrystopher L. Nehaniv. The algebra of time. In *Proc. National Conf. Japan Soc. for Industrial and Applied Math.*, pages 127–128, September 1993.

[16] Chrystopher L. Nehaniv. What's your story? — irreversibility, algebra, autobiographic agents. In *Socially Intelligent Agents: Papers of the AAAI Fall Symposium (Cambridge, Massachusetts, 8-10 November 1997)*, pages 150–153. American Association for Artificial Intelligence, 1997.

[17] Chrystopher L. Nehaniv and John L. Rhodes. Krohn-Rhodes theory, hierarchies and evolution. In B. Mirkin, F.S. Roberts F.R. McMorris and, and A. Rzhetsky, editors, *Mathematical Hierarchies and Biology*, pages 29–42, Providence, RI, USA, 1997. DIMACS Series in Discrete Mathematics and Theoretical Computer Science. American Mathematical Society.

[18] Paul O'Rorke and Andrew Ortony. Explaining emotions. *Cognitive Science*, 18:283–323, 1994.

[19] Stephen John Read and Lynn Carol Miller. Stories are fundamental to meaning and memory: for social creatures, could it be otherwise? In Robert S. Wyer, editor, *Knowledge and memory: the real story*, pages 139–152. Lawrence Erlbaum Associates, Hillsdale, New Jersey, 1995.

[20] Roger C. Schank and Robert P. Abelson. Knowledge and memory: the real story. In Robert S. Wyer, editor, *Knowledge and memory: the real story*, pages 1–85, Hillsdale, New Jersey, 1995. Lawrence Erlbaum Associates.

Proc. of Third Int. Symp. on Artificial Life, and Robotics (AROB III' 98),
Oita, Japan, 19-21, January, 1998,

Artificial Visual System Evolution for Stereo Perception by GA

Wen Nian Kozo Okazaki
FUKUI UNIVERSITY
3-9-1 Bunkyo, Fukui 910,Japan

Shinichi Tamura
OSAKA UNIVERSITY
2-2 Yamadaoka,Suita,Osaka 565,Japan

Abstract

The visual function is easy to visualize its function, and therefore is most easy to understand the brain function among various human activities. We use the genetic algorithm to verify the proposition by a natural manner that it is necessary to have consciousness and abstract consideration ability to carry out higher order functions of the human activities. It may give partly a solution to the question of why the consciousness exists. In this paper, we propose a binocular stereopsis model to derive the stereo perception ability of the creature and further examine the acquisition process of space perception by neural network able to predict future target position which we can regard one of a spatial reasoning function.

1. Introduction

Pattern recognition is one of the important tasks in intelligent information processing. The ability of recognizing pattern is the most principal tasks in intelligent system, e.g.a robot. However, ability of conventional pattern recognition system is generally limited. Then it may be valuable to learn from the function of creatures. Here, there is questions whether the vision system of creature is the optimum, or whether another methods can exist. Therefore, to check the necessity of vision system of a creature, we have been studying the evolution of visual system on a computer assuming that the visual organ of a creature is composed of neural network with arbitrary structure. The structure of the system is determined and evolved by a genetic algorithm .

The visual function is easy to make visualize its function, and therefore most easy to understand the brain function among various human activities. We use the genetic algorithm to verify the proposition by a natural manner that it is necessary to have consciousness and abstract consideration ability to carry out higher order functions of the human activities. It may give partly a solution to the question of why the consciousness exists.

In this paper, we propose a binocular stereopsis model (Fig.1) to derive the stereo perception ability of the creature and further examine the acquisition process of space perception by neural network able to predict future target position which we can regard a spatial reasoning function.

2. Binocular stereopsis and other recognition maps

A binocular stereopsis model is shown in Fig.1. The visual depth is obtained by Eq.1.

$$d = \frac{Lf}{X_L - X_R} \qquad (1)$$

where X_L and X_R denote the positions in left and right eye images corresponding to the point P, respectively, L is the base line length, and f is the focal length.

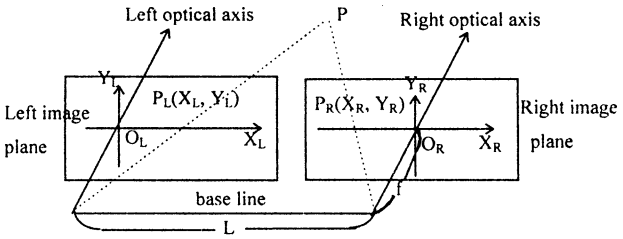


Fig.1 Model of binocular stereopsis

2.1 Stereo perception

The neural network that can output simply the parallax or the distance inversely proportional to the parallax of inputs (only two one-dimensional images corresponding to epipolar lines for simplicity) will be constructed from binocular images. Here, output plane is one-dimensional array as shown in Fig.2 or a two-dimensional position map with direction axis and distance axis.

2.2 Prediction of moving object

The neural network that can predict the object position in the next time from two one-dimension images which express position directions at the two consecutive times will be constructed. Though the structure is the same as Fig.2, the output is only one-dimensional image.

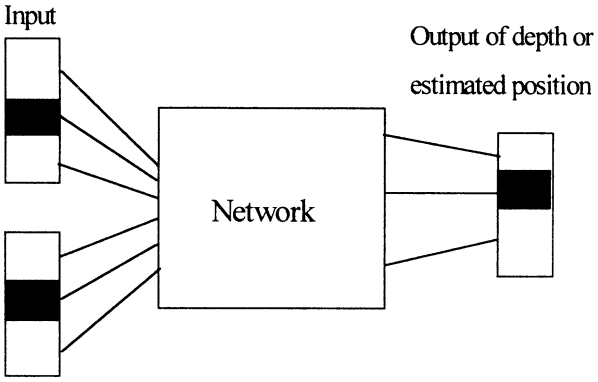


Fig.2 Stero perception and moving object prediction

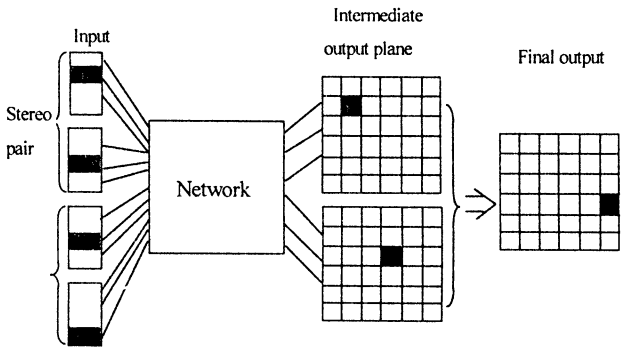


Fig.3 Generation of recognition map for 2-D moving object position prediction or subject-object relation

2.3 2D prediction map and environmental map

By combining **2.1** and **2.2**, the neural network that can output distance and direction of the predicted object position from four one-dimensional images or two one-dimensional stereo images in consecutive times can be constructed. Intermediate output is two one-dimensional arrays corresponding to distance at each time. As an alternative expression, we can obtain two two-dimensional recognition maps. Finally they will be converted to a position prediction map

at the next time. The structure is shown in Fig.3.

This structure is also applicable to generate environmental map including positions of target (enemy) and the creature itself.

3 Experiment

If we start with outputting the distance to the target position which is proportional to the inverse of the parallax of inputs, it is difficult because of the nonlinearity of the inverse calculation. So we examine the neural network which can output the parallax itself instead of the distance of inputs from a binocular images. The configuration of the network is the same as shown Fig.2, where inputs are two one-dimensional array expressing X_L and X_R. The numbers of input units corresponding to X_L and X_R are 6. We assume the middle layer is composed of a mutually connected network. Each connection between two units is bidirectional with the same weight. Calculation is done asynchronously. The output (or state) of an unit excited or suppressed is determined by a threshold value. Here, the threshold is set as 0. The weight's value is set by taking one in the set {-2,-1,0,1,2}. The weights of connection between the units are determined by GA. Thus the neural network of the vision system is evolved by genetic algorithm.

3.1 Individual genotype

We must set form of creature's gene when we apply the genetic algorithm. Here, we assign the connection weights among all pairs of units to the gene code. Thus the visual system of virtual creature composed of the neural network is represented by the gene.

3.2 Generation replacing regulation

We assume that the values of the input X_L, X_R are in the set {8,7,6,5,4,3,2,1} and $X_L \geqq X_R$ so that the number of combinations is 36. Therefore, the correct parallax detection rate of the initial random network may be only 1/36 at each time. We set the condition that the creature will survive if it is correct to detect the distance for the input images, and it will die if it is wrong. In this case, however, all of the creatures will die out soon ,even thought we set the initial number of creatures as 1000. Therefore, we divide the creatures into two groups to improve survival and evolution : number of creatures in a children's group is 500 and that of an adult group is 250. We adopt the criterion function (correct detection value /ages) as shown in Eq.2. Here, we set one generation one year and the creature's correct detection value is added 1 for every one generation when the detection is correct. The creatures with ages lower than 11 belong the children's group. In this group, all of the creatures are calculated its criterion, and no operation of death-life and multiplication is applied. When the creature's age is over 10, they are shifted to the adult group and are applied the operation of death-life and multiplication as shown in fig.4.

The number of creatures generated in every generation was set 50. The initial genes are generated randomly from the first to fifteenth generation. In the adult group, the creatures are arranged in the order of priority (criterion function) . The 50 creatures of the next generation are generated from the best 50 creatures by crossing with another 50 creatures in the adult group randomly.

$$priority_order = \frac{correct_detection_value}{ages} \quad (2)$$

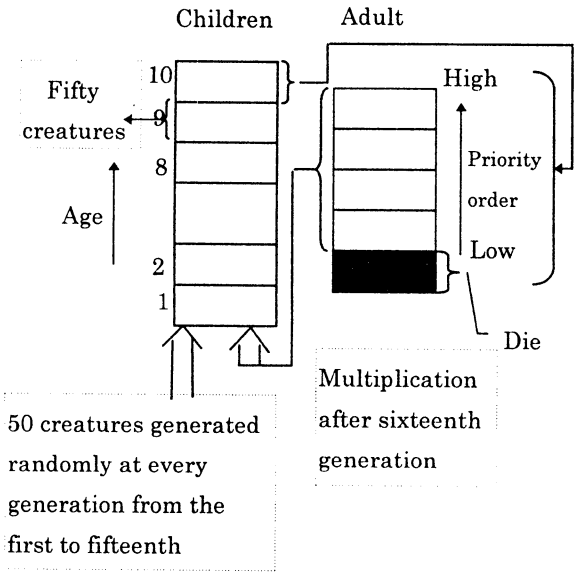


Fig.4 Creature's multiplication

4 Results and conclusive remarks

A network obtained after 50,000 generations recognized correctly 31 out of 36 patterns. The correct recognition rate is 86%.

We come up to implement the first stage of two dimensional spatial recognition map. The second stage of our task is to configure the neural network with which human being objectify oneself and make model one's action in brain.

We will also apply the recognition map to carry out such activities that several targets emerge in time series individually or simultaneously. These situations correspond to the emergence of plural baits or enemies.

We are considering

(1-1) present position calculation (objectified oneself) based on one's action on the past recognition map (say, absolute map), and

(1-2) matching of relative map obtained from present visual information for position confirmation or complement,

(2) drawing up the action plan based on these situations.

References

[1] W. Nian, K. Okazaki, and S. Tamura, "Evolution of Vision System by Genetic Algorithm", PROCEEDINGS OF INTERNATIONAL SYMPOSIUM ON ARTIFICIAL LIFE AND ROBOTICS (AROB '97), pp.9-13.

[2] Hopfield, J.J., " Neurons with graded response have collective computational properties like those of two-state neurons", Proceedings of the National Academy of Sciences, 81, pp.3088-3092, 1984.

[3] Yoh-Han Pao, " Adaptive Pattern Recognition and Neural Networks", Addison Wesley, 1989.

[4] J.H.Holland, " Adaptation in Natural and Artificial Systems", The Univ. Michigan Press (1975), MIT Press (1992).

[5] T.Nagao, T.Agui and H.Nagahashi, "Structural evolution of neural networks having arbitrary connections by a genetic method", IEICE Trans. INF. & SYST. Vol. E76-D, No.6, pp.689-697. 1993.

Proc. of Third Int. Symp. on Artificial Life, and Robotics (AROB Ⅲ'98),
Oita, Japan, 19-21, January, 1998,

The Application of Neurocomputer for a Control Problem

Masanori Sugisaka and Zhi-Jun Liu

Department of Electrical and Electronic Engineering
Faculty of Engineering
Oita University

Tel: +81-975-54-7831, Fax:+81-975-54-7841
msugi@cc.oita-u.ac.jp, zjliu@cc.oita-u.ac.jp

Keywords: Artificial Neural Networks, Neurocomputer, Back Propagation Model, Multi-input Nonlinear Systems, Control Systems.

ABSTRACT: We used the neurocomputer called MY-NEUPOWER made by HITACHI MICROCOMPUTER SYSTEM LTD.(Tokyo, Japan) in our research to carry out the artificial neural networks (ANN's) calculating. We developed an application software on back propagation (BP) model under the UNIX platform using the specified computer language named MYPARAL which was provided by HITACHI MICROCOMPUTER SYSTEM. This model was used to simulate the cooler system in steel plant which is a multi-input and single output nonlinear system.

1 Introduction

1. 1 ANN's in Control System

Although there are a lot of kinds of ANN's structures, a typical ANN's consist of many interconnected simple nonlinear systems called neuron or unit. Each neuron can process individually. All or part of neurons in the same layer may calculate simultaneously under the system command. The terms of ANN's are typically used to distinguish them from biological networks of neurons.

Because ANN's have such features as massive parallelism, learning ability, nonlinear function and fault tolerance, they offer the better solution for control systems than conventional alternatives. So, It can be seen as a natural step to use ANN's in control systems to meet new challenges[1][2]. ANN's have found growing success in many kinds of industrial control application. For example, using neurocontroller in active vision system [3], ANN's was used as state feedback controller that learns the time-optimal actions by means of optimization process[4]. Also ANN's was used as a nonlinear self-tuning adaptive controller[5].

1.2 Neurocomputer Used in ANN's

As the important developing tool, traditional and general purpose computer has much limitation used in artificial neural networks(ANN's) development [6]. The main reason is that the hardware and software(operation system and application software) in general purpose computer operate serially that makes it much different from the function of ANN. Although there are some parallel processing computer systems, such as the UNIX system, the number of processing element(PE) are much less than the neural units in a simple ANN model. So that, with the general purpose computer, it is difficult to simulate the function of ANN and impossible to realize the real time control using more complicated ANN algorithms.

We used neurocomputer called MY-NEUPOWER [7] in our research. This is a real parallel calculating computer designed for the purpose of artificial neural networks' simulation. In this neurocomputer, there are 512 physical neural units. Each neural unit has one ALU(32bits), 16 special registers(32bits), 512 RAM (16bits) and other registers such as the flag register and group register. Besides the RAMs and registers in each neural unit, 4M RAM(10bits) are provided in data buffer. The data exchanging between neural units is carried out by means of data buffer. The system clock frequency is 25MHz. The computer language named as MY PARALL was particularly developed under the UNIX platform by HITACHI MICROCOMPUTTER SYSTEM for this kind of neurocomputer. It combines the parallel calculating and serial calculating together. Each neuron in the same group(layer) can calculate simultaneously under one command.

We developed the application software of BP model using the neurocomputer under the UNIX platform to simulate the cooler system in steel plant[8]. The simulation was carried out and simulation result was analyzed. The output of BP model converges after 880 times training. The standard deviation σ is equal to 0.02. Further improvements that will be carried out in the future are pointed out.

2 Model Structure

2. 1 Model Topology

There are many kinds of ANN's existing by now. The main categorization of these methods is the distinction between supervised and unsupervised training or learning. As for the supervised training, there are back propagation(BP), learning vector quanti-

zation(LVR)[6], etc. As for unsupervised training, there are adaptive resonance theory(ART)[6], counterpropagation (CPN)[6] and so on.

In our work, the BP model was selected because of its simplicity of model structure and training algorithm to simulate the cooler system. The model

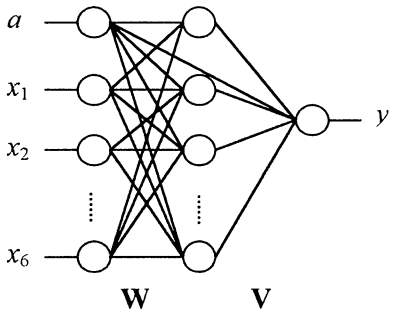


Fig.1 BP model

structure is shown as Fig.1.

This is a two layers(with one hidden layer) BP model, with 6 input units in input layer, 10 neurons in hidden layer and one neuron in output layer. The model input vector is $\mathbf{X}=[x_1\ x_2\ x_3\ x_4\ x_5\ x_6]$, y is the output of model. The weight matrix between input layer and hidden layer, hidden layer and output layer is **W** and **V**, respectively.

$$\mathbf{W}=\begin{bmatrix} w_{11} & w_{12} & \dots & w_{1\,10} \\ w_{21} & w_{22} & \dots & w_{2\,10} \\ \dots & \dots & \dots & \\ w_{71} & w_{72} & \dots & w_{7\,10} \end{bmatrix} \qquad \mathbf{V}=\begin{bmatrix} v_1 \\ v_2 \\ \dots \\ v_{11} \end{bmatrix}$$

Besides the input vector **X**, there is a constant input named a. a is input to each neuron in hidden layer and output layer as the neuron's bias. In our simulation, $a = 1$. The activation function in each neuron is sigmoid function given by Eq.(1).

$$f(s) = \frac{1}{1+\exp(-s/T)} \tag{1}$$

where s is the summation of the inputs of one neuron multiplied by associated weights, T is the artificial temperature which changes the slope of sigmoid function, and f(s) is the output of one neuron.

The multi-layer ANN can be used to realize arbitrary nonlinear functions theoretically although encountering some technical difficulties. The training algorithm is one of the important factors in real applications

2.2 Training Algorithm

The training algorithm of BP model uses an objective function which is defined to be the summation of square errors between the desired outputs and the network outputs. It then employs a steepest-descent search algorithm to seek the minimum of the objective function[9].

The variable coefficient training algorithm was used in our simulation. The training algorithm is described below. It is the kind of supervised training algorithm, so it needs the system real inputs and outputs as training pairs. The training of the weights in output layer is shown by Eq. (2).

$$\delta_o = y(1-y)(y_t - y) \tag{2a}$$
$$\Delta v_j(n+1) = \alpha \cdot \Delta v_j(n) + \beta \cdot \delta_o \cdot o_{hj} \quad (j=1\text{-}10) \tag{2b}$$
$$\Delta v_{11}(n+1) = \alpha \cdot \Delta v_{11}(n) + \beta \cdot \delta_o \cdot a \tag{2c}$$
$$v_j(n+1) = v_j(n) + \eta \cdot \Delta v_j(n+1) \quad (j=1\text{-}11) \tag{2d}$$

where y is the output of BP model in output layer, y_t is the target output in output layer, δ_o is the output error $(y_t - y)$ multiplied by $y(1-y)$, $v_j(n)$ is the j-th weight element at n-th training time, $v_j(n+1)$ is the j-th weight element at (n+1)-th training time, $\Delta v_j(n)$ is the error of j-th weight element at n-th training time, $\Delta v_j(n+1)$ is the error of j-th weight element at (n+1)-th training time, a is constant factor(a=1, here), α and β are the constant coefficients and η is the variable coefficient. The value y is shown by Eq.(3)

$$y = f\left(\sum_{j=1}^{10} o_{hj} \cdot v_j + a \cdot v_{11}\right) \tag{3}$$

o_{hj} is the output of j-th neuron in hidden layer, shown by Eq.(4).

$$o_{hj} = f\left(\sum_{i=1}^{6} x_i \cdot w_{ij} + a \cdot w_{7j}\right) \quad (j=1\text{-}10) \tag{4}$$

where f( ) is sigmoid function.

The training of weights in hidden layer is shown by Eq.(5).

$$\delta_{hj} = o_{hj}(1 - o_{hj})\,\delta_o \cdot v_j \quad (j=1\text{-}10) \tag{5a}$$
$$\Delta w_{ij}(n+1) = \alpha \cdot \Delta w_{ij}(n) + \beta \cdot \delta_{hj} \cdot x_i \quad (i=1\text{-}6, j=1\text{-}10) \tag{5b}$$
$$\Delta w_{7j}(n+1) = \alpha \cdot \Delta w_{7j}(n) + \beta \cdot \delta_{hj} \cdot a \ (j=1\text{-}10) \tag{5c}$$
$$w_{ij}(n+1) = w_{ij}(n) + \eta \cdot \Delta w_{ij}(n+1) \quad (i=1\text{-}7, j=1\text{-}10) \tag{5d}$$

where δ_{hj} is the error of j-th neuron multiplied by $o_{hj}(1 - o_{hj})$, $w_{ij}(n)$, $w_{ij}(n+1)$ is ij-th element of weight matrix **W** at n-th and (n+1)-th training, respectively. $\Delta w_{ij}(n)$, $\Delta w_{ij}(n+1)$ is the error of ij-th element of weight matrix **W** at n-th and (n+1)-th training, respectively.

3 Cooler System

3.1 System Description

The cooler system in steel plant is a multi-input and single output nonlinear system. In real system, there are 8 inputs and one output. To simplify the problem, we consider the average of two outputs temperature Out-TempA and Out-TempB as Out-Temp, and ignore the input of WB-19R Temp, so that to reduce the system inputs to 6 which named as **X.**

Table 1 The data normalized

	Input Mass *(T/H) Max:1200* x 1	Coller Level *(mm) Max:1500*	Coller Rotate *(rpm) Max:1200*	Out Temp *(^0C) Max: 400*	Atmosphere Temp *(^0C) Max: 50*	WB-20 Temp *(^0C) Max: 500*	Damper Stroke *(%) Max:100*
original value	1014.57	1431.62	553.83	56.45	19.7	442.38	43.10
normalized value	0.845	0.954	0.461	0.141	0.394	0.884	0.431

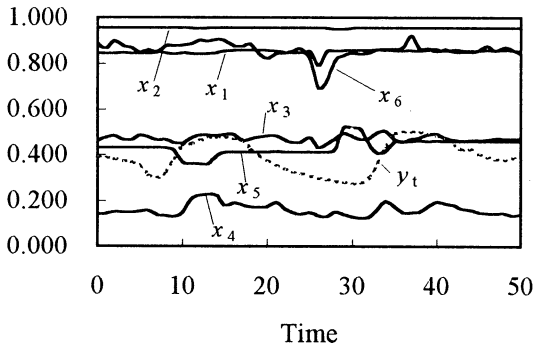


Fig.2 The cooler system

X=[x_1 x_2 x_3 x_4 x_5 x_6]. The system inputs and output are illustrated as Fig.2. In Fig.2, there are 50 sets of inputs and output which will be used as training pairs in the training process of BP model.

3.2 Data Normalization

To satisfy the need of BP model and the demand of neurocomputer calculation, we normalized the inputs and output data of the real system by dividing the maximum value of the original value for each input and output. Table 1 shows the data normalized for one set of input and output data. After the data normalization, the maximum of each variables(inputs and output) in BP model is limited to 1.

Because the data length of input and output in neurocomputer is limited to 10 bits, from -512-511 for decimal value, the normalized value in table 1 is limited to 3-digit after the decimal point. This reduction may cause error because the original value is 6-digit. In table 1, there are six inputs, named Input Mass(x_1), Cooler Level(x_2), Cooler Rotate(x_3), Out Temp(x_4), Atmosphere Temp(x_5), WB-20 Temp(x_6), one output named Damper Stroke(y_t). The original data and normalized data for inputs and output are listed in Table 1. The normalized data will be used as training pairs in the training process.

Fig.2 illustrates the inputs and output of the system after normalization. X=[x_1 x_2 x_3 x_4 x_5 x_6] in Fig.2 will be the target input vector, y_t will be the target output in BP model

4 Training of BP Model

4.1 Convergence Condition for Training Process

We trained the BP model on the method described above using the training pair X=[x_1 x_2 x_3 x_4 x_5 x_6] and y_t. There are 50 sets of training pair selected to train the BP model. The standard deviation σ is calculated below as the training error given by

$$\sigma = \sqrt{\frac{\sum_{i=1}^{n} (y_{ti} - y_i)^2}{n(n-1)}} \qquad (6)$$

where n is the number of training pairs. In this paper, n=50. The standard deviation σ is calculated by Eq. (6) for each step of the training process. The convergence condition is defined by Eq. (7).

$$\begin{array}{ll} \sigma_0 \leqq \sigma & \text{training continues;} \\ 0 \leqq \sigma < \sigma_0 & \text{convergence, training stops.} \end{array} \qquad (7)$$

In our simulation , σ_0 is set to be 0.02.

4.2 Variable Coefficient

The variable coefficient η is adjusted according to the value of σ in training process by Eq. (8).

$$\begin{array}{lll} \eta = 0.031, & \text{while} & 0.05 \leqq \sigma \ ; \\ \eta = 0.0625, & \text{while} & 0.03 \leqq \sigma < 0.05; \\ \eta = 0.125, & \text{while} & 0.02 \leqq \sigma < 0.03. \end{array} \qquad (8)$$

The value of coefficient η is set to small value(0.031, in this paper) to prevent the summation of neuron saturating quickly at the beginning of training. The value of coefficient η increases while the standard deviation σ becomes small at the end of training to avoid the paralysis phenomenon.

4.3 Selection of Initial Values

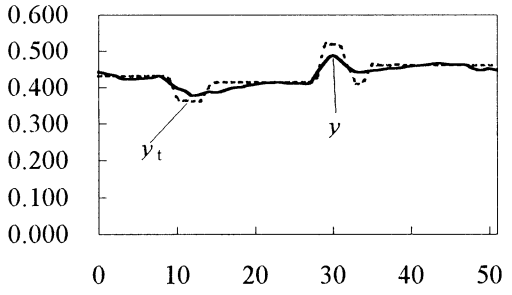
The initial values of weight matrix **W** and **V** were selected to be small random values. The selection of the initial values has much influence on the convergence and training times of the BP model. If the initial values are much large, for any inputs, the summation of each neuron in hidden layer will saturate quickly, and the neuron output will be always be 1 because of the nature of sigmoid function. If the initial

values are very small, the summation of each neuron in hidden layer will be very small, the neuron output in hidden layer will be about 0.5 because of nature of sigmoid function. As a result, the neurons in hidden layer can not correctly distinguish the input vectors because of the poor initial values of weights.

5 Simulation Result and Analysis

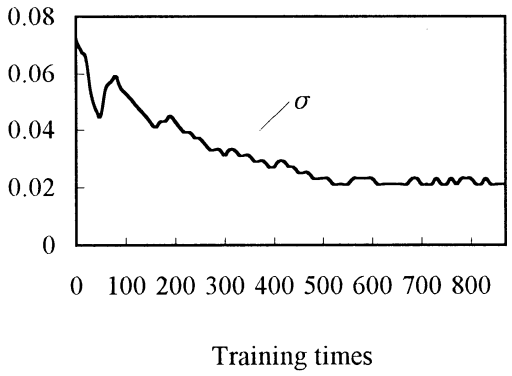
5.1 Simulation Result

The simulation results are illustrated as Fig. 3 and Fig. 4. Fig.3 is output y of BP model after 880 times training comparing with the target output y_t. Fig.4 is the standard deviation σ varying with training times.



The number of training pairs

Fig.3 The output of BP model



Training times

Fig.4 The training standard deviation

5.2 Analysis

From the simulation results shown by Fig.3 and Fig.4, we can see that the output y of BP model converges after 880 times training. The standard deviation σ is equal to 0.02. The value of standard deviation σ is still little large. The first reason is that the input and output data length is limited to 10 bits in this neurocomputer, less than the length of original data. The second one is that maybe the structure of BP model is not complex enough.

In the further research, we will make effort to improve the property of this algorithm as following.

① To adjust the software to be more concise and simple. Because for one more sentence in program, it will cycle m×n times in training process. Where, m is the number of sets of teacher pair, n is the training times. In this paper, m=50, n=880, so m×n=44,000. So that, the more simple the program is, the training process will be more quick. It is a very important factor to improve the training quickness.

② To adjust the structure of BP model, for example, the number of hidden layers, the number of neurons in each hidden layer, to obtain more accurate model for this cooler system.

③ To solve the problem of data transforming between UNIX work station and the PC. Because the neurocomputer operates under the UNIX platform, all the input and output data are UNIX format that is not compatible to PC format, so it took a long time to treat the simulation result in PC.

④ To use this trained model in the controlling of cooler system in steel plant.

6 Conclusion

In this paper, we used BP model to simulate the cooler system in steel plant with neurocomputer. This algorithm is suitable to the nonlinear system and the simulation result is reasonable. In next step, we will improve the program and the model structure to get more accurate result and to apply this model to the cooler control system.

References

[1] M. Agarwal, "A Systematic Classification of Neural-Network-Based Control", IEEE Control Systems, Vol. 17, No. 2, pp.75-93,1997.

[2] P. J. Antsaklis, "Neural Networks in Control Systems", IEEE Control Systems Magazine, Vol. 10, No. 3, pp. 3-5, 1990.

[3] N. Srinivasa and R. Sharma, "Execution of Saccade for Active Vision Using a Neurocontroller", IEEE Control Systems, Vol. 17, No. 2, pp. 18-29, 1997.

[4] T. R. Niesler and J. J. Duplessis, "Time-Optimal Control by Means of Neural Networks", IEEE Control Systems, Vol. 15, No. 5, pp.23-33, 1995.

[5] F. C. Chen, "Back-Propagation Neural Networks for Nonlinear Self-Tuning Adaptive Control", IEEE Control Systems Magazine, Vol. 10, No. 3, pp.44-48, 1990.

[6] V. N. Reinhold, Neural Computing—Theory and Practice, New York, Library of Congress Press, Ch. 3, pp. 43-57, 1989.

[7] MY-NEUPOWER----User Manual, HITACHI MICROCOMPUTTER SYSTEM LTD., 1995.

[8] Tokuda, "The Research on the Temperature Control of Cooler", Nippon steel plant in Oita, pp. 1-9, March 12,1996.

[9] S. C. Huang and Y. F. Huang, "Learning Algorithms for Perceptrons Using Back-Propagation with Selective Updates", IEEE Control Systems Magazine, Vol. 10, No. 3, pp. 56-61, 1990.

Proc. of Third Int. Symp. on Artificial Life, and Robotics (AROB III' 98),
Oita, Japan, 19-21, January, 1998,

Automatic Path planning of Spray Robot for a Die Casting Process by Using Genetic Algorithm

Tatsuo Sakamoto, Katsutoshi Kuribayashi, Susumu Matsumoto*, Marcelo G. Franco*, Jun Tang*, Kousei Murakami, Hideo Komeya*

Ube Industries Co., Ltd. Machinery Div.
1981 Okinoyama, Ube, 755 Japan

*Yamaguchi University
2557 Tokiwadai, Ube, 755 Japan

Abstract

In die casting operation, die spray is the key for the quality and for the productivity. But die spray operation depends it's parameter setting such as spray path and volume on operator's experiences even the robot sprayer is adopted.

This paper purposes an algorithmic rule base which can perform the spray path planning . The spray path, created through the genetic algorithm method has been compared with operator's work then transferred to a spray robot as an off-line teaching and demonstrated the actual spraying.

The unique spray system which consists of a small wrist robot with spray nozzles attached to a main robot was developed to perform actual spray work.

The results show good matching with operator experience and forecast good application in actual casting operation.

Key words: Die Cast, Spray, G.A., Robot, Path-Planning

1. Introduction

Die Casting is the most effective production process to make net shape parts for use in automobiles, appliances, etc. This process is the high pressure casting which injects the molten metal into the die cavity and quickly solidify. Die spray is the key for this process. The spray provides thermal insulation, a cooling effect and aids the release of the part from the die[1]. The spraying operation is usually done manually or by 1 to 2 axis automatic spray device. Recently the system is converting to the articulated robot.

But the spray path is by teach pendant and the operating parameters are set based on the operator's experiences, because the parameters on spray operation are to be considered in various conditions as listed below:

(1) Die cavity configuration is complicated.
(2) Die surface temperature distribution is deeply depend on spray condition and the casting quality and productivity are heavily rely on it.
(3) Time for spray is always to be minimum.

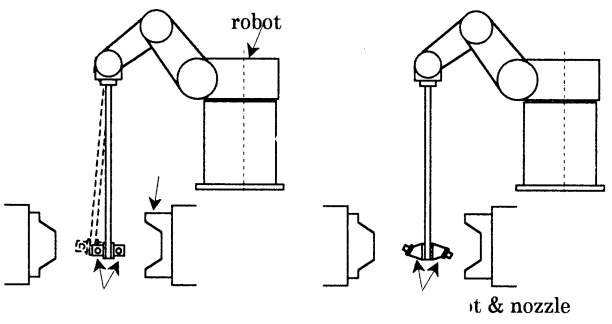
The purpose of this study is to create the optimum spray path by calculation through the genetic algorithm method, considering above conditions[2][3].

The created spray path has been compared with that of operator's work then transferred to a spray robot by an off-line teaching and the actual spraying by the spray robot was demonstrated.

2. The system configuration of spray robot

[Fig. 2-1] shows the arrangement of spray robot on die casting machine. Die casting die is consisted in moving and stationary halves, therefor spray system is to be equipped with wrist robot to spray the both die surface simultaneously.

Spray nozzle is attached on the wrist, and spray lubricant perpendicularly to the die surface.

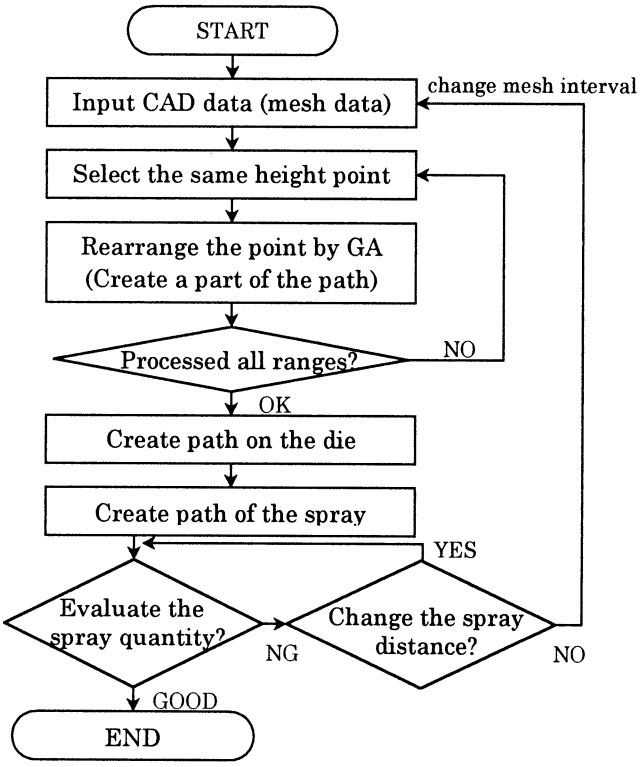


[Fig.2-1] Spray robot layout

3.Path calculation by G.A.

3.1 Good spray procedure

In actual die spray operation, operator will spray die from high temperature area to uniform temperature distribution on die, also will create minimum path to reduce overall spray time.
To realize this spray operation, the procedure as shown in [Fig.3-1] was prepared.



[Fig.3-1] Path calculation flow chart

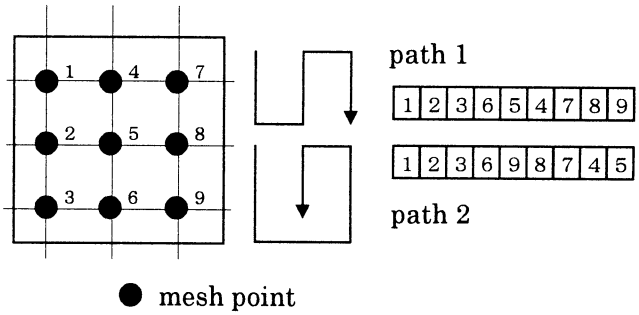
The procedure starts from input the die cavity configuration which is the mesh point on the CAD data Following 6 data on each point are obtained, coordinate (x,y,z), posture (rotation on x-axis, on y-axis) and cavity thickness.
Then calculation starts, as shown in the flow chart, some of preset rules are applied to simplify the calculation. For example the same height points were selected first, because as an assumption in this calculation, the height represents the die temperature. To maintain the continuity, the start point of the path for next height is set to the nearest to the end point of previous height. The last portion of the flow chart is for the conversion of completed path on the die to the spray nozzle path to evaluate the spray mist deposition.

3.2 Calculation method

In this study, the spray path is described as a string of gene. The each mesh point represents gene, and the spray path is represented by the series of gene.
The calculation procedure is as follows:

(1) Initialization of the parameters, and set the start point
(2) Creates individuals randomly and selects the population.
(3) According to pre-determined probability, procures crossover and mutation.
(4) Evaluates the individuals with fitness
(5) Selection

This procedure is iterated for preset generations.



[Fig.3-2] Mesh point and examples of the path

3.3 G.A. parameter setting

In this study, following parameters are selected.

(Ng) = Number of Generation
(Np) = Number of Population
(Pc) = Probability of Crossover
(Pm) = Probability of Mutation
(GENE)= Number of mesh point which represents the individuals
(a,b,c) = Weight coefficients on the fitness

Then, through the G.A. calculation , following 3 kinds of the fitness were used for the selection of next generation.

(1) Die temperature
This fitness is to give the path priority on the die temperature distribution, ie., the thickness of die represents temperature.
If the path is point a→b→c, and temperature at each point is t_a, t_b, t_c ,then set the temperature fitness 《t》 as a difference of the temp erature on each points.

$t_{ab} = t_a - t_b \quad (t_a \geqq t_b)$
$t_{ab} = -2(t_a - t_b) \quad (t_a < t_b)$

Here, t_{ab} is the fitness on point a and b, small value is better and if the path go to lower point it suffers penalty of double

temperature difference. This 《t》 fitness is sum up through all the path as 《t total》 .

(2) Path length

This fitness is to evaluate total path length. When path is a→b→c, and each coordinates are (X_a, Y_a ,Z_a) (Y_b ,Y_b ,Y_b) (X_c, Y_c, Z_c), 《L》 is the fitness of path length.

$$L_{ab} = \sqrt{(x_a - x_b)^2 + (y_a - y_b)^2 + (z_a - z_b)^2}$$

The accumulated path length is 《L total》 and small 《L total》 has a higher priority.

(3) Path smoothness

This is to give the priority on the path the minimum direction change for the robot to avoid useless motion. When path is a→b→c, and each coordinates are (X_a, Y_a ,Z_a), (Y_b ,Y_b ,Y_b) (X_c, Y_c, Z_c),the directional vector between [a and b], [b and c] are shown as :

V_{ab}= ($X_b - X_a$, $Y_b - Y_a$, $Z_b - Z_a$)

V_{bc}= ($X_c - X_b$, $Y_c - Y_b$, $Z_c - Z_b$)

Then with these vector and L_{ab} and L_{bc}, the angle consisted by 2 vectors 《 θ 》 is obtained.

$$\theta_{abc} = \cos^{-1}\left[\frac{V_{ab}}{L_{ab}}\frac{V_{bc}}{L_{bc}}\right]$$

The smaller accumulated 《 θ total》 has a higher priority.

(4) Total criterion

Finally total fitness is shown as :

$f\text{-}_{total}$ =a($t\text{-}_{total}$) + b($L\text{-}_{total}$) + (θ -$_{total}$)

here a, b, c is the weight coefficients for each fitness to decide the criterion $f\text{-}_{total}$, which is used for selects of next generation.

In this study, the selection was performed by selecting the better $f\text{-}_{total}$ individuals from the best value to the size of population, after crossover and mutation have been procured.

3.4 Spray mist distribution model

After the best path is calculated, the spray mist deposition on the die surface is evaluated. Assuming the shape of mist from the nozzle is the corn shape, and the mist distribution is as normal distribution, the total deposition of the mist was calculated. The mist distribution f(r, σ) is shown as follows:

$$f(r,\sigma) = \frac{1}{\sigma\sqrt{2\pi}}\exp\left\{-\frac{r^2}{2\sigma^2}\right\}$$

here, r =distance from nozzle center

σ = standard deviation

Through the test, actual spray volume and above estimation is compared to certify the spray mist deposition.

The assumption show good matching with test, the result is shown in [Table 3-1].

g/mm^2	Spray distance		
	100mm	200mm	300mm
Assumption	30.6	15.3	10.2
Test	39.0	15.0	9.3

[Table 3-1] Spray mist deposition test

3.5 Calculation result by G.A.

The calculation was done in several cases, the result on two models are shown below.

(1) Model die- I

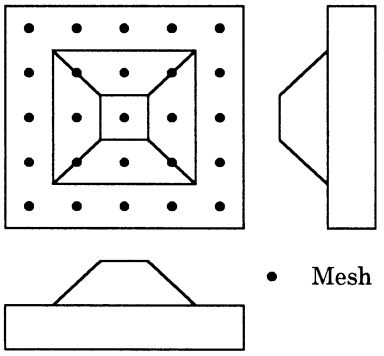
Simple model shown in [Fig.3-3] was used for the calculation and the result was compared with operator's path.

On this model, the weight coefficients have been varied to see the influence on the path.

The parameters in this calculation are:

Ng = 300, Np = 20, Pc = 1.0, Pm = 0.3.

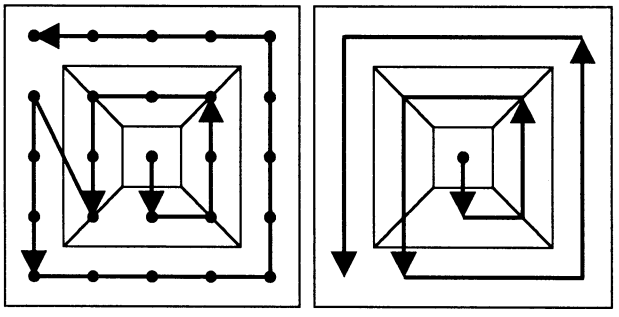
The geometry of the model is 40mm x 40mm pitch and total point is 25.



[Fig.3-3] Model die- I

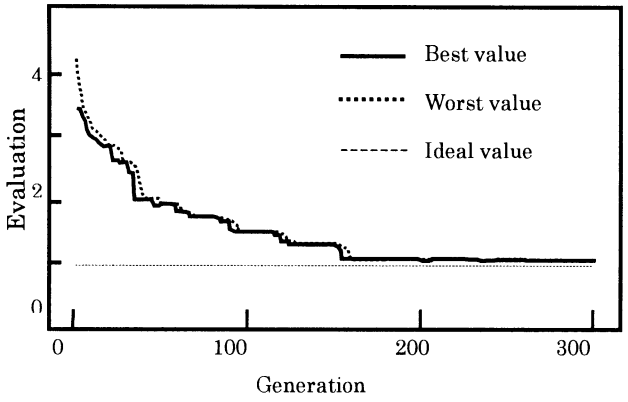
The calculated path and operator's path are compared in [Fig.3-4].

In in [Fig.3-5], the relation of generation and fitness is shown.



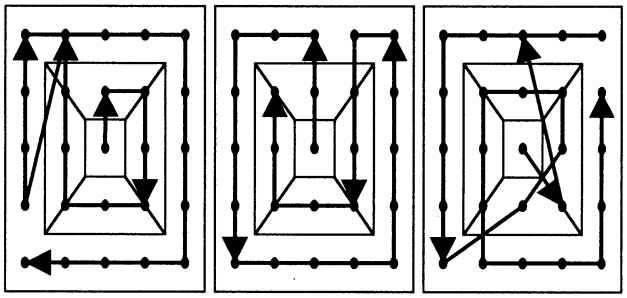
Calculation Operator's path

[Fig.3-4] Comparison of spray path]



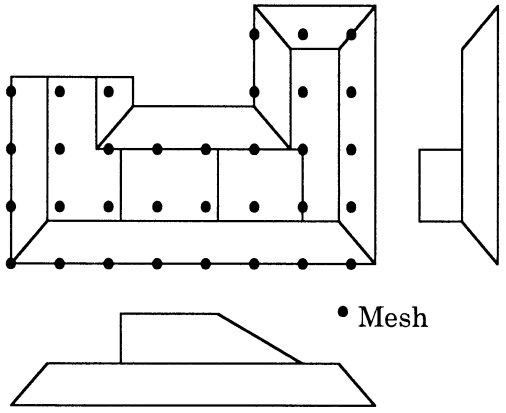
[Fig.3-5] Relation of fitness vs generation

[Fig.3-6] is the example of the influences of the fitness priority difference. According to priority, the spray path varies.
Those are, from left to right, the die temperature priority, minimum path length oriented and the most smooth robot path.



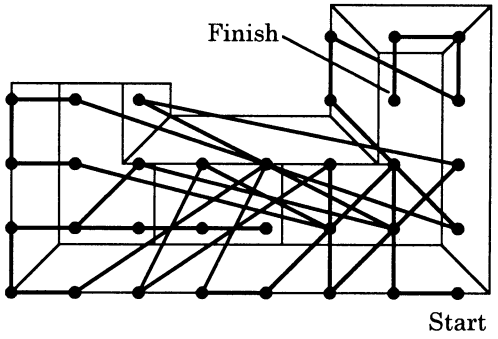
[Fig. 3-6] Example of path variation according to different fitness coefficients

(2) Model die - II
The other calculation is shown below.
The result of the path calculation was used for spray test to evaluate the spray mist on the die. [Fig. 3-7] is the shape and mesh point.

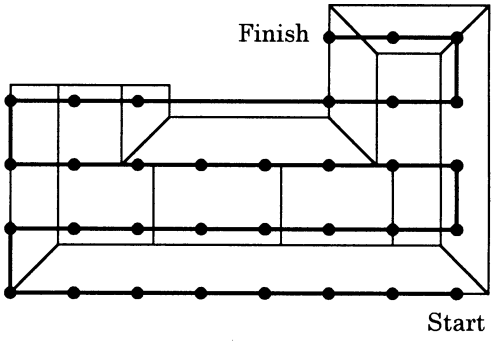


[Fig. 3-7] Model die - II

The parameters in this calculation are:
Ng = 500, Np = 20, Pc = 1.0, Pm = 0.3.
The geometry of the model is 40mm x 40mm pitch and total point is 35.
[Fig.3-8] and [Fig.3-9] are the result of the calculation at zero generation and at 500th generations respectively.



[Fig.3-8] Result at zero generation

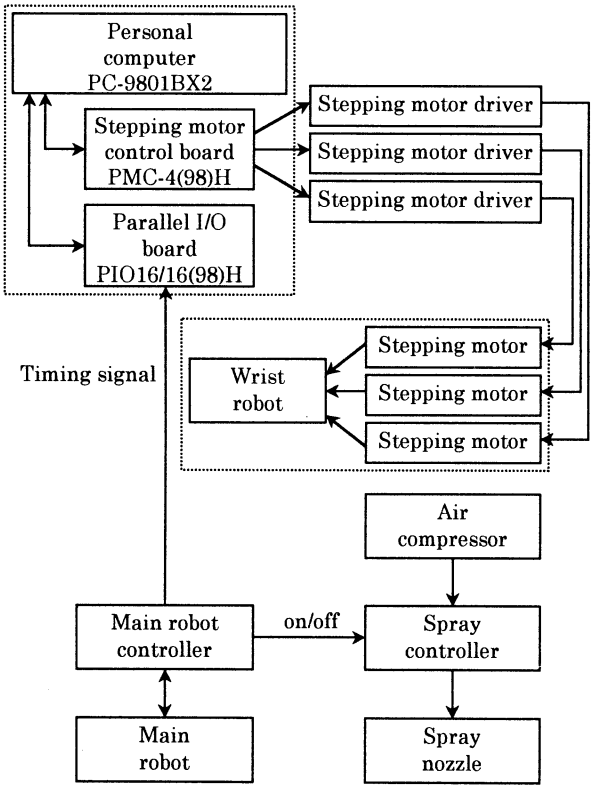


[Fig.3-9] Result at 500th generation

4. Testing equipment

4.1 System arrangement

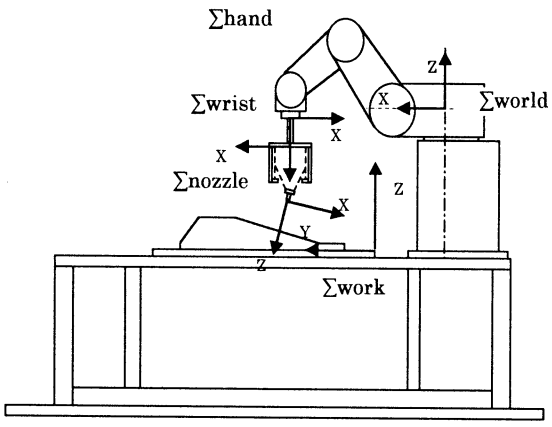
To evaluate the calculation result, the system shown in [Fig.4-1] was developed for the spray test.
This system is to realize actual spray automatically, i.e., from the path planning to wrist robot data conversion.
As stated in the introduction, die casting die is consisted in two die halves, those are stationary and moving halves.
Therefor, if the mere robot is used, simultaneous spray onto the both die surface is impossible.
The arrangement is to utilize wrist robot to maintain the spray angle perpendicular to the die surface on both die halves, in accordance to the movement of main robot. Thus the maintaining the calculated result, the total spray time could be reduced by half incase of one wrist robot on each side. If necessary, the number of the wrist robot is increased.



[Fig.4-1] System for spray test

4.2 Algorithm to convert path for robot

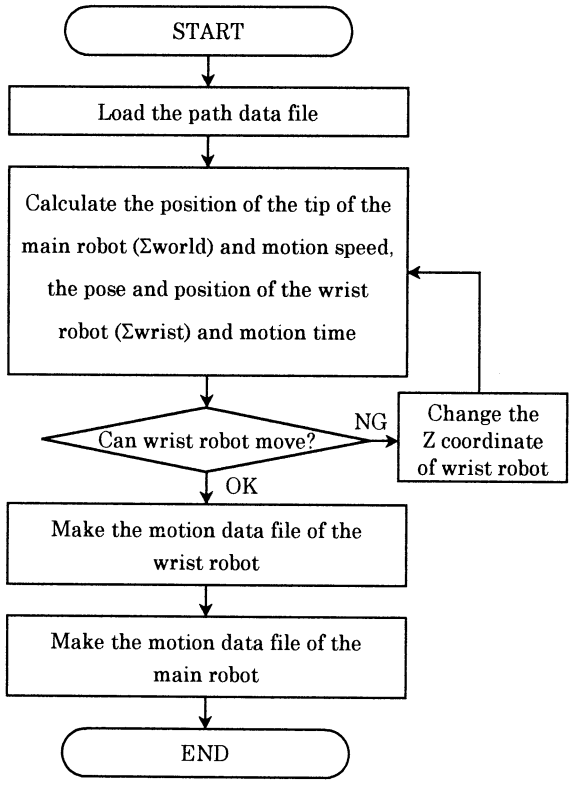
To perform the spray path on the robot, path data need to be converted for the robot.
[Fig.4-2] shows the coordinates on the test system. Here, Σworld represents main robot coordinates which becomes the base coordinates in the system, and Σwork is for the die.



[Fig.4-2] Relation of coordinates in test system

The path which is created by G.A. has following data:
(1) Mesh number
(2) Coordinate (X, Y, Z)
(3) Posture (W, P, R)
(4) Velocity
Through the flow chart which is shown in [Fig.4-3], the path data is converted to the robot data. From the path data on the die mesh point, the spray nozzle position, posture and velocity are calculated, then those are converted to the main robot coordinates (World Coordinates).

To complete the spray work, the main robot and the wrist robot must be synchronized. The procedure in this system is as follows, when the main robot reaches each path point which is converted from mesh point, it send synchronous signal to the wrist robot. The wrist robot receives the signal and procures it's motion toward to the next path point.

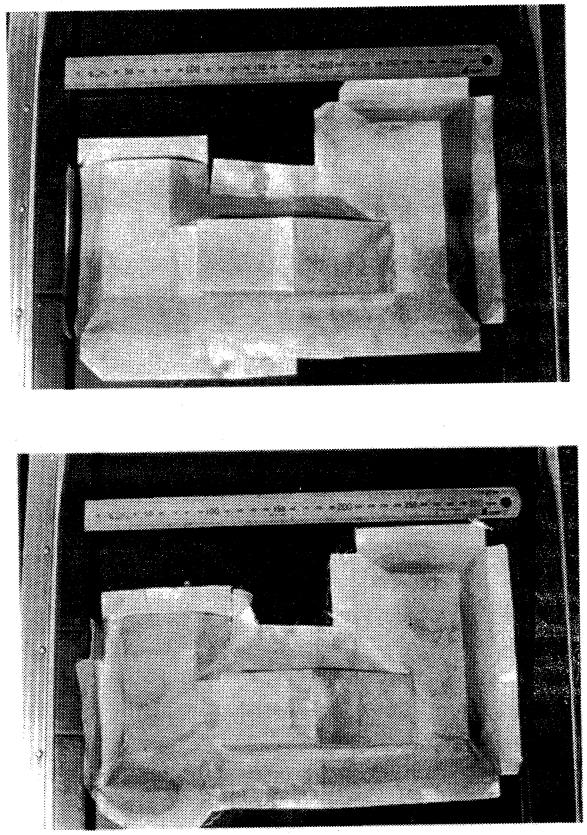


[Fig.4.3] Flow chart for path converting.

4.3 Spray experiment

The spray test was achieved on the plastic test die which is shown in [Fig.3-7].
In the test, the synchronous movement of the main robot and the wrist robot was confirmed.

The result was in the all path, the spray angle was kept perpendicular to the die surface.
The mist distribution was evaluated on both path which was created by calculation and by operator. The result is shown in [Fig.4-4]. It show good matching.



[Fig.4-4] Spray results

5. Conclusion

As a result of this study the following was accomplished.

(1) Assuming the spray path as an individual, Genetic Algorithm was applied on spray path planning with plural fitness evaluation. And results show good matching with the path which was created by operator.
(2) For the ideal spray condition, unique robot system which has small wrist robot on it's end-effector was proposed.
(3) The direct path conversion program and off-line teaching system demonstrated fully automated spray operation.
(4) Actual spray operation was done on the model die, it show good spray mist distribution.

This study show the good possibility to perform automatic path creation in actual die casting.

References

(1) Y.Takemoto, T.Nakamoto : The prospect of die casting production system. ALTOPIA 1993. 12 (in Japanese)
(2)T.Shibata, T.Fukuda, K.Kosuge, F.Arai : Path Planning using Genetic Algorithm. J.S.M.E. 58-553 (1992. 2) (In Japanese)
(3)T.Abe, T.Shibata, K.Tanie, M.Nose : Motion Planning for a Redundant Manipulator by Genetic Algorithm. 1994 IEEE Symposium on Emerging Technologies & Factory Automation

Proc. of Third Int. Symp. on Artificial Life, and Robotics (AROB III' 98),
Oita, Japan, 19-21, January, 1998,

Cooperative Behavior and Control of Collective Autonomous Mobile Robots using Reinforcement Genetic Programming

Hyo-Byung Jun, Dae-Joon Kim, and Kwee-Bo Sim

Robotics and Intelligent Information System Lab.
Dept. of Control and Instrumentation Eng., Chung-Ang University
221, Huksuk-Dong, Dongjak-Ku, Seoul 156-756, Korea
Tel : +82-2-820-5319, Fax : +82-2-817-0553,
E-mail : kbsim@cie.cau.ac.kr, URL : http://rics.cie.cau.ac.kr

Abstract

In this paper, we propose a genetic programming with reinforcement as the scheme that makes a program group for cooperative behavior of distributed autonomous robotic systems(DARS). Evolution and learning are two different ways in which the behavior, and other characteristic, of organisms can change. The combination of learning with traditional genetic algorithm is called as hybrid genetic algorithm. There are two different types of hybrid genetic search: Lamarckian evolution and Baldwin effect. In this paper, to improve performance of the whole system through the behavioral evolution of each robot, we use Genetic Programming with reinforcement based on Natural Selection. We combine learning with evolution to assign the mutation probability of each node in a program. We verify the effectiveness of the proposed scheme applying to the two examples for cooperative behavior of distributed autonomous robotic system.

1. Introduction

In recent, artificial life concept was proposed by C. Langton and has become one of the most popular research area as a solution of intelligent information processing system under uncertain, complex and dynamic environment. Main issue in artificial life is to implement something lifelike with computer and roots by synthesizing phenomena normally associated with natural living systems. The evolutionary computation based on the natural selection theory plays an important role in artificial life.

Distributed autonomous robotic system(DARS) is composed of several agents, autonomous mobile robots, which perceive surroundings individually and perform given task cooperatively. Up to now, single robot system has been researched widely, in recent days much attention is payed to the swarm intelligence and collective behavior found in distributed system. Many papers about this topic, for example distributed autonomous robots, multi-robot system, self-organizing robot, and cooperation of multi-robot etc., are being published[1].

In this paper, we propose the genetic programming with reinforcement as the scheme that makes a program group for cooperative behavior emergence. Genetic algorithm(GA), genetic programming(GP), evolution strategies(ES), evolutionary programming (EP) belong to the category of evolutionary computation, and each of them could be applied to the distributed system[2][3]. Especially genetic programming is expected to have good result in the group behavior of the distributed autonomous mobile robots, agent's behavior being expressed by program tree, and the program size being variable.

The GP with reinforcement is based on the Darwinian evolution theory, and Baldwin effect the modifications due to environment, if constant and lasting, would be inherited and produce a new type. The chromosome in genetic programming is composed of tree structured programs. In conventional genetic programming, the node for mutation is selected randomly, so the crossover point is. But we assign the reinforcement value to each node of a program depending on the state-action relations while it is interacting with environment. And then each node's mutation probability is calculated using the reinforcement value. If a program is selected for mutation, each node should be mutated not randomly, but in proportion to its mutation probability. By applying the each node's reinforcement to generate next population, the acquired characteristic for the lifetime could be inherited, in the long run the best solution could be found faster and more effective than conventional GP with relatively small population.

Although each agent has several simple rules, from the result of interactions between a agent and environment including other agents that rules are changed, therefore the whole system's objective has directly effect on each agents' behavior rule. So each individual has relatively simple function, but when a kind of group is formed intellectual and complex behavior of the group is emergent.

We show the validity of the proposed algorithm by showing some experimental results.

2. Evolution and Learning

Generally evolution and learning are two distinct kinds of change which occur at two different levels. Evolution process in natural system is change at the population level. Each individual in the population reproduces selectively and subject to mutation and sexual recombination which maintain interindividual variability. And learning is another way in which the behavior, and other characteristics, of organisms can change. Learning is change at the individual level. By interacting during its life time with a specific environment an individual can change its behavior by incorporating, through its experience, aspects of the environment in its internal structure.

The combination of learning with traditional genetic algorithm is called as hybrid genetic algorithm. The common form of hybrid genetic searching algorithm uses learning, that occurs during the lifetime of individual, to improve the initial population as well as the genotype produced by genetic recombination. There are two different types of hybrid genetic search. The first uses Lamarckian evolution, in which the resulting improvements are coded onto the genotype processed by the genetic algorithm.

Instead of coding the improvements back onto the genotype, the fitness value of the improvement can be transferred to the individual. This has the effect of changing the fitness landscape, but the resulting form of evolution is still Darwinian in nature. Various phenomena associated with this form of combining learning and evolution are collectively known as the Baldwin effect. In 1896, James Mark Baldwin proposed that individual learning can explain evolutionary phenomena that appear to require Lamarckian inheritance of acquired characteristics. The ability of individuals to learn can guide the evolutionary process. In effect, learning smooths the fitness landscape, thus facilitating evolution. Baldwin further proposed that abilities that initially require learning are eventually replaced by the evolution of genetically determined systems that do not require learning. Thus learned behaviors may become instinctive behaviors in subsequent generations, without appealing to Lamarckian inheritance.

Hinton and Nolan[4] illustrated the Baldwin effect using a genetic algorithms a simple random learning process that develops a simple neural network.

In this paper, we combinate learning with genetic process in the context of Baldwin effect. But our method is different with original Baldwinian in that the improvements by learning are transferred to genetic operation frequency especially mutation probability not to the fitness.

By the sexual recombination each individual's characters are inherited to the next generation. Mutation in natural systems is the source of plasticity to enable a individual to adapt dynamic environment. But traditional genetic process mutation are occurred randomly according to the given probability. Also, in conventional genetic programming, the node for mutation is selected randomly, so the crossover point is. But we assign the reinforcement value to each node of a program depending on the state-action relations while it is interacting with its environment. This reinforcement is obtained by learning and this process is considered as credit assignment. According to this reinforcement value each node's mutation probability can be obtained.

3. Swarm Intelligence and Group Behavior

The insects like ants or bees take group actions or do a thing on system, in other words they have social behavior. But they do not have any absolute being or instructor making an order to maintain the public order, on the contrary they set up against an invader and get food by the intersection between the members, so the whole system is sustained. Like this, it is called swarm intelligence or collective intelligence that individual's actions are collectively effect on the entire objective[1][5].

Recently this swarm intelligence is widely studied in biology and robotics, and many people are trying to implement the artificial swarm intelligence because it has a lot of merit to the single robot system. Several agents could do a task which can't be done by single robot, further more this system could get unpredictable, but nice ability due to the interactions between the agents. Mataric at MIT suggested basic group behavior based on the interaction of the mobile robots which could perceive the other robots and obstacles by only it's sensors. He proposed Collision Avoidance, Following, dispersion, Aggregation, Homing, and Flocking as the basic group behavior. For example, a task finding and gathering food in a wide area could be accomplished by following and flocking in high density area, and by dispersion and homing in opposite case[3].

On the other hand, a new approach is interesting by introducing artificial life concept to this field that self-organization and evolution of the autonomous mobile robots could make group behavior and swarm intelligence[6][7]. In order to solve the complicated problem by cooperation of the multi autonomous mobile robots, each robot need to determine its action appropriately from the relative relation with the other robots. These group behavior from the interaction between the individual robots could be took as emergent characteristic of the self-organization system with several interaction rules.

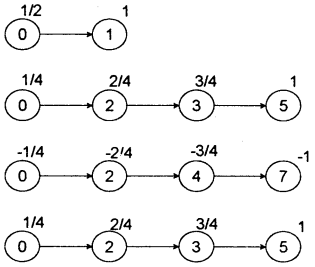
4. Genetic Programming with Reinforcement

On genetic programming, the computer program is generated automatically by the computer introducing the Darwinian evolution theory[8]. Genetic algorithm, evolutionary strategy, and evolutionary programming are shown up in 1960-1970, but genetic programming is developed the early 1990 by the John Koza at Stanford university.

The chromosome in genetic programming is composed of tree structured programs, S-expression of the LISP function. In the same way as the other evolutionary computation, the initial population is constructed by randomly generated tree structured programs, and then selected according to the fitness proportionate to construct next generation. But genetic programming differs from traditional genetic algorithm in that it uses hierarchical genetic material and this is not of fixed size.

There are three basic operators for the genetic programming: mutation, crossover, and inversion.

In traditional genetic programming, the node for mutation is selected randomly, so the crossover point is. But we put the reinforcement to each node by the expression (1) as shown in Fig. 1, and then calculate the each node's mutation probability as shown in Fig. 2. A terminal node executed at the current state will be got 1 as reward or -1 as penalty depending on the state-action relations.



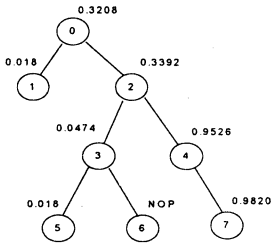


Fig. 1 Node's Reinforcement Fig. 2 Mutation Prob.

After the lifetime, the reinforcement calculation of each node in a program is made by,

$$R_i = \frac{\sum_{t=0}^{T} r_i(t)}{N} \qquad (1)$$

where N is i_th node's executing number for its life time, T a program's lifetime, $r_i(t)$ i_th node's reward/penalty value at time t. Then the mutation probability of i_th node is calculated by the equation

$$p_m(i) = \frac{1}{2}(1 - \tanh(2R_i)) \qquad (2)$$

If a program is selected for mutation, every node would be mutated not randomly, but in proportion to it's mutation probability calculated above. And the crossover points are determined by the same way. By applying the each node's reinforcement to generate next population, the acquired characteristic for the lifetime could be inherited, in the long run the best-so-far individual could be found faster than conventional GP. Additionally Editing, Encapsulation, and Decimation could be used according to the aim of task.

The five major preparatory steps in applying genetic programming to a problem involve determining

(1) the set of terminals
(2) the set of primitive functions
(3) the fitness measure
(4) the parameters for controlling the run
(5) the method for designating a result and the criterion for terminating a run

Genetic programming is applied to various field, such as a robot's program creation, game, image recognition, artificial intelligence, and the convergency of that algorithm has been proved. We use the genetic programming with reinforcement as the scheme that makes a program group for cooperative behavior of DARS.

In the next section, some experimental results will be illustrated about the learning effect on evolution.

5. Computer Simulation

5.1 Artificial Ant

At first we consider a task devised by Jefferson et al.[7] for an artificial ant attempting to find the food lying along an irregular trail. We use the Santa Fe trail designed by Christoper Langton, which is an irregular winding trail with food in 89 of the 1024 cells. In this problem, we compare the performance of GP with reinforcement proposed in this paper with that of conventional GP.

The environment setting for the problem is a 32× 32 toroidal grid in the plane. The artificial ant begins in the cell identified by the coordinates (0,0) and is facing East. The simulation results are shown below for the two different population size.

We tried 300 times for each population case, and the vertical axis represent the mean fitness of all trials for each generation. As shown in the Fig. 3, Fig. 4 GP with reinforcement has better performance with small population, it means we could save the memory for the computation and the convergence time.

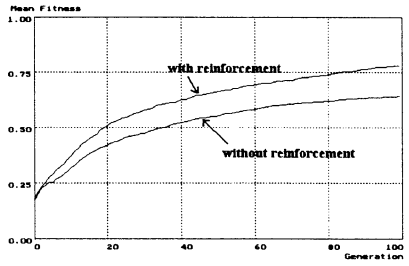


Fig. 3 Population : 100

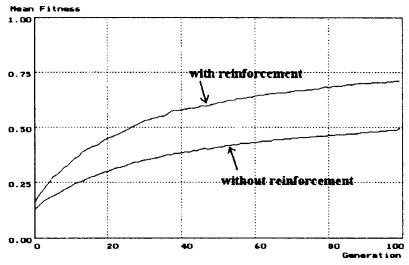


Fig. 4 Population : 50

5.2 Cooperative search problem

We verify the effectiveness of the proposed learning and evolution algorithm by applying it to cooperative search experiment. For the purpose of learning and evolution of the autonomous mobile robots, the simulation environmental conditions are set as follows,

- Working area : 20×20m
- Robot Size : 5×5cm
- Number of robots : 25 units
- Number of food : 100 units
- Number of obstacle : 30 units
- Evaluation time: 250 steps
- Communication Radius : 30cm

Robots are expected to avoid obstacles and get the objects as many as possible in shorter time. And the function set is composed of IF_FOOD_AHEAD, IF_OBSTACLE_AHEAD, PROGN2, and PROGN3. The terminal set is composed of MOVE_FORWARD, LEFT_TURN, RIGHT_TURN, and MOVE_RANDOM.

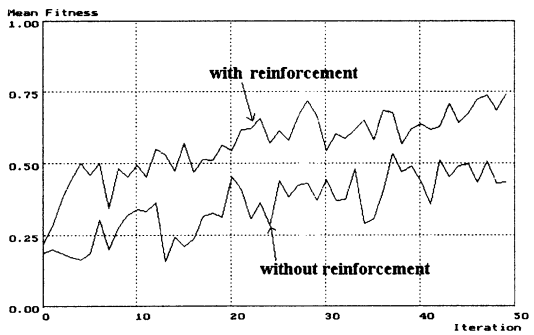


Fig. 5 Fitness changes versus iteration

The simulation result shows that the genetic programming with reinforcement has better performance then traditional genetic programming. It means that where and how much times mutation occurs are determined by interacting with environment.

Acknowledgement

This research was supported by grants from Institute of Information Technology Assessment (No. 97-G-0214).

6. Conclusions

In this paper, GP with reinforcement was proposed as the scheme to make group behavior emergent from the simple behavior rule of each individual without any central instructor.

The GP with reinforcement is based on the Darwinian evolution theory, and Baldwinian. We compared the proposed method's performance with the convention GP first, and applied it to making group behavior emergent in DARS.

However, to realize more excellent swarm intelligence in DARS, the proposed method should be extended to more complicated problems, and generalized. It remains the future work.

References

[1] "Special Issue on Multiple Intelligent Robots," J of SICE, Vol. 31, No. 11, 1992.

[2] Fukuda, "A Study on Dynamically Reconfigurable Robotic System," Trans. of JSME, Vol. 59-C, No. 568, pp. 3837-3844, 1993.

[3] M. J. Mataric, "Designing Emergent Behaviors: From Local Interactions to Collective Intelligence," Proc. of 2nd I.C. on Simulation of Adaptive Behavior, pp. 432-441, 1993.

[4] G.E. Hinton, S.J. Nolan, "How learning can guide evolution," Complex Systems, Vol. 1, pp. 495-502, 1987.

[5] C. R. Kube and H. Zhang "Collective Robotic Intelligence," Proc. of 2nd International Conference on Simulation of Adaptive Behavior, pp. 460-468, 1993.

[6] E. Horiuchi, K. Tani, "Behavior Learning of Group of Mobile Robots with a Distributable Genetic Algorithm," *J of RSJ(Japan)*, vol. 11, no. 8, pp. 1212- 1219, 1993.

[7] R. J. Collins and D. R. Jefferson, "Ant Farm: Towards Simulated Evolution," Artificial Life II, vol. X, Addison -wesley, pp. 579-601, 1991.

[8] J. R. Koza, "Genetic Programming: On the Programming of Computers by Means of Natural Selection," MIT PRESS, 1992.

Proc. of Third Int. Symp. on Artificial Life, and Robotics (AROB III' 98),
Oita, Japan, 19-21, January, 1998,

A Genetic Algorithm for Design of Boundary Filter In Subband Coding by Using Wavelet Transform

Jinshan Tang
(Beijing University of Posts and Telecommunications, Beijing , China)
E-mail: stang@iss01.iss.ac.cn

Yongguang Zhang
(Institute of Systems Science, Academia Sinica ,Beijing , China)
Yzhang@iss01.iss.ac.cn

Abstract

This paper describes a genetic algorithm to design boundary filters for image coding by subband decomposition with wavelet filter bank. Wavelet transform has been introduced to image coding for a long time. But there are still some problems to solve, one of which is the processing of boundary[1]. Although there have proposed several methods to deal with this problem, a good answer is still difficult to find. In this paper, we propose a scheme for constructing high-performance boundary filter by genetic algorithm。 In our scheme, the design of high-performance boundary filter is implemented by choosing a boundary filter from a set of boundary filters. Experimental results prove its efficiency.

Keywords: Genetic algorithm, Wavelet transform. Boundary proccessing, Subband coding, Filter bank

1 Introduction

In recent years, there has been increased interest in the field of image coding based on wavelet transform . Wavelet transform has been proved to be more efficient than DCT. But there are still some problems for image coding by using wavelet transform. One is the boundary processing. In wavelet transform theory, the signals are supposed to be infinite, but in application, image signals are generally finite, so the signals have to be extended before transforming. There have been many papers to deal with this problem, however, so far we didn't find some paper which presented an effective design of boundary filter for image coding。 In[2], boundary processing methods were tested and some results were shown., but the experiments were done only for a few special cases such as zero-padding, boundary replication and so on , it didn't discuss common design method. In[3], although a theoretical framework of designing boundary filter was developed in which all the possible boundary processing methods can be considered, it did not give a real design scheme. In this paper, a real design scheme is provided. The scheme is implemented by choosing an adequate boundary processing matrix from a set of 0-1 boundary processing matrices. Optimization is by genetic algorithm.

2. Subband Coding System with Wavelet Filter And Boundary Processing

Subband coder scheme with wavelet filters can be described by Fig.1. It consists of two parts: the

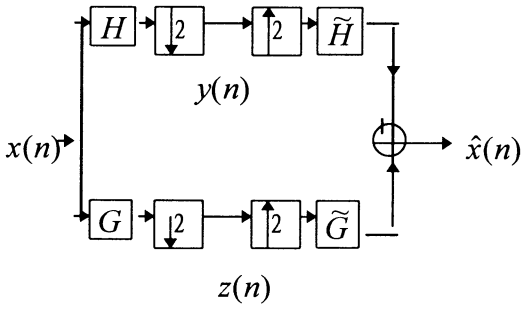


Fig1. Subband system for infinite-signal

analysis part and the synthesis part. The subband coder provides zero distortion

$$\hat{x}(n) = x(n).$$

In analysis part, the relationship of $x(n)$, $y(n)$ and $z(n)$ can be described as:

$$y(n) = \sum_k h_{2n-k} x(k)$$
$$z(n) = \sum_k g_{2n-k} x(k) \quad (1)$$

where (2)

$$\sum_k h_k = 1$$

In synthesis part, x(n)can be reconstructed by

$$x(l) = 2 \times (\sum_n \tilde{h}_{2n-l} y(n) + \sum_n \tilde{g}_{2n-l} z(n)) \quad (3)$$

where $\tilde{h}$, $\tilde{g}$ can be different from h, g.

The case of infinite signals is described in Fig1. If we want to consider the case of finite signal, we should extend the signal to infinite by using boundary processing mentioned in[2].

For convenience, we introduce some notations

here. We consider one-dimensional signal and biorthogonal wavelet. Let the support of the wavelet filter be [-M,M] (M≠0), the length of finite signal be N (N>>M). The low-pass filter in analysis part is

$$\{h_{-M}, h_{-M+1}, \cdots, h_{-1}, h_0, h_1, \cdots, h_M\}$$

and the high-pass filter is

$$\{g_{-M}, g_{-M+1}, , \cdots, g_{-1}, g_0, g_1, \cdots, g_M\}$$

Let the input signal in the analysis part be $x = \{x_0, x_1, x_2, x_3, \cdots, x_{N-1}\}$ [$N=2^p$, p is an integer] and the output signals be $y = \{y_0, y_1, \cdots, y_{\frac{N}{2}-1}\}^T$, $z = \{z_0, z_1, \cdots, z_{\frac{N}{2}-1}\}^T$.

If we use (1)(2) to calculate the output signals, we must extend x as $\hat{x}$ so that the operation can be carried on, because these equations involve undefined x_k that is, those values for $-M \le k < 0$ and for $N \le k < N+M$. Generally, linear extension is used. First, we divided x into three regions as $x^T = [x_l^T, x_c^T, x_r^T]$ and the extended signal is formed by $\hat{x}^T = [x_{e,l}^T, x^T, x_{e,r}^T]$. Then, the extended signal can be described as:

$$\hat{x}^T = [x_{e,r}^T, x_l^T, x_c^T, x_r^T, x_{e,r}^T]$$

where

$x_{el} = R_l\, x_l$

$x_{er} = R_r\, x_r$

The sizes of x_l, x_c, x_r are M, N-2M, M respectively. and R_R and R_L is MxM matrix. Let

$$H=\begin{pmatrix} h_M & h_{M-1} & h_{M-2} & \cdots & h_{-M+1} & h_{-M} & 0 & 0 & 0 & \cdots & 0 \\ 0 & 0 & h_M & \cdots & h_{-M+3} & h_{-M+2} & h_{-M+1} & h_{-M} & 0 & \cdots & 0 \\ \vdots & \vdots & \vdots & \vdots & \cdots & \vdots & \vdots & \vdots & \vdots & \cdots & \vdots \\ 0 & 0 & \cdots & h_M & h_{M-1} & h_{M-2} & \cdots & h_{-M+1} & h_{-M} & 0 & 0 \\ 0 & 0 & \cdots & 0 & 0 & h_M & \cdots & h_{-M+3} & h_{-M+2} & h_{-M+1} & h_{-M} \end{pmatrix}_{\frac{N}{2}\times(N+2M} \quad \text{.....(5)}$$

$$G=\begin{pmatrix} g_M & g_{M-1} & g_{M-2} & \cdots & g_{-M+1} & g_{-M} & 0 & 0 & 0 & \cdots & 0 \\ 0 & 0 & g_M & \cdots & g_{-M+3} & g_{-M+2} & g_{-M+1} & g_{-M} & 0 & \cdots & 0 \\ \vdots & \vdots & \vdots & \vdots & \cdots & \vdots & \vdots & \vdots & \vdots & \cdots & \vdots \\ 0 & 0 & \cdots & g_M & g_{M-1} & g_{M-2} & \cdots & g_{-M+1} & g_{-M} & 0 & 0 \\ 0 & 0 & \cdots & 0 & 0 & g_M & \cdots & g_{-M+3} & g_{-M+2} & g_{-M+1} & g_{-M} \end{pmatrix}_{\frac{N}{2}\times(N+2M} \quad \text{.....(6)}$$

$$R = \begin{pmatrix} R_L & 0 & 0 \\ I & 0 & 0 \\ 0 & I & 0 \\ 0 & 0 & I \\ 0 & 0 & R_R \end{pmatrix}, \qquad (7)$$

$$T = \begin{pmatrix} H\,R \\ G\,R \end{pmatrix} = \begin{pmatrix} \overline{H} \\ \overline{G} \end{pmatrix} \qquad (8)$$

$$Y = \begin{bmatrix} y \\ z \end{bmatrix}, \qquad (9)$$

Now subband analysis can be described as

$$Y = T\,X \qquad (10)$$

We call the matrix es R_R and R_L as a boundary processing matrixes.

3. Problem Formulation

From[2], we know that the choice of boundary processing matrix R is very important, because the performance of subband coding system dependes on them. In fact, the band-pass properties of $\overline{H}$ and $\overline{G}$ are affected by R. For example, the low-pass properties in $\overline{H}$ may become worse than that in H . This will lead the performance of image coding to be worse. Thus , a good boundary processing should posses the following properties:

Try to keep the low-pass properties of $\overline{H}$ and the high-pass properties of $\overline{G}$ as good as H and G.

Let $V_1, V_2, \ldots, V_M$ be the row vectors in matrix $\overline{H}$ which are different from the same rows in H . Let

$W_1, W_2, ..., W_M$ be the row vectors in matrix $\overline{G}$ which are different from the same rows in G . Then the property means trying to keep the following equation [4]:

$$\frac{\left|V_m^{'T} J\right|}{\left|V_m^{'T} I\right|} = \frac{\left|W_m^{,T} I\right|}{\left|W_m^{,T} J\right|} \qquad (11)$$

where

m=1,2,...,M

$I = (1,1,1,\ldots,1)^T$

$J = (1,-1,1,\ldots,-1)^T$

Then, our problem can be formulated as:

Try to find R_R and R_L such that

$$F = \sum_m \left| \frac{\left|V_m^{'T} J\right|}{\left|V_m^{'T} I\right|} - \frac{\left|W_m^{,T} I\right|}{\left|W_m^{,T} J\right|} \right| \qquad (12)$$

is minimized.

4. Optimization of boundary processing matrixes by using genetic algorithm

4.1 0-1 boundary processing matrix

We define a matrix as a 0-1 matrix if the elements in it are 0's or 1's. A boundary processing matrix is called 0-1 boundary processing matrix if it is 0-1 matrix. It is not difficult to see that 0-1 boundary processing matrix method includes symmetric extension, boundary value replication and some of other methods as its special case. From this fact we know that 0-1 boundary processing matrix method represents a more bigger class of boundary processing methods. Thus , it is not sure that the popular methods studied in [2] are optimal such that (12) is minimized. The problem is how to find the optimal 0-1 boundary processing matrix. which minimizes (12).

Obviously, it is impractical to test every 0-1 boundary processing matrix one by one as [2], because the number of 0-1 boundary processing matrices is very large. For example , if the size of a 0-1 matrix is 4X4, then the number is 2^{16}; if the size of a 0-1 matrix is 8X8, then the number is 2^{64}.

Besides, general optimization method such as gradient method is not suittable either here, because the value of 0-1 matrix is discrete, it is difficult to find a suitable transition rule to move from a point in the decision space to next one. One way to solve this problem is to adopt genetic algorithm. In genetic algorithm, the point in decision space is generally coded a string, the elements of which are 0's or 1's, in the case of 2 dimensions this is a 0-1 matrix.

4.2. Optimization by GA

Our genetic algorithm can be described as follows:(for simplicity, we only consider Left border)

Step 1. Generate an initial population of M indivitual randomly. A 0-1 boundary processing matrix is a indivitual.

Step 2. Calculating Fitness Value

From(8), we obtain matrices $\overline{H}, \overline{G}$. Since we have M sets of 0-1 boundary processing matrices, using (12), we have M values of the fitness which is defined as:

$$F_i = F(R_L^i) = \frac{1}{\sum_m \left| \frac{\left|V_m^{'T} J\right|}{\left|V_m^{'T} I\right|} - \frac{\left|W_m^{,T} I\right|}{\left|W_m^{,T} J\right|} \right|} \qquad (13)$$

$(i = 1,2,\ldots,M)$

Step3. Genetic operations

Reproduction, crossover and mutation operators are used in this paper to generate new population. The probability of mutation is 0.08. The crossover operation in this paper showed in Fig2. The mutation operation showed in Fig3 .

Step4. step1-step3 are repeated from generation to generation such that the fitness value of the population increases until the termination criterion is satisfied.

5. Results of Simulations

Our simulation was carried out on biorthogonal wavelet. The biorthogonal wavelet filter is nine-seven taps, the impulse response coefficients for the analysis filters are shown in Table.1. The parameters of the GA are given as follows:

(1)population size is 100;

(2) crossover probability Pc=0.7;

(3) Mutation probability Pm=0.08;

The algorithm Stops when the following condition are satisfied:

$$F=\sum_{m}\left|\frac{\left|V_m^{'T}J\right|}{\left|V_m^{'T}I\right|}-\frac{\left|W_m^{'T}I\right|}{\left|W_m^{'T}J\right|}\right|<\varepsilon$$

or the iteration times t satisfies t>N

where ε is small real number and N is a fixed integer. In this paper ε =0.0001 and N=100. The results of optimization are shown in Fig.4

Table 1. Analysis biorthogonal wavelet filters

Filter(H)	h_0	$h_{\pm1}$	$h_{\pm2}$
	0.8526987	0.377403	-0.110624
	$h_{\pm3}$	$h_{\pm4}$	
	-0.0238495	0.037828	
Filter(G)	g_{-1}	$g_{-2,0}$	$g_{-3,1}$
	0.788485616	-0.41809227	-0.040689
	$g_{-4,2}$		
	0.0645389		

Reference

[1]Jinshan Tang, Yongguang Zhang, "*Wavelet transform for finite signals processinga and image coding* International conference on CAD/Graphics, Shen Zhen,China,1997.

[2] G.Karlsson and M.Vetterli, "*Extension of finite length signals for subband coding* ,signal processing , vol.17, pp. 161-168, 1989.

[3]Veyis Nuri and Roberto H.Bamberge, "*Sized-limited filter banks for subband image compression*", IEEE Trans. on image processing , vol. 4, No. 9, Sept. 1995.

[4] Jia Pei-Zhang, "The vector-space algorithm of orthonormal wavelet transform" ,J.Sys. Sci.& Math.Scis.

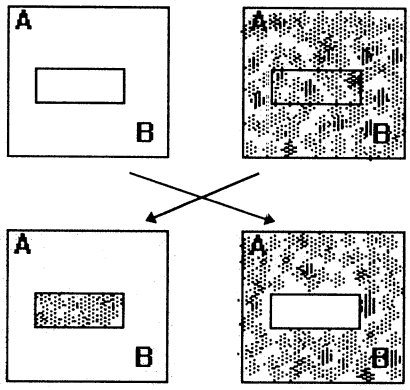


Fig. 2. Crossover operations

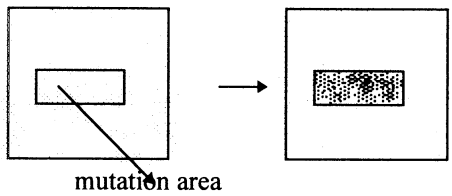


Fig. 3. Mutation operation

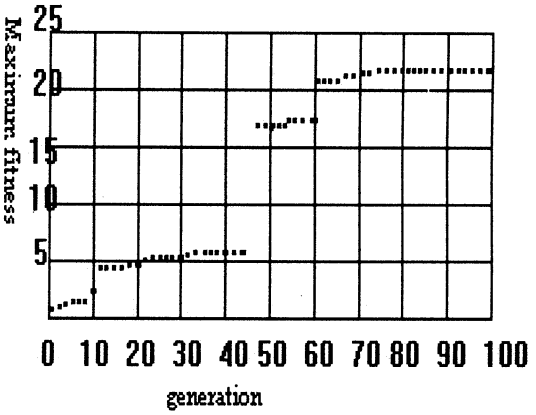


Fig.4 Maximum fitness for each generation

Proc. of Third Int. Symp. on Artificial Life, and Robotics (AROB III' 98),
Oita, Japan, 19-21, January, 1998,

Structure Optimization and Learning of Neural Networks by Co-Evolution

Dong-Wook Lee, Sang-Hwan Lee, Kwee-Bo Sim

Robotics and Intelligent Information System Lab.
Dept. of Control and Instrumentation Eng., Chung-Ang University
211, Huksuk-Dong, Dongjak-Ku, Seoul 156-756, Korea
Tel : +82-2-820-5319, Fax : +82-2-817-0553, http://rics.cie.cau.ac.kr/
E-mail : dwlee@cau.ac.kr, kbsim@cau.ac.kr

Abstract

Usually, Evolutionary Algorithms are considered more efficient for optimal system design. However, the performance of the system is determined by fitness function and system environment. In this paper, in order to overcome the limitation of the performance by this factor, we propose a coevolutionary method that two populations constantly interact and coevolve.

In this paper, we apply coevolution to neural networks' evolving. So, one population is composed of the structure of neural networks and other population is composed of training examples. The structure of neural networks evolve to optimal structure and, at the same time, training examples coevolve to feature pattern. This method prevent the system from the limitation of the performance by random design of neural network structure and inadequate selection of training examples. In this time neural networks are trained by evolution strategies that can be applied to the unsupervised learning. And in the coding of neural networks, we propose the method to maintain nonredundancy and character preservingness that are essential factor of genetic coding.

We show the validity and the effectiveness of the proposed scheme by applying it to the visual servoing of RV-M2 robot manipulators.

1. Introduction

Evolution by natural selection is a central idea in biology, and the concept of natural selection has influenced our view of biological systems tremendously. Evolutionary Algorithms(EAs) are computational models of evolution that play a important role in many artificial life models. Usually, EAs are considered more efficient for optimal system design because EAs can provides higher opportunity for obtaining the global optimal solution. But the performance of the system is determined by the fitness function. In this paper we propose a coevolutionry method that two populations constantly interact and coevolve. In this case, the fitness of the system changes according to other population's evolving. This coevolutionary method is more similar to biological evolution in nature than other evolutionary algorithms.

In this paper, one population is composed of the structure of neural networks and other population is training examples. Most conventional neural learning algorithms assume training examples to be provided by external teacher. However, in order to improve the generalization performance in dynamic environments, it is important to select or generate training examples. In this coevolutionary method, useful examples are generated by genetic search process. And also the structure of neural networks coevolve with training examples.

In general, it is important to decide the number of neurons and weights of hidden layer. Too many neurons or weights cause delay of response time and learning time, and increase free degree of network that occurs learning noise. On the contrary, too small number of neurons and weights cause insufficient memory of network and reduction of the probability of convergency to optimal solution. In order to find optimal network structure, structure of neural networks need to be evolved. In coding of chromosome, nonredundancy and character preservingness is necessary condition to evolve. So, in order to maintain nonredundancy and character preservingness, we propose new coding method of neural networks. To realize character preservingness, a neuron and its weights become one gene, so crossover point is not taken in weight level but neuron level. And to achieve nonredundancy of network coding, all neuron are rearranged according to the value of weights which connected a neuron. And for learning of weights of neuron, Evolution Strategies(ESs), which is useful method of real value optimization, are used. By using ESs, unsupervised learning is realized.

We will show the validity and the effectiveness of the proposed scheme by applying it to the visual serving of RV-M2 robot manipulators.

2. Mechanism of Co-Evolution

2.1 Concept of Co-Evolution

The evolutionary process in nature is often described as if one population of individuals is trying to adapt to a fixed environment. This description is however, only a first-order approximation to the actual situation[2]. In actual state, the evolution is a result of mutual effect between multiple populations or environments. So, all living things in nature coevolve with other individuals by interaction.

Genetic algorithms are computational algorithm that is modeled based on nature's evolution phenomena. Most cases of application of this algorithm, it was used optimization problem in given fixed environment. However, GAs requires a fitness function which accurately reflect the usefulness of any proposed solution and can reduce its relative merits a single numerical value. In this point of view, coevolutionary method is expected to the solution of this defect. In coevolutionary method, fitness is affected by other population's evolving. so two or more populations interact through their fitness.

The method of coevolution is classified into competitive coevolution[1~3] that is predator-prey relation and cooperative coevolution[4].

2.2 Process of Co-Evolution

In general, the coevolution is depicted that multiple populations interact and evolve each other, but in our case two populations are considered. However for multiple populations, the proposed algorithm can be used by some extension.

Proposed coevolutionary algorithm that used in this paper, is as follows.

Step 1 : Let the evolving two populations are primary population and secondary population for convenience's sake. And the object of the evolution becomes primary population and the exterior factor, for example an environment, becomes secondary population.

Step 2 : Fitness evaluation

The fitness of primary population and secondary population are as follows.

$$f(P_i)=\frac{\sum_{j\in A} f(P_i,S_j)}{L} \tag{1}$$

$$f(S_j)=\frac{\sum_{i\in B} f(P_i,S_j)}{K_j} \tag{2}$$

And the notations of variables that used, are as follows.

N : number of primary population
P_i : i-th individual of primary population, where $i=0\cdots N$
M : number of secondary population
S_j : j-th individual of secondary population, where $j=0\cdots M$
L : evaluation times of P_i
$f(H_i)$: fitness of P_i
$f(P_j)$: fitness of S_j
$f(H_i,P_j)$: mutual fitness of primary individual i and secondary individual j
A : index set of secondary individuals that are selected by primary individual i
B : index set of primary individuals that select secondary individual j
K_j : selected times of secondary individual j

That is to say, the fitness of the primary individual is calculated by average of mutual fitness for L secondary individuals, and the fitness of secondary individual is calculated by average of mutual fitness for K_j primary individuals that select it.

Step 3 : For each population, we take process of selection, crossover, mutation and reproduce next generation's population.

Step 4 : Step 2 and step 3 are repeated, until sufficient result is obtained or limited generation is passed.

3. Evolution of Neural Networks

3.1 Encoding Method of Neural Networks

We adopt a dynamic neuron for neuron model, because dynamic neuron is more similar to biological neuron. The characteristic of dynamic neuron[5] is represented by equation (3) and (4).

$$\tau\frac{dx_i}{dt}=-x_i+g\left(\sum_{j=0}^{N-1} w_{ij}y_j\right)+r_i \tag{3}$$

$$y_i=f(x_i) \tag{4}$$

where $g(\cdot)$, $f(\cdot)$ is sigmoid function.

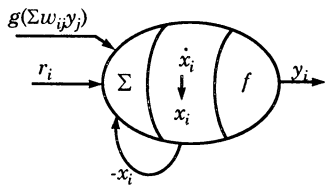


Fig. 1 Dynamic Neuron

In general, the number of hidden layer of multi-layer neural networks is one or two, because too many neuron or layer cause delay of response time and learning time, and increase free degree of network that occurs learning noise. So. in our problem, we use one hidden layer.

In order to find optimal structure of neural networks, we use GAs. In cording of chromosome, to realize character preservingness, a neuron and its weights are one gene, so crossover point is not taken in a weight level but a neuron level. And to achieve nonredundancy of network coding, all neuron are rearranged according to the summation of weight values which connected a neuron. If the number of input neuron is N_i and output is N_o, then one gene is compose of N_i+N_o bits. And if number of hidden neuron is N_h, then the necessary number of bits is $(N_i+N_o)\times N_h$.

3.2 Learning of Neural Networks

For the purpose of learning neural networks' weight, We use evolution strategies(ESs) that is one of the evolutionary algorithms for searching optimal real values[6]. If exact teaching signal is not calculated, the networks can be learned by ESs. This method is one of the unsupervised learning. So, in our cases, it is needed to calculate only the fitness of the system.

The individual of ESs is composed of real vector, namely $(\vec{x}, \vec{\sigma})$. where $\vec{x}$ is the position vector of state space and $\vec{\sigma}$ is the vector of standard deviation. The individual of next generation is depicted as equation (5) that represents mutation process. where $N(\vec{0}, \vec{\sigma})$ is random number that average is $\vec{0}$ and standard deviation is $\vec{\sigma}$.

$$\vec{x}^{t+1} = \vec{x}^{t} + N(\vec{0}, \vec{\sigma}) \tag{5}$$

In order to maximize the performance of the learning, we use following three strategies.

1. 1/5 success rule : if successive mutation rate is more than 1/5, search would continue large steps, if not, the step would be shorter.

$$\vec{\sigma}^{t+1} = \begin{cases} c_d \times \vec{\sigma}^{t} & \text{if } \varphi(k) < 0.1 \\ c_i \times \vec{\sigma}^{t} & \text{if } \varphi(k) > 0.3 \\ \vec{\sigma}^{t} & \text{if } 0.1 \le \varphi(k) \le 0.3 \end{cases} \tag{6}$$

where $c_d = 0.82$, $c_i = 1.22 = 1/0.82$

2. Change the probability of mutation :

$$p_m = \begin{cases} -0.5f + 0.5 & \text{if } f < 0.9 \\ 0.05 & \text{if } f \ge 0.9 \end{cases} \tag{7}$$

If the fitness is low, in order to improve the exploration ability, the probability of mutation sets large value, and if the fitness is high, in order to improve the exploitation ability, probability of mutation sets small value.

3. According to the length of chromosome, maximum generation is limited like below.

$$g_{max} = l + 10 \tag{8}$$

where g_{max} is maximum generation, l is length of chromosome.

3.3 Encoding Method of Training Examples

In order to evolve the training examples, training examples is encoded to bit string that is chromosome of GAs.

4. Simulation Result and Discussion

4.1 Problem

In order to verify the effectiveness of the proposed scheme, we applied the visual servoing of RV-M2 robot manipulator.

The object is $50\times50\times30$㎜ cube and has four feature point in camera image. It assumes that the ideal image is already known. And the objective of the system is to conform the actual image to the ideal image by moving robot manipulators. If the actual image corresponding to the ideal image, a robot catch it using griper.

Table 1 shows the joint angle range and the maximum velocity of RV-M2 robot manipulators.

Table 1. Joint angle range(°) and maximum velocity(°/sec) of RV-M2 robot manipulator

Joint	θ_1	θ_2	θ_3	θ_4	θ_5
angle	-150~150	-30~100	-120~0	-200~20	-180~180
velocity	140	79	140	163	223

The eight inputs of neural network controller are deviation of four feature point between ideal image and object image. And the outputs are variation of RV-M2's 5 joint angles. Training example is put the 300×400㎜ plane and height is 80㎜. It is the condition that robot manipulators moving maximally. So, working area is (165,-200,80) to (465,200,80).

It is very important to determine the number of training examples and what is training examples. In most cases, training examples are given by system designer. In this system, training examples evolve to feature pattern, so neural network trained well by these evolving pattern.

4.2 Structure Search and Learning of Neural Networks by Co-evolution

1. Evolution of neural networks

Minimum number of neuron is 14(8 input, 1 hidden, and 5 output neuron) and maximum number of neuron is 24. therefore, hidden layer has minimum 1 to maximum 10 neurons.

The number of primary population, the network structure, is 20. Probability of crossover and probability of mutation is 0.8 and 0.02 respectively. And we use elitist preserving rule.

2. Evolution of training examples

Training example has coordinate of center point of cube and rotate angle. the range of x coordinate is 300㎜, y is 400㎜, and the range of rotate angle is -45° to 45°. And each value is encoded as 5, 5, 6bits respectively. Where precision of each value is 9.375㎜, 12.5㎜, 1.4°.

The number of secondary population, the training examples, is 20. And reproduction is steady-state method that is some lower rank individuals replace new ones.

3. Fitness evaluation

The fitness of individual of primary and secondary population is calculated by equation (1) and (2). where number of training example(L) is 5.

The mutual fitness between structure and example is defined as equation (9). So, regardless of initial position, all examples are evaluated same weight.

$$f(P_i, S_j) = \begin{cases} 0.01 & \text{if } f(P_i, S_j) \le 0.01 \\ 1 - \dfrac{e_{i,total}}{e_{i,init}} & else \end{cases} \quad (9)$$

where $e_{i,init} = T \times \sum_{t=0}^{N-1} d_i(0)$, $e_{j,total} = \sum_{t=0}^{T-1} \sum_{i=0}^{N-1} d_i(t)$, and $d_i(t)$ is distance of i-th feature point between ideal and actual images at time t, T is total time.

4.3 Simulation Result

As a result coevolving network structure and training example for 30 generation, we obtain quasi optimal structure(node : 6; weight : 33) and feature examples. Fig. 2~4 show the some simulation results of neural networks and training examples.

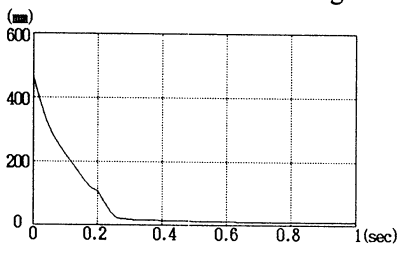
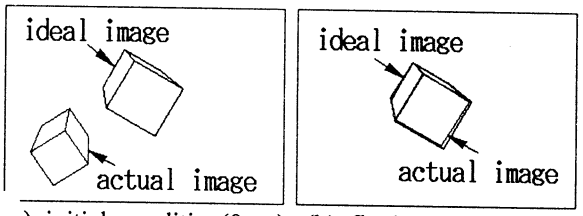
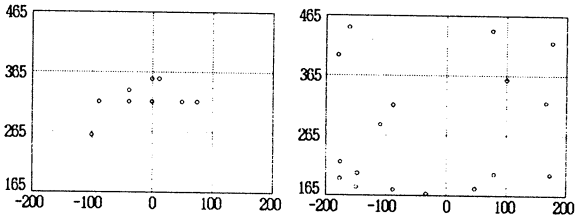


Fig. 2 Error curve of a training example($\sum_{i=0}^{3} d_i$)



(a) initial condition(0sec) (b) final condition(1sec)

Fig. 3 The tracking result of robot manipulators



(a) 15 generation (b) 30 generation

Fig. 4 The distribution of evolved training examples

5. Conclusions

In general, the structure of neural network and training examples(or environment) are given by system designer. So the performance of the system is limited by this one. In this paper, in order to overcome the limitation, we propose the coevolutionary method that optimal structures and feature training examples are coevolving. And we proposed the encoding method to realize nonredundancy and character preservingness. The effectiveness of the proposed method was verified by computer simulations.

Acknowledgements

This paper is supported by Institute of Information Technology Assessment(No. 97-G-0214), Korea.

References

[1] W. Daniel Hillis, "Co-Evolving Parasites Improve Simulated Evolution as an Optimization Procedure," *Artificial Life II*, Addison-Wesley, 1991.

[2] John R. Koza, "Genetic Evolution and Co-Evolution of Computer Programs," *Artificial Life II*, Addison-Wesley, 1991.

[3] Jan Paredis, "Coevolutionary Computation," *Artificial Life*, vol. 2, no. 4, pp. 355-375, 1995.

[4] H. Handa, T. Horiuchi et.al., "Genetic algorithms Including a Mechanism of Co-evolution," *Proceeding of system/information joint symposium*(SICE), pp. 7-10, 1996.(Japanese)

[5] C-T Lin and C.S. George Lee, *Neural Fuzzy Systems*, Prentice Hall, 1996.

[6] T. Bäck, H.P. Schwefel, "An Overview of Evolutionary Algorithms for Parameter Optimization," *Evolutionary Computation*, vol.1, no.1, pp.1-23, 1993.

[7] M. Mitchell, S. Forrest, "Genetic Algorithms and Artificial Life," *Artificial Life*, vol. 1, no. 3, pp. 267-289, 1994.

Proc. of Third Int. Symp. on Artificial Life, and Robotics (AROB III' 98),
Oita, Japan, 19-21, January, 1998,

Discovery of Intelligence
-Beyond Discrimination between Artificial and Natural-

Tohru Moriyama

Graduate School of Science and Technology,
Kobe University, Nada, Kobe, 657, Japan

Abstract

Intelligence is not a property of an object but a name declared in a situation in which capacity of solving a problem and the very problem can not be divided. In such situation, one can see aspect that the object discover problem and solve it by itself. I demonstrate such aspect by an experiment of pill bug (*Armadillidium vulgare*) in this paper and suggest that the notion will help to find intelligence in machines.

Key words: intelligence, problem solving,
uncontrollability

1. Introduction

In order to find out intelligence in an object (animals, robots,...etc.), we usually constitute problem solving situation and observe how the object perform. But the object which solves one especial problem can not be regarded as intelligent one. We recognize intelligence when the object solve a lot of problem efficiently. In machinery-thinking, the object must have a lot of programs to solve various problems, and capacity (i.e. the programs) and environment (i.e. the problems) are independent each other. If one divide the capacity and the problem in this way, intelligence is regarded as the amount of programs and development of intelligence is regarded as increasing of memory size to stack the programs. In this viewpoint, one considers all objects as machines even if they are animals. But the object can have finite number of programs at most, the object can not solve unknown problem and we can not see universality which is the main concept of intelligence.

To avoid being attracted to machinery-thinking and missing universality of problem solving, we must admit the idea that capacity of problem solving and the problem can not be divided. This idea which is contrary to machinery-thinking require us to understand uncontrollability of the object. If one accepts the idea, we will see aspect that as if the object find problem by itself and solve it autonomously. In another word, uncontrollable object performs as if it has universal program to solve problems.

In this paper, I demonstrate the aspect by a biological experiment of pill bug (*Armadillidium vulgare*). The experiment can also be model to consider intelligence in technology and robotics.

2. Experiment of pill bug

(*Armadillidium vulgare*)

2.1 Experiment 1

It is known that in continuous two-arm maze, *Armadillidium vulgare* select the arm alternately, i.e. ...left-right-left-right... . But the mechanism has not been investigated in detail. I invented continuous two-arm maze by pairing two turn tables each of which mounts a two-arm maze (Fig.1). Eighteen individuals were tested.

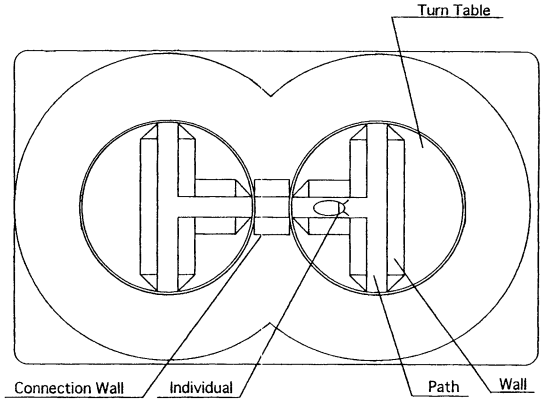


Fig.1 Apparatus

Each individual was made experienced 201 selections of arms and all of them exactly selected arms alternately, and I found mechanism of the alternate selection of arms as shown in Fig.2. At the first turn, an antenna of out-corner touches the wall at first (1) and the antenna memorize the wall. I call this antenna 'leading antenna' in this paper. The animal locomotes the arm with the leading antenna touching on the wall (2), and at the

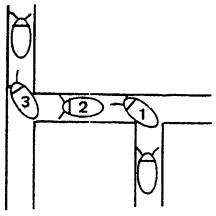


Fig.2 Mechanism of alternate selection of arms.

next intersection the antenna is released and the animal turns to the direction of the released leading antenna (3). This process continues. In this way, selection of arm is determined by this elemental rule. There are eight elemental rules as shown in Fig.3. The rule 1 and 2 appeared continuously in the experiment in twelve individuals (rule obeyed ones) and I concluded that in the process of evolution *A. vulgare* acquired the mechanism of memorizing the object which touches at first. But in six individuals, a lot of the other rules (3, 4,...,8) appeared (rule unobeyed ones) in spite they basically obeyed rule 1 and 2. Then

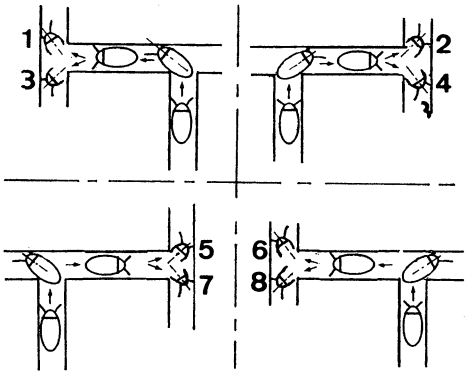


Fig.3 Elemental rules for turning intersection.

time sequential change of adopted rules was investigated and typical results are shown in Fig.4 (a) and (b). Fig.4(a) shows typical change of emergent rate of rule 1 and 2 of an individual of rule obeyed ones. The average rate is 0.76 (max=1.0) and σ^2=0.154, so the two rules are stable and only a little statistical noise (i.e. the other rules) is observed. Fig.4(b) shows typical result of an individual of rule unobeyed ones. The average rate is 0.62 and σ^2=0.376, so the two rules are unstable. But in this animal, we can find aspect of learning because the rate gradually increases from session 1 to 8 significantly (Spearman; rs=0.72619 α<0.05). So the animal seems to try to memorize the wall

which touches at first. But after the learning, it comes to adopt the other rules again in spite condition of the experiment does not change. In this way, while rule obeyed ones are regarded as well controlled good machines, rule unobeyed ones are regarded as bad controlled ones because we can assume that they have learning program to adopt rule 1 and 2, whereas we can also assume that they have contradictory program to break the learning program. Now I call rule obeyed ones controllable type and rule unobeyed ones uncontrollable type.

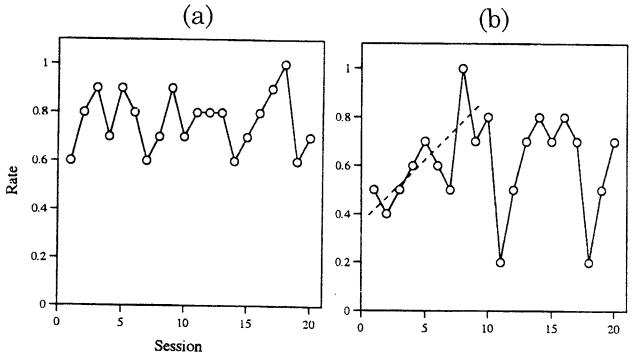


Fig.4(a) Change of sum of emergent rate of rule 1 and 2 of controllable type. After the experiment, we got sequence constituted by 200 elemental rules for each individual. The sequence was divided into 20 sessions each of which consists of 10 elemental rules. Number of rule 1 and 2 in each session were counted and sum of them were divided by 10. Vertical line: emergent rate. Horizontal line: sessions.

Fig.4(b) Change of sum of emergent rate of rule 1 and 2 of uncontrollable type. Dashed line is a regression line.

2.2 Experiment 2

Next the same individuals were examined in another apparatus as shown in Fig.5. The structure of the apparatus is as same as that of Fig.1 but the walls are covered with teflon sheet except for connection wall. They can not climb the covered walls. Each individual was examined for 50 trials and from the 51st trial, it was led to blind alleys after turning the intersections. When they led to a blind alley, they locomoted backward, turned, and then locomoted forward and were led to another intersection, and after they turned they were led to blind alley again. In this way, they locomoted in closed space. The walls of blind alleys are also covered with teflon sheet. The result is that while individuals of controllable type continued locomoting in the apparatus, those of uncontrollable type climbed the connection wall after several trials and escaped from the apparatus. In the previous experiment, all walls of the apparatus (Fig.1) were made of wood but a few animals climb the wall, and I previously investigated that they climbed the wall of corner point but seldom did at plane wall. This aspect seems that as if individuals of uncontrollable type recognized that they were confined in the apparatus and then escaped from it. If the experiment continued for hours, the controllable individuals would die of water deficit whereas the

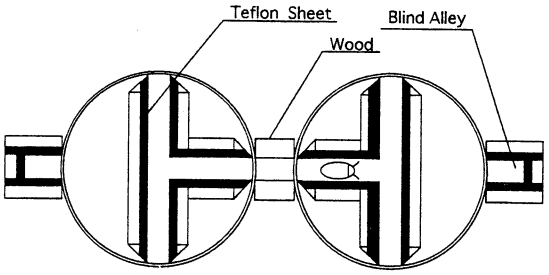


Fig.5 Apparatus with teflon walls and blind alleys.

uncontrollable ones had opportunity to seek moist place in the outside of the apparatus.

3. Conclusion

In the above experiment, we can see the aspect that uncontrollability constitute problem and solve it autonomously. In experiment 2, the individuals which locomote forward by using leading antenna suddenly came across blind alley. The situation means that they locomoted by obeying program which conduct to memorize the wall that had touched at first and kept touching on it, but suddenly the program is inhibited by the blind alley. Then they locomoted backward, turned and locomoted forward again. Of course that is the solution to escape from the blind alley but the behaviour is programmed mechanistic one. This situation seems that the problem exists outside of the object (environment), and capacity of solving the problem exists in the object as program, i.e. the problem and the capacity are divided. But individuals of uncontrollable type refereed to the environment, i.e. confining state, and recognized it as problem and escaped from the environment as solution. In this situation, constitution of problem is capacity by itself and so we can not divide the problem and capacity of solving at all, but can find intelligent aspect.

Generally when one try to find capacity of problem solving in animals, one set problem and observes its performance and if the animals reach the solution which is as same as observer's, he thinks he finds intelligent capacity in it. But such capacity is the same as program. On the contrary, if we recognize the capacity as ability to constitute problem, and the problem and the capacity can not be divided, we must accept that the object is uncontrollable, but can find intelligence which implies universality. Recently alike experiment using octopus which have higher nervous system also was reported[1]. More theoretical notion about unprogrammability constituting autonomy was reported by Gunji[2].

In this paper, through experiment of animal, I illustrated the aspect that intelligence is discovered, but the experiment is not only models for animals but also for machines because if one considers that behaviour of animals is determined by genetic programs, they become the very machines. As long as we assume programs in animals and machines, we are destined to meet frame problem.

If we require intelligence to machines, we will have to consider how to use uncontrollable but not broken machines.

Acknowledgment

I am grateful to Professor K. Ito and Dr. Y. P. Gunji for helpful suggestion and much advice.

References

1. Moriyama, T. and Gunji, Y.P.(1997) Autonomous learning in maze solution by *Octopus*. Ethology 103: 499-513

2. Gunji, Y.P.(1993) Forms of life: unprogrammability constitutes the outside of a system and its autonomy. Appl. Math. Comp. 57: 19-76

Proc. of Third Int. Symp. on Artificial Life, and Robotics (AROB III' 98),
Oita, Japan, 19-21, January, 1998,

Variation of Activation Functions for Accelerating the Back-Propagation Algorithm

Byungdo Lee and Minho Lee
Department of Electrical Engineering
Korea Maritime University
1 Dongsam-Dong, Yeongdo-ku, Pusan 606-791, Korea
Email : mhlee@hanara.kmaritime.ac.kr Tel : +82-51-410-4413

Abstract

In this paper, a new learning method is proposed for enhancing the learning speed of the error back propagation learning algorithm. In order to cope with the premature saturation phenomenon at the initial learning stage, a variation scheme of activation functions is introduced by using higher order functions, which does not need much increase of computation load. It naturally changes the learning rate of interconnection weights to a large value as the derivatives of sigmoid function abnormally decrease to a small value during the learning epoch. Also, we suggest the hybrid learning method incorporated the proposed method with the Delta-bar-Delta training algorithm. Computer simulation results show that the proposed learning algorithm outperforms the conventional methods such as momentum and Delta-bar-Delta algorithms.

Keywords : Higher order activation functions, local minima, hybrid learning algorithm, premature incorrect saturation

1. Introduction

The multilayer neural network models have been successfully used in many engineering problems including computer vision, signal and image processing, speech and character recognition, and control of a nonlinear system.[1-3] Although various architectures and learning algorithms have been introduced, the error back-propagation learning algorithm has been still popularly used in many real applications. This algorithm provides a revival chance of "Perceptron" model, but it is a first order approximation of the steepest descent technique in the sense that it depends on the gradient of the instantaneous error surface in weight space, and thus the rate of learning convergence tends to be relatively slow.[3]

There have been some researches on improving the convergence speed of the back-propagation algorithm. The Conjugate gradients and Quasi-Newton algorithms use the second order gradient,[4-6] but these are much more computationally expensive, and these are impractical methods especially when the scale of the problem is large. Other approximation methods to reduce the computational load have been introduced, but the applicability of these methods depends on how well the diagonal Hessian approximation models the true Hessian.[5] Another attempt to enhance the learning speed is so called "Quickprop".[7] It uses the difference between two successive gradient of error function as a measure of the change of curvature, and this information is used to change the step size. Since the Quickprop algorithm had reported to considerably reduce the training time, several training algorithms to adaptively change the step size have been introduced. The delta-bar-delta learning method and the differential step size back-propagation(DSBP) algorithm are the examples of those.[8-10] It is well known that the variation of learning rate is necessary to increase the learning speed on flat learning curve.

In this paper, we propose a new learning method to cope with the incorrect premature saturation problem without loss of computation time. When the interconnection weights abnormally grow to a large value, an activation function output is automatically replaced by the output of higher order activation function. It naturally produces the larger learning rate value by derivation of learning algorithm based on steepest descent method. Also, a hybrid learning method is introduced by incorporating the conventional Delta-bar-Delta learning method with higher order activation function scheme. The following section describes the representative conventional methods to speed up learning process, and the proposed learning algorithms are followed. In section 4, 4 bit parity check is used as bench mark problem, and the learning speeds of the proposed method and conventional ones are compared by computer simulation.

2. Learning trajectories of conventional methods

In this section we describe procedures for increasing the rate of convergence while maintaining the locality constraint that is an inherent characteristic of back propagation learning.[11-14]

2.1 Momentum algorithm

One way to speed up the off-line training in general back propagation is to use the so-called momentum algorithm.[6] The value of weight variation in the momentum algorithm at a k learning stage can be written as follows,

$$\Delta \mathbf{v}^{k} = \alpha\, \delta_z\, \mathbf{x}^{k} + \beta\, \Delta \mathbf{v}^{k-1} \qquad (1)$$
$$\Delta \mathbf{w}^{k} = \alpha\, \delta_y\, \mathbf{z}^{k} + \beta\, \Delta \mathbf{w}^{k-1}$$

where α , β are the momentum constants and v and w are the interconnection weights of first and second layer, respectively. Also, δ_z, δ_y are the error signals of hidden layer and output neuron, respectively. Consequently, the updated weights using the momentum rule at a $k+1$ learning stage are as follows,

$$\mathbf{v}^{k+1} = \mathbf{v}^{k} + \alpha\, \delta_z\, \mathbf{x}^{k} + \beta\, \Delta \mathbf{v}^{k-1} \qquad (2)$$
$$\mathbf{w}^{k+1} = \mathbf{w}^{k} + \alpha\, \delta_y\, \mathbf{z}^{k} + \beta\, \Delta \mathbf{w}^{k-1}$$

2.2 Delta-bar-Delta($\Delta - \overline{\Delta}$) algorithm

Other way to speed up the off-line training in general back propagation is the Delta-bar-Delta algorithm.[3] The value of weight variations in the output layer and hidden layer can be written as follows,

$$\Delta_{\mathbf{w}}^{k} \equiv -\delta_y\, \mathbf{z}^{k} \qquad (3)$$
$$\overline{\Delta}_{\mathbf{w}}^{k} \equiv (1-\beta)\Delta_{\mathbf{w}}^{k} + \beta\, \overline{\Delta}_{\mathbf{w}}^{k-1}$$
$$\Delta_{\mathbf{v}}^{k} \equiv -\delta_z\, \mathbf{x}^{k} \qquad (4)$$
$$\overline{\Delta}_{\mathbf{v}}^{k} \equiv (1-\beta)\Delta_{\mathbf{v}}^{k} + \beta\, \overline{\Delta}_{\mathbf{v}}^{k-1}$$

and the new learning rate at a $k+1$ stage are given as following equations.

$$\alpha^{k+1} = \begin{cases} \alpha^{k} + \nu & ; \overline{\Delta}^{k-1} \cdot \Delta > 0 \\ (1-\gamma)\alpha^{k} & ; \overline{\Delta}^{k-1} \cdot \Delta < 0 \\ \alpha^{k} & ; \overline{\Delta}^{k-1} \cdot \Delta = 0 \end{cases} \qquad (5)$$

where ν, γ are arbitrary positive constants. The updated weights using the Delta-bar-Delta rule at a $k+1$ learning stage become

$$\mathbf{w}^{k+1} = \mathbf{w}^{k} + \Delta \mathbf{w}^{k} = \mathbf{w}^{k} + \alpha^{k+1}\, \delta_y\, \mathbf{z}^{k} \qquad (6)$$
$$\mathbf{v}^{k+1} = \mathbf{v}^{k} + \Delta \mathbf{v}^{k} = \mathbf{v}^{k} + \alpha^{k+1}\, \delta_z\, \mathbf{x}^{k}$$

3. Variations of activation functions with higher order

In this section, we propose a new adaptation method of learning rate that is effective to enhance the learning speed without increase of the computation load. The slow convergence in error back-propagation is mainly due to the premature saturation. That is, if the net value of a neuron, $net_j = \mathbf{x}_i\, \mathbf{w}_{ji}^{T}$, abnormally grows a large value of sigmoid function $f'(net_j)$ is small. where $\mathbf{x}_i$ and $\mathbf{w}_{ji}$ denote an input or an output of the previous layer and the interconnection weight, respectively. Thus, the chaining rate of interconnection weight tends to decrease. To overcome the incorrect saturation, the DSBP algorithm omitted the $f'(\cdot)$ in the back propagation learning algorithm, and others used a constant value instead of the value $f'(\cdot)$ during the back propagation learning process when the $f'(\cdot)$ is smaller than a threshold value. However, these methods seem to be unnatural, and also the oscillation phenomena always occurs in final stage of learning.

We suggest a new learning method to cope with the incorrect saturation problem. If the differential value of a activation function is smaller than a threshold value while the output error does not decrease to a desired accuracy, we use the higher order activation function value such as $f^{3}(\cdot)$ instead of the conventional sigmoid function $f(\cdot)$ as the output of the neuron.

The learning procedure of proposed neural network is as follow. Let's define the error function as Eq. (7)

$$E = \frac{1}{2} \sum_{k=1}^{m} (d_k - y_k)^2 \qquad (7)$$

where k is a input pattern and m is the number of desired input pattern. The d_k and y_k are the desired output and the output of neural network, respectively. The weighted sum of neuron and the output $\mathbf{z}_j$ are

$$net_j = \mathbf{x}_i\, \mathbf{w}_{ji}^{T}, \quad \mathbf{z}_j = [f(\mathrm{net}_j)] \qquad (8)$$

where $\mathbf{x}_i$ is the i-th input neuron vector, $\mathbf{w}_{ji}$ is a weight between the i-th input neuron and the j-th hidden neuron. T represent transpose matrix and f is the sigmoid function. If the error E is larger than a desired value and the $\frac{\partial E}{\partial \mathbf{w}_{ji}}$ is smaller than a threshold value, the neuron output changes to the following equation.

$$net_j = \mathbf{x}_i \mathbf{w}_{ji}^T \quad \mathbf{z}_j = [f(net_j)]^3 \tag{9}$$

The training algorithm using the above activation function is as follows. The error signal propagated to the weight which connects between the $\mathbf{z}_j$ in Eq. (9) and the output of the previous layer is

$$\begin{aligned} \delta_z &= -\frac{\partial E}{\partial \mathbf{z}_j}[\mathbf{z}_j]' \\ &= -3[f(net_j)]^2 \frac{\partial E}{\partial \mathbf{z}_j} f'(net_j) \end{aligned} \tag{10}$$

The updated weight using the backpropagated error in Eq. (10) is

$$\begin{aligned} \mathbf{w}_{ji}^{k+1} &= \mathbf{w}_{ji}^k + \Delta \mathbf{w}_{ji}^k \\ &= \mathbf{w}_{ji}^k + \alpha \delta_z \mathbf{x}_{ki}^k \end{aligned} \tag{11}$$

As show in Eq. (10), when the premature saturation occurs during the back-propagation learning, the learning rate naturally changes form a constant value α to $3f(net_j)^2\alpha$ using the proposed algorithm.

In order to enhance the learning speed, we use a hybrid method incorporated the conventional Delta-bar-Delta method with the proposed higher order activation functions. Since the conventional Delta-bar-Delta learning algorithm does not sufficiently reflect the premature incorrect saturation phenomenon at the sigmoid function and also the proposed higher order activation function method uses the changing tendency of weight values in the learning process by virtue of Delta-bar-Delta algorithm, the hybrid method considerably speeds up at the flat region of learning curve.

Resultantly, the hybrid learning algorithm is to use the update law shown in Eq. (6) with the error signal δ_z, δ_y as shown in Eq. (10).

4. Simulation results

In this section, in order to show the effectiveness of the proposed learning algorithm, the 4 bit parity check problem is used as a bench mark example. The parameter values used for the simulations are shown in Table 1. DBD in Table 1 means Delta-bar-Delta algorithm.. Table 2 shows the 4 bit parity check problem.

We use the multilayer neural network with 1 hidden layer and 5 hidden neurons.[15] Many trials with different initial conditions were tested for several conventional learning algorithms. Simulation results are shown in Figs. 1 and 2. We compare the learning speed of the proposed hybrid method with general back-propagation, momentum method, and Delta-bar-Delta algorithm.

Table 1. Parameter values in the simulation

	constent	value	
		Fig. 1	Fig. 2
momentum	β	0.40	0.500
DBD	β	0.50	0.410
	x	0.59	0.408
	γ	0.29	0.300
New	β	0.50	0.410
	x	0.59	0.408
	γ	0.29	0.300

Table 2. 4 bit parity problem

x_1	x_2	x_3	x_4	y^k
1	1	1	1	-0.9
1	1	1	-1	0.9
1	1	-1	1	0.9
1	1	-1	-1	-0.9
1	-1	1	1	0.9
1	-1	1	-1	-0.9
1	-1	-1	1	-0.9
1	-1	-1	-1	0.9
-1	1	1	1	0.9
-1	1	1	-1	-0.9
-1	1	-1	1	-0.9
-1	1	-1	-1	0.9
-1	-1	1	1	-0.9
-1	-1	1	-1	0.9
-1	-1	-1	1	0.9
-1	-1	-1	-1	-0.9

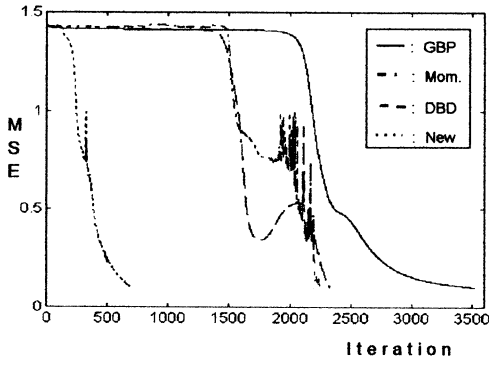


Fig. 1 Comparison of convergence using the learning parameters of first case in Table 1.

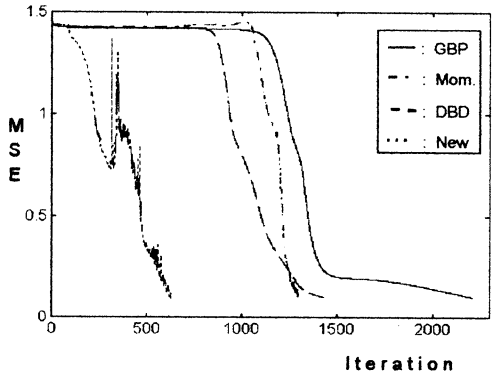


Fig. 2 Comparison of convergence using the learning parameters of second case in Table 1.

As shown in these figures, the proposed hybrid algorithm gives the best results

5. Conclusions

In this paper, we proposed a new learning algorithm to enhance the learning speed of error back propagation learning method. The higher activation functions protect the incorrect premature saturation by simple change of conventional learning method without much increase of computation time. A hybrid method incorporating the conventional Delta-bar-Delta method with the proposed learning algorithm gives excellent result by reducing the training time. As a further work, we are considering a new criterions for hidden representation to enhance the learning speed and generalization performance.

References

1. Philip D. Wasserman(1989) Neural Computing, Theory and practice.. Van Nostrand Reinhold, New York, pp. 43-60.
2. Philip D. Wasserman(1993) Advanced methods in neural computing, Van Nostrand Reinhold, New York, pp. 97-118.
3. Simon Haykin(1994) Neural Networks A Comprehensive Foundation, Macmillan, Toronto, pp. 138-229.
4. A. R. Webb, David Lowe, M. D. Bedworth(1988) A Comparison of Nonlinear Optimistion Strategies for Feedforward Adaptive Layered Royal Signals and Radar Establishment Memorandum 4157.
5. Sue Becker, Yann le Cun(1988) Improving the Convergence of Back-Propagation Learning with Second Order Methods Proc. 1988 Summer School on Connectionist Model, Carnege-mellon Univ., pp. 22-37.
6. J. S. R. Jang, C. T. Sun and E. Mizutani(1977) Neuro-Fuzzy and Soft Computing, Prentice Hall.
7. Scott E. Fahlman(1988) Fast-Learning Variations on Back-propagation : An Empirical Study Proc. 1988 Summer School on Connectionist Model, Carnege-Mellon Univ., pp. 38-51.
8. J. R. Chen and P. Mars(1990) Stepsize Variation Methods for Accelerating the Back-Propagation Algorithm. International Joint Conference on Neural Networks, 1990, vol. 1, pp.601-604.
9. S. Haykin(1986) Adaptive Filter Theory Englewood Cliffs, NJ, Prentice-Hall.
10. Robert A. Jaobs(1988) Increased Rates of Convergence Through Learning Rate Adaptation Neural Network vol. 1, pp. 195-307.
11. Seung-Joon Lee and Dong-Jo Park(1993) New accelerated learning algorithm motivated for novel shape of error surfaces for multilayer feedforward neural networks. International Joint Conference on Neural Networks, 1993, vol. 1, pp. 553-556.
12. Peter GECZY and Shiro USUI(1997) Learning Performance Measures for MLP networks. IEEE International Conference on Neural Networks, vol. 3, pp. 1845-1850.
13. Yao Zhang(1993) Updating Learning Rates for Backpropagation Network. International Joint Conference on Neural Networks. , 1993, vol. 1, pp. 569-572.
14. Marcus Pfister and Raul Rojas(1993) Speeding - up Backpropagation - A Comparison of Orthogonal Techniques. International Joint Conference on Neural Networks, 1993, vol. 1, pp. 517-522.
15. R. A. Jacobs(1988) Increased Rates of Convergence through Learning Rate Adaptation. Neural Networks. 1:pp. 295-307.

Proc. of Third Int. Symp. on Artificial Life, and Robotics (AROB III' 98),
Oita, Japan, 19-21, January, 1998,

An Architecture of an Artificial Mind for Collaborating and Communicating Robots

Akira Ito Hideki Kozima
Communications Research Laboratory
588-2, Iwaoka-cho, Iwaoka, Nishi-ku,
Kobe 651-2401 Japan
{ai, xkozima}@crl.go.jp

Abstract

Hitherto artificial communication systems have been manufactured based on the code model — the model which assumes the sharing of communication protocols or "codes" among participants. Human communication, on the other hand, seems to be based on an entirely different mechanism — interpreting information using "the theory of mind." In this paper we discuss what kind of architecture is required for creating an artificial mind capable of a human-like flexible communication.

1 Introduction

Recently autonomy of machine systems (robots) is widely investigated in the hope that autonomous robots can act flexibly and can adapt to an ever-changing environment. Autonomous robots with learning capability are being developed by a number of researchers. These learning robots are often interacting with other robots, and need to cooperate for achieving their own goals.

A serious problem arises, however, for collaboration and communication of learning robots. If all the robots can be developed based on a well-defined design principle, the remaining problem is to develop efficient protocols for collaboration and communication. Former researches on collaboration and communication of multi-agent (robot) system have mostly focused on this topic[1].

But what happens, if robots are allowed to develop or modify their rules and protocols independently. The environment may differ from robots to robots, and consequently they may come to develop more or less different protocols and rules. Machine system is very fragile for such inconsistency of protocols and rules. Of course, it is easy to prohibit these modifications, but then robots cannot learn from, or adapt to the environment, as far as communication or collaboration is concerned.

We humans can collaborate and communicate more flexibly. Of course, our communication heavily depends on the use of language. However, we can communicate without a common language. Suppose a man adrift on an unknown island who is trying to communicate with the natives. Why can we communicate? How can we understand others? If we want to make robots communicate with human beings, we must investigate the basic mechanism underlying these human communication abilities.

2 The code model of communication and the theory of mind

Communication is accomplished by transmitting to the hearer (i.e., reproducing in the hearer's mind) the speaker's thought. The code model explains this process as follows (see Fig. 1): The speaker's thought is transformed by the language generator (encoder) into speech, and is transmitted to the hearer. The hearer decodes the speech into a thought using his own language interpreter. Here the sharing of linguistic knowledge (coding protocols) is assumed. This code model has, however, a number of problems.

- The information contained in an utterance seems too poor for reproducing the speaker's thought. The situation does not improve much even if we take into consideration non-verbal information from the speaker. As Sperber argues[2], the utterance may be just a clue for reproducing the speaker's thought.
- How can we realize the sharing of the linguistic knowledge. Many theories have been proposed

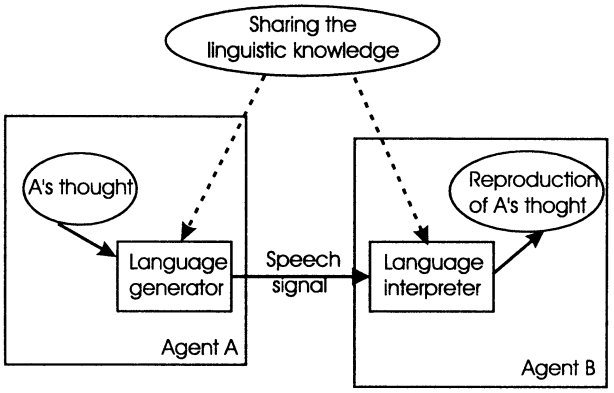


Fig. 1 The code model of communication

for the language acquisition of infants, but here again the information available for infants seems too poor for their language acquisition task.

- In real dialogue, the mapping between a thought and an utterance seems too arbitrary. A single expression can convey multiple meanings, while many expressions are possible for conveying a single thought. This kind of many-to-many mapping is the source of the efficiency of language [3], but nobody succeeded in formulating the rules for this mapping.

Hence Sperber proposed "the inference by relevance " [2] instead of the code model. He does not explain, however, what the mechanism or algorithm for this inference really is. Probably the sharing of a common "hardware" is assumed. If we assume this common "hardware" as mind, then the relevance theory reduces to the following assertion: We humans have a common "mind" in each of us, and interpret others' utterances using this common mind.

When we want to understand others' behaviors or utterances, we try to read others' mind. The importance of mindreading in communication comes to be recognized with the advance of the "Theory of Mind" research[4]. The theory of mind is a model of mind we ordinary people have, and with which we interpret other people's behaviors or utterances. In plain words, the theory of mind says that others have the same mind as we have, and we read the mind of others (interpret the action of others) using our own mind as a model of others' mind (see Fig. 2).

The Theory of Mind is first proposed by Premack & Woodruff[5] in a paper "Does the Chimpanzee Have a Theory of Mind?" After its publication, researchers have investigated if animals and children of a specific ages have the theory of mind or not. But there seems

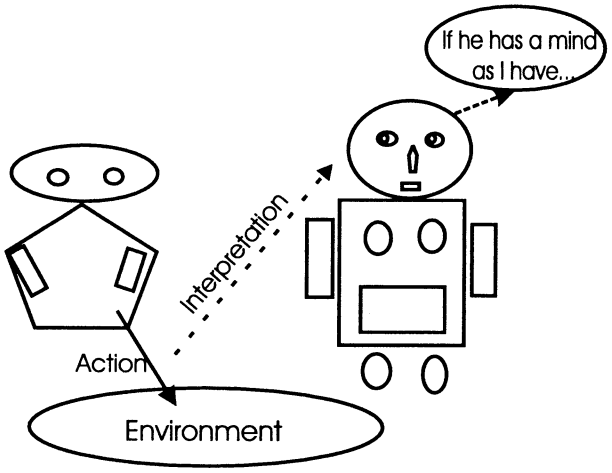


Fig. 2 Interpreting other's action with "The Theory of Mind"

to be no consensus on what the theory of mind really is, and nobody succeeded in implementing it as a computer software.

3 Mind as a communication tool

Here we investigate mind as a design problem for communication in an evolutionary world. What is the best design for communication system, when nature has to invent one for living beings.

Let me explain this with Fig. 3. Genetic system produces minds according to the genetic code for a mind. The end products (minds) may differ more or less depending on the environment of their ontogeny. Next minds learn from the environment and acquire various knowledge as their growth process. The innate part may correspond to the Operating System, while learned part to the program & data in a computer system.

Now suppose these minds want to communicate each other. If each mind is produced exactly alike and shares all the communication protocols (how to encode information into utterances, behaviors etc.), the correctness of the communication is assured. This is what engineers have been aiming at in designing the modern communication system, whose efficiency has been proved in many fields.

This design has, however, a drawback, i.e., the system lacks the ability to adapt flexibly to the environment. An artificial system can be re-designed by humans when it become out-of-date. Natural system, on the other hand, cannot expect such an intervention from outside. When a new phenomenon, concept, or

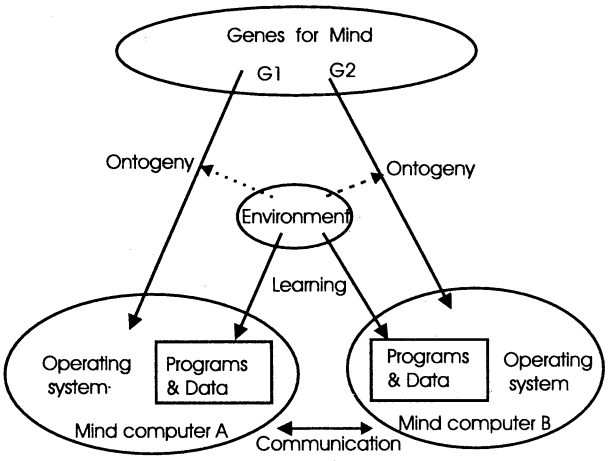


Fig. 3 Design of mind in an evolutionary world

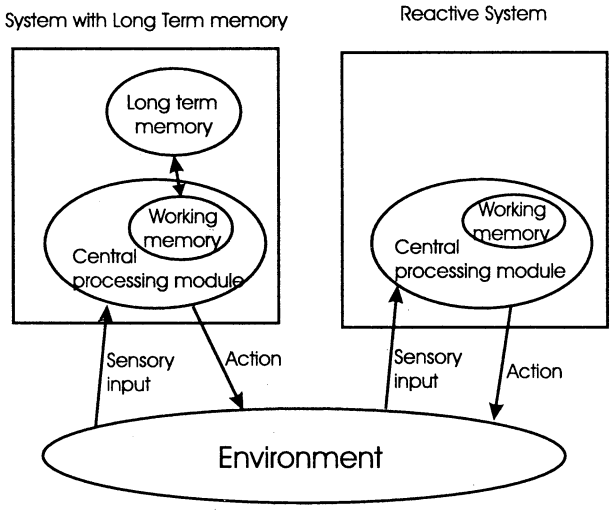


Fig. 4 System with long term memory and reactive system

idea needs to be communicated, a natural system with pre-defined design (code model) cannot cope well.

The system can adapt to an environment by learning, i.e., modifying its rules and protocols appropriately. But the environment appears differently for each individual (agent) in the system, and we cannot expect that each individual maintains the same protocols after the learning. The ability to adapt to the environment is a powerful weapon for the race of evolution, but it demands a special mechanism for communication.

The departure from the code model is also requested by the evolution mechanism itself. As the evolution works by making the slightly different individuals compete for survival, the complete matching of protocols cannot be expected.

Thus the communication based on the code model is applicable only in simple animals such as bees, where the evolutionary speed is relatively slow. To put it another way, human being could acquire a surprising speed of evolution by developing a communication mechanism other than that based on the code model.

Next section discusses what kind of architecture is required for an artificial mind for communication.

4 Requisites for an artificial mind

How do we know that other people really have minds. It is often argued that mind can be detectable from the observation of other's behaviors. But when we have to determine if an agent (robot, animal, etc) has a mind or not, what features do we search for its clues?

One of the requisites for mind is that it does not allow an easy modeling of itself by other agents. Modelablility by a simple automaton is a disadvantage in a battle for survival. Modelablility means that other agents can predict its behavior, which leads to the exploitation by parasites, or betrayal by mate agents. It is known that an automaton with a relatively small memory (reactive system) can be determined from its action sequences. Hence an agent must have a practically unlimited amount of (long-term) memory for making its behavior unpredictable mathematically.

Once an unlimited amount of memory is obtained, then it can also be used for modeling of other agents, i.e., predicting others' behavior from the observation of their actions. Modeling others while denying to model itself, a powerful weapon for interactions with others, is one of the chief functions of mind.

This marvelous mind has, however, a drawback. The larger memory agents have, the more advantageous it is in modeling others. If every agent try to surpass other agents by memory size, it leads to a boundless arm race and ultimately to an exhaustion of agents' resources. The process cannot be continued indefinitely. After all, the equipment of a large memory itself is of no help for modeling of mate agents, and consequently for improving communication between mate agents.

An escape path to overcome this difficulty must be built in the function of mind. Our assertion is that the theory of mind is just the escape path we are searching for. The theory of mind works roughly as follows. Each mind can be a model of others' mind, and can simulate the behavior of others' mind using itself.

The processing of simulation requires some kind of stack mechanisms, and the existence of large amount of memory is again essential.

If this mind is simple enough, it can be modeled easily by mindless agents. If it is too difficult, it cannot be modeled by mate agents. Here the theory of mind works as a built-in secret password. For those agents who share the theory of mind, modeling of other's mind is comparatively easy. But it is very difficult for those lacking the theory of mind. The trick lies in the fact that the theory of mind cannot be deduced just from the observation of agents with mind.

5 Evolving robot's mind

If we try to make a model of other mind with a rule-based approach, we are trapped in a classical AI difficulty: We cannot write down all the rules which constitute "the mind," for we ourselves do not know well what mind really is. This is very natural if the mind is as we explained in the previous section. The mind is not the thing we can learn by observing it from outside, but what we must develop by ourselves.

Hence we are developing an artificial mind by making robots (agents) learn their mind through the interaction with other robots. Robots are given some communication and collaboration tasks and each robot is forced to search the best strategy for the task. Robots who can collaborate and communicate well can only survive.

A search strategy takes into account the theory of mind, i.e., each robot regards that other robots also have a mind as it has, which means — in computer science terminology — that other robots have nearly the same search strategy as that of itself. The task is such that in order to accomplish it they have to understand or interpret others' actions and messages correctly. But the system lacks an *a priori* language or protocols for communication and collaboration.

Of course, nothing new will emerge if we call some software module as "mind". The point is that we forced a restriction on searching algorithm: It must model others using its own algorithm as a model of others. This method proved to be effective for developing collaboration strategies in the model of the Prisoner's Dilemma Game[6].

Of course, the mind thus developed is very different from that of human beings. It is another mind, or would-be mind, in Artificial Life terminology. The important point is that this another mind must have the property we ascribed to mind in this paper, i.e., modeling others while denying to be modeled, easing the communication with the mate agents, etc.

6 Conclusion

We explained why the code model for communication is insufficient for learning robots (agents), and suggested a flexible mechanism for communication based on the theory of mind. Next we described the requisites for an artificial mind and how to create a mind through evolution. Our research is preliminary but its effectiveness is verified in a simple model for collaboration.

References

[1] *Proc. First Intl. Conf. on Multi Agent Systems, (ICMAS'95)*, pp.201-208, San Fransisco, 1995.

[2] Sperber, D. and Wilson, D.: *Relevance: Communication and Cognition*, Blackwell, 1986.

[3] J. Barwise and J. Perry: *Situations and Attitudes*, The MIT Press, 1983.

[4] Baron-Cohen, S.: *Mindblindness: An Essay on Autism and Theory of Mind*, MIT Press, 1995.

[5] Premack, D. and Woodruff, G.: "Does the Chimpanzee Have a Theory of Mind?", *The Behavioral and Brain Sciences*, 4, pp.515-526, 1978.

[6] Ito, A.: "How Do Selfish Agents Learn to Cooperate?" *Proc. of 5th Intern. Conf. on Artificial Life (ALife V)*, Nara, pp.142-149, MIT Press, May 1996.

Proc. of Third Int. Symp. on Artificial Life, and Robotics (AROB III' 98),
Oita, Japan, 19-21, January, 1998,

Towards Mindreading by an Attention-Sharing Robot

Hideki Kozima Akira Ito
Communications Research Laboratory
588-2, Iwaoka-cho, Iwaoka, Nishi-ku,
Kobe 651-2401 Japan
{xkozima,ai}@crl.go.jp

Abstract

This paper describes our model of "mindreading" and its implication for human-robot communication. Mindreading is an activity of estimating others' mental states (e.g. belief and desire) by means of observing their behavior. We here focus on "attention-sharing" as a basic device for observing others' behavior. Attention-sharing is an activity of paying one's attention to someone else's attentional target. This enables one to observe others' stimuli (what they are perceiving from the target) and responses (what they are doing on the target). Being inspired by lack of attention-sharing in autism, we assume that attention-sharing plays an indispensable role in mindreading. As a test-bed for mindreading, we are developing a robot that can follow people's attentional target by means of monitoring their gaze direction.

1 Introduction

Human-robot communication is one of the most challenging target in AI and robotics. A number of computational devices for image processing, speech processing, and higher information processing have already been developed. Integrating these devices, however, no one has achieved natural human communication like that of HAL.

We emphasize here that the essence of human communication is "mindreading" [1], i.e. estimating others' mental states (belief, desire, intentions, etc.). By mindreading one can predict others' behavior, so that he or she can do well in competition and cooperation with others. This may be one of the reasons why human beings acquired language, which is a useful device for mindreading.

But we often try to mindread others in terms of their non-verbal behavior. For example, you may intentionally glance at your watch when you want to make someone hurry. As Sperber [2] claimed, an explicit utterance is just a clue for mindreading. Also infants, who cannot use language, do mindread. This is so-called "social referencing", in that an infant refers to facial expressions of his or her caretaker so as to make a decision in an ambiguous situation.

These facts suggest that mindreading is achieved by a cognitive module that is independent from any individual language and is functioning before infants' language acquisition. The aim of this research is to understand the function and structure of the mindreading module.

The following section introduces "autism" as a communication disorder. Autism is also known as "mindblindness" [1], i.e. a disability of mindreading. Section 3 describes "attention-sharing" and our model of mindreading based on attention-sharing. Attention-sharing is an activity of sharing attentional target with someone else; infants and children with autism do not show attention-sharing with others. Section 4 introduces the attention-sharing robot being developed as a test-bed for human-robot communication by mindreading. Section 5 draws implication of mindreading for future human-robot communication.

2 Autism: Communication Disorder

Autism, which used to be an enigmatic mental disease, is a developmental disorder caused by specific (and mainly inherited) brain damage [3]. Recent statistical reports show that about 0.1% of children are autistic; the ratio of boys to girls is about 4:1.

Children with autism have serious impairment in non-verbal communication, e.g. use of gaze, pointing, and facial/gestural expression in communication, as well as in verbal communication, e.g. language acquisition and appropriate use of language [4]; they keeps other abilities like rote memory and spatial recognition. Autism is therefore called "a communication disorder".

Why do children with autism lack communication abilities? To find an answer to the question, develop-

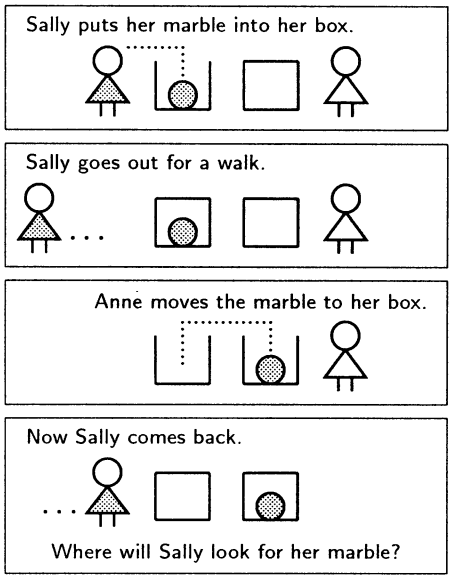


Figure 1. The Sally-Anne experiment

mental psychologists devised "the Sally-Anne experiment" [1, 3], which is a version of false-belief tasks. The experiment is as follows. First, the experimenter shows a simple puppet play, as is illustrated in **Figure 1**, to children. After the play, the experimenter ask them a simple question: "Where will Sally look for her marble?"

The answer is "In Sally's box". Normal 4-year-old children can solve this problem effortlessly and almost unconsciously. Also children with Down's syndrome (verbal MA, mental age, above 4 years) can do it. However, children with autism (verbal MA above 4 years) fail in the task [1]. They answered "In Anne's box", instead of showing random responses.

What is missing in autistic children? We assume that they do not understand "each person has his or her own mental state" and "the mental state determines the person's behavior". They cannot imagine others' belief or desire, so that they cannot predict others' behavior. What they can understand is the physical reality observed by themselves.

3 Attention-Sharing and Mindreading

How can normal children effortlessly and unconsciously ascribe mental states to others' behavior? We assume that "attention-sharing" plays an indispensable role in it, since its absence distinguishes autistic children from normal children.

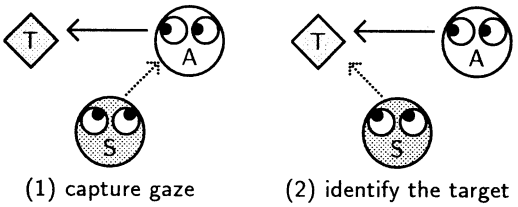


Figure 2. Attention-sharing through gaze

3.1 Shared attention and shared world

Attention-sharing is an activity of paying one's attention to someone else's attentional target. We call the attention thus shared "shared attention" (some psychologists call it "joint attention" instead). Shared attention spotlights things and events being attended to by two persons or more, creating shared world in front of them. As clues for the attentional target, one can use direction of others' pointing, gaze, face, and so on.

Figure 2 illustrates how self (S) creates shared attention with an agent (A) in terms of gaze direction. First, the self captures the agent's gaze direction. Then, the self searches in the direction and identifies the target (T) of the agent's attention. To maintain the shared attention thus created, the self often goes back and checks the agent's gaze direction.

Children with autism do not create shared attention with others, as we mentioned above. Being instructed by an experimenter, however, they can identify someone else's attentional target. This suggests that children with autism do not have motivation to identify and share the target.

Normal infants and children can easily read others' attentional targets and can also guide others' attention by using gaze and pointing. Attention-sharing is observed in infants at the pre-verbal stage; its development starts before 6 months old and completes around 18 months old [5]. This implies the course of its ontogeny.

In addition, attention-sharing can be observed in some species of non-human higher primates. Chimpanzees and orangutans can use gaze and pointing for attention-sharing; species of lower primates, e.g. macaques, can follow human pointing [6]. This implies the course of phylogeny of attention-sharing.

3.2 Observing others' behavior

We think that the major function of attention-sharing is observation of others' behavior. In other words, shared attention works as a probe for observing

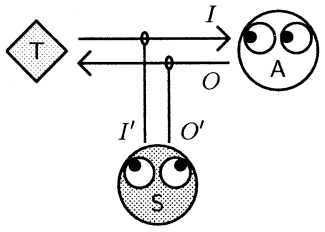


Figure 3. Observing other's behavior

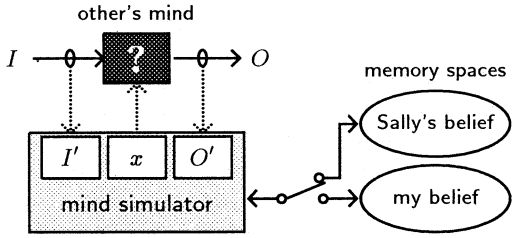


Figure 4. Simulation of other's mind

someone else's stimulus (what he or she is perceiving) from the environment and response (what he or she is doing) to the environment.

Let us assume that an agent (A) is interacting with a target (T), as illustrated in **Figure 3**. Attention-sharing with the agent enables self (S) to observe the agent's sensory-input I and motor-output O. Since the self and the agent are paying attention to the same target T (from slightly different angles), the self's sensory-input I' becomes approximately equivalent to I. Also the shared attention enables the self to observe the agent's motor-outout O; this requires to map it onto the self's motor image O'.

These functions of attention-sharing can be summarized as "empathy", i.e. to imagine oneself in the position of someone else. Empathy enables us to explain others' behavior and predict others' next behavior.

3.3 Simulating others' mind

How can we explain and predict others' behavior? It is difficult to predict an agent's response only from the agent's stimulus observed, since the mapping between them is heavily dependent on the agent's mental states. Different beliefs make different actions, as we have seen in the Sally-Anne story.

How can we estimate others' mental states? We think that "a mind simulator" can estimate others' mental states, as illustrated in **Figure 4**. First, the simulator observes an agent's input I' and output O' by attention-sharing. Then, from the past experiences in one's memory, the simulator selects the most likely state x which was produced by I' and produced O'.

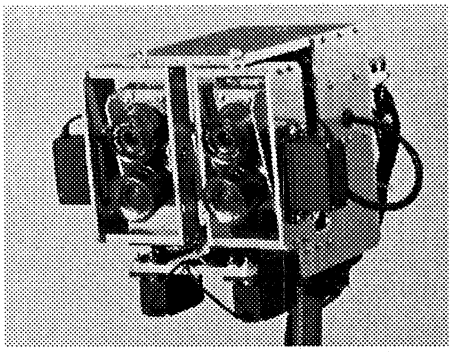


Figure 5. The attention-sharing robot

Once the agent's current mental state $x(t)$ is estimated, the simulator can predict the agent's next behavior. Observing the agent's next input $I'(t+1)$, the simulator selects the most likely output $O'(t+1)$ which was produced by $I'(t+1)$ and $x(t)$.

The memory is organized into several belief spaces, as shown in **Figure 4**; the simulator refers to an appropriate one for mindreading and modifies it according to the simulation result. Thus one can feel and think in Sally's position and maintain Sally's belief.

4 The Attention-Sharing Robot

We are developing a robot, *Infanoid*, that can create and maintain shared attention with humans. The robot is intended as a test-bed for human-robot communication, especially for mindreading.

The robot has an active-vision head with an anthropomorphic shape, as is shown in **Figure 5**. Each eye on the head has two different CCD cameras (like those on *Cog* [7]). The lower with a wide lens spans the visual field (approx. 70 degs horizontally) and the upper with a zoom lens takes the precise image on the fovea (approx. 25 degs horizontally). Four servo motors drive the direction (pan and tilt) of the eyes; the eyes can perform a saccade of 45 degs within 100 msec.

What we are going to do with *Infanoid* is "gaze-monitoring", i.e. identifying an attentional target of a human being in terms of his or her gaze direction. As described in **Figure 6**, the gaze-monitoring process includes the following tasks.

1. First, the robot detects a human face in a complex scene taken by the wide-lens cameras.
2. Once the face has been detected, the robot saccades to it. This enables the zoom-lens cameras to take the precise image of the face.

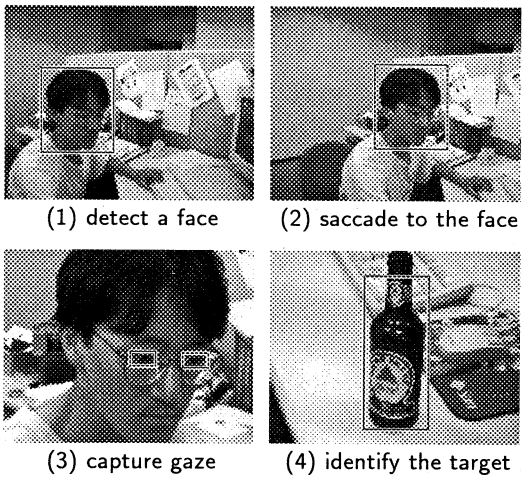


Figure 6. Gaze-monitoring process

3. On the zoomed image, the robot detects eyes and captures their gaze-direction in terms of the position of the pupils. If impossible, the robot captures the face-direction instead.
4. Then, the robot starts searching for a target in that direction. If something with a clear boundary is found (by using stereo vision), the robot identifies it as the target.

We have implemented a saccade controller and a real-time face/eye detector. The detector employs template matching with lighting correction on the hierarchically layered images; it performs detection for 10 templates at frame-rate (more than 20 frames/sec).

The gaze-monitoring system will realize attention-sharing between humans and the robot. Currently we are working on capturing gaze-direction and target identification. Our preliminary experiments revealed that human precision of gaze-monitoring is not so high that we often rely on semantic and pragmatic clues, like "relevance" [2], for target identification.

5 Conclusion and Future Research

We described here our preliminary model of mind-reading based on shared attention. Mindreading is one of the most fundamental methods for human communication. Attention-sharing, which is a device for observing others' behavior, is required in mindreading, since children with autism do not show attention-sharing and cannot mindread others.

For our future research, we would like to investigate how observation of others' behavior (by shared attention) works in infants' social development.

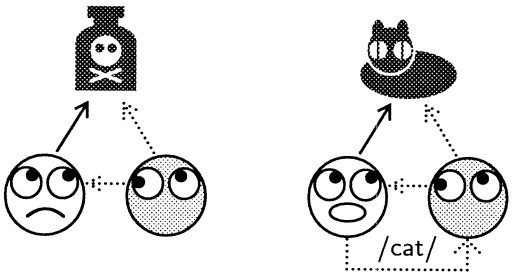


Figure 7. Learning social conventions

First, observation of others' behavior could be a basis for "social referencing". When an infant faced an unknown object, as illustrated in **Figure 7** (left), the infant refers to the caretaker's facial expression in order to check if the object is safe. Also this scheme will work on learning social behavior by "mimic".

Secondly, observation of others' behavior will be required in "language acquisition", that is acquisition of a conceptual system (or symbolic system) of one's native language. A conceptual system is a system of social conventions which articulates things and events in the world into "categories" and gives different names (phonological representations) to them. As illustrated in **Figure 7** (right), observing both the agent's sensory-input (sensory-input from the cat) and motor-output (the caretaker's speech), the self can make association between them.

References

[1] S. Baron-Cohen: *Mindblindness: An Essay on Autism and Theory of Mind*, MIT Press, 1995.

[2] D. Sperber and D. Wilson: *Relevance: Communication and Cognition*, Blackwell, 1986.

[3] U. Frith: *Autism: Explaining the Enigma*, Blackwel, 1989.

[4] *The ICD-10 Classification of Mental and Behavioral Disorders World Health Organization*, World Health Organization, 1993.

[5] G. Butterworth and N. Jarrett: What minds have in common is space, *British Journal of Developmental Psychology*, Vol.9, pp.55–72, 1991.

[6] S. Itakura: An exploratory study of gaze-monitoring in nonhuman primates, *Japanese Psychological Research*, Vol.38, pp.174–180, 1996.

[7] R. A. Brooks and L. A. Stein: Building Brains for Bodies, *MIT AI Lab. AI Memo*, No.1439, 1993.

Proc. of Third Int. Symp. on Artificial Life, and Robotics (AROB III' 98),
Oita, Japan, 19-21, January, 1998,

The Effect of Self Organization in the Trade Cycle

Masayoshi Tabuse and Mieko Tanaka-Yamawaki

Department of Computer Science and Systems Engineering
Faculty of Engineering, Miyazaki University, Miyazaki 889-21 Japan
E-mail: tabuse@eagle.cs.miyazaki-u.ac.jp
mieko@eagle.cs.miyazaki-u.ac.jp

Abstract

We examine a model of trading agents that one of the present authors considered some time ago, with a special attention to clarify its dynamical nature. The model exhibits a global oscillation of the entire system which can be identified as a trade cycle if the parameters are appropriately chosen, and a sudden collapse of the cycle in a certain parameter region which is sometimes followed by its recovery to a global cycle. Moreover, these patterns have similarity with the behavior of a living organs such as heart beats, as frequently seen in other chaotic systems of coupled oscillators[1].

It is found that the strength of positive feedback incorporated in this model works as a driving power of the cycles, which in turn works as coupling of each agent as an element of coupled oscillators. The sudden collapse is triggered by chance if the time-lag is minimum and the coupling constants of the agents have appropriate strengths. We introduce a global index named 'n-down curve' and show that the behavior of the n-down curve explains the above-mentioned cycles. Namely, the cycle occurs whenever one of the n-down curves passes zero and the cycle collapses when no n-down curve cuts zeros.

Keywords: self organization, trade cycle, computer simulation, coupled oscillators, chaos

1 Introduction

Economics forecast is believed to be extremely difficult. Its difficulty is believed to be due to the complexity of the object. Conventional theories of price determination based on the equilibrium is too idealized to explain dynamical phenomena such as trade cycles. We have investigated this problem by studying a dynamical model of trading agents with a constant time-lag, and observed by means of computer simulations that a global cycle indeed occurs if we choose the parameters of the model carefully, and observed that this cycle is stabilized as the time-lag increases. When the time-lag takes its minimum value which is equal to one, on the other hand, the cycle tends to decay suddenly after a long period of seemingly stable oscillations[2].

Though the model was originally meant for studying the trade cycle, the above-mentioned behavior motivates us to compare this phenomena to biological motions with a hope to understand the underlying mechanism of life versus death.

2 Chaotic Time Series from a Model of Trade Cycles

We shall briefly survey the basic assumptions of our model. The model is made of N uniform agents who trade a single kind of goods with a constant time delay. The system has 2N independent variables which are not determined by a single decision maker, but are fixed by each agent distributively according to its own situation. They are the price for each agent to sell the goods it owns and the budget for each agent to prepare to buy (the same kind of) goods from other agents within this artificial economic society.

We first looked at the chaotic structure of the average price in the case of the minimum time-lag as a function of time[3]. In the model the minimum time-lag (one unit) corresponds to selling the purchased goods at the next trade without keeping them in the storage. Typical time series keeps global oscillations for a considerably long time and then suddenly changes its pattern to a random oscillation with small amplitude (as in Figure 3-(3a)). By reconstructing an attractor from this time series we have

estimated the first Lyapunov exponents by the method of Sato et. al.[4] and found that they take small positive values (range of 0.001) and increases (to the range of 0.015) when the pattern of the time series drastically changes. We have also computed the correlation dimensions [5] and found that they jump by a factor of two when the pattern of the average price changes.

3 Driving Force for Oscillations

In order to understand the mechanism of oscillations in this model more closely, we proceed to look at the motions of individual agents. First we ask what values of the parameters cause the oscillation. There are three parameters in the model, $\{ a, b, \ell \}$, where ℓ is the time-lag between the purchase of goods and the time to put them for sale. At each trading time, each agent decides its own price for sale and its budget to buy goods from the others according to the following rule:

new price = last price + b

new budget = last budget + b

if the agent was able to sell goods in the last trade, and

new price = last price / $(1+a)$

new budget = last budget / $(1+a)$

if the agent could not sell goods due to the high price.

If nothing was sold due to the lack of merchandise the price and budget are kept unchanged.

Because all the agents follow the same rule, their prices change similarly each other.

The main issue is to show how this rule set for individual agent works to create a global cycle of the entire system in a self-organized manner. Figure 1 shows a typical pattern of a global cycle of the average price simultaneously drawn with the price of one agent. It can be seen from this figure that the price of each agent moves as a collection of n-down elements. Namely, the price of one agent, after rising by one step, falls by n steps continuously before turning to a rise again (see Figure 2). Figure 1 begins with 9-down element, then shifts to 8-down element, 5-down element, and 4-down element, then after reaching the bottom of the cycle it moves to 3-down element then to 2-down element as the average rises.

Practically we can use the following quantity

$< n-down >= (\overline{price} + b) / (1+a)^n - \overline{price}$

without tracing the prices of individual agents. We name this as 'n-down curve'. We can show that the cycle occurs if one of the n-down curves passes zero, and the cycle decays as that curve moves away from zero as we change the parameter a and b. Fig 3 (1b)-(3b) show the n-down curves for a and b corresponding to Fig 3 (1a)-(3a), respectively. It is convenient to remember in the following discussion that n-down curve is approximately

$< n-down > \cong b - n \cdot a \cdot \overline{price}$.

The self-organization mechanism to make the average price fall in the trade cycle is as follows:

[step 1] As the average price falls, the decrement of individual price in one step decreases.

[step 2] The curve of the average price turns gentler.

[step 3] n-down curve crosses zero from negative to positive.

[step 4] Go to step 1.

This process causes avalanche of the prices and eventually brings the average price to the bottom of the cycle.

The following phase is the shift from the falling pattern to the rising pattern of the average price. This occurs only when some individual prices become slightly below zero and the n-down curve closest to zero is located just above zero and still not touching the zero line. This situation makes that agent to be able to sell its goods.

Once the average price begins to go up, again a self organization works to make a global rise of the prices:

[step 1] As the average price rises, the increment of individual price in one step increases.

[step 2] The curve of the average price turns sharper.

[step 3] n-down curve crosses zero from positive to negative.

[step 4] Go to step 1.

In this cycle the relevant (crossing zero) n-down curve shifts from larger n to the smaller n like n=3,2,1. As the average price goes up it passes the turning point of the curve and the slope begins to decrease. Correspondingly the relevant n-down curve shifts as n=1,2,3, etc. until the average price passes the top of the cycle and moves to the falling phase.

4 Cases of Large Time-lag

As the time delay increases from one, more

goods are kept in the storage as inventory and the total amount of merchandises for sale decrease accordingly. This effect makes the oscillation of the average price with more sensitively.

When the price is low, the above mentioned self organization mechanism to increase the price is in action. The detail is as follows. As the average price goes down, more goods are sold and sent to the storage, which makes the amount of merchandises for sale decrease and each agent can buy with its budget more merchandises from the larger number of other agents, which in turn increases the number of agents whose price goes up. Thus the average price increases.

As the price goes up, on the other hand, the self organization mechanism to decrease the price becomes in action. As the price increases, less goods are sold due to high price thus the amount of merchandises for sale increases and each agent can buy with its budget merchandises from the smaller number of other agents, and the number of unsold agents increases who lower the price at the next sale.

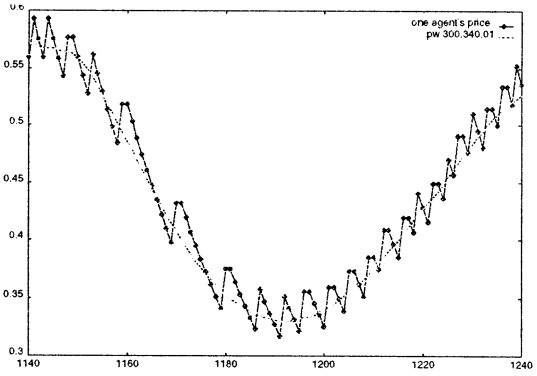
In conclusion, larger time-lag makes both the price raising power and the price lowering power stronger compared to the case of minimum time-lag.

6 Summary

We considered the nature of the peculiar oscillatory pattern appeared in a model of trading agent. We are particularly interested in the long-term cycles followed by a sudden collapse and (occasional) recovery. First we investigated various chaotic features of the time series of the average price by reconstructing an attractor. It was found that the first Lyapunov exponent takes small positive values and increases whenever the average price changes its pattern. Also the correlation dimension jumps at the same points. Next, we studied the individual prices. We found that the trade cycle occurs for the parameter region where one of the n-down curves crosses zero.

Thus we can roughly foresee the region of a and b for which the cycle is generated.

Figure 1 The price of one agent and the average price as a function of time. (N=100, a=0.030, b=0.034, ℓ=1)



References

[1]e.g. K. Keneko and I. Tsuda(ed.), Physica D75 (1994), pp.1-450.

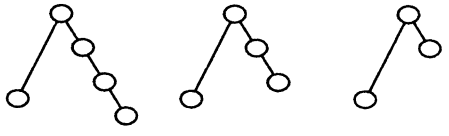
[2]M. Tanaka-Yamawaki, K. Hasebe and L.C.Jain, 'A Dynamical Model of the Trade Cycle and Its Computer Simulation', Edited Proceedings of ETD2000, IEEE Computer Society Press, pp.571-577.

[3]M. Tanaka-Yamawaki and M. Tabuse, 'Chaotic Time Series from a Model of Trading Agents', to be published in Proceedings of Nolta'97 (Hawaii, November 1997)

[4]M. Ding, C. Grebogi, E. Ott, T. Sauer, and J. A. Yorke, Physical Review Letters, vol.70 (1993), pp.3872-3875; P. Grassberger and I. Procaccia, Physical Review Letters, vol.50 (1983) pp.346-349; Physica, vol.9D (1983),pp.189-208.

[5] S. Sato, M. Sano and Y. Sawada, Progress of Theoretical Physics, vol.77(1987)pp.1-5.

Figure 2 n-down elements (n=3,2,1) of the price of one agent.



3-down element 2-down element 1-down element

Figure 3 The average price and n-down curves as a function of time, for the case of one hundred agents (N=100), ℓ =1, a =0.030 and b =0.027, 0.034, 0.045.

Figure 3-(1a) The average price for ℓ =1, a =0.030, b =0.027.

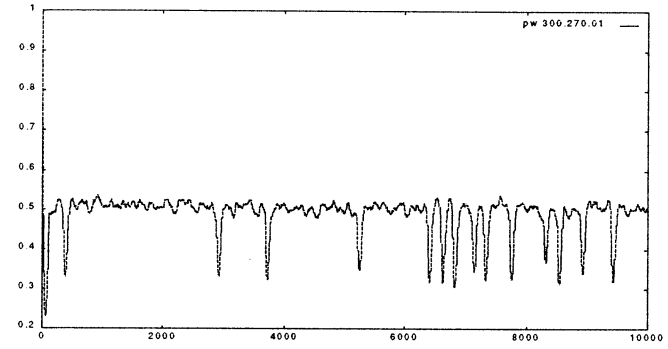


Figure 3-(1b) The n-down curves (n=1,2,3,4) for ℓ =1, a =0.030, b =0.027.

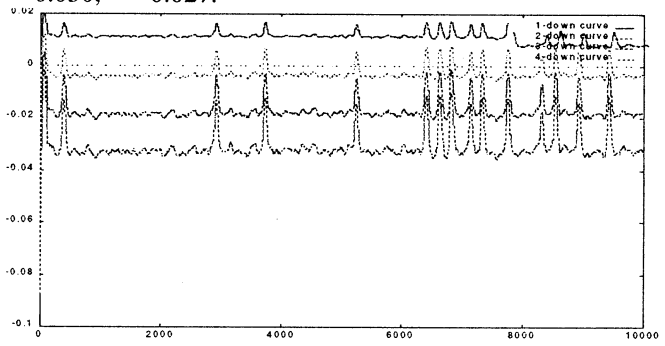


Figure 3-(2a) The average price for ℓ =1, a =0.030, b =0.034

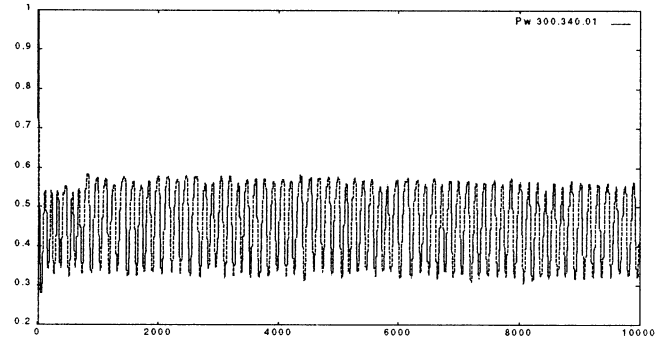


Figure 3-(2b) The n-down curves (n=1,2,3,4) for ℓ =1, a =0.030, b =0.034.

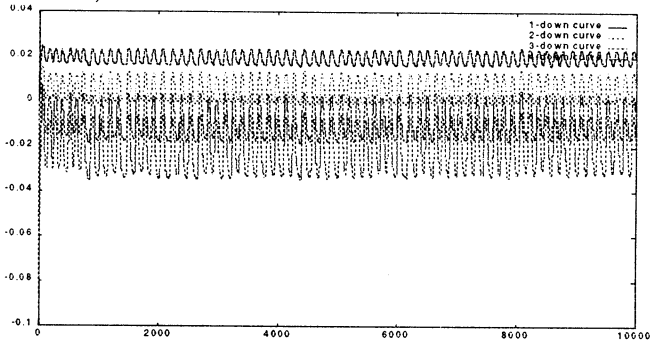


Figure 3-(3a) The average price for ℓ =1, a =0.030, b =0.045

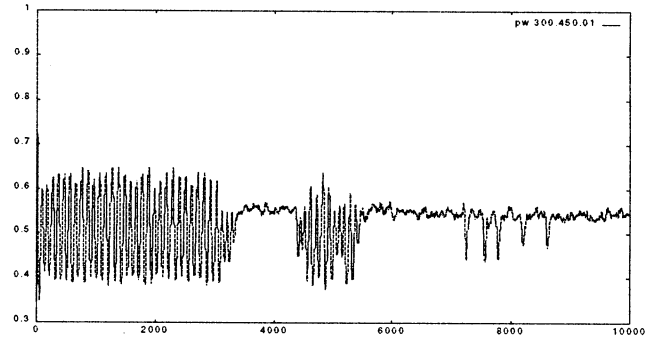
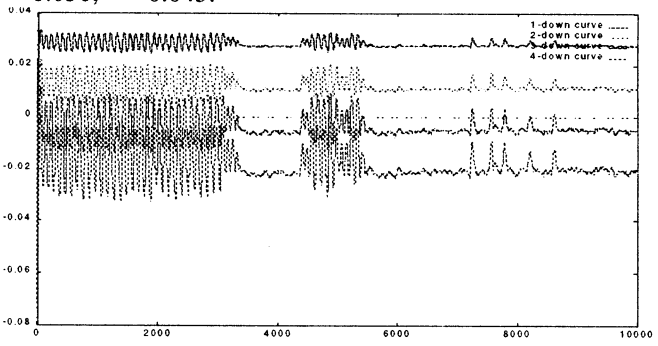


Figure 3-(3b) The n-down curves (n=1,2,3,4) for ℓ =1, a =0.030, b =0.045.



Proc. of Third Int. Symp. on Artificial Life, and Robotics (AROB III' 98),
Oita, Japan, 19-21, January, 1998,

Introduction of Functional Boundary Model for Emergent Organization

Keita SHONO † Keiji SUZUKI † Azuma OHUCHI †

† Research Group of Complex Systems Engneering,
Graduate School of Engneering, Hokkaido University,
North-13 West-8, Sappro 060, Japan
{shono, suzuki, ohuchi}@complex.eng.hokudai.ac.jp

Abstract

In this paper, we introduce the functional boundary face model into the autopoietic self-organizing system. The concept of the autopoiesis has recently been receiving increased attention as new concept of the dynamical systems. Then, several computational models were developed which indicate the emergent properties arisen from the autopoietic self-organizations. The autopoietic self-organizations in these models, however, are hard to control the organizing process of them. One of the reasons seems to be that the sub-structures in the organizations can't be kept and reused. Namely, even if the emerged sub-structures derive the interested properties, we can't pick up them without changing the properties of themselves. Because such sub-structures tightly and dynamically join with the other structures in the whole organizations. Thus, toward the controllable organizing process of autopoietic systems to be developed, we try to introduce the functional boundary face model as new element in the Atomoid which is one of the autopoietic models[1]. The introduced model has the function of peculiar permeability like as the biological boundaries of cells. We will expect the model to become the dividing factor between the sub-structures contained in it and others.

1 Introduction

In this paper, we introduce the functional boundary face model into the autopoietic self-organizing system.

Complex systems in nature have the self-organizing properties based on the interaction between a lot of component elements. In addition, the systems flexibly change the organization and the dynamical processes of them affect to produce the new organization processes of other complex systems. The dynamics of the organizing process seems to be one of the sources of the complex and emergent phenomena in nature.

To explain the property of such dynamics in the complex systems, the concept of the autopoiesis is introduced. Moreover, to realize the artificial autopoietic behavior, several computational models are developed which indicate the emergent properties based on the autopoietic self-organizations [1][2]. The autopoietic self-organizations in these models, however, are hard to control the organizing process of them. One of the reasons seems to be that the sub-structures in the organizations can't be kept and reused. Namely, even if the emerged sub-structures derive the interested properties, we can't pick up them without changing the properties of themselves. Because such sub-structures tightly join with the other structures in the whole organizations.

Thus, toward the controllable organizing process of autopoietic systems to be developed, we try to introduce the functional boundary face model as new element in the Atomoid. Thus the boundary model is expect to perform the functions as follows: First, it keeps the specific components into the inside according to its peculiarity. Second, the model divides the tightly joined all interactions into the inside organaizing interactions among the inside components and the outside interactions. Namely, the function of the peculiar permeability in the model will works as the interface between the interactions of both sides. Therefore, we will expect the model to become the dividing factor between the sub-structures contained in it and others.

2 Atomoid

In this experiment, we use Atomoid[1] as the phenotype. Atomoid is a reaction-formation model which has a reaction-dynamics similar to reaction based on energy level observed in physical world.

Each atom in Atomoid has its own hands and can bond with those of others when inner states of bond-

ing hands satisfy bond condition. Furthermore, this bond may cause separation because of changing inner states. Thus Atomoid has very simple reaction rules, but Atomoid can realize complex atomic reactions. Furthermore, we can observe the emergence of self-reproductive hypercycle, because of its dissipated structural properties.

2.1 Model of atom

When M denote the kind of atom, an atom whose atomic number is $k(k = 1, \cdots, M)$ is described as follows.

$$a_k = (hd(k), \varphi_j(k), r_j(k), \theta_j, s_j | j = 1, \cdots, hd(k)) \quad (1)$$

$hd(k)$: the number of bonding hands
$\varphi_j(k)$: the operator which operates the other atoms
$r_j(k), \theta_j$: the operand which represents the bonding hand structure
s_j : the energy state of the bonding hand, and it takes only two states { ground(0) , excited(1)}

2.2 Relationship between the bonding hand structure and the energy structure

The ground state energy e_0 and the excited state energy e_1 are defined as follows with the complex form $z = re^{i\theta}$

$$e_0 = \min(r\cos\theta, r\sin\theta), \quad -r \leq e_0 \leq r \quad (2)$$

$$e_1 = \max(r\cos\theta, r\sin\theta), \quad -r \leq e_1 \leq r \quad (3)$$

When operated by the operator $e^{i\varphi(h)}$ of atom h, the bonding hand structure $z = re^{i\theta}$ is changed as follows.

$$z' = ze^{i\varphi(h)} = re^{i(\theta+\varphi(h))} \quad (4)$$

With this change, its energy structure, that is, its energy level change from (e_0, e_1) to (e'_0, e'_1).

$$e'_0 = \min(r\cos(\theta+\varphi(h)), r\sin(\theta+\varphi(h))) \quad (5)$$

$$e'_1 = \max(r\cos(\theta+\varphi(h)), r\sin(\theta+\varphi(h))) \quad (6)$$

2.3 Reaction between two atoms

If the hand of atom α and one of atom β are to bond with each other, the possibility for bonding is calculated as follows.

Bonding hands of atom α are to be regarded as $z_i = r_i e^{i\theta_i}$ $(i = 1, \cdots, hd(\alpha))$

$$z'_i = z_i e^{i\varphi(\beta)} \quad (7)$$

and bonding hands of atom β are set similarly.

At the time of bond, under the assumption that the energy states of every hand are transited to the ground state at the new energy level on being operated on by the other. The sum of all energy changes relating to both atom α and β is calculated as follows.

$$\Delta E = \sum_{j \in \alpha,\beta} (e'_0(j) - e'_{s_j}(j)) \quad (8)$$

If the sum of all energy change ΔE and activation energy ΔE_f holds following condition,

$$\Delta E + \Delta E_f < 0 \quad (9)$$

then both hands are bonded with each other. Bonding makes the energy structure more stable as a whole. And then, α's bonding hand structure θ_i and β's θ_j are updated as follows.

$$\theta_i \Leftarrow \theta_i + \varphi(\beta) \quad (i = 1, \cdots, hd(\alpha)) \quad (10)$$

$$\theta_j \Leftarrow \theta_j + \varphi(\alpha) \quad (j = 1, \cdots, hd(\beta)) \quad (11)$$

2.4 Reaction between atom and molecule

When atom and molecule are bonded, energy structure in the molecule is changed in the same way as the reaction between the two atoms, as the result, it may cause separation of molecule. Separation changes the structure by $-\varphi$. The possibility of separation is calculate as follows.

When atom α and atom β which is a member of the molecule bond together, and defining $conc(a(\beta))$ as an atom which has previously bonded with atom β, if $conc(a(\beta))$ exists and the following condition is hold, the connection between atoms is broken.

$$e_{s_j}(j) + e_{s_k}(k) > e'_1(j) + e'_1(k) \quad (12)$$

$e_{s_j}(j)$: β's energy before separation
$e_{s_k}(k)$: $conc(a(\beta))$'s energy before separation
$e'_1(j)$: β's exsited energy after separation
$e'_1(k)$: $conc(a(\beta))$'s excited energy after separation

β's bonding hand θ_j and $conc(a(\beta))$'s hand θ_k are update by $-\varphi$ inversely at the bond of atoms.

2.5 Reaction between molecules

Basically algorithm is similar to reaction between atom and molecule.

2.6 Reaction of photon

Photon is energy resource, and moves under no influence of boundary face. A photon ρ is modeled with its energy range γ and phase ϕ as follows.

$$\rho = (\gamma, \phi) \tag{13}$$

When photon hits the bonding hand, if the following conditions are hold, it causes the energy state of hand change from ground to excited.

$$\gamma > \Delta e \quad \text{and} \quad |\phi - \varphi| < \psi \tag{14}$$

Δe: sufficient energy to cause excitation
ψ :parameter which restricts the absorption of photon

When photon hits the bonding hand and gives its energy to the hand, photon's energy γ, so γ decrease Δe.

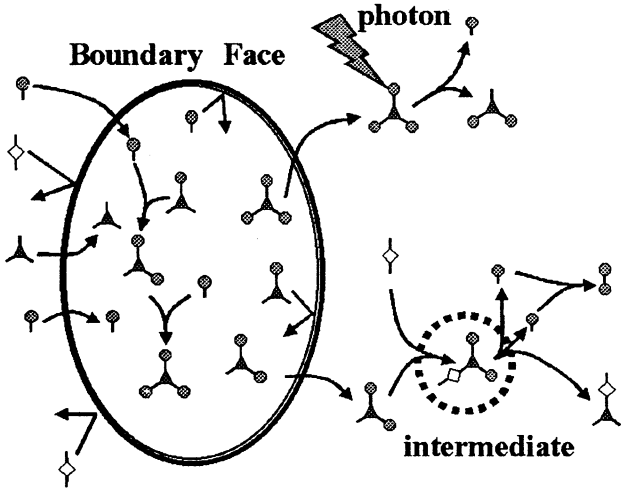


Fig.1 Reaction of Atomoid with Boundary Face model

3 Introducing boundary face

This section presents functional boundary face which we introduce into Atomoid. Boundary faces have peculiar permeability respectively, so let atoms and molecules which match permeability only through. We expect these boundary faces make hierarchical structure.

3.1 Permeability of boundary face

The boundary face has a feature that permeable number of atoms as to every kind of atom. If the atom or molecule whose composition is in permeable domain of the boundary face, it can pass through this face. We provide two permeability types, one is limited permeability, and the other is limited impermeability. Moreover the permeability of the boundary face is different between inside and outside of the boundary face. A boundary face M_i whose face number is $i (i = 1, \cdots)$ is described as follows.

$$M_i = (\alpha_{k_{in}}, \alpha_{k_{out}}, \beta_{k_{in}}, \beta_{k_{out}}, \sigma_{k_{in}}, \sigma_{k_{out}} | k = 1, \cdots, M) \tag{15}$$

$$\sigma = \begin{cases} 0 & : \text{limited permeability} \\ 1 & : \text{limited impermeability} \end{cases}$$

α : upper bounding of limited domain
β : lower bounding of limited domain

For example, the molecule whose components are $N(a_1)$ pieces of atom a_1 and $N(a_2)$ pieces of atom a_2 can pass through the boundary face that is set $\sigma_{1_{out}} = 0, \sigma_{2_{out}} = 1$ from outside of the face to inside, if following condition are hold.

$$\alpha_{1_{out}} < N(a_1) < \beta_{1_{out}} \tag{16}$$

$$\alpha_{2_{out}} > N(a_1) \quad or \quad \beta_{2_{out}} < N(a_1) \tag{17}$$

3.2 Generation and removal of the boundary face

Generation and removal of the boundary face depend on the number of atoms in the face. If the number of atoms in the face decrease under the limit of removal($L_{k_{rm}}$ | k : face number), then the face is removed. On the other hand, if the number of atoms in the boundary face increase over the limit of generation($L_{k_{gn}}$ | k : face number), then new boundary face is generated in the face. Permeability, limit of removal and limit of generation of generated face are determined in random. The range of each parameter is shown at Table.2 in section4.

3.3 Change of the boundary face

When the atom or molecule pass through the boundary face, each permeability of α_k or β_k and σ_k are changed randomly with probability P_{fa}. Furthermore, the removal limit $L_{k_{rm}}$ and the generation limit $L_{k_{gn}}$ change at the same time.

4 Simulations

At this simulation, we confirm the behavior of boundary face model and investigate the influence of

peculiar permeability. Therefore, we simulated two cases as follows.

- boundary face has peculiar permeability
- boundary face has unlimited permeability

4.1 Parameter setting

Parameter of this simulation is shown in Table.1,2. Table.2 indicates the range of parameter setting. These parameters are set randomly in this range.

kind of atoms	4
r and θ of atoms	random
ϕ of photons	random
population	10000
activation energy	$\Delta E_f = 1.0$
threshold for absorbing photons	$\psi = \frac{\pi}{6}$
probability of permeability change	$P_{fa} = 0.001$

Table.1 : Parameters of the simulation

α and β	$0 \sim 4$
L_{rm}	0 ~Population / 10
L_{gn}	0 ~Population / 10 but $L_{rm} < L_{gn}$

Table.2 : Managing Parameters of Peculiar Permeability

4.2 Results and discussions

Fig.2 shows that boundary face which has peculiar permeability tend to contain more atoms than the face with unlimited permeability. Moreover, to survey in detail, we give the number of atoms in the face at the 10000th step Fig.3. This figure shows that the peak of the number of atoms in the face with peculiar permeability is biased toward large size as compared with the case which the face has unlimited permeability. The reason of this result is considered as follows. The boundary face with peculiar permeability has different permeability between its inside and outside, and therefore, there are some kinds of atoms or molecules which come into inside of the face easily, and go out to outside difficulty. If these kinds of atoms or molecules exist at the outside of face in large, the face takes in atoms or molecules effectively, so keeps a lot of atoms or molecules in itself relatively to the face with unlimited permeability. Conversely, if the face has the feature that is easy to go out and difficult to come in, then the face emits atoms and molecules rapidly and is removed, therefore the face having few atoms does not exist much more.

Thus the face with peculiar permeability will gather atoms and molecules which is matched its feature, so make a specific environment in the face. If such phenomenon occurred in the face, we can pick up the substructure in the face.

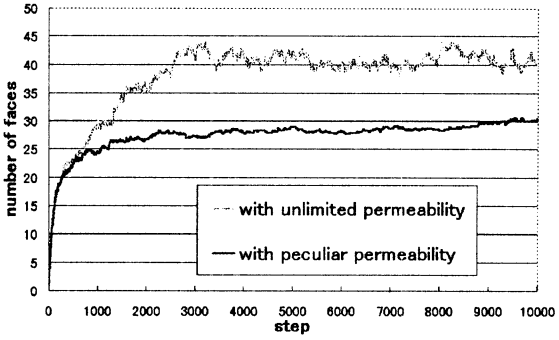


Fig.2 The average of number of faces in the system (The value in this figure is average of five trials)

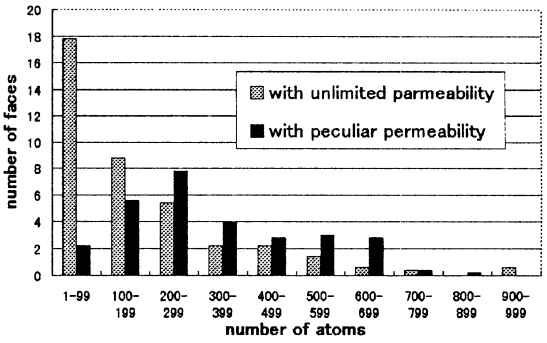


Fig.3 The average of distribution the number of atoms in the face at the 10000th step (The value in this figure is average of five trials)

5 Conclusion

In this paper, we introduce the concept of boundary face into reaction-formation model called "Atomoid", and inspect the behavior of such boundary face model and influence of peculiar permeability through the simulation.

References

[1] Shinichiro YOSHII, Hiroaki INAYOSHI and Yukinori KAKAZU: Atomoid: A New Prospect in Reaction-Formation System Spontaneous Hypercycles Guided by Dissipative Structural Properties, Christopher G.Langton and Katunori Shimohara (Ed.), Artificial Life V, pp.418-425(1996).

[2] Wolfgang Banzhaf Self-organisation in a system of binary strings, Rodney A.Brooks and Pattie Maes (Ed.),Artificial LifeIV, pp.109-118(1994)

Proc. of Third Int. Symp. on Artificial Life, and Robotics (AROB III' 98),
Oita, Japan, 19-21, January, 1998,

UNCERTAIN VARIABLES AND LEARNING ALGORITHMS IN KNOWLEDGE-BASED CONTROL SYSTEMS

Z. Bubnicki

Institute of Control and Systems Engineering,
Wroclaw University of Technology,
Wyb. Wyspianskiego 27, 50 – 370 Wroclaw, POLAND
phone: +48 (071) 320 33 28 , +48 (071) 21 62 26 ; fax: +48 (071) 320 38 84
email: bubnicki@ists.pwr.wroc.pl

Keywords: knowledge-based systems, learning systems, uncertain systems, uncertain variables

Abstract

The paper concerns a class of knowledge-based control systems with unknown parameters in the knowledge representation describing the plant. For the deterministic case the logic-algebraic method of the determination of the control decisions has been developed. The purpose of this paper is to present an extension of this method for the case with unknown parameters. In the first part an approach based on uncertain variables is presented. In the second part the method and algorithms of the current knowledge updating in the learning system are proposed. The main idea of this approach consists in step by step estimation of the unknown parameters in the knowledge representation, using the successive values of the control decisions and their results. This concept may be considered as an extension of the known ideas of identification and adaptation for the traditional case [1,4].

1. Introduction

Logic-algebraic method has been developed for a class of knowledge-based systems with a logical knowledge representation [2,3,7,8,11,14]. In this approach the knowledge representation is considered as an extension of a traditional mathematical model. In the traditional case for a static plant described by a function $y = \Phi(x)$ where x, y are input and output vectors, respectively – the analysis problem consists in finding the value y for the given value x , and in the decision making problem one should find the decision x for the given value y. In our case the plant is described by a set of relations which have the form of the facts F , i.e. the logical formulas concerning x, y and some additional variables. The analysis problem consists in finding the output property (i.e. the logical formula F_y concerning y) for the given input property F_x concerning x , and in the decision making problem one should find the logical formula F_x for the given formula F_y. The main idea of the logic-algebraic method consists in replacing individual reasoning concepts based on inference rules by unified algebraic procedures based on the rules in two-value logic algebra. The results may be considered as a unification and generalisation of the different reasoning procedures.

The purpose of this paper is to present an extension of the logic-algebraic approach for the systems with unknown parameters in the knowledge representation. In the first part an approach based on the definition of so called uncertain variables is presented. The uncertain (or approximate) variables [9,12,15] – related to random and fuzzy variables – are based on uncertain logics and are described by the certainty factors (or certainty distributions) which correspond to probabilities (or probability distributions) for the random variables or to membership functions for the fuzzy numbers. The second part of the paper is concerned with the situation when we have no *a priori* knowledge on the unknown parameters. In this case the method and algorithms of the knowledge validation and updating in the learning control system are proposed. The main idea of this approach consists in step by step estimation of the unknown parameters in the knowledge representation, using the successive values of the control decisions and their results. This concept may be considered as an extension of the known ideas of identification and adaptation for the traditional case [1,4].

2. Knowledge-based control for deterministic case

Let us introduce the following notation for the plant under consideration:

1) x, y, c – input, output and unknown parameter vector, respectively; $x \in X$, $y \in Y$, $c \in C$; **2)** $\alpha_{xi}(x,c)$ – simple formula (i.e. simple property) concerning x and c, e.g. $\alpha_{x1}(x,c) =$ "$x^{\mathrm{T}}x < c^{\mathrm{T}}c$" where x and c are column vectors, $i = 1, 2, \ldots, n_1$; **3)** $\alpha_{wr}(x,y,c)$ – simple formula concerning x, y and c, $r = 1, 2, \ldots, n_2$; **4)** $\alpha_{ys}(y,c)$ – simple formula concerning y and c, $s = 1, 2, \ldots, n_3$; **5)** $\alpha_x = (\alpha_{x1}, \ldots, \alpha_{xn_1})$, $\alpha_w = (\alpha_{w1}, \ldots, \alpha_{wn_2})$, $\alpha_y = (\alpha_{y1}, \ldots, \alpha_{yn_3})$; **6)** $\alpha = (\alpha_x, \alpha_w, \alpha_y)$ – sequence of all simple formulas in the knowledge representation; **7)** $F_j(\alpha)$ – j-th fact given by an expert. It is a logic formula composed with the subsequence of α and the logic operations: $\vee$ – **or**, $\wedge$ – **and**, $\neg$ – **not**, $\rightarrow$ – **if** ... **then**, $j = 1, 2, \ldots, k$. E.g. $F_1 = \alpha_1 \wedge \alpha_2 \rightarrow \alpha_3$, where α_1 = "$x^{\mathrm{T}}x < c^{\mathrm{T}}c$", α_2 = "the temperature is small", α_3 = "$y^{\mathrm{T}}y > 2c^{\mathrm{T}}c$";
8) $F(\alpha) = F_1(\alpha) \wedge F_2(\alpha) \wedge \ldots \wedge F_k(\alpha)$; **9)** $F_x(\alpha_x)$ – input property, i.e. the logic formula using α_x; **10)** $F_y(\alpha_y)$ – output property; **11)** $a_m \in \{0, 1\}$ – logic value of α_m, $m = 1, 2, \ldots, n$; $n = n_1 + n_2 + n_3$;
12) $a = (a_1, a_2, \ldots, a_n)$; **13)** $F(a)$ – the logic value of $F(\alpha)$. All facts given by an expert are assumed to be true, i.e. $F(a) = 1$.

Decision making (control) problem: For the given $F(\alpha)$ and the output property $F_y(\alpha_y)$ find the best input property (control decision) $F_x(\alpha_x)$ such that the implication $F_x \rightarrow F_y$ is satisfied. If it is satisfied for F_{x1} and F_{x2}, and $F_{x2} \rightarrow F_{x1}$ then F_{x1} is better than F_{x2}.
It may be shown [4,7] that finding F_x is reduced to solving two sets of equations:

$$\left.\begin{aligned} F(a_x, a_w, a_y) &= 1 \\ F_y(a_y) &= 1 \end{aligned}\right\} \quad \text{and} \quad \left.\begin{aligned} F(a_x, a_w, a_y) &= 1 \\ F_y(a_y) &= 0 \end{aligned}\right\} \qquad (1)$$

with respect to a_x. If S_{x1} denotes the set of all solutions of the first equation (i.e. the set of all a_x for which there exists a_w, a_y such that F=1 and F_y=1), and S_{x2} denotes the set of all solutions of the second equation – then F_x is determined by $S_x = S_{x1} - S_{x2}$. In general, solving the equations (1) requires to test all 0-1 sequences a. The algorithm generating the solution may be more effective when the following **decomposition** of the set of facts is applied:

$$F(a) = \bar{F}_1(\bar{a}_0, \bar{a}_1) \wedge \bar{F}_2(\bar{a}_1, \bar{a}_2) \wedge \ldots \\ \ldots \wedge \bar{F}_p(\bar{a}_{p-1}, \bar{a}_p) \wedge \ldots \wedge \bar{F}_N(\bar{a}_{N-1}, \bar{a}_N)$$

where $\bar{a}_0 = (a_x, a_y)$, $\bar{F}_p$ is the conjunction of all facts containing the variables from the sequence $\bar{a}_{p-1}$ and $\bar{a}_p$ is the sequence of all other variables in $\bar{F}_p$ ($p = 1, 2, \ldots, N$). Then the set $\bar{S}_0$ of all solutions (a_x, a_y) of the equation $F(a_x, a_w, a_y) = 1$ may be determined by the following recursive procedure

$$\bar{S}_{p-1} = \left\{ \bar{a}_{p-1} \in S_{p-1} : \bigvee_{\bar{a}_p \in \bar{S}_p} \left[\bar{F}_p(\bar{a}_{p-1}, \bar{a}_p) = 1 \right] \right\} \qquad (2)$$

where S_p is the set of all $\bar{a}_p$, $p = N, N-1, \ldots, 1$, $\bar{S}_N = S_N$. Then, for the given $\bar{S}_p$ (starting from $p=N$) the next set $\bar{S}_{p-1}$ is generated by testing $\bar{F}_p$, i.e. by finding all $\bar{a}_{p-1}$ for which there exists $\bar{a}_p \in \bar{S}_p$ such that $\bar{F}_p = 1$. Having $\bar{S}_0$ we can determine S_x (and consequently F_x):

$$S_x = \left\{ a_x : \bigvee_{a_y \in S_y} (a_x, a_y) \in \bar{S}_0 \right\} - \left\{ a_x : \bigvee_{a_y \notin S_y} (a_x, a_y) \in \bar{S}_0 \right\}$$

where

$$S_y = \left\{ a_y : F_y(a_y) = 1 \right\}.$$

3. Knowledge-based control for uncertain case

Now we assume that the parameter c is unknown and that c is a value of so called "uncertain variable". The definition of the **uncertain variable** is based on multi-value logics and the definition of certainty factor. Let us consider a set X with a variable $x \in X$ and a property (a statement) $\varphi(x)$ concerning x. In two-value logics $w[\varphi(x)] \in \{0,1\}$ where w is the logical value of $\varphi(x)$. In multi-value logics $w[\varphi(x)] \in [0,1]$. The value $w[\varphi(x)] \triangleq v[\varphi(x)]$ will be called here a **certainty factor** of the property $\varphi(x)$. The following operations will be used in the next considerations:

$$v(\neg\varphi) = 1 - v(\varphi), \quad v(\varphi_1 \vee \varphi_2) = \max[v(\varphi_1), v(\varphi_2)], \\ v(\varphi_1 \wedge \varphi_2) = \min[v(\varphi_1), v(\varphi_2)].$$

Assume now that X is a subspace of m-dimensional real number vector space, i.e. $X \subseteq R^m$.
Definition: The uncertain variable $\bar{x}$ is defined by the set of its values X and a certainty distribution $h(x)$. The certainty distribution $h(x)$ for a fixed x denotes the certainty factor of the property: "$\bar{x}$ is approximately equal to x", i.e. $h(x) = v(\bar{x} \cong x)$ □
Then

$$v(\bar{x} \in D_x) = \max_{x \in D_x} h(x).$$

Let us turn now to our control problem for the knowledge representation described in Sec.2. The unknown parameter c is assumed to be a value of the uncertain variable $\bar{c}$ described by the certainty distribution $h(c)$. The knowledge representation consists of $F(\alpha)$ and

$h(c)$. The properties $F_x(\alpha_x)$ and $F_y(\alpha_y)$ determine the relations

$$R_x(x,c)=\{(x,c)\in X\times C:\ F_x[a_x(x,c)]=1\}\ , \quad (3)$$

$$R_y(y,c)=\{(y,c)\in Y\times C:\ F_y[a_y(y,c)]=1\}\ . \quad (4)$$

The result R_x may be used to determine the decision x for which the desirable output property is satisfied with the largest certainty factor. For the fixed x, the certainty factor of the property $(x, c)\tilde{\in}R_x$

$$v(x)=\max_{c\in D_c(x)} h(c) \quad (5)$$

where $$D_c(x)=\{c\in C:(x,c)\in R_x\} \quad (6)$$

Since the implication $F_x\rightarrow F_y$, i.e. $(x, c)\in R_x\rightarrow (y, c)\in R_y$ has the certainty factor = 1, then (5) is the certainty factor of output property $(y, c)\tilde{\in}R_y$ for the given x. If $x\notin\Delta_x$ (where Δ_x is the set of all possible x, i.e. all x for which there exists c such that $(x, c)\in R_x$) then $D_c(x)$ is an empty set and $v(x) = 0$. The final result is the control decision x_{opt} such that

$$v(x_{opt})=\max_{x\in\Delta_x}\left[\max_{c\in D_c(x)} h(c)\right]\ . \quad (7)$$

4. Example for the system with uncertain parameter

Let us consider a simple example with $x, y, c\in R^1$. The simple formulas: $\alpha_{x1}=\alpha_1=$ "$x\le 3c$", $\alpha_{x2}=\alpha_2=$ "$x^2+c^2\le 1$", $\alpha_{w1}=\alpha_3=$ "pressure is high", $\alpha_{w2}=\alpha_4=$ "humidity is small", $\alpha_{w3}=\alpha_5=$ "temperature is less than $x+y+c$", $\alpha_{y1}=\alpha_6=$"$y^2+(c-\frac{1}{2})^2\le\frac{1}{4}$", $\alpha_{y2}=\alpha_7=$"$-c\le y\le c$".

The knowledge representation: $F_1=\alpha_1\wedge(\alpha_4\vee\neg\alpha_6)$, $F_2=\alpha_2\wedge\alpha_4\rightarrow\alpha_6$, $F_3=\neg\alpha_4\vee\neg\alpha_3\vee\alpha_5$, $F_4=\alpha_4\wedge(\alpha_3\vee\neg\alpha_5)$, $F_5=(\alpha_4\wedge\neg\alpha_2)\rightarrow\alpha_7$, c is a value of an uncertain variable $\bar{c}$ and $h = 2c$ for $0\le c\le\frac{1}{2}$, $h=-2c+2$ for $\frac{1}{2}\le c\le 1$, $h = 0$ otherwise. E.g. F_3 means: "humidity is not small or pressure is not high or temperature is less than $x+y+c$". Substituting a_i in place of α_i we obtain the expressions $F_i(a)$. In our case $\bar{a}_0=(a_x, a_y)=(a_1, a_2, a_6, a_7)$ and as a result of the decomposition we have $\bar{F}_1=F_1\wedge F_2\wedge F_5$, $\bar{F}_2=F_3\wedge F_4$, $\bar{a}_1=a_4$, $\bar{a}_2=(a_3, a_5)$. Using (2) one can obtain $\bar{S}_0=\{(1,1,1,1),(1,1,1,0),(1,0,1,1),(1,0,0,1)\}$.

If $F_y=a_6$ then $F_x=a_1\wedge a_2$, i.e.: If $x\le 3c$ and $x^2+c^2\le 1$ then $y^2+(c-\frac{1}{2})^2\le\frac{1}{4}$.

$$R_x(x,c)=\{(x,c):\ x\le 3c\ \text{ and }\ x^2+c^2\le 1\},$$

$$R_y(y,c)=\left\{(y,c):\ y^2+(c-\frac{1}{2})^2\le\frac{1}{4}\right\}.$$

It is easy to obtain $\Delta_x=\left[-1,\frac{3}{\sqrt{10}}\right]$ and for $x\in\Delta_x$ according to (6) $D_c(x)=\left[\frac{x}{3},\sqrt{1-x^2}\right]$. The maximization in (5) leads to the following result

$$v(x)=\begin{cases}1 & \text{for } \frac{-\sqrt{3}}{2}\le x\le\frac{\sqrt{3}}{2}\\ 2\sqrt{1-x^2} & \text{otherwise in } \Delta_x\end{cases}$$

Finally, as the control decision x_{opt} we can choose any value from $\left[\frac{-\sqrt{3}}{2},\frac{\sqrt{3}}{2}\right]$ and the output property is satisfied with the certainty factor = 1.

5. Learning control system

The method presented in Sec.2 is based on *a priori* knowledge on c: c is an uncertain variable with the known certainty distribution $h(c)$. Now we assume that the parameter c has the value $c=\bar{c}$, $\bar{c}$ is unknown and we have no additional *a priori* knowledge on our parameter. The main idea of the method presented in this section consists in step by step knowledge updating in the learning control system with control decisions based on the result of knowledge evaluation. In Sec.3, for the given requirement $D_y(c)$ we obtain the result $D_x(c)$ such that

$$x\in D_x(c)\rightarrow y\in D_y(c)$$

$$x\notin D_x(c)\rightarrow y\notin D_y(c)$$

where

$$D_x(c)=\{x\in X: F_x(a_x)=1\}\ ,\quad D_y(c)=\{y\in Y: F_y(a_y)=1\}.$$

Assume for the further consideration that the parameter c does not occur in α_y, i.e. in the formulation of D_y, and that $D_x(c)$ is a continuous and closed domain in X. To know if x_i (i = 1,2, ... , n, ...) is a correct decision it is necessary to put x_i at the input, to measure the output y_i and to prove if $y_i\in D_y$. If $y_i\in D_y$ then $x_i\in D_x(\bar{c})$, if $y_i\notin D_y$ then $x_i\notin D_x(\bar{c})$. We propose here two concepts of the knowledge validation and updating.

A. Off-line knowledge validation and updating

According to this approach two time intervals are introduced. In the first interval the knowledge validation and updating is based on the sequence of inputs x_n chosen

randomly from X and the sequence of corresponding outputs y_n. In the second interval the control is based on the result of learning, i.e. x_n are chosen randomly from $D_x(c_n)$ where c_n is the value of $\bar{c}$ obtained at the end of learning. Let us denote by $\bar{x}_i$ the subsequence for which $y_i \in D_y$ and by $\hat{x}_i$ the subsequence for which $y_i \notin D_y$, and introduce the sets:

$$\bar{D}_c(n) = \{ c \in C : \text{ each } \bar{x}_i \in D_x(c) \},$$
$$\hat{D}_c(n) = \{ c \in C : \text{ each } \hat{x}_i \in X - D_x(c) \}.$$

The set

$$\bar{D}_c(n) \cap \hat{D}_c(n) \triangleq \Delta_c(n) \qquad (8)$$

is proposed here as the estimation of $\bar{c}$. E.g. for the plant with k inputs, one parameter c and $D_x(c)$ determined by $(x^{(1)})^2 + (x^{(2)})^2 + \ldots + (x^{(k)})^2 \le c^2$ where $x = [\, x^{(1)} \ldots x^{(k)} \,]^T$ – we have $\bar{D}_c(n) = [c_{\min,n}, \infty)$, $\hat{D}_c(n) = [0, c_{\max,n})$ and $\Delta_c(n) = [\, c_{\min,n}, c_{\max,n} \,)$ where

$$c_{\min,n}^2 = \max_{i \in \overline{1,n}} \bar{x}_i^T \bar{x}_i, \quad c_{\max,n}^2 = \min_i \hat{x}_i^T \hat{x}_i.$$

Assume that x_n is chosen randomly from X with probability density $f(x)$. If $f(x) > 0$ for each $x \in X$ and for each $c \ne \bar{c}$ $D_x(c) \ne D_x(\bar{c})$ then it may be proved that $\Delta_c(n)$ converges to $\{\bar{c}\}$ with probability 1.

Consequently, we can use the following recursive **learning algorithm** for $n > 1$:

Choose randomly x_n, put at the input, measure y_n. If $y_n \in D_y$ – **knowledge validation for $x_n = \bar{x}_n$**

Prove if

$$\bigwedge_{c \in \bar{D}_c(n-1)} [\, x_n \in D_x(c) \,].$$

If yes then $\bar{D}_c(n) = \bar{D}_c(n-1)$. If not – determine new $\bar{D}_c(n)$.

Knowledge updating for $x_n = \bar{x}_n$

$$\bar{D}_c(n) = \{ c \in \bar{D}_c(n-1) : \; x_n \in D_x(c) \}.$$

Put $\hat{D}_c(n) = \hat{D}_c(n-1)$.

If $y_n \notin D_y$ – **knowledge validation for $x_n = \hat{x}_n$**

Prove if

$$\bigwedge_{c \in \hat{D}_c(n-1)} [\, x_n \in X - D_x(c) \,].$$

If yes then $\hat{D}_c(n) = \hat{D}_c(n-1)$. If not – determine new $\hat{D}_c(n)$.

Knowledge updating for $x_n = \hat{x}_n$

$$\hat{D}_c(n) = \{ c \in \hat{D}_c(n-1) : \; x_n \in X - D_x(c) \}.$$

Put $\bar{D}_c(n) = \bar{D}_c(n-1)$, $\Delta_c(n) = \bar{D}_c(n) \cap \hat{D}_c(n)$.

For $n = 1$, if $x_1 = \bar{x}_1$ determine

$$\bar{D}_c(1) = \{ c \in C : x_1 \in D_x(c) \},$$

if $x_1 = \hat{x}_1$ determine

$$\hat{D}_c(1) = \{ c \in C : \; x_1 \in X - D_x(c) \}.$$

B. Knowledge validation and updating in learning control system

Now the successive x_n is the control decision based on the current knowledge of the plant, i.e. x_n is chosen randomly from $D_x(c_n)$ where c_n is chosen randomly from $\Delta_c(n)$. The control algorithm is the same as in point A with the difference that x_n is chosen from $D_x(c_n)$ and not from X. The block scheme of the learning control system is presented on Fig.1. For the random choice of c_n and x_n the generators G_1 and G_2 of the random numbers are required. Their probability distributions are precised currently for $\Delta_c(n)$ and $D_x(c_n)$.

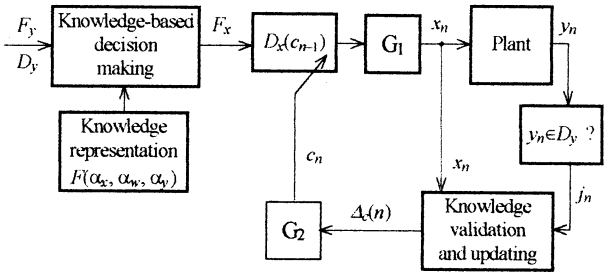


Fig. 1

6. Example for the learning system

Consider the example from Sec.4 with the same form of the facts F_i and with the following simple formulas: $\alpha_{x1} = \alpha_1 =$ "$(x^{(1)})^2 + (x^{(2)})^2 \le c^2$", $\alpha_{x2} = \alpha_2 =$ "$x^{(1)} \le 3c$", $\alpha_{w1} = \alpha_3 =$ "pressure is high", $\alpha_{w2} = \alpha_4 =$ "humidity is small", $\alpha_{w3} = \alpha_5 =$ "temperature is less than $x^{(2)} + y + c$", $\alpha_{y1} = \alpha_6 =$ "$y \ge 5$", $\alpha_{y2} = \alpha_7 =$ "$2 \le y \le 3$". For $F_y = a_6 \vee a_7$ one can obtain $F_x = a_1$. The result is then as follows: If $(x^{(1)})^2 + (x^{(2)})^2 \le c^2$ then $2 \le y \le 3$ or $y \ge 5$. In our example $D_x(\bar{c})$ is determined by the inequality

$$(x^{(1)})^2 + (x^{(2)})^2 \le \bar{c}^2,$$

$x_n = (x_n^{(1)}, x_n^{(2)}) = \bar{x}_n$ if x_n satisfies this inequality,

$$\bar{D}_c(n) = [c_{\min,n}, \infty), \quad \hat{D}_c(n) = [0, c_{\max,n})$$

where

$$c_{\min,n}^2 = \max_i \left[(\bar{x}_i^{(1)})^2 + (\bar{x}_i^{(2)})^2 \right],$$
$$c_{\max,n}^2 = \min_i \left[(\hat{x}_i^{(1)})^2 + (\hat{x}_i^{(2)})^2 \right],$$

$$\Delta_c(n) = [\, c_{\min,n} \,,\, c_{\max,n} \,) \,.$$

The control and learning process has been simulated for the different probability distributions $f(x)$ and the different numerical values of x_1 and c. The results of the simulations for $c = 2$ and for version B are presented on Fig.2. The distribution $f(x)$ was constant in the corresponding circle and equal to 0 outside this circle; c_n is chosen randomly with the rectangular distribution for $c \in [c_{\min,n} \,,\, c_{\max,n}]$.

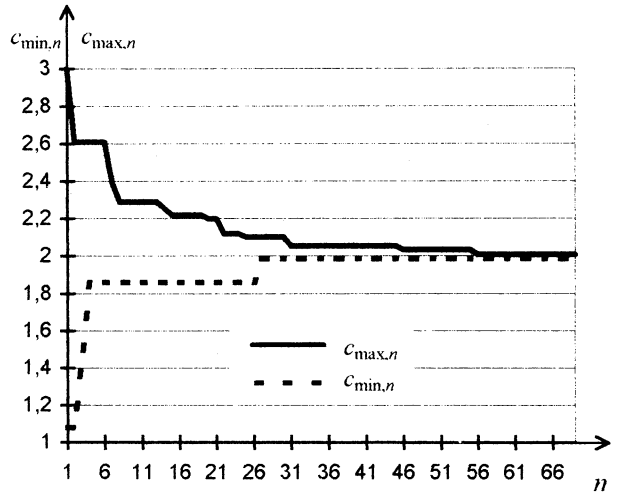


Fig. 2

7. Final remarks

In the first part of the paper it was shown how to use *a priori* information on the knowledge parameters in the form of the certainty distribution $h(c)$. In the second part it was described how to update the knowledge and to use the current knowledge in closed-loop learning control system without *a priori* information on the knowledge parameters. It may be interesting to combine these two approaches and to show how to update step by step the *a priori* information in the form of certainty distribution, probability distribution or membership function) using the successive values $(x_n \,,\, y_n)$ in learning system.

The logic-algebraic method in the deterministic version has been applied for specific problems of pattern recognition and operation systems [5,6] and for the dynamical knowledge representation [10]. Consequently, the ideas and algorithms described in this paper may be extended for this case with the unknown parameters in the knowledge representation.

It is important to note that the algorithms based on the logic-algebraic method may be connected with great computational difficulties for the high size of the problems. The application of the decomposition mentioned in Sec.2 leads to the significant improvement of the effectiveness (decrease of the execution time). The further increasing of the effectiveness may be achieved when the multiprocessor system is applied to execute the logic-algebraic algorithms [13].

References

[1] Z. Bubnicki, "Identification of Control Plants", Elsevier, Oxford, Amsterdam, New York, 1980.

[2] Z. Bubnicki, "Algebraic approach to some class of reasoning problems", *Proc. of IFIP Workshop on Automated Reasoning*, Beijing, pp. 12-16, 1992.

[3] Z. Bubnicki, "Decomposition of a system described by logical model", In: Cybernetics and System Research, World Scientific, London, New Jersey, pp. 121-128, 1992.

[4] Z. Bubnicki, "New problems and directions in the area of control and identification for knowledge-based systems", In: Modelling, Identification and Control, Acta Press, Zurich, pp. 1-4, 1993.

[5] Z. Bubnicki, "Knowledge-based approach as a generalization of pattern recognition problems and methods", *Systems Science*, Vol. 19 , No. 2, pp. 5-21, 1993.

[6] Z. Bubnicki, "Logic-algebraic foundations of knowledge-based operation systems", *Proc. of IX Int. Conf. on Systems Eng.*, Las Vegas, pp. 360-364, 1993.

[7] Z. Bubnicki, "Logic-algebraic method for knowledge based control systems", In: Modelling, Identification and Control. Acta Press, Zurich, pp. 253-256, 1995.

[8] Z. Bubnicki, "Logic-algebraic foundations of a class of knowledge based control systems", *Proc. of II World Automation Congress*, TSI Press, Montpellier, pp. 89-94, 1996.

[9] Z. Bubnicki, "Logic-algebraic approach to a class of knowledge based fuzzy control systems", *Proc. of European Control Conference*, Brussels, 1997.

[10] Z. Bubnicki, "Logic-algebraic method for a class of dynamical knowledge-based systems", *Proc. of IMACS Congress*, Berlin, pp. 101-106, 1997.

[11] Z. Bubnicki, "Logic-algebraic method for a class of knowledge based systems", *Proc. of Eurocast 97*, Lecture Notes on Computer Science, Springer Verlag, 1997 (to be published).

[12] Z. Bubnicki, "Uncertain variables in knowledge-based systems", *Proc. of IASTED Int. Conf. on Intelligent Systems and Control*, Halifax, Canada, 1998 (to be published).

[13] Z. Bubnicki, "Structures of distributed expert systems with parallel processing", *Proc. of XII Int. Conf. on Systems Eng.*, Coventry, 1997.

[14] Z. Bubnicki, "Logic-algebraic method for knowledge-based relation systems", *Systems Analysis Modelling and Simulation*, 1998 (to be published).

[15] Z. Bubnicki, "Uncertain logics, variables and systems", *Proc. of The Third Workshop of The International Institute for General Systems Studies* (IIGSS), Beidaihe, Qinhuangdao, China, 1998 (to be published).

Proc. of Third Int. Symp. on Artificial Life, and Robotics (AROB III' 98),
Oita, Japan, 19-21, January, 1998,

Cognitive Robotics: A New Approach to Artificial Intelligence

Thomas Christaller
GMD- German National Research Center for Information Technology
D-53754 Sankt Augustin
http://www-fit-ki.gmd.de/

Abstract

This paper describes a research program about how to achieve artificial intelligence by building robots. It is part of the behavior-oriented AI approach but differs in some of its hypotheses and the methodological approach from others.

Key words: behavior-based robotics, artificial intelligence, cognition.

1 Introduction

(Natural) Intelligence is a phenomena, which we (until now) seem only be able to observe for biological systems, i.e. living forms, especially for primates like the homo sapiens sapiens. Like for any biological phenomena we can assume that intelligence appears for different living forms and this to different degrees. It seems very unlikely, that we–the human beings– should be the only living form with intelligence and there is of course the question, if there are not more intelligent living forms than us. Intelligence is seen as an achievement of the organ brain. A survey of the actual state of neural science is given by [11]. But how can we start on this basis and design and construct an artifically intelligent artefact?

2 Artificial Intelligence. Some definitions

In a recent paper about "Strategic directions in Artificial Intelligence" [5] four scientific and practical aims are given as a definition of Artificial Intelligence research:

> constructing intelligent machines, whether or not these operate in the same way as people do;
>
> formalizing knowledge and mechanizing reasoning, both commonsense and refined expertise, in all areas of human endeavor;
>
> using computational mdoels to understand the psychology and behavior of people, animals, and artifical agents;
>
> and making working with computers as easy and helpful as working with skilled, cooperative, and possibly expert people.

This definition or characterization of the field of AI makes really sense if only one underlying concept can be grasped: what is human (or more general: biological or natural) intelligence? In this strategic paper and to our knowledge in all of the textbooks about AI there is no discussion about the natural phenomena of intelligence. Only Matt Ginsburg goes into a deeper discussion about this issue as can be seen by the following citations:

> Artificial Intelligence is the enterprise of constructing an intelligent artifact. ...So what is intelligence? As a first cut, let me take the rather egoistical view that tasks demonstrating intelligence are those that people do well. ...There is something else outside the scope of AI that people are good at. People are good at being people. ...AI is the enterprise of constructing a physical-symbol system that can reliably pass the Turing test. In [7, pp.3-17]

He starts with a commonsense definition, questions it but in the end he also joins the mainstream and leaves any discussion about natural intelligence out of his textbook. But before blaming the AI researchers we should have a look into the Cognitive Sciences which are coping with natural intelligence. And there we cannot find any common definition of intelligence but only the understanding that so-called higher mental processes like abstract thinking, representation,

and problem solving are subsumed by the concept of intelligence. This is true also in textbooks about neural sciences like [11] where the brain and all its (known) processes are extensively discussed but only very careful statements are made on these higher level mental processes and there correlation with nervous tissues [11, pp.828-883].

3 Why does it pay off to be intelligent?

With having only a commonsense definition of intelligence (or cognition) it is of course difficult to create artificial intelligent systems because the only way to tell something about the intelligence of the artefact is to compare it with human intelligence, which is Alan Turings proposal. Could we do better than this?

The answer is yes, we suggest, if we change the question from "What is intelligence?" into "Why does it pay off to be intelligent?". In the latter case we have to consider the fact that intelligence is not for free, e.g. the human brain draws about on third of blood oxygen. Only few living systems can take this burden and utilize it to their fortune. This is already a departure of many approaches in behavior-oriented AI and Artificial Life where survival is the criteria for saying that a behavior is intelligent or not. The difficulty with such an approach is that it depends on the time interval in which a behavior is judged as intelligent or not. In the end, taken the fact that an individual as well as a species has to die, no behavior or all behaviors has to be counted as intelligent.

The following quotation from the work of one of the most successful primatologists may give us a different way of looking at intelligence:

> We suggest that vervets and other primates make good primatologists. They observe social interactions, recognize the relations that exist among others, and classify relationships into types. ...(Primate intelligence) originally evolved to solve social problems and was only later extended to problems outside the social domain. [2]

The need of observing each another is given if the alternatives of reacting or initiating some action in a specific social (and physical) setting is large enough to make it impossible to handle this completely by reflexes or simple stimulus-response schemata.

A very prelimenary answer to "Why does natural intelligence pay-off?" is the following: If an individual can only survive in a social group with individualized social relationships and the variety of possible behaviors is beyond some threshold it must develop intelligence as a means to forecasting the behaviors of other individuals, primarely in the same group, and imagine its own behaviors as possible responses.

The social realm is the major source for the evolution of intelligence. It needs more pressure to transfer the social intelligence into other areas like using and constructing tools, doing science, or developing a global economy. And so it takes no wonder that for biological systems to have intelligence is not a yes-no question but to take a point on a wide continuum.

The consequences for AI are–as many other researchers already said–to build robots to achieve its ultimate goal and consider robots as instances of an artificial life form [12]. To make this a serious effort, one might be forced to let robots be evolved. Today evolution or genetic algorithms are already used to "create" control programs for robots and even take the controller hardware into account using field programmable gate array (FPGA) chips [13]. Nevertheless, the mechatronics and the sensors are still designed and constructed in the old-fashioned engineering way. There are no genes for cognitive robots.

4 Cognitive Robotics

The essence of this research program is to take the findings in science seriously especially about the circumstances, factors, and reasons in which and why cognition and intelligence evolved in nature. But to make it clear from the beginning: We do not believe that robots, whose behaviors are emulating that of ants or similar beings, are a good starting point. And we do not believe that building humanoid robots is an achievable goal.

This is to say that understanding the motor control, e.g. in stick insects, can really be helpful to realize interesting controllers for legged robots [3]. But it is not at all obvious how to do the scaling-up into tasks where intelligence should or must be involved. There are some proposals to build a humanoid robot as means to achieve at a humanoid level of intelligence. The best known is Cog [1]. While it is of course a challenge to emulate a human body as a mechatronic construction this is not the real starting point where intelligence starts to be needed.

The question then is where to start and finding a good set of assumptions is perhaps the most difficult task. In the following two of them are discussed. First, we describe sewage systems as a habitat for cognitive

robots. Second, a methodological approach is sketched based upon experiences with the dynamic system approach in behavior-oriented AI.

4.1 Sewers as natural habitat for artificial intelligence

Communal sewers in Germany amounts to roughly 400,000 km while a town like Hamburg has 5,000 km, a huge infrastructure which must be maintained. One essential task is the inspection which is done today via teleoperated platforms which are connected by a cable with a control unit above ground. The usual distance such a platform can go ahead if there are no curves or obstacles are 100 m. Beyond that the friction of the cable is too high and the platform must be salvaged and brought into the sewer using the next inlet. This procedure is time and personel intensive and therefore costs a lot of money.

The sewers are a challenge for sensors and motors of a robot because there is no natural light source, the material used for the pipes differ widely, and depending on usage and weather conditions a sewer might be nearly dry or flooded. Despite the fact that sewer systems are man-made a lot of unforseen situations may occur: illegal inlets, broken or blocked pipes, undocumented junctions, roots of tree, any type of obstacle.

The major and focussing application for our Cognitive Robotics research is the development of sewer robots, which in the long run should be able to inspect autonomously a sewer. The vision is to develop learnable autonomous sewer inspection robots, which stay for days or even weeks inside the sewage system, cooperating with each another in a team and communicate their findings to human operators. In a feasability study, LAOKOON, we elaborated a ten years research program to achieve this vision [6]. Recently we started the first project, MAKRO, to develop a multi-segmented robot which is capable to drive and navigate autonomously in a cleaned sewer, performing inspection via a video camera, can take usual junctions and steeps up to 30 cm.

To perform controlled experiments a test sewage system was erected in the backyard of the institutes building with a total length of 90 m and most of the standard types of junction. This test system was used to develop a first sewer robot prototype, KURT, which is able to navigate in it [8].

4.2 Self-Organizing Behaviors and Sensors in Robots

In taking physical robots as testbed for AI theories or models means to cope with all sorts of constraints to any type of resource and produce an overall meaningful behavior. One of the first hypothesis we explored is that intelligence in biological systems has been evolved out of social needs in groups of conspecifics and forecasting the very next movements of each another by a kind of inner rehearsal [4].

Therefore we worked upon senso-motoric feedback-loops as building blocks for movements of ever rising complexity. E.g. Sir Arthur is a six-legged robot with 16 degrees of freedom (often behavior-oriented robots have two degrees). It served as a design study for the future sewer robot in MAKRO which may have at least as much degrees as Sir Arthur. By traditional analytical means the control problem is unsolvable. We applied successfully hierarchical Q-learning (a kind of reinforcment learning) such that Sir Arthur first learned how to move one leg and then how to coordinate them.

A major task in building robots is to achieve a rich repertoire of behaviors–robots that can do many interesting things. Current methods basically rely on hand-coding. However, human designers cannot master the interactions of more than, say, 10 behaviors. A mathematical model of the interplay of behaviors has been developed, called "dual dynamics" [10]. Bifurcation theory is applied to explain how behaviors change from one into the other. This gives not only a theoretical foundation to the field, but also a transparent scheme for design. It allows to specify a robots behaviors in ordinary differential equations. Debugging is much facilitated due to the scheme's clarity.

Robots observe their environment, and humans observe robots. Both wish to understand what they observe. In a deep sense, understanding is connected to the ability to predict. The robot understands its environment when it can predict the consequences of its actions; the human understands the robots when he can foresee what it will do. Mathematically, learning to predict from observations is the field of stochastic time series modelling. A new class of such stochastic models has been developed, called observable operator models [9]. These models are more expressive than the current state of the art models, namely, than hidden Markov models. They are also simpler to learn. Where a hidden Markov model requires hours to be approximated, an observable operator model can be aquired in a one-step algorithm in the fraction of a second. This amounts to a veritable breakthrough in time series modeling.

5 Discussion

The Cognitive Robotics research framework presented here consists of three parts:

- Why does it pay off to be intelligent for biological systems? The major hypothesis is, that evolving an intelligence for social needs in a group of conspecifics. In such a group an individual is personally known by the others and the alternatives to act are so high that stimulus-response schemas do not suffice any longer.
- How complex must a habitat be to enforce intelligence? To transfer a social intelligence into other realms a similar complex situation must be given. Our habitat are the communal sewage systems with the great advantage that they have a large practical impact beside the basic research questions we are striving for.
- How can we scale-up the prototypes? Here we propose something like Dual Dynamics for the dynamic system approach in behavior-oriented AI. but right now extensive testing is still missing. We acknowledge that other principles must be developed or applied to rise the complexity of the control programs in a significant way. i.e. there are until now on

Acknowledgements

This work would not be possible if the author had not the chance to discuss aspects of this together with Joachim Hertzberg, Herbert Jaeger, Rolf Pfeifer, Luc Steels, and the members of the Cognitive Robotics group at GMD and the student project about robot construction at the university of Bielefeld.

References

[1] R. A. Brooks and L. A. Stein. Building brains for bodies. *Autonomous Robots*, (1):7–25, 1994.

[2] D. L. Cheney and R. M. Seyfarth. Precis of how monkeys see the world. *Behavioral and Brain Sciences*, 15(1):135–182, 1992.

[3] H. Cruse, C. Bartling, J. Dean, T. Kindermann, J. Schmitz, Michael Schumann, and Hendrik Wagner. Coordination in a six-legged walking system. Simple solutions to complex problems by exploitation of physical properties. In: P. Maes et al. (eds.), *From animals to animats 4.* pp. 84–93, Cambridge (MA), The MIT Press, 1996.

[4] K. Dautenhahn and T. Christaller. *Remembering, rehearsal and empathy: Towards a social and embodied cognitive psychology for artifacts.* In: S. ONuallain et al. (eds.), Two sciences of mind. Readings in cognitive science and consciousness., pages 257–282. John Benjamins, Amsterdam, 1997.

[5] J. Doyle and T. Dean et al. Strategic directions in artificial intelligence. *ACM Computing Surveys*, 28(4):653–670, 1996.

[6] J. Hertzberg et al. BMBF feasability study laokoon (in german). Technical report, BMBF, Bonn, 1996.

[7] M. Ginsberg. *Essentials of Artificial Intelligence.* Morgan Kaufmann, San Francisco, 1993.

[8] J. Hertzberg and F. Kirchner. Landmark-based autonomous navigation in sewerage pipes. *Proc. of the first Euromicro workshop on advanced mobile robots.*, pp. 68–73. IEEE Computer Society Press, 1996.

[9] H. Jaeger. Observable operator models and conditioned continuation representations. Technical Report 1043, GMD – Forschungszentrum Informationstechnik GmbH, Sankt Augustin, 1997.

[10] H. Jaeger and T. Christaller. Dual dynamics: Designing behavior systems for autonomous robots. In: M. Sugisaka (ed.), *Artificial life and robotics.* 1997.

[11] E. R. Kandel, J. H. Schwartz, and T. M. Jessell. *Principles of neural science.* Prentice Hall, Englewood Cliffs (NJ), 1991.

[12] R. Pfeifer and C. Scheier. The autonomous agents approach to cognitive science. *Theory in Biosciences.* to appear.

[13] A. Thompson. Evolving electronic robot controllers that exploit hardware resources. In: F. Moran et al. (eds.), *Advances in Artificial Life. Third European Conference on Artificial Life.*, LNCS 929, pp. 640–656, Berlin, 1995. Springer.

Proc. of Third Int. Symp. on Artificial Life, and Robotics (AROB III' 98),
Oita, Japan, 19-21, January, 1998,

A Modification of (M-R) Systems and Its Simulation

Y.G. Zhang
(Inst. of Syst. Science,
Academia Sinica,
Beijing China)

M.Sugisaka
Dept. of E. & E. Engineering,
Oita University,
Oita, Japan)

C.M.Xu
(Inst. of Syst. Science,
Academia Sinica,
Beijing China)

ABSTRACT

Cell is the basic form of living systems. Metabolism and repair function are the very basic for cells. (M-R) systems is an abstract discription of this kind of living systems. In this paper, we proposed a modified Metabolism-Repair system to the one presented by [1-3]. The main change are : repair do not recover a individual cell, but repair the the function of the whole living system, and ignor the part of Bf. We try to combine the activity of cells with the formation of organization. And the simulation experiment on the network of (M-R) system has been done, it shown that the model here is more reasonble.

Key words: Metabolism-Repair system, living systems, replication, split, growth, organization

I. Introduction

Cell is the basis of all living subjects existed in the world. It is also the basic form of life. A starting point to describe a living system or any organization is the basal function of the cell. There are some important features about cells. Basically, the cell has two functions: one is a metabolism representing the basal biochemical process in a cell, the other is a maintenance or repair function to ensure continued viability of the living system or organization at the situation of some cell to be died and existence of external disturbances. In a living systems, the metabolism and repair functions are always together with growing , cell splitting and dying. A abstract description for the living systems and organization is so-called **Metabolism-Repair Systems**, or (M-R) systems. The metabolism-Repair system is such a system that containing an internal model of itself. In [1,2] R. Rosen presented the concept of M-R network; J. Casti presented a linear M-R system in [2]; and in [4] we proposed a modified system based on the nature of cell's activity.

According to the result of [1-3], One can represent the metabolic activity of the cell as a map: $f : \Omega \to \Gamma, \quad \omega \to \gamma$. The fundamental role of metabolism is to keep the biochemical process by using absorbing external subjects and energy, and excreting the wastes generated in the biochemical process and make the living system growing up to certain shape. The repair role is to make a copy of the cell which to be dead according to the genotypic information in the cell, and restore the metabolism f of the living system or organization when some cells failed or to be dead. Thus, one suppose that the repair function can be abstractly represented by the map: $P_f : \Gamma \to H(\Omega,\Gamma), \quad \gamma \to f$. The P_f is called as the repair machinery. However, how to deal with the error made by P_f? One can represent the reproductive machinery of the cell by the map: $\beta_f : H(\Omega,\Gamma) \to H(\Gamma,H(\Omega,\Gamma)), \quad f \to P_f$. One can summarize the discussion in[2,3] by the diagram shown in the following:

$$\underset{\text{(metabolism)}}{\Omega} \xrightarrow{f} \Gamma \xrightarrow[\text{(repair)}]{P_f} \underset{\text{(translation)}}{H(\Omega,\Gamma)} \xrightarrow[\text{(replication)}]{\beta_f} \underset{\text{(transcription)}}{H(\Gamma,H(\Omega,\Gamma))}$$

Fig.1 The diagram of (M-R)-systems

In this paper we try to give some modification for the modeling of (M-R)-systems in order to make the model of linear (M-R)-systems more reasonable. The main parts of modification are as the following:

1) Due to the life of a cell is finite and limited, the discrete model to metabolic machinery should be finite degree but not infinite. Of cause, it may be a big finite.

2) The repair process to a living system means to keep the function of the living system rather than to recover a cell to be dead

3) the repair function itself includes two stages: one is to make a copy of the metabolic map f , and then a repairable cell splits itself into two parts which have the same behaviors and structure with the dying cell when it received a control signal from it. To make a copy of metabolic map f means to restore the information hidden in genes, it similar to that process in DNA. Mathematically, it is Systems Identification.

4) There are some cells which are non-repairable, they can not be repaired while they failure or dead.

5) The map β_f to repair the repairer mentioned in [2,3] is unnecessary.

Based on our opinion and understanding to Metabolism-Repair systems The metabolism-repair systems we proposed here has the following scheme:

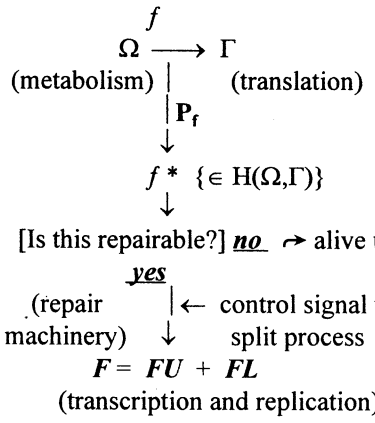


Fig. 2 The scheme of repair mechanism for a cell

The simulation for a living system or organization based on this model has been done and the result shown this model is more reasonable.

II. Modified Model of Metabolism

Essentially, the metabolic process in a cell is a biochemical reaction process and the life of a cell is finite, so y_i , the output of metabolic machinery, should be a finite bounded and stationary sequence. If y_i is a vector, $y_i \in \Re^p$, then

$$\| y_i \| \le C, \quad i = 1, 2, 3, ..., T$$

and $$\| y_i \| = 0, \quad i > T, \qquad (2.1)$$

where C is a some constant and T is the lifetime of the cell. (2.1) is a necessary constrain condition to characterize the metabolic process. Based on this view, the metabolic process can be thought of as a map: $$y_t = f(u_i, i < t) \qquad (2.2)$$

where f may be linear or nonlinear and the input u_i may be deterministic or stochastic. Usually, f is genotypic and implicit, we can not describe it exactly so far. What we could do is to describe and identify it by using some mathematical models. Especially, if we consider a linear (M-R)-system, it can be described as $\gamma = F\omega$ subject to (2.1), or,

$$\begin{pmatrix} y_1 \\ y_2 \\ y_3 \\ \vdots \\ y_N \\ \vdots \\ y_t \end{pmatrix} = \begin{pmatrix} A_1 & 0 & 0 & \cdots & 0 & 0 \\ A_2 & A_1 & 0 & 0 & \ddots & 0 \\ A_3 & A_2 & A_1 & 0 & 0 & \ddots \\ \ddots & \ddots & \ddots & \ddots & \ddots & 0 \\ A_N & & \cdots & & A_2 & A_1 \\ A_1 & & & & A_3 & A_2 \\ \vdots & & \vdots & & \vdots & \vdots \\ A_{L-1} & \cdots & A_2 & A_1 & A_N & \cdots \end{pmatrix}_{t \times N} \begin{pmatrix} 0 & 0 & \cdots & 0 & 1 \\ 1 & 0 & 0 & \cdots & 0 \\ 0 & 1 & 0 & \cdots & 0 \\ \vdots & \vdots & \vdots & \vdots & \vdots \\ 0 & \cdots & 0 & 1 & 0 \end{pmatrix}^k \begin{pmatrix} u_{k-N} \\ u_{k-N+1} \\ u_{k-N+2} \\ \vdots \\ u_{k-2} \\ u_{k-1} \end{pmatrix}_{N \times 1} \qquad (2.3)$$

where k=1, 2, 3,..., t and L= t mod(N) +1,

$$\text{or} \quad y_k = \sum_{i=1}^{N} A_{i+L}\, u_{k-i} \ , \quad \text{if } k>N,$$

where L= k mod(N)

$$\text{or} \quad = \sum_{i=1}^{N} A_i\, u_{k-i} \ , \quad \text{if } k \le N,$$

(here $u_j = 0$, if $j < 0$),

subject to (2.1). (2.3)'

Where F is a finite Toeplitz matrix and it has the size of t x N , t is the aliving time, T is the livetime, t < T and N is the length of the finite map f. In this model, $f = \{A_1, A_2, A_3, ..., A_N\}$. Usually, T>>N and N>>1. The reason is that the biochemical process in a cell, i.e. its lifetime, will keep a longer time compare with its transient time N, although the model is linear but not means the process is very simple, so N >>1.

If we want to describe a metabolism as a essential nonlinear (M-R) systems according to (2.2), the Artificial Neural Networks model is one of selections.

III. Repairableness of Cells and Repair

The repair subsystem introduced in [2,3] has a basic function that to restore the metabolic subsystem while a cell is failure. It means that to make a copy of the map f when the metabolic subsystem (cell) is alive and substitute it when the cell go to dead. However, the real repair process is much more complicated In fact, from the observations of biologists the repair can not recover a cell which is dying, but reproduce a new cell by splitting a cell into two almost the same parts which has the same functions and structure with the dying cell.

Here we explain the repair map P_f in [2,3] as **system identification**, the function of P_f is to make f^*, which is a copy of the information included in f, by using the output γ of metabolic machinery (in fact, including the input ω also!). If we accept (2.3) as the model of linear (M-R)-systems, then there are several method to identify $f = (A_1, A_2, ... A_N)$. Of cause, some mathematical conditions should be satisfied, for example, the condition of permanent exciting. (2.3) can be rewritten as

$$\gamma = Uf$$

and $$\hat{f} = U^+ \gamma, \qquad (3.1)$$

where U^+ is the pseudo-inverse of U. we can take $\hat{f}$ as f^*. We say map f^* is a copy of f that means $\| f^*(\omega) - f(\omega) \| < \varepsilon$, for given small $\varepsilon > 0$. If input u_i would be stochastic, then we have to use the density of power spectrum to identify f. If this system can not be identified or $\| f^*(\omega) - f(\omega) \| > \varepsilon$, We call this

cell **non-repairable.** Otherwise, it is **repairable.** The **stabilization** problem of repair machinery P_f discussed in [2,3] become the **consistency** problem here. If a cell is repairable but not stabilized or not consistence, then this cell would be "**Cancer cell**".

IV. Description of Living System

The failure of a metabolic machinery.

In the model (2.3) if $y_t = 0$, as $t \geq T$ and $y_t \neq 0$, as $t < T$, then we call the metabolic machinery is **dead at time T**. It implies that $\|A_j\|$, i = 1, 2, ... N. become smaller and smaller since certain time $t^* < T$ and then $\|A_j\| = 0$, i = 1, 2, ... N ultimately at time T. More exactly speaking, the failure of a metabolic machinery means that some change is happened in map f or in inputs.

Based on our opinion, the replication means the split of the matrix F into two parts: upper and lower. For example, if the cell received a replication start signal then the follows:

$$F = \begin{pmatrix} A_1 & 0 & 0 & \cdots & & 0 & 0 \\ A_2 & A_1 & 0 & 0 & & \ddots & 0 \\ A_3 & A_2 & A_1 & 0 & 0 & \ddots & \vdots \\ \ddots & \ddots & \ddots & \ddots & \ddots & 0 & 0 \\ A_N & & \cdots & & \cdots & A_2 & A_1 \\ A_1 & & & & & A_3 & A_2 \\ \vdots & & \vdots & & \vdots & \vdots & \vdots \\ A_{L-1} & \cdots & A_2 & A_1 & A_N & \cdots & A_L \end{pmatrix}_{t \times N} \Rightarrow$$

$$FU = \begin{pmatrix} A_1 & 0 & 0 & \cdots & & 0 & 0 \\ A_2 & A_1 & 0 & 0 & & \ddots & 0 \\ A_3 & A_2 & A_1 & 0 & 0 & \ddots & \vdots \\ \ddots & \ddots & \ddots & \ddots & \ddots & 0 & 0 \\ A_N & & \cdots & & \cdots & A_2 & A_1 \\ \vdots & & & & & \vdots & \vdots \\ A_{r-1} & \cdots & \cdots & \cdots & \cdots & A_{r+1} & A_r \end{pmatrix}_{m \times N} \quad \text{and}$$

$$FL = \begin{pmatrix} A_r & \cdots & A_1 & A_N & \cdots & A_{r+2} & A_{r+1} \\ \vdots & & \vdots & & \vdots & & \vdots \\ A_{L-1} & \cdots & A_2 & A_1 & A_N & \cdots & A_L \end{pmatrix}_{(t-m) \times N} \qquad (3.2)$$

We call the both as FU and FL. Obviously, the two metabolic machinery consisted of FU and FL have the same behaviors with F, the replication process finished.

Of cause, we could give other splitting form which is more similar to the process from DNA, it means that the split of matrix F could be vertical split and two half part belong to two cells resulted in from splitting. It is easy to recover the each half part of F to the whole matrix F.

Living system -- Network of (M-R) systems

The model above we have proposed is for a single cell's M-R system. It is well known that Living system or organization is made up of the cells. That is, in fact, an abstract living system is a network of (M-R) systems. It should have the process of growing up, stable growing, getting old and going to death. More important is the living system should have immunity function, that means the living system has the ability to keep from reproduction of the nonrepairble cells. Otherwise nonrepairable cells will become more and more and the living system will has cancer. In an organization, when it is stable, there are stable number of cells; the death and replication of cells are in dynamic balance. In living system the cells consisted of the organization must be in collaboration.

V. Simulation of a living system

We have done the simulations for a network of this modified (M-R) System. It has functions of metabolism, growing up, splitting of cells and repairing the system while some cells to be dead. The whole process is controlled by the gene information.

The initial parameters we appointed as follows:
1)CELLNUM—the number of basic cells to promulgate, in this experiment we appoint it 5.
2)CELLLIFE — the cells' lifelimit. When a cell gets to the limit, it will be splet or die.
3)N—the dimension of metabolism function f( ), in the linear M-R system, $f = (A_1, A_2, A_3, ..., A_N)$.

We also need to determine two threshold functions d1(t) and d2(t) to decide whether the cell will die, split, or repair.

At the beginning, we input U[CELLLIFE] and A[N] of each cell. According to (2.3) computing the cell's output Y[ ] at given t. Then we use Householder algorithm to get $f^*( ) = (A_1', A_2', A_3', ..., A_N')$ according to (2.4).

If t<N, the process is in transient state. During this period, if $\|f'( ) - f( )\| < d1(t)$, thus the cell grows, otherwise it will die.

If t > = N, the cell become material. When t < CLEAVE, we use d2(t) to determine whether it can be repaired and use d1(t) to determine whether it grows. The functions d1(t) and d2(t) are time-dependent. When a metabolic machinery will fail, we use d1(t) to determine whether it is in the repair scope. If t = CLEAVE, the cell can be spilt or die, determined by the situation whether it is in which domain. The choice of them has obvious impact on the simulation result.

Besides the choice of above functions, there are also others factors that influence the result, such as input U[CELLLIFE] and A[N]. Here U[CELLLIFE] means the environment, sometimes it can call further

enormous change. The genetic change is revealed in the disturbances on A[N]. Some of them can be igorned, some are handed down on and, of cause, some cells die with the disturbances.

There are some restricts on the inputs. Because we can appoint different N and CELLLIFE, and there are variances in the computation of Householder algorithm, we may get the shiftiness of f( ) and f*( ) at any level. So if we want to get ideal results, we must make a good analysis for inputs, N, CELLLIFE, d1(t) and d2(t).

In Fig.3 the simulation results are shown, we use a rectangle to denote a organism and ellipse drawing to denote cells. With the number of cells growing, the organism also grows up, then it become a stable shape.

In this model there are two factors which may result in a cell's failure: one is u(t), the other is Ai, i=1,2,....N. Those two factors denote the changes of external environment and internal situation.

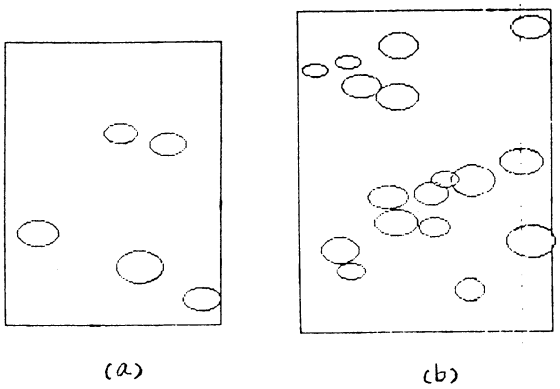
References

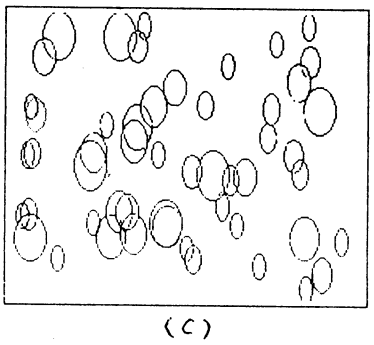
[1] Rosen.R, "Some relational cell models: the metabolism-repair systems." In: Foundations of Mathematical Biology, Vol.2, edited by R.Rosen, Academic Press, New York, 1972, pp.217-253.

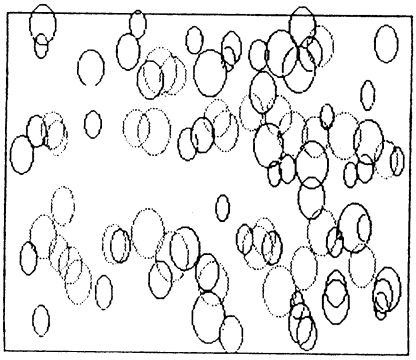
[2] Casti, J. L, "Linear Metabolism-Repair Systems", Int. J. General Systems, Vol.14, pp.143-167, 1988

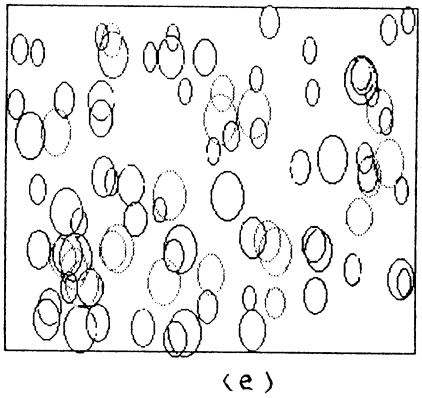
[3] Casti, J. L, REALITY RULES: Picturing the World in Mathematics, Chapter 7, JOHN WILEY & SONS. INC, 1992,

[4] Zhang, Y.G. and Sugisaka, M., "Some new look on Metabolism-repair systems", proceedings of Artificial Life and Robotics (AROB97'), 1997, Beppu, Japan









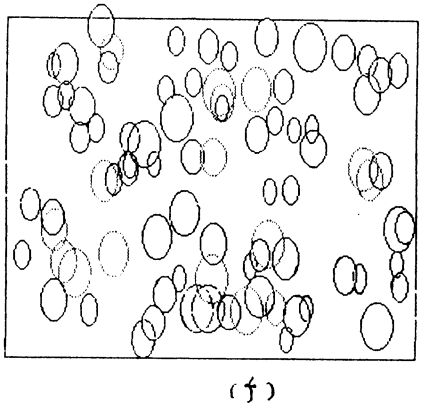


Fig. 3 The results of simulation experiement on network of (M-R) systems

(a) t=3 (b) t=20 (c) t=30 (d) t=40
(e) t=60 (f) t=90

Proc. of Third Int. Symp. on Artificial Life, and Robotics (AROB III' 98),
Oita, Japan, 19-21, January, 1998,

Robot Football, Artificial Life, and Complexity

Jeffrey Johnson
Department of Design and Innovation, The Open University, Milton Keynes, MK7 6AA, England.
Tel: 01908-583284, Fax: 01908-282660, email: j.h.johnson@open.ac.uk

Abstract

Autonomous football-playing robots provide a stimulating research challenge in the sciences of Complexity and Artificial Life. Currently the game is dominated by problems of making the robots move sufficiently accurately. Even so, the dynamics of robot football are clearly chaotic, requiring some higher level control strategy. A mathematics of the *relations* between the robots, ball, and the pitch is introduced. This mathematics supports a theory of structural time necessary for higher level dynamics and cognitive functions. On comparison with computer chess, robot football is more complex and may supplant it as a benchmark test. Many systems considered to be complex have behaviour which emerges from interacting autonomous agents. *Simulation* is a new paradigm on which a science of such systems is being built. However, simulation currently suffers from the 'can you trust it' syndrome: for many systems it is impractical to do experiments to test the simulation. However, robot football is a system which can be both simulated and built. It is suggested that this makes it an important scientific laboratory subject for understanding the relationship between simulation and real complex system behaviour.

1. Introduction

Robot football is fast and exciting, easy to understand, and presents a wide variety of advanced research problems in engineering science and the science of complex systems.

One version involves blue and yellow robots with maximum dimension 8 cm playing on a green 130 x 90 cm pitch with an orange golf ball. Each team has a television camera above the pitch which is used to give robot and ball position information. The camera is connected to a computer, which communicates with the robots by wireless links (Figure 1). In the MIcro RObot SOccer Tournament (MIROSOT) version the robots look like Rubik cubes with wheels. Other versions use larger robots with on-board cameras. The robots are autonomous, with no human intervention during play. As such they are an important research focus in the science of Artificial Life.

Currently robot football is dominated by engineering problems such as miniaturisation of the electromechanical components, their computational control hardware, their communications systems, and programming their vision systems.

Moving robots fast and with precision is difficult. Making them strike a moving ball or pass the ball to another player is more difficult still. And carrying out complicated sequences of movements such as those executed by human players has not been achieved by most teams. These control problems are dicussed in Section 2.

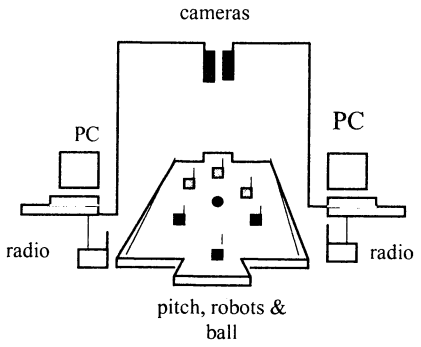


Figure 1 The general setup for MIROSOT

These problems give a major research impetus in many engineering disciplines, but for many people the really interesting challenge in robot football comes later in the context of autonomous agents, self-organising systems, and emergent behaviour.

Section 3 shows that the dynamics of a football-playing robot are clearly chaotic, in the technical sense of the word. The simplest experiments show that precise movements are not exactly *repeatable* for a totally autonomous machine. Set the system going from apparently the same starting position, and it will diverge from the previous trajectory.

In Section 4 robot football is used to develop some general ideas in the science of complexity. In particular I will consider the *relational structure* which underlies higher level constructs used to analyse and reason about the game. The essential idea is that this relational structure constrains the dynamics of the game: it allows and forbids, but does not require (Gould, '84). This is related to

frequency distributions, and some structural configurations being more or less pre-disposed to desirable outcomes than others.

Section 5 introduces a notion of structural time for planning higher level cognitive strategies. This is related to clock time which governs the physics of the system, but it is the events of the game rather than the tick of the clock which govern the higher level dynamics.

Section 6 discusses the importance of pattern recognition when applying rules and higher level cognitive knowledge, and suggests that the structural ideas developed in Section 5 can be naturally applied in this context.

Chaos means that brute-force search may not be applied to robot football as it has successfully been applied in computer chess. In Section 7, I suggest that the Artificial Life game of robot football may be a natural successor to the benchmark problem of chess in Artificial Intelligence.

As discussed in Section 8, an important aspect of robot football is the contribution it can make to our understanding of *simulation* in the science of complexity. Simulation is a new scientific paradigm enabling predictions to be made of systems which would otherwise be impossible.

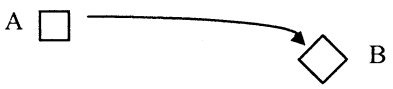
For many complex systems it may be difficult or impossible to set up experiments to verify the theoretical simulation predictions. In robot football we can both simulate the system by computer, and implement it in reality. In this way robot football becomes a research topic in artificial life; and it also becomes a new *laboratory* for the science of simulation and complex systems.

2. Robot Football and Control

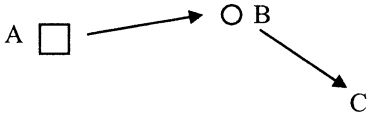
There are two types of control problem in robot football, (1) 'low-level' control of the motors to move the vehicles as required, and (2) 'higher level' control in which the movement has some purpose and may involve collaboration between the robots. In terms of interacting autonomous agents the second is most interesting, but for most teams the first is the limiting factor.

To focus the research, FIRA (Federation of International Robot Football Associations) has defined a set of benchmark problems. These are based on control problems such as those shown in Figure 2. The better teams can move their robots quite well, but few teams would claim to be able to execute (c) in a consistent way.

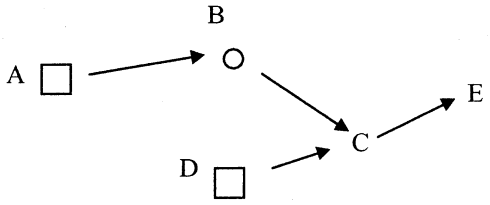
Low level control of a small robot is difficult because there are many variables, and some are difficult to measure. Even supposing one had a good mathematical model of the relationship between the power applied to the motors, as required by conventional control theory (Bissell, 1994) there are other problems, e.g. modelling and measuring wheel skid, etc..



(a) move a robot from A to B



(b) Move robot from A to strike the ball at B to make it go through point C.



(c) Move a robot from A to strike the ball at B to be struck at point C by a robot at point D to pass through point E.

Figure 2. Benchmark Problems

It is interesting to note a divergence between conventional control approaches in which humans design in all the low-level control behaviour, and other approaches.

Ideally, in the context of Artificial Life, one would like a control strategy based on simple interactions from which the desired motions emerge. This could be approached from the perspective of the machine learning how to move, probably in the context of some selection mechanism.

Conventional control theory is not applicable to the higher level control required in robot football, because it is not practical to devise a mathematical model which embodies all possible relationships and states of the system.

3. Discrete Chaos in Robot Football

Arrowsmith (1991) characterises chaos as follows: "The basic ingredient of *chaos* is the *sensitive dependence* of the future evolution of the system on the initial conditions". Figure 3 shows a simple experiment in which one of our robots was sent

forward twenty times from a set position. The lines represent the front of the robot. From this it can be seen that the robot had variation in both its motion and its final orientation. Thus one expects the system to be *chaotic* in the technical sense that trajectories will diverge from almost identical initial conditions while remaining bounded.

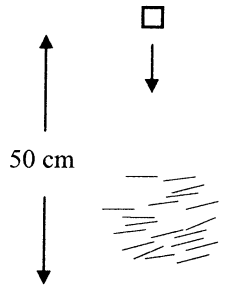


Figure 3. Uncertainty in positioning a robot.

Suppose then that a *trajectory* for a robot is a sequence of states (s_0, s_1, s_2, ..., s_t) through some equally spaced set of time intervals, such as the frames of a digital camera observing the motion. Then another trajectory, (s'_0, s'_1, s'_2, ..., s'_t), can be defined to be 'almost identical' at s_i if there exists some δ such that $| s'_i - s_i | < \delta$ (Figure 4).

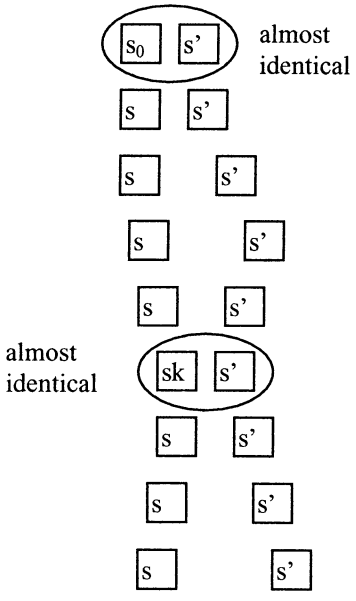


Figure 4. Almost identical states in discrete chaos

Consider two sequences S and S' which have the property that for some k, s_k and s'_k are not be 'almost identical' as the motions diverge. The interesting question is then whether there exists a later k for which s_k and s'_k are again 'almost identical'. In practice, two system states are *almost identical* when the observational instruments do not allow them to be discriminated with respect to some prescribed set of properties.

For example, when we placed our robots for the experiment illustrated in Figure 4, we carefully put the 'same' robot in the 'same' initial position and observed the motion. Of course we knew that the robots and their initial positions were at best 'almost identical', with δ about 1 mm.

In robot football we want a relatively small set of strategies and tactics which can be applied when the circumstances are 'appropriate'. This means classifying the system states as 'almost identical', and this involves the relations between the players, ball, and parts of the pitch.

4. Relational Structure

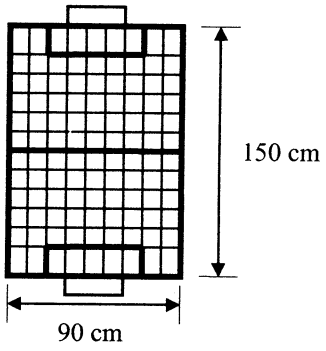


Figure 5 The pitch divided into cells

In human football the pitch is divided by lines into areas such as the halves of the pitch and the goal areas. More subtle divisions exist in peoples minds, e.g. we talk of a play moving "down the wing", which means an area at the side of the opponents' half of the pitch. This is absolutely typical of the way human beings form linguistic constructs to represent abstract aspects of systems, in order to be able to describe and reason about them.

In robot football the pitch is divided into areas which facilitate the positioning of the robot when play is restarted after a foul, goal, or free ball (Figure 5). But this artificial and arbitrary partitioning of the pitch takes on a life of its own, and many people use this as part of their representation of the system.

Then, robots can be allocated to squares, and the cognitive problem of planning where to position a robot begins to look like the problem of positioning a piece in chess, as discussed in Section 7.

The geometric relationships between a set of robots can be viewed as *n*-ary relations, which generalises the better known binary relations represented in

graph and network theory. A set of n robots under a relation R defines what is called a simplex in a simplicial complex. For example, the robots a, b, and c being R-related by their relative positions can be expressed algebraically as $\langle a, b, c; R \rangle$.

Simplices have geometric realisations as polyhedra: triangles for 3-ary relations, tetrahedra for 4-ary relations, and so on (Figure 6).

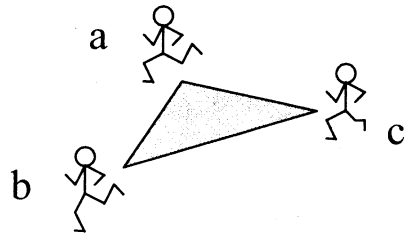


Figure 6 The relationship between three players represented by a triangle (2-simplex).

In robot football these simplices form and disappear dynamically. Any sequence of moves determines a trajectory of polyhedra in multidimensional space, as illustrated in Figure 7.

The simplices are important because they may support interesting outcomes such as goal-scoring: some simplices may be more predisposed to a goal being scored than another. If this is so, then teams using this representation in their cognitive subsystems will be able to define sub-goals in terms of creating certain geometric configurations with desirable polyhedra. This may put them at an advantage compared to teams which do not use this representation and the knowledge it allows to be accumulated and exploited by the cognition subsystem.

For example, every robot is related to the set of squares, or cells, which it attacks or defends. Let $C_A = \{ c_{0A}, c_{1A}, c_{2A}, ..., c_{pA} \}$ denote this set of cells for robot A. Robot A defines a relation, R_A on the cells, assembling them into a structure represented by the simplex $\langle c_0, c_1, c_2, ..., c_p; R_A \rangle$. By an abuse of language this simplex will be represented by the notation $\langle C_A; R_A \rangle$.

In general $C_A \cap C_B \neq \varnothing$ for two robots, A and B, and there is a subset of cells attacked by both. This is of course exactly the part of the system where the robots can interact Thus we can write

$$\langle C_A; R_A \rangle \cap \langle C_B; R_B \rangle = \langle C_A \cap C_B; R_A \cap R_B \rangle$$

which is the assembly of cells attacked or defended by robots A and B. If A and B are on the same side this may be part of a defensive substructure; if A and B are on opposite sides it reflects that part of the structure on which they may compete for access or possession of the ball.

5. System Events in Structured Time

Given that a system like football is chaotic, it becomes axiomatic that one does not attempt to predict its long term behaviour in the terms of that chaotic representation. Does this then mean the system is, for practical purposes, unpredictable? Of course not. But now the system has to be represented within in a different kind of time.

Twenty years ago R. H. Atkin (1977) suggested that social time is a *structural* concept rather than a continuous topological construction. Most complex systems have a pulse measured in terms of their natural *events*. Atkin suggested that an event is marked by the formation of a simplex, *i.e.* when the parts are all present, and the relation between them can be observed to hold.

In many systems, including robot football, these events *evolve* through clock time, and they are 'locally' related to clock time. But they sometimes have discrete jumps, when the continuous description becomes out of clock-phase, but after which the continuous description again become locally coherent. Presumably these phase shifts are related to our human feelings that things are moving very fast, or that time is beginning to drag.

Suppose it takes a robot t second to move from A to B, subject to an error distribution, Δt, which is often Guassian. In principle we can plan a sequence of motions with a total time of $\Sigma(t_i + \Delta t_i) = \Sigma t_i + \Sigma \Delta t_i$. As the number of t_i increases, the variance of $\Sigma \Delta t_i$ increases. When it is of the order of magnitude as single events, predictions of system state involving $\Sigma \Delta t_i$ become useless from a planning perspective: given the combinatorial number of things that might happen in the meantime, any particular state may have probability almost zero of occurring at time $\Sigma(t_i + \Delta t_i)$.

This means that any plan must be a sequence of positions, ordered in clock time but not mapped precisely into clock time. Let a *plan* be a sequence of states $(S_0, S_1, ..., S_n)$, where S_0 is the initial state and S_n is the target state.

Any plan has a control probability sequence, $(p_0, p_1, ..., p_n)$ where the probability of s_i occuring is p_i. Since p_i is conditional on p_{i-1}, it follows that $p_{i-1} \geq p_i$, and the further one looks into the future

for any particular trajectory, the less likely is any particular outcome.

However, this is not so over large numbers of trials, when the distribution of particular outcomes may be more predictable. In football it does not matter precisely when a goal is scored. The problem is to structure the universe so that one or more goals can be scored within the ninety minutes allotted to humans, or ten minutes allotted to robots.

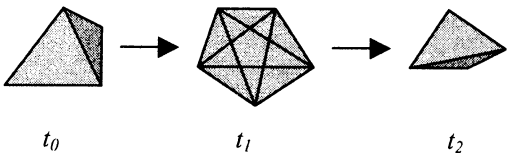


Figure 7. The evolution of events marks time in robot football.

Following Atkin, we see a robot football games as sequence of events, where each event is represented by a simplex (Figure 7). Then the time flow of the game is determined by these events. The only relationship that they have with clock time is their dependence on the low level control that moves the robots to attain short term positional goals.

In physical systems there is constant struggle to keep the high-level states of the system aligned to the clock time of the low-level states of the system. This highlights the need for a theory of high-level control which can mesh with the feedback techniques of conventional control theory.

6. Pattern Recognition in Strategic Control

It is very attractive idea to build robots with a small number or rules from which their behaviour emerges, rather like a cellular automaton. But the result could be like a schoolboy kick-and-run game in which there is very little strategic overview.

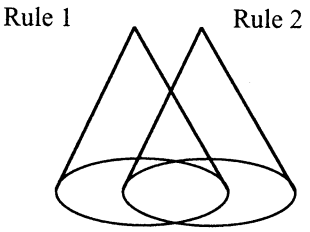
To apply any rule, it is necessary to test to see if the rule can be applied to the particular situation. In other words, pattern recognition is necessary. As shown in Figure 8, each particular situation may be unique, but by ignoring some of the details, they can be classified as 'equivalent' to other members of their class (Schreider, 1975).

As noted in Section 2, system states may be almost identical, and there may be generalisations that can be made about the best control strategy for particular representative states.

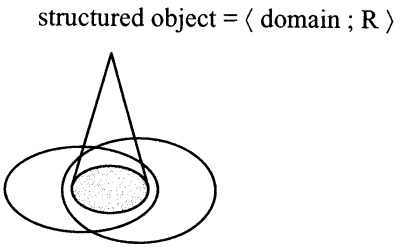
For example, in human football there are various 'set piece' movements which are designed to score goals. These set pieces have certain similarities, but of course they are never absolutely identical. Thus despite the combinatorially many states that may occur in football, there may be classes of states which are representative of some unifying property.

This is important because higher level cognitive processes may be able to reason about these states, and even create sequences of intermediate states likely to bring about some particularly desirable archetype. However, this means the system must have the ability to recognise emergent patterns as the game proceeds.

The relational mathematics described earlier is essential for this: patterns are by definition sets of related objects.



(a) hierarchical aggregation through rule-defined patterns



(b) Rules are generalisations, individuals have eccentric features excluded in the rule definition

Figure 8. Pattern recognition as classifying objects by their parts and relationships between those parts.

7. Robot Football & Computer Chess

Robot football has all the combinatorial problems of computer chess, but it is much more complex. It extends the problem of positioning pieces to achieve some long term goal into a system where chaotic behaviour is normal and the search space for the 'best' move may be infinite. Then repeated iteration of rules may not be a practical strategy for long term control, and different kinds of cognitive functions are required.

Robot football is chaotic in a way which chess is not: start the robots from the 'same' positions and give the same commands, and there will be rapid divergence between the system trajectories.

An important consequence of this is that brute-force search methods may not be applicable in the same way that they have successfully been applied in computer chess. In the year that the world champion human chess player was defeated by a computer (plus human programmers), the Artificial Life game of robot football may be seen as the natural successor to this benchmark problem in Artificial Intelligence

8. Robot Football and Simulation

A very important aspect of robot football is the contribution it can make to our understanding of simulation in the science of complexity. Simulation is a new scientific paradigm enabling predictions to be made of systems which would otherwise be impossible.

A major problem arises for many of the complex systems of interest in that it may be difficult or impossible to set up experiments to verify the theoretical simulation predictions. Casti (1997) has called this the "Can you trust it?" problem. Casti sets out the following axes along which the validity of models can be evaluated:

- *Operational:* Is the model able to provide answers to the questions for which it has been built?
- *Empirical:* Does the model agree with observed data that are relevant to the problem under consideration?
- *Theoretical:* Does the model contradict any established theories?
- *Consistency:* Does the model contain any logical contradictions?
- *Faith:* Do specialists in the area being modeled agree that the model produces believable results?
- *Testing:* Can the model be tested in the real world.

In robot football we can both simulate the system by computer, and build it in reality. Thus we can indeed test the simulation model against the real world, and evaluate it according to these criteria.

In this way robot football becomes more than a research topic in artificial life; and it also becomes a new laboratory for the science of simulation and complex systems.

9. Conclusion

Robot football has been presented as an important new scientific laboratory for the study of complex systems and simulation:

- it exhibits emergent behaviour from the interaction of autonomous agents
- it is chaotic in its low level dynamics and more complex than chess as a benchmark problem
- relational structure is important in understanding and controlling higher level dynamics
- both clock time and structural time are necessary for low-level and high-level control
- it is a system that can both be built and simulated, making it an important laboratory subject for research into complexity.

Acknowledgement: This research was supported by the Engineering and Physical Science Research Council of Great Britain.

References

Arrowsmith, D. K., 'The mathematics of chaos', in *The Mathematical Revolution Inspired by Computing*, The Clarendon Press, Oxford, J. Johnson & M. Loomes (eds), 1991.

Atkin, R. H., *Combinatorial Connectivities in Social Systems*, Birkhauser (Basel), 1977.

Bissell, C. C., 1994, *Control Engineering*, Chapman Hall (London).

Casti, J., 1997a, 'Robots on the football field', *New Scientist*, March 1997

Casti, J, 1997b, 'Can you trust it?', *Complexity*, **2**(5), May/June 1997

Gould, P., Johnson, J., Chapman, G., *The structure of television*, PION (London), 1984.

Johnson, J. H., 1997, 'Design and control of self-organising complexes', *Control mechanisms for complex systems*, M. Coombs & M. Sulcoski, Santa Fe Institute Press, 1997.

Johnson, J. H., Booth, M. J., 1997, 'Robot Football: emergent behaviour in nonlinear discrete systems', *Proc. Microsot-97*, J-H Kim & J.J.Lee (eds), KAIST, 1997.

Johnson, J. H., 'Robot Football: New Frontiers in Control and Complexity Theory, *Proc. Int. Conf. Systems Engineering*, ICSE97, James (ed), Coventry, 1997.

Kim, J-H, J.J. Lee, 1996, (eds) *Proceedings of the Micro-Robot World Cup Soccer Tournament*, 9-12 November 1996, Korea Advanced Institute of Science and Technology, Taejon, Korea.

Kim, J-H, J.J. Lee, 1997, (eds) *Proceedings of the Micro-Robot World Cup Soccer Tournament*, 1996, KAISTechnology, Taejon, Korea.

Schreider, J. A., (1975) *Equality, reemblance, and order*, Mir Publishers (Moscow).

Proc. of Third Int. Symp. on Artificial Life, and Robotics (AROB III' 98),
Oita, Japan, 19-21, January, 1998,

Robocup challenge

H. Kitano
Sony Computer Science Laboratory
Takanawa Muse Building, 3-14-13 Higashi gotanda, Shinagawa-ku,Tokyo, Japan
+81-3-5448-4380, E-mail: kitano@csl.sony.co.jp

The manuscript of this talk will be distributed at the symposium.

Proc. of Third Int. Symp. on Artificial Life, and Robotics (AROB III'98),
Oita, Japan, 19-21, January, 1998,

Initial Configuration Dependence in a Self-Organizing Robot

Kiyotaka Izumi*, **Hodaka Tamura****, **Yasuhiro Ikeda*****, and **Keigo Watanabe***

* Department of Mechanical Engineering,
Faculty of Science and Engineering,
Saga University, 1-Honjomachi, Saga 840, Japan.
Email: izumi@me.saga-u.ac.jp
** Graduate School of Science and Engineering,
Saga University, 1-Honjomachi, Saga 840, Japan.
*** Mitsubishi Electric Corporation

Abstract

In this paper, we describe the dependence of an initial state in a self-organizing robot on an optimal structure configuration, where a "fractum" is used as a basic unit. Each robot is operated on a genetic algorithm (GA) by itself, and all of them will produce a desired configuration. But, the problem such as a deadlock state happens by an initial configuration. The deadlock state means a state in which all robots can not move because each robot moves autonomously. It is shown from simulations that a difference of initial configuration affects on both the deadlock rate and the number of movement of fracta for obtaining an optimal structure configuration.

KeyWords: Self-Organizing Robot, Initial Configuration, Deadlock State, Genetic Algorithm

1 Introduction

In recent years, autonomous distributed robot systems have been studied. The whole systems consist of robots which make decision and act independently, keeping their order intact. These systems are autonomous distributed robot systems [1]. There are some systems that realize useful function by considering a robot as a unit and combining many of them as a robot system. This robot system can carry out self-repairing if one unit can change the combination with other adjacent units autonomously: it is just a self-organizing robot system. We call the robot that constructs such a system as a self-organizing robot. This system has also a structure configuration as steps to perform a self-repairing.

We considered a self-organizing robot, consisting of a basic unit called "fractum", proposed by Murata et al. [2]. We have already solved a shortest procedure of the self-organizing robot movement by using a centralized genetic algorithm (GA) [3]. The centralized genetic algorithm wholly controls the swarm composing of many fracta.

In this paper, we consider an optimal structure configuration problem for the self-organizing robot mentioned above by using a decentralized GA. The optimal configuration is obtained by making decisions of each fractum autonomously. In this approach, each robot is operated by a GA, and it cooperates each other from any initial state, and consequently a swarm composing of many fracta will produce a desired structure configuration. However, a deadlock state that implies a state in which all robots can not move anymore is often appeared, because each robot moves autonomously. From this fact, we also consider the initial configuration dependence on a deadlock state through several simulations.

2 Configuration Structure

A fractum used in this paper is a minimum unit for a structure configuration and any fractum can be used at any place for the structure configuration. An initial state and a desired state are shown in Fig. 1 for a structure configuration. The initial configuration can be set freely, but there exists a constraint that each fractum must always connect with each other. There are 12 kinds fractum states, depending on the connecting location and number of the adjacent fractum. We call them "Type"[2]. In Fig. 1, the fracta are shown as a hexagonal shape, in which the letter in the shape represents the adjacent type (i.e., fractum type). Given an initial state, the swarm of fractum decides a movable fractum among the fractum types {e, o, ϵ }. The fractum always connects other fractum while one fractum moves at once. There is only 2 kinds of mov-

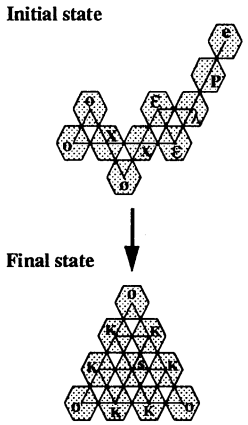


Figure 1: Fractum assembly

ing direction; one is the case when the fractum moves rightward and the other is the case when the fractum moves leftward.

2.1 Optimal configuration

We define a desired configuration as an optimal configuration. By repeating a movement, movable fracta change the state and try to configure the desired state, where the optimal configuration is represented by the type of each fractum. In Fig. 1, the set of types is {s, K, K, K, K, K, K, o, o, o}, which is regarded as the statement of a desired configuration, and whose element is regarded as the desired type. It is considered that the swarm of fractum configures the desired configuration, if all fracta have their desired types. In order to obtain the optimal configuration, it is required to recognize how far the configuration structured by the swarm of fractum from the optimal configuration. This information can be determined by using a type length [2]. The type length stands for the number of operation from one type to another. The shorter the length between each type of all fracta and the desired types is, the closer the structure configuration to the optimal configuration is.

2.2 Deadlock state

Since each fractum moves autonomously, it obtains only the local information so that a state happens in the case when all fracta can not move anymore. We call such a configuration constructed by the swarm of fractum a deadlock state. For example, there are 4 types of deadlock state for a case of 10 fracta, as shown in Fig. 2.

3 Genetic Algorithm

Genetic algorithm is a stochastic search method which imitates a process of biological evolution with gene information [4]-[5]. In the GA, after coding, some candidate solutions are represented by individual with

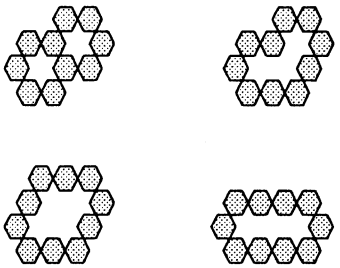


Figure 2: Deadlock states

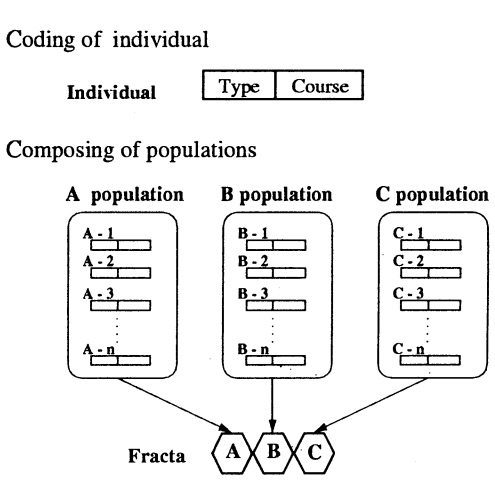


Figure 3: Coding of individuals and the composition of populations

some gene array, and the GA uses a fitness as a performance cost. The initial population consists of some individuals generated by random numbers. Some individuals which have high fitness value can survive by operating selection, crossover and mutation. Thus, the GA can produce the best individual (optimal solution) by iterating generations.

3.1 Coding

The usual GA needs a coordinator coordinating individuals, because the GA searches all individuals and carries out a selection [6]. If one population is assigned to a swarm of fractum, it is naturally coordinated by a coordinator. It does not mean that each fractum acts on its own judgment autonomously. Therefore, one population is assigned to each fractum. Figure 3 shows the coding of individuals and the composition of populations. An individual is represented by {Type, Course}. The "Type" means a fractum type and the "Course" denotes the moving direction.

3.2 Fitness

Although we have already defined that the swarm of fractum acquires an optimal configuration when all of fractum types are consistent with the statement of an optimal configuration, it is difficult to obtain an optimal configuration, if all of fracta move randomly.

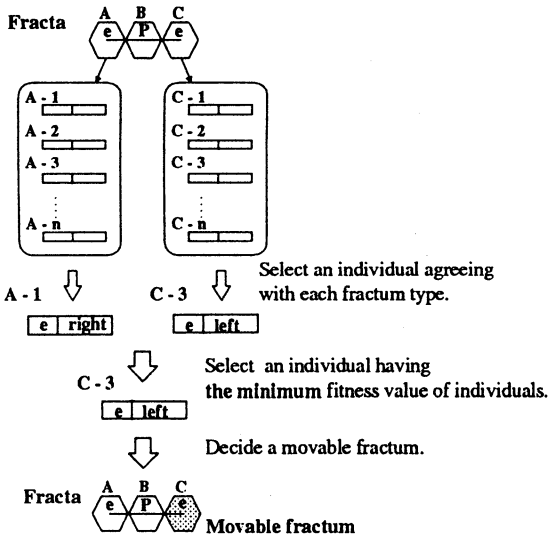


Figure 4: Decision of a movable fractum

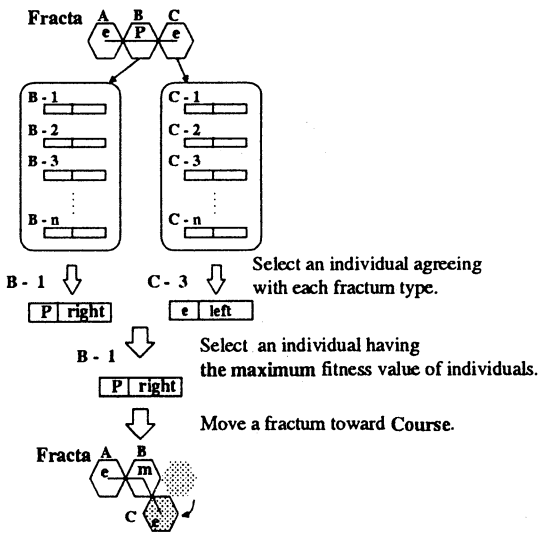


Figure 5: Decision of a course of movable fractum

Therefore, we define an individual as the better one when it has a shorter length between its own type and the desired type or it has a type matching the desired type.

Thus, the fitness is described by

$$Fitness(i) = \frac{0.5\ type(i)}{\min\limits_{j \in J} d(type^d(j), type(i))} + ntype^d(k, j) \quad (1)$$

where

$Fitness(i)$	:	fitness of ith individual
$type(i)$	:	type of ith individual
$type^d(j)$	:	jth desired type in a desired configuration
J	:	discrete number $[1, \ldots, N]$
N	:	fractum number
$d(a, b)$	:	length between type a and type b
$ntype^d(k, j)$	:	kth adjacent fractum type

Here 1.0, 2.0, 3.0, ..., 12.0 are substituted into $type(i)$ and $ntype^d(k, j)$ in order of e, o, m, p, ε, λ, Y, K, Ψ, X, f and s. Note that $ntype^d(k, j)$ is added to the fitness function only if the kth adjacent fractum type of a movable fractum matches the jth desired type in the statement of optimal configuration.

4 Procedure of Structure Configuration

The individuals of all fracta are first generated by random numbers. As shown in Fig. 4, the individuals which match each fractum type are selected from movable fracta (**Fractum A**, **Fractum C**) in a configuration by a swarm of fractum. Among them, a fractum which has an individual with the minimum fitness value is selected as a movable fractum. Next, as can be seen in Fig. 5, each individual whose type matches each fractum type is selected from the movable fractum (**Fractum C**) and the adjacent fractum (**Fractum B**). A moving direction of the movable fractum is decided by the "Course" in the individual which has a higher fitness value, and the movable fractum moves toward the "Course". Since a change of the adjacent fractum and connecting location alters the fractum type, the individual that was used for moving is evaluated by the fitness. When the adjacent fractum type matches the desired type by moving, we define the adjacent fractum as one with a desired achievement. Individuals whose types match the adjacent fractum types are evaluated by the fitness, so as not to change a fractum type which is consistent with a desired type by moving. Thus, iterations of moving change the configuration, but the generation of GA is altered after some moving. The stopping condition is in the case when the lengths among fracta located at an apex of a desired configuration (e.g., triangle state) are same, after completing that any fractum type matches one with a maximum combination number in the desired configuration statement.

5 Simulations

The computer simulations were carried out by using 10 fracta, where a triangle configuration shown in Fig. 1 was set as an optimal configuration. The initial configurations as shown in Fig. 6 are a string state as α initial configuration, a V letter as β initial configuration, a state of fracta collected in center as γ initial configuration, a state being similar to a deadlock state as δ initial configuration. The mutation rate was 0.1 and the number of individuals was 10 for each fractum. The alternation of generation

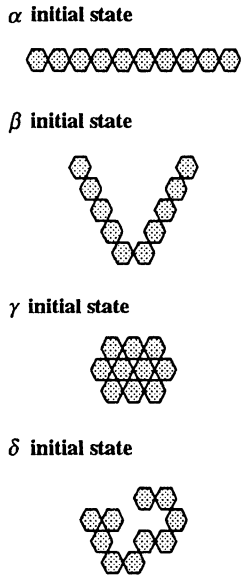


Figure 6: Initial states

was carried out per 10 moving of any fractum. The computer simulations were carried out 50 times for each initial state. The results are shown in Table 1, in which the "*average movement*" denotes the average movement number of all fracta when obtaining the desired configuration, the "*shortest movement*" is the shortest movement number within 50 simulations to obtain the desired configuration. In addition, the "*deadlock rate*" denotes the rate of deadlock evaluated by

$$deadlock\ rate = \frac{n_d + n_o}{50} \qquad (2)$$

where n_d is the number of times that some fracta become a deadlock state and n_o is the number of times that all fracta did not construct a desired configuration up to 2000 movements.

Table 1: Simulations results

Initial state	α	β	γ	δ
Average movement	437	344	262	360
Shortest movement	85	45	16	23
Deadlock rate	0.18	0.57	0.11	0.34

The deadlock state happened mostly exists in the part of configuration; it is not composed of all fracta as shown in Fig. 2. Some examples of the deadlock state structured by a part of all fracta are shown in Fig. 7, in which the black shadowed fracta denote the deadlock state. We observe that after structuring the ringlike deadlock state by 6 fracta, the resting fracta move around the deadlock state in any initial configuration. In the α initial configuration, the number of movement

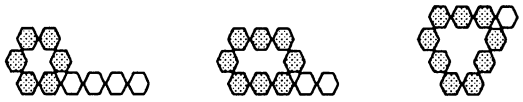


Figure 7: Deadlock states consisting of partial fracta

is much more but the deadlock rate is less than the other initial configuration, because of the string state. The β initial configuration has a high deadlock rate because the parts fracta at the acute angle in the V letter can easily construct a deadlock state. In the γ initial configuration, since it is very similar to the optimal configuration and collected in one place, it has a low number of movement and a low deadlock rate, compared to the other configuration. Although the δ initial configuration is similar to a spectacle like deadlock state, the deadlock rate is less compared to the β initial configuration. This reason seems that this deadlock state is avoided by moving of a movable fractum into the center, before constructing the part of ringlike deadlock state.

6 Conclusion

In this paper, we have considered the initial configuration dependence in self-organizing robot on the optimal structure configuration, where the fractum studied by [2] was used as a unit. By using several simulations with different initial configuration, it was proved that a difference of initial configuration affects on both the deadlock rate and the number of movement of fracta for obtaining an optimal structure configuration.

References

[1] Nagata, T.,"*Robot Systems Aiming at Autonomous Decentralization*,"Ohmsha, Tokyo, 1995.

[2] Murata, S., Kurokawa, H., and Kokaji, S.,"Self-Repairable Machine," *Trans. SICE*, vol. 31-2, pp.254-262, 1995.

[3] Watanabe, K. and Ikeda, Y.,"Optimal structure configuration of self-organizing robots using genetic algorithms," *Proceeding of The 14th SICE Kyushu Branch Annual Conference*, pp.317-320, 1995.

[4] Kitano, H.,"*Genetic Algorithms*," Sangyo-Tosho, Tokyo, 1993.

[5] Iba, H.,"*Introduction to Genetic Algorithms*," Ohmsha, Tokyo, 1994.

[6] Horiuchi, E. and Tani. K.,"A Learning Architecture of Collective Behavior for Mobile Robots in Non-stationary Environments," *Journal of the Robotics Society of Japan* , vol. 14-2, pp.305-312, 1996.

Proc. of Third Int. Symp. on Artificial Life, and Robotics (AROB III' 98),
Oita, Japan, 19-21, January, 1998,

An Incest Prevented Evolution Strategy and Its Application in Optimal Gain Tuning for a Mobile Robot Control System

M.M.A. Hashem*, Keigo Watanabe**, Kiyotaka Izumi** & Takehide Miyazaki*

* Graduate School of Science and Engineering,
Faculty of Engineering Systems and Technology,
Saga University, 1-Honjomachi, Saga 840, Japan.
** Department of Mechanical Engineering,
Faculty of Science and Engineering,
Saga University, 1-Honjomachi, Saga 840, Japan.
Email: watanabe@me.saga-u.ac.jp

Abstract

The success and progress of an evolutionary search algorithm mostly depends upon the balance between population diversity and selective pressure. In this paper, we introduced a new probabilistic incest prevention mechanism to ensure the considerable population diversity and to offset the monotonic selective pressure of our previously developed evolution strategy algorithm. To demonstrate its effectiveness, we applied this algorithm to solve the stable and optimum gain tuning problem of a mobile robot control system.

KeyWords: Evolutionary Computation, Incest Prevention, Mobile Robot Control, Optimum Control, Intelligent Systems.

1 Introduction

Recently, a wide variety of Evolutionary Algorithms (EAs) has been proposed to solve different kinds of optimization problems and for machine learning [1]~[5]. Among them, the Evolution Strategies (ESs) [1]~[4] proved to be able to efficiently solve difficult optimization problems numerically. The effectiveness and simplicity of ES algorithms have induced many people to believe that they are the methods of choice for hard real-life problems superseding traditional search techniques [2]~[4]. However, they are not without their limitations. In particular, the choice of a good evolutionary operator can make a considerable difference to the exploration and exploitation and often even the feasibility of the evolutionary search [1]~[3]. To cope with this problem, we already have developed a novel Evolution Strategy (ES) algorithm [6, 7] in which $(\mu + \mu)$-ES was used. With a view to enhancing its capability to a great extend, we further introduced a new technique called "Incest Prevention" (i.e., prevention in mating of similar individuals). This method insures a considerable balance between population diversity and selective pressure in the ES.

It is very tedious task to find optimal stable-gain which will make the system stable as well as provide with minimum trajectory error of a mobile robot control system by off-line trial and error method [8]. If the gain-dimension of the controller is increased substantially, it is also very difficult to maintain both criteria at the same time. However, to demand stability and miminum trajectory error, one has to come to terms with this seemingly contradictory requirements. On the other hand, it is possible to tune the optimal stable-gain set automatically without tedious repeative trial and error method by using ESs.

The objective of this paper is to tune a set of optimal gain which will provide with stability as well as minimum type-1 servo error for the control system of a mobile robot. To meet these objectives, we used our proposed ES to solve the above problem.

2 The Evolution Strategy(ES)

The general procedure of our developed ES is given in **Table 1** and it is described below briefly.

Table 1: A novel evolution strategy

1. Initialize the population
2. Evaluate the population
3. Apply subpopulation-based max-mean arithematical crossover(SBMAC)
4. Apply time-variant mutation (TVM)
5. Evaluate the population
6. Alternate the generation
7. If termination condition is not satisfied, then go to step 3

Initial population will be generated by using a Uniform Random Number (URN) within desired domain of the parameters.

Subpopulation-based max-mean arithmetical crossover (SBMAC) [6, 7] is employed in the crossover in which each subpopulation's elite and the mean strength of that subpopulation except the elite are used. We devide the μ populations into l number of

subpopulations. We define $\psi_{j,\max}$ as an elite individual that maximizes a cost function within the j-th subpopulation and $\bar{\psi}_j$ as a mean strength of the j-th subpopulation except the $\psi_{j,\max}$, we define the crossover for the subpopulation j as follows :

$$\zeta_1 = \alpha\psi_{j,\max} + (1-\alpha)\bar{\psi}_j \quad (1)$$

$$\zeta_2 = (1-\alpha)\psi_{j,\max} + \alpha\bar{\psi}_j \quad (2)$$

where α is selected from URN[0,1]. Note that the children are generated for each subpopulation by using $(\frac{\mu}{l} + \frac{\mu}{l})$-ES.

Time-variant mutation (TVM) [7] plays a significant role towards fine local tuning. It is proposed to reduce the disadvantage of uniform mutation [3]. The TVM is defined for a child i, as

$$\zeta_i' = \zeta_i + N(0, \sigma^2(t)) \quad (3)$$

where $\boldsymbol{\sigma}(t) = [\sigma(t), \ldots, \sigma(t)]^T$ is the time-variant standard deviation vector at the generation t, and $\sigma(t)$ is defined as

$$\sigma(t) = \left(1 - r^{(1-\frac{t}{T})^\gamma}\right) \quad (4)$$

where r is selected from the URN[0,1], T is the maximal generation number, γ is a real-valued parameter determining the degree of dependency on the generations. The function $\sigma(t)$ returns a value in the range [0, 1], which falls within the evolution window [4] such that the probability of $\sigma(t)$ being close to 0 increases as age of the population, t increases. This property of $\sigma(t)$ causes to search the problem space uniformly initially (when t is small) and very locally at t larger stages.

Evaluation is performed after mutation operation. Each child is evaluated to its cost function (fitness) for a possible solution in each generation.

Alternation of generation is carried out by using $(\mu+\mu)$-ES. That is, among μ parents, which were evaluated at the former generation, and μ children which are evaluated in the current generation, the $\mu + \mu$ individuals are ordered in proportional to the amount of the cost function, and the best μ individuals are selected for the next generation.

3 Proposed Incest Prevention Method

Our developed ES monotonically collects the best individuals by using $(\mu + \mu)$-ES which imposes considerable selective pressure. With a small population size, however, the population converges to the point that it begins to more or less reproduce many of the same individuals and the time-variant standard deviations of the mutation becomes so small, it is unable to perturb the object variables of the individuals to maintain the population diversity. At this instant, we proposed a Highly Disruptive Mutation (HDM) operation with the help of $Gauss(0, 1)$ noise. Some of the individuals (typically $17\% - 34\%$ of the individuals), except that the best individual is preserved intact, undergo HDM operation with a probability of incest prevention, P_{ip} depending on the optimization problem. After this HDM operation, the evolutionary search continues with the SBMAC and TVM as usual. This form of incest prevention is designed to promote the population diversity during the evolution process. The rationale behind it is to have a very aggressive search (by using monotonic selection through survival of the best individuals over the generations) and to offset the aggressiveness of the search by using HDM operation. Now, the modified ES algorithm can be viewed as shown in the **Table 2.**

Table 2: Proposed incest prevented evolution strategy

1. Initialize the population
2. Evaluate the population
3. Apply subpopulation-based max-mean arithematical crossover(SBMAC)
4. Apply time-variant mutation (TVM)
5. Evaluate the population
6. Alternate the generation
7. Calculate the similarity of the population
8. If the population similarity exceeds the given threshold, then apply HDM with given P_{ip} except the best individual
9. If termination condition is not satisfied, then go to step 3

4 A Mobile Robot with Two Independent Driving Wheels

Let the state variable of a mobile robot with two independent driving wheels be $\boldsymbol{x} = [v \quad \phi \quad \dot{\phi}]^T$, the manipulated variable be $\boldsymbol{u} = [u_r \quad u_l]^T$ and the output be $\boldsymbol{y} = [v \quad \phi]^T$ where ϕ is the azimuth angle, v is the moving velocity. Then the corresponding state-space model is described by

$$\dot{\boldsymbol{x}} = A\boldsymbol{x} + B\boldsymbol{u} \quad (5)$$

$$\boldsymbol{y} = C\boldsymbol{x} \quad (6)$$

where

$$A = \begin{bmatrix} a_1 & 0 & 0 \\ 0 & 0 & 1 \\ 0 & 0 & a_2 \end{bmatrix}, \quad B = \begin{bmatrix} b_1 & b_1 \\ 0 & 0 \\ b_2 & -b_2 \end{bmatrix}$$

$$C = \begin{bmatrix} 1 & 0 & 0 \\ 0 & 1 & 0 \end{bmatrix}$$

$a_1 = -2c/(Mr^2 + 2I_w), \quad a_2 = -2cl^2/(I_v r^2 + 2I_w l^2)$
$b_1 = kr/(Mr^2 + 2I_w), \quad b_2 = krl/(I_v r^2 + 2I_w l^2)$
where M is the mass of the robot; l is the distance between any wheel and c.g. of the robot; c is the viscous friction factor for the wheel; r is the radius of the wheel; I_v is the moment of inertia around the c.g. of the robot; I_w is the moment of inertia of the wheel around the driving shaft; and k is the driving gain factor.

5 Type-1 Optimal Servo for the Robot

The continueous-time model (5)-(6) can be expressed by

$$\boldsymbol{x}(k+1) = A_d\boldsymbol{x}(k) + B_d\boldsymbol{u}(k) \quad (7)$$

$$\boldsymbol{y}(k) = C\boldsymbol{x}(k) \quad (8)$$

where A_d and B_d are the system and distribution matrices respectively in the discrete-time and they will be calculated by using the sampling width, 50 [ms] and by the following physical parameter conditions of the robot:
$M = 25.5$ [kg]; $l = 0.165$ [m]; $I_v = 0.6541$ [kgm^2];
$I_w = 4.419 \times 10^{-4}$ [kgm^2]; $k = 90.0$; $r = 0.05$ [m];
$c = 0.0479$ [kgm^2/s].

When designing type-1 optimal servo system, an augmented system is needed and we need the time transition operator described by $f(z^{-1}) = 1 - z^{-1}$. Here z^{-1} denotes the one step-delay operator. We define the reference error vector $\boldsymbol{e}(k)$ for the output error vector $\boldsymbol{y_d}(k)$ as

$$\boldsymbol{e}(k) = \boldsymbol{y_d}(k) - \boldsymbol{y}(k) \tag{9}$$

Since $\boldsymbol{y_d}(k)$ is constant and when $f(z^{-1})$ is applied, it yields to $f(z^{-1})\boldsymbol{y_d}(k) = \boldsymbol{y_d}(k) - \boldsymbol{y_d}(k-1) = 0$. Operating $f(z^{-1})$ on the discrete time model (7)-(8) and the reference error vector (9), it follows that

$$f(z^{-1})\boldsymbol{x}(k+1) = A_d f(z^{-1})\boldsymbol{x}(k) + B_d f(z^{-1})\boldsymbol{u}(k) \tag{10}$$

$$f(z^{-1})\boldsymbol{e}(k) = -f(z^{-1})\boldsymbol{y}(k) \equiv -Cf(z^{-1})\boldsymbol{x}(k) \tag{11}$$

When defining $\boldsymbol{x_a}(k) = [f(z^{-1})\boldsymbol{x}(k) \quad \boldsymbol{e}(k-1)]^T$ as the state variable vector for the augmented system, we have

$$\boldsymbol{x_a}(k+1) = A_a \boldsymbol{x_a}(k) + B_a f(z^{-1})\boldsymbol{u}(k) \tag{12}$$

where

$$A_a = \begin{bmatrix} A_d & 0_{2\times 3} \\ -C & I_{2\times 2} \end{bmatrix}, \quad B_a = \begin{bmatrix} B_d \\ 0_{2\times 2} \end{bmatrix}.$$

In order to design the optimal servo for the augmented system, we will consider a quadratic cost function of the states and the control inputs, that is,

$$J = \sum_{k=0}^{\infty} (\|\boldsymbol{x_a}(k)\|_Q^2 + \|f(z^{-1})\boldsymbol{u}(k)\|_R^2) \tag{13}$$

where Q and R are the symmetric weighting matrices to be selected by the designer. From the augmented system, we can get optimal feedback gain G which will minimize the cost function (13) and it is given by

$$G = (B_a^T P B_a + R)^{-1} B_a^T P A_a \tag{14}$$

where P is the solution of popsitive definite matrix on the algebraic Riccati equation given by

$$P = A_a^T P A_a - A_a^T P B_a (B_a^T P B_a + R)^{-1} B_a^T P A_a + Q \tag{15}$$

Anyhow, if P is computed, then optimal feedback law can be realized by

$$f(z^{-1})\boldsymbol{u}(k) = -G\boldsymbol{x_a}(k) = -[F \quad K]\boldsymbol{x_a}(k) \tag{16}$$

Now dividing both sides of (16) by $f(z^{-1})$, we have

$$\boldsymbol{u}(k) = -F\boldsymbol{x}(k) - K\boldsymbol{z}(k-1) \tag{17}$$

where $(f(z^{-1}))^{-1}\boldsymbol{e}(k-1) = \boldsymbol{z}(k-1)$ and the corresponding type-1 optimal servo system for the robot is shown in **Fig. 1**.

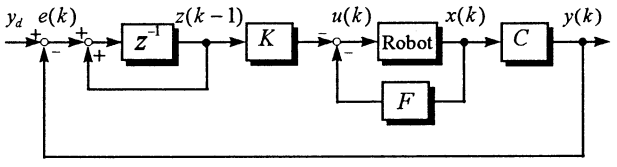


Figure 1: Block diagram for type-1 optimal servo system of the mobile robot

6 The Fitness Function

In order to obtain stable-optimum gains for the robot controller, we have designed the following bidirectional fitness function in which stability as well as trajectory tracking criterion is considered so that both the errors are minimized simultaneously.

$$f(G) = \begin{cases} \dfrac{1}{aE_c + bP_c} & \text{if the system is unstable} \\ \dfrac{1}{E_s} & \text{Otherwise} \end{cases} \tag{18}$$

where E_c is the total unit circle error, P_c is a penalty factor based on the number of unit circle error, a and b are the scalling constants and E_s is the total of the absolute servo tracking errors.

7 Simulations and Results

To simulate the above control system for a straight line trajectory, 4 [m] with a constant velocity, $v_d = 0.2$ [m/s] and a constant azimuth, $\phi_d = 0.0$ [rad], it is assumed that total simulation time is 20 [s] with a sampling width of 50 [ms], and initial state vector $\boldsymbol{x}(0) = [0\ 0\ 0]^T$.

7.1 ES Implementation

The ESs are implemented by using a population size of 60, $l = 10$, $\gamma = 8.0$ and $T = 400$. The similarity metric of the population is calculated as the standard deviation, σ of the population fitnesses. The P_{ip} and the similarity threshold for incest prevention are assumed to be 0.2 and 0.001 respectively. An individual is represented by the gain, G components of the controller. When the fitness function (18) is maximized, the desired gain, G is found.

7.2 Results

By application of the proposed IPES on the fitness function (18), we found the following tuned stable and optimum gain set:

$$G = \left[\begin{array}{ccc:cc} F_{11} & F_{12} & F_{13} & K_{11} & K_{12} \\ F_{21} & F_{22} & F_{23} & K_{21} & K_{22} \end{array}\right]$$

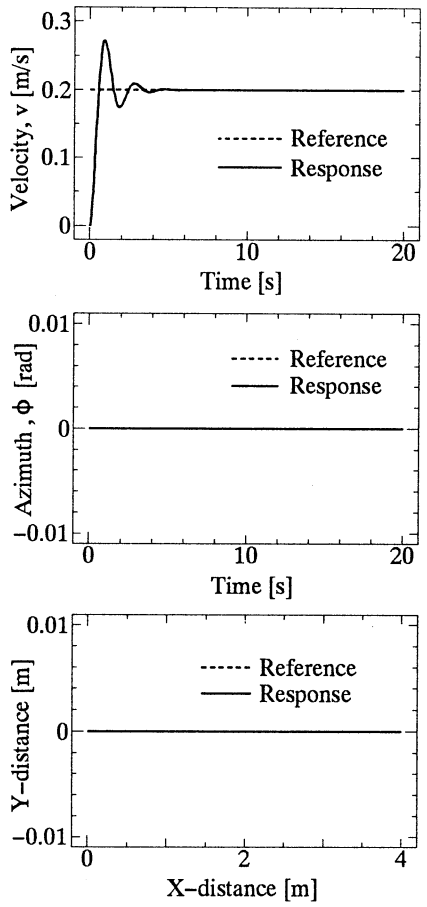


Figure 2: Control results

$$= q \begin{bmatrix} 8.9251 & 8.0602 & 3.1523 & \vdots & -4.2907 & 0.2205 \\ 8.9251 & -4.8231 & -8.7618 & \vdots & -4.2907 & 0.9059 \end{bmatrix}$$

where $q = 1.0 \times 10^{-3}$. And this gain set produces the stable pole locations within the unit circle as $[(0.9804, \pm 0.0456), (0.7003, 0.000), (0.9344, \pm 0.1565)]$. The corresponding control results are shown in **Fig.2**. In spite of velocity overshoot for few seconds, we found good trajectory tracking results. The evolutionary results in **Fig. 3** shows that the convergence of proposed IPES is faster than that of previously developed ES and it can also maintain a fair population diversity.

8 Conclusions

In this paper, we have studied a new ES algorithm to solve stable-optimal gain tuning problem of a type-1 servo control system. The gains are tuned automatically by IPES without iterative trial and error method. The obtained type-1 controller gave the satisfactory control responses. It can be inferred from the presented evolutionary results that the proposed IPES can outperform the previously developed ES. The similarity metric is considered as the standard deviation of the population fitnesses. This is, somewhat, a macro-level similarity. However, a better similarity metric yet to be developed, it may be based on the micro-level, i.e., parameter level. Now, it seems that this algorithm will be more general in practice.

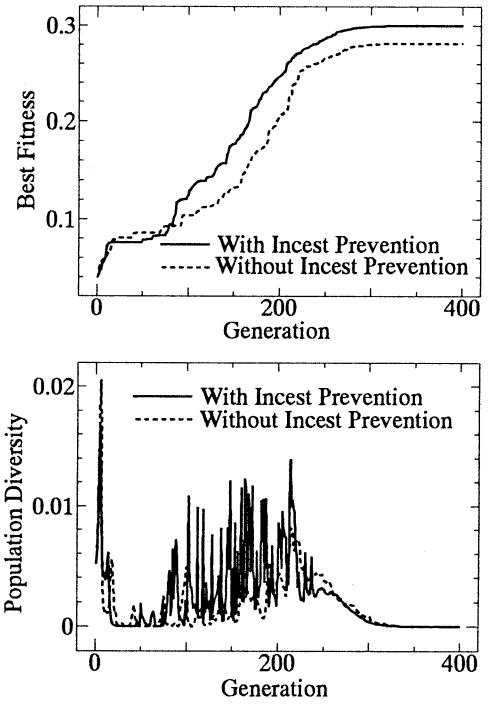


Figure 3: Evolutionary results

References

[1] Schwefel, H.-P., Rudolph, G. and Bäck, T. "*Contemporary Evolution Strategies*," In Advances in Artificial Life, Springer-Verlag, Berlin, pp.893-907, 1995.

[2] Schwefel, H.-P.,"*On the Evolution of Evolutionary Computation*," In Computational Intelligence: Imitating Life, IEEE Press, New York, pp.116-124,1994.

[3] Michalewicz, Z.,"*Genetic Algorithms + Data Structures = Evolution Programs*,"-3rd. rev., and ext. edition, Springer-Verlag, Berlin, 1996.

[4] Rechenberg, I.,"*Evolution Strategy*, "In Computational Intelligence: Imitating Life, IEEE Press, New York, pp.147-159, 1994.

[5] Whitley, D.,"*A Genetic Algorithm Tutorial*," Statistics and Computing, Special issue on Evolutionary Computation, vol.4, pp.65-85,1994.

[6] Izumi, K., Hashem, M.M.A. and Watanabe, K., "*An Evolution Strategy with Competing Subpopulations*," Procs. of the IEEE CIRA'97, Monterey, USA, pp.306-311, 1997.

[7] Hashem, M.M.A., Watanabe, K. and Izumi, K., "*Evolution Strategy: A New Time-Variant Mutation for Fine Local Tuning*," Procs. of 1997 SICE Int'al Sessions, Tokushima, Japan, pp.1099-1103, 1997.

[8] Han-Xiong Li and Gatland, H.B., "*A New Methodology for Designing a Fuzzy Logic Controller*," IEEE Trans. on Syst., Man and Cyber., Vol.25, No.3, pp.505-512, 1995.

Proc. of Third Int. Symp. on Artificial Life, and Robotics (AROB III' 98),
Oita, Japan, 19-21, January, 1998,

Construction of Fuzzy Behavior-Based Control Systems for a Mobile Robot

Keigo Watanabe and Kiyotaka Izumi
Department of Mechanical Engineering
Faculty of Science and Engineering
Saga University
1-Honjomachi, Saga 840, Japan
watanabe@me.saga-u.ac.jp

Abstract

A fuzzy behavior-based control system is proposed for a mobile robot by applying the concept of subsumption architecture and using the softcomputing techniques, in which a simple fuzzy reasoning is assigned to one elemental behavior consisting of a single input-output relation, and then two consequent results from two behavioral groups are competed or cooperated. Here, it is assumed that the order of the input in a behavioral group is the same as that of the output and other behavioral groups have the same condition. For the competition or cooperation between behavioral groups or elemental behaviors, a suppression unit is constructed as a neural network by using a sign function or saturation function. Furthermore, a Jacobian net is introduced to transform the results obtained from the competition or cooperation to the joint coordinate systems. Finally, we consider one example for a mobile robot with two independent driving wheels.

KeyWords: Fuzzy Set Theory, Behavior-Based Control, Fuzzy-Neural Networks, Learning, Reactive Behavior, Subsumption Architecture

1 Introduction

In the control of mobile robots and manipulators, behavior-based control has been actively studied [1]-[3], whose control system is intelligently constructed by running the robot in a given complex environment. This approach is different from conventional approaches such as a regulator problem and a servo problem in the construction of control system. As a representative, there exists the so-called subsumption-architecture [4]. The main features of this concept are that the control system is divided into behavioral elements (or modules), instead of dividing it into functional elements, and the behavioral fusion is taken through the competition and cooperation between behavioral elements. There have been already several studies, depending on how to realize such a fundamental concept.

Although a fusion method between behavioral elements was fixed in advance, Maes [5] proposed a behavior net approach, in which all behavioral elements are connected by the network and the causality relation between behavioral nodes is learned. Oka *et al.* [6] studied an extended approach that combined the Maes behavior net with conventional feedforward and feedback control methods. Since these approaches need the so-called regional knowledge, it is necessary that the detailed behavioral knowledge and strategy are provided in advance.

On the contrary, there exits the Koza GP (Genetic Programming) approach [7], as a method which acquires the behavioral knowledge from actual behaviors, instead of providing a priori regional knowledge. A dynamic behavioral knowledge is evolutionarily obtained through this approach. Note, however, that it needs more number of individuals and generations, and the resultant rules do not seem to be robust against behaviors, because their rules are not generated from fuzzy reasoning techniques.

To acquire the learning behavior of obstacle avoidance control problem for a mobile robot, Furuhashi *et al.* [8] had studied a GA (Genetic Algorithm) approach similar to the Pittsburgh approach that is well-known as a machine learning, in which all control rules are represented using one individual. However, in this approach, the fuzzy reasoning mechanism is constructed using the fusion of several sensor information as conventional control, so that it does not seem to be a behavior-based control, even if it is regarded as a learning-type control, because a reasoning is not generated using the behavioral element and there are no competitions and cooperations between behavioral elements

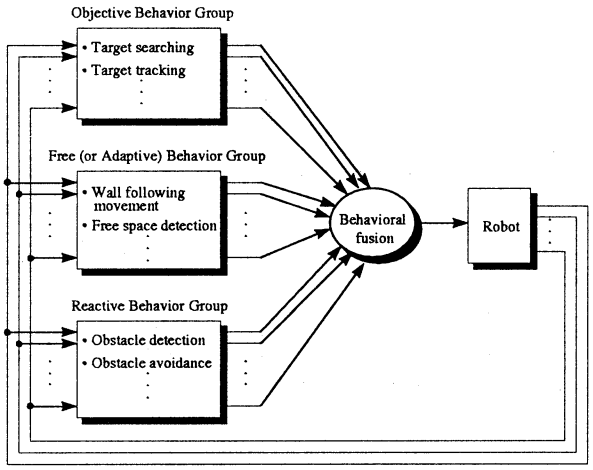


Figure 1: A behavior-based control system using multiple behavior groups for a mobile robot

In this paper, a fuzzy behavior-based control is described using the subsumption architecture as a basic concept, introducing a simple fuzzy reasoning to one behavioral element consisting of single-input and single-output, and making the competition and cooperation of fuzzy reasoning consequents between behavioral groups. Here, it was assumed that, for the simplicity of problem, the number of input and output order is same for any behavioral group and it is also same between behavioral groups

In what follows, we first explain the input-output relation of any behavioral group and its fuzzy rules within such a behavioral group. Next, the fusion method is described by using the competition and cooperation between behavioral groups or elements. In particular, a suppression unit is proposed as a neural network using a sign or saturation function. Furthermore, we introduce a Jacobian net to transform the fuzzy reasoning results obtained from the competition and cooperation into the quantities in the motor (or joint) coordinates. Finally, an example is demonstrated through an obstacle avoidance problem for a mobile robot with two independent drive wheels.

2 Input-Output Relation of Behavior Group and Its Fuzzy Rules

Figure 1 shows an example of the behavior-based control system consisting of three behavior groups for a mobile robot [9]. The reactive behavior group basically consists of some behavioral elements that detect or avoid obstacles. The free (or adaptive) behavior group is composed of some behavioral elements that move following the wall or detect a free space; these behavioral elements connect with a higher level behavior. The objective behavior group consists of some behavioral elements that search or track a target, which is an essential purpose of the robot. The behavioral fusion (unification) part fuses the behavioral results generated from each behavior group by using the competition and cooperation.

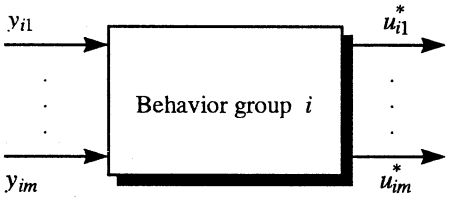


Figure 2: Input-output relation for a behavior group

It should be noted that this figure is persistently a basic concept for the behavior-based control system, so that we have to consider how to use the sensor information obtained from the robot and how to construct each behavior group for each problem.

2.1 Input-output relation of behavior group

In the construction of a behavior group, the following assumptions are assumed:

- The number of input-output order is same for a behavior group.
- The sensor information is generated from the absolute (or work-space) coordinates.
- The force or torque in the absolute coordinates is generated from a behavior group.
- Other behavior groups have the same conditions described above.

As an additional assumption, it is assumed that if the sensor information is once used in a behavior group, then the same sensor information is never used in other behavior group. The input-output relation of this behavior group is shown in Fig. 2.

2.2 Fuzzy rule relation of behavior group

As can be seen from Fig. 3, in a behavior group, a simple fuzzy reasoning is applied to one behavioral element using one sensor information y, and it generates one reasoning result u^*. We use a Gaussian-type function as the membership function, and use the simplified reasoning [10]. The resultant fuzzy reasoning

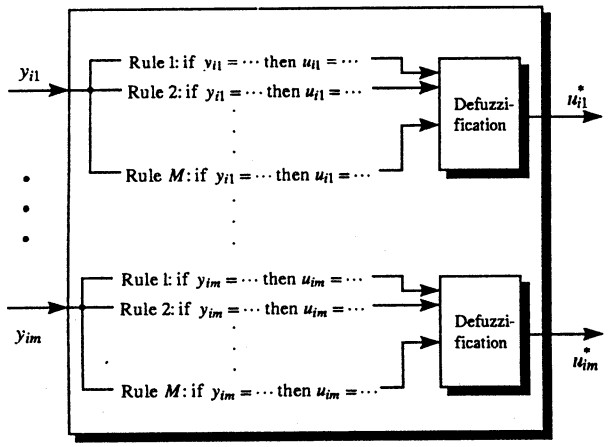


Figure 3: Internal fuzzy rules for a behavior group i

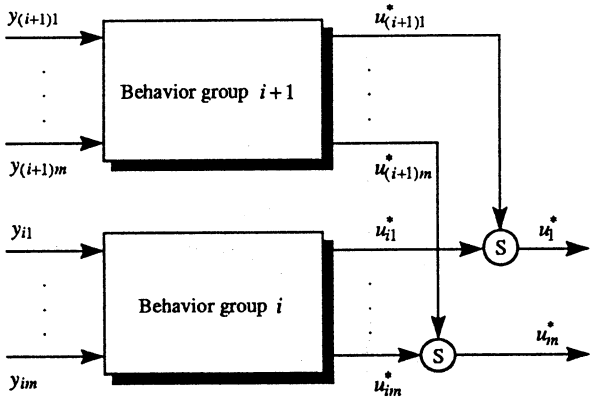


Figure 4: Fusion of two behavior groups

consequent is obtained as

$$u^* = \sum_{i=1}^{M} p_i w_{bi} \tag{1}$$

where M denotes the total number of rules, w_{bi} the constant in the conclusion of the i-th rule, and p_i the normalized rule confidence such as

$$p_i = \frac{\mu_i}{\sum_{j=1}^{M} \mu_j} \tag{2}$$

$$\mu_i = \exp\{\ln(0.5)(y - w_{ci})^2 w_{di}^2\} \tag{3}$$

Here, w_{ci} denotes the center value (e.g. the mean value of a Gaussian like membership function) associated with the i-th membership function, and w_{di} denotes the reciprocal value of the deviation from the center w_{ci} to which the i-th Gaussian function of the input data on the standardized support set has value 0.5.

In a conventional reactive behavior, a number of rules are driven in parallel by using only one sensor information and a suitable rule that satisfies a condition is selected. On the other hand, using a simple fuzzy reasoning technique gives a consequent result as a weighted sum of multi-rules. In other words, using M fuzzy divisions of a behavioral element gives a tolerance to the determination of the behavioral element; as a result, our approach may acquire a more robust behavior against a change of environment.

3 Fusion of Behavior Groups

Here, we explain how to fuse the reasoning results obtained from each behavioral element. That is, the forces or torques in the absolute coordinate systems are fused by using the competition and cooperation of the reasoning consequents for the behavioral elements between the behavior groups, and the associated fusion units are constructed using the neural network.

3.1 Subsumption relation of behavior group outputs

Consider the two behavior groups i and $i+1$ shown in Fig. 4. Let the two forces (or torques), which have the same output number in their behavior groups, be described as a and b, and their signs be compared. If they have the same sign, then it is regarded as the cooperation and the output from the upper group $i+1$ is treated as the fusion result $c = b$. Otherwise, if they have the opposite sign, then it is regarded as the competition and the output from the lower group i is treated as the fusion result $c = a$.

In case of more than three groups, the similar fusion procedure is taken from the top group and proceeded to the lower group; thus, the force or torque that is fed to the Jacobian net is finally determined in the absolute coordinate systems. It should be noted that the fusion method described above has not necessarily been applied to the conventional subsumption architecture. For example, let a and b be the lower and the upper behavior outputs respectively, if either a or b has the OFF state, then the either ON state is generated as the fusion result, whereas if both a and b have the ON state, then the ON state in the lower behavior is generated as the fusion result.

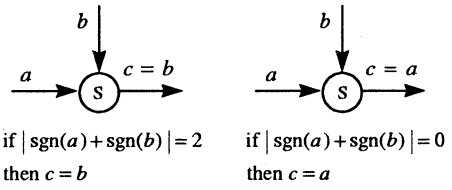


Figure 5: Logic for a suppression unit

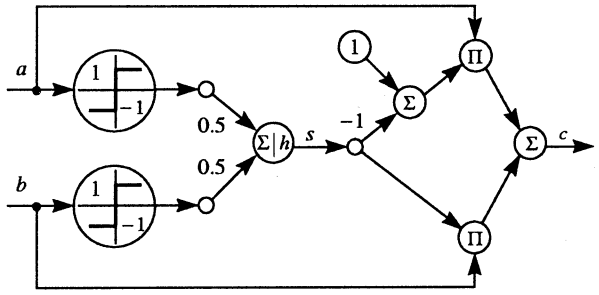


Figure 6: Sgn function-type suppression unit realized as a NN

3.2 Construction of suppression unit as a neural network

We refer to the unit with the logic described above as suppression unit. If we use the following sign function

$$\mathrm{sgn}(x) = \begin{cases} 1 & \text{for } x > 0 \\ -1 & \text{for } x < 0 \end{cases} \tag{4}$$

the cooperation taking the same sign is written by

$$\text{if } |\mathrm{sgn}(a) + \mathrm{sgn}(b)| = 2 \text{ then } c = b \tag{5}$$

whereas the competition taking opposite sigh is written by

$$\text{if } |\mathrm{sgn}(a) + \mathrm{sgn}(b)| = 0 \text{ then } c = a \tag{6}$$

Figure 5 depicts this concept. Introducing a switching variable s and summarizing the above results gives

$$c = (1 - s)a + sb \tag{7}$$

$$s = |\mathrm{sgn}(a) + \mathrm{sgn}(b)|/2 \tag{8}$$

This suppression logic circuit is shown in Fig. 6, if used the neural network.

This sign function (or hard limiter) type suppression unit may not give a practical fusion result, if the output from both groups or either group is very small. Therefore, it seems to be practical that the above logic is applied to the reasoning results a and b having the

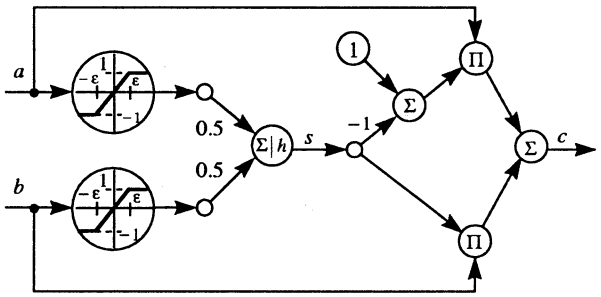


Figure 7: Saturation function-type suppression unit realized as a NN

larger magnitude than a fixed order, otherwise the fusion unit is composed of the weighted sum of both reasoning results. For this purpose, it is reasonable to introduce the following saturation function:

$$\mathrm{sat}(x) = \begin{cases} \mathrm{sgn}(x) & \text{for } |x| > \epsilon \\ x/\epsilon & \text{for } |x| \le \epsilon \end{cases} \tag{9}$$

where ϵ denotes a small positive number. Consequently, following the same manner as in (7), the output expression of the unit results in

$$c = (1 - s)a + sb \tag{10}$$

$$s = |\mathrm{sat}(a) + \mathrm{sat}(b)|/2 \tag{11}$$

Figure 7 shows the suppression logic circuit based on using the saturation functions, which is realized by using the neural network.

4 Jacobian Net

The force or torque in the absolute (or work-space) coordinate systems is obtained by fusing the reasoning results generated from each behavior group by using the nonlinear suppression unit. To transform the above quantity to the torque in the motor (or joint) coordinate systems, we use the Jacobian net as shown in Fig. 8. If the Jacobian matrix is known, then the net structure is fixed as J^T; this is a simple coordinate transformation. In a practical robot operation, we have to further transform the torque input to the associated voltage or current, so that the transformation gain to the actuator driver should be determined in advance. However, for the case when the Jacobian matrix or transformation gain is unknown, the Jacobian net must be trained as a net with the changeable connection weights.

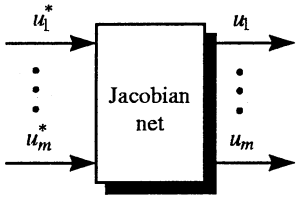


Figure 8: Jacobian net; it is just J^T, if the Jacobian is known

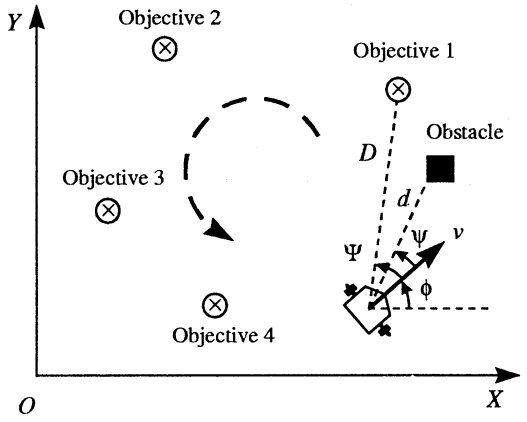


Figure 9: Behavior model for a mobile robot with two independent driving wheels

5 A Construction Example

Now, following the method described above, let us try to construct a control system in the obstacle avoidance problem for a mobile robot with two independent driving wheels.

Suppose that the sensor information of the robot is given by Fig. 9. Here, ϕ is the azimuth angle of the robot, v the forward velocity, ψ the relative angle between the forward direction of the robot and the obstacle, d the distance between the robot and the obstacle, Ψ the relative angle between the forward direction of the robot and the objective point, and D the distance between the robot and the objective point. The task given for the robot is that the robot travels to all objective points only one time, but proceeds in order from the point 1 to the point 4. In addition, if the obstacle is found, then the robot must avoid it.

Figure 10 shows a construction example of the fuzzy behavior-based control system for the above problem. Here, note that the sensor information supplied to each behavior group are not shared, as described before. Figure 11 shows one sample behavioral element, expressed by a fuzzy neural network (FNN) [11], for the velocity change behavior in the free behavior group, in which the behavioral element is divided into three fuzzy regions. In this model, the center value w_{vci}, the reciprocal value of the deviation w_{vdi}, and the constant value in the conclusion w_{vb} must be learned by using any method. Furthermore, the Jacobian matrix for this type of mobile robots is known as

$$\begin{bmatrix} u_r \\ u_l \end{bmatrix} = J^T \begin{bmatrix} u_v \\ u_\phi \end{bmatrix} \tag{12}$$

$$J^T = \frac{r}{2} \begin{bmatrix} 1 & 1/l \\ 1 & -1/l \end{bmatrix} \tag{13}$$

where u_v denotes the force for changing the robot velocity, u_ϕ denotes the torque for changing the azimuth angle of the robot, r is the radius of the wheel, and l is the length from the center of gravity of the robot to the one wheel.

Thus, if J is known, then the Jacobian net is fixed as shown in Fig. 12. However, if the Jacobian matrix is unknown or the transformation gain to the driver is also learned, then four connection weights must be learned as shown in Fig. 13.

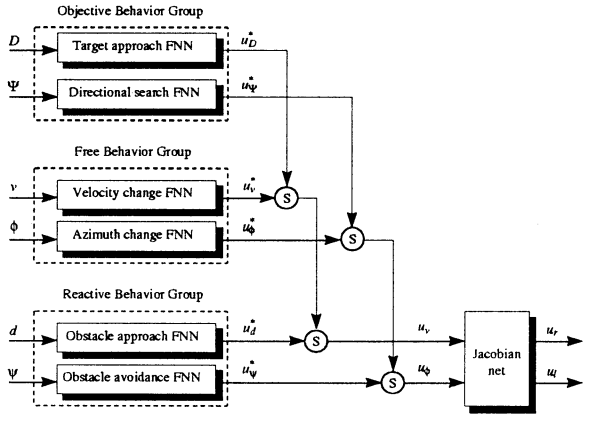


Figure 10: Fuzzy behavior-based control system for a mobile robot

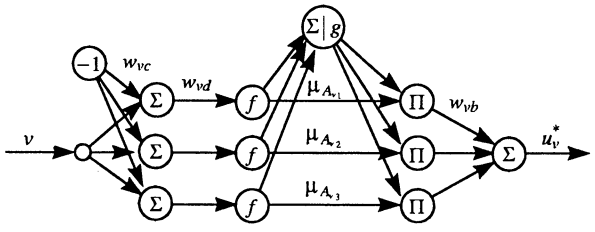


Figure 11: A FNN for an elemental behavior

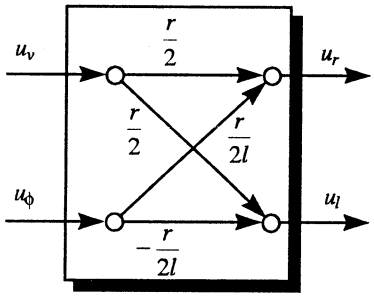


Figure 12: Jacobian net: known case

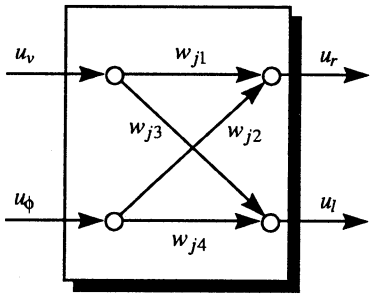


Figure 13: Jacobian net: unknown case

6 Conclusions

In this paper, we have described a fuzzy behavior-based control system, which is basically based on the concept of subsumption architecture and realized by the softcomputing technique. The proposed method has been based on introducing a simple fuzzy reasoning to one behavioral element consisting of single-input and single-output, and making the competition and cooperation of fuzzy reasoning consequents between behavioral groups. However, it was assumed that the number of input and output order is same for any behavioral group and it is also same between behavioral groups.

To make a fusion of fuzzy reasoning results by using the competition and cooperation between behavioral groups or elements, a suppression unit was also described as a neural network using a sign or saturation function. In addition, a Jacobian net was introduced to transform the fuzzy reasoning results obtained from the competition and cooperation into the quantities in the motor (or joint) coordinates. Finally, an example was demonstrated through an obstacle avoidance problem for a mobile robot with two independent drive wheels.

References

[1] S. Yamada: "Learning for Reactive Planning," *J. of the Robotics Society of Japan*, vol. 13, no. 1, pp. 38-43, 1995 (in Japanese).

[2] Y. Kuno: "Behavior of Behavior-based Robots," *J. of the Robotics Society of Japan*, vol. 11, no. 8, pp. 1178-1184, 1994 (in Japanese).

[3] N. Yoshida: "Robot Motion Control Using Subsumption Architecture," *J. of the Robotics Society of Japan*, vol. 11, no. 8, pp. 1118-1123, 1993 (in Japanese).

[4] R.A. Brooks: "A Robust Layered Control Systems for a Mobile Robot," *IEEE Robotics and Automation*, vol. 2, no. 1, pp. 14-23, 1986.

[5] P. Maes: "Learning Behavior Networks from Experience," *Procs. of 1st European Conf. on Artificial Life*, pp. 48-57, 1992.

[6] T. Oka, M. Inaba and H. Inoue: "Designing Hierarchical Motion Systems for Autonomous Robots based on BeNet," *Procs. of JSME Annual Conf. on Robotics and Mechatronics*, vol. B, pp. 1361-1364, 1996 (in Japanese).

[7] J.R. Koza: "Evolution of Subsumption using Genetic Programming," *Procs. of 1st European Conf. on Artificial Life*, pp. 110-119, 1992.

[8] T. Furuhashi, K. Nakaoka, H. Maeda and Y. Uchikawa: "A Proposal of Genetic Algorithms with a Local Improvement Mechanism and Finding of Fuzzy Rules," *J. of Japan Society for Fuzzy Theory and Systems*, vol. 7, no. 5, pp. 978-987, 1995 (in Japanese).

[9] M. Watanabe, K. Onoguchi and Y. Kuno: "Control of Mobile Robot by Cooperation with Multiple Behavior-Based Agents," *Toshiba Review*, vol. 47, no. 7, pp. 540-543, 1992 (in Japanese).

[10] K. Tanaka: *Advanced Fuzzy Control*, Kyoritsu-syuppan, 1994 (in Japanese).

[11] K. Watanabe, K. Hara, S. Koga, and S.G. Tzafestas: " Fuzzy-neural network controllers using the mean-value-based functional reasoning", *Neurocomputing*, vol. 9, pp. 39-61, 1995.

Proc. of Third Int. Symp. on Artificial Life, and Robotics (AROB III' 98),
Oita, Japan, 19-21, January, 1998,

Fuzzy Behavior-Based Tracking Control for an Omnidirectional Mobile Robot

Kiyotaka Izumi and Keigo Watanabe
Department of Mechanical Engineering
Faculty of Science and Engineering
Saga University
1-Honjomachi, Saga 840, Japan
izumi@me.saga-u.ac.jp

Abstract

In this paper, we newly develop a fuzzy behavior-based control system that combines the concept of subsumption architecture and fuzzy reasoning technique, and then apply it for an omnidirectional mobile robot with three orthogonal wheel mechanisms. The present behavior-based control system is fundamentally similar to the system due to the subsumption architecture, but has a competition or cooperation unit consisting of a saturation function to generate a suitable consequent result. Thus, the proposed behavior-based control system is realized as a soft-computing. We discuss the concrete strategy for the fuzzy behavior-based control system. The effectiveness of the present method is illustrated with a simulation example for the acquisition of an objective point.

KeyWords: Fuzzy Behavior-Based Control, Subsumption Architecture, Genetic Algorithm, Omnidirectional Mobile Robot

1 Introduction

A behavior-based control system, which can intelligently construct a controlled system for a mobile robot or manipulator, is now being attractive in the field of robotics [1]-[3]. One very interesting approach is known as a subsumption architecture [4]. In this method, the controlled system is separated into each elemental behavior, and then several results from elemental behaviors are competed or cooperated.

In this paper, we newly develop a fuzzy behavior-based control system that combines the concept of subsumption architecture and fuzzy reasoning technique, and then apply it for an omnidirectional mobile robot with three orthogonal wheel mechanisms. The present behavior-based control system is fundamentally similar to the system due to the subsumption architecture, but has a competition or cooperation unit consisting of a saturation function to generate a suitable consequent result. Thus, the proposed behavior-based control system is realized as a soft-computing.

Concretely, the simplified fuzzy reasoning is assigned to each elemental behavior consisting of a single input-output relation. The mean value and inverse value of standard deviation for Gaussian membership function, and a constant value in the conclusion part are learned by a genetic algorithm (GA). Thus, the total parameters associated with a fuzzy controller are encoded within one chromosome, like a Pittsburgh approach. We discuss the concrete strategy for the fuzzy behavior-based control system. The effectiveness of the present method is illustrated with a simulation example for the acquisition of an objective point using an omnidirectional mobile robot.

2 Omnidirectional Mobile Robot

2.1 Dynamical Model of Robot

An omnidirectional mobile robot has a horonomic property. Such a mobile robot is expected to be applied for a cart in the confused environment. The nonlinear dynamical equation is given by

$$\dot{\boldsymbol{x}} = A(\boldsymbol{x})\boldsymbol{x} + B(\boldsymbol{x})\boldsymbol{u} \tag{1}$$

where $\boldsymbol{x} = [x_w, y_w, \phi, \dot{x}_w, \dot{y}_w, \dot{\phi}]$. Here, x_w and y_w are the positions on the absolute coordinate system, ϕ is the rotational angle of the moving coordinate system with respect to the absolute coordinate system, $\boldsymbol{u} = [u_1, u_2, u_3]$, u_i $(i = 1, 2, 3)$ is a driving input torque for

each assembly. Coefficient matrices are expressed by

$$A(\boldsymbol{x}) = \begin{bmatrix} 0 & 0 & 0 & 1 & 0 & 0 \\ 0 & 0 & 0 & 0 & 1 & 0 \\ 0 & 0 & 0 & 0 & 0 & 1 \\ 0 & 0 & 0 & a_1 & -a_2\dot{\phi} & 0 \\ 0 & 0 & 0 & a_2\dot{\phi} & a_1 & 0 \\ 0 & 0 & 0 & 0 & 0 & a_3 \end{bmatrix},$$

$$B(\boldsymbol{x}) = \begin{bmatrix} 0 & 0 & 0 \\ 0 & 0 & 0 \\ 0 & 0 & 0 \\ b_1\beta_1(\phi) & b_1\beta_2(\phi) & 2b_1\cos\phi \\ b_1\beta_3(\phi) & b_1\beta_4(\phi) & 2b_1\sin\phi \\ b_2 & b_2 & b_2 \end{bmatrix},$$

with

$$\begin{aligned} a_1 &= -3c/(3I_w + 2Mr^2), \\ a_2 &= 3I_w/(3I_w + 2Mr^2), \\ a_3 &= -3cL^2/(3I_wL^2 + I_vr^2), \\ b_1 &= kr/(3I_w + 2Mr^2), \\ b_2 &= krL/(3I_wL^2 + I_vr^2), \\ \beta_1(\phi) &= -\sqrt{3}\sin\phi - \cos\phi, \\ \beta_2(\phi) &= \sqrt{3}\sin\phi - \cos\phi, \\ \beta_3(\phi) &= \sqrt{3}\cos\phi - \sin\phi, \\ \beta_4(\phi) &= -\sqrt{3}\cos\phi - \sin\phi, \end{aligned}$$

where L is the distance between any assembly and the center of gravity of the robot; c is the viscous friction factor for the wheel; I_v is the moment of inertia for the robot; M is the mass of the robot; r is the radius of the wheel; I_w is the moment of inertia of the wheel around the driving shaft; and k is the driving gain factor.

2.2 Jacobian Matrix

The Jacobian matrix J of the mobile robot satisfies

$$\begin{bmatrix} u_1 \\ u_2 \\ u_3 \end{bmatrix} = J^T \begin{bmatrix} u_x \\ u_y \\ u_\phi \end{bmatrix}, \tag{2}$$

$$J^T = \frac{r}{3}\begin{bmatrix} \beta_1(\phi) & \beta_3(\phi) & 1/l \\ \beta_2(\phi) & \beta_4(\phi) & 1/l \\ 2\cos\phi & 2\sin\phi & 1/l \end{bmatrix} \tag{3}$$

where u_x is the input force for x direction, u_y is the input force for y direction and u_ϕ is the input torque for the rotational angle.

3 Fuzzy Behavior-Based Control

In this section, a procedure of the fuzzy behavior-based control is shown about a terminal control problem in which an omnidirectional mobile robot travels to a goal point, as illustrated in Fig. 1. Here, $\sum_w$ is the absolute coordinate, $\sum_m$ is the moving coordinate, d_x and d_y are the errors between the center of mass for the robot and the objective point about each direction, i.e., $d_x = x_d - x_w$ and $d_y = y_d - y_w$, where x_d and y_d are the terminal point. To solve this problem, we construct a fuzzy behavior-based control system which has an objective behavior group and a free behavior group as shown in Fig. 2. In Fig. 2, u_x^* denotes the force to change the goal distance of x direction, u_y^* is the force to change the goal distance of y direction, u_{vx}^* is the force to change the velocity of x direction, u_{vy}^* is the force to change the velocity of y direction, u_x is the force to change the x position of the robot, u_y is the force to change the y position of the robot and u_ϕ denotes the torque to change the rotational angle of the robot. The symbol S denotes a suppression unit that implies the cooperation and competition for the output results of two behavioral elements. If two reasoning results are expressed by a and b, then the suppression logic can be written by

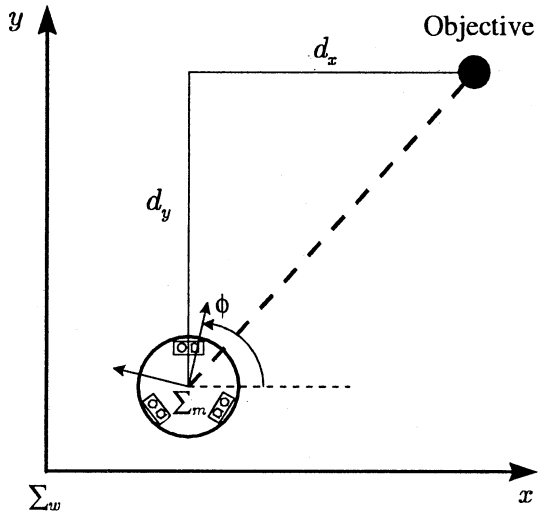


Figure 1: Behavior model for an omnidirectional mobile robot

$$c = (1-s)a + sb, \tag{4}$$

$$s = |\mathrm{sat}(a) + \mathrm{sat}(b)|/2, \tag{5}$$

where c denotes the result of competition or cooperation and $\mathrm{sat}(\cdot)$ is a saturation function

$$\mathrm{sat}(x) = \begin{cases} \mathrm{sgn}(x) & \text{for } |x| > \epsilon \\ x/\epsilon & \text{for } |x| \le \epsilon \end{cases} \tag{6}$$

in which ϵ is a small positive constant. In this problem, the case in which the output results of two behavior

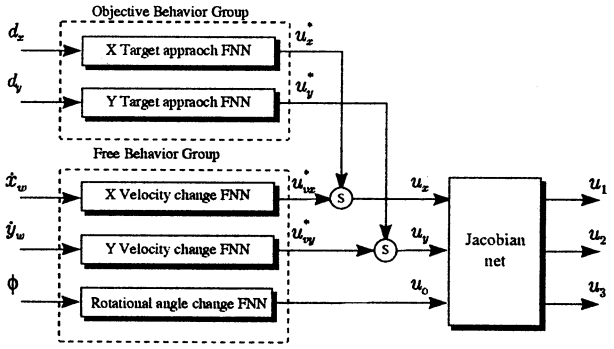


Figure 2: Fuzzy behavior-based control system

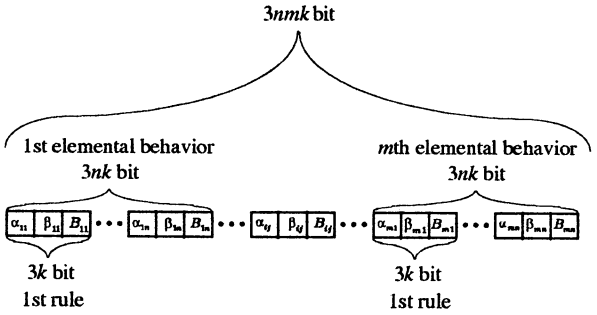


Figure 3: Individual structure

groups have same sign is defined as the cooperation, whereas the case in which those results have opposite sign is defined as the competition. This logic differs from that in the conventional subsumption.

4 Learning of Fuzzy Rules Using GA

Each elemental behavior is expressed by single-input and single-output as shown in Fig. 2. It is assumed that the fuzzy reasoning for each behavioral element consists of a simplified reasoning with single input and output and that a Gaussian type function is used as the membership function, so that learned parameters are the center value of the membership function, the reciprocal value of the standard deviation and the constant value of conclusion part. If the number of label is n and the number of elemental behavior is m, then the number of learned parameters is $3nm$. A bit size of an individual is $3nmk$, where a learned parameter is represented by k bits, as shown in Fig. 3. The transformation from the genotype to the phenotype for a learned parameter is given by

$$x = x_{\min} + (x_{\max} - x_{\min}) \frac{\text{gcode}}{2^k - 1} \qquad (7)$$

Table 1: Min and max values of central value

	Min	Max
d_x and d_y	-3	3
$\dot{x}_w$ and $\dot{y}_w$	-1	1
ϕ	$-\pi$	π

Table 2: Min and max values of standard deviation

	Min	Max
d_x and d_y	2/3	10/3
$\dot{x}_w$ and $\dot{y}_w$	2	10
ϕ	$2/\pi$	$10/\pi$

where x is the center value of membership function or the reciprocal value of standard deviation or the constant value of conclusion, $x_{\min}$ and $x_{\max}$ denote the minimum and the maximum values for each parameter, and "gcode" denotes the value obtained by transforming the genotype into the integer with a gray code.

5 Simulation

5.1 Parameter Setting

The objective point is $(x_d, y_d) = (2.0[\text{m}], 2.0[\text{m}])$ in the absolute coordinate system and the objective rotational angle is $\phi_d = \pi/6[\text{rad}]$. The initial value of state is $[0, 0, 0, 0, 0, 0]^T$. The sampling interval is 50 [ms].

The fitness function for the objective behavior is

$$fitness = D_{\text{end}} + |\Delta\phi|, \qquad (8)$$

where D_{end} is the distance between the final point of the robot and the objective point, $\Delta\phi$ is the error between the the final rotational angle and the objective rotational angle, i.e., $\Delta\phi = \phi_d - \phi_{\text{end}}$. Acquiring the objective behavior is equivalent to solving the minimization problem of equation (8).

The maximum and minimum values of the center value and the reciprocal value of the standard deviation for the membership function in the antecedent part are shown in Table 1 and Table 2, respectively, and those of the constant value in the consequent part are also shown in Table 3.

The GA parameter is set as follows. The population size is set to be 60. The selection method is a

Table 3: Min and max values of consequent part

	Min	Max
d_x, d_y, $\dot{x}_w$ and $\dot{y}_w$	-10	10
ϕ	-0.01	0.01

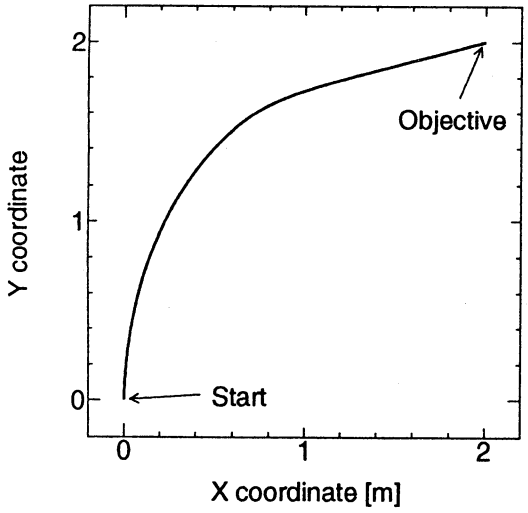


Figure 4: Resulting mobile robot path

tournament type with three individuals. The crossover method is a uniform type with its probability 0.6. The mutation probability is fixed to be 1/600. The number of generation is fixed to be 300. The boundary layer value ϵ, which is used in the saturation function to make a competition or cooperation of the reasoning result, is set to be 1.0×10^{-5}.

5.2 Simulation Result

The resulting path is illustrated in Fig. 4. The mobile robot has reached to the final goal point. Figure 5 illustrate the rotational angle. It is found that the robot slowly turns up to $\pi/6$ within the whole simulation time. Finally, the history of learning for the control system is shown in Fig. 6. The fitness approach to the optimal value which is zero.

6 Conclusions

The fuzzy behavior-based control system has been applied to the acquisition problem of a goal point for an omnidirectional mobile robot. The efficacy of this method was shown by a simulation.

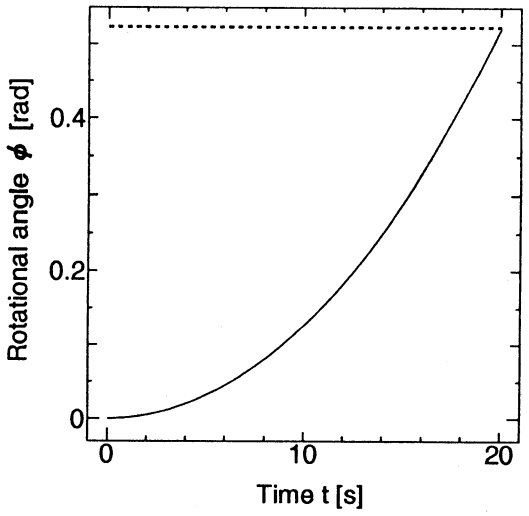


Figure 5: Resulting rotational angle of robot

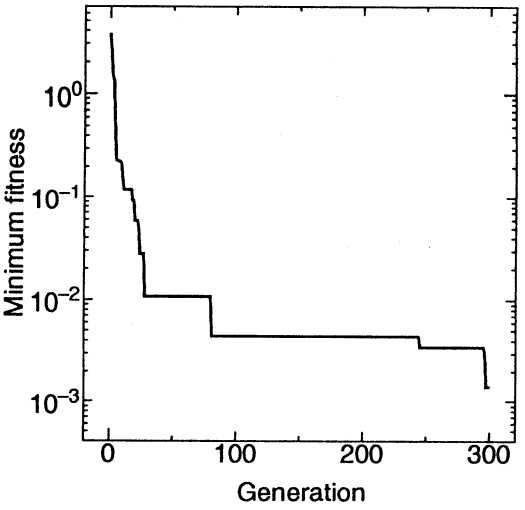


Figure 6: History of minimum value of fitness

References

[1] S. Yamada, Learning for Reactive Planning, *Journal of the Robotics Society of Japan*, Vol.13, No.1, pp.38-43, 1995 (in Japanese).

[2] Y. Kuno, Behaviors of Behavior-Based Robots, *Journal of the Robotics Society of Japan*, Vol.11, No.8, pp.1178-1184, 1993 (in Japanese).

[3] N. Yoshida, Robot Motion Control Using Subsumption Architecture, *Journal of the Robotics Society of Japan*, Vol.11, No.8, pp.1118-1123, 1993 (in Japanese).

[4] R.A. Brooks, A Robust Layered Control Systems for a Mobile Robot, *IEEE Robotics and Automation*, Vol. 2, No. 1, pp. 14-23, 1986.

Proc. of Third Int. Symp. on Artificial Life, and Robotics (AROB III' 98),
Oita, Japan, 19-21, January, 1998,

Neuro-Approach to Motion Control

Sigeru Omatu
Department of Computer and Systems Sciences,
College of Engineering, Osaka Prefecture University,
Sakai, Osaka 593, Japan
Email:omatu@cs.osakafu-u.ac.jp

Abstract-----In this paper, we consider neur-approach to motion control based on a PID(propotional plus integral plus derivative) control method to stabilize the pendulum. This controller requires the determination of PID control gains, but it is difficult to select the best gains theoretically. Here, we propose a method to use the neural networks to tune the PID gains such that human operators tune the gains adaptively according to the environmental condition and systems specification. As an example of self-tuning the PID gains, we consider the torque control of electric vehicle.

1. Introduction

Computational intelligence like fuzzy theory, neural network, genetic algorithm, artificial life, etc. has been well-developed and applied to many real control problems in an efficient way[1]-[2]. As in real control processes, the PID controller has been used as a major control method and the operators are selecting a suitable PID gains from time to time based on their experience and knowledge, it is required to find a suitable PID gains automatically. The main reason is that its structure is simple and PID controllers are robust with noise and parameter variations. But to use the controller, we must tune the PID gains which have been determined by experience and knowledge. In this paper, we propose a tuning method of the PID gains by using neural networks and apply it to torque control of an electric vehicle.

2. Neur–control approach

Recently, many neuro-control schemes have been proposed [1]-[3] where a neural network can be trained to perform as a controller by learning an inverse model of the plant or as an emulator by identifying the forward model. Among many neural network learning methods, the back-propagation algorithm[1] is the most widely used in a wide variety of applications. In control problems, there has been development on neuro-control for robots control problems. Although various intelligent control methods may be applied to this problem, PID control is a major approach since it is robust to noise and stable for parameter change.

Using the back-propagation method, various kinds of neuro-controllers could be trained in such a way that the desired plant output is attained as much as possible. The basic control scheme is depicted as Fig.1 where feedforward controller(FFC) and feedback controller(FBC) are adjusted. The neuro-controller is used in FFC or FBC instead of a conventional controller. In Fig.2 three typical neuro-controllers are illustrated where (a) is called a series type, (b) is called a parallel type, and (c) is called a self-tuning type. In this paper, we consider the self-tuning type of (c) in Fig.2 when FFC is neglected and the PID structure is adopted for FBC.

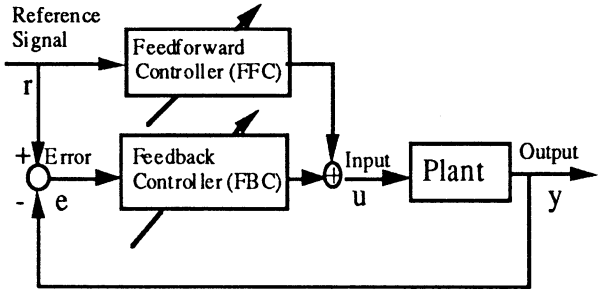


Fig. 1. General control scheme.

3. Self-tuning neuro-PID Controller

The control structure of the self-tuning neuro-PID controller can be shown in Fig.2 where the outputs of the neural network are proportional(P), integral(I), and derivative(D) gains and the inputs are selected in a suitable way according to the specific problem.

In order to derive the self-tuning neuro-PID control algorithm, we will define mathematical notations of neuron models. Total input to neuron j is denoted by *net* j and given by

$$net_j = \sum_{i=1}^{n} w_{ji} O_i + \theta_j$$

where θ_j denotes a threshold. Then the output of neuron i becomes

$$O_j = f(net_j), \quad f(x) = \frac{1}{1+e^{-x}}$$

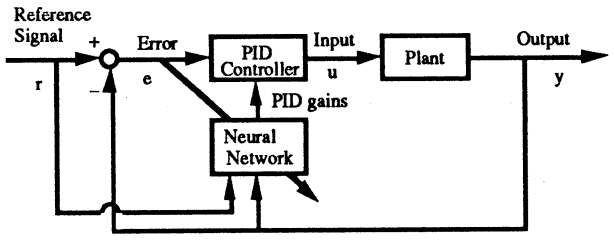


Fig. 2. Self-tuning neuro-PID control scheme.

By connecting many neurons in a layered array, we can derive a learning rule based on the gradient method, which is called the error-back-propagation(BP) method. The BP method is described as follows:

Step 1. Find the generalized error δ_k at the output layer

$$\delta_k = (t_k - O_k) f'(net_k)$$

and the generalized error at the hidden layer

$$\delta_j = f'(net_j) \sum_{k=1}^{K} \delta_k w_{kj}$$

where t_k is the target pattern, O_k is the actual output of neural networks, $f'(x)$ denotes a derivative of $f(x)$ with respect to x, and w_{ji} denotes the connection weight from neuron i to neuron j.

Step 2. Change the connection weights by w_{ji} in the following way.

At the output layer

$$\Delta w_{kj}(n+1) = \eta \delta_k O_j + \alpha \Delta w_{kj}(n) + \beta \Delta w_{kj}(n-1)$$

and at the hidden layer

$$\Delta w_{ji}(n+1) = \eta \delta_j O_i + \alpha \Delta w_{ji}(n) + \beta \Delta w_{ji}(n-1)$$

where a modified BP method has been used to avoid the local minimum problem.

Step 3. If the error becomes smaller than a predetermined value, then stop and if not, then n is replaced by n+1 and go to *step* 1.

Using the above BP algorithm, we can derive the self-tuning neuro-PID control algorithm. First, note that the PID controller in discrete-time is described as

$$u(n) = u(n-1) + K_P \ (e(n)-e(n-1)) + K_I \ e(n) + K_D \ (e(n)-2e(n-1)+e(n-2)) \quad (1)$$

where K_P, K_I, and K_D are proportional, integral, and derivative gains, respectively, u(n) denotes the plant input at nT, and e(n) is the error between a desired value r(n) and the actual output y(n), that is,

$$e(n) = r(n) - y(n).$$

Here, T denotes a sampling interval.

In order to adjust K_P, K_I, and K_D adaptively, we use a three layered neural network based on the BP method. Each layer consists of N_1, N_2, and N_3 neurons where N_1 and N_2 can be selected by trial and error according to complexity of the plant and N_3 is three which are equal to the number of PID gains. For the BP method, we need a cost function E which should be minimized. Here, the following E is adopted such that the PID controller can decrease the error e(n+1) at (n+1)T,

$$E = \frac{1}{2} \ e(n+1)^2.$$

The connection weights w_{kj} at the output layer are updated by the following relation.

$$\Delta w_{kj}(n) = \eta \delta_k O_j + \alpha \Delta w_{kj}(n-1) + \beta \Delta w_{kj}(n-2)$$

where

$$\delta_k = - \frac{\partial E}{\partial net_k}.$$

Using the chain rule for derivative, we get

$$\delta_k = e(n+1) \frac{\partial y(n+1)}{\partial u(n)} \frac{\partial u(n)}{\partial O_k} \frac{\partial O_k}{\partial net_k}$$

Furthermore, we have from (1)

$$\frac{\partial w(n)}{\partial O_k} = \begin{cases} e(n)-e(n-1), & \text{for } k=1 \\ e(n), & \text{for } k=2 \\ e(n)-2e(n-1)+e(n-2), & \text{for } k=3 \end{cases}$$

where $O_1 = K_P$, $O_2 = K_I$, and $O_3 = K_D$.

If the plant is unknown, two approximation algorithms to calculate the system Jacobian $\frac{\partial y(n+1)}{\partial u(n)}$.

The first one is to use the following relation:

$$\frac{\partial y(n+1)}{\partial u(n)} = \text{sign}\left(\frac{\partial y(n+1)}{\partial u(n)}\right) \left| \frac{\partial y(n+1)}{\partial u(n)} \right|.$$

Thus, if we know only the sign of the Jacobian, we can adjust the learning rate η such that $\left| \frac{\partial y(n+1)}{\partial u(n)} \right|$ is included into η.

The second way is to build the emulator which can simulate the input/output map of the plant. Then we regard the emulator as the true plant. Using the BP method, we can adjust the connection weights by combining the neural network to tune the PID gains with a neural network to simulate the plant. The total configuration for the second approach is given by adding the emulator to the plant in a parallel way. Using the control scheme, we have obtained fine tuning of the PID gains in many cases. The total configuration of the neuro-PID controller with an emulator is shown in Fig.3 where inputs of the emulator are past plant input and output data.

Using the control scheme of Fig.3, we have obtained fine tuning of the PID gains in many cases. But it took much time to get convergence results even though the results obtained were similar to those by human operators who have engaged for a long time to control the process and obtained much experience how to tune the PID gains when unknown circumstances came out. Therefore, the only problem for the above approach is to shorten the computational time to find the fine tuning values. The convergence time depends on the initial values of the PID gains and connection weights, we can use the genetic algorithm to find them roughly.

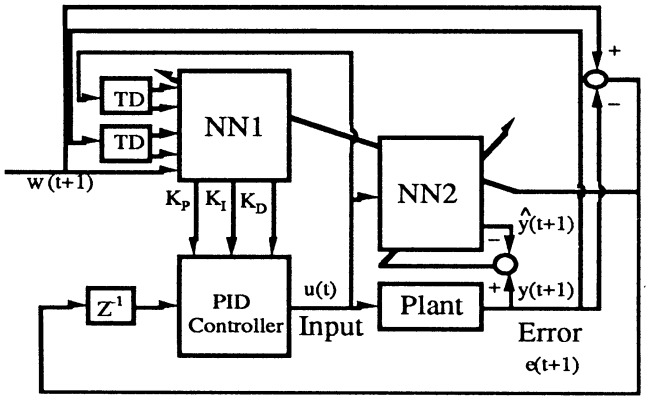


Fig. 3. Neuro-PID controller configuration.

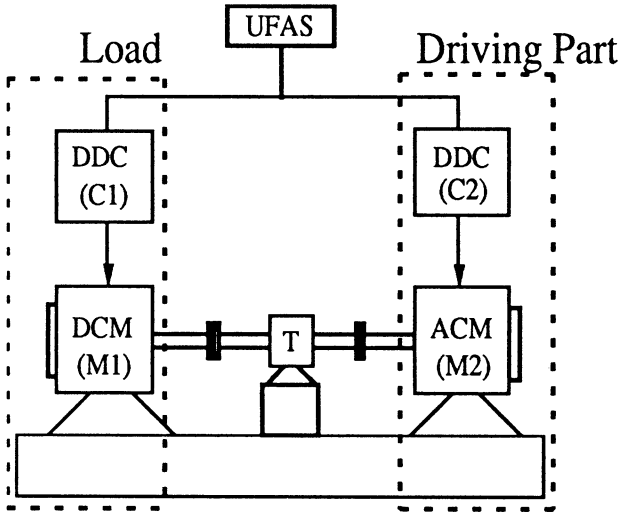
4. Torque and spped control of electric vehicle

We will consider the torque control by the self-tuning neuro-PID control approach stated in Section 3. Control system of the electric vehicle has been shown in Fig.4 where load can produces any type of road conditions and driving part shows the driving mechanism of the vehcle

The configuration of the neuro-PID control system for torque control is illustrated in Fig.5. The inputs for the NNM are the plant output, plant input,and desired value togetherwith rotation speed of the vehicle. Figure 6 shows the experimental result for torque control by using neuro-PID control and Fig.7 illustrates the speed control results where (a) shows the initial stage and (b) shows the final stage. From these results, the proposed self-tuning neuro-PID controller could offer the efficient scheme for motion control.

5. Conclusions

In this paper, we have considered the self-tuning neuro-PID control approach to motion control. Since it needs some trials to find the initial values of PID gains and the initial values of connection weights, we must consider some approach to find them. One of them may be suitable to apply the genetic algorithm and we will consider the method in the future.



D C M : DC Motor
A C M : Inductive Motor
D D C : Direct Digital Controller
U F A S : Universal FA System
T : Torque Meter

Fig.4. Torque control system of the electric vehicle.

Rerefences

[1] W. T. Miller III, R. S. Sutton, and P. J. Werbos, "Neural Networks for Control", MIT Press, 1990.

[2] D. A. White and D. A. Sofge Edited, "Handbook of Intelligent Control", Neural, Fuzzy, and Adaptive Approaches, Van Nostrand Reinhold, 1992.

[3] S. Omatu, M. Khalid, and R. Yusof, "Neuro-Control and Their Applications", Advances in Industrial Control, Springer-Verlag, 1995.

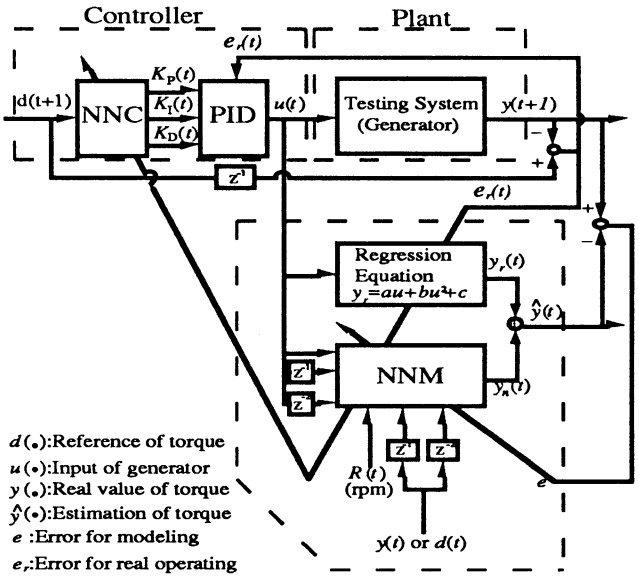


Fig.5. Control structure of the electric vehcle.

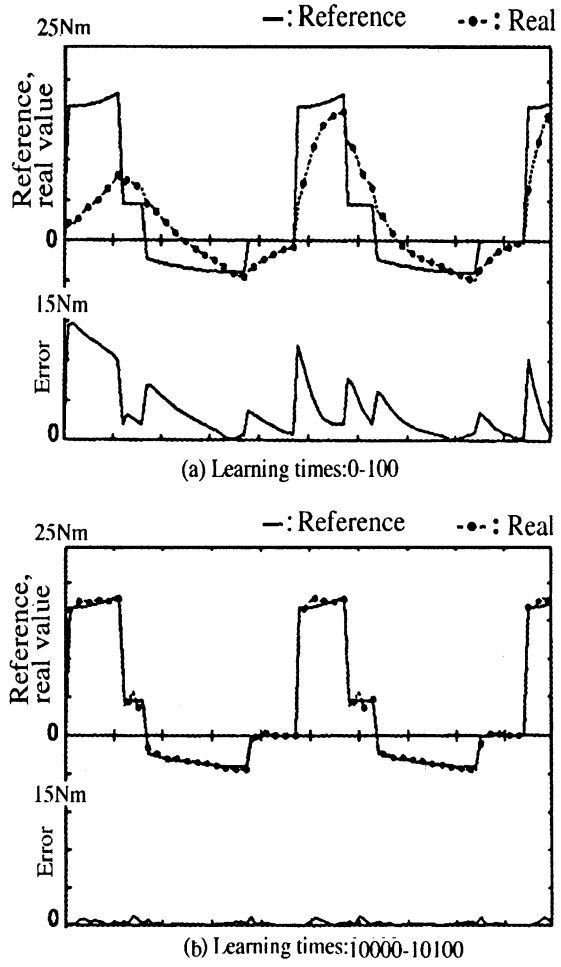


Fig.6. Torque control results where (a) shows the initial stage and (b) shows the final stage.

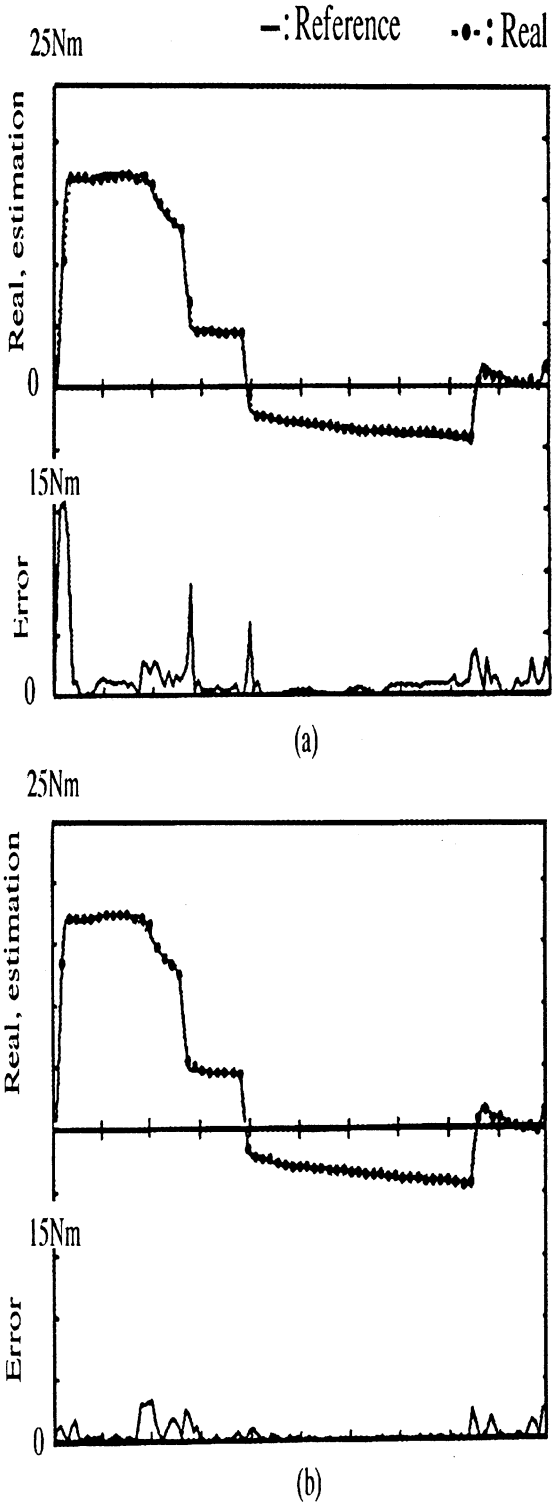


Fig. 7. Speed control results by using the proposed method where (a) and (b) show the same meaning as Fig.6.

Proc. of Third Int. Symp. on Artificial Life, and Robotics (AROB III' 98),
Oita, Japan, 19-21, January, 1998,

A Proposal of Human-Machine Interactive System through Linguistic Instructions Using Fuzzy Classifier System

Makoto FUJII Takeshi FURUHASHI

Dept. of Information Electronics, Graduate School of Eng., Nagoya University
Furo-cho, Chikusa-ku, Nagoya 464-01, JAPAN
E-mail:{fujii, furu}@bioele.nuee.nagoya-u.ac.jp

Abstract

If systems are capable of understanding natural language, communications between humans and systems will be very efficient. However, natural language are often very vague and/or inaccurate, and it has been very difficult to construct a capable system. This paper presents a system which can understand linguistic instructions given by a human operator and extract the intentions from the linguistic instructions using a Fuzzy Classifier System(FCS). By extracting the intentions, the proposed system can generalize the instructions for different conditions. The proposed system is applied to an obstacle avoidance problem. Simulations are done to show that the system can extract intentions, and the extracted rules have generalities.

1 Introduction

Natural language is one of the most useful communication means for humans, and if systems are capable to understand natural language, efficient communications between humans and the systems will be realized. For instance, if systems can learn linguistic instructions given by users, these systems will be very usable. However, natural language are often very vague and/or inaccurate, and it has been very difficult to construct such a capable system.

Fuzzy inference can handle vagueness and inaccuracy, and learnable human-machine interfaces using fuzzy inference have been studied. Sugeno and Park[1]proposed FULLINS(FUzzy-Learning based on Linguistic INStruction). FULLINS is a learning system which has the capability of knowledge acquisition from linguistic instructions using *a priori* knowledge. FULLINS has been applied to trailer truck backer-up control[1] and helicopter flight control[2]. Miyamoto et al.[3] proposed a learning method based on linguistic instructions using a qualitative linguistic model, and applied the method to the fuzzy control of a chemical reaction process. These systems can communicate with humans using natural language, but humans' evaluations on linguistic instructions are needed to acquire implications of linguistic instructions.

Knowledge discovery method using Fuzzy Classifier System(FCS) has been proposed[4, 5]. The capability of knowledge finding and a method of payoff and apportionment of credits for the FCS are studied in [4] and [5]. The authors have proposed a learing system using the FCS which can understand linguistic instructions from humans and modify its actions based on the interpretations[6, 7].

This paper presents a new system which can extract humans' intentions from linguistic instructions using the FCS. In this paper, humans' intentions are defined as rules with needed variables selected from input variables. When a human gives linguistic instructions to this system, it selects related variables in the antecedent of the acquired fuzzy rules. Using these intentions, the system can act properly under different conditions.

Simulations of obstacle avoidance are done to show that the proposed system can extract intentions and the extracted rules have effectiveness in improving the avoidance actions.

2 Proposed System

2.1 System for understanding linguistic instructions

This system is based on the Fuzzy Classifier System(FCS)[6, 7]. The structure is shown in Fig.1. The FCS is a learning system having the following four blocks: rule generation mechanism, fuzzy rule base, fuzzy inference system and apportionment of credit[4, 5]. The proposed FCS in [6, 7] has a basic rule base which corresponds to the fuzzy rule base in the FCS, and has another two rule bases for understanding linguistic instructions: instruction condition rule base and instruction interpretation rule base.

1. Basic Rule Base: This is a fuzzy rule base for basic actions of the system.

2. Instruction Condition Rule Base: This rule base memorizes linguistic instructions given by humans and conditions under which they gave the instructions to the system.

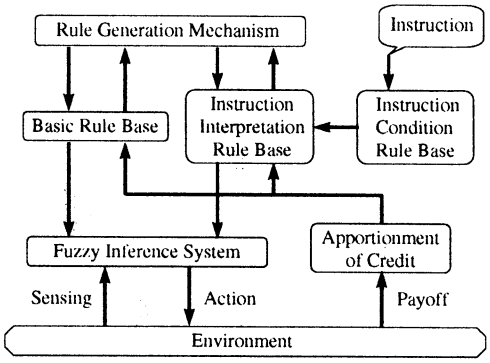


Figure 1: Fuzzy Classifier System in [6,7]

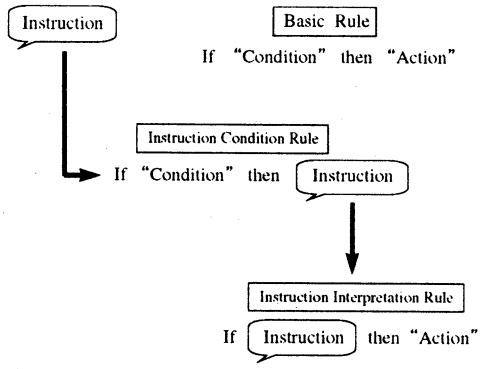


Figure 2: Instruction condition rule and instruction interpretation rule

3. Instruction Interpretation Rule Base: This rule base determines the correspondance between the linguistic instructions and the system actions.

To find rules for proper actions, the following two steps are taken: First, basic rules are found. The FCS acquires basic rules. It is hard for only the basic rules to achieve all the tasks required for the system. Therefore, at the second step of finding rules, a human interacts with the system to improve its actions. When an instruction is given, the system generates two fuzzy rules: an instruction condition rule and an instruction interpretation rule. The instruction condition rule has the condition in the antecedent part under which the human gives the instruction, and has the symbol in the consequent part representing the linguistic instruction. The instruction interpretation rule has the symbol of the linguistic instruction in the antecedent part and the action corresponding to the instruction in the consequent part. These rules are illustrated in Fig.2. The fuzzy inference system calculates the truth values of instruction condition rules. These truth values are the degrees of coincidence to the conditions under which the human gave the instructions. These truth values are used as those of corresponding instruction interpretation rules. Calculating the center of gravity of outputs of both the basic rules and the instruction interpretation rules, the action is outputted to the environment. If the action fails, the rule ganeration mechanism generates a new candidate of instruction interpretation rule. The system can acquire proper actions indicated by the linguistic instructions.

2.2 Extraction of humans' intentions

In this paper, extraction of intentions from the linguistic instructions are defined as to select only needed variables from the instruction condition rules. Needless variables in the antecedent part of the instruction condition rules are deleted, and conditions which the human kept in mind for the instructions are extracted.

Extraction of intentions are done by the following steps:

1. Asterisk(∗) is inserted into each input variable of the instruction condition rule one by one. That is, the grade of membership of the variable with ∗ is set at 1.
2. Using the instruction condition rule with ∗, the system acts in the environment.
3. If the action is successful, the instruction condition rule is memorized.
4. The steps 1∼3 are repeated. The rules having the ∗ as many as possible are considered to be the rules with human's intentions.

For the simplification of the elimination of needless variables, this paper proposes a new geometric-mean method to calculate the truth value of fuzzy rule. The truth value ω of fuzzy rule using the geometric-mean method is defined as folows:

$$\omega = \sqrt[(n-a)]{\prod_{k=1}^{n} h(x_k)} \qquad (1)$$

where x_k is the *k-th* input variable, n is the number of input variables in the antecedent of fuzzy rule, a is the number of ∗ in the antecedent and $h(x_k)$ is a swiching function. If the label of the *k-th* variable is ∗, $h(x_k)$ is 1, otherwise $h(x_k)$ is the grade of membership. The feature of this geometric-mean method is that a $(n\text{-}a)$ root for actually used $n\text{-}a$ number of variables is calculated. The system can treat rules equally which has different numbers of variables in the antecedent. The conventional methods of calculation of the truth value are product

operation, minimum operation, etc. By the product operation, the truth value drastically changes if an * is inserted into the antecedent. This means it is impossible to treat the truth values of rules equally having different numbers of input variables in the antecedent. Therefore the product operation is not suitable for the extraction of intentions. On the other hand, the minimum operation determines the truth value by the least grade of membership. Every rule having a different number of input variables in the antecedent can be treated equally. But the variable with the least grade is the one the human considers least likely in giving the instruction. For this reason, the minimum operation is not suitable for the extraction of intentions.

3 Simulation

3.1 Simulation condition and parameters

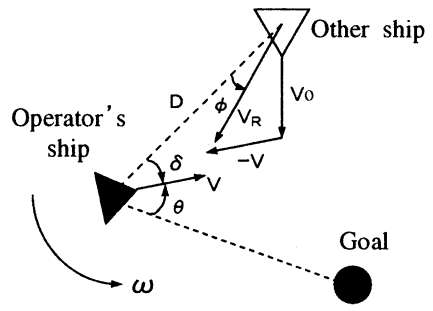


Figure 3: Denotations of parameters

The proposed system in this paper is applied to an obstacle avoidance problem. In this paper, the problem is just to steer the operator's ship to go into the goal avoiding the other ship. Fig. are 3 shows the parameters among the operator's ship, the other ship and the goal. The speed of the operator's ship and the other ship are $|V|$,$|V_o|$, respectively, and both are set to be constant. The distance between the operator's ship and the other ship is denoted by D. The angle between the direction of operator's ship and the direction of the other ship viewed from the operator's ship is denoted by δ. In the same way, the angle between the direction of operator's ship and the goal is θ. V_R is the relative velocity between the two ships. The angle between the relative velocity V_R and the direction of operator's ship from the other ship is ϕ. When ϕ is nearly zero, it means that the other ship comes toward the operator's ship. The angular velocity of operator's ship is ω. Fig. are 4 shows the simulation environment. The operator's ship starts from the left side and goes to the goal. The other ship goes across from top to bottom. In this simulation, success is

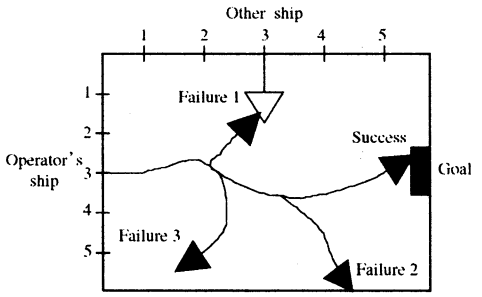


Figure 4: Simulation environment

that the operator's ship reaches the goal avoiding the other ship and failures are; 1)The operator's ship clashes with the other ship; 2)The operator's ship runs out of the simulation environment; 3)The absolute value of θ which is the angle between the direction of operator's ship and the goal is over 90 degrees. Changing the start point of the operator's ship and the other ship by five times, simulations were done.

3.2 Simulation results

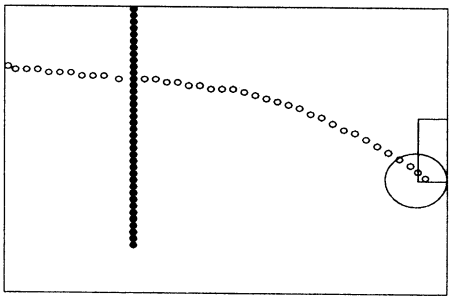
The proposed system acquired basic rules by the FCS. The inputs of the system were the relative distance D, the angle ϕ, the relative angle δ, θ, the anguler velocity ω. The output of the system was the steering angle $\Delta\omega$. Five membership functions(Negative Big(NB), Negative Small(NS), Zero(ZO), Positive Small(PS), Positive Big(PB)) ware used. The geometric-mean method was used for the calculation of the truth values of fuzzy rules.

Fig. are 5 shows the tracks of ships using the basic rules acquired by the FCS. When the controlled ship could reach the goal at least once, the simulation was stopped. In the case of start point 5, the human gave three linguistic instructions to the system(Fig.5(b)), while he was looking at the CRT-screen. As a result, the controlled ship could reach the goal as shown in Fig.6.

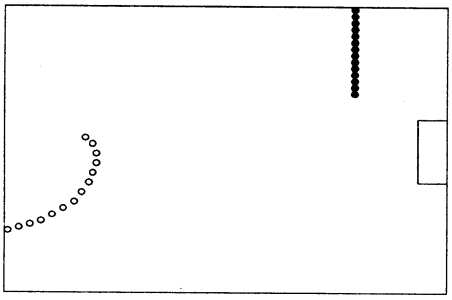
The system acquired three linguistic instruction rules as follows: Instruction condition rules(A)~(C) correspond to ↓ signs of (A)~(C) in Fig.6, respectively.

Instruction condition rules:

- If D is PB, ϕ is ZO, δ is ZO, θ is ZO, ω is ZO then Instruction is "A" (A)
- If D is NB, ϕ is ZO, δ is ZO, θ is ZO, ω is NS then Instruction is "B" (B)



(a)Start point 1



(b)Start point 5

Figure 5: Actions by basic rules

- If D is NB, ϕ is ZO, δ is NS, θ is ZO, ω is ZO
  then Instruction is "C" (C)

Instruction interpretation rules:

- If Instruction is "A" then $\Delta\omega$ is PS
- If Instruction is "B" then $\Delta\omega$ is PB
- If Instruction is "C" then $\Delta\omega$ is PS

To extract human's intentions in linguistic instructions, the system eliminated needless variables in the antecedent of linguistic instruction rules. $*$'s

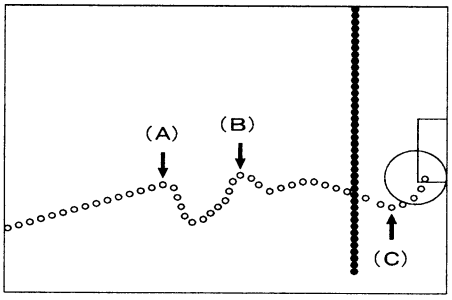


Figure 6: Actions after linguistic instructions were given(Start point 5)

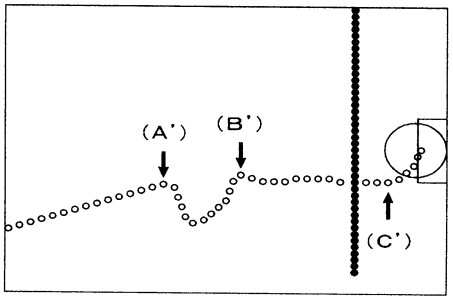


Figure 7: Actions after extraction of intentions from linguistic instructions (Start point 5)

were inserted into the antecedent parts of the three linguistic instruction rules, and simulations were done again. In the case where the controlled ship could reach the goal even with $*$, these variables were judged unnecessary.

Extracted intentions which have the largest numbers of $*$ for each rules are shown below. The variables with $*$ are not shown.

Rules with extracted intentions:

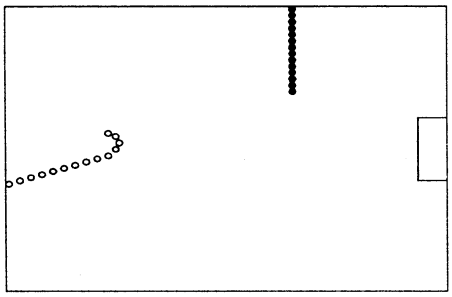
- If D is PB, θ is ZO
  then Instruction is "A" (A')
- If D is NB, ϕ is ZO, ω is NS
  then Instruction is "B" (B')
- If ϕ is ZO, δ is NS, ω is ZO
  then Instruction is "C" (C')

Rule A' which was obtained from instruction condition rule A has only two parameters in the antecedent, and other three parameters were deleted. Rule A' reads that, when the distance D between the operator's ship and the other ship is large and the relative angle between the direction of the operator's ship and the goal is nealy zero, the system understood that the intention of the linguistic instruction "A" was to steer the controlled ship to right a little. In (B'),(C'), the needed parameters were also extracted and the intentions in the linguistic instructions were clarified.

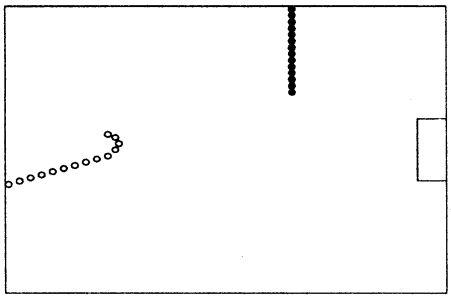
Fig. are 7 shows the tracks of ships using the extracted intentions. There was little difference between the tracks in Fig.6 and Fig.7.

3.3 Effectiveness of extracted intentions

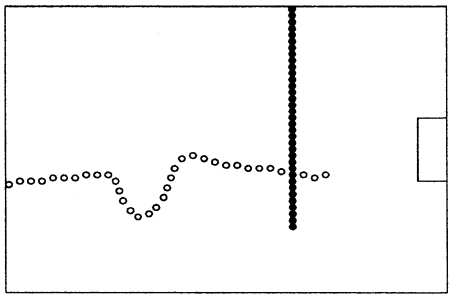
Next, to show the effectiveness of extracted intentions, the operator's ship started from the start point 4(Fig.4) using linguistic instruction rules(A)~(C) and extracted intentions(A')~(C'). Fig. are 8(a) shows the actions using only the basic



(a)Actions using only basic rules



(b)Actions using basic rules and linguistic instruction rules



(c)Actions using basic rules and extracted intentions

Figure 8: Actions from Start point 4

rules. Fig. are 8(b) shows the case where both the basic rules and the linguistic instruction rules were used. The linguistic instruction rules did not fire, and the steering failed. In Fig.8(c), the basic rules and the extracted intentions were used. The system could steer the ship to approach the goal.

4 Conclusion

This paper presented a new system to extract human's intentions from vague linguistic instructions. Simulations were done to show that human's intentions could be extracted from the linguistic instructions, and als the effectiveness of the extracted intentions. The extracted rules worked well under different conditions.

References

[1] Sugeno, M., Park, G. "Learning Based on Linguistic Instructions Using Fuzzy Theory", the J. of Japan Society for Fuzzy Theory and Systems Vol.4, No.6, pp.1164-1181(1992)

[2] Sugeno, M., Park, G. "An Approach to Linguistic Instruction Based Learning and its Application to Helicopter Flight Control", Proc. of fifth Int'l Fuzzy Systems Assoc. World Congress'93 (IFSA'93), pp.1082-1085(1993)

[3] Miyamoto, A., Goto, K., Itoh, O., Migita, H., Sugeno, M. "Method for Adjustment Control Rules by Linguistic Instructions", Japanese Journal of Fuzzy Theory and Systems, Allerton Press, Inc. Vol.8 No.5 pp.847-861(1996)

[4] Nakaoka, K., Furuhashi, T., Uchikawa, Y. "A Study on Apportionment of Credits of Fuzzy Classifier System for Knowledge Acquisition of Large Scale Systems", Proc. of third IEEE Int'l Conf. on Fuzzy Systems(FUZZ-IEEE'94), pp.1797-1800(1994)

[5] Furuhashi, T., Nakaoka, K., Uchikawa, Y. "A Study on Fuzzy Classifier System for Finding Control Knowledge of Multi-Input System", Journal of Studies in Fuzziness and Soft Computing, Vol.8, pp.489-502(1996)

[6] Hasegawa, T., Kamei, D., Furuhashi, T., Uchikawa, Y. "A Study on Autonomous Understanding of Linguistic Instructions and Behavior Improvement Using Fuzzy Classifier System", 12th Fuzzy System Symposium in Japan pp.459-462(1996)

[7] Fujii, M., Hasegawa, T., Furuhashi, T., Uchikawa, Y. "A Study on Understanding of Linguistic Instructions and Behavior Improvement", 6th Intelligent System Symposium in Janan pp.185-188(1996)

Proc. of Third Int. Symp. on Artificial Life, and Robotics (AROB III' 98),
Oita, Japan, 19-21, January, 1998,

Trajectory Prediction and Catching System of Moving Target under Fuzzy Reasoning Method

T. Yasuno, T. Kamano, T. Suzuki, and K. Kumabe
Dept. of Electrical and Electronic Eng.
The University of Tokushima
2-1 Minamijyosanjima-cho, Tokushima-city, 770, Japan

Y. Kataoka
Kataoka Machine Co., LTD.
4765-46 Sangawa-cho, Iyomishima-city, 799-04, Japan

Key words: Trajectory prediction, Catching motion, robot manipulator, Fuzzy reasoning

Abstract

This paper describes a method to predict a trajectory of a moving target on the 3D-coordinates and catching algorithm using a vertical-type multi-joint robot manipulator. The trajectory of the moving target is estimated by a fuzzy prediction system using the positions of the moving target for past five sampling periods as input signals, of which prediction rules are automatically tuned so that a prediction error converges to zero. To realize excellent catching motion, the robot manipulator is moved by a catching algorithm from initial position to catching position on the predicted trajectory ahead of the moving target. Some experimental results demonstrate the effectiveness of the proposed fuzzy trajectory prediction system and the catching algorithm using the robot manipulator.

1 Introduction

One of the fundamental problems in intelligent robot manipulators is catching or pick up motion of moving targets. As an example, an excellent catching motion results the high efficiency of operations. In the catching motion, if the trajectory of the moving target is known in advance or the moving speed of the robot manipulator is higher than that of the moving target, it is possible to successfully pick up the moving target without the prediction of the trajectory of the moving target. However, since the trajectories are frequently unknown in advance and the target moves more speedily than the robot manipulator, the prediction of the trajectory is required to achieve an excellent catching motion.

Recently, some investigates on the prediction and catching problems have been reported. The most typical prediction method is the Kalman filter based on the formalized linear model of the moving object. On the other hand, Pierre Payeur et. al.[1] proposed the trajectory prediction method of the moving object by applying artificial neural networks and the cubic model. Moreover, Zhi-wei Luo et. al. have experimentally studied that the visual information is effective to catch a high speed moving target [2].

In this paper, to realize excellent catching motion by using a six degree-of-freedom vertical-type robot manipulator, a fuzzy prediction method of the position of the moving target which moves along a periodical unknown path on the 3D-coordinates is described. In general, fuzzy reasoning system consists of a collection of many reasoning rules which is the relationship between the fuzzy input and the fuzzy output information and the fuzzy reasoning engine. All reasoning rules are used in parallel, and the reasoning results are combined according to the fuzzy rules, which are weighted by the degree of satisfaction of the antecedent. This implies that the fuzzy reasoning has the ability to predict the trajectory by using the tuned rules for uncertainly or unknown trajectory of the moving target.

This paper contains five sections in addition to the introduction and a short conclusion. Following this introduction, Section 2 introduces the structure of the trajectory prediction system using the fuzzy reasoning. Furthermore, a tuning algorithm of the fuzzy rules is described. Section 3 explains the catching algorithm from the initial position to the catching point, which is decided by the predicted trajectory of the moving target. Section 4 presents some experimental results of the trajectory prediction and catching motion using the vertical-type robot manipulator. Final remarks are concluded in Section 5.

2 Fuzzy prediction method

2.1 Basic module

In this section, we propose a basic module for the trajectory prediction system of the moving target using a self-tuning fuzzy reasoning system (STFRS), as shown in Fig.1. The objective of the basic module is to estimate the position of the moving target along the

only x-axis after one sampling period.

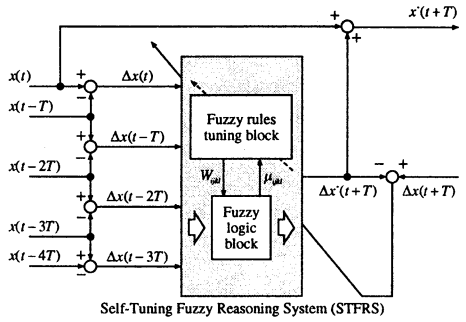


Fig. 1: Basic module.

The STFRS is functionally divided into a fuzzy rules tuning block and a fuzzy logic block. Input signals to the STFRS are displacements at the present and the past four sampling periods : $\Delta x(t)$, $\Delta x(t-T)$, $\Delta x(t-2T)$, and $\Delta x(t-3T)$, and converted into suitable linguistic variables, such as PB(Positive Big), ZO(Zero) and NS(Negative Small), etc., which correspond to labels of fuzzy sets. Fuzzy sets are defined by assigning the grade of membership functions. In this application, the triangular-shaped membership functions shown in Fig. 2 are used because the implementation of these membership functions is easy for programming on the personal computer. As results

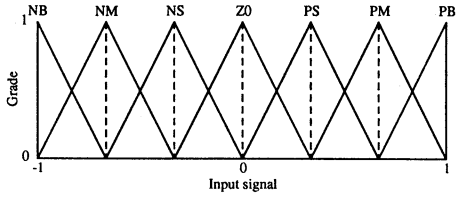


Fig. 2: Membership functions.

of combination of fuzzy sets, 16 rules are selected, and then we will employ the singleton method, proposed by Sugeno [3], which utilizes only the weights W_{ijkl} for each output fuzzy sets. However, weights W_{ijkl} are adjusted by the following tuning law at every sampling period so that the prediction error decreases.

$$\frac{dW_{ijkl}(t)}{dt} = \gamma e_f(t)\mu_{ijkl}(t) \tag{1}$$

where $\gamma > 0$ is the tuning gain and e_f is the prediction error which is given by

$$e_f(t) = \Delta x(t+T) - \Delta x^*(t+T) \tag{2}$$

μ_{ijkl} is the grade for the tuning parameters given by

$$\mu_{ijkl}(t) = \mu_i(t)\mu_j(t)\mu_k(t)\mu_l(t) \tag{3}$$

where μ_i, μ_j, μ_k and μ_l correspond to the grade of the membership functions.

The final output of the STFRS is calculated by

$$\Delta x^*(t+T) = \frac{\sum_{i,j,k,l=1}^{7} \mu_{ijkl}(t)W_{ijkl}(t)}{\sum_{i,j,k,l=1}^{7} \mu_{ijkl}(t)} \tag{4}$$

This means that the relative displacement at the next sampling, $\Delta x(t+T)$ is obtained by fuzzy prediction rules. Consequently, the position of the moving target after one sampling is calculated by

$$x^*(t+T) = x(t) + \Delta x^*(t+T) \tag{5}$$

2.2 Fuzzy prediction system

Fig.3 shows the proposed prediction system, in which m tuned basic modules are connected in series. The number of modules, m, corresponds to the prediction periods, and is decided so that the speed of the end-effector is kept within bounds under maximum speed conditions of the end-effector.

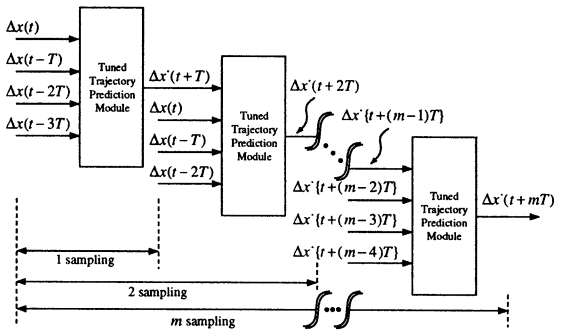


Fig. 3: Trajectory prediction system.

In the first basic module, the displacement after one sampling period, $\Delta x^*(t+T)$, is estimated from four input signals, $\Delta x(t)$, $\Delta x(t-T)$, $\Delta x(t-2T)$ and $\Delta x(t-3T)$. The estimated displacement $\Delta x^*(t+T)$ is added to the next module. In the second basic module connected with the first basic module, the displacement after two sampling periods $\Delta x^*(t+2T)$ is predicted. By repeating this procedure, the displacement after m sampling periods $\Delta x^*(t+mT)$ is obtained by the proposed fuzzy prediction system shown in Fig.3. Therefore, the position after m sampling periods is given by

$$x^*(t+mT) = x^*\{t+(m-1)T\} + \Delta x^*(t+mT) \quad (6)$$

The proposed method implies that the accuracy of the proposed prediction system depends on that of the basic module or the tuned fuzzy prediction rules. Therefore, it is noted that the adequate tuning of the fuzzy rules is required to achieve the high accuracy prediction. However, the accurate position after m sampling periods is not necessarily in catching motion because the path of the robot manipulator can be modified while approaching.

3 Catching Algorithm

Fig. 4 shows a typical catching motion using a robot manipulator. Generally, when the catching position which the moving target will go through after m sampling periods is given, many paths from the current position to the catching point can be planned. In this application, we use the most simple catching method which is planned so that the robot manipulator goes straight to the catching position. The predicted position of the moving target, however, may include a few prediction error. Therefore, at the next sampling period, the robot manipulator moves toward the catching position where the target will be on the path after $m-1$ sampling periods. However, since the catching position is updated as the prediction process progresses, the path of the robot manipulator is modified at every sampling period. By repeating the movement and the modification, the robot manipulator can approach and catch the target after m sampling periods.

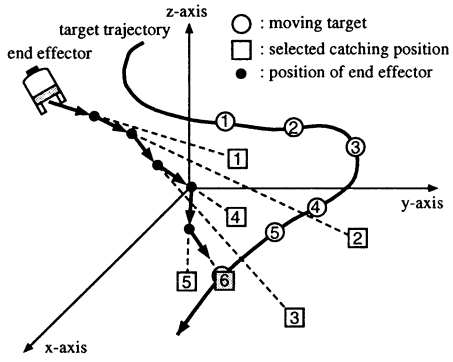


Fig. 4: Catching motion of the robot manipulator.

4 Experimental results

4.1 Robot manipulator system

In order to verify the proposed fuzzy prediction system and catching algorithm, performances are measured by means of an AC servo motor drive robot manipulator system shown in Fig.5. The specifications of the tested robot manipulator is listed in Table 1. The manipulator is controlled by the specialized open robot controller under the point-to-point (PTP) control method. A main computer is connected with the open robot controller by local area network (ARCNET) through the real-time interface board, and is used to manage several tasks such as measurement of the absolute rotary encoder signal, tuning of fuzzy rules for the trajectory prediction of the moving target and the path planing for the catching target. All of the robot control sequence are carried out for every sampling period T=0.1[s].

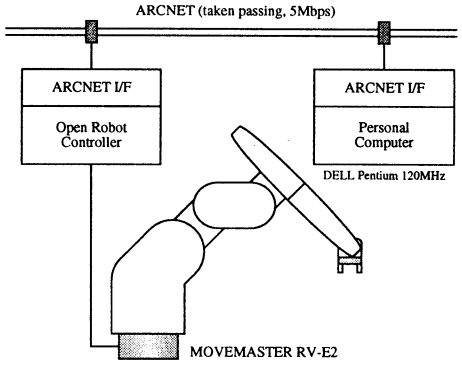


Fig. 5: An open architecture robot system.

Table 1: Specifications of tested robot manipulator.

type			RV-E2
rated load		N	19.6
composed max. speed		mm/s	3500
arm length	shoulder shift	mm	100
	upper arm	mm	250
	fore arm	mm	±0.04
	elbow shift	mm	250
	wrist length	mm	250

4.2 Results of trajectory prediction

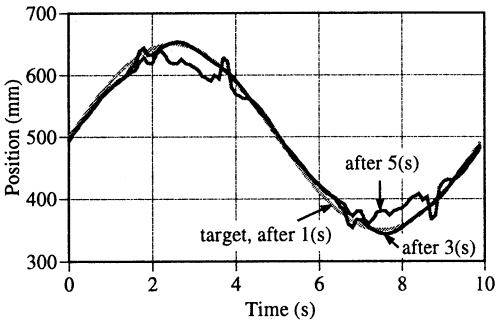
To confirm the validity of the proposed fuzzy prediction method and the catching algorithm, first, the trajectories of the moving target given by

$$\begin{cases} x = 500 + 150\sin(0.2\pi t) \\ y = -150 + 150\cos(0.2\pi t) \\ z = 400 + 150\sin(2\pi t) \end{cases} \quad (7)$$

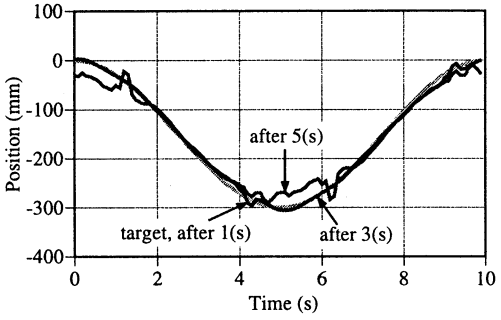
are predicted. Fig.6(a), (b) and (c) show predicted positions along each axis in cases where the prediction time are 1(s), 3(s) and 5(s). As can be seen from these results, the prediction errors between target and predicted trajectories increase with prediction time.

4.3 Results of catching motion

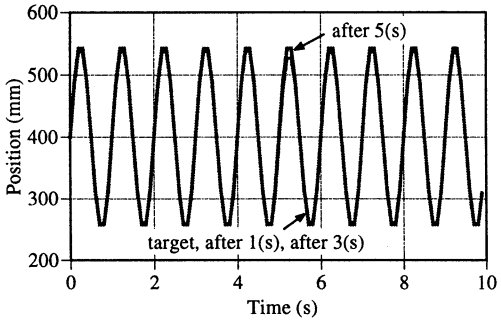
Fig.7 shows some catching motions of the robot manipulator on the 3D-coordinate. In the case of prediction time is long, although the moving direction of the robot manipulator is different from the desired direction at beginning, the robot manipulator can successfully catch the moving target because of updating the catching position at every sampling period. This implies that the prediction accuracy increases as the manipulator approaches the desired catching position.



(a) Positions along X-axis.



(b) Positions along Y-axis.



(c) Positions along Z-axis.

Fig. 6: Results of the trajectory prediction.

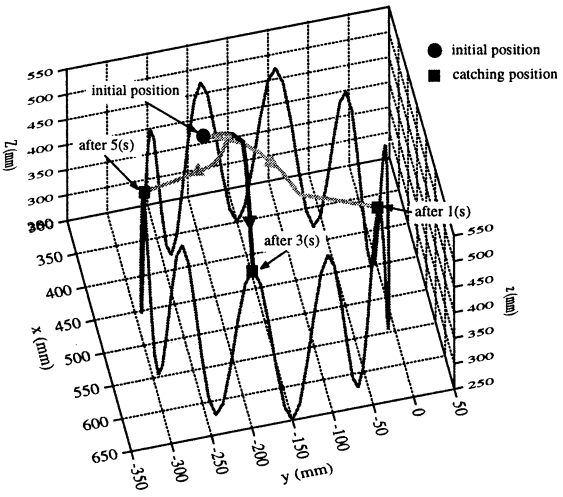


Fig. 7: Results of the catching motion.

5 Conclusions

In this paper, we present a new trajectory prediction method of the moving target under the self-tuning fuzzy reasoning approach and the catching algorithm using the vertical-type robot manipulator. The validity of the proposed system has been demonstrated for the tested experimental robot control system. As a result, the self-tuning fuzzy reasoning approach is effective for the trajectory prediction of the moving target. Although there is a limit of the capability of the proposed trajectory prediction system, it is possible to catch the moving target by using the catching algorithm. A future work is to apply the proposed trajectory prediction method and the catching algorithm to a sensor-based robot control system in unknown or uncertain dynamic environment.

References

[1] Pierre Payeur, Hoang Le-Huy, and Clement M. Gosselin, "Trajectory Prediction for Moving Objects Using Artificial Neural Networks", IEEE Transaction on industrial electronics, vol.42, no.2, pp.147-158, April 1995

[2] Zhi-wei Luo, Osamu Simada, and Masami Ito, "Control Design of a Robot for Catching a Moving Object", Proc. of SICE Conf., pp.513-514, Tottori in Japan, July 1996

[3] Sugeno Michio, "Fuzzy Control", Japan, Nikkan-kogyou-shinbunsya, 1991

Proc. of Third Int. Symp. on Artificial Life, and Robotics (AROB III' 98),
Oita, Japan, 19-21, January, 1998,

Improving Vehicle Performance Using Adaptive Control Techniques

D J G James†, K J Burnham†, M J Richardson††, R A Williams††
† Control Theory and Applications Centre, Coventry University, Coventry, UK
†† Jaguar Cars Ltd, Coventry, UK

Abstract: The paper reviews a collaborative research programme aimed at improving vehicle performance using adaptive control techniques. Initially the design of active suspension systems are considered and the benefits of using a non-linear controller model with an adaptive control scheme considered. Adaptive schemes for active roll control are then considered and the merits of incorporating a Smith predictor, to accommodate for system delays, highlighted. Preliminary research in adaptive cruise control and collision avoidance is discussed and plans for further developments outlined.

Keywords: active suspension systems, anti-roll control, adaptive cruise control

1 Introduction

All motor car manufacturers are currently engaged in research and development to ensure that they remain at the competitive edge, both in terms of vehicle performance and the perceived human factors such as comfort and driveability. Current developments include active suspension systems, anti-roll control, adaptive cruise control, lane tracking, steer and brake by wire, engine management systems, and automatic heating, ventilation and air-conditioning systems.

As a leading manufacturer of high quality luxury cars, Jaguar Cars Ltd based at Coventry in the UK, are at the forefront in the development and implementation of such new technologies. Over a number of years the research centre at Coventry University has collaborated with the company in some of these areas, particularly in those making use of adaptive control techniques. This paper reviews some of these collaborative activities as well as giving an indication of future directions for continuing research.

2 Active suspension systems

Conventional vehicle suspension systems consist of a passive spring in parallel with a damper; their main functions being to support the body mass and to provide both passenger comfort and road holding. It has a number of limitations due to the fixed nature of the components used and the requirements for the vehicle to function over a wide variety of operating conditions. It is well known, for example, that ride may be improved by softening the suspension, whilst handling is improved by increasing the suspension stiffness; furthermore all suspension movement is constrained by the available working space. An acceptable road vehicle suspension design is one of compromise between passenger comfort and handling. To provide a comfortable ride it is desirable to provide large suspension movements, in order to isolate the vehicle from road inputs, thus requiring a soft suspension. A suspension is also required to react to changes in vehicle load, a constraint which requires a stiff suspension. The introduction of active elements into the suspension allows the compromise to be redefined, providing an all round improvement in performance. Two forms of active suspension systems (ASS) are generally recognised, namely high bandwidth and low bandwidth configurations as depicted in Figure 1, in which USM denotes the unsprung mass. In the high bandwidth ASS the actuator, which sits in parallel with the road spring, is required to control both the body motion (circa 1Hz) and the wheel hop motion (circa 12Hz).

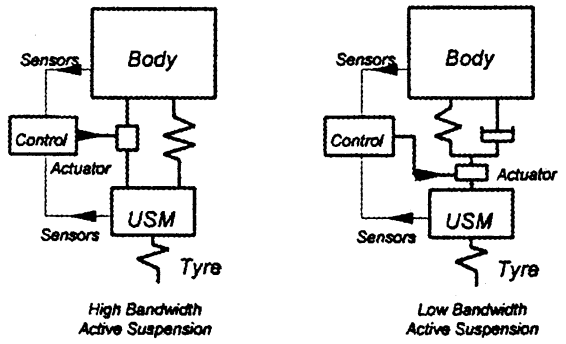


Figure 1 Active Suspensions

In the low bandwidth ASS the actuator sits in series with the road spring and damper and is required to control the body motion only, with wheel hop control being provided by the passive damper. A good summary of some of the developments in the design and control of automotive systems may be found in Jurgen[1], Sharp and Crolla[2] and Williams[3].

Preliminary work in this area was concerned with the design of computer controlled ASS, with specific attention being attached to implementation issues and the trade off between ride and handling. The high frequency 'wheel hop' mode at 12Hz being controlled using passive elements and the low frequency body mode actively controlled via a computer, with various control strategies considered. Whilst interaction between the two fundamental frequencies restricted the use of on-line adaptive control techniques such as self-tuning control, simulation studies, using a quarter car model, demonstrated the feasibility of low bandwidth active schemes[4]. Following on from this work longitudinal

and lateral half car models were developed to investigate pitch and roll respectively; with the control strategy adopted utilising manually tuned fixed gain three term PID controllers. The performance of the overall system was found to vary when subject to differing load and road input conditions[5], suggesting that an element of adaptivity could be used to advantage.

The vehicle model was then extended to the full nonlinear case[6] incorporating an oleo-pneumatic actuator[7] at each wheel. Such an actuator has a proven service history and combines the spring and damper of a conventional suspension system into a single unit and thus lends itself well to the low bandwidth active suspension configuration. The actuator has nonlinear characteristics being dependent on both temperature and displacement. The control strategy applied was based on that proposed by Williams et al[8], in which use is made of ride filters which effectively model the vehicle and can thus be modified or adapted by changing the parameters. An element of skyhook damping was also introduced to enhance the ride performance. To apply the strategy to a full vehicle a multi modal, having bounce, pitch and roll as modes, was used as shown in Figure 2. The summed terms from the accelerometer and displacement transducers at each wheel are then fed into their respective ride filters which are designed such that they match the actual vehicle transfer function.

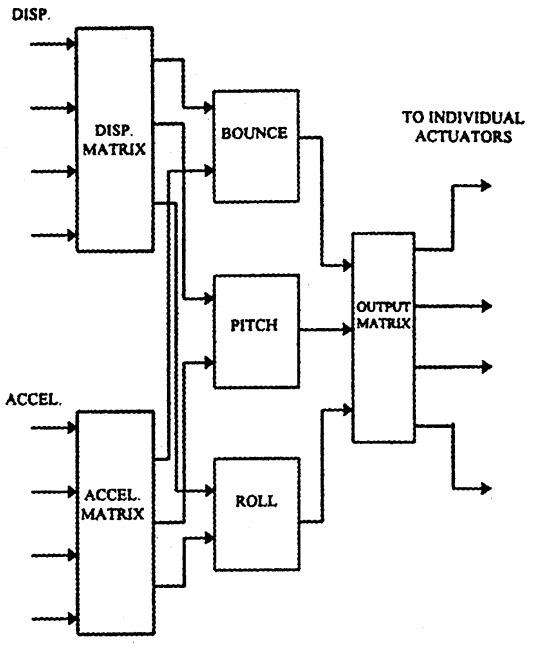


Figure 2 Modal Controller

The resulting signals are fed into an output matrix which determines the demand to the control valve at each wheel. In addition a pressure transducer is added at each wheel station, with the signals being fed into a 'pressure matrix' where they are summed. By using the pressure signal, a further filter to control the corner-to-corner 'warp' mode is used. This prevents the load from being carried on diagonally opposite corners of the vehicle. In order to improve the performance of the controller an element of adaptation is introduced in order to accommodate for changes in the suspension frequency caused by change in vehicle mass and its distribution and change in gas spring temperature. To achieve this the filter coefficients are adjusted on-line to match the actual values which in practice may be obtained from measurements and observations. Overall the strategy provides an effective and robust control[9], whilst the introduction of adaptivity produces only marginal improvements in terms of reduced deflection and body acceleration it leads to a marked reduction in the total fluid flow, hence power, required[10, 11].

3 Active roll control

A conventional vehicle is fitted with torsion bars to restrict its roll degree of freedom and to assist in bringing the vehicle back to the level position. Since active suspension systems suffer from inherent problems of cost, weight, complexity and refinement there has been renewed interest over recent years in active roll control (ARC)[12]. In the work reported in this paper the ARC considered is outlined in Figure 3[13] and essentially consists of rotary hydraulic actuators set within split front and rear anti-roll bars.

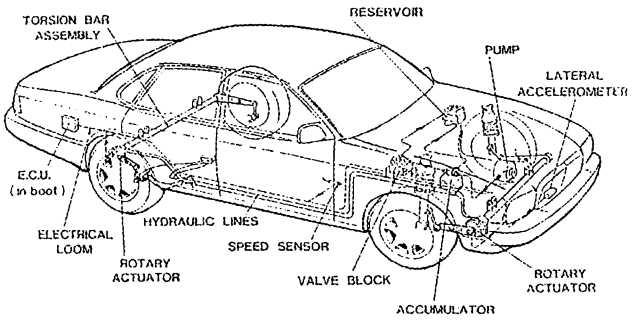


Figure 3 ARC installation

These actuators apply a torque into the suspension system in opposition to the torque caused during vehicle manoeuvres, such as cornering or lane changing, with the aim to maintaining the desired anti-roll performance of the vehicle. The amount of torque that must be produced is calculated by an electronic control unit (ECU). This incorporates a microprocessor which executes a control algorithm based on information received from a lateral acceleration sensor mounted on the vehicle body at some point in the plane of symmetry and from rotary potentiometers in the anti-roll bars. The lateral acceleration sensor signal can be thought of as the input signal to the ARC. A rotary potentiometer in the anti-roll bar senses the twist between the casing and blade of the rotary actuator and this is used in a simple negative feedback loop to enable close correspondence

between lateral acceleration at the sensor and actuator rotations. The output control signal from the ECU drives the single electro-hydraulic flow control valve, which controls the flow of fluid to the rotary hydraulic actuators so that anti-roll behaviour is maintained.

Simulation studies using a mathematical model of an ARC Jaguar XJ6 were undertaken, adopting a conventional three term PID controller within the ARC, and results compared with the behaviour of the development vehicle[14]. Having established good correlation between the model and the vehicle further simulation studies were undertaken adopting modified controllers with a view to improving vehicle performance. Measurements showed that there was significant transport delay within the system. By incorporating a Smith predictor[14] within the control algorithm significant improvements in the system performance was achieved.

4 Adaptive cruise control

The impetus for the work on adaptive cruise control (ACC) was the PROMETHEUS (**PRO**gra**M**me for a **E**uropean **T**raffic with **H**ighest **E**fficiency and **U**nprecedented **S**afety) project, a collaborative pre-competitive research programme initiated by the European automobile industry, of which Jaguar Cars Ltd was a partner. In setting objectives for improving traffic it was recognised at the outset that:

'Modern information and communication technologies will permit the implementation of intelligent, flexible and reliable solutions, which will eliminate information deficits of to-day's traffic. The major advances in microelectronics,sensor engineering,telecommunications and information technology will pave the way for significant improvements in vehicle and traffic engineering. They will allow solutions which were previously impossible or not reasonably feasible for either technical or economic reasons. These will include technical solutions which combine on-board systems with roadside facilities. To put it in a nutshell: Technical progress will allow intelligent vehicles on intelligent roads'.

Conventional cruise control, which performs the function of speed control, is an established and well known feature, particularly in the United States where the combination of long driving distances and low traffic density makes it particularly useful to the driver. In operation a desired speed is selected by the driver and a control system operates the throttle to maintain the desired speed. The disadvantage of such systems is that in heavy traffic the driver must frequently adjust the desired (set) speed or disengage the system so as not to encroach on slower, preceding traffic in the same lane. ACC, whose main components are illustrated in the block diagram of Figure 4, is a system designed to overcome this disadvantage.

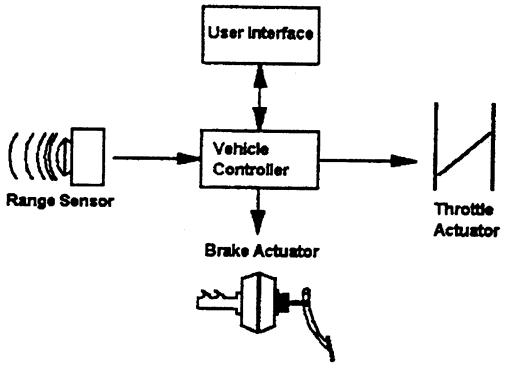


Figure 4 ACC system components

It incorporates a distance sensor which is added to a conventional cruise control system to realise a distance keeping function. Limited authority braking may also be incorporated so that both the throttle and brake actuators can be used to control the distance and relative velocities between vehicle and the target vehicle, thus reducing the need for driver intervention. ACC can then be conceived of as an extension, or enhancement, to standard cruise control which aids the driver in the task of driving a vehicle at a comfortable distance from the car in front.

A key technology for ACC is the sensor, as it dominates both cost and the performance that can be achieved. Fundamental to an ACC system is a sensing system that can reliably detect the road ahead, objects in the vehicle path and their dynamics. In addition it must handle the traffic environment, which presents a large variety of conditions, is constantly changing, and in most cases is unconstrained. The sensors should be capable of performing these functions reliably for the life of the vehicle, in an autonomous manner, and in all the environmental conditions that driving normally occurs. There are a number of possible sensor technologies which might be capable of fulfilling this role, these include: millimetre wave radar, infra-red ladar or lidar and computervision. In each case the sensor specification will include range, relative velocity, field of view and specification of objects which have to be detected. The effectiveness of such systems have been investigated[15] and radar systems would seem to be favoured by the automobile industry at this time.

ACC systems are designed primarily to fulfill a comfort and convenience function. They are not designed to prevent collisions and will not necessarily prevent an ACC equipped vehicle from running into the car in front under extreme braking conditions, so it is important that the driver is ready to intervene in particular situations. Typically, ACC with braking is intended to function where there is a maximum relative velocity of around 30mph. If the relative velocity is greater than this then the driver is required to intervene. In addition the current limitation of the sensing

technology prevents the system from detecting stationery or very slow moving targets at long range.

5 Collision warning

With the installation of a forward looking distance sensor, the vehicle can determine the existence of obstacles within the vehicle's path. Since the sensor also determines the rate of change of this distance, potential collisions may be detected. A driver support system that provides a warning, such as an audio tone, in the event of these situations is therefore a feature that might be implemented on ACC equipped vehicles relatively easily. The problem remains, however, to determine the situations in which the alarm is to be triggered. A number of metrics for identifying the criticality of the situation have been considered and include[15].

i) Time to collision $T_1(t) = d(t) / \dot{d}(t)$ where $d(t)$ is the relative distance at time t. This estimates the time remaining before a collision assuming constant relative speed persists. Clearly this is not always the case, and on-line display of time to collision can show small values (less than a few seconds) during normal driving.

ii) Similar metrics can be formulated by assuming the persistence of one of the higher derivatives of relative distance $d(t)$. For example, assuming a constant relative acceleration leads to an estimate

$$T_2(t) = \left[-\dot{d}(t) \pm \sqrt{\dot{d}^2(t) + 2d(t)\,\ddot{d}(t)} \right] \;/\; \ddot{d}(t)$$

of line to collision, where the earlier of the two roots has to be taken.

iii) An alternative form of metric related to the reaction time $T_r(t)$ required of the driver to react to the leading vehicle decelerating, perhaps at a level only limited by the road friction. If at time t, when it is travelling with speed $v_l(t)$, the lead car were to brake with deceleration A_l then

$$T_r(t) = \left[\frac{v_l(t)^2}{2A_l} - \frac{v_f(t)^2}{2A_f} + d(t) \right] \Big/ v_f(t)$$

where $v_f(t)$ is the speed of the following car at time t and A_f is its braking deceleration after a reaction time $T_r(t)$. Normal driving can lead to negative values of this metric; for example, on a wet road the lead car could brake with A_l = 4m/s^2, and the following car could achieve a maximum A_f = 4m/s^2. With initial velocities of v_f = 40m/s (80mph) and v_l = 35m/s (70mph) and a time headway of 1s ($d(t)$ = 40m), a reaction time of -0.2s is required. That is, if the lead vehicle decelerates at the maximum adhesion level, there is no chance of avoiding a collision.

The above metrics can be computed on-line, in the vehicle, as the situation evolves. The strategy is to issue a warning to the driver on one of these metrics passing a threshold level. Depending on this threshold, the warning could either be annoying to the driver, who would find the warning going off continually under normal driving, or too late in critical circumstances. The metric $T_r(t)$ also introduces an important limitation of the system, that of reaction time. The electronic systems will have a discrete time (sampled) nature and so an inherent delay time, coupled with the driver's reaction time to an audio tone, could be a second or more. This delay can be significantly reduced if the intervention is automatically applied. This would also have the advantage of controlling the critical situation correctly without panic braking, which may adversely affect the vehicles behind, or insufficient braking due to the driver being unable to assess rapidly the situation.

So far, only one dimensional geometry has been considered in that the path of the following vehicle is assumed to be the same as that of the lead vehicle. Clearly the driving task is a two-dimensional one, and early forward looking sensors suffered from the inability to distinguish between obstacles in the vehicle's path and those in adjacent lanes, or off the side of the road. Significant advances were demonstrated using yaw rate gyroscopes to predict the curvature of the road, on the assumption that the road remained on a circular path, as illustrated in Figure 5.

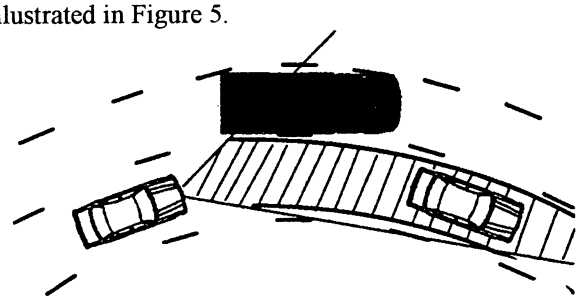


Figure 5 Reducing the area of interest based on an assumption about the road curvature

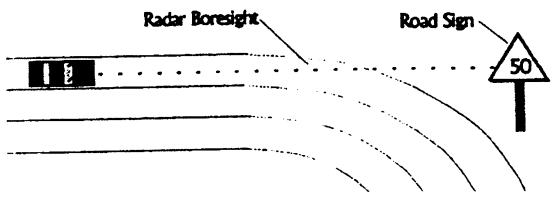


Figure 6 Potential identification of an obstacle

from inaccuracies of the prediction of the road geometry, during changes in the road curvature. This can lead to obstacles being falsely identified as being on the

vehicle's path, as illustrated in Figure 6. Because of this ACC systems are deliberately programmed to ignore obstacles that are stationary, thus rejecting all road-side obstacles. For the ACC to function this has no consequence, since it is not intended to cruise behind stationary obstacles. For collision avoidance strategies, however, stationary targets may be the most important. Advanced sensor techniques such as vision processing systems to measure the road trajectory in front of the vehicle are being investigated to improve the accuracy of determining whether the obstacle is indeed on the vehicle's path[16].

Even having the ability to measure the road trajectory and the precise location and velocity of all the obstacles in front of the vehicle the prediction problem associated with collision avoidance still remains. One of the issues with collision avoidance by longitudinal intervention considered so far is the difficulty of only intervening when the situation is critical. There would be little merit in performing an emergency braking action in the situation, for example, where the driver is approaching a road sign at high speed and in the normal course of action would simply steer out of the way. A fundamental question which has to be answered is: at what point is it impossible for the driver to steer clear of an obstacle?

Initially this question was considered using a simple static model, coupled with the assumptions that the optimum avoidance trajectory is based on a circular path and that the vehicle can instantaneously achieve a maximum lateral acceleration limited only by the adhesion of the tyres to the road, which on a good road surface can be as much as one gravity. Under these assumptions a relationship between the vehicle's speed and 'strike distance' is simply calculated, where 'strike distance' represents the distance at which, whatever action the driver takes, it is no longer possible to avoid a collision[15]. Alternatively this may be viewed as a set of speed and road condition dependent risk zones in front of the vehicle where, independent of any driver action, collision avoidance by lateral action is impossible. Whilst this analysis does not take into consideration the dynamics of the vehicle, environmental conditions and driver response time, it does represent the limiting case and implies that it is possible to get extremely close to an obstacle before avoidance is impossible. For example at a speed of 20m/s the vehicle gets to within 9 metres of the obstacle before a crash cannot be avoided. This proposed lateral avoidance manoeuvre would be practically impossible to achieve and a more realistic estimate of vehicle behaviour can be achieved by taking into consideration the dynamic behaviour of the vehicle. As a first step a simple two degree of freedom bicycle model capable only of sidewise translation and yawing rotation, was adopted. Assuming that the vehicle is subjected to a force system which is dominated by the tyre forces modified risk zones in front of the vehicle were obtained[15], tending to increase the amount of the time during which it is possible to intervene (or to warn the driver).

6 Future work

Work on the collision avoidance problem is on-going with a view to combining aspects of ACC, ASS and ARC to develop adaptive control strategies which can handle a variety of situations and environmental conditions. It is planned that the overall distributed control system will employ data fusion techniques drawing information from a model/knowledge-based system to compliment sensor-based inputs relating to the physical state of the vehicle and its environment. It is anticipated that fuzzy logic and/or Kalman filtering procedures will be applied to combine model/knowledge-based information and measured sensor data, in order to provide useful and structured inputs which can be used effectively by the controller.

Acknowledgements: The authors are pleased to acknowledge the contribution of former students Colin Paterson, Adam Webb and Steve Miller.

References

(1) Jurgen RK (1995) The electronic motorist, *IEEE Spectrum*, March, pp 37-48
(2) Sharp RS, Crolla DA (1987) Road vehicle suspension design - a review, *Vehicle System Dynamics*, 16, pp 167-192
(3) Williams RA (1994) Electronically controlled automotive suspensions, *IEE Computing and Control Engineering Journal*, June, pp 143-148
(4) Paterson CA (1993) Computer controlled suspension systems, PhD Thesis, Coventry University, UK
(5) Webb AC, Burnham KJ, James DJG, Williams RA (1995) A comparative study of passive and low bandwidth active suspension systems, *J Systems Science*, 21(4), pp 27-41
(6) Webb AC, Burnham KJ, James DJG, Williams RA (1996) On-line adaptive control of a low bandwidth active suspension system, *Proc UKACC Int Conf on Control '96*, IEE Conference Publication No 427, pp 1154-1159
(7) Moulton AE, Best A (1979) Hydragas suspension, *SAE 790374*
(8) Williams RA, Best A, Crawford IL (1993) Refined low frequency active suspension, *IMechE, C 446-028-93*
(9) Williams RA, Burnham KJ, Webb AC (1996) Developments for oleo-pneumatic active suspension, *Proc IEEE Symp Computer Aided Control System Design*, Dearborn, MI, USA, pp 44-49
(10) Webb AC, Burnham KJ, James DJG, Williams RA (1996) Adaptive multi-modal control of a low bandwidth active suspension system, *Proc IFAC World Congress 96*, San Francisco, Vol Q, pp 255-260
(11) Webb AC (1996) Self-tuning low bandwidth active suspension systems, PhD Thesis, Coventry University, UK
(12) Sharp RS, Pan D (1993) On the design of an active roll control system for a luxury car, *Proc Inst Mech Engr, Part D: J Automobile Engineering*, 207, pp 275-284
(13) Miller SA, Williams RA, Burnham KJ (1994) Active-roll control, simulation and experimentation, *Proc 10th Int Conf on Systems Engineering*, Coventry University, UK, pp 851-860
(14) Warwick K, Rees D (1986) Industrial digital control systems, IEE Control Engineering Series, *Peter Peregrinus Press*
(15) Richardson M, Barber P, David L (1997) Knowledge based collision avoidance manoeuvres, *Proc 12th Int Conf on Systems Engineering*, Coventry University, UK, pp 565-570
(16) Tribe RH, Young E, Conlong R (1992) Improved obstacle detection by sensor fusion, *IEE Prometheus & Drive Colloquium*, London

Proc. of Third Int. Symp. on Artificial Life, and Robotics (AROB III' 98),
Oita, Japan, 19-21, January, 1998,

Sliding Mode Cooperative Motion Control of Dual Arm Manipulators

Woosoon Yim, Manoharan Selvarajan, and William R. Wells
Department of Mechanical Engineering
Howard R. Hughes College of Engineering
University of Nevada, Las Vegas
Las Vegas, NV 89154
U.S.A.

Abstract

This paper presents a method to realize a cooperative control of dual arm manipulators (RM-10A by Remotec Inc.) handling the same object in the presence of dynamic parameter uncertainties of robots and object. When multiple robots handle the same object, both position and internal forces between robots and an object should be controlled. In this paper, a sliding mode controller is derived for trajectory tracking of object position and internal forces. To show the effectiveness of the proposed controller numerical simulations are performed for 12 axis dual arm manipulators.

1. Introduction

Cooperative control of multiple manipulator system involves dynamics of multiple manipulators and an object. Even if we have accurate knowledge of multiple manipulator dynamics, dynamic properties of the object handled by these manipulators should be known for trajectory tracking of object position and internal forces. Algorithms of cooperation control of robots can be categorized into centralized and decentralized approaches. In a centralized approach, the controller is designed in the state space of the total system, and in a decentralized approach, each robot is controlled by its own controller without communications [1,2]. In the latter case, co-operations between robots are realized by controlling their interactive forces. Dynamic cooperation control using nonlinear feedback is reported in [4,5] This paper extends the centralized dynamic hybrid controller to robust sliding mode controller which is insensitive to dynamic parameter uncertainties of robots and an object.

2. Dynamics of Cooperative System

Dynamics of two manipulators working together to move a single object is derived. Suppose the two arms graspe an object rigidly and cooperatively handle it as shown in the Fig.1. The dynamic equation of the arm i (i =1 for right arm; i =2 for left arm) in the joint space $\mathbf{q}_i$ has the form:

$$\mathbf{M}_i\ddot{\mathbf{q}}_i + \mathbf{h}_i + \mathbf{g}_i = \tau_i + \mathbf{J}_i^T\lambda_i \tag{1}$$

where λ_i is the force exerted by the object on robot i in Cartesian space, $\mathbf{J}_i$ is manipulator Jacobian, $\mathbf{M}_i$ is 6x6 positive definite mass matrix, $\mathbf{h}_i$ is vector representing centrifugal and Coriolis forces, and $\mathbf{g}_i$ is a vector representing gravity load. For the control of the manipulator end effector, it is useful to rewrite the manipulator dynamics in Cartesian space The position and orientation of the end effector can be represented in the Cartesian space using a vector $\boldsymbol{X}$ as

$$\mathbf{X} = [x \quad y \quad z \quad \gamma \quad \beta \quad \alpha]^T$$

where x, y, and z are three and γ, β, and α are three rotation angles. The kinematics of the object can be written as

$$\mathbf{X} = \phi_1(\mathbf{q}_1) = \phi_2(\mathbf{q}_2) \tag{2}$$

where ϕ_i is nonlinear function and $\mathbf{q}_i$ is joint position vector of each arm. Differentiating (2) with respect to time yields

$$\dot{\mathbf{X}} = \mathbf{R}_i\dot{\mathbf{q}}_i \tag{3}$$

$$\ddot{\mathbf{X}} = \dot{\mathbf{R}}_i\dot{\mathbf{q}}_i + \mathbf{R}_i\ddot{\mathbf{q}}_i \tag{4}$$

Using (3) and (4), $\ddot{\mathbf{q}}_i$ can be written as

$$\ddot{\mathbf{q}}_i = \mathbf{R}_i^{-1}\left(\ddot{\mathbf{X}} - \dot{\mathbf{R}}_i\mathbf{R}_i^{-1}\dot{\mathbf{X}}\right) \tag{5}$$

Let $\mathbf{u}_i$ be the equivalent force applied on the mass center of the object by the joint torque τ_i. The τ_i is related to $\mathbf{u}_i$ by the Jacobian matrix $\mathbf{R}_i$ defined on the object frame as

$$\tau_i = \mathbf{R}_i^T\mathbf{u}_i \tag{6}$$

where $\mathbf{R}_i$ is the Jacobian of the object frame to the world frame. Using (3), (4), and (6), (1) becomes

$$\begin{aligned}\ddot{\mathbf{X}} = {} & \dot{\mathbf{R}}_i\mathbf{R}_i^{-1}\dot{\mathbf{X}} - \mathbf{R}_i\mathbf{M}_i^{-1}\left(\mathbf{h}_i + \mathbf{g}_i\right) + \\ & \mathbf{R}_i\mathbf{M}_i^{-1}\left(\mathbf{R}_i^T\mathbf{u}_i + \mathbf{J}_i^T\lambda_i\right)\end{aligned} \tag{7}$$

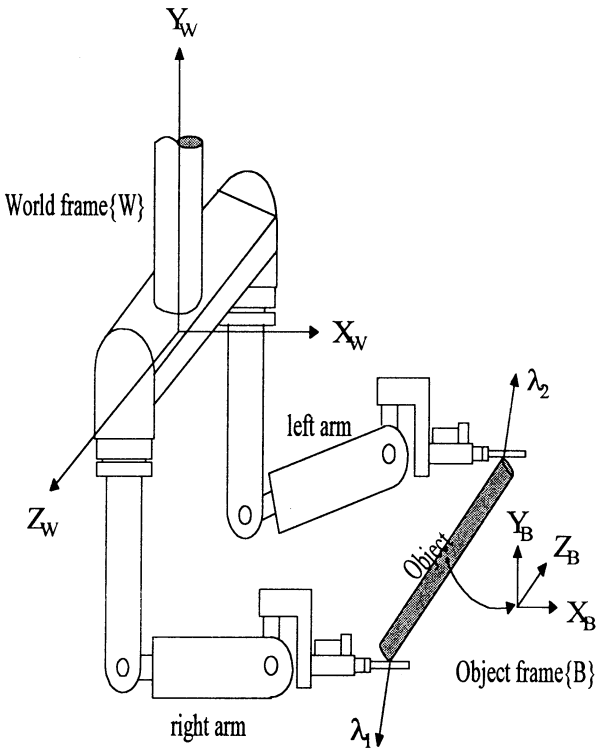


Figure 1 Dual Arm Manipulator, RM-10A

Let $\mathbf{f}_i$ be the equivalent force acting on the mass center of the object to λ_i. Then λ_i and $\mathbf{f}_i$ are related by

$$\lambda_i = \mathbf{J}_i^{-T}\mathbf{R}_i^T\mathbf{f}_i \tag{8}$$

Substituting (8) into the equation (7) results in the equations of motion of the object in terms of operational coordinate [3]

$$\ddot{\mathbf{X}} = \dot{\mathbf{R}}_i\mathbf{R}_i^{-1}\dot{\mathbf{X}} - \mathbf{R}_i\mathbf{M}_i^{-1}\left(\mathbf{h}_i + \mathbf{g}_i\right) + \mathbf{R}_i\mathbf{M}_i^{-1}\mathbf{R}_i^T\left(\mathbf{u}_i + \mathbf{f}_i\right) \tag{9}$$

The $\mathbf{f}_i$ in equation (9) can be decomposed into internal force $\mathbf{f}_{i\,\mathrm{IN}}$ and external force $\mathbf{f}_{i\,\mathrm{OUT}}$. That is

$$\mathbf{f}_i = \mathbf{f}_{i\,\mathrm{IN}} + \mathbf{f}_{i\,\mathrm{OUT}} \tag{10}$$

The external force, $\mathbf{f}_{i\,\mathrm{OUT}}$, contributes to the motion of the object but the internal force, $\mathbf{f}_{i\,\mathrm{IN}}$, does not. Since the internal forces exerted by the left and right arm cancel each other $\left(\mathbf{f}_{1\,\mathrm{IN}} + \mathbf{f}_{2\,\mathrm{IN}} = 0\right)$ the net force acting on the object mass center becomes summation of $\mathbf{f}_{1\mathrm{OUT}}$ and $\mathbf{f}_{2\mathrm{OUT}}$. The object dynamics can be written as

$$\mathbf{M}_o\ddot{\mathbf{X}} + \mathbf{g}_o = -\mathbf{f}_{1\,\mathrm{OUT}} - \mathbf{f}_{2\,\mathrm{OUT}} \tag{11}$$

where $\mathbf{M}_o$ is 6x6 mass matrix of the object and $\mathbf{g}_0$ is 6x1 vector representing gravity load on the object. It should be noted that velocity terms are neglected in object dynamics for simplicity. Let $\mu_1(t)$ and $\mu_2(t)$ be the load distribution for the right and left arms respectively.

$$\mathbf{f}_{1\,\mathrm{OUT}} = -\mu_1(t)\left[\mathbf{M}_o\ddot{\mathbf{X}} + \mathbf{g}_o\right] \tag{12}$$

$$\mathbf{f}_{2\,\mathrm{OUT}} = -\mu_2(t)\left[\mathbf{M}_o\ddot{\mathbf{X}} + \mathbf{g}_o\right] \tag{13}$$

where $\mu_1(t) + \mu_2(t) = 1$. Using equations (10). (12), and (13) and defining $\Lambda_i = \left(\mathbf{R}_i\mathbf{M}_i^{-1}\mathbf{R}_i^T\right)^{-1} = \mathbf{R}_i^{-T}\mathbf{M}_i\mathbf{R}_i^{-1}$ the equation (9) can be written as [2]

$$\Lambda_i\ddot{\mathbf{X}} + \mathbf{R}_i^{-T}\left(\mathbf{h}_i + \mathbf{g}_i\right) - \Lambda_i\dot{\mathbf{R}}_i\mathbf{R}_i^{-1}\dot{\mathbf{X}} = \mathbf{u}_i + \mathbf{f}_{i\,\mathrm{IN}} - \mu_i(t)\left[\mathbf{M}_o\ddot{\mathbf{X}} + \mathbf{g}_o\right]$$

or

$$\mathbf{A}_i\ddot{\mathbf{X}} + \mathbf{B}_i + \mathbf{C}_i = \mathbf{u}_i + \mathbf{f}_{i\,\mathrm{IN}} \tag{14}$$

where

$$\mathbf{A}_i = \Lambda_i + \mu_i(t)\mathbf{M}_o$$

$$\mathbf{B}_i = \mathbf{R}_i^{-T}\mathbf{h}_i - \Lambda_i\dot{\mathbf{R}}_i\mathbf{R}_i^{-1}\dot{\mathbf{X}} = \mathbf{R}_i^{-T}\mathbf{h}_i - \Lambda_i\dot{\mathbf{R}}_i\dot{\mathbf{q}}_i$$

$$\mathbf{C}_i = \mathbf{R}_i^{-T}\mathbf{g}_i + \mu_i(t)\mathbf{g}_o$$

Therefore the dynamics of the arms shown in Fig.1 in terms of operational coordinates $\mathbf{X}$ can be written as

right arm

$$\mathbf{A}_1\ddot{\mathbf{X}} + \mathbf{B}_1 + \mathbf{C}_1 = \mathbf{u}_1 + \mathbf{f}_{1\,\mathrm{IN}} \tag{15}$$

left arm:

$$\mathbf{A}_2\ddot{\mathbf{X}} + \mathbf{B}_2 + \mathbf{C}_2 = \mathbf{u}_2 + \mathbf{f}_{2\,\mathrm{IN}} \tag{16}$$

3. Sliding Mode Control

The cooperation dynamics of the arms in the operational space are derived in (15) and (16). Adding these two equations,

$$A\ddot{\mathbf{X}} + B + C = u_1 + u_2 \tag{17}$$

where $A = A_1 + A_2, B = B_1 + B_2, C = C_1 + C_2$. Here it should be noted that the internal forces $\mathbf{f}_{1\,\mathrm{IN}}$ and $\mathbf{f}_{2\,\mathrm{IN}}$ cancel each other. From equations (15) and (17), $\mathbf{f}_{1\,\mathrm{IN}}$ can be expressed in terms of input force $\mathbf{u}_1$ and $\mathbf{u}_2$ as

$$\mathbf{f}_{1\,\mathrm{IN}} = \mathbf{A}_1\left\{-\mathbf{A}^{-1}(\mathbf{B}+\mathbf{C}) + \mathbf{A}^{-1}(\mathbf{u}_1 + \mathbf{u}_2)\right\} + \mathbf{B}_1 + \mathbf{C}_1 - \mathbf{u}_1 \tag{18}$$

Then equations (17) and (18) can be rewritten in the matrix form of

$$\begin{bmatrix} \ddot{\mathbf{X}} \\ \mathbf{f}_{1\,IN} \end{bmatrix} = \begin{bmatrix} -\mathbf{A}^{-1}[\mathbf{B}+\mathbf{C}] \\ -\mathbf{A}_1\mathbf{A}^{-1}(\mathbf{B}+\mathbf{C})+\mathbf{B}_1+\mathbf{C}_1 \end{bmatrix} + \begin{bmatrix} \mathbf{A}^{-1} & \mathbf{A}^{-1} \\ \mathbf{A}_1\mathbf{A}^{-1}-\mathbf{I} & \mathbf{A}_1\mathbf{A}^{-1} \end{bmatrix} \begin{bmatrix} \mathbf{u}_1 \\ \mathbf{u}_2 \end{bmatrix} \tag{19}$$

or

$$\begin{bmatrix} \ddot{\mathbf{X}} \\ \mathbf{f}_{1\,IN} \end{bmatrix} = \mathbf{G}+\mathbf{H}\mathbf{u} \tag{20}$$

Here we assume that robot and object dynamics parameters are not known exactly, but robot kinematic parameters are known. Let

$$\begin{aligned} \mathbf{G} &= \mathbf{G}^* + \Delta\mathbf{G} \\ \mathbf{H} &= \mathbf{H}^* + \Delta\mathbf{H} \end{aligned} \tag{21}$$

where G^* and H^* are the nominal values of matrices G and H, and ΔG and ΔH represent the unknown portions of G and H, respectively.

For the design of variable structure control system, we select a switching surface S(t)=0 in the state space as a function of the output trajectory error, its derivative, and the integral of the tracking error.

$$\mathbf{S}(t) = \begin{bmatrix} \dot{\tilde{\mathbf{X}}} + 2\zeta\omega_n\tilde{\mathbf{X}} + \omega_n{}^2 \int \tilde{\mathbf{X}}dt \\ \int \tilde{\mathbf{f}}_{1IN}\,dt \end{bmatrix} \tag{22}$$

where $\tilde{\mathbf{X}} = \mathbf{X} - \mathbf{X_r}$ is output position trajectory error, $\tilde{\mathbf{f}}_{1IN} = \mathbf{f}_{1IN} - \mathbf{f}_{1IN_r}$ is internal force error, ζ is the damping ration, and $\omega_n>0$ is the natural frequency. In the sliding phase, the trajectory is confined to the surface $S(t)=0$, which implies that $\dot{\mathbf{S}}(\mathbf{t}) = \mathbf{0}$, and $\tilde{\mathbf{X}} \to 0$ and $\mathbf{f}_{1IN} = \mathbf{f}_{1IN_r}$ as $t \to \infty$.

Now we consider the design of a discontinuous controller, such that trajectory reaches the switching surface $S(t)=0$ in a finite time from any initial condition. The derivative of $S(t)$ is given by

$$\begin{aligned} \dot{\mathbf{S}} &= \mathbf{G}^* + \Delta G + \begin{bmatrix} -\ddot{\mathbf{X}}_r + 2\zeta\omega_n\dot{\tilde{\mathbf{X}}} + \omega_n{}^2\tilde{\mathbf{X}} \\ -\mathbf{f}_{1IN_r} \end{bmatrix} + (\mathbf{H}^* + \Delta\mathbf{H})\mathbf{u} \\ &= \mathbf{P}^* + \Delta\mathbf{G} + (\mathbf{H}^* + \Delta\mathbf{H})\mathbf{u} \end{aligned} \tag{23}$$

where $\mathbf{P}^*$ denotes the known function in (23). In view of (23), we choose a variable structure control law of the form

$$\mathbf{u} = \mathbf{H}^{*-1}[-\mathbf{P}^* - \mathbf{K}\,\mathrm{sgn}(\mathbf{S})] \tag{24}$$

where $\mathrm{sgn}(\mathbf{S}) = [\mathrm{sgn}(s_1)\cdots\mathrm{sgn}(s_{12})]^T$ and $\mathrm{sgn}(s_i) = 1$ for $s_i > 0$ and $\mathrm{sgn}(s_i) = -1$ for $s_i < 0$. Here, the detailed proof of stability and bounds on uncertainty functions are omitted. In this controller, it is assumed that X and f_{1IN} are available for feedback and high frequency chattering problem due to a discontinuous controller input can be avoided by replacing $\mathrm{sgn}(s_i)$ continuous function of $sat(s_i)$.

$$sat(s_i) = \begin{cases} \mathrm{sgn}(s_i), & |s_i| > \varepsilon_i \\ s_i/\varepsilon_i, & |s_i| \le \varepsilon_i \end{cases} \tag{25}$$

4. Simulation Results

Computer simulation was done to verify the proposed controller. Initial position and internal forces are

$X=[0.62\ -0.414\ 0\ 0\ 1.5708\ 0]^T$ (m)

$f_{1IN}=[0\ 0\ 0\ 0\ 0\ 0]^T$ (N)

and the final position and the desired internal forces are

$X_c=[0.610\ -0.404\ 0.01\ 0.01\ 1.58\ 0.01]^T$ (m)

$f_{1cIN}=[10\ 10\ 10\ 1\ 1\ 1]^T$ (N, Nm)

Control parameters used in the simulation are

$\zeta=0.707$, $\omega n=5$, $\varepsilon=0.1$

Figure 2 and 3 show the simulation results of object motion and internal forces for uncertain object inertia properties of 50%.

5. Conclusions

Cooperative control of dual arm manipulators handling the same object in the presence of dynamic parameter uncertainties object is studied. In this paper, a sliding mode controller is derived for trajectory tracking of object position and internal forces. To show the effectiveness of the proposed controller numerical simulations are performed for 12 axis dual arm manipulators.

References

[1] Y Liu, S. Arimoto, V.Parra_Vega, and K. Kitagaki,"Adaptive distributed cooperation controller for multiple manipulators,", 1995 IEEE ICRA, pp489-494,

[2] Y Liu, S. Arimoto, and T. Ogasawara,"Decentralized cooperation control: Non-communication object handling," 1996 IEEE ICRA, pp2414-2419, Minneapolis, MN

[3] O. Khatib, "A unified approach for motion and force control of robot manipulators: the operation space formulation", IEEE Trans. Robotics and Automation, Vol RA-3, No.1, pp43-53, 1987

[4] T.J. Tarn, A.K.Bejzcy and X.Yun,"Design of dynamic control of two cooperating robot arms:closed chain formulation," IEEE ICRA, pp 7-13, 1987

[5] T. Yoshikawa and X.Zheng, "Coordinated dynamic hybrid position/force control of multiple robotic manipulators handling one constrained object," IEEE ICRA, pp 1091-1096, 1989

[6] M. Selvarajan, "Cooperative control of dual arm manipulator," MS thesis, University of Nevada, Las Vegas, 1997.

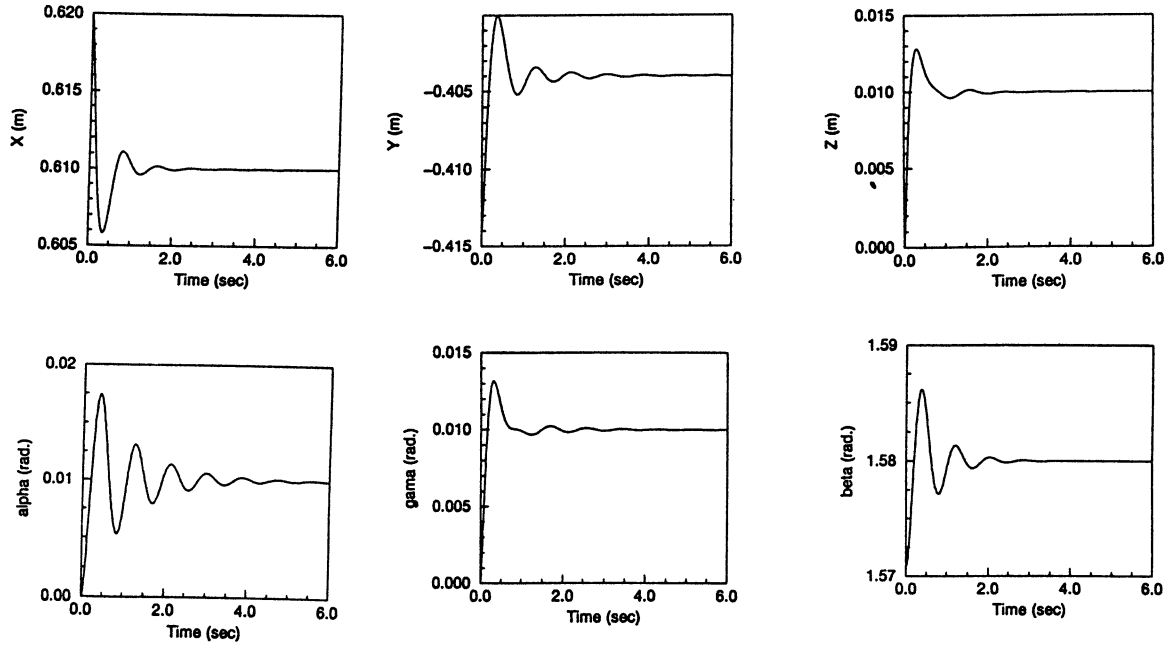


Figure 1. Motion of Object

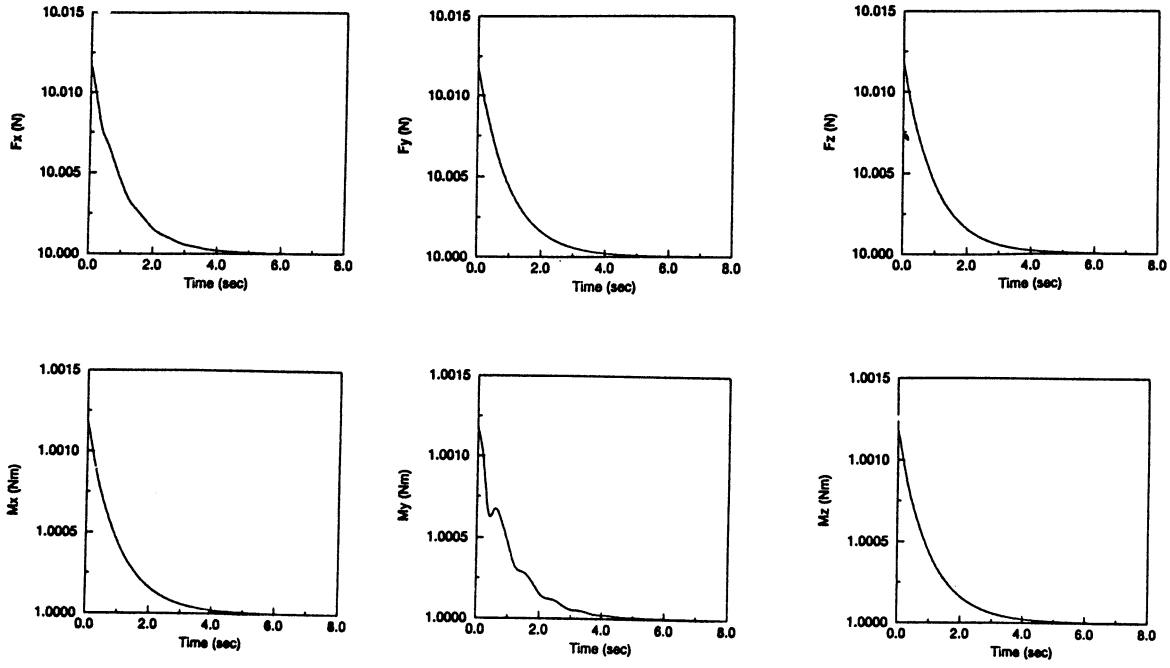


Figure 2. Plots of internal forces

Proc. of Third Int. Symp. on Artificial Life, and Robotics (AROB III' 98),
Oita, Japan, 19-21, January, 1998,

Real-Time Control Schemes for MiroSot

Jong-Hwan Kim, Kwang-Choon Kim, Dong-Han Kim, Yong-Jae Kim and Prahlad Vadakkepat
Dept. of Electrical Engineering, KAIST, Taejon-shi, 305-701, Republic of Korea
{johkim,kckim,dhkim,yjkim,prahlad}@vivaldi.kaist.ac.kr
http://www.mirosot.org/, http://www.fira.net/

Abstract

The vector field based path planning and role selection using Petri-net state diagrams are proposed for real-time control of soccer robots. The roles of robots will get changed from attack mode to defense mode based on the angles between the moving direction of ball, the distance between robots and ball, and the heading angles of robots. The path planning is carried out with overall vector fields. Vector fields generated according to ball position and the goal point are used, and the robots will be allowed to follow the same.

The MIRO II team using the above role selection mechanism and strategies was placed in third position in the second Micro-Robot World Cup Soccer Tournament (MiroSot) competitions held in KAIST, Korea, between June 1-5, 1997.

Keywords: multi-agent, robot soccer, MiroSot, vector fileds, Petri-net.

1 Introduction

Developing a multi-agent system amounts to the search for a method for implementing an intelligent system composed of multiple agents, with independent motion control and cooperating each other. Multi-agent systems are more flexible and fault tolerant as several simple robot agents are easier to handle and cheeper to build compared to a single powerful robot for different tasks.

MiroSot is a suitable test bench for multi-agent system research. The soccer game is different from other multi-agent systems, in that the robots of one team have to cooperate, while facing competition from the opponent team. The multi-agent control algorithm, in such an active environment, must comprise of low level kinematics and dynamics, and high level strategies to avoid obstacles and to compete with opponent robots. Such an environment needs fast processing algorithms and suitable robot structure.

This paper proposes a novel real time vector field based path plannig for attack mode robot and a Petri-net state diagram approach for robots' (attack,defense and goalie) role selection for MiroSot. The robots used in MiroSot are small in size (7.5cm $\times$ 7.5cm $\times$ 7.5cm), fully/semi autonomous and without any human operators. MiroSot involves multiple robots that need to collaborate in an adversarial environment to achieve specific objectives. In multi-robot systems the environment's dynamics can be determined by other robots in addition to the uncertainty that may be inherent in the domain. They have dynamic environments as other robots intentionally affect the environment in unpredictable ways. The key aspect being the need for robots not only to control themselves, but also to track and control the ball which is a passive part of the environment. The interesting theoretical issue behind MiroSot experiments is the use of soccer as a prototype example of a complex, adaptive system.

Different types of schemes for soccer robot control are available. In a remote-brainless vision-based soccer robot scheme a host computer controls the robots by commanding the robot velocities like a radio-controlled car. In the brain on-board vision-based soccer robot system, the robots move as per the vision data, keeping away from obstacles autonomously. A robot-based scheme, wherein each autonomous robot can make a decision based on information it collects with its sensors and if needed, can communicate with other robots. Robots which can be operated autonomously are needed for the robot-based system. The control structure, behaviors and actions of robots will influence their performance in a big way in robot-soccer games. This paper deals with the remote brainless robot system.

The effectiveness of proposed algorithm is shown through MiroSot competition, and our team was awarded 3rd place in MiroSot'97, held in KAIST, Korea, June 1-5, 1997.

2 Control of Mobile Robots

In this section, we develop a method for path generation and control of robots. The conventional path generation and motion control have complex algorithm. Therefore real time and high speed control is difficult.

In MiroSot competitions, there are many conditions to be satisfied. It must be possible,

- for real time control,
- to control the robot speed while moving fast,
- to avoid obstacles and,
- to deal with error and noise for robust control.

2.1 Modeling of a mobile robot

Two wheeled mobile robots with non-slipping and pure rolling are considered in this work [1]. The velocity vector

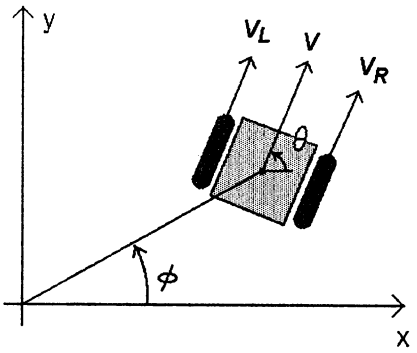


Figure 1: Modeling of kinematics.

consists of translation velocity of the center of robot and rotational velocity with respect to the center of robot. The pose vector $\overrightarrow{P}$ and velocity vector $\overrightarrow{Q}$ associated with the robot kinematics are given in equation 1:

$$\overrightarrow{P} = \begin{bmatrix} \dot{X} \\ \dot{Y} \\ \dot{\theta} \end{bmatrix} = \begin{bmatrix} cos(\theta) & 0 \\ sin(\theta) & 0 \\ 0 & 1 \end{bmatrix} \cdot \begin{bmatrix} V \\ \omega \end{bmatrix} = J(\theta)\overrightarrow{Q}. \quad (1)$$

To get robot position and angle, equation 1 should satisfy the following nonholonomic constraint:

$$\begin{aligned} G.\overrightarrow{P} &= [sin(\theta) \quad -cos(\theta) \quad 0] . \begin{bmatrix} \dot{X} \\ \dot{Y} \\ \dot{\theta} \end{bmatrix} \\ &= \dot{X}sin(\theta) - \dot{Y}cos(\theta) = 0. \end{aligned} \quad (2)$$

This means that the instant heading direction is the same as the angle of the front side of robots. The associated Lagrange's equation is given as follows:

$$\begin{aligned} \frac{d}{dt}\frac{dL}{d\dot{q}} - \frac{dL}{dq} &= \tau\,[F_L \quad F_R] \\ &= \begin{bmatrix} \frac{M}{4} + \frac{I}{L^2} & \frac{M}{4} - \frac{I}{L^2} \\ \frac{M}{4} - \frac{I}{L^2} & \frac{M}{4} + \frac{I}{L^2} \end{bmatrix} \cdot [a_L \quad a_R] \\ &= Hq \end{aligned} \quad (3)$$

where M is the mass of robot, I is the rotational inertia and, the mass and rotational inertia of the wheels are approximated to zero. F_L and F_R are forces acting on the left and right wheels and, a_L and a_R are the wheel accelerations. The force supplied by both wheels and associated acceleration are coupled. If $\frac{M}{4} = \frac{I}{L^2}$ is satisfied, both wheels will get decoupled.

2.2 Re-analysis of existing method on vector field

In the Potential Field Method an agent can move in proportion to the resultant force with an attractive force from the desired position and a repulsive force from the obstacle to be avoided. This method, generallly used in robot control, is simple and helps to control the robots in real time. However, when a constant velocity can not be maintained and the obstacle is too big, it is possible for the robot to oscillate and the direction at the final point can not be guaranteed [2]. Figure 2 shows the force direction at each position, with an obstacle in the vicinity.

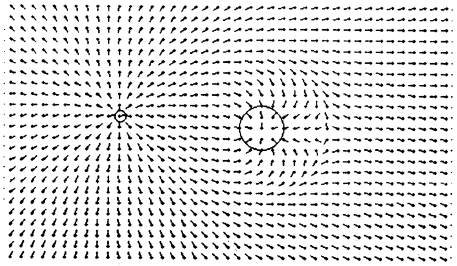


Figure 2: Potential field method

The vector field in Figure 2 shows the directions that the robot can follow from its present position. The magnitude of field will vary as per robot position. It is possible to control the robot better with a modified vector field.

In this work, we assume that the magnitude of vector is the same at all positions. The following method is used to reduce the error in angle, between the robots and field vectors:

$$\begin{aligned} \omega &= K_P(\angle\overrightarrow{V(x,y)} - \theta) \\ \overrightarrow{V(x,y)} &: the\ vector\ field\ at\ position\ (x,y) \\ &\quad with\ magnitude\ unity. \\ K_P &: feedback\ gain, \end{aligned} \quad (4)$$

while the translational velocity V is constant. The discrete time implementation is given as:

$$\begin{aligned} \theta[n+1] &= (1 - K_P T)\theta[n] + K_P F(\overrightarrow{P}) \\ where \quad F(\overrightarrow{P}) &= \angle\overrightarrow{V(x[n], y[n])} \\ T &: sampling\ time \\ \theta &: heading\ direction\ angle. \end{aligned} \quad (5)$$

2.3 Control method development for defense and goal keeper robots

The defense and goal keeper robots are controlled using position and angle fields. Figures 3 and 4 show the position and angle fields, respectively.

The meaning of position field is basically the same as that of the potential field. The robot can move to the desired goal point but the final heading direction can't be guaranteed. When orientation of robot is not important in its final position, this field can be used. On the other hand, angle field is used to control only the angle without translation. At that the time translation velocity of robot must be zero, so V in equation (4) must be zero. The

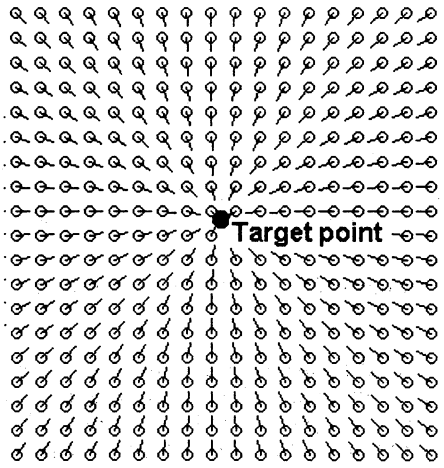


Figure 3: Position field

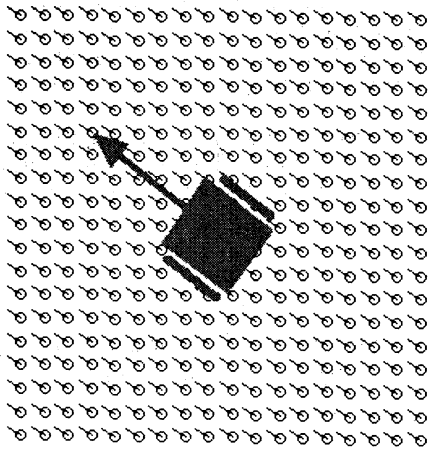


Figure 4: Angle field

movements of the defender and goal keeper robots are made based on these two vector fields and the detailed algorithm is provided in section 3.

2.4 Development of control methods for attacking robot

The attacking robot's vector field heads towards the final position and the associated angle of robot is shown in Figure 5.

The final position of the robot is the center of the field and the final angle is to the right. The circle and straight lines shown in Figure 5 correspond to the initial position and angle of the robot, and the curved lines correspond to the path that is simulated by equation (4).

In the soccer game, the attacker is programmed to get more acceleration by making its final position 10 pixels ahead of ball position and its final direction as the goal post. As a result, the attacker may kick or dribble the ball. As the ball moves, the vector field gets modified.

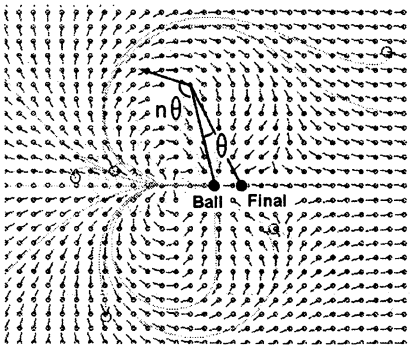


Figure 5: Vector field for final position.

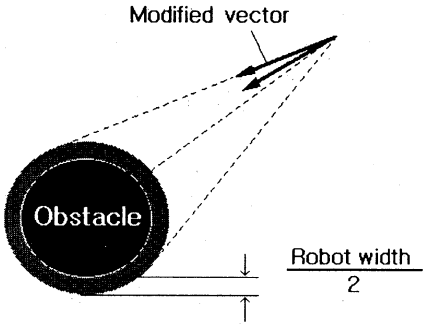


Figure 6: Modification of vector.

The robot can move behind, and kick or dribble the ball towards the goal.

2.5 Modified vector field with obstacles

Obstacle avoidance behaviour is obtained by modifying the vector field as in Figure 6. When the vector at a position is oriented towards an obstacle, it is reformed to orient to the boundary of the obstacle. At that time, it is considerd that the size of the obstacle is larger than its real size and assumed to have a size as the width of the robot. The modified vector field is shown in Figure 7.

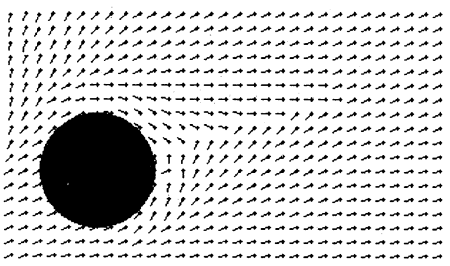


Figure 7: Field Modified by Obstacle

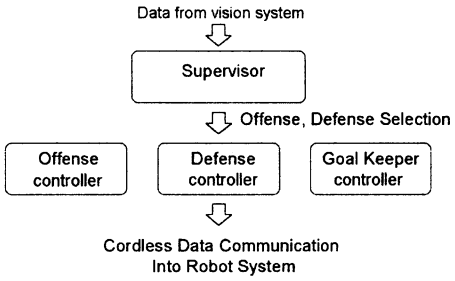


Figure 8: Structure of supervisory controller.

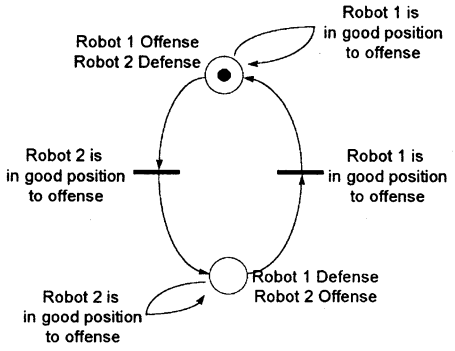


Figure 9: Petr-net model of the supervisor.

3 Petri-net Based Modelling and the Strategy Adapted

3.1 The objectives and scope of research

The objective of this paper is to get an effective controller for the robot soccer environment. In this section, we will consider controllers for attacking, defending and goal keeping robots.

The following conditions are assumed, at each sampling time:

- the host computer receives the position and orientation informations of attacking, defending and goal keeping robots from the vision system,
- the host computer receives the position information of the ball from vision system and,
- the host computer sends commands to each robot which are generated efficiently from a knowledge base made from experience and by observing human behaviours.

In this paper, a supervisory controller using Petri-net is designed and the same is implemented in real system to confirm the efficacy of the developed method.

3.2 Structure of the supervisory controller

It is assumed that the left half is the attacking side and the right is defending. The reference origin of the playground is taken as the left upper corner. A flexible border region which moves according to the ball position is considered with its flexible center line. It is assumed that the robot in the goal area as the goal keeper, the robot on the left side of the flexible center line as the attacking robot, and the one on the right side as the defending robot. The structure of supervisory controller is given in Figure 8.

3.2.1 Supervisor

The supervisor in Figure 8 receives the information of the robots and ball, and decides the role of each robot. In other words, supervisor doesn't fix the attacking and defending robots beforehand, but their roles are decided and allocated according to the situation. The following states are defined for modeling the system in Petri-net:

- Robot 1 is attacking, Robot 2 is defending.
- Robot 1 is defending, Robot 2 is attacking.

The state diagram can be modeled in simple Petri-net as in Figure 9. The Petri-net in Figure 9 is programmed, and the subroutine is used for normal game. Which robot is in an advantageous position with the distance and angle from the ball can be determined. The robots used in our system have good straight moving capability, but are not so good in turning. So, when a robot is close to the ball and is oriented towards it, it can attack more effectively than the other robot. The following switching condition is used.

"It is assumed that, there are two robots, a defense and an attack robot. r_1 *is the distance from the attack robot to the ball and* r_2 *is that from the defense robot to the ball.* Ang_1 *and* Ang_2 *are angles between the heading direction of each robot and the ball. So, If* $r_2 < 2 * r_1$ *and* $-45Deg. < Ang_2 < 45Deg.$*, then the roles of robot1 and robot2 get interchanged."*

3.3 Defense controller

The robot with a role to defend, should block the ball before the opponent robots can kick the ball. So, it is reasonable that the defense robot must move to the right side of the ball as soon as possible. Four simple states are assumed:

(a) Defense robot behind the ball.
(b) Defense robot kicks the ball.
(c) Self goal position.
(d) Defense robot in contact with the ball and behind.

Figure 10 shows the above four states in detail. In state (a) the defense robot is in a probable kicking position, in state (b) it is kicking the ball, in state (c) it is in front of the ball, so should be careful to avoid self goal, and in state (d) it is in contact with the ball.

With these four states, the Petri-net of the defense controller is formed. In Figure 11, *'Angle'* refers to the

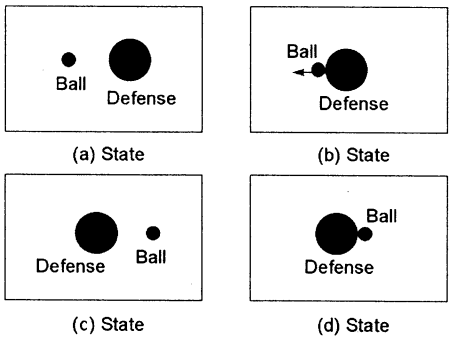


Figure 10: States of defense controller.

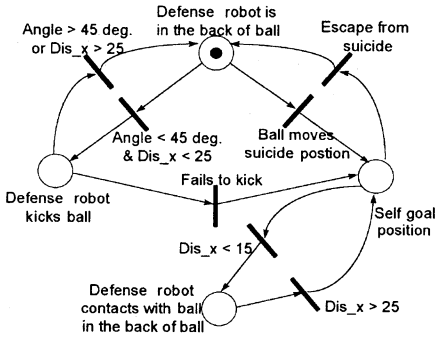


Figure 11: Petri-net model for defense controller.

angle between the heading direction of the defense robot and the ball. $'Dis'_x$ is the distance between the defense robot and the ball in pixels. In state (a), the defense robot is ordered to move to the ball and kick it. In state (b), if angle is above 45 deg., or $'Dis'_x$ is more than 25 pixels, the defense robot goes to state (a). In state (a), if the ball is on the right side of the defense robot (self goal position), it should go to state (c). In state (b), if the defense robot fails to kick the ball, the robot goes to state (c). In state (c), the defense controller orders the robot to move sideways and come behind the ball without touching the ball and it goes to state (a). In state (c), if $'Dis'_x$ is below 15 pixels, the robot goes to state (d), so, it should move away from the ball until $'Dis'_x$ is above 25 pixels and then gets into state (c).

3.4 Goal keeper controller

The goal keeper robot is assumed to move only within the goal area. The major objective of the goal keeper is to block the ball effectively. In this work, the goal keeper controller is designed according to the distance between the goal and the ball. The three states considered are:

- Far distance
- Medium distance
- In goal area.

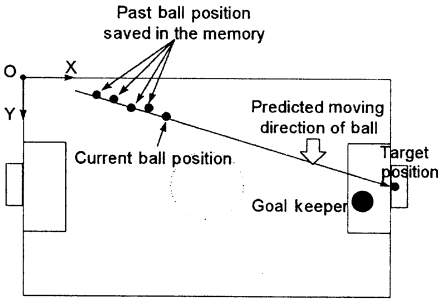


Figure 12: Subroutine 'predictor()'.

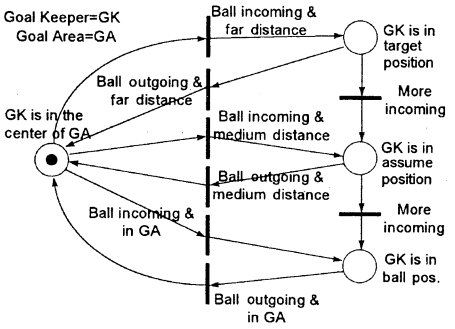


Figure 13: Petri-net model of goal keeper controller.

'Far distance' means, the distance between the goal area and the ball is above 60 pixels, 'Medium distance' means, it is above 20 pixels and within 60 pixels, and 'In goal area' means, it is below 20 pixels.

The subroutine predictor() predicts the ball direction using a linear equation. It is assumed that the ball always goes straight. With the five past positions of the ball, the predictor derives an equation for the line of movement of the ball using curve fitting algorithm. Figure 12 shows the role of predictor().

Four states are assumed for the goal keeper controller as follows:

1. Goal keeper at the center of goal area
2. Goal keeper in target position
3. Goal keeper in assume position
4. Goal keeper in ball position.

State 1 represents a case where goal keeper is located at the center of goal area for 'kick off' when the play resumes. The ball doesn't move toward the goal keeper at this situation. The 'target' position of state 2 is represented in Figure 13. In other words, the 'target' position is the direction of the moving ball that the predictor() predicts. The 'assume' position of state 3 means the point that links the present position of ball and the center of

goal post. State 4 represents a situation of emergency, so goal keeper should move to ball position. Figure 13 shows a Petri-net model for the goal keeper controller with these states.

In Figure 13, the goal keeper robot is located at the center of goal area for kick-off. If ball moves toward the goal area and the distance between them is 'Far Distance', goal keeper controller invokes the predictor() subroutine and moves to the predicted 'target' position. At that time, if the distance is bigger than 'Far Distance', the goal keeper moves to the center again.

If the distance between a ball and goal area is 'Medium Distance' with opponent robots around, the controller directs the goal keeper to move to 'assume' position. When the emergency situation is over, the goal keeper retuns back. If the ball comes within the goal area, the goal keeper should move to the position of the ball. If ball comes closer when goal keeper is located in 'target' position, then the goal keeper moves to 'assume' position.

In this study, the situation that is represented in Figure 13 is implemented using Goalie() subroutine.

3.5 Attack controller

The attack controller uses the vector field method explained in section 2.5 to implement a fast attacking strategy. If the goal position of the vector field is that of ball position and the direction is towards the opposite goal, the home robot can dribble the ball towards it. It is possible to control very fast movement using this method. If the condition is satisfied, the home attacker must attack fast.

4 Conclusion

In this paper, supervisor controller and defense mode controller using Petri-net are proposed, and the controller using vector field is studied for the low level controller. As a result using these controllers, the team, Miro got third prize in MiroSot'97 held in KAIST, June 1-5, 1997.

The controller did not use any information on the opponent team, and the robots did not use full duplex communication scheme. But these will have to be studied to bring in more cooperation among robot agents.

References

[1] Guy Campion, Georges Bastin and D'Andrea-Novel, "Structural Properties and Classification of Kinematic and Dynamic Models of Wheeled Mobile robots", IEEE Trans., RNA, Vol. 12, No. 1, pp 47-62, Feb. 1996.

[2] J.Borenstein and Y.Koren, "Real-time Obstacle Avoidance for Fast Mobile Robots", IEEE Trans. on Syst. Man and Cyber., Vol. 20, No. 4, pp 1179-1187, 1989.

[3] J.-H. Kim, H.-S. SHim, H.-S. Kim, M.-J. Jung, I.-H. Choi and K.-O. Kim, "A Cooperative Multi-Agent System and Its Real Time Application To Robot Soccer," Proc. of the IEEE Int. Conf. on Robotics and Automation, Albuquerque, New Mexico, 1997.

[4] H.-S. Shim, H.-S. Kim, M.-J. Jung, I.-H. Choi, J.-H. Kim and J.-O. Kim, "Designing Distributed Control Architecture for Cooperative Multi-agent System and Its Real-Time Application to Soccer Robot", Journal of Robotics and Autonomuos Systems, Vol. 21, No.2, pp. 149-165,10 September 1997.

[5] Allessandro Giva and Frank DiCesare, "Supervisory Design Using Petri-nets", Proc. of the 30th Conference on Decision and Control, pp 92-97, Brighton, England, 1991.

[6] Tadao Murata, "Petri-nets: Properties, Analysis and Applications", Proc. of the IEEE, Vol. 77, No. 4, pp 541-580, April 1989.

[7] J.-H. Kim (ed.), Proceedings of MiroSot'96, KAIST, Taejon, Korea, November 1996.

[8] J.-H. Kim and J.-J. Lee (ed.), Proceedings of MiroSot'97, KAIST, Taejon, Korea, June 1997.

[9] J.-H. Kim (ed.), Special Issue: First Micro-Robot World Cup Soccer Tournament, MiroSot, Robotics and Autonomous Systems, Elsevier, Vol. 21, No. 2, Sept., 1997.

Proc. of Third Int. Symp. on Artificial Life, and Robotics (AROB III' 98),
Oita, Japan, 19-21, January, 1998,

Estimation Problems in Artificial Intelligence*

Fathalla S. Mistiri
Faculty of Science
University of Garyounis
Benghazi, Libya

Alan P. Wang
Department of Mathematics
Arizona State University
Tempe, Arizona 85287-1804

Sueo Ueno
Information Science Lab
Kyoto School of Computer Science
Kyoto 606, Japan

Abstract

In this paper we shall investigate estimation problems in an artificial intelligence system by considering an inputs and outputs system, in the sense of introducing the system as composed of internal and external states. The advantage of the two states is to get the Kalman filters equation, as well as a complete set of equations, for which the star-product theory (as defined by Mistiri and Wang [20]) is applied to derive and organize new and old results for the estimation problem.

1 State Estimation

To investigate the estimation problem, to be treated in this paper, we consider the following stochastic integral equation on some Hilbert space:

$$u(t) = u(a) + \int_a^t A(s)u(S)\,du + \int_a^t \phi(s)\,dW(s), \quad z \in [a,b], \tag{1}$$

where $A(t)$ is a deterministic linear bounded operator, ϕ is a suitable transformation valued stochastic process, and $W(t)$ is a Hilbert space valued Wiener process.

To discuss the integral equation (1) we need some basic abstract probability theory. We consider throughout that $(\Omega, \mathcal{A}, \mu)$ is a probability space, where $\mathcal{A}$ is a Borel field and μ is a probability measure. We let H be a Hilbert space and $[a,t]$ to be a finite interval.

Then an H-valued random variable $x(\omega)$ is a map $x : \Omega \to H$ which is measurable relative to μ; furthermore, if $x \in L(\Omega, H)$ then its expectation is given by

$$Ex = \int_\Omega x(\omega)\,d\mu.$$

An H-valued stochastic process is a transformation $x(t,\omega) : [a,b] \times \Omega \to H$ which is measurable in both t and ω. Another important notion is the conditional expectation, $E[x|\mathcal{F}]$, of an H-valued variable relative to a subsigma field $\mathcal{F} \subset \mathcal{A}$. $E[x|\mathcal{F}]$ is such that

$$\int_C x(\omega)\,d\mu = \int_C E[x|\mathcal{F}]\,d\mu$$

for all C in $\mathcal{F}$.

If $\mathcal{F} = \mathcal{A}[y; y \in H]$, that is, if $\mathcal{F}$ is generated by an H-valued random variable y on $(\Omega, \mathcal{A}, \mu)$ then in this case we write $E[x|y]$ for the conditional expectation of x given y, and $E[x|y]$ is called the *best global estimate* of x given y.

If $\mathcal{F} = \mathcal{A}[y; y \in H]$ and both x and y are in $L_2(\Omega, H)$ and $L_2(\Omega, \bar{H})$, respectively, ($\bar{H}$ is a Hilbert space) then $E[x|y]$ is the projection of X on the subspace H_y of $L_2(O, H)$ where

$$H_y = \{u(\omega) \in H : u(\omega) = F(y(\omega), F : \bar{H} \to H\}$$

is measurable relative to the measure induced by y on $(\bar{H}, B(\bar{H}))\}$.

In the following, we give a brief introduction to the notions of covariance, independence, orthogonality, and Wiener process in Hilbert space (for more details see [12], [5, 7] and [9]).

The covariance operator of H-random operators x and y which is denoted by $\mathrm{cov}(x,y)$ and is given by

$$\mathrm{cov}(x,y) = E(x \cdot y) - (Ex) \cdot (Ey),$$

where $\mathrm{cov}(x,y) \in L(H,H)$ and $(x \cdot y) : H \to H$ defined by $(x \cdot y)h = x\langle y, h\rangle$ for all $h \in H$ with $\langle\ ,\ \rangle$ as the inner product associated with H.

where $\hat{X}(s)$ is known as the filtered estimate of $X(s)$ and $n(s) = n(s,\omega)$ is a process with orthogonal increments. Now, with all of the above information, we are in a position to state our estimation problem.

2 Estimation Problem

With the standing assumptions on equations (3) and (4) and with the innovations process (5):

(i) We wish to find the *best global estimate* of $X(s)$ given the observation process $Y(s)$, with $a < s < t < b$ where t is considered fixed. That is, we want to find the linear estimate of $X(s)$ given by

$$\hat{X}(s|t) = \int_a^t K(s,u)dn(u)$$

where $K(s,\cdot) \in L(H,H)$ and such that it minimizes

$$E\langle h, (X(s) - \hat{X}(s|t))\rangle^2 \text{ for all } h, H.$$

If $s < t$, then $\hat{X}(s|t)$ is known as the *smoothed estimate* of $X(s)$, and if $s = t$ then $\hat{X}(s|s) = \hat{X}(s)$ is the *filtered estimate* of $X(s)$.

(ii) For a given observation $Y(s)$ we wish to use the input-output method to establish some relations between the smoothed and filtered estimates of $X(s)$.

3 Propositions

Part (i) of the estimation problem depends heavily on the following proposition which we state without proof (see Curtain [5] and Falb [12]), also keeping in mind that since $X(a)$, $W(t)$ and $Z(t)$ are Gaussians, $\hat{X}(s|t) = E[X(s)|Y_t]$, where $Y_t = \{Y(s) : a \le s \le t\}$.

Proposition 1 *The*

$$\hat{X}(s|t) = \int_a^t K(s,u)\, dn(u)$$

is the best linear estimate *if and only if*

$$E(X(s) - \hat{X}(s|t) \cdot (n(\sigma) - n(\tau)) = 0 \text{ for } a \le \tau \le \sigma < t.$$

Furthermore, $K(s,u) = R(s,u)H(u)$ is the unique solution which satisfies the estimation problem (i), where

$$H(u) = C^*(u)(D(u)D^*(u))^{-1}$$

and

$$\begin{aligned} R(s,u) &= E((\hat{X}(s) - X(s)) \cdot (\hat{X}(u) - X(u))^*) \\ &= \begin{cases} \phi(s,u)R(u), & s > u \\ R(s)\phi^*(u,s), & s < u \end{cases} \end{aligned}$$

with $\phi(s,u)$ being the fundamental solution associated with $(A(s) - R(s)H(s)C(s))$ and $R(u) = R(u,u)$ satisfying the following Riccati equation

$$\begin{aligned} \frac{d}{du}R(u) &= B(u)B^*(u) + A(u)R(u) \\ &\quad + R(u)A^*(u) - R(u)H(u)C(u)R(u). \end{aligned} \tag{6}$$

From the above proposition, it follows that

$$\hat{X}(s|t) = \hat{X}(s) + R(s)\lambda(s|t) \tag{7}$$

where

$$\lambda(s|t) = \int_s^t \phi^*(u,s)H(u)dn(u) \tag{8}$$

with $\lambda(t|t) = 0$.

Before proceeding with our approach which uses (7) and (8), we state some known results for the given system (3) and (4) under the standing assumptions.

(I) The filtered estimate $\hat{X}(s)$ satisfies the celebrated Kalman filters equation:

$$d\hat{X}(s) = A(s)\hat{X}(s)ds + R(s)H(s)dn(s). \tag{9}$$

For details, see Bucy and Joseph [4] and Davis [10] for the finite dimensional case and Falb [12] and Curtain [5] for the infinite dimensional case.

(II) The smoothed estimate $\hat{X}(s|t)$ and the *adjoint state* $\lambda(s|t)$ satisfy the *Hamiltonian system* given by

$$d\hat{X}(s|t) = A(s)\hat{X}(s|t)\, ds + B(s)B^*(s)\lambda(s|t)ds \tag{10}$$

$$\begin{aligned} -d\lambda(s|t) &= -H(s)C(s)\hat{X}(s|t)ds + A^*(s)\lambda(s|t)ds \\ &\quad + H(s)dY(s) \end{aligned} \tag{11}$$

where (10) and (11) were derived by Bryson and Frazier [3] and by Jazwinski [13] using variational methods.

(III) The partitioned equations of Lainiotis [17], obtained by him in a classical approach, are given by

$$\hat{X}(s) = \hat{X}_0(s) + \phi_0(a,s)\hat{X}(a|s) \tag{12}$$

$$\hat{X}(a,s) = (E - R(a)O_0(a,s))^{-1}(\hat{X}(a) + R(a)\lambda_0(a|s)) \tag{13}$$

$$\begin{aligned} R(s) &= R_0(S) + \phi_0(a,s)R(a) \\ &\times (E - O_0(a,s)R(a))^{-1}\phi^* \circ (a,s) \end{aligned} \tag{14}$$

where

(i) $R_0(s)$ is the solution of (6) with $R(a) = 0$,

(ii) $\hat{X}_0(s)$ is the filtered estimate of $X(s)$ when $\hat{X}(a) = 0$ and $R(a) = 0$,

(iii) ϕ_0, O_0 and λ_0 are given, respectively, by

$$\frac{d}{ds}\phi_0(a,s) = (A(s) - R_0(s)H(s)C(s))\phi_0(a,s), \quad \phi_0(a,a) = E \tag{15}$$

$$\frac{d}{ds}O_0(a,s) = \phi_0^*(a,s)H(s)C(s)\phi_0(a,s), \quad O_0(a,a) = 0 \tag{16}$$

$$\lambda_0(a|s) = \int_a^s \phi_0^*(u,a)H(u)dn_0(u) \quad \text{with}$$

$$dn_0(u) = dY(u) - C(u)\hat{X}_0(u)du.$$

(iv) Kailath and his colleagues approach (see [18], [16], [14]) in deriving Lainiotis equations using Redheffer scattering theory for the Hamiltonian system (10) and (11) with the boundary conditions $\lambda(s|s) = 0$ and $\hat{X}(a|s) = \hat{X}(a) + R(a)\lambda(a|s)$ associated with the scattering picture as in Figure 1, with

$$S_0(a,s) = \begin{pmatrix} t_0(a,s) & \rho_0(a,s) \\ r_0(a,s) & \tau_0(a,s) \end{pmatrix}$$

as the operator associated with the generator:

$$M(s) = \begin{pmatrix} A(s) & B(s)B^*(s) \\ -H(s)C(s) & A^*(s) \end{pmatrix}$$

when $R(a) = 0$ and

$$S_a = \begin{pmatrix} E & R(a) \\ O & E \end{pmatrix},$$

as the constant operator where E is the identity operator, for the boundary layer with the fact that $S(a,s) = S_a^* S$. Hence, Lainiotis and other results follow.

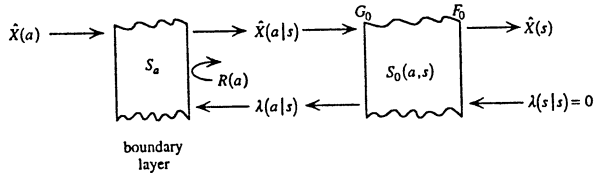


Figure 1. Kailath Scattering Picture

Now we are ready to present our results for the estimation problem (ii), but first we set:

$$\tilde{X}(s|t) = \hat{X}(s|t) - \hat{X}(s) = R(s)\lambda(s|t).$$

Then we have the following:

Proposition 2 *$\tilde{X}(s|t)$ and $\lambda(s|t)$ satisfy the Hamiltonian system given by*

$$d\tilde{X}(s|t) = \mathcal{A}(s)\tilde{X}(s|t)ds + B(s)B^*(s)\lambda(s|t)ds - R(S)H(s)dn(s) \tag{17}$$

$$-d\lambda(s|t) = -H(s)C(s)\tilde{X}(s|t)ds + A^*(s)\lambda(s|t)ds + H(s)dn(S) \tag{18}$$

Proof:

From

$$\lambda(s|t) = \int_s^t \phi^*(u,s)H(u)dn(u)$$

it follows that

$$-\frac{d}{ds}\lambda(s|t) = H(s)\frac{d}{ds}n(s) + \int_t^s \left(\frac{d}{ds}\phi^*(u,s)\right)H(u)dn(u),$$

$$\frac{d}{ds}\phi^*(u,s) = -A^*(s) - C(s)H(s)R(s))\phi^*(u,s); \tag{19}$$

hence

$$\begin{aligned} -\frac{d}{ds}\lambda(s|t) &= H(s)\frac{dn}{ds}(s) \\ &\quad -(A^*(s) - C(s)H(s)R(s)) \\ &\quad \times \int_t^s \phi^*(u,s)H(u)dn(u) \\ &= H(s)\frac{dn}{ds}(s) + (A^*(s) \\ &\quad -C(s)H(s)R(s))\lambda(s|t), \end{aligned}$$

or

$$\begin{aligned} -d\lambda(s|t) &= -C(s)H(s)\tilde{X}(s|t)ds + A(s)\lambda(s|t)ds \\ &\quad +H(s)dn(s). \end{aligned}$$

On the other hand,

$$\frac{d}{ds}\tilde{X}(s|t) = \left(\frac{d}{ds}R(s)\right)\lambda(s|t) + R(s)\frac{d}{ds}\lambda(s|t)$$

and, by (6),

$$\begin{aligned} \frac{d}{ds}\tilde{X}(s|t) &= (B(s)B^*(s) + A(s) + R(s)A^*(s) \\ &\quad -R(s)H(s)C(s)R(s))\lambda(s|t) \\ &\quad +R(s)[-H(s)dn/ds(s) - A^*(s) \\ &\quad -C(s)H(s)R(s))\lambda(s|t)] \\ &= A(s)\tilde{X}(s|t) + B^*(s)\lambda(s|t) \\ &\quad -R(s)H(s)\frac{d}{ds}n(s) \end{aligned}$$

and hence we get (17).

Equations (17) and (18) can be written in matrix form as follows:

$$
\begin{aligned}
& d\begin{pmatrix} \tilde{X}(s|t) \\ -\lambda(s|t) \\ E \end{pmatrix} \\
&= \begin{pmatrix} A(s) & B(s)B^*(s) & -R(s)H(s)\frac{d}{ds}n(s) \\ -H(s)C(s) & A^*(s) & H(s)\frac{d}{ds}n(s) \\ 0 & 0 & 0 \end{pmatrix} \\
&\times \begin{pmatrix} \tilde{X}(s|t) \\ \lambda(s|t) \\ E \end{pmatrix} ds.
\end{aligned}
$$

Since $\tilde{X}(s|t) = \hat{X}(s|t) - \hat{X}(s)$ and $\lambda(s|s) = 0$, then (19) becomes

$$
\begin{aligned}
& d\begin{pmatrix} \hat{x}(s|t) \\ -\lambda(s|t) \\ E \end{pmatrix} \\
&- \begin{pmatrix} A(s) & B(s)B^*(s) & 0 \\ -H(s)C(s) & A(s) & H(s)\frac{d}{ds}Y(s) \\ 0 & 0 & 0 \end{pmatrix} \\
&\times \begin{pmatrix} \hat{X}(s|t) \\ \lambda(s|t) \\ E \end{pmatrix} ds \\
&= d\begin{pmatrix} \hat{X}(s) \\ -\lambda(s|s) \\ E \end{pmatrix} \\
&- \begin{pmatrix} A(s) & B(s)B^*(s) & R(s)H(s)\frac{d}{ds}n(s) \\ -H(s)C(s) & A^*(s) & H(s)\frac{d}{ds}(Y(s) - n(s)) \\ 0 & 0 & 0 \end{pmatrix} \\
&\times \begin{pmatrix} \hat{X}(s) \\ \lambda(s|s) \\ E \end{pmatrix} ds
\end{aligned}
\tag{20}
$$

From the input-output point of view, if we consider $\tilde{X}(s|t)$ and $\lambda(s|t)$ as waves through a slab located between α and t, where t is fixed, then from $\tilde{X}(s|t) = \hat{X}(s|t) - \hat{X}(s)$, $\lambda(s|t) = \lambda(s|t) - \lambda(s|s)$ then physically the waves $X(s|t)$ and $\lambda(s|t)$ can be decomposed in internal and external intensities, that is,

$$\begin{pmatrix} \hat{X}(s|t) \\ -\lambda(s|t) \\ E \end{pmatrix}$$

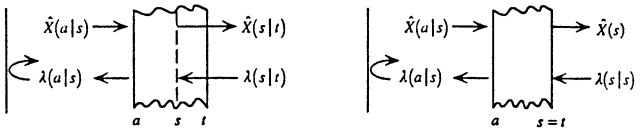
will be considered as the internal intensity of

$$\begin{pmatrix} \tilde{X}(s|t) \\ -\lambda(s|t) \\ E \end{pmatrix},$$

and

$$\begin{pmatrix} \hat{X} \\ -\lambda(s|s) \\ E \end{pmatrix}$$

as the external intensity, as seen in Figure 2.



Internal intensities External intensities

Figure 2.

The decomposition of the waves $X(s|t)$ and $\lambda(s|t)$ into internal and external intensities along with (20) suggests the decomposition of (19) into internal and external states represented, respectively, by

$$
\begin{gathered}
d\begin{pmatrix} \hat{X}(s|t) \\ -\lambda(s|t) \\ E \end{pmatrix} = N_1(s)\begin{pmatrix} \hat{X}(s|t) \\ -\lambda(s|t) \\ E \end{pmatrix} ds, \\
a \le s < t \ (t \text{ fixed})
\end{gathered}
\tag{21}
$$

where $N_1(s)$ is the matrix on the left hand side of (20) and

$$
d\begin{pmatrix} \hat{X}(s) \\ -\lambda(s|s) \\ E \end{pmatrix} = N_E(s)\begin{pmatrix} \hat{X}(s) \\ \lambda(s|s) \\ E \end{pmatrix} ds, \quad a \le s = t
\tag{22}
$$

where $N_E(s)$ is the right hand side matrix of (20).

Proposition 3 *The decomposition of system (19) into internal state (21) and external state (22) is necessary and sufficient.*

Proof: The proof of sufficiency is trivial. To prove the necessity, we note that since $dn(s) = dY(s) - C(s)\hat{X}(s)\,ds$, then equation (18)

$$-d\lambda(s|t) = -H(s)C(s)\hat{X}(s|t)ds - \hat{X}(s))ds$$

becomes

$$
\begin{aligned}
& A^*(s)\lambda(s|t)ds + H(s)(dy(s) - C(s)\hat{X}(s)ds \\
&= -H(s)C(s)\hat{X}(s|t)ds + A^*(s)\lambda(s|t)ds + H(s)dy(s)
\end{aligned}
$$

and hence we get the equation of $\lambda(s|t)$ in (21). $\lambda(s|s)$ in (22) is trivial since $\lambda(s|s) = 0$.

Now since $\hat{X}(s|t) = \hat{X}(s) + R(s)\lambda(s|t)$, then

$$\begin{aligned} d\hat{X}(s|t) &= d\hat{X}(s) + \left(\frac{d}{ds}R(s)\right)\lambda(s|t)ds \\ &\quad +R(s)d\lambda(s|t) \\ &= d\hat{X}(s) + \left(\frac{d}{ds}R(s)\right)\lambda(s|t)ds \\ &\quad +R(s)H(s)C(s)\hat{X}(s|t)ds \\ &\quad -A^*(s)\lambda(s|t)ds - H(s)dY(s)) \end{aligned}$$

and hence

$$d\hat{X}(s|t)|_{t=s} = d\hat{X}(s) - R(s)H(s)dn(s).$$

On the other hand, we have from (21)

$$d\hat{X}(s|t)|_{t=s} = A(s)\hat{X}(s)ds;$$

hence

$$d\hat{X}(s) - R(s)H(s)dn(s) = A(s)\hat{X}(s)ds$$

and the last equation is the equation of $\hat{X}(s)$ in (22).

Lemma 1 *The internal state (21) gives the Hamiltonian system (10), (11) for the smoothed estimate $\hat{X}(s|t)$ and the adjoint state $\lambda(s|t)$. The external state (22) gives the Kalman filter equation (9) for the filtered estimate $\hat{X}(s)$. The proof is straightforward and is omitted; when we examine the internal state (21), that is,*

$$N_t(s) = \begin{pmatrix} A(s) & B(s)B^*(s) & 0 \\ -H(s)C(s) & A^*(s) & H(s)\frac{dY}{ds}(s) \\ 0 & 0 & 0 \end{pmatrix}$$

has an operator

$$P_0(a,s) = \begin{pmatrix} t_0(a,s) & \rho_0(a,s) & F_0(a,s) \\ r_0(s,a) & t_0^*(a,s) & G_0(a,s) \\ 0 & 0 & E \end{pmatrix}$$

when $R(a) = 0$.

From Mistiri [19] it can be shown that:

$$\begin{aligned} \frac{d}{ds}t_0(a,s) &= A(s) - \rho_0(a,s)H(s)C(s)t_0(a,s), t_0(a,a) \\ &= E \end{aligned} \tag{23}$$

$$\begin{aligned} \frac{d}{ds}\rho_0(a,s) &= B(s)B^*(s) + A(s)P_0(a,s) + \rho_0(a,s)A^*(s) \\ &\quad -\rho_0(a,s)H(s)C(s)\rho_0(a,s), \\ &\quad \rho_0(a,a) = 0 \end{aligned} \tag{24}$$

$$\frac{d}{ds}r_0(a,s) = t_0^*(a,s)H(s)C(s)t_0(a,s), \quad r_0(a,a) = 0 \tag{25}$$

$$\begin{aligned} dF_0(a,s) &= (A(s) - \rho_0(a,s)H(s)C(s))F_0(a,s)ds \\ &\quad +\rho_0(a,s)H(s)dY(s), \\ F_0(a,a) &= 0 \end{aligned} \tag{26}$$

$$\begin{aligned} dG_0(a,s) &= t_0^*(a,s)H(s)(dY(s) - C(s)F_0(a,s)ds), \\ G_0(a,a) &= 0. \end{aligned} \tag{27}$$

We note that equation (24) is the same as equation (6) with $\rho_0(a,a) = 0 = R(a)$, hence $R_0(s) = \rho_0(a,s)$. Also, equation (23) is the same as equation (15) and this gives $\phi_0(a,s) = t_0(a,s)$ and equations (25) and (16) imply that $O_0(a,s) = r_0(a,s)$.

Now if

$$P(a,s) = \begin{pmatrix} t(a,s) & \rho(a,s) & F(a,s) \\ r(a,s) & t^*(a,s) & G(a,s) \\ O & O & E \end{pmatrix}$$

is the operator associated with the generator $N_r(s)$ when $\rho(a,a) = R(a) = 0$, $t(a,a) = t_a$, $r(a,a) = 0$, $F(a,a) = F_a$ and $G(a,a) = G_a$, then $P(a,s) = P_a * P_0(a,s)$, where

$$P_a = \begin{pmatrix} t_a & R(a) & F_a \\ O & t_a^* & G_a \\ O & O & E \end{pmatrix}$$

is the modified initial condition matrix, and provided $(E - R(a)r_0(a,s))^{-1}$ exists in which case we have

$$P_{(a,s)} = \begin{pmatrix} t_0(a,s)Pt_a \\ t_a^*r_0(a,s)Pt_a \\ O \\ \rho_a(a,s) + t_0(a,s)R(a)qt_0^*(a,s) \\ t_a^*qt_0^*(a,s) \\ O \\ t_0(a,s)PF_a + t_0(a,s)R(a)qG_0(a,s) + F_0(a,s) \\ t_a^*r_0(a,s)PF_a + t_a^*qG_0(a,s) + G_a \\ E \end{pmatrix} \tag{28}$$

with $P = (E - R(a)r_0(a,s))^{-1}$ and $q = (E - r_0(a,s)R(a))^{-1}$.

The elements of $P(a,s)$ satisfy the same differential equations as those of $P_0(a,s)$; in particular, we need

$$\begin{aligned} dF(a,s) &= (A(s) - \varphi(a,s)H(s)C(s))F(a,s)dS \\ &\quad +\varphi(a,s)H(s)dY(s), \\ F(a,a) &= F_a \end{aligned} \tag{29}$$

$$
\begin{aligned}
dG(a,s) &= t^*(a,s)H(s)(dY(s) - C(s)F(a,s)dS), \\
G(a,a) &= G_a. \qquad (30)
\end{aligned}
$$

We consider the internal state (21) as pictured in Figure 3 with an arbitrary boundary condition,

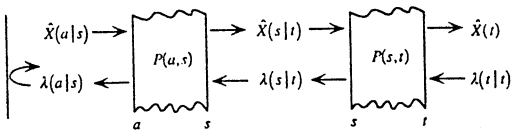


Figure 3. Internal state.

Then

$$
\begin{pmatrix} \hat{X}(s|t) \\ \lambda(a|s) \\ E \end{pmatrix} = P(a,s) \begin{pmatrix} \hat{X}(a|s) + \gamma \\ \lambda(s|t) \\ E \end{pmatrix}, \quad a \le s < t
$$

or

$$
\begin{aligned}
\hat{X}(s|t) &= t(a,s)(\hat{X}(a|s) + \gamma) + \rho(a,s)\lambda(a|t) \qquad (31) \\
&\quad + F(a,s)
\end{aligned}
$$

$$
\begin{aligned}
\lambda(a|s) &= r(a,s)(\hat{X}(a|s) + \gamma) + t^*(a,s)\lambda(s|t) \qquad (32) \\
&\quad + G(a,s).
\end{aligned}
$$

Lemma 2 *The internal state given by (31) and (32) with zero inputs implies that*

$$
\begin{aligned}
\hat{X}(s) &= F(a,s) \\
\lambda(a|s) &= G(a,s).
\end{aligned}
$$

Proof:

Zero inputs means that $\hat{X}(a|s) = 0$ and $\lambda(s|t) = 0$ as $s \to t$ and $\gamma = 0$ and the proof then becomes trivial.

If we denote the solutions of the internal state with zero inputs by $\underline{\hat{X}}(s)$ and $\underline{\lambda}(a|s)$, then as an immediate consequence of the previous lemma, which satisfies the Kalman filters equation since equation (3) gives:

$$
\begin{aligned}
d\underline{\hat{X}}(s) = dF(a,s) = (A(s) - \rho(a,s)H(s))C(s)\underline{\hat{X}}(s)ds \\
+\rho(a,s)H(s)dY(s), \quad \underline{\hat{X}}(a) = F_a
\end{aligned}
$$

and that equation (3) also gives

$$
\begin{aligned}
nd\underline{\lambda}(a|s) = dG(a,s) = t^*(a,s)H(s)(dY(s) \\
-C(s)\underline{\hat{X}}(s)ds), \\
\underline{\lambda}(a|a) = G_a.
\end{aligned}
$$

Proposition 4 *The internal state given by (31) and (32) with $s \to t$ gives*

$$
\hat{X}(s) = t(a,s)(\hat{X}(a|s) + \gamma) + \underline{\hat{X}}(s) \qquad (33)
$$

$$
\begin{aligned}
\lambda(a|s) &= r(a,s)(\hat{X}(a|s) + \gamma)\underline{\lambda}(a|s) \qquad (34) \\
\hat{X}(a|s) &= (E - R(a)(r(a,s))^{-1}[X(a) \\
&\quad + R(a)(\underline{\lambda}(a|s)) + r(a,s)
\end{aligned}
$$

Proof:

Since $\hat{X}(s)$ and $\underline{\lambda}(a|s) = G(a,s)m$, then with $s \to t$ (33) and (34) follow immediately from (31) and (32), respectively.

To establish (34) we get from $\hat{X}(a|s) = \hat{X}(a) + R(a)\lambda(a|s)$ and from (33) the following:

$$
\hat{X}(a|s) = \hat{X}(a) + R(a)[r(a,s)(X(a|s) + \gamma) + \underline{\lambda}(a|s)]
$$

and

$$
\begin{aligned}
\hat{X}(a|s) &= (E - R(a)r(a,s))^{-1}[\hat{X}(a) + R(a)(\underline{\lambda}(a|s) \\
&\quad + r(a,s)\gamma)]
\end{aligned}
$$

provided that $(E - R(a)r(a,s))^{-1}$ exists.

We should note that we can have a zero input $\hat{X}(a|s)$ by having $\hat{X}(a) = 0$ and $R_0(a) = 0$. In this case we denote the solution of the dynamic system, given by (3) and (4) by $X_0(s)$ and the adjoint state by $\lambda_0(s|t)$, and if $t_0 = E$, $\gamma = F_a = G_a = 0$, then we get the Kailath and Lainiotis results mentioned earlier, that is,

$$
\begin{aligned}
\hat{X}_0(s) &= \hat{X}(s) = F(a,s) = F_0(a,s) \\
\lambda_0(a|s) &= \lambda(a|s) = G(a|s) = G_0(a,s)
\end{aligned}
$$

and equations (33) and (34) become, respectively,

$$
\hat{X}(s) = t_0(a,s)\hat{X}(a|s) + \hat{X}_0(s)
$$

and

$$
\hat{X}(a|s) = (E - R(a)r_0(a,s))^{-1}(\hat{X}(a) + R(a)\lambda_0(a|s))
$$

which are Lainiotis equations (12) and (13), respectively Lainiotis equation (14), namely:

$$
\rho(a,s) = \rho_0(a,s) + t_0(a,s)R(a)(E - r_0(a,s)R(a))^{-1}t_0(a,s)
$$

can be obtained directly from (28).

Now we examine the external state given by (22) where the generator $N_E(s)$ can be rewritten as

$$
\underline{N}_E(s) = \begin{pmatrix} A(s) - R(s)H(s)C(s) & B(s)B^*(s) & \\ O & A^*(s) & \\ O & O & \\ & & R(s)H(s)\frac{dY}{ds} \\ & & O \\ & & O \end{pmatrix}
$$

and we assume that the generator $\underline{N}_E(s)$ has an operator $P_0(a,s)$ when $R_0(a,s)=0$ with

$$N_E(s)=\begin{pmatrix} \underline{t}_0(a,s) & \rho_0(a,s) & \underline{F}_0(a,s) \\ \underline{\tau}_0(a,s) & \underline{\tau}_0(a,s) & \underline{G}_0(a,s) \\ O & O & E \end{pmatrix}, \quad a \le s = t$$

it can be shown, see Mistiri [19], that

$$d\underline{t}_0/ds(a,s) = (A(s) - R_0(s)H(s)C(s))\underline{t}_0(a,s), \quad t_0(a,a)=E$$

hence $\phi(a,s)=t_0(a,s)=\underline{t}_0(a,s)$,

$$\begin{aligned} d\underline{\rho}_0/ds(a,s) &= B(s)B^*(s)+A(s) \\ &\quad -R_0(s)H(s)C(s))\rho_0(a,s) \\ &\quad +\underline{\rho}_0(a,s)A^*(s), \quad \underline{\rho}_0(a,a)=0. \end{aligned}$$

But this implies that we must have $\underline{\rho}_0(a,s)=R_0(s)$, $d\underline{\tau}_0/ds(a,s)=0$, $\underline{\tau}_0(a,a)=0$, hence $\underline{\tau}_0(a,s)=0$, $d\underline{\tau}_0/ds(a,s)=\underline{\tau}_0(a,s)A^*(s)$, $\underline{\tau}_0(a,a)=E$, $d\underline{F}_0(a,s)=(A(s)-R_0(s)H(s)C(s))\underline{F}_0(a,s)\,ds + R_0(s)H(s)\,dY(s)$, $\underline{F}_0(a,a)=0$ hence $uF_0(a,s)=F_0(a,s)$, $d\underline{G}_0(a,s)=0$, $\underline{G}_0(a,a)=0$, hence $\underline{G}_0(a,s)=0$. In the case where the operator $\underline{P}(a,s)$ corresponds to the generator $N_E(s)$ when $R(a)\neq 0$, we have

$$\underline{P}(a,s)=\underline{P}_a * \underline{P}_0(a,s)$$

where

$$\underline{P}_a=\begin{pmatrix} \underline{t}_a & R(a) & \underline{F}_a \\ O & \underline{\tau}_a & O \\ O & O & E \end{pmatrix}$$

is the modified initial condition,

$$\underline{P}(a,s)=\begin{pmatrix} \underline{t}_0(a,s)\underline{t}_a \\ 0 \\ 0 \\ \underline{\rho}_0(a,s)+\underline{t}_0(a,s)R(a)\underline{\tau}_0(a,s) \\ \underline{\tau}_0\underline{\tau}_0(a,s) \\ 0 \\ \underline{\tau}_0(a,s)\underline{F}_a+\underline{F}_0(a,s) \\ 0 \\ E \end{pmatrix}$$

We note also here that the elements of $\underline{P}(a,s)$ satisfy the same differential equations as those of $\underline{P}_0(a,s)$, and in particular we need:

$$\begin{aligned} d\underline{F}(a,s) &= (A(s)-R(s)H(s)C(s))\underline{F}(a,s)\,ds \\ &\quad +R(s)H(s)\,dY(s), \underline{F}(a,a)=\underline{F}_a \end{aligned} \quad (35)$$

The external state (22) with arbitrary boundary conditions can be pictured as in Figure 4.

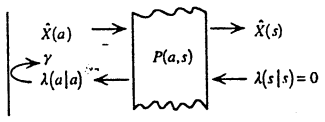


Figure 4. External state $a \le s = t$.

that is, the external state is equivalent to

$$\begin{pmatrix} \hat{X}(s) \\ \lambda(a|a) \\ E \end{pmatrix} = \underline{P}(a,s) \begin{pmatrix} \hat{X}(a|\,)+\gamma \\ \lambda(s|t) \\ E \end{pmatrix},$$

or

$$\hat{X}(s)=\underline{t}(a,s)(\hat{X}(a)+\gamma)\underline{F}(a,s) \quad (36)$$

Lemma 3 *The external state given by (36) with zero inputs implies that*

$$\hat{X}(s)=\underline{F}(a,s).$$

The proof is trivial since for the zero inputs we need only to have

$$\hat{X}(a)=0 \quad \text{and} \quad \gamma=0.$$

Now if we denote the solution of the external state (36) with zero inputs by $\hat{X}(s)$, then (36) becomes

$$\hat{X}(s)=t(a,s)\hat{X}(a)+\hat{X}(s); \quad (37)$$

furthermore, $\hat{X}(s)$ satisfies the Kalman filter equation since (35) gives:

$$\begin{aligned} d\hat{X}(s) &= d\underline{F}(a,s)=(A(s)-R(s)H(s)C(s))X(s)ds \\ &\quad +R(s)H(s)dY(s), \quad \hat{X}(a)=\underline{F}a. \end{aligned}$$

If $\underline{F}_a=0$ and $\underline{t}_a=E$, then $\underline{t}(a,s)=\underline{t}_0(a,s)$ and $\hat{X}_0(s)=\underline{F}(a,s)=\underline{F}_0(a,s)$, and then (37) becomes

$$\hat{X}(s)=t_0(a,s)\hat{X}(a)+\hat{X}_0(s)$$

but this is just the Lainiotis equation (12) with $\lambda(a|s)=0$ and $\hat{X}(a|s)=\hat{X}(a)+R(a)\lambda(a|s)=\hat{X}(a)$.

4 Conclusion

We used the star-product theory of 3×3 scattering matrix, an extension of classic 2×2 scattering matrix, to construct and to analyze the estimation problems. We are able to give a physical model with inputs and outputs and obtain some new and old results. For example, we established the basic relations between the smooth and filter estimates, the decomposition properties of system (19) into internal and external states. The external state is the well-known Kalman's filter.

References

[1] L. Arnold, *Stochastic differential equations: Theory and applications*, John Wiley, New York, 1973.

[2] A.T. Bharucha-Reid, *Random integral equations*, Academic Press, New York, 1972.

[3] A.E. Bryson and M. Frazier, Smoothing for linear and nonlinear dynamic systems, Aero. Sys. Div., Wright-Patterson Air Force Base, Oh, TDR 63-119, pp. 353–364, 1963.

[4] R. Bucy and P.D. Joseph, *Filtering for stochastic processes with applications to guidance*, Interscience Publ., New York, 1968.

[5] R.F. Curtain, Estimation theory for abstract evolution equations excited by general white noise processes, *SIAM J. Control and Optimization*, Vol. 14, pp. 1124–1150, 1976.

[6] R.F. Curtain, Infinite dimensional estimation theory for linear systems, Control Theory Cent. Rep. No. 38, University of Warwick, Coventry, England, 1976.

[7] R.F. Curtain, Infinite-dimensional filtering, *SIAM J. Control*, Vol. 13, pp. 89–103, 1975.

[8] R.F. Curtain, Stochastic differential equations in Hilbert space, Ph.D. Dissertation, Browman University, Providence, R.I., 1969.

[9] R.F. Curtain and P.L. Falb, Stochastic differential equations in Hilbert space, *J. Differential Equations*, Vol. 10, pp. 412–430, 1971.

[10] M.H.A. Davis, *Linear estimation and stochastic control*, John Wiley, New York, 1977.

[11] J.L. Doob, *Stochastic processes*, John Wiley, New York, 1953.

[12] P.L. Falb, Infinite dimensional filtering: The Kalman-Bucy filter in Hilbert space, *Information and Control*, Vol. 11, pp. 102–137, 1967.

[13] A.H. Jazwinski, *Stochastic processes and filtering theory*, Academic Press, New York, 1970.

[14] T. Kailath, Redheffer scattering theory and linear state space estimation problems, *Ricerche di Automatica*, Vol. 10, pp. 135–163, 1979.

[15] T. Kailath, An innovations approach to least-square estimation. Part I: Linear filtering in additive white noise. Part II: Smoothing in additive white noise (with P. Frost), IEEE, *Trans. Automatic Control*, Vol. AC-13, pp. 646–660, 1968.

[16] T. Kailath and L. Ljung, *A Scattering theory frame work for fast least-squares algorithms, multivariant analysis* VI, North-Holland, Amsterdam, The Netherlands, 1977, 387–406.

[17] D.G. Lainiotis, Partitioned estimation algorithms, II: Linear estimation, Information Science, Vol. 7, pp. 317–340, 1974.

[18] L. Ljung, T. Kailath and B. Friedlander, Scattering theory and least squares estimation, Part I: Continuous-time problem, *Proc. IEEE*, Vol. 64, pp. 131–138, 1976.

[19] F. Mistiri, Star-product and linear dynamical systems, Ph.D. Dissertation, Arizona State University, 1983.

[20] F. Mistiri and Alan P. Wang, The star-product and its algebraic properties, *J. of the Franklin Institute*, Vol. 321, pp. 21–38, 1986.

Proc. of Third Int. Symp. on Artificial Life, and Robotics (AROB III' 98),
Oita, Japan, 19-21, January, 1998,

An area filling algorithm for autonomous sweeping robot

W.K.Hyun* , Jiny.Cho**, T.K.Park***, and C.S.Park**

*Dept. Electronics Eng. of Honam Univ, KwangJu, KOREA
**Dept. Computer Science Eng. of Honam Univ, KwangJu, KOREA
*** Automatic Control Lab, KIMM, KOREA
E-mail: wkhyun@honam.honam.ac.kr

Abstract

An OFF-LINE path planning algorithm for an autonomous sweeping robot which executes the area filling task is proposed. This algorithm generates subgoals at the contact position with the obstacle and environment wall while the robot tracking whole workspace, and finds sequential tracking line which links the subgoals continuously and is never crossed. If the line pass through the obstacle, hierarchical collision free algorithm proposed is implied. The proposed algorithm consists of (1) collision detection procedure, (2) obstacle map making procedures, (3) tracking points generation procedures for subgosls, (4) tracking points scanning procedures, and (5) obstacle avoidance procedure.

1. Introduction

The development of specialized service robots was brought about by the increasing demand to economize on several kinds of services. A representative application fields are floor-cleaning or smearing of construction. Most of today's cleaning and smearing machines are guided by human operators along extended and fixed motion patterns in areas often greater than some hundreds of square meters. Due to increasing machine maintenance and personal costs this cleaning or smearing task could be performed in future by an autonomous robot. Many researcher have been devoted to the path planning algorithm[1,2,3,4,5]. In these methods, the methods in [1,2,3] developed semi-autonomous sweeping robot and applied it to the floor-cleaning tasks. These robots may meet dead-lock station in some environment with obstacles owing to local collision avoidance approach based on sensors. Hofner proposed a heuristic path planning algorithm using potential field function[5] which is bounded in local planning approach. This method also can not solve the dead-locking problem.

In this paper, a path planning algorithm for an autonomous sweeping robot which executes the area filling task is proposed. This algorithm generates subgoals at the contact position with the obstacle and environment wall while the robot tracking whole workspace, and finds sequential tracking line which link the subgoals continuously and is never crossed. If the line pass through the obstacle, hierarchical collision free algorithm proposed in [6] is implied.

2. Area Filling Algorithm

Since a sweeping robot works for floor-cleaning or smearing in 2 dimensional space, a mobile robot and objects in workspace are modeled in 2 dimensional space. It is assumed that (1) the mobile robot move in omni-direction, (2) the robot is a polygon shape and obstacles in workspace have polygon or circle shape.

Area filling algorithm consists of obstacle map making procedure, and tracking point generation procedure, tracking point scanning procedure, and robot language generation procedure. Fig. 1 represents the sequential procedure of the proposed area filling algorithm. The sweeping robot can have translational and rotational motion in 2 dimensional work space. Therefore the configuration space of the robot in which the robot is described as a point is 3 dimensional space. This configuration space is called as obstacle map.

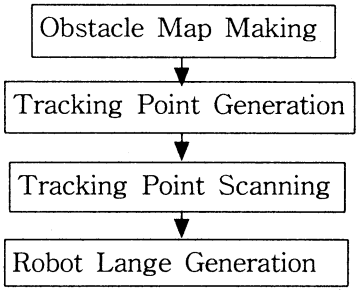


Fig. 1 The sequential procedure of area filling Algorithm

The obstacle map making procedure is to make the obstacle map by scanning the whole work space. And then the configuration space is quantized as a equal size cell. A cell in the grid-based configuration space is identified as FREE cell or OBSTACLE cell. The grid-based configuration space is utilized for finding a collision free path by using Two Level path planning algorithm proposed in [6] which is a kind of graph search algorithm. Tracking point generation procedure tracks the whole workspace with an adjustable scanning width and records tracking points as subgoals and then the path planner shift to the tracking point scanning procedure. This procedure link the recorded tracking points continuously under the condition that a tracked point is never tracked and the linked path is never crossed. The next procedure is robot motion generation procedure.

2.1 Tracking point generation procedure

Tracking point generation procedure tracks the whole workspace with an adjustable scanning width and records tracking points as subgoals. In this tracking, the separation of each track is set to be half of the width of the robot. The separation can be varied and with smaller separation of the tracks, the degree of overlap increases. If, for example, the width is the same as the width of the robot, then there is no overlap between the tracking lines. While the robot tracks the whole workspace, tracking point generation procedure records the contact positions and collision status between robot and wall of workspace, and robot and obstacles. These positions are utilized as subgoals to take area filling. The data structure of tracking points is as follows.

```
struct trackPoint {
                int    position[DIMENSION];
                char   status;
                char   tracked_flag;
                int    obstacleNo;
} *TrackingPoint;
```

Where position[DIMENSION] is the contact position between robot and wall and robot obstacle, and status represents contact types which are LEFT_WALL, RIGHT_WALL, LEFT_OBSTACLE, and RIGHT_OBSTACLE. Each means contact state between left side of robot and wall, right side of robot and wall, left side of robot and obstacle, and right side of robot and obstacle, respectively. And tracked_flag implies that tracking point is tracked or not. It will be utilized when the robot tracks these tracking points for finding area filling path. In tracking point generation processor, the robot moves from left top to right bottom in workspace to record the tracking points and the orientation of the robot is fixed as 0 degree. The algorithm of tracking points generation is as follows;

For given robot initial position $(x, y, \theta) = (0, 0, 0^0)$, and scanning width Δy and Δx.

x and y mean positions along x axis and y axis, respectively.

STEP 1: Set x and y to 0, respectively, And find a initial robot position in the workspace by increasing x with Δx and y with Δy, respectively, while orientation of the robot if fixed as 0 degree. And record its position and status as LEFT_WALL.

STEP 2: Move the robot from left to right with y position fixed. If the robot contacts the wall, record its position and status, where the status is RIGHT_WALL. Else if the robot collides with obstacle, record its position and status as RIGHT_OBSTACLE and obstacle number. Move the robot until it meets right wall.

STEP 3: If the robot meets right bottom of the workspace, goto STEP 5. Move the robot as

Δy along y axis while x position is fixed. And then move the robot from right wall to left wall. If the robot collides with obstacle, record its position at the contact position and recode the status which are LEFT_OBSTACLE and obstacle number. And move the robot until the robot meets left wall. And record the status and position.

STEP 4: Move the robot as Δy along y axis and goto STEP 1.

STEP 5: Sort the recoded data.

2.2 Tracking point scanning procedure

Tracking point scanning procedure links the recorded tracking points continuously under the condition that a tracked point is never tracked and the linked path is never crossed. The next procedure is robot motion generation procedure.

Tracking point scanning procedure find a continuously linked line by connecting all tracking points in such a way that (1) a tracked point should not be tracked, and (2) the integrated length of linked line should be as short as possible. Tracking point scanning procedure find a tracking point to be next linked with respect to the status of the current tracking point. The tracking strategy is as follows;

For given scanning width , and minimum length of the workspace along y ax $\Delta y$is, y_{max}.

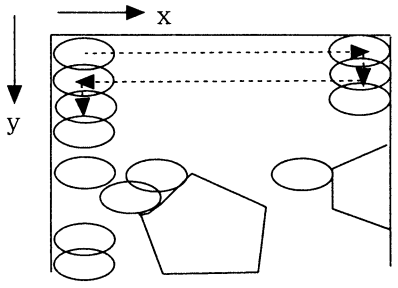


Fig. 3 An example of tracking point scanning

Step 1: Search TP's(Tracking Points) of RIGHT_WALL or RIGHT_OBSTACLE TP

Step 2: Find minimum distance TP from current TP in Step 1, and if it $y=0$is not tracked and not collided with obstacle when current moves to the TP goto Step 6 else goto Step 3

Step 3: $y \leftarrow y - \Delta y$, if goto Step 5

Step 4: Search the same status, RIGHT_WALL and RIGHT_OBSTACLE TP's, and find minimum distance and untracked one. If there is no one, goto the next Step else goto Step 6.

Step 5: $y \leftarrow y+\Delta y$, if $y > y_{max}$, then goto Step 6

Step 6: Find next TP to be linked which is minimum distance one between current TP and the next TP to be linked in whole untracked TP's. In this case collision free path planning procedure is requested.

Step 7: If the number of the linked tracked points is the same as tracking points stored in tracking point generation procedure, then end, else goto link the TP and mark the TP tracked.

(2) When the status of the current tracking point is RIGHT_WALL:
the process is the same as the case when the current TP is LEFT_WALL except that in Step 1 and Step 4, LEFT_WALL and LEFT_OBSTACLE are replaced with LEFT_WALL and LEFT_OBSTACLE, respectively.

(3) When the status of the current tracking point is LEFT_OBSTACLE:
the process is the same as the case when the current TP is LEFT_WALL except that in Step 1 and Step 4, RIGHT_WALL and RIGHT_ OBSTACLE are replaced with LEFT_WALL and LEFT_OBSTACLE, respectively, all candidate TP should be the same obstacle number state.

(4) When the status of the current tracking point is RIGHT_OBSTACLE:
the process is the same as the case when the current TP is LEFT_OBSTACLE except that in Step 1 and Step 4, LEFT_WALL and LEFT_OBSTACLE are replaced with LEFT_WALL and LEFT_OBSTACLE, respectively.

2.3 Collision free path planning procedure

When tracking point scanning procedure can not search a TP to be linked near the current TP. It find a minimum distance TP from current TP in whole untracked TP. If the current TP collide with the

minimum distance TP when current TP moves linearly to the minimum distance one, collision free path planning procedure in [6] is requested.

3. Simulation results

The area filling algorithm has been tested with mobile robot of octagon type. In test-bed example as shown in Fig. 5, there are 5 obstacles in workspace and it is the received draft data from GUI interface. The workspace is 50m×50m square meter. It is assumed that the robot can move in omni-direction. The results for sequential procedures of the proposed algorithm are shown in Fig. 6 through Fig. 9. Subgoals generated by tracking point generation procedure are shown in Fig. 6. Fig. 7 shows that the resulting path of tracking point scanning procedure without collision free path planning. The 5 collision situations are occurred in the test-bed example. Planned collision free path by TLPPA are illustrated for each collision situation in Fig. 8. Fig. 9 show that the proposed area filling can plan a successive path. The time cost for planning the final path is about 3 sec.

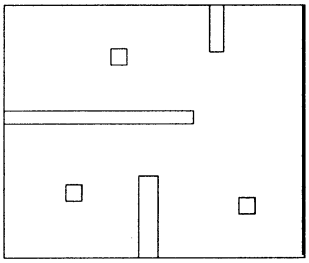


Fig. 5 An exemplary map

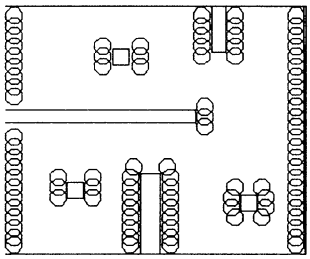


Fig. 6 Generated tracking points

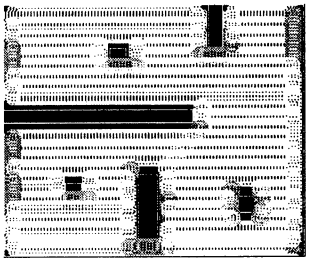


Fig.7 Area Filling without Obstacle avoidance

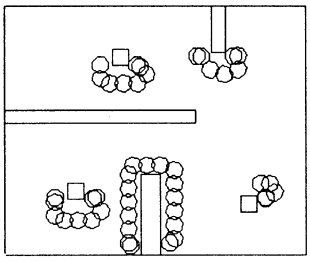


Fig. 8 Collision free path

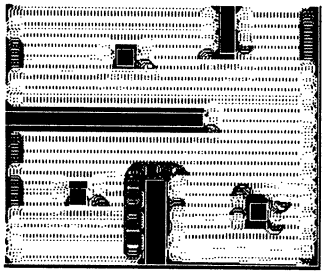


Fig. 9 Final Result

4. Concluding remarks

In this paper, an OFF-LINE area filling algorithm is proposed. The proposed area filling algorithm can fill successfully whole workspace without deadlocking and collision in spite even though obstacles are in workspace. In the algorithm, tracking point generation procedure to find subgoal for filling path, and tracking scanning procedure to link the subgoals without discontinuity and collision for finding filling path are proposed. As a future work, the area filling path planning algorithm works in an environment with unknown obstacles will be investigated.

[Reference]

[1] F.Yasutomi, D.Takao, M.Yamada, K.Tsukamoto, "Celaning robot control," *proc. if IEEE International Conference on Robotics and Automation*, vol.3, pp1839-1841, 1988

[2] T.Fukuda, S.Ito, N.Oota, F.Arai, Y.Abe, K.Tanaka, Y.Tanaka, "Navigation system based on ceilling landmark recording for autonomous mobile robot," *proc. of international Conference on Industrial Electronics, Control, and Instrumen- tation*, vol. 3, pp.1466-1471, 1993

[3] W.Li,"Preception-action behavior control of a mobile robot in uncertain environments using fuzzy logic," *proc. of IEEE/RSJ/GI International Conference on Intelligent Robots and Systems*, vol.1, pp439-461, 1994

[4] D.Kurabayashi, J.Ota, T.Arai, and E.Yoshida ,"Cooperative Sweeping by Multiple Mobile Robots," *proc. of IEEE Conference on Robotica and Automation*, vol. 2, pp1744-1749, 1996

[5] C.Hofner and G.Schmidt,"Path planning and guidance techniques for an autonomous mobile cleaning robot," *proc. of IEEE Conference on Intelligent Robots and Systems*, vol. 1, pp610-617, 1994

[6] W.K.Hyun, "A Hierarchical Collision-Free Path Planning Algorithm for Robots," *IEEE IROS '95*, Vol.2. pp.837-845, 1995.

Proc. of Third Int. Symp. on Artificial Life, and Robotics (AROB III' 98),
Oita, Japan, 19-21, January, 1998,

An Appropriate Parameter Selection for Designing Motor and Servo Controller of Robot Manipulator to Achieve Precise Contour Control

Naruto EGASHIRA
Department of Control and Information Systems Engineering
Kurume National College of Technology
Komorinomati, Kurume 830, Japan

Masatoshi NAKAMURA and Satoru GOTO
Department of Electrical Engineering
Saga University
Honjomachi, Saga 840, Japan

Nobuhiro KYURA
Department of Electrical Engineering
Kinki University
Kashiwanomori, Iizaka 820, Japan

Abstract

Contour control of robot manipulators are implemented in a wide range of fields and performances of contour control are required to achieve high accuracy and high speed of work. Servo controller design and motor selection for the industrial robot manipulators are usually carried out in an intuitive manner by engineers in the industry based on their experiences. This paper describes a reasonable selection of motor and servo controller parameters for robot manipulators by introducing a new model for widely used industrial robot manipulators.

1 Introduction

In our laboratory, human skills were mathematically analyzed and the solutions to the problems were attained through long term collaboration works. Through collaboration works with the researchers in university and industry, the authors have theoretically solved many problems which had been encountered in the actual industry[1]. This paper proposed a methodology for artificial realization of human skill.

Contour control of the robot manipulators are implemented in a wide range of fields such as grinding, cutting, welding and sealing, and performances of contour control are required to achieve high accuracy and high speed of work. Servo controller design and motor selection for industrial robot manipulators are usually carried out by engineers in the industry based on their experiences in an intuitive manner.

This paper describes a reasonable selection of motor and servo controller parameters for robot manipulators by introducing a new model which can be widely used for industrial robot manipulators. Concretely, in this paper a mathematical model for industrial robot manipulators is constructed and the relationship between torque saturation and motor parameters of robot manipulators is analyzed. Further the direction of the selection of the motor for industrial robot manipulators is proposed.

2 Modeling of an Industrial Robot Manipulator

2.1 Industrial Robot Manipulator

The industrial robot manipulators are constructed by mechanical connections between servo systems for each axis, and these servo systems are controlled for each axis, independently. Angle and angular velocity of the motors of the robot manipulators are measured by using sensors such as potentiometers, tachogenerators and encoders which are attached to the motors. The motors are controlled by servo controllers based on the measurement data of the motors. Thus, the servo controllers of industrial robot manipulators do not directly control the position and the velocity of the mechanism but they control the angle and the angular velocity of the motor. Such kind of control technique is called as a semi-closed loop type control. The control performance of robot manipulators mainly depend on the servo systems of each link.

2.2 Mathematical Model of Industrial Robot Manipulator

A mathematical model of industrial robot manipulators was derived for servo controller design and motor selection. The industrial robot manipulator was modeled in two parts separately, i.e., the servo controller part, and the motor and mechanical load part. In the derivation of the model, only crucial factors, such as reference input generator, position control part, velocity control part, current control part, power

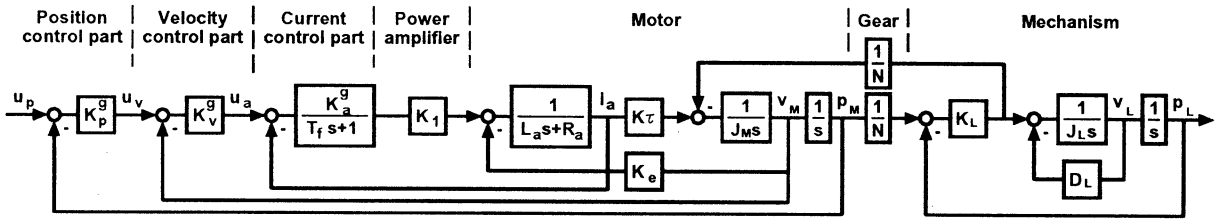


Figure 1: Structure of the industrial robot manipulator

amplifier, motor, gear and mechanism, were taken into account.

In the reference input generator, the position input signal u_p for each axis position is calculated from the data of start point, end point and work velocity. In the position control part, the velocity input signal u_v for the velocity of the motor is released to the velocity control part by using the position input signal u_p, the motor position response p_M and the position loop gain K_p^g. In the velocity control part, the current input signal u_a for the current of motor is released to the current control part by using the velocity input signal u_v, the motor velocity response v_M and the velocity loop gain K_v^g. In the current control part, the instruction signal for the motor is released to the power amplifier by using the current input signal u_a, the motor current response i_a and the velocity loop gain K_a^g. Then the servo motor is driven, following the instruction signal and the mechanism is worked appropriately.

In robot manipulators, the filter for delaying axis resonance is included to the current control part. The frequency of the axis resonance is about $5\omega_L$, then, the time constant T_f of the filter is about $1/5\omega_L$ [2].

Usually, the reference input generator and the position control part are structured by the digital controller, and velocity control part and the current control part are structured by the analogue controller[4].

The model for the industrial robot manipulators is constructed by a 6th order model(see Fig.1). In Fig.1, K_1 is the amplification rate of the amplifier, L_a is the inductance of the motor armature, R_a is the resistance of the motor armature, K_τ is the torque constant of the motor, K_e is the back electromotive force constant of the motor, N is the gear rate between the motor and the mechanism, K_L is the damping constant of the mechanism part, D_L is the viscosity friction coefficient of the mechanism part, J_L is the inertia of the mechanism part.

Usually, the objective trajectory for contour control is a ramp input. The position input signal u_p is released at each reference time interval ΔT. The position loop is digitally controlled with a sampling time Δt_p. In the holder for the sample-and-hole device of the reference input generator, the 1st order hold device is used for suppression of velocity ripples and contour ripples at each reference input time interval ΔT [4].

In industrial robot manipulators, the inferiority of contour control performance is occurred at transient period. Then, the mathematical model of industrial robot manipulator can be composed without its position loop. Hence, the velocity input signal $U_v(\mathbf{s})$ is

$$U_v(\mathbf{s}) = \frac{v_{ref}\,\Delta T\,K_p^g}{\mathbf{s}}. \tag{1}$$

In Fig.1, the transfer function $G_M(\mathbf{s})$ from U_v to the current response I_a is derived as

$$G_M(\mathbf{s}) = \frac{I_a(\mathbf{s})}{U_v(\mathbf{s})} = \frac{Z_a(\mathbf{s})}{P_v(\mathbf{s})} \tag{2}$$

$$\begin{aligned} Z_a(\mathbf{s}) &= K_1 K_a^g K_v^g \\ &\quad \times \{J_M J_L \mathbf{s}^3 + J_M D_L \mathbf{s}^2 \\ &\quad + K_L \left(J_M + J_L/N^2\right) \mathbf{s} \\ &\quad + K_L D_L/N^2\} \end{aligned} \tag{3}$$

$$\begin{aligned} P_v(\mathbf{s}) &= J_M J_L L_a T_f \mathbf{s}^5 \\ &\quad + \{J_M J_L L_a + J_M J_L R_a T_f \\ &\quad + J_M D_L L_a T f\} \mathbf{s}^4 \\ &\quad + \{J_M J_L \left(R_a + K_1 K_a^g\right) + J_M D_L L_a \\ &\quad + J_M D_L R_a T_f \\ &\quad + \left(J_M + J_L/N^2\right) K_L L_a T_f \\ &\quad + J_L K_\tau K_e T_f\} \mathbf{s}^3 \\ &\quad + \{J_M D_L \left(R_a + K_1 K_a^g\right) \\ &\quad + \left(J_M + J_L/N^2\right) K_L L_a \\ &\quad + J_L K_\tau \left(K_e + K_1 K_a^g K_v^g\right) \\ &\quad + K_L \left(J_M + J_L/N^2\right) R_a T_f \\ &\quad + K_L D_L L_a T_f/N^2 + D_L K_\tau K_e T_f\} \mathbf{s}^2 \\ &\quad + \{K_L \left(J_M + J_L/N^2\right) \left(R_a + K_1 K_a^g\right) \\ &\quad + K_L D_L L_a/N^2 \\ &\quad + D_L K_\tau \left(K_e + K_1 K_a^g K_v^g\right) \\ &\quad + K_L D_L R_a T_f/N^2 + K_L K_\tau K_e T_f\} \mathbf{s} \\ &\quad + K_L D_L \left(R_a + K_1 K_a^g\right)/N^2 \\ &\quad + K_L K_\tau \left(K_e + K_1 K_a^g K_v^g\right) \end{aligned} \tag{4}$$

where

$$K_p \simeq K_p^g \tag{5}$$

$$J = J_M + J_L/N^2 \quad (6)$$

$$K_v = \frac{K_v^g K_\tau}{J} = \frac{K_v^g K_\tau}{J_M + J_L/N^2} \quad (7)$$

$$K_a' = K_a^g K_1 \quad (8)$$

$$K_a = \frac{K_a'}{L_a} = \frac{K_a^g K_1}{L_a} \quad (9)$$

From equation (1) and (2), the motor current response I_a is

$$I_a(\mathbf{s}) = G_M(\mathbf{s})\, U_v(\mathbf{s}). \quad (10)$$

Hence, the torque response τ_M of the motor is derived as

$$\tau_M(\mathbf{s}) = K_\tau\, I_a(\mathbf{s}). \quad (11)$$

The torque response τ_M is used for the following servo controller design and motor selection.

3 Servo Controller Design and Motor Selection

In the traditional procedure of design of an industrial robot manipulator, the inertia J_L, the viscosity friction coefficient K_L and the damping constant K_L of the mechanism part and work conditions such as objective velocity are given. The inertia J_M, the inductance of the armature L_a, the resistance of the armature R_a, the torque constant K_τ and the back electromotive force constant of the motor and the gear rate N is determined by those conditions. According to experience in the industry, the relationship between the motor inertia J_M and the inertia of the mechanism J_L is given as

$$J_M > \frac{1}{5\sim 8}\, J_L/N^2. \quad (12)$$

If the mechanism inertia J_L is large and equation (12) can't be hold, an extended inertia is attached to the motor shaft or the change of the motor of which inertia is large enough, is recommenced. Parameters of the servo driver which fits the motor is adjusted to an appropriate current response and velocity response[2]. The desired contour control performance of the robot manipulator is checked. If enough performance can't be obtained, the motor and its servo driver are recommenced to be changed. Thus, in the traditional procedure of design of the industrial robot manipulators, the control performances can't be understood until inspecting them. Accordingly, selection of a motor and parameters of servo driver from desired control performance K_p and K_v of the robot manipulator is discussed. The human selects the motor and its servo driver which has enough control performance, position loop gain K_p and velocity loop gain K_v by using J_L, D_L, K_L, v_{ref} and N.

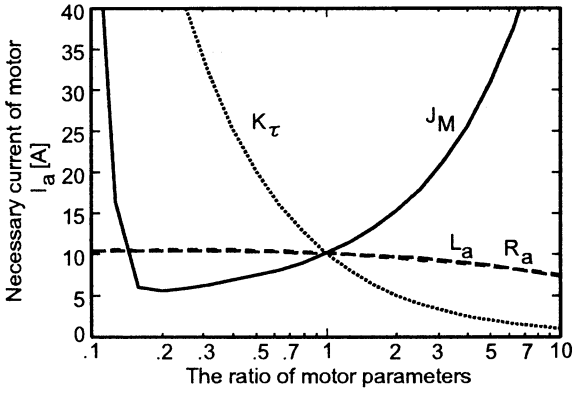


Figure 2: Relationship between the ratio of motor parameters and the necessary current of the motor

3.1 Relationship between Servo Parameters and Contour Control

Contour control performance was evaluated by using a mathematical model of industrial robot manipulators for each servo parameter. In robot manipulators, one of the reason of inferiority contour control performance is torque saturation. And in most causes, the torque saturation is occurred due to the current saturation in the servo driver.

Accordingly, the necessary current and torque are analyzed by using simulation results of the current and torque response from the model (10) and (11).

The experimental device DEC-1 consists of a servo controller and a servo motor and a load generator (mechanism). The DC servo motor and servo controller are the same device which are used robots and NC machine tools in industry.

Relationship between the necessary current for DEC-1 experiment system composed by an industrial DC servo motor and servo driver are located at 1 in horizontal axis of Fig.2. The parameters of DEC-1 experiment system are $J_L = 6.53 \times 10^{-3}$[kgm^2], $K_L = 57.9$[Nm], $D_L = 2.46 \times 10^{-3}$[Nms], $N = 1$[1], $J_M = 6.53 \times 10^{-3}$[kgm^2], $K_\tau = K_e = 0.291$[Nm/A], $L_a = 10.76 \times 10^{-3}$[H] and $R_a = 1.5$[Ω][3]. For the motor inertia J_M, the lowest current is obtained at the ratio 0.18.

Relationship between the necessary torque and parameters of the motor is shown in Fig.3. The shape of the curves in Fig.3 is same as those in Fig.2 except for K_τ.

Relationship between J_M and poles of the transfer function as in (2) is shown in Fig.4 If J_M is smaller than $\frac{1}{5.5}\, J_L/N^2$, two poles move to negative region from positive region. Then, current response oscillates and the control becomes inefficient. Using the parameters of DEC-1, without oscillation of the cur-

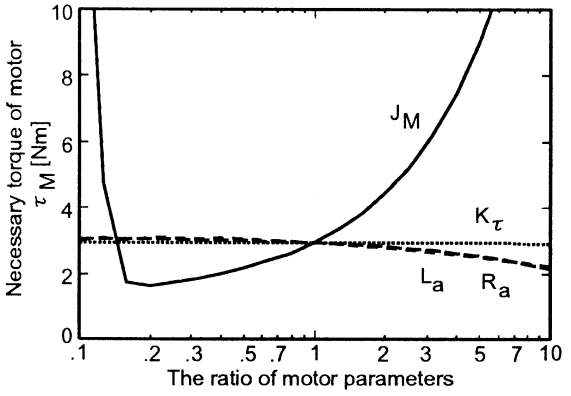


Figure 3: Relationship between the ratio of motor parameters and the necessary torque of the motor

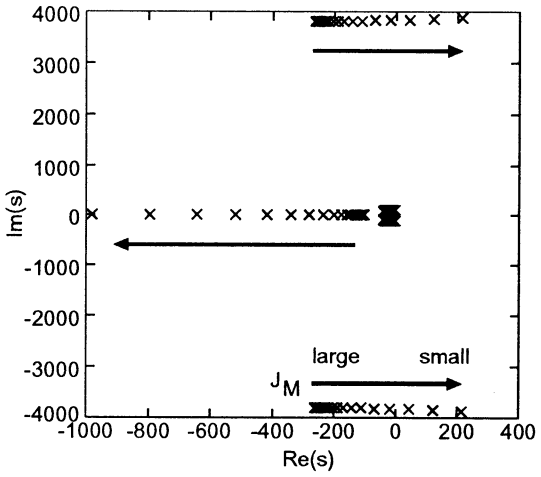


Figure 4: Relationship between motor inertia J_M and poles of the 6th order model for the industrial robot manipulator

rent response, J_M must be satisfied with

$$J_M > \frac{1}{5.5} J_L/N^2. \tag{13}$$

This result coincides with the industrial experience as explained in (12). If J_M larger than $\frac{1}{5.5} J_L/N^2$, an extension inertia to increase insufficiency inertia is attached to the motor shaft.

3.2 Selection of Servo Parameters and Motors

By using the relationship between the servo parameters and contour control performance, we obtained a rule of an appropriate selection of the servo parameters and motors. The rule enables any engineers to an appropriate selection of the motors and their parameters to achieve precise contour control of robot manipulators.
(1) Select a motor temporarily from J_L, D_L, K_L, v_{ref} and N by using traditional method[2].
(2) Select the velocity loop gain K_v below the natural angular oscillation and ω_L. The position loop gain K_p should be equal to $K_v/6.8$[2].
(3) Determine the reference input time interval ΔT from the relationship between ΔT and velocity ripples or contour ripples[4].
(4) Inspect the servo motor by relationship between motor parameters in Fig.3 and equation(13). Select the servo driver which is corresponds to the servo motor.
(5) Adjust parameters of the servo driver which fit to the motor to become appropriate current response and velocity response.

By following the above procedure, a human can construct the robot manipulator to achieve a desired control performance.

4 Conclusion

This paper proposed a procedure for the selection of the motor for industrial robot manipulator by constructing the mathematical model for industrial robot manipulators and analyzed the relationship between torque saturation and motor parameters of the robot manipulators.

References

[1] M.Nakamura, S.Goto, K.Kyura, *Artificial Realization of Human Skill for Robot Manipulator Control*, Proceeding of International Symposium on Artificial Life and Robotics, 1996.

[2] Yaskawa Electric Mfg. Co., Ltd., *Introduction to Servo Techniques for Mechatronics*, Nikkankogyo-shimbunsha 1986 (in Japanese).

[3] N.Egashira, M.Nakamura, K.Kyura, *Analysis of Performance in Mechatronic Software Servo Systems with Servo Motor Parameters*, The 15th SICE Kyushu Branch Annual Conference, 1996.11 (in Japanese).

[4] N.Egashira, M.Nakamura, K.Kyura, *Analysis of Stational Velocity Ripples at each Reference Input Time Interval for Mechatronic Servo Systems*, Journal of the Robotics Society of Japan, vol.16, no.1, 1998 (in Japanese)(accepted).

Proc. of Third Int. Symp. on Artificial Life, and Robotics (AROB III' 98),
Oita, Japan, 19-21, January, 1998,

Real-Time Control of a SCARA Robot by Visual Servoing with the Stereo Vision

S. H. Han
Mechanical Eng.
Kyungnam Univ.,
Masan, Korea. 631-701

M. H. Lee
Mechanical Eng.
Pusan National Univ.
Pusan, Korea. 609-735

J. I. Bae
Mechanical Eng.
Pukyung National Univ.
Pusan, Korea. 609-735

K. S. Yoon
Mechanical Eng.
Tokyo Univ.
Tokyo, Japan

Abstract

This paper presents a new approach to visual servoing with the stereo vision. In order to control the position and orientation of a robot with respect to an object, a new technique is proposed using a binocular stereo vision. The stereo vision enables us to calculate an exact image Jacobian not only at around a desired location but also at the other locations. The suggested technique can guide a robot manipulator to the desired location without giving such priori knowledge as the relative distance to the desired location or the model of an object even if the initial positioning error is large. This paper describes a model of stereo vision and how to generate feedback commands. The performance of the proposed visual servoing system is illustrated by the simulation and experimental results and compared with the case of conventional method for a SCARA robot.

KEYWORDS : Visual servoing, Stereo vision, Feedback command, Real-time control, Image Jacobian

1 Introduction

There are mainly two ways to put the visual feedback into practice.[1,2] One is called look-and-move and the other is visual servoing. The former is the method which transforms the position and orientation of an object obtained by a visual sensor into those in the world frame fixed to an environment and guides the arm of the manipulator to a desired location in the world frame. In this method, precise calibration of a manipulator and camera system is needed. On the contrary, visual servoing uses the Jacobian matrix which relates the displacement of an image feature to the displacement of a camera motion and performs a closed-loop control regarding the feature as a scale of the state. Therefore, we can construct a servo system based only on the image and can have a robust control against the calibration error because there is no need to calculate the corresponding location in the world frame.[2,3,4] A hand eye system is often used in visual feedback and there are two ways of arranging the system. One is placing a camera and a manipulator separately; the other is placing the camera at the end-tip of the manipulator. The former motion strategy of the manipulator becomes more complicated than the latter. In the latter, it is easy to control the manipulator using a visual information because the camera is mounted on the manipulator end-tip.[5,6]

This paper presents a method to solve this problem by using a binocular stereo vision. The use of stereo vision can lead to an exact image Jacobian not only at around a desired location but also at the other locations. The suggested technique places a robot manipulator to the desired location without giving such priori knowledge as the relative distance to the desired location or the model of an object even if the initial positioning error is large. This paper deals with modeling of stereo vision and how to generate feedback commands. The performance of the proposed visual servoing system was evaluated by the simulations and experiments and obtained results were compared with the conventional case for a SCARA robot.

2 Visual Servoing System

2.1 Stereo Vision Model

We define the frame of a hand-eye system with the stereo vision and use a standard model of the stereo camera whose optical axes are set parallel each other and perpendicular to the baseline. The focal points of two cameras are apart at distance d on the baseline and the origin of the camera frame Σ_c is located at the center of these cameras. Fig. 1 represents the schematic diagram of a suggested visual servoing system. In Fig. 1 two DSP

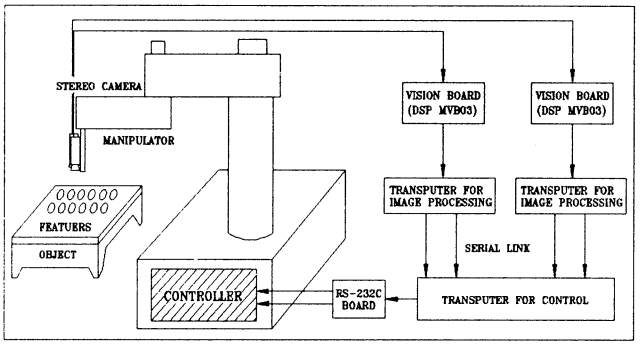


Fig. 1 Schematic diagram of visual servoing system

vision boards (MVB03) are used, which were made Samsung Electronics Company in Korea based-on the TMS320C30 chips.

An image plane is orthogonal to the optical axis and apart at distance f from the focal point of a camera and the origins of frame of the left and right images, Σ_l and Σ_r, are located at the intersecting point of the two optical axes and the image planes. The origin of the world frame Σ_w is located at a certain point in the world. The x, y, and z axes of the coordinate frames are shown in Fig. 2.

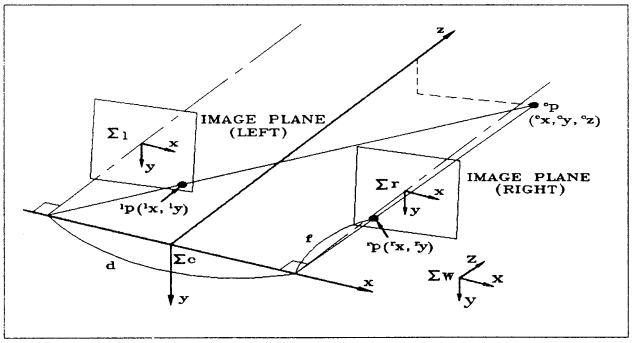


Fig. 2 The coordinates system of stereo vision model.

Now let ${}^l p = ({}^l x, {}^l y)$ and ${}^r p = ({}^r x, {}^r y)$ be the projections onto the left and right images of a point p in the environment, which is expressed as ${}^c p = ({}^c x\ {}^c y\ {}^c z)^T$ in the camera frame. Then the following equation is obtained (see Fig. 2).

$$ {}^l x\ {}^c z = f({}^c x + 0.5d) \tag{1-a} $$

$$ {}^r x\ {}^c z = f({}^c x - 0.5d) \tag{1-b} $$

$$ {}^l y\ {}^c z = f\ {}^c y \tag{1-c} $$

$$ {}^r y\ {}^c z = f\ {}^c y \tag{1-d} $$

Suppose that the stereo correspondence of feature points between the left and right images are found. In the visual servoing, we need to know the precise relation between the moving velocity of camera and the velocity of feature points in the image, because we generate a feedback command of the manipulator based on the velocity of feature points in the image. This relation can be expressed in a matrix form which is called the image Jacobian.

Let us consider n feature points $p_k (k = 1, \cdots, n)$ on the object and the coordinates in the left and right images are ${}^l p_k({}^l x_k, {}^l y_k)$ and ${}^r p_k({}^r x_k, {}^r y_k)$, respectively. Also define the current location of the feature points in the image ${}^I p$ as

$$ {}^I p = ({}^l x_1\ {}^r x_1\ {}^l y_1\ {}^r y_1\ {}^r y_1 \cdots {}^l x_n\ {}^r x_n\ {}^l y_n\ {}^r y_n)^T \tag{2} $$

where each element is expressed with respect to the virtual image frame Σ_P.

First, to make it simple, let us consider a case when the number of the feature points is one. The relation between the velocity of feature point in image ${}^I \dot{p}$ and the velocity of camera frame ${}^c \dot{p}$ is given as

$$ {}^I \dot{p} = {}^P J_c\ {}^c \dot{p} \tag{3} $$

where ${}^P J_c$ is the Jacobian matrix which relates the two frames.

Now let the translational velocity components of camera be σ_x, σ_y and σ_z the rotational velocity components be w_x, w_y, w_z, then we can express the camera velocity V as

$$V = [\ \sigma_x\ \sigma_y\ \sigma_z\ w_x\ w_y\ w_z\ ]^T = [\ {}^c v_c\ {}^c w_c\ ]^T \quad (4)$$

Then the velocity of the feature point seen from the camera framed ${}^c\dot{p}$ can be written

$${}^c\dot{p} = \frac{d^c p}{dt} = \frac{d}{dt}\,{}^c R_w({}^w p - {}^w p_c) \quad (5)$$
$$= {}^c R_w\{-{}^w w_c \times ({}^W p - {}^w p_c)\} + {}^c R_w({}^W\dot{p} - {}^w\dot{p_c})$$

where ${}^c R_w$ is the rotation matrix from the camera frame to the world frame and ${}^w p_c$ is the location of the origin of the camera frame written in the world frame. As the object is assumed to be fixed into the world frame, ${}^w\dot{p} = 0$. The relation between ${}^c\dot{p}$ and V is

$${}^c\dot{p} = {}^c R_w\{-{}^w w_c \times ({}^w p - {}^w p_c)\} - {}^c R_w\,{}^w\dot{p_c}$$
$$= -{}^c w_c \times {}^c p - {}^c\dot{p_c} \quad (6)$$
$$= \begin{bmatrix} -w_y\,{}^c z + w_x\,{}^c y - \nu_x \\ -w_z\,{}^c x + w_x\,{}^c z - \nu_y \\ -w_x\,{}^c y + w_y\,{}^c x - \nu_z \end{bmatrix}$$

Therefore, substituting Eq. (6) into Eq. (3), we have the following equation.

$${}^I\dot{p} = {}^I J_c\ {}^c\dot{p} = J\ V \quad (7)$$

In Eq. (7) matrix J which expresses the relation between velocity ${}^I\dot{p}$ of the feature point in the image and moving velocity V of the camera is called the image jacobian.

From the model of the stereo vision Eq. (1), the following equation can be obtained.

$${}^c x\,(2\,{}^l x - {}^r x) = d\,{}^l x + {}^r x \quad (8)$$
$${}^c y\,({}^l x - {}^r x) = {}^l y\ d = {}^r y\ d \quad (9)$$
$${}^c z\,({}^l x - {}^r x) = f\ d \quad (10)$$

Above discussion is based on the case of one feature point. In practical situation, however, the visual servoing is realized by using plural feature points. When we use n feature points, image Jacobian $J_1, \cdots, J_n$ are given from the coordinates of feature points in the image. By combining them, we express the image Jacobian as

$$J_{im} = [\ J_1 \cdots\cdots J_n\ ]^T \quad (11)$$

Then, it is possible to express the relation of the moving velocity of the camera and the velocity of the feature points even in the case of plural feature points, that is,

$${}^I\dot{p} = J_{im}\ V \quad (12)$$

where we suppose that the stereo and temporal correspondence of the feature points are found.

In the case of the monocular, the image Jacobian J has the following form.

$$J = f\begin{bmatrix} -\frac{1}{{}^c x} & 0 & \frac{{}^c x}{{}^c x^2} & \frac{{}^c x\,{}^c y}{{}^c z} & -(1+\frac{{}^c x^2}{{}^c x^2}) & \frac{{}^c y}{{}^c z} \\ 0 & -\frac{1}{{}^c x} & \frac{{}^c y}{{}^c x^2} & 1+\frac{{}^c y^2}{{}^c z^2} & -\frac{{}^c x\,{}^c y}{{}^c x^2} & -\frac{{}^c x}{{}^c z} \end{bmatrix} \quad (13)$$

We now introduce the positional vector of the feature point in the image of monocular vision using the symbol ${}^m P = ({}^m x,\ {}^m y)$. This is the projection of the point expressed as ${}^c P = ({}^c x\ {}^c y\ {}^c z)^T$ in the camera frame into the image frame of the monocular vision, and has the following relation.

$${}^m x = f\ {}^c x\ {}^c z^{-1} \quad (14\text{-a})$$
$${}^m x = f\ {}^c y\ {}^c z^{-1} \quad (14\text{-b})$$

Substituting Eq.s (14-a) and (14-b) into Eq. (13) yields another expression of the image Jacobian for the monocular vision.

$$J = f\begin{bmatrix} -\frac{1}{{}^c z} & 0 & \frac{{}^m x}{{}^c z} & \frac{{}^m x\,{}^m y}{f} & -\frac{{}^m x^2+f^2}{f^2} & {}^m y \\ 0 & -\frac{f}{{}^c x} & \frac{{}^m y}{{}^c x} & 1+\frac{{}^m y^2+f^2}{f^2} & -\frac{{}^m x\,{}^m y}{f} & -{}^m x \end{bmatrix} \quad (15)$$

A disparity which corresponds to the depth of the feature point, is included in J in the case of the stereo vision, but s-term expressed in the camera frame ${}^c z$ is included in J in the case of the monocular vision.

In the stereo vision, as all elements of J can be described in the image frame, a feedback command can be computed with only the image information. On the other hand, variables in the image frame and the depth ${}^c z$ in the camera frame are combined together in J for the monocular vision. Therefore, it is unable to

accomplish feedback control with only information of image and it is necessary to employ either modeling of the object or the desired location in the depth direction ${}^{c}z$ in the camera frame. To cope with this problem, the visual servoing with the monocular vision conventionally uses a pseudo-inverse matrix of the image Jacobian fixed at the desired point. In the stereo vision, however, there is no need to consider the stability problem, because it is possible to calculate a correct value at every sampling period. Furthermore, to determine the relative location and orientation uniquely, at least four feature points are required in the case of the monocular vision. On the other hand, three feature points are sufficient for the case of the stereo vision.

2.2 Feedback Command

In the visual servoing, the manipulator is controlled so that the feature points in the image reach their respective desired locations.

We define an error function between the current location of the feature points in image ${}^{I}p$ and the desired location ${}^{I}p_d$ as

$$E = Q({}^{I}p - {}^{I}p_d) \tag{16}$$

where Q is a matrix which stabilizes the system. Then the feedback law is defined as following equation

$$V = -G\,E \tag{17}$$

where G corresponds to a feedback gain.

To realize the visual servoing, we must choose Q so that convergence is satisfied with the error system can be satisfied with

$$\begin{aligned} \dot{E} &= \frac{\partial E}{\partial t} = Q\frac{\partial\,{}^{I}p}{\partial t} = Q\,{}^{I}\dot{p} \\ &= Q\,J_{im}V = -G\,Q\,J_{im}\,E \end{aligned} \tag{18}$$

We use pseudo-inverse matrix of the image Jacobian J_{im} for Q to make $Q\,J_{im}$ positive and not to make an input extremely large, that is,

$$Q = J_{im}^{+} = (J_{im}^{T}J_{im})^{-1}J_{im}^{T} \tag{19}$$

Therefore, the feedback command is given as

$$V = -G\,J_{im}^{+}\,({}^{I}p - {}^{I}p_d) \tag{20}$$

Fig. 3 shows a block diagram of the control scheme described by Eq. (20).

Note that the feedback command u is sent to the robot controller and both the transformation of u to the desired velocity of each joint angle $\dot{q}_d$ and its

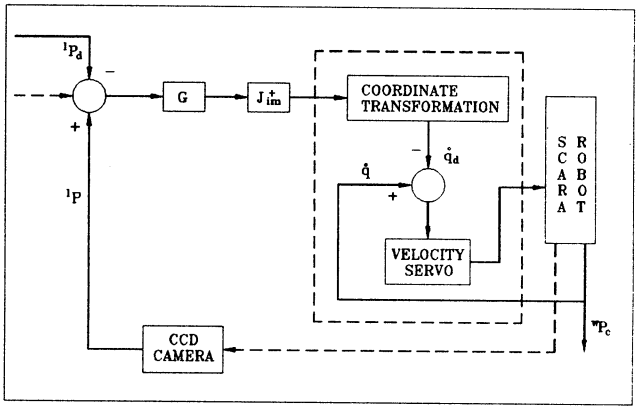


Fig. 3 Block diagram of visual feedback system.

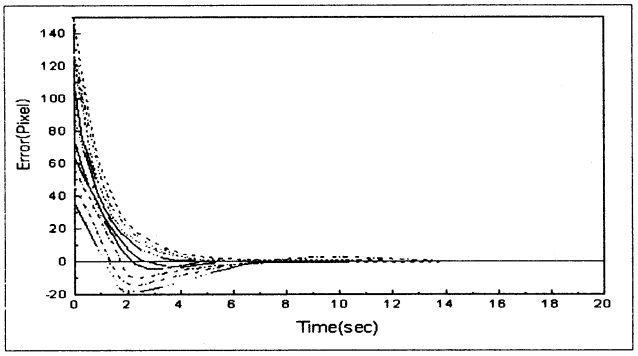
velocity servo are accomplished in the robot controller as show in Fig. 3. Futhermore, as J_{im} is a $4n\times6$ matrix and pseudo-inverse matrix J_{im}^{+} is a $6\times4n$ matrix, a feedback command Eq. (20) of 6 degrees of freedom is obtained.

3 Simulation and Experiments

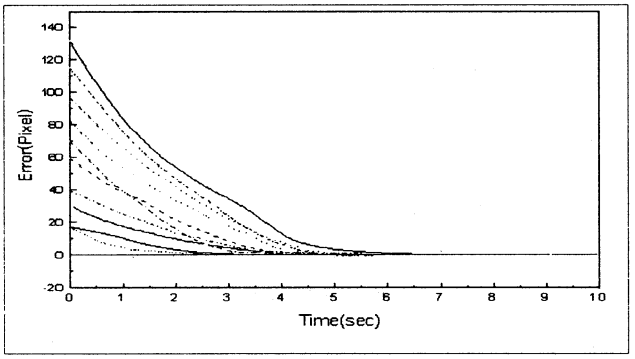
3.1 Simulation

We have compared the visual servoing using the monocular vision with that using the stereo vision by the simulation. In the simulation, feature points of an object are the four corners of a square whose side dimension is 300 mm. In the same condition, we used four feature points even in the stereo vision. Parameters used the focal length, f=16 mm, baseline d=130 mm, sampling time of 50 msec, gain λ=1, desired location ${}^{c}P_d = (100\ 100\ 500)^{T}$mm desired orientation in Euler angle $(\varphi, \theta, \psi) = (0,0,0)$rad, initial error $(-50\ -50\ -50)^{T}$mm in the translation and $(\varphi, \theta, \psi) = (20,20,20)$rad in the orientation.

The error between the desired location and the current location of the feature points in cases of the monocular and stereo visions are shown in Fig. 4. Next, we will show the results for the change of the way to choose the feature points and set the initial.



(a) Monocular



(b) Stereo

Fig. 4 Positional Error in x and y axes in the case of the stereo and monocular vision.

error image. We select the four corners of a rectangle whose size is 200×200 mm as the feature points and set the translational error as (-150 -150 -450) mm and the other values are the same as before (Fig. 5).

In Fig. 5, we can see that the result diverges in the case of the monocular vision, but converges in the case of the stereo vision. This is because the image Jacobian is fixed at the desired location in case of the monocular vision. Therefore, a correct feedback command can not be generated when the initial error is large. On the other hand, the image Jacobian can be updated at every in the case of the stereo vision, thus it is possible to generate a correct feedback command which assures the stability visual servoing.

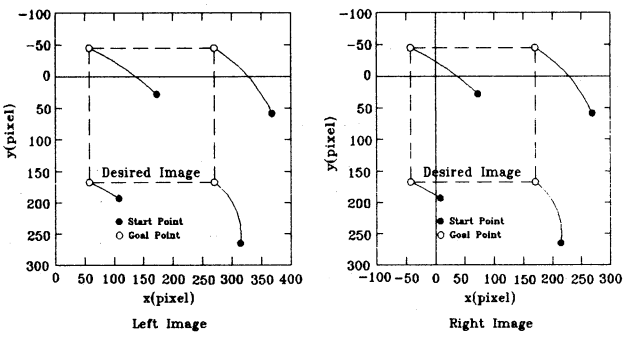


Fig. 5 Trajectories of the feature points on the images.

3.2 Experiments

In experiments, we used a four-axis SCARA Robot (SM5 Model) made in Korea with a stereo camera attached to the end tip of the arm. The feature points are three circular planes of 20 mm radius on three corners of a equilateral triangle, one side 87 mm and are placed on the board. Precise calibration had not been done for the stereo camera attached to the end-tips.

Two stereo images were taken and transformed to the binary images in the real time and in parallel by two image input devices and the coordinate of the gravitational center of each feature point was calculated in parallel by two transputers. We gave the stereo correspondence of the feature point in the first sampling.

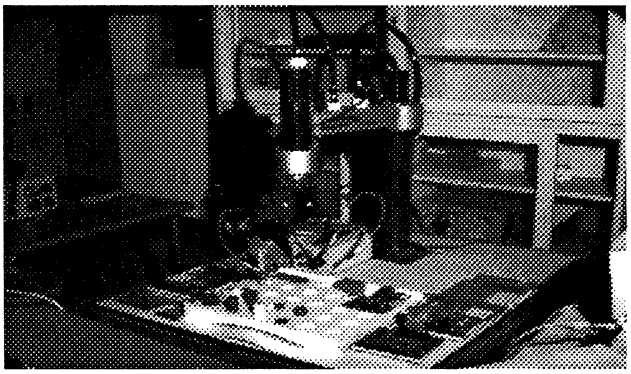


Fig. 6 The Experimental equipment set-up.

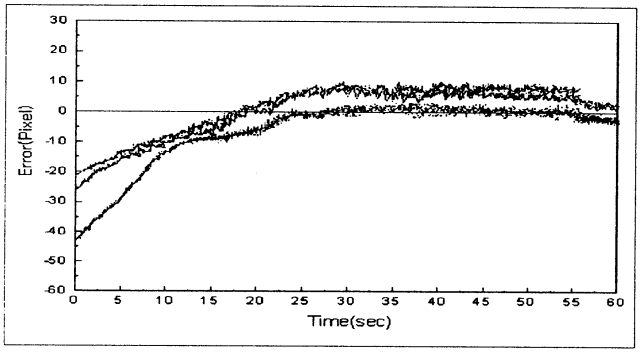
However, the stereo and temporal correspondence of the feature points in the succeeding sampling were found automatically by searching a nearby area where there were the feature points in the previous sampling frame.

The coordinates of the feature points were sent to a transputer for motion control and it calculated a feedback command for the robot. The result was sent to the robot controller by using RS-232C, and the robot was controlled by a velocity servo system in the controller.

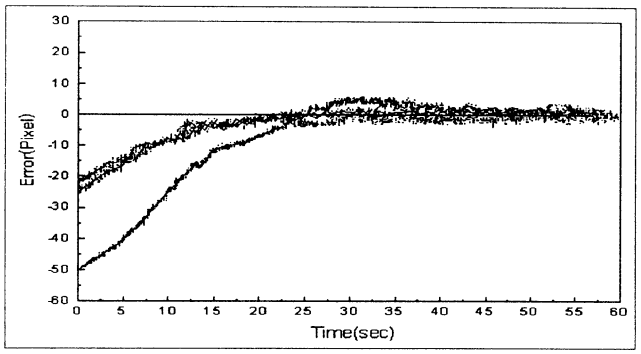
The sampling period of visual servoing was about 50 msec. Details were 16 msec for taking a stereo images, about 1 msec for calculating the coordinates of the feature points, 3 msec for calculating feedback command, about 16 msec for communicating with the robot controller. If we send a feedback input to the robot controller without using RS-232C, the faster visual servoing can be realized.

The desired location was $(0, 0, 500)^T$mm and the desired orientation in Euler angle, (ϕ, θ, ψ)= (0, 0, 0)degree and the initial error was $(50, 50, 50)^T$mm for translation.

The other parameters were the same as in the simulation. The error of current and desired location of the feature points are shown in Fig. 7 From these experimental results, we can see that the manipulator converges toward a desired location even if the calibration is not precise.



(a) Left image



(b) Right image

Fig. 7 Position Error in x and y axes.

4 Conclusion

This paper proposes a new method of visual servoing with the stereo vision to control the position and orientation of a SCARA robot with respect to an object. The method overcomes the several problems associated with the visual servoing with the monocular vision. By using the stereo vision, the image Jacobian can be calculated at any position. So neither shape information nor desired distance of the target object is required. Also the stability of visual servoing is assured even when the initial error is very large. We have shown the effectiveness of this method by simulation and experiments.

References

[1] L. E. Weiss, , A. C. Sanderson, , and C. P. Neuman, , "Dynamic sensor-based control of robots with visual feedback," *IEEE Journal of Robotics and Automation*, RA-3(5), pp.404-417, 1987.

[2] K. Hashimoto, T. Kimoto, T. Edbine, and H. Kimura, "Manipulator control with image-based visual servo". *In Proceedings of IEEE International Conference on Robotics and Automation*, pp. 2267-2272, 1991.

[3] F. Chaumette, P. Rives, and B. Espiau, "Positioning of a robot with respoect to an object, tracking it and estimating its velocity by visual servoing". In Proceedings of the IEEE International Conference on Robotics and Automation, pp. 2248-2253, 1991.

[4] K. Hashimoto, T. Edbine, and H. Kimura, "Dynamic visual feedback control for a hand-eye manipulator". *In Proceedings of the IEEE/RSJ International Conference on Intelligent Robots and Systems*, pp. 1863-1868, 1992.

[5] E. Bernard, C. Francois, and R. Patrick, "A new approach to visual servoing in robotics". *IEEE Transactions on Robotics and Automation*, Vol. 8, No. 3, pp.313-326, 1992.

[6] P. K. Allen, B. Toshimi, and A. Timcenko, "Real-Time Visual Servoing". *In Proceeding of the IEEE International Conference on Robotics and Automation*, pp. 851-856, 1991.

Proc. of Third Int. Symp. on Artificial Life, and Robotics (AROB III' 98),
Oita, Japan, 19-21, January, 1998,

Detection of Human's Confusion from Their Unconscious Action with Neural Networks

Kimihiko NAKATSUKASA, Hideki HASHIMOTO, and Fumio HARASHIMA

Institute of Industrial Science, University of Tokyo
7-22-1 Roppongi, Minato-ku, Tokyo 106, Japan.
E-mail: {tsukasa, hideki, fumio}@vss.iis.u-tokyo.ac.jp

Abstract

We proposed and constructed "Human's confusion detection system" [1], and did some experiments with it. The system to detect confusion in operating ATM machine, which are in banks or other places, was supposed and we show that our system judges whether people are confused or not from only their simple movements of hands with Back-Propagation Neural Networks and Radial Basis Function networks.

1 Introduction

Today, because of the development of science and technology, many intelligent systems have appeared to support our society. This tendency will continue in the next generations. There exist many machines which have various utilities and our life becomes convenient more and more.

On the other hand, some people say, "We can't use such systems because they are too complicated for us." Some expensive computers with the latest OS are not easy or convenient to users, especially for the elder.

One of the friendly systems for us may be the system with a function that can understand our intension without special input actions. For example, how about a computer which can tell us what to do next with their voice when we are at a loss to use it? How about the machine which shows its message at a high speed when we are going well, but changes speed slowly when we are confused? These are only some examples, but the system which can understand our action, can judge our intension, and can work based on it, must be indispensable for our comfortable life.

As a first stage of this purpose, we propose the system to detect human confusion with Neural Networks and 3D tracking eye system of our laboratory. The imaginary figure of this system is shown in Fig.1.

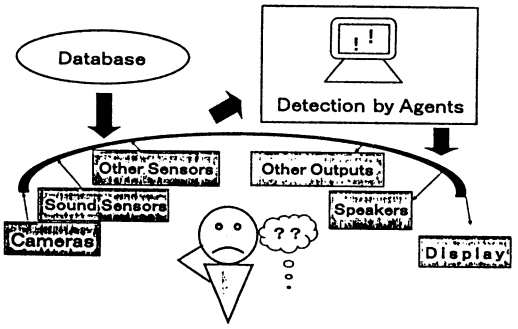


Figure 1: The concept of detection System of human confusion

2 Human Confusion Detecting System

In this section, the structure of our detection system is to be explained. The system is devided into two parts; information input part and judgement algorithm part. Using the information from the input part, the judgement part decides whether he is confused or not. The structure of this system is shown in Fig.2.

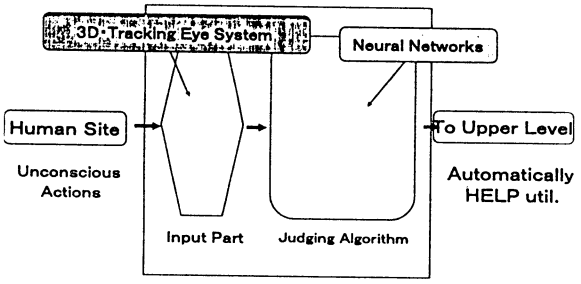


Figure 2: The structure of detection system of human confision

2.1 Information Input Part

To identify human's status automatically, their unconcious actions or movements are very important. For example, if he does same action iteratively, it may mean that he is confused. How about the following case : machine is waiting for next inputs, however he does not have any action. Adding to these things, the expression or bodily temperature will be important information. In this research, we noticed human's unconsious action (mainly movements of their hands) as a clue.

To get such information, our 3D tracking eye system is used as information input part of the system. In our laboratory, the eye system to track human's position by detecting human's skin color is being developed [2]. To detect skin color, an eye system uses two simple algorithms, and this system has realtime characteristic;

- detection of color using only RGB ratio information
- separation of standstill area as the background

With this system, the position coordinate, velocity, and acceleration of target are transferred to algorithm part.

One scene of our eye system is shown in Fig.3.



Figure 3: 3D Tracking Eye System : detection skin color

2.2 Judgement Algorithm Part

The role of judgement algorithm part is to calculate "the index number of confusion (INC)" of target. INC is a number between 0 and 1. If INC is close to 0, it means that he is not confused, and if INC is close to 1, it means that he is very confused.

To calculate INC, we applied neural networks. Neural Networks are well-known for thier good performance to identify the complicated mapping relations. The inputs of networks are human's unconscious movement of their hands or head, and output of networks is INC. With the eye system, human's movement (x, y, z) are expressed in 2D/3D coordinate form, and thier velocity $(V_{x,y,z})$ and acceleration $(A_{x,y,z})$ are calculated. If we adopt 2D coordinate, input information of networks are made from 6 parameters for every one time step. In the following experiment, we use information of three time steps for inputs, so inputs of networks are made from 18 parameters and outputs is 1 parameter (INC).

3 Realization of Detection System

3.1 Confusing People Using ATM machine

The first problem to realize the detection system is to define the confusion. Every person has different expression way of confusion and those ways change case by case. First, we try to limit the case to apply this system. We suposed the confusion detection system for users of auto teller machines (ATM). ATM are seen at banks or other places, but most of them are complicated because of their many functions. So we took video pictures of some people operating ATM, and we sought the typical action of them. Some of such typical actions are shown in the following;

- Waving hands in the air
- Leaning thier heads
- Looking around restlessly
- Doing same action again and again
- Stoping their action

We expressed such movement in 2D coordinate form, and Fig.4 shows an example of it. They are a part of network inputs.

3.2 Pretuning of Neural Networks

What we did next is pretuning neural networks. With every 100 data sets of confusing status and normal status, neural networks are pretuned. In the following experiment, we constructed 3 neural networks. They are, a)Simple Back-Propagation type Neural Network (BP1), b)Neural Network with Levenberg-Marquadt Method (BP2), c)Radial Basis Function type Network (RBF) with Gaussian [3].

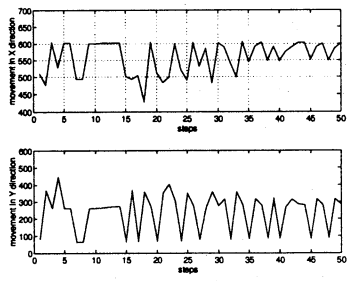


Figure 4; One example of inputs:movement of hand

4 Studies on Network Performances

To certificate the performance of constructed networks, we compare the real outputs and expected outputs to some inputs. If real outputs are enough close to expected ones, we can say that network has good parformance to identify INC, that is, to detect human's confusion.

4.1 Performance with Closed Data

First, we measured the performance of every networks with closed data. Closed data means the data which were used for pretuning of networks. Results are shown in Fig.5-7.

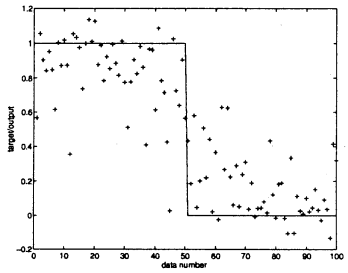


Figure 5: real and expected outputs of BP1 [with closed data]

These figures show that BP2 and RBF are well pretuned, but BP1 was not pretuned enough. BP1 and BP2 adopts same algorithm principly, so the bad performance of BP1 may be caused of the computer performance and not-essencial reasons. In the following experiments, we adopt BP2 and RBF which are suitable for this kind of datasets.

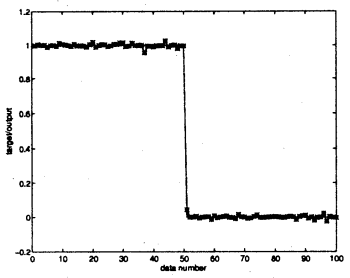


Figure 6: real and expected outputs of BP2 [with closed data]

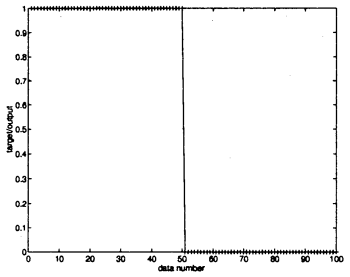


Figure 7: real and expected outputs of RBF [with closed data]

4.2 Performance with Open Data

Next, we measured the performance of every networks with open data. Open data means the data which were not used for pretuning of networks. These experiments mean to measure the network performance to unknown data sets. Results are shown in Fig.8-9.

These figures mean that our system separetes human's status roughly from inputs. If we set 0.5 as the threshold, 97% of inputs are separeted collectly into normal or confused in BP2, 93% in RBF.

However considering the characteristics of neural networks, this rough threshold may be not good. Selectiong proper threshold is a one of the big problems.

5 Problems at present and Future Plans

In this section, problems at present and research plans to them are shown;

- Instability of input information from 3D eye system

Outputs of our eye system are influenced by illuminance or other surroundings. We must improve it to get information stably.

- Definition of "confusion" is too vague

  At present, confusion means the status thst most of us feel it's really confusion. This method is one of the definitions indeed, but is there any other good idea? Fig.10 shows the concept of identfying human's inner status, that is, in this paper, confusion.

- Sometimes network error diverges while pretuning

  We want to input many information into network, but it becomes the causes of divergence of network outputs error. We must make studies on more efficient way of giving teaching data.

- To select proper threshold is difficult

  How to understand the outputs close to 0.5, for example 0.55 or 0.45. Do they show confusion or not? One of the solution may be taking statistics by asking many people.

6 Conclusion

In this paper,we proposed and constructed "Human confusion detection system". To be specific, the system to detect confusion in operating ATM machine was supposed and we showed that "it is possible to identify human's inner status from only their simple movements of hands". This will be great step to make intelligent human interface or robots in the next generation. We will continue the research on this theme, to get better performance of the system and new ideas about these problems.

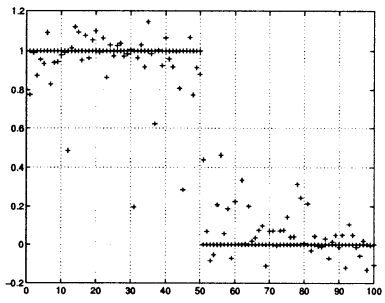


Figure 8: real and expected outputs of BP2 [with open data]

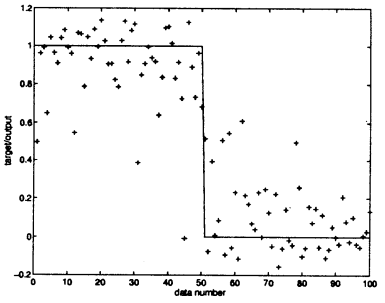


Figure 9: real and expected outputs of RBF [with open data]

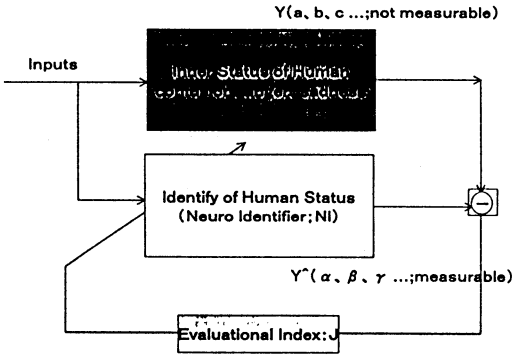


Figure 10: concept of identfying human's inner status

References

[1] K.Nakatsukasa,G.Appenzeller,H.Hashimoto ;Detection of Human's Confusion with Neural Networks(in Japanese),the 7th Intelligent System Symposium (FAN'97),1997

[2] G.Appenzeller,J.H.Lee,H.Hashimoto;Building Topological Maps by Looking at People: An Example of Cooperation between Intelligent Spaces and Robots,IROS97,1997

[3] S.Chen et al;Orthogonal Least Squares Learning Algorithm for Radial Basis Function Networks,IEEE Trans. on NN,1991

Proc. of Third Int. Symp. on Artificial Life, and Robotics (AROB III' 98),
Oita, Japan, 19-21, January, 1998,

Robust Robot Controller through Feedback Sliding Mode Observer

Kang-Bark Park, Ju-Jang Lee
Department of Electrical Engineering
Korea Advanced Institute of Science and Technology
373-1 Kusong-dong, Yusong-gu, Taejon 305-701 Korea

Teruo Tsuji
Department of Electrical Engineering
Kyushu Institute of Technology
1-1 Sensui-cho, Tobataku, Kitakyushu, 804 Japan

Abstract

In this paper, a continuous sliding mode controller(SMC) for robot robot mainpulator is proposed. The proposed method guarantee that the tracking error converges to zero maintaining the smoothness of the actual control signal. In order to estimate the acceleration data, a sliding mode observer is used.

1 Introduction

The basic theory of a switching control system was proposed in the Soviet Union in 1950's [1] and thereafter the term "variable structure system (VSS)" and "sliding mode control (SMC)" have been used for such systems [2].

Even though the SMC has the invariance property against system uncertainties and external disturbances, it has the drawback so called "*chattering phenomena*". Since the SMC uses switching functions to get an invariance property under the existence of system uncertainties and disturbances, it is inevitable for the control input to show the chattering phenomena.

Almost all of the researchers has used continuation techniques to overcome the chattering problem. The continuation techniques are focused on the smoothing of switching function. The switching function has been replaced by the saturation function and/or a sigmoid function.

However, all of these methods suffer from the same difficulty, that is, there is no quantitative rule for assigning boundary layer thickness of their algorithms. Thus, the corresponding effects of the chattering alleviation may not be guaranteed. In addition, these approaches can not guarantee the error convergence to zero, i.e., only the boundedness of the error within some predetermined boundary layer thickness can be guaranteed.

Thus, in this paper, a smooth sliding mode controller that guarantees the error convergence to zero is proposed for robot manipulators. The main concept is to consider the combination of a low pass filter (LPF) and the robot as a *virtual* plant, and design a virtual sliding mode controller u for this virtual plant as shown in Fig. 1. In this figure, τ is a *real* control signal and u means a virtual control signal. Then, although the virtual control signal u shows chattering phenomenon due to the switching function, the *real* control signal τ shows a smooth curve because it is an output of a LPF whose input is u.

The control scheme mentioned above, however, has to use the *acceleration* data which is not easy to obtain in usual case. In this paper, thus, the smooth sliding mode controller using sliding mode observer is proposed to estimate the acceleration of the joint of the robot manipulators. The closed-loop system is locally exponentially stable and region of attraction is also analyzed.

2 Virtual Plant Dynamics

The dynamic equation for an n-link robot manipulator is linearly parameterizable as follows:

$$M(q)\ddot{q} + C(q,\dot{q})\dot{q} + G(q) = Y(q,\dot{q},\ddot{q})\theta = \tau \qquad (1)$$

where $q, \dot{q}, \ddot{q} \in \Re^n$ are the joint angular displacements, velocities, and accelerations, respectively. $M(q)$ is the $n \times n$ positive definite inertia matrix, $C(q,\dot{q})$ is the $n \times n$ matrix corresponding to Coriolis and centrifugal factors, $G(q)$ is the $n \times 1$ vector of gravitational torques, τ is the $n \times 1$ input torque vector, θ is a constant p-dimensional vector of inertia parameters and Y is an $n \times p$ matrix of known functions of the generalized coordinates and their higher derivatives. It can be assumed that the parameter vector θ is uncertain and there exists $\theta_0 \in \Re^p$ and $\rho \in \Re_-$, both known, such that $\|\tilde{\theta}\| := \|\theta - \theta_0\| \leq \rho$ [4].

From the LPF's input-output relation, the following equation can be obtained. $\dot{\tau} + \Lambda\tau = u$ where $\Lambda = diag(\lambda_1, \lambda_2, \ldots, \lambda_n)$, and $\lambda_i > 0$, $i = 1, 2, \ldots, n$. Thus, for the virtual control signal u, the dynamic equation of the virtual plant can be described by

$$M\dddot{q} + \dot{M}\ddot{q} + \Lambda M\ddot{q} + C\ddot{q} + \dot{C}\dot{q} + \Lambda C\dot{q} + \dot{G} + \Lambda G = u \qquad (2)$$

where u is the $n \times 1$ virtual control input vector.

Introducing the tracking error state vectors $x_1 = q - q_d$, $x_2 = \dot{q} - \dot{q}_d$, $x_3 = \ddot{q} - \ddot{q}_d$ where $q_d \in \Re^n$ represents the desired trajectory vector, the virtual plant(2) can be rewritten in the following state-space representation:

$$\begin{aligned} \dot{x}_1 &= x_2 \\ \dot{x}_2 &= x_3 \\ \dot{x}_3 &= \beta(x_1 + q_d, x_2 + \dot{q}_d, x_3 + \ddot{q}_d) + M^{-1}u - \dddot{q}_d \end{aligned} \qquad (3)$$

where

$$\begin{aligned} \beta(\overline{x}_1, \overline{x}_2, \overline{x}_3) &= -M(\overline{x}_1)^{-1}\left\{\left(\dot{M} + \Lambda M + C\right)\overline{x}_3 \right. \\ &\quad \left. + \left(\dot{C} + \Lambda C\right)\overline{x}_2 + \dot{G} + \Lambda G\right\} \end{aligned} \qquad (4)$$

which defines a locally observable representation in the sense of the lie-algebra, as defined by Hermann and Krener [7] and $q_d^i \in C^3[0,\infty)$.

It is obvious that the above representation can be rewritten as the following:

$$\dot{x} = \begin{bmatrix} 0 & I_n & 0 \\ 0 & 0 & I_n \\ 0 & 0 & 0 \end{bmatrix} x + \begin{bmatrix} 0 \\ 0 \\ I_n \end{bmatrix} (y + \beta_1) \qquad (5)$$

where $x^T = \left[x_1^T, x_2^T, x_3^T\right]$, $y = M_0^{-1}u$, $\beta_1 = \beta - \ddot{q}_d + (M^{-1}M_0 - I_n)y$, and and $I_n \in \Re^{n\times n}$ is an identity matrix. The following assumption is assumed to be valid.

Assumption 1 *There exists a known function $\overline{\beta} > 0$ and a posotive known constant $c_0 > 0$ such that*

$$||\beta - \hat{\beta}|| \le \overline{\beta}, \qquad \left\|M^{-1}M_0 - I_n\right\| \le c_0 < 1 \qquad (6)$$

for all their arguments where $\hat{\beta}$ is the estimate of β.

3 Design of SMC using Full States

Consider the following function augmented sliding surface $s \in \Re^n$ so that $s(0) = 0$ is assured.

$$s = x_3 + \Lambda_1 x_2 + \Lambda_2 x_1 - Ne^{-\Lambda_3 t} \qquad (7)$$

where $\Lambda_i = diag(\lambda_{i1}, \lambda_{i2}, \ldots, \lambda_{in})$, $\lambda_{ij} > 0$, $i = 1, 2, 3$, and $j = 1, 2, \ldots, n$, $N = x_3(0) + \Lambda_1 x_2(0) + \Lambda_2 x_1(0)$. Then, the control law can be obtained from the sliding mode existence condition $s^T\dot{s} \le 0$, that is, $\dot{s} = y + \beta_1 + \Lambda_1 x_3 + \Lambda_2 x_2 + N\Lambda_3 e^{-\Lambda_3 t}$. Therefore, the control law can be given by

$$y = \ddot{q}_d - \Lambda_1 x_3 - \Lambda_2 x_2 - N\Lambda_3 e^{-\Lambda_3 t} - \hat{\beta} - \Psi s - \rho \cdot sgn(s)$$

where ρ is a scalar positive bounding function satisfying the following inequality:

$$||\beta - \hat{\beta} - \left(M^{-1}M_0 - I_n\right) y|| \le \rho \qquad (8)$$

From the Assumption 1, ρ can be obtained by

$$\rho = c_0 \left\|\ddot{q}_d - \hat{\beta} - \Psi s - \Lambda_1 x_3 - \Lambda_2 x_2 - N\Lambda_3 e^{-\Lambda_3 t}\right\| + c_0\rho + \overline{\beta}.$$

Then, for the virtual control law $u = M_0 y$, the following theorem can be stated.

Theorem 1 *Applying the following virtual control input (9) to the virtual plant (5), the closed-loop system is globally exponentially stable.*

$$\begin{aligned} u &= M_0 \left(\ddot{q}_d - \Lambda_1 x_3 - \Lambda_2 x_2 - N\Lambda_3 e^{-\Lambda_3 t}\right. \\ &\quad \left. -\hat{\beta} - \Psi s - (\rho + \eta) \cdot sgn(s)\right) \end{aligned} \qquad (9)$$

where $\eta = [\eta_1, \eta_2, \ldots, \eta_n]^T$, $\eta_i > 0$, $i = 1, 2, \ldots, n$.

Proof For the Lyapunov function candidate $V = \frac{1}{2}s^T s$, its time derivative can be derived as the following:

$$\begin{aligned} \dot{V} &= s^T\dot{s} = s^T\left(\dot{x}_3 + \Lambda_1 x_3 + \Lambda_2 x_2 + N\Lambda_3 e^{-\Lambda_3 t}\right) \\ &\le -\Psi s^T s - \sum_{i=1}^{n} \{\eta_i |s_i|\}. \end{aligned}$$

Thus, it is easy to know that V is a positive definite function of s and $\dot{V}$ is a negative definite function of s. Therefore, V is a Lyapunov function. Furthermore, since $s(0) = 0$, $V(0) = 0$ and hence $s = 0\ \forall t \ge 0$. Hence, it is obvious that the tracking error exponentially converges to zero. ■

Corollary 1 *The system is in the sliding mode all the time, that is, $s \equiv 0\ \forall\ t \ge 0$.*

4 Design of Sliding Mode Observer

Based on the general scheme for the sliding mode observer [6], the following state observer can be designed:

$$\begin{aligned} \dot{\hat{x}}_1 &= K_1\tilde{x}_1 + \hat{x}_2 + \Gamma_1 sgn(\tilde{x}_1) \\ \dot{\hat{x}}_2 &= K_2\tilde{x}_2 + \hat{x}_3 + \Gamma_2 sgn(\tilde{x}_2) \\ \dot{\hat{x}}_3 &= K_3\tilde{x}_2 + \Gamma_3 sgn(\tilde{x}_2) \end{aligned} \qquad (10)$$

where $\hat{x}_1, \hat{x}_2$, and $\hat{x}_3$ are the estimated values of x_1, x_2, and x_3, respectively, $\tilde{(\cdot)} = (\cdot) - \hat{(\cdot)}$, $K_1, K_2, K_3, \Gamma_1, \Gamma_2$, and Γ_3 are $n \times n$ positive definite matrices. M_0 is the "nominal" inertia matrix. In the simplest case, it will be only a diagonal constant matrix, e.g., $M_0 = m_0 I$ where $m_0 > 0$. The nonlinear function $\hat{\beta}$ is introduced to cope with the influence of β in (4) and to account for differences between the tracking errors and the observation errors.

By subtracting the observer equations (10) from the virtual plant equations (4), the following equations can be obtained

$$\dot{\tilde{x}}_1 = -K_1\tilde{x}_1 + \tilde{x}_2 - \Gamma_1 sgn(\tilde{x}_1) \qquad (11)$$

$$\dot{\tilde{x}}_2 = -K_2\tilde{x}_2 + \tilde{x}_3 - \Gamma_2 sgn(\tilde{x}_2) \qquad (12)$$

$$\dot{\tilde{x}}_3 = -K_3\tilde{x}_2 - \Gamma_3 sgn(\tilde{x}_2) + y + \beta_1. \qquad (13)$$

Since the angular position and velocity can be obtained from the encoder and the tachometers, respectively, it is assumed that x_1 and x_2 are measureable as described in the following assumption.

Assumption 2 *The angular position(x_1) and the angular velocity(x_2) are measureable.*

For the simplicity's sake consider Γ_1, Γ_2 to be the diagonal matricies, i.e., $\Gamma_1 = \gamma_1 I$, $\Gamma_2 = \gamma_2 I$. Then the following lemma can be obtained.

Lemma 1 *The region $\{(x_1, x_2)|\tilde{x}_1 = \tilde{x}_2 = 0\}$ is invariant as long as $|\tilde{x}_3^i| < \gamma_2$.*

Proof Since the proof is so obvious, it is omitted. ■

The generalized notion of the solution of a differential equation with discontinuities on the right-hand side such as (11)–(13) is given by [3]; the dynamics on the switching surface is an average of the dynamics on each side of the discontinuity surface. The region within which the switching surface is invariant is called "sliding patch"[6]. For the sliding patch, the following lemma can be obtained.

Lemma 2 *On the region of $\mathcal{R} = \{(x_1, x_2, x_3)|\tilde{x}_1 = \tilde{x}_2 = 0, |\tilde{x}_3^i| < \gamma_2\}$, which is called the sliding patch, $x_3 = \hat{x}_3 + \Gamma_2 sgn(\tilde{x}_2)$, and the error dynamics of $\left[\tilde{x}_1^T, \tilde{x}_2^T, \tilde{x}_3^T\right]^T$ is given by the following reduced-order dynamics:*

$$\dot{\tilde{x}}_3 = -\Gamma\tilde{x}_3 + y + \beta_1 \qquad (14)$$

where $\Gamma = \Gamma_3\Gamma_2^{-1} = \gamma I$ with $\gamma > 0$.

Proof Since the proof is so obvious, it is omitted. ■

Remark 1 *From the above Lemma, it can be known that the acceleration data can be estimated as the following in the sliding patch $\mathcal{R}$:*

$$x_3 = \hat{x}_3 + \Gamma_2 sgn(\tilde{x}_2) \tag{15}$$

5 Stability Analysis for the Closed-Loop System

It will be analyzed in this section that the stability of the closed loop system with the sliding mode controller (9) using the estimated state through the state estimator (10) in place of the true state. Since x_1 and x_2 are assumed to be measureable in Assumption 2, they can be used directly. The acceleration, however, is not accessible directly. From Remark 1, it was proved that the acceleration x_3 is given by (15) in the sliding patch $\mathcal{R}$.

Instead of the vector x, therefore, $\left[x_1^T,\, x_2^T,\, (\hat{x}_3 + \Gamma_2 sgn(\tilde{x}_2))^T\right]^T$ is used in the controller (9). Let us define the new state vector $\overline{z} = \left[x_1^T,\, x_2^T,\, \zeta_3^T\right]^T$ where $\zeta_3 = \hat{x}_3 + \Gamma_2 sgn(\tilde{x}_2)$, and the modified sliding surface $\overline{s} = \zeta_3 + \Lambda_1 x_2 + \Lambda_2 x_1 - \overline{N} e^{-\Lambda_3 t}$ where $\overline{N} = \zeta_3(0) + \Lambda_1 x_2(0) + \Lambda_2 x_1(0)$. Then, the control law using the full states (9), can be modified by

$$\begin{aligned} u \;=\; & M_0(\ddot{q}_d - \Lambda_1\zeta_3 - \Lambda_2 x_2 - \overline{N}\Lambda_3 e^{-\Lambda_3 t} - \Psi\overline{s} \\ & -\hat{\beta}(x_1 + q_d, x_2 + \dot{q}_d, \zeta_3 + \ddot{q}_d) - (\overline{\rho} + \eta)\cdot sgn(\overline{s})) \end{aligned} \tag{16}$$

where $\overline{\rho}$ is defined as

$$\begin{aligned} \overline{\rho} \;=\; & \frac{c_0}{1-c_0}\left\|\ddot{q}_d - \hat{\beta} - \Psi\overline{s} - \Lambda_1\zeta_3 - \Lambda_2 x_2 - \overline{N}\Lambda_3 e^{-\Lambda_3 t}\right\| \\ & + \frac{1}{1-c_0}\overline{\beta}(x_1 + q_d, x_2 + \dot{q}_d, \zeta_3 + \ddot{q}_d). \end{aligned} \tag{17}$$

Using the above control law (16), the following theorem can be derived.

Theorem 2 *The closed-loop system with the plant (5) and the proposed control law (16) using the observer (10) is exponentially stable provided that the state is in the sliding patch $\mathcal{R}$.*

Proof From Remark 1, in the sliding patch $\mathcal{R}$, $x = \overline{z}$, $s = \overline{s}$, and the control law (16) is identical with (9). Therefore, in the sliding patch $\mathcal{R}$, the closed-loop system dynamics of (5) and (10) is described as:

$$\dot{z} = \overline{A}z + \overline{B}\,(y + \beta_1) \tag{18}$$

where $z = [x_1^T,\, x_2^T,\, x_3^T,\, \tilde{x}_3^T]^T \in \Re^{4n}$

$$\overline{A} = \begin{bmatrix} 0 & I_n & 0 & 0 \\ 0 & 0 & I_n & 0 \\ 0 & 0 & 0 & 0 \\ 0 & 0 & 0 & -\Gamma \end{bmatrix} \quad \overline{B} = \begin{bmatrix} 0 \\ 0 \\ I_n \\ I_n \end{bmatrix}. \tag{19}$$

In the sliding patch $\mathcal{R}$, it is obvious that the sliding mode existence condition $s^T\dot{s} < 0$ can be guaranteed when the control law (16) is used. In addition, since it is also clear that $s(0) = 0$ is guaranteed in the sliding patch $\mathcal{R}$, the system is in the sliding mode all the time, that is, $s \equiv 0 \;\; \forall\; t \geq 0$ as Corollary 1. Therefore, one of the resulting dynamics can be obtained from $s = 0$ as the following:

$$s = x_3 + \Lambda_1 x_2 + \Lambda_2 x_1 - Ne^{-\Lambda_3 t} \;=\; 0. \tag{20}$$

Obviously, the above resultant dynamics (20) is exponentially stable.

For the simplicity of the analysis, let us assume that $\Lambda_1 = 3\Lambda$, $\Lambda_2 = 3\Lambda^2$, $\Lambda_3 = \Lambda^3$ so that the poles of the resultant dynamics are placed on $-\Lambda$.

The other dynamics can be obtained from the last equation of (18) which is obtained from (14). Since the condition $s \equiv 0$ implies $\dot{s} = 0$ as well as $s = 0$,

$$\dot{s} = \dot{x}_3 + \Lambda_1 x_3 + \Lambda_2 x_2 + N\Lambda_3 e^{-\Lambda_3 t} \;=\; 0.$$

This implies the following equation:

$$y + \beta_1 = -\Lambda_1 x_3 - \Lambda_2 x_2 - N\Lambda_3 e^{-\Lambda_3 t}. \tag{21}$$

Using the above equations (20) and (21), the last equation of (18) which is obtained from (14) can be rewritten as follows:

$$\begin{aligned} \dot{\tilde{x}}_3 &= -\Gamma\tilde{x}_3 + y + \beta_1 \\ &= -\Gamma\tilde{x}_3 + \left(\Lambda_1^2 - \Lambda_2\right)x_2 + \Lambda_1\Lambda_2 x_1 - (\Lambda_1 N - N\Lambda_3)\,e^{-\Lambda_3 t} \end{aligned} \tag{22}$$

Thus, from the equations (20) and (22), it is obvious that $q \to q_d$ and $\hat{x}_3 \to x_3$ exponentially as $t \to \infty$. ■

Since the exponential stability is guaranteed in the sliding patch $\mathcal{R}$, the region of attraction has to be determined. For the simplicity of the analysis, it is assumed that $s = \hat{\Lambda}x = x_3 + 2\Lambda x_2 + \Lambda^2 x_1$ where $\hat{\Lambda} = [\Lambda^2 \;\; 2\Lambda \;\; 1] \in \Re^{n\times 3n}$, $\Lambda = \lambda I_n$, and $\Psi = \psi I_n$. The following lemma will be used.

Lemma 3 *There exists a positive definite matrix $Q = Q^T \in \Re^{4n\times 4n}$ such that $\overline{B}^T P = \overline{\Lambda}$ where $\overline{\Lambda} = \left[\hat{\Lambda} \;\; 0_n\right] \in \Re^{n\times 4n}$, $0_n \in \Re^{n\times n}$ is the zero matrix, P is the unique positive definite matrix satisfying the Lyapunov equation $\overline{A}_0^T P + P\overline{A}_0^T + Q = 0$ where $\overline{A}_0 = \left(I_{4n} - \overline{B}\overline{\Lambda}\right)\overline{A} - \overline{B}\Psi\overline{\Lambda}$.*

Proof Since the proof is so obvious, it is omitted. ■

Now, let us define the Lyapunov function candidate as $V(z) = z^T P z$. Differentiating the $V(z)$ with respect to time, we have

$$\begin{aligned} \dot{V} \;=\; & z^T\left(P\overline{A}_0 + \overline{A}_0^T P\right)z - 2\rho z^T P\overline{B}sgn(s) + 2z^T P\overline{B}\,(\eta - \beta_1) \\ \leq\; & -z^T Q z \;\leq\; -\lambda_{min}(Q)\,\|z\|^2 \;\leq\; 0 \end{aligned}$$

where $\lambda_{min}(\cdot)$ means the minimum eigenvalue of $(\cdot)$. Since the above inequality is satisfied provided that the system is in the sliding patch $\mathcal{R}$, it sould be guaranteed that z is always in the sliding patch $\mathcal{R}$. It is clear that V is bounded as $\lambda_{min}(P)\,\|z\|^2 \leq V \leq \lambda_{max}(P)\,\|z\|^2$ where $\lambda_{max}(\cdot)$ means the maximum eigenvalue of $(\cdot)$. Thus, a region of attraction, where z remains in the sliding patch $\mathcal{R}$ and z is asymptotically stable, is given by

$$\Omega = \left\{ z \;\middle|\; \|z\| \leq \gamma_2\sqrt{\lambda_{min}(P)/\lambda_{max}(P)} \right\}.$$

6 Simulation Results

The simulation has been carried out for a two-link robot manipulator model used by Yeung and Chen [5]. The parameter values are also the same as those of Yeung and Chen.

The results are shown in Figs. 2~4 .

The tracking error, velocity, and acceleration of the proposed controller is presented in Fig. 2. One can easily know that the tracking error converges to zero.

In Fig. 3, the virtual control signal u is given. Because of the switching function($sgn(\cdot)$), it chatters with the high frequency. However, as in Fig. 4, the *real* control signal τ applied to the robot(real plant) shows the smooth curve.

7 Conclusions

In order to overcome the *chattering problem*, first order LPF and the concept of a virtual controller/plant has been used. The proposed control scheme guarantees the invariance property against parameter uncertainties maintaining the smoothness of the *real* control signal without sacrificing the tracking accuracy. That is, although the proposed controller generates a smooth control signal τ, the system is in the sliding mode all the time and the tracking error converges to zero exponentially under the existence of parameter uncertainties. The closed-loop system has been shown to be globally exponentially stable.

Since the chattering-free sliding mode controller uses the acceleration data, a smooth control law using the estimated acceleration is proposed and the stability for the closed-lop system has been verified.

References

[1] S. V. Emelyanov, "A technique to develop complex control equations by using only the error signal of control variable and its first derivative," *Avtomatika i telemekhanika*, vol. 18, no. 10, p. 873–885, 1957.

[2] S. V. Emelyanov, *Theory of Variable Structure Systems*, Moscow: Nauka(*in Russian*), 1970.

[3] F. A. Filippov, "Differential equations with discontinuous right-hand side," *Matematicheskii Sbornik*, vol. 51, no. 1, pp. 99–128, 1960.

[4] Mark W. Spong, "On the robust control of robot manipulators," *IEEE Trans. Automat. Contr.*, vol. AC-37, no. 11, pp. 1782–1786, 1992.

[5] K. S. Yeung and Y. P. Chen, "A new controller design for manipulators using the theory of variable structure systems," *IEEE Trans. Automat. Contr.*, vol. AC-33, no. 2, pp. 200–206, 1988.

[6] J. J. E. Slotine, J. K. Hedrick, and E. A. Misawa, "Sliding observers for nonlinear systems," *ASME J. Dynamic Syst., Measurement, Contr.*, vol. 109, pp. 245–252, 1987.

[7] R. Hermann and A. J. Krener, "Nonlinear controllability and observability," *IEEE Trans. on Automat. Contr.*, vol. 22, pp. 728–740, 1977.

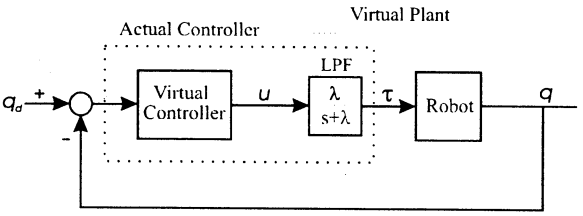


Fig. 1. Block Diagram of the Virtual System

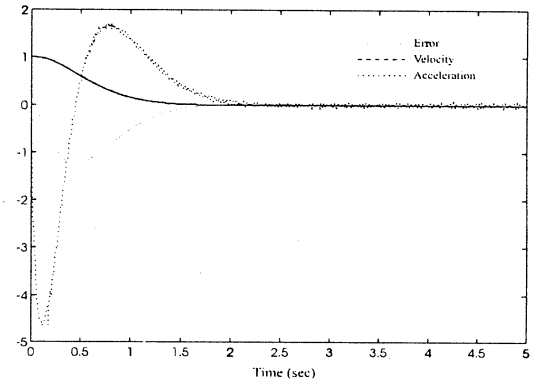


Fig. 2. Tracking Error, Velocity, and Acceleration

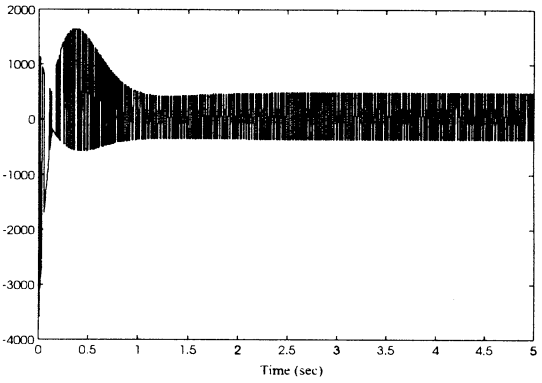


Fig. 3. Virtual Control Signal u

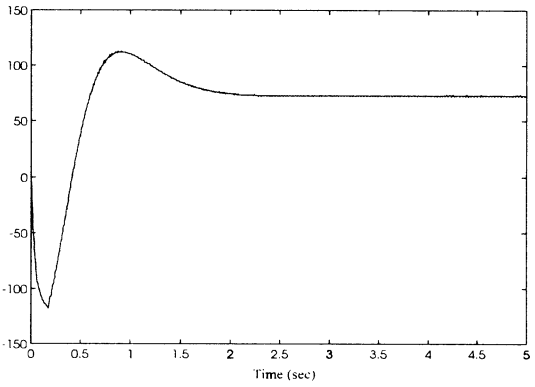


Fig. 4. Actual Control Signal τ

Proc. of Third Int. Symp. on Artificial Life, and Robotics (AROB III' 98),
Oita, Japan, 19-21, January, 1998,

Implementation of Multilayer Neural Network with Threshold Neurons

Kazuo Sato, Hiroomi Hikawa
Dep. of Computer Science and Intelligent Systems, Oita University, Oita, 870-11, Japan
kazuo@csis.oita-u.ac.jp; hikawa@csis.oita-u.ac.jp
Fax +81-975-54-8786

Abstract

In this paper, the implementation of Multilayer Neural Network (MNN) with threshold neurons is discused. To reduce the circuit size, simple function is used as the activating function of neurons. The proposed MNN has on-chip learning capability. As the learning algorithm, backpropagation algorithm is modified for effective hardware implementation. The proposed MNN is implemented on Field Programmable Gate Array (FPGA) to evaluate the learning performance and circuit size.

1 Introduction

In recent years, Artificial Neural Networks (ANN) have been used in many applications such as image processing, speech processing, high-speed communication network control, etc. For widespread practical use of ANNs in these and other applications, it is necessary to implement them in efficient custom hardware. The advantage of using digital approach is that it can use state-of-the-art VLSI and ULSI implementation techniques, and many researchers have focused on the digital neural networks[1][2]. One of the major problems in implementing neural networks in hardware is the activating function of neurons, Multilayer Neural Network (MNN) architecture with threshold neuron has been proposed[3]. In this paper, the implementation of MNN with threshold neurons on Field Programmable Gate Array (FPGA) is discused. To reduce the circuit size, simple function is used as the activating function of neurons. Also the threshold neuron MNN has on-chip learning capability which is based on modified backpropagation algorithm[3].

2 Multilayer Neural Network with Threshold function

MNN is one of the most widely used neural network models. The operation of the MNN is divided into two phases, i.e., learning phase and retrieving phase. During the learning phase, weights are adjusted to perform a particular application. The learning phase consists of forward and backward operation. Every learning phase, forward operation is executed to obtain the output response against particular input training pattern. Then error between the teaching data and the actual output value is propagated in backward to update the weight values. In the retrieving phase, the same operation as the forward operation is performed.

2.1 Forward operation

Let $o_k^{(s)}$ denote the output of k-th neuron in s-th layer, and the layers are numbered from 0 to M, then the computation performed by each neuron is:

$$H_k^{(s)} = \sum_{j=1}^{N_{s-1}} w_{kj}^{(s)} o_j^{(s-1)} + \theta_k^{(s)} \quad (1)$$

$$o_k^{(s)} = f(H_k^{(s)}) \quad (2)$$

where $H_k^{(s)}$ is the weighted sum of the k-th neuron in s-th layer and $w_{kj}^{(s)}$ is the synaptic weight. Neuron output $o_k^{(s)}$ is obtained by computing an activating function $f(\cdot)$ on the weighted sum. Usually, sigmoid function is used as the activating function $f(\cdot)$, but threshold function $g(\cdot)$ shown in Figure 1(A) is used as the activating function. The function $g(\cdot)$ can be easily implemented in hardware by using comparators.

2.2 Backward operation

Learning algorithm is performed in the backward operation. The back-propagation algorithm[4] is ex-

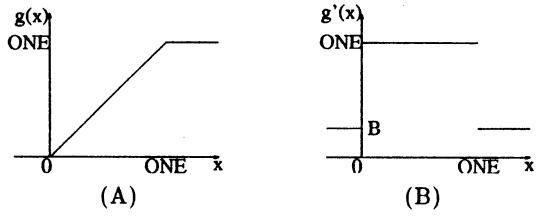


Figure 1: Function used as (A)the threshold function and (B)the derivative function

pressed as:

$$\sigma_k^{(s)} = \begin{cases} t_k - o_k^{(s)} & s = M \\ \sum_{j=1}^{N_{s+1}} w_{kj}^{(s+1)} \delta_j^{(s+1)} & \\ & s = 1, \cdots, M-1 \end{cases} \quad (3)$$

$$\delta_k^{(s)} = \sigma_k^{(s)} f'(H_k^{(s)}) \qquad s = 1, \cdots, M \quad (4)$$

$$\Delta w_{kj}^{(s)} = \eta \delta_k^{(s)} o_j^{(s-1)}$$
$$k = 1, \cdots, N_s \quad j = 1, \cdots, N_{s-1} \quad (5)$$

Function $f'(\cdot)$ in (4) is the derivative of the activating function. In the proposed neurons, the function $g'(\cdot)$ depicted in Fig. 1(B) is used. Strictly, B should be 0, because the function $g'(\cdot)$ is the derivative function of $g'(\cdot)$. However, when B is set to 0, in some cases, error signals may be completely terminated in hidden layers, and the learning fails because the weights in lower layer are not adjusted[3]. Consequently, non-zero value is used for B.

3 System architecture

The architecture of the proposed network is shown in Fig. 2. The forward operation is straightforward. Each neuron calculates its output from the weighted sum of the neuron output in the lower layer and its output is weighted and transferred to the neurons in the upper layer. In the backward operation, modified back-propagation algorithm is performed. First, the error term δ and σ are represented by pulse width modulated signal. A Pulse width Modulator (PWM) shown in Fig. 3 is used to convert the error into pulse width modulated signal which is used to enable weight registers. PWM consists of an up-down counter and a register. First, the error term is shifted to the right by m-bit, and is loaded into the counter at the end of foward phase. The up-down counter generates the error signal until terminal count(TC) becomes *High*. Thus the time during which the error signal is high

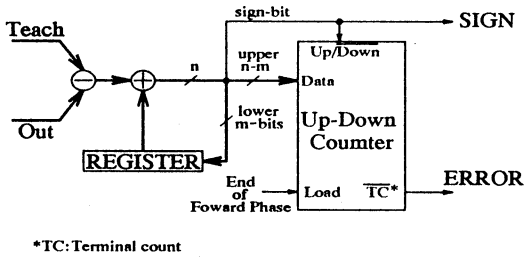


Figure 3: Pulse Width Modulator (PWM)

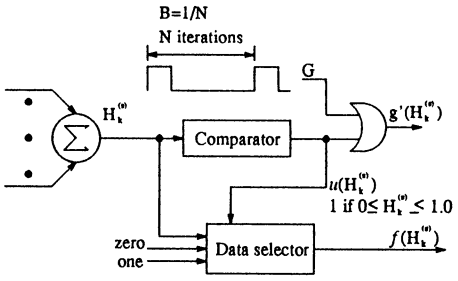


Figure 4: Neuron unit

level is proportional to the error δ or σ. The lower m-bits is used for the next error calculation. $\sigma_k^{(s)} g'(H_k^{(s)})$ in (4) can be realized by AND gates and, the error signals are transferred to the lower layer when $g'(H_k^{(s)})$ is *High* level.

The block diagram of the proposed neuron is depicted in Fig. 4. The function $g'(H_k^{(s)})$ used in (4) is realized by combining two signals, one is the signal $u(H_k^{(s)})$ which is given by a comparator, and the other is the signal **G**. The $u(H_k^{(s)})$ gives *High* output when $H_k^{(s)}$ is between 0.0 and 1.0. The signal **G** is periodically turns *High* and opens the AND gates so that a constant value $B(< 1.0)$ is added to the function $u(H_k^{(s)})$. As shown in Fig. 5, in the learning process, training patterns are applied to the network repeatedly, and all the patterns form a pattern set. The signal **G** gives *High* level output every N pattern set. Therefore, B is equivalent to $1/N$. For example, to have $B = 0.25$, **G** turns *High* every four iterations.

To calculate $w_{kj}^{(s+1)} \delta_j^{(s+1)}$ in (3), instead of the actual weight value, the sign-bit of the weight is multiplied with the error term $\delta_j^{(s+1)}$. As the sign-bit takes two values, the circuit to perform the operation is a exclusive-OR which inverts **SIGN** signal when the sign-bit of the weight is *one*.

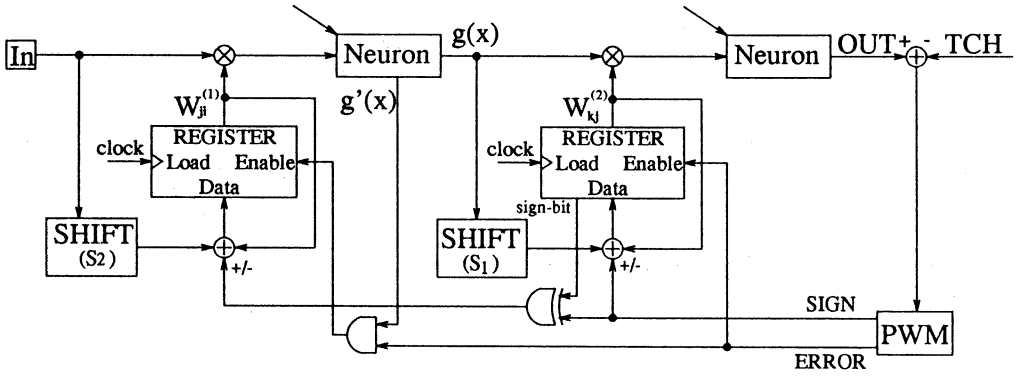


Figure 2: Network configuration

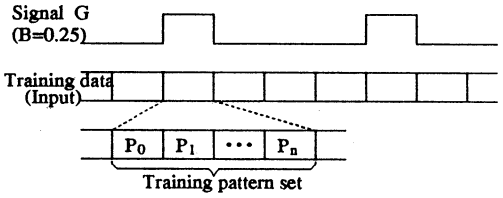


Figure 5: Generation of B

number of iteration	# of successful learning cace (out of 200,000 trial)	success rate(%)
100	79,687	39.8
500	128,127	64.1
1000	159,376	79.7

Table 1: Learning performance, B=0.25, m=5, 2 neurons in the hidden layer

The multiplication, $\delta_k^{(s)} o_j^{(s-1)}$ in (5), and the update of weights are performed as follows; when **ERROR** signal is *high* and clock signal is applied, $o_j^{(s-1)}$ is shifted to the right by S bit, and it is added to the weight if **SIGN** is zero (error is positive value), otherwise it is subtracted from the weight value. The proposed MNN is implemented on FPGA to evaluate the learning performance.

4 Learning performance

Using the system model discussed in the previous section, system-level computer simulations are conducted to test the learning performance of the proposed MNN. Weights values are expressed in fixed point 16-bit signed format and the neuron output is represented in 8-bit unsigned integer format.

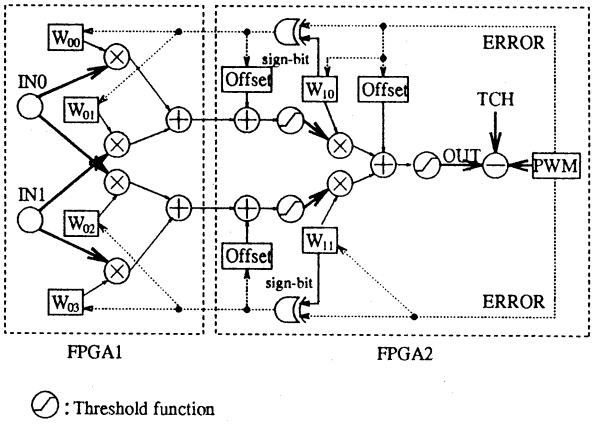


Figure 6: 2 input 1 output neural network

Table 1 shows the rate of successful lerning. The network is trained to perform exclusive-OR function until error term becomes zero. Table 1 shows nearly 80% of 200,000 trials has been trained within 1,000 iterations.

5 Experiment

The proposed MNN is implemented on FPGAs as shown in Fig. 6. In Fig. 6, The thick arrows indicates bit-parallel operation, the others indicate bit-serial operation. The multipliers in Fig. 6 use bit-serial operation. The number of CLBs for each FPGAs are following: FPGA1 has 35% (280 of 800) CLB FG function generators and 35% (278 of 800) CLB flip-flops. FPGA2 has 69% (552 of 800) CLB FG function gen-

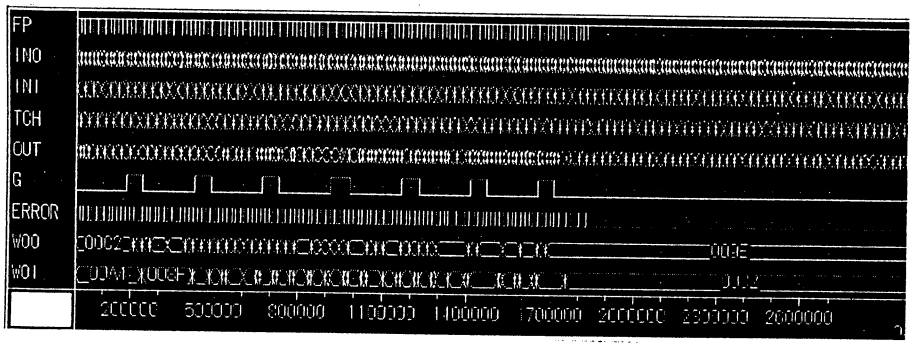


Figure 7: Logic-level simulation result

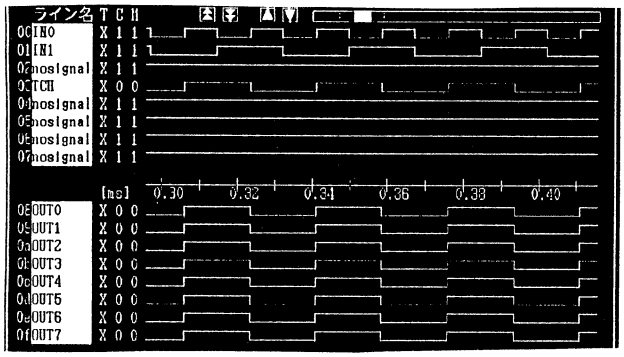


Figure 8: Signals in the experimental MNN on FPGA

erators and 50% (398 of 800) CLB flip-flops.

Fig. 7 shows the logic-level simulation result. The functions of signals in Fig. 7 are:

FP *HIGH* during the forward operation, *LOW* when the MNN is in the backward operation.

IN0,IN1 inputs.

OUT MNN output.

TCH teaching data.

G signal *G* shown in Fig. 1(B).

ERROR error signal.

W00, W01 synaptic weights.

Fig. 7 shows the whole learning phase, and one can notice that the error signal **ERROR** stops at around time index 1850000. Fig. 8 shows the signals in the experimental circuit after lerning. In the figure, **IN0**, **IN1** and **TCH** are represented in single-bit. **OUT** is represented in 8-bit. Fig. 8 shows all **OUT** signals equal to **TCH**. Therefore, the proposed MNN successfully learns the exclusive-OR function.

6 Conclusion

In this paper the implementation of MNN with threshold neurons on FPGA has been discussed. To reduce the circuit size, threshold function is used as the activating function of neurons. For the on-chip learning, back-propagation algorithm is also modified to reduce the circuit size.

The proposed architecture has been tested by system-level simulation and logic-level simulation as well as the experiment which uses the threshold neuron based MNN implemented on FPGA. Implementation result indicate that proposed MNN is very small.

References

[1] B. A. White, M. I. Elmasry, "The digi-neocognitron: a digital neocognitron neural network model for VLSI, " *IEEE Trans. on Neural Networks*, Vol. 3, pp. 73-85, Jan. 1992.

[2] C. Lehmann, M. Viredaz and F. Blayo, "A Generic Systolic Array Building Block For Neural Networks with On-Chip Learning," *IEEE Trans. on Neural Networks*, Vol. 4, No.3, May. 1993.

[3] H. Hikawa, "Learning Performance of Multilayer Neural Network with Threshold Neurons," *ITC-CSCC'97*, VOL. II, pp.1065-1068, 1997.

[4] R. P. Lipmann, "An introduction to computing with neural nets," *IEEE Acoustics, Speech, and Signal Processing Magazine*, pp.4-22, April 1987.

[5] H. Hikawa, "Implementation of Simplified Multi-Layer Neural Networks with On-chip Learning," *IEEE ICNN'95*, VOL.4, pp.1633-1637, 1995.

Proc. of Third Int. Symp. on Artificial Life, and Robotics (AROB III' 98),
Oita, Japan, 19-21, January, 1998,

Motion planning in dynamic environments – A parallel online approach

Heinz WÖRN, Dominik HENRICH and Christian WURLL[1]

Abstract

This paper presents a new approach to parallel motion planning for industrial robot arms with six degrees of freedom in an on-line given 3D environment. The method is based on the A-search algorithm and needs no essential off-line computations. The algorithm works in an implicitly descrete configuration space. Collisions are detected in the Cartesian workspace by hierarchical distance computation based on the given CAD model. By decomposing the 6D configuration space into hypercubes and cyclically mapping them onto multiple processing units, a good load distribution can be achieved. We have implemented the parallel motion planner on a workstation cluster with 9 PCs and tested the planner for several benchmark environments. With optimal discretisation, the new approach usually shows linear speedups. In on-line provided environments with static obstacles, the parallel planning times are only a few seconds.*

Keywords: industrial robots, motion planning, on-line algorithms, distributed and parallel processing, search algorithms

1 Introduction

The issue of robot motion planning has been studied for a couple of decades and many important contributions to the problem have been made [10]. Motion planning algorithms are of great theoretical interest, but are rarely used in practice because of their computational complexity [11].

Future robotic tasks (i.e. recycling, robot guidance, tele-operation, assembly and disassembly, medical surgery) can often only be solved in dynamic environments. Therefore, powerful on-line motion planners for industrial robots with six degrees of freedom (DOF) are needed. The *on-line* capability means that the planner does not require any time-consuming off-line computations in order to react directly to dynamic changes in the environment.

For dynamic environments, three different cases can be distinguished. In the first case, the environment contains dynamic obstacles (i.e. objects on a conveyor belt, or additional robots) with known or partially known movements. In the second case, the robot gripps different objects. There, the kinematic chain of the robot, including the gripped object, will change. The third case occurs in the area of virtual engineering. After every assembly operation, the product, or the environment will change its geometry. All three cases of dynamic environments implicate a modification of the configuration space (C-space), which has to be considered during planning motions.

An extensive introduction to this problem is presented by Fujimura. In several examples he explains the different approaches basically for the motion planning problem of autonomous, mobile robots [5]. Fiorini discusses a motion planner for industrial robots based on velocity adaptation, but he plans only with a 2 DOF workspace with two robots and known movements, but without any other obstacles [4]. Ralli proposes a potential-field approach based on the explicit calculation of the workspace and C-space. If a new object appears, the new path is searched in a few seconds, but the planner works for 5 DOF in a very small search space, which is unfavourable for industrial robots [15].

Generally speaking, speeding up the computation will enable the motion planner to cope better with dynamic environments in practice. One approach is based on the introduction of parallel processing. Mazer reports good planning times based on parallel genetic algorithms for 6 DOF robots in simple problems, but the planner is unfavourable for industrial environments [13]. Challou presents a parallel formulation of the informed randomised search and achieves good results [3]. But the necessary precomputed heuristics are unfavourable for dynamic environments. An extensive overview and a classification of the different parallel methods can be found in [7, 9]. The result of the overview is that parallel processing is an efficient method for speeding up motion planning.

Summarising, up to now, no planners for 6 DOF robots exist, which have the ability of dealing with dynamic obstacles and having low on-line computation times. Our motivation has been the development of a planner for industrial robots satisfying these requirements. We focus on industrial robots, which constitutes a considerable part of robots being used.

The remainder of the paper is organised as follows: In Section 2 the basic approach of our motion planner is introduced. Section 3 describes the necessary enhancements for parallelising the sequential approach. Section 4 shows the experimental results, and the paper ends with the conclusion and an outlook to the future investigation in Section 5.

2 Sequential Approach

Most of the off-line motion planners are based on an explicit representation of the *free C-space*. The free C-space computation consists of the obstacle transformation into the C-space and the construction of a free-space representation. Both tasks are very time- and memory consuming, and their calculation effort increases exponentially with the robot's DOF. In order to avoid these time consuming obstacle transformations, one can search in an

[1] Institute for Real-Time Computer Control Systems & Robotics (IPR), o. Prof. Dr.-Ing. H. Wörn, o. Prof. Dr.-Ing. U. Rembold, and Prof. Dr.-Ing. R. Dillmann, University of Karlsruhe, Faculty for Informatics, P.O. Box 69 80, D-76128 Karlsruhe, Germany, E-Mail: dHenrich@ira.uka.de. Further information can be found in the Web pages of the PaRo group (Parallel Robotics) of the IPR at http://wwwipr.ira.uka.de/~paro/

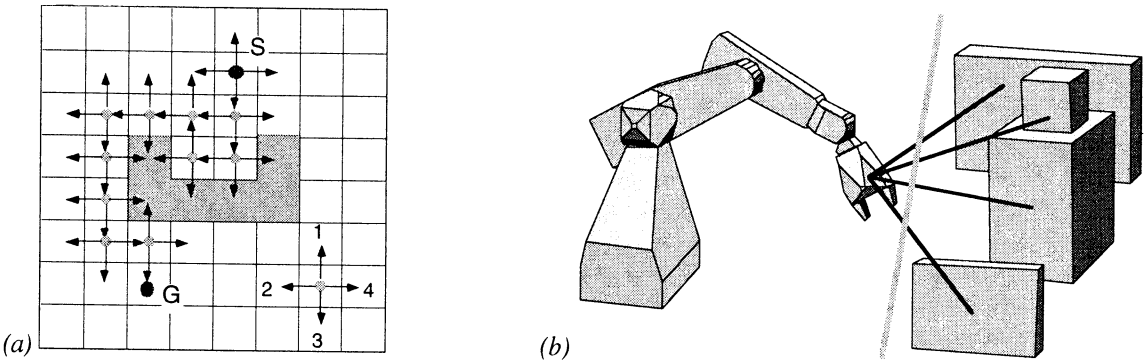


Figure 1: (a) A-search in the implicit C-space from the start configuration S to the goal configuration G, (b) collision detection by distance computation in the workspace*

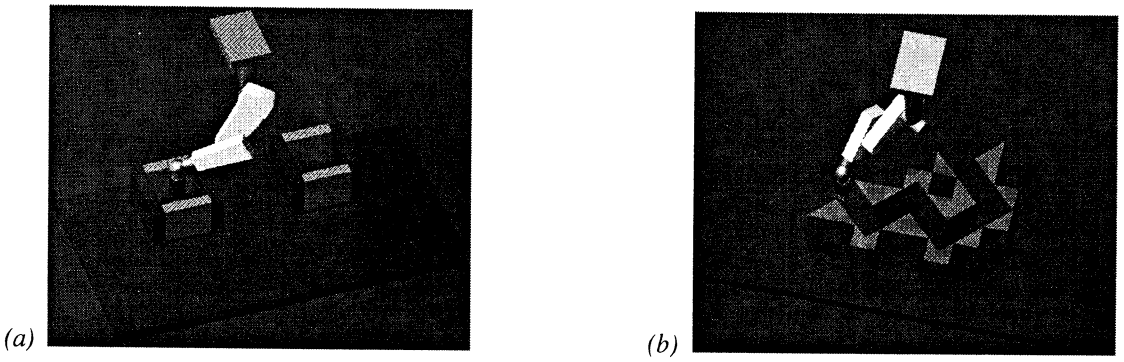


Figure 2: The benchmark problems STAR (a) and DETOUR (b) for the 6 DOF robot Puma260

implicitly represented C-space and detect collisions in the workspace. This strategy enables the planner to cope with on-line provided environments and moving obstacles.

For searching in the implicit C-space, we apply the well known A*-search algorithm [Hart86]. The main task of the A*-algorithm consists of the expansion and the processing of configurations, which are stored in the priority list OPEN. In every iteration, the best configuration of OPEN is expanded.

According to a heuristic evaluation function, these successors will be considered in the following iterations. After the expansion, the parent configuration is saved in the hashing table CLOSED. The search continues until the goal is found, or the OPEN list is empty. In the latter case the algorithm stops with no solution. In Figure 1a, an example for a 2D search is given. The dots indicate investigated configurations and the arrows give reference to the corresponding successors.

Collisions are detected by a fast, hierarchical distance computation in the 3D workspace, based on the given CAD model of the environment and the robot [6, 8] (see Figure 1b). With the help of the "maxmove-tables", introduced in [12], the Cartesian distances are then transformed into joint intervals in order to define the state ("free" or "prohibited") of the regarded configuration. For obtaining similar joint intervals, thus implicating an efficient distance exploitation, the optimal joint discretisation is automatically computed based on the method of [14].

3 Parallel approach

For parallelizing the A*-algorithm, the configurations in OPEN and CLOSED must be accessible to all processors, in order to distribute the whole work. These lists can either be managed by one dedicated processor or each processor can have its own local lists. In a message passing system, each access to a global list would lead to an enormous communication effort, thus, the local method was preferred.

The work distribution is the key aspect of parallelization. Therefore, the C-space is decomposed into d-dimensional hypercubes of size b in each dimension. For parallel processing, the hypercubes are cyclically mapped on the p available processors by the following function[2]:

$$f(\Theta) := 1 + \left(\sum_{i=1}^{d} \left\lfloor \frac{\theta_i}{\Delta\theta_i * b} \right\rfloor \right) \bmod p$$

According to the automatically computed discretisation $\Delta\Theta_i$, every configuration $\Theta = [\Theta_1, \ldots, \Theta_d]$ is mapped uniquely to one hypercube or to one processor. Thus, the OPEN list of each processor contains configurations of the multiple mapped hypercubes.

4 Experimental Results

We have implemented the parallel motion planner on a workstation cluster. The cluster consists of 9 PC's, each with 133 Mhz Intel Pentium processors and 64 Mbyte memory. The parallel communication is established by an Ethernet based bus network. For more details see [18].

For testing the motion planner, we have developed five benchmark problems for a 6 DOF robot, a Puma260.

[2] The operator $\lfloor \bullet \rfloor$ denotes the next lower integer number.

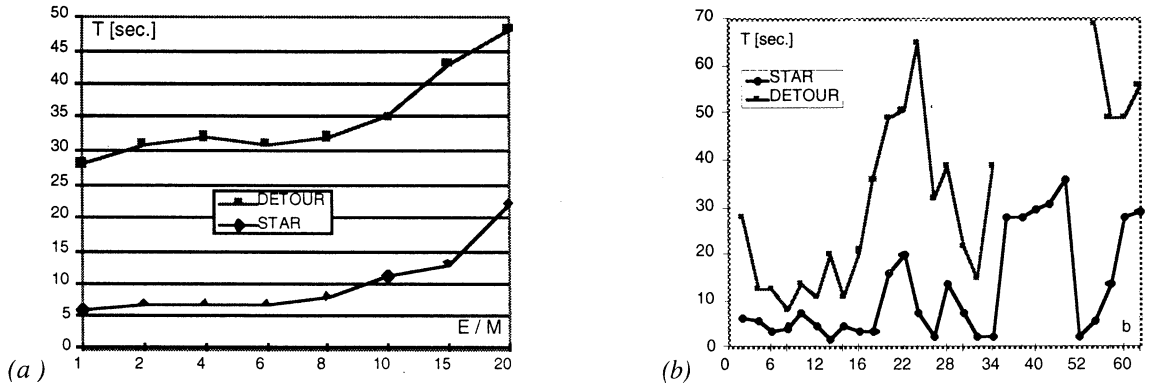


Figure 3: Analysis of the parallel motion planner: (a) Run-time T for different number of expansions E per message M (b)Run-time T for increasing cube sizes b

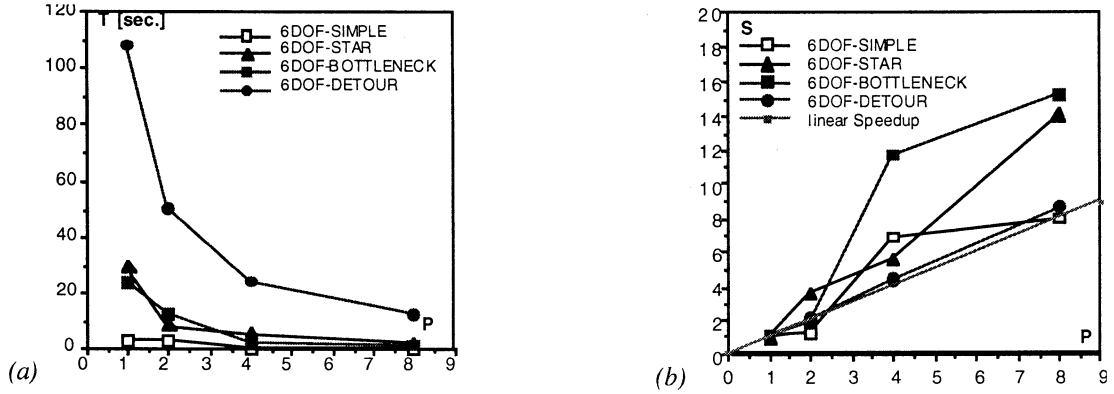


Figure 4: Planning time T (a) and the speedup S (b) with P processors for the different benchmark problems

As an example, the benchmark problems STAR and DETOUR are shown in Figure 2, developed in [12][3].

Concerning communication, lower cube sizes result in a good load distribution, but increase the number of messages. Too many messages, however, usually leads to a bottleneck in the communication network and slows down the calculation times. Combining several messages to form one message seems to be a way out of this problem.

Evaluation runs for the benchmark problems STAR and DETOUR are given in Figure 3a. Here, a cube size $b = 2$ and $p = 8$ processors are used. The results show that the combining of configurations to one message over several iterations leads to longer planning times. For example, without combining, the benchmark problem STAR was solved in 8 sec, but with the combining of messages over 20 iterations the planner has needed 20 sec [16].

This is mainly due to the fact, that the remote configurations are sent too late. Thus, every processor does not receive better configurations and expands the worse ones. At this stage, no message combining was included in the further runtime tests.

The performance of the parallel algorithm essentially depends on the load balancing mechanism. In our approach, we have implemented a static distribution mechanism, which can be influenced by modifying the cube size b. Considering the C-space decomposition, small sizes lead to more cubes (in different areas of the C-space) being mapped on to a single processor. Thus, implicating a good load distribution. In contrast, larger sizes will worsen the load balancing. This is mainly due to the coarse decomposition, thus, the processors are longer idle, until they receive work. Additionally, larger cube sizes lead to less cubes being mapped on to one processor.

For validating the performance of this load balancing mechanism, we have solved benchmark STAR with different cube sizes b. On each of the $p = 8$ processors, we measured the number of collision detections, which is the most expensive function. Figure 3b shows the experimental results. For larger values, the coarse C-space decomposition leads to an irregular load distribution. In some cases, only a few cubes are covering the complete solution space, thus, some processors becomes idle. Additionally, due to the sparse mapping, the searching processors expand unnecessary configurations, because they receive no better ones. For smaller cube sizes, the load is nearly equally distributed. For the rest of the experiments we choose $b = 16$.

To compare the run-times, we have run every benchmark problem 12 times, deleted the lowest and highest planning times and computed the average of the remaining 10 values. The Cartesian resolution was chosen to be 20 *mm*, which leads (for a Puma260) to the discretisation $\Delta\Theta = [1.91°, 1.96°, 2.79°, 5.66°, 5.66°, 20.66°]$. According to the upper and lower joint limits of the Puma260, the C-space consists of $2.99*10^{11}$ states, which

[3] These benchmark problems can be downloaded from the Web page at http://wwwipr.ira.uka.de/~paro/skalp/

is at least 3 magnitudes greater, than in the examples of the references.

To calculate the speedups, we have run 8 parallel processes of the parallel algorithm on 1, 2, 4 and 8 processors, thus, guaranteeing an identical C-space decomposition. This method of measuring was necessary in order to obtain a fair comparison, because the search performance essentially depends on the C-space decomposition.

Figure 4 presents the parallel planning times and the achieved speedups for the benchmark problems. It can be seen that the parallelizing results in a reduction in planning times, and that the speedups are linear, and sometimes even superlinear. Three of four planning times range below 5 seconds. Only the benchmark problem DETOUR needs about 20 seconds planning time [19].

5 Conclusion and Future Work

In this paper, we have introduced a new approach to parallel motion planning for industrial robot arms with 6 DOF. The algorithm works in an implicit and discretisized C-space and the collision detection is done in the Cartesian workspace by distance computation. This avoids the time- and memory consuming obstacle transformation and C-space calculation. The method is based on the A*-search algorithm and needs no essential off-line computation. This approach enables the motion planner to work reasonably fast in dynamic environments.

The parallelization with static load balancing results in an equal load distribution and shows linear and sometimes even superlinear speedups. Further acceleration of the motion planner is possible by distributing communication, which can be done using a mesh-based communication network [18].

Based on these results, we now focus on developing a motion planner which is able to cope with moving obstacles, such as other robots. With some modification, our approach is also suitable for tasks in the area of virtual engineering. Instead of planning the path for robots, we are able to search a trajectory for the sub-components, which have to be mapped onto another object.

To further increase the speed of the algorithm, we are currently working on a hierarchical on-line discretisation of the C-space, thus reducing the enormous size of the search space [19]. The planning strategy will also be enhanced by a multi-directional search [1]. Additionally, for running the computed trajectories on a real robot, we are working on a path smoothing algorithm [2].

6 Acknowledgement

The project "Scalable algorithms for parallel motion planning in dynamic environments" is funded by the German Basic Research Framework (DFG-Schwerpunktprogramm) "Efficient algorithms for discrete problems and their applications".

7 References

[1] Beeh F.: „Erweiterung des parallelen Bewegungsplaners", Master's Thesis, Insitute for Real-Time Computer Control Systems and Robotics, University of Karlsruhe, 1997.

[2] Bordon U.: „Parallele Glättung von Robotertrajektorien", Bachelour's Thesis, Insitute for Real-Time Computer Control Systems and Robotics, University of Karlsruhe, 1997.

[3] Challou D.J.; Boley D.; Gini M.; Kumar V. : „A parallel formulation of informed randomized search for robot motion planning problems", IEEE Int. Conf. on Robotics and Automation, Nagoya, Japan, May 21-27, 1995.

[4] Fiorini P., Shiller Z.: „Time optimal trajectory planning in dynamic environments", IEEE Int. Conf. on Robotics and Automation, vol. 2, pp. 1553-1558, 1996.

[5] Fujimura K.: „Motion planning in dynamic environments", Berlin, Heidelberg, Springer, 1991.

[6] Henrich D., Cheng X., "Fast Distance Computation for On-line Collision Detection with Multi-Arm Robots", IEEE Int. Conf. on Robotics and Automation, Nice, France, May 10.-15., pp. 2514-2519, 1992.

[7] Henrich D.: "A review of parallel processing approaches to motion planning", In: Proceedings of the IEEE International Conference on Robotics and Automation, Minneapolis, Minnesota, USA, April 22-28, 1996, pp 3289-3294.

[8] Henrich D., Gontermann St., Wörn H.: „Schnelle Kollisionserkennung durch parallele Abstandsberechnung" In: 13. Fachgespräch Autonome mobile Systeme (AMS´97), Stuttgart, 6. + 7. Oktober, Springer-Verlag, Reihe „Informatik Aktuell", 1997.

[9] Henrich D.: "Fast motion planning by parallel processing – A review", In: Journal of Intelligent and Robotic Systems, vol 20, no 1, pp 45-69, Sept 1997.

[10] Hwang Y. K., Ahuja N., "Gross motion planning – A survey", ACM Computing Surveys, vol 24, no 3, Sept. 1992.

[11] Kamal L., Gupta K., del Pobil, A.P.: „Practical motion planning in robotics: Current approaches and future directions", IEEE Robotics & Automation Magazine, Dec. 1996.

[12] Katz G.: „Konzeption einer Entwicklungsumgebung unter ROBCAD für die parallele Bewegungsplanung", Insitute for Real-Time Computer Control Systems and Robotics, University of Karlsruhe, 1997.

[13] Mazer E., Ahuactzin J.M., Bessiere P., Chatroux T.: „Parallel motion planning with the Ariadne´s clew algorithm", ISER-93, 1993.

[14] Qin C., Henrich D.: „Path planning for industrial robot arms - A parallel randomized approach", In Proc. of the Int. Symp. on Intelligent Robotic Systems (SIRS´96), Lissabon, Portugal, pp. 65-72, July 22-26, 1996.

[15] Ralli E., Hirzinger G.: „A global and resolution complete path planner for up to 6 DOF robot manipulators", IEEE International Conf. on Robotics and Automation, Minnesota, 1996.

[16] Sandmann St.: „Entwicklung eines parallelen Bewegungsplaners", Insitute for Real-Time Computer Control Systems and Robotics, University of Karlsruhe, 1997.

[17] Verwer B.J.H.: „A muliresolution work space, multiresolution configuration space approach to solve the path planning problem", IEEE Conf. on Robotics and Automation, 1990.

[18] Wurll C., Henrich D.: „Ein Workstation-Cluster für paralleles Rechnen in Robotik-Anwendungen", In: APS´97, 4. ITG / GI - Fachtagung Arbeitsplatz-Rechensysteme, Koblenz-Landau, 1997.

[19] Wurll C., Henrich D., Wörn H.: „Parallele Bewegungsplanung in dynamischer Umgebung", Technical Report, no. 20/97, Faculty for Informatics, University of Karlsruhe, 1997.

Proc. of Third Int. Symp. on Artificial Life, and Robotics (AROB III' 98),
Oita, Japan, 19-21, January, 1998,

The Consciousness of Artificial Life

Roy Ascott
Centre for Advanced Inquiry in the Interactive Arts
University of Wales College
Newport NP6 1YG

Abstract

This paper addresses the relationship of consciousness to Artificial Life set in the context of art. Artificial Life is as much a part of our quest for self definition as an instrument in the construction of reality. In exploring the technology of life we are exploring the possibilities of what we might become. In our hypermediated, telematic culture, the self acquires an essentially non-linear identity. Telepresence, Virtual Reality, the avatars of Net life, present us with a distributed, multiple identity which in turn is producing a radically new art. This embodies an 'interstitial practice' set within the domain of Artificial Life, located at the intersections of cognitive science, bio engineering, telematics, and metaphysics.

Can artists find in Artificial Life, nanotechnology, robotics, molecular engineering the means towards a re-materialization of art, after its post-modern, screen based dematerialization? Just as ideas of the "immaterial" have dominated art discourse of the last fifteen years, so questions of emergent form, intelligent structures and Artificial Life are shaping a new discourse, from which art is moving off the screen and back into the material world. Will the real significance of art's re-materialization will be at the level of mind? Will Artificial Life only gain cultural significance when it gives rise to artificial mind and the construction of consciousness?

Introduction

In classical art, the Aesthetic of Appearance directed us only to the surface appearance of things. Our attention throughout this century has turned increasingly towards the invisible, to forces and fields, processes of chaos and complexity, and to the coming-into-being of form, meaning and consciousness [1]. Artificial Life, self-aware systems, the ubiquitous Net, Virtual Reality, Augmented Reality, intelligent architecture, things that think, are elements in an emergent world view which opens up unprecedented pathways for development in art and science, as well as demanding new moral and ethical values for the kind of worlds we can envisage and eventually construct. Equally, they challenge the immutability of human identity, offering the prospect of transformation and distribution of the self.

The history of this changing attitude has had as much to do with developments in science and technology as with aesthetics, philosophy or art practice. From the artist's point of view, our cultural immersion in interactivity, transformative systems and hyperlinked structures, set in virtual spaces, with world wide connectivity, is opening up immense possibilities of cultural innovation and artistic creativity. All fields of knowledge have become permeable, all systems connect. The paradox is that, after the gross materialism of the old industrial culture, relentlessly fueled by technology and science, the issues of consciousness, mind and spirit which are rising to the top of the artist's agenda are themselves instituted by technology and science. It is technology which is both informing and challenging our models of mind. It is hard science which is confronting the soft questions of philosophy.

The ways in which Art has responded to all of this and in a sense had anticipated it, is to be found in its conceptual provenance and in its embrace of digital and telematic systems. Art now is invested in what can be called a Technoetic Aesthetic, which is emerging from a substrate provided by the technology of Artificial Life, telecommunications and noetics, a technology which is bringing about a new human faculty, which I have called cyberception [2], and new models of mind.

The Matter of Mind

Mind is process not substance, or as William James pointed out, not a thing. Art which is invested primarily in qualities of connectivity, transformation and emergence, while not insubstantial, is full of mind. It is more than the apogee of the conceptual imperative which has shaped the art of this century, not withstanding the works of high artistic merit that this new field is producing. It is more than the triumph of process over thing. And while, as an end game, it may not yet compare with the 'great moments' of Western art history, it holds the promise of an art more radical and more transformative than any of the precursors of the 20th century avant-guard. And what promise! If Artificial Life and Artificial Intelligence will be the commanding technologies of the early part of the next century, then Artificial Consciousness will define the aesthetic. As the science of consciousness develops in consort with advances in biology and technology, art will increasingly inhabit the bio-telematic domain and illuminate the technoetic principle that informs it. Mind in telematic space is not only leading to new forms of human communication but to the reframing of consciousness itself.

To invoke 'artificial consciousness' is not to speak simply of the modification, augmentation or replacement of the human brain as it is presently understood, whether such processes be bionic or abiotic.

Nor is it only to recognise the increasingly cognitive quality of the tools, products and buildings that are now invested with intelligence: we are surrounded by things that think, or that at least are smarter than they used to be (and learning fast!). It is to place art at the centre of the cultivation of new fields of consciousness, creating conditions for emergent mind. And here I am pointing as much to new states of consciousness as to new acts of consciousness, states of mind supervenient on cyberception. There are acts of consciousness, functionally directed mental behaviour, which can be modeled and simulated by technology and to some degree transformed by it. David Chalmers [3] suggests that awareness is a better word to use for this aspect of consciousness, leaving the word consciousness itself to designate the much more enigmatic, unexplained and mysterious area of subjective experience, which he identifies as presenting the 'hard' problem.

The hard problem deals with the much more interesting issue of experience, about which Nagel has famously asserted 'there is something that it is like to be a conscious organism'[4]. Philosophers discuss the state of subjective experience or phenomenal consciousness in terms of *qualia*, the 'sensible qualities' of touch, smell, taste, hearing, sight, like redness or sweetness, for example. To which are added the qualia of felt emotion, bodily sensations, mental imagery, and the feeling of the flow of conscious thought. Qualia may be independent of physics, or at least of Newtonian physics (since who knows what quantum causalities there may be?). They may belong in the non physical realm of the mind. Or they may be epiphenomena causally dependent, or 'supervenient' on brain events but not straightforwardly identified with such events. *Techno-qualia*, new sensations and qualities of feeling resulting from technologically mediated experience need now be added to our repertoire. The 'easy' problems of consciousness, according to Chalmers, are those which seek to explain the ability to discriminate, categorize and react to environmental stimuli, the integration of information into cognitive systems, the reportability of mental states, the deliberate control of behaviour, the difference between wakefulness and sleep. They are those problem that cognitive science, using computational or neural models, can expect to deal with.

To understand why we are conscious in the way that we are, when seemingly a zombie could in many ways function as effectively in the world as we do without this add-on of subjective experience, poses the most intractable problems for philosophers. Why do we need this dimension of consciousness, what is it 'for'? How do I know you are not a zombie? I have only your verbal accounts to say you are not. How can I possible share your experience of yourself, your consciousness of self, to know what it is like to be you? How can a scientist or philosopher possibly 'understand' these states of experience. This is the 'hard' problem. It is our inner sense of being that cannot be explained. And because of our Western intellectual history, our felt sense of becoming is even more difficult for science to comprehend. But whereas the scientist seeks to understand consciousness, the artist seeks to construct it.

Art and Mind

From the artist's point of view, what is of interest in all of this is not just to play with the zombie aspect of awareness, the artistic exploitation of robots, androids, artificial brains, however fascinating their sensory or affective behaviour might be, but to work creatively with subjective consciousness, the state of consciousness in which someone or *something* knows what it I like to be itself....at least provisionally. It is worth emphasizing that this knowledge is provisional, not just because all knowledge 'about' the world is subject to revision, but because, as artists whose practice is invested in hypermedia and virtual space, in interaction with agents and avatars, and in the emergence of Artificial Life, we know so well that identity can be endlessly transformed. The immutability and unity of the self, so dearly prized in the European tradition, is giving way to an understanding of how we each can be involved in our own creation and re-creation, how even consciousness itself might be transformed, and how an artificial consciousness might be constructed. Just as we are now more interested philosophically in the nature of becoming rather than of being, so we see the self as an ongoing creation. And in cyberspace, the self is open to tele-differentiation, distribution and planetary dissemination. In consequence, a kind of non-linear identity is emerging.

Thus, as artists, our central interest in consciousness is the extent that we might reframe it, transform it, re-build it: the extent to which, in adopting a diversity of identities, modulating our sense of self, constructing new mental states, extending our range of qualia, we might play creatively with consciousness itself. We seek through technology to escape the constraints of the body, extend the mind, navigate the Net's planetary field of consciousness, seed Artificial Life , in order to reach a better understanding of our own capabilities and to create other ways of being. My computer is a sub-system of the system which is me, its processes are structurally coupled with my organic processes, together we constitute a whole autopoietic system. We share, in short, a field of consciousness. But my computer is also a network which is a node of a larger network, the Internet , the sum of all those networks sharing in a larger structural coupling with the world, in what might be seen as a planetary field of consciousness. My computer is an intrinsic part of me at two levels. At the general level, it is integral to all those technological tools and instruments of seeing, prostheses of the senses, that augment our view of the world. On the particular level, it is the interface to my communication with others, apart from those with whom I live or work in close physical proximity. It is where most of my memory is located. It prompts essential actions. It enables me to plan and configure. It checks for accuracy, it assists my imagination, it gives me access to databanks in every

realm of thought in every part of the world. Both scientists and artists are interested in what it is to be like this extended organism. The scientist wants to understand it, the artist wants to cultivate it, play with it, create with it, transform it. This extended organism is now integrally my self.

This extended organism, in its relationship with the emergent structures and complex systems of Artificial Life, enters the domain of an extended consciousness, artificial consciousness and constructed mind. Similarly, its habitat, an intelligent environment, will of necessity consist in an architecture which is seeded, grown and cultivated, bottom up.

Although the subject of intensive, consciousness remains an enigma. For art there can be no more compelling mysterium to work within. The space of technologically expanded consciousness is where artists will become most intensively involved, moving between these two spaces, the artificial and the psychic, frequently confusing the two, creating a double consciousness, a hybridization of the technoetic and natural mental states.

Cyberception

Cyberception is an emergent human faculty in which cognition and perception are not simply augmented by technology but are moved to another level of efficacy by the radical nature of the technologies involved. At a general level, we need only think of the collective intelligence of our planetary networks, what I have referred to as the Hypercortex, to see how profoundly this technological augmentation of memory, thought and perception is transforming our lives. At a more specific level , an important example is found in the technologically assisted perception of matter at the atomic level . The scanning tunneling microscope (STM) enables single atoms on a surface to be imaged, providing a view of matter at atomic scales. Significant as that undoubtedly is to the artist concerned to penetrate the material surface of reality, the more radical implication of this device is that it is at the same time used to manipulate single atoms, to move them about on a surface, and build atomic scale structures atom by atom . In this development, the eye's prosthesis becomes an instrument of material manipulation. In this sense the famous textual inscription in single atoms of xenon on a nickel surface which spelt out 'IBM' (an image roughly one nanometre square) was more than the ultimate miniaturization of the written word, it was the beginning of a process which, eventually, may lead to the word, as it were, becoming flesh, or at any rate the nanotechnological structuring of new material entities which may grow eventually to inhabit the world of Artificial Life.

What then is the significance of STM, and other reality building technologies, to human consciousness? Does it mean that to see is to build? To envision is thereby to realize? It may well be in the gardens of molecular biochemistry that the 21st century artist will play, rather than in the darkened vaults of computer science. But then, computer science itself is set to move from the bunker into the data garden, as interfaces become more humanly oriented and more subtly integrated into the information ecology.

The re-materialization of may eventually find a place in this quantum world. Art will then have moved decisively from the more or less passive perception and expression of the surface of the world to the active cyberception and bottom-up construction of quantum reality. The quantum computer along with the implications of coherent quantum matter and atom optics will eventually inform a future discourse of art, but these developments demand artistic and theoretical consideration now, just as the digital computer as it is presently constituted, called for an initial cybernetic discourse well before the technology had advanced to bring about its present common currency. Art is as much anticipation as reflection. Its antennae are always directed towards the future.

Art's Conceptual Provenance

The legacy of the art of this century, despite its existential anxiety and the pessimism wrought by gross industrialization, is that of reaching for the spiritual, plumbing the depths of the mind, navigating the immensity of memory, channeling the complexities of associative thought, finding ways to make visible the invisible. It has led to what we might now call the fluidity of identity and the hypermediation of knowledge and experience - the unconscious desire of post-modernism before it began its decline into a click-on culture. Because even post-modernism, rightly seen in its present form as the most malignant of cultural growths, began with a promise: to celebrate ambiguity, to reveal the multi-layered structures of reality, to release the self from its paralyzing singularity. Post-modernism started with the engagement of the viewer in the evolution of the thing viewed, and only at its demise saw the dis-engagement of the viewer from authentic experience and from life itself. It is this dis-engagement which vitiates the interactivity of the Net. It is this dis-engagement which leads to aimless surfing on the Net's insubstantiality rather than seeking in its productive potency routes towards the re-materialization of art.

Mind, organic and telematic, is inseparable from the activity of its interface. While mind is ubiquitous, it is only evident to us in the presence of matter. Thus to speak of art becoming material again or to assert that the process of becoming will be the material of art is not in contradiction to its conceptual provenance. Indeed the re-materialization of art is the necessary outcome of this period of immateriality. This process will not be confined to a silicon substrate, or the computer screen. Reframed consciousness, a planetary consciousness, is emerging in the Net but will find its fullest realization in Artificial Life, particularly as Artificial Life attains a more 'moist' identity, integrating with our own wet biology. Similarly, the technological externalization of the means by which meaning might materialize in a work of art (in the

frame of interactivity) corresponds to the telematic externalization of memory and the sensorium from the body (in the frame of connectivity). Interactivity, transformation and emergence form the canon of an art which is as much implicate as material, as much transient as continuous, and whose technoetic principle brings passion, reason and chance into a dynamic whole, affecting the shape of consciousness, the substance of behaviour, and thereby the construction of reality.

Towards Nature II

Finally, in a paper exploring consciousness and Artificial Life something must be said about Nature, and Art's fascination with mimesis, realism and the representation of life. It is often noted that we have lost touch with Nature. It is not so much that Nature has retreated, or that we destroyed or denied it. It is simply that the metaphors it has long supported no longer hold. The shelf life of all metaphors is limited, and Nature seems to be past its sell by date. It has served us well in many respects. The ultimate appeal, for example, in questions of justice, human behaviour, as in those of representation and figuration in the arts has always been - *is it natural?* Thus the popular artistic icon has been Van Gogh and for higher brows Cézanne, who, we are reminded, spent most of their time in the fields, *immersed* in nature . The scenario conveniently ignores Cezanne's comment that "all things, particularly in art, are *theory* developed and applied in contact with nature". Advanced imaging and telemetry systems, are yielding an entirely new kind of nature - its transformations of energy, its emergent behaviours, its order in chaos, the birth and death of galaxies, molecular life, quantum events - none of which is observable directly by the human eye, and none of which previously had been observed by human beings in the whole of recorded history. All of which presents a picture of nature quite unlike that 'staged' for our viewing by Western artists and writers for the past five hundred years. It is what I have called *Nature II* [5].All of this however, is nothing compared to the challenge that the advent of Artificial Life presents to art both in its practice and in its theory.

It was not always so. Sir Kenneth Clark, one of the last apologists of the old order, rejected artists who merely "refurnished their repertoire of forms from the laboratories (which) does not compensate for the loss of intimacy ... with which it was possible to contemplate the old anthropocentric nature. *Love of creation cannot really extend to the microbe...*[6] (my italics). Earlier, with the same patrician certainty, Bernard Berenson [7] , in trying to account for the "living force" which he found in the painting of Giotto, asserted that "there must exist surely a *viaticum* which bears its possessor to our own hearts , across the wastes of time, some secret which Giotto possessed....What is this life conserving virtue - in what does it consist? The answer is brief - *in life itself.* If the artist can cunningly seize upon the spirit of life and emprison it in his paintings, his works....will live forever". These two texts, sentimental and superstitious in turn, spoke for both the confusion and the desires of a culture at its turning point, in confronting the questions: how do we *realise* nature and *evoke* life, in what do they consist, how may they be re-created and transmitted? These questions remain those which artists today prioritize , but the advent of Artificial Life, and new models of reality provided by physics and biology, combined with our insight into ancient forms of based in mysticism and psychic awareness, lead us instead to ask , " what might nature *become*?" . And with knowledge and perception increasingly mediated by computer-based systems, bionic prostheses and telepresence, the question " what is reality?" is being replaced by "how do we interact with a proliferation of separate realities" .

Conclusions

In a paper which has had significant influence on art thinking, Christopher Langton has described how 'life emerges out of the organised interaction of a great number of non living molecules, with no global controller responsible for the behavior of every part'[8]. This equally describes the emergence of meaning from the interactivity of the Net, whose art has no overall author. Here the art, the artist and the viewer are one. Similarly, the 'moist' materialization of art in the post-biological culture of Artificial Life will integrate symbiotically with our own wet biology rather than stand separate as a discrete entity or art object. While science is redefining our ideas about the nature of the world and of ourselves, the artist is creating an art which sees its content and meaning as the product of the viewer's interaction and negotiation. Here is an art which is unstable, shifting and emergent; an art which parallels life, not through surface representation, but in its processes of unfolding and transformation; an art which favors the ontology of becoming, rather than the assertion of being; an art embracing Artificial Life and building bottom up on its principles; an art, finally, which reframes consciousness, while proposing new realities. At the centre of these developments is the technoetic principle, with consciousness, given and constructed, as the field of art's unfolding.

References

[1] Ascott R (1995)Apparitional Aesthetics.In: Leopold-seder H (ed) Internationales Kompendium der Computer-künste '95. Östereichister Rudfunk,Linz pp.15-22..

[2] Ascott R (1995). The Architecture of Cyberception. In: M. Toy (ed) Architects in Cyberspace. Academy Editions, London, pp 38-41

[3] Chalmers D (1996) The Conscious Mind. Oxford University Press, New York.

[4] Nagel T (1974) What is it like to be a bat? Philosophical Review, **83**, pp. 435-51

[5] Ascott R (1993) Zurück zur (künstlichen) Natur. In: Kaiser G, et al (eds) Kultur und Technik im 21. Jahrhundert. Campus Verlag, Frankfurt, pp. 341-355

[6] Clark K (1953) Landscape into Art . Murray, London

[7] Berenson B (1897) The Central Italian Painters of the Renaissance. Putnam, London.

[8] Langton CG (1989) Artificial Life. In: Langton CG (ed) Artificial Life. Addison-Wesley, Redwood City,p.2

Proc. of Third Int. Symp. on Artificial Life, and Robotics (AROB III' 98),
Oita, Japan, 19-21, January, 1998,

Artistic Communication for A-Life and Robotics

Naoko Tosa
ATR Media Integration & Communications Research Laboratories
2-2, Hikaridai, Seika-cho, Soraku-gun, Kyoto, 619-02 Japan
tosa@mic.atr.co.jp

Abstract

In researches concerning communication between machine and man involving artificial life and robotics today, realization of sensitive communication by introducing an artistic interface is drawing attention. In this session, we would like to discuss about the artistic human like communication researches applying artificial life and robotics researches which would become necessary with increasing need for man-machine communication. I have invited an artist involved with this theme, a critic in media art, a scientist, and a biologist. They will introduce their researches from their view points, and we will introduce our artificial intelligence works capable of communicating with humans.

1. Introduction

Humans cannot live alone. A human is basically a creature who longs for communication with humans and things. By showing affection to someone or something, teasing someone, or personalizing things, a human is spiritually satisfied. In the future, humans will tend love or hate the computers that will fill our lives. In order to co-exist with computers, we are forced to change our lifestyles. In our life today, however, it is nearly impossible to avoid communication with computers.That is why sensitive communication with computers becomes important. Although, computers are essentially unfriendly, they can be made friendly by the skillful design of computer software and hardware. In this paper, we introduce an AI computer system featuring an interactive theater in which a person can create an impromptu poem and participate in a play while communicating with AI characters capable of sensing human emotion.

2. Interactive Poem

We propose a new type of speech-based interaction system called "Interactive Poem" (Fig. 1). A human and a computer agent create a poetic world by exchanging poetic phrases, thus realizing emotion-based communications between computers and humans. As a first step toward emotion-based communications between computer agents and humans, we have developed several computer agents such as "Neuro Baby"[1] and "MIC and MUSE"[2]. These are computer characters that are capable of recognizing several emotions in speech and reacting to them by changing their facial expressions and body motions. Fortunately, these agents have been very successful and have been demonstrated at various exhibitions. As a next step toward the realization of feeling-based communications between computer agents and humans, we selected "poem" as a means of communications.



Fig. 1 Interactive Poem

There are several reasons for this approach. The main reason is that in a poem not only the meaning of words or phrases but also the rhythms and moods created by their sequence plays an essential role. Therefore, the poem is intended to transmit feeling information such as mood and sensitivity rather than logical information. The second reason is that poems were originally expressed by oral reading rather than in writing. This means that a poem is suitable for interaction between computers and humans. Recently, researchers have shown increased interest in the realization of feeling-based interactions and communications between computers and humans[3][4][5]. However, only a few have worked on voice communications, despite the fact that voice is an essential means of feeling-communications. This is the third reason for our interest in developing communications based on an uttered poem. This paper next explains the basic principles of the Interactive Poem system we have developed based on the above concept. The software configuration and hardware configuration are then described in detail. Finally, a typical installation of the Interactive Poem system is introduced. "Interactive poem" is a new type of poem that is created by a participant and a computer agent collaborating in a poetic world full of inspiration, emotion and sensitivity.

3. Concept of Interactive Poem

My interest is in how to generate feeling in communication between people and intelligent characters. Also, I'm interested in creating an intelligent character's consciousness. The computer-generated poet "Muse" can make a poem with you interactively and in real time. Interactive poetry has its roots in old Japanese culture as a type of poem called "renga" . "Renga" is a kind of haiku. Haiku was created in the Edo era "beginning in the 1600's" and is a typical expression of Japanese sensibility. "Renga" is a combination of short poems and generated by multiple people. For example, one person makes the first short poem, and another person makes the second short poem.

A computer agent called "MUSE", who has been carefully designed with a face suitable for expressing the emotions of a poetic world, appears on the screen. She will utter a short poetic phrase to the participant. Hearing it allows him/her to enter the world of the poem and, at the same time, feel an impulse to respond by uttering one of the optional phrases or by creating his/her own poetic phrase. Exchanging poetic phrases through this interactive process allows the participant and MUSE to become collaborative poets who generate a new poem and a new poetic world.

4. Software Configuration

The system used to create the interactive poem consists of four main units: system control, speech recognition, computer graphics generation and speech output (Fig. 2).

The system control unit manages behavior of the whole system by utilizing the interactive poem database. In this system, the most important issue is constructing the interactive poem, so we must first explain how the interactive poem database is constructed. A conventional poem is considered a sequence of poetic phrases. In other words, the basic construction of a conventional poem can be expressed by a simple state-transition network where each phrase corresponds to a given state, and for each state there is only one successive state (Fig. 3-A).

The basic form of the interactive poem is expressed by this simple transition network, but it differs from a conventional poem in that phrases uttered by the computer agent and phrases uttered by a participant appear in turn. This corresponds to a simple interaction where the computer agent and the participant alternately read a predetermined sequence of poetic phrases (Fig. 3-B).

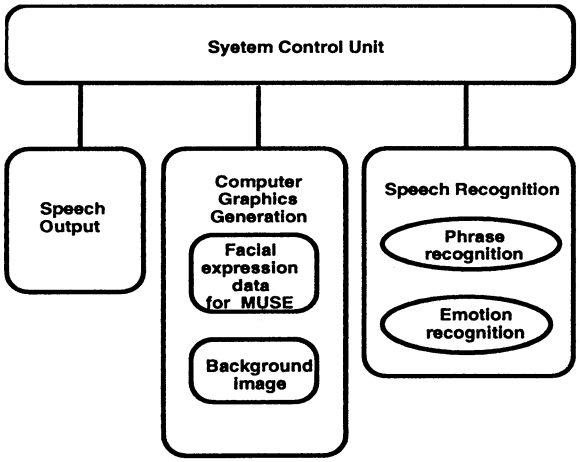


Fig. 2 Block diagram of the Interactive Poem

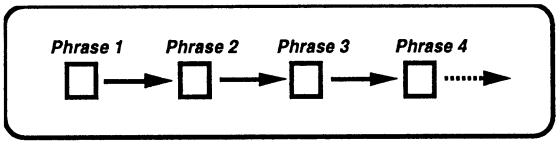


Fig. 2-A Conventional poem

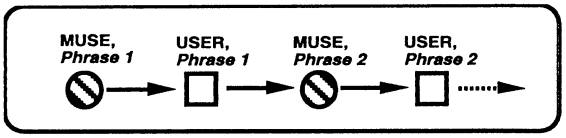


Fig. 3-B Construction of the Interactive poem(a)

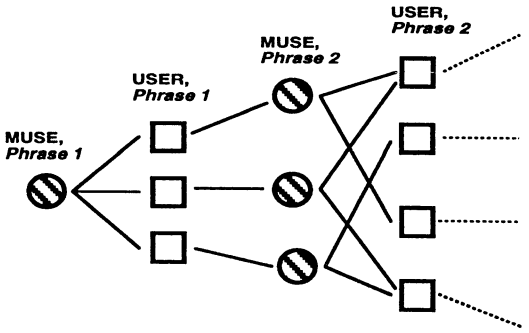


Fig. 3-C Construction of the Interactive Poem(b)

To introduce improvisational interaction into our system, we modified this simple transition so that multiple phrases are connected to each phrase of the computer agent (Fig. 3-C). These phrases are carefully created and chosen by taking into account how well their rhythms are formed and the meaning of each phrase. This transition network is stored in the interactive poem database and used to control the whole process.

The speech recognition unit has two different speech recognition functions: phrase recognition and emotion recognition. To recognize each phrase uttered by a participant, we have adopted HMM (hidden Markov model) based speaker-independent speech recognition technology. Each phrase to be uttered is represented in the form of a phoneme sequence and stored in the lexicon (Fig. 4). To simultaneously detect the emotional state of a participant, an emotion recognition function is introduced. A neural network architecture has been adopted as the basic architecture for emotion recognition. This neural network is trained with the utterances of many speakers to express the eight emotional states of joy, happiness, anger, fear, teasing, disgust, disappointment and emotionlessness. As such, speaker-independent and content-independent emotion recognition is realized (Fig. 5).

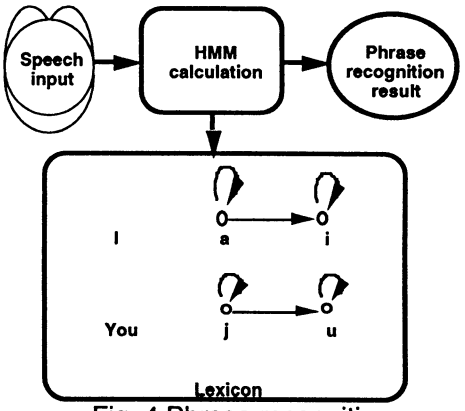


Fig. 4 Phrase recognition

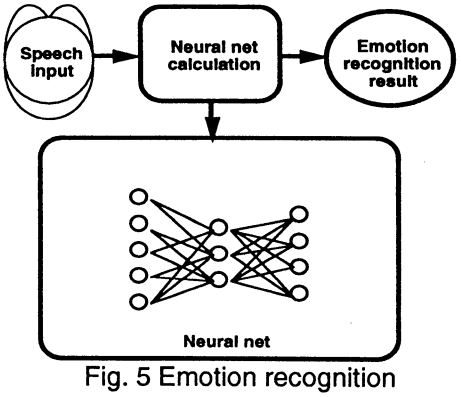


Fig. 5 Emotion recognition

Reaction of the computer agent to utterances of a participant is expressed through her speech and by images. In the speech output unit, speech data for each phrase to be uttered by the computer agent is digitally stored and generated when necessary.

The computer graphics generation unit controls image reaction of the computer agent. Image reaction consists of two kinds of images: facial expressions for the computer agent "MUSE" and various scenes. The facial expressions of MUSE express her reactions to the emotional state of the participant. These images are represented by keyframe animations, each of which corresponds to the eight emotions (Fig. 6). To express the atmosphere of the interactive poem, several kinds of scenes are digitally stored. Each scene image corresponds to a group of states in the transition network, and each correspondence is carefully determined in advance.

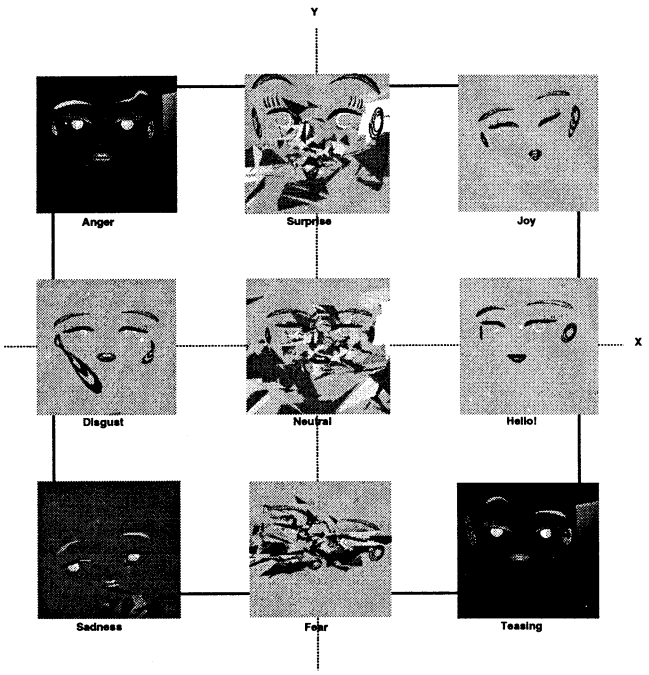


Fig. 6 Muse's emotional expression

5. Hardware Configuration

This mainly consists of several workstations and a PC: a workstation for computer graphics generation, a workstation for both system control and phrase recognition, a workstation for emotion recognition, and a PC for speech output. For the participant's convenience, optional phrases that may be uttered following an utterance of MUSE appear on the display. The participant can choose one of these phrases based on their feelings and sensitivity, or they can create their own poetic phrase. Regardless, the emotion recognition function can produce a result. In addition, the phrase recognition function selects the pre-existing phrase that most closely resembles the uttered phrase. Therefore, the participant feels as if the interactive poem process continues in a natural way (Fig. 7).

6. Interactions

The interaction mechanism operates as follows.
(1) When MUSE utters a phrase, the recognition process is activated. A participant then utters a phrase and it is

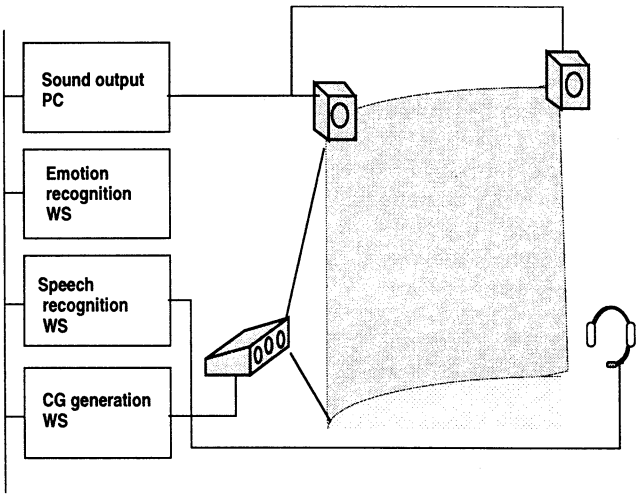


Fig. 7 Interactive Poem hardware configuration

recognized by the phrase recognition function, which uses the lexicon subset corresponding to the next set of phrases in the transition network. At the same time, the emotion contained in the utterance is recognized by the emotion recognition function.
(2) Based on information pertaining to recognition and the transition network, the system's reaction is decided. The facial expression of MUSE changes according to the results of emotion recognition, and the phrase MUSE utters is based on the results of phrase recognition and the transition network. The background scene changes as the transitions continue.
(3) In the above manner, poetic phrases between MUSE and the participant are consecutively produced.

7. Interactive cinema with emotion recognition

As a media artist, I've always been fascinated by the idea of entering the world of movies I created myself. In interactive art, one can interact with movies in virtual reality. My vision was to create a work in which I can talk to characters of my own creation as if they were alive and feel the excitement of dramatically changing a virtual reality world. One could say this experience resembles the world of dreams. In a dream, we autonomously communicate with the characters and objects we encounter, and the world is a series of fragments of images with or without context. Characters in a dream fascinate us with their mysterious behavior. What happens in a dream resembles being emotionally involved with movies in a movie theater. The difference is that we are more autonomous in dreams. We have begun research on this electronic daydreaming as the next generation of cinema. In this paper, we introduce the design of attractive characters that are capable of recognizing emotion from the tone of a human voice.

7. 1. Interactive Character's design

"MIC" is a male child character. He has a cuteness that makes humans feel they want to speak to him. He is playful and cheeky, but doesn't have a spiteful nature. For example he is the quintessential comic character.

7.2 Emotion

(1) MIC recognizes the following emotions from intonations in the human voice. An asterisk indicates how the user should make intonations. The physical form of intonations is called prosody, and how to treat prosody will be discussed in Section 4.

a. Joy (happiness, satisfaction, enjoyment, comfort, smile)
 * exciting, vigorous, voice rises at the end of a sentence
b. Anger (rage, resentment, displeasure)
 * voice falls at the end of a sentence
c. Surprise (astonishment, shock, confusion, amazement, unexpectedness)
 * screaming, excited voice
d. Sadness (sadness, tearful, sorrow, loneliness, emptiness)
 * weak, faint, empty voice
e. Disgust
 * sullen, aversive, repulsive voice
f. Teasing
 * light, insincere voice
g. Fear
 * frightened, sharp, shrill voice

7.3 Communication

In most cases, the content of a media transmission conceals the actual functions of the medium. This content is impersonating a message, but the real message is a structural change that takes place in the deep recesses of human relations. We aim for this kind of deep communication. People use a microphone when communicating with MIC. For example, if the participant whistles, MIC's feeling is positive and he responds with excitement. If the speaker's voice is low and strong, MIC's feeling is bad and he gets angry.

8. Processing

This section describes the principles and operational details for the recognition of emotions included in speech. It also, explains the generation process of Neuro Baby's reactions, which correspond to the emotions it receives.

8.1 Basic principle

NB has advanced from its original version through several stages[1][6] to "MIC & MUSE." In our present research, we tried to realize higher-level processing that can achieve more sophisticated interactions between NB and humans. For this purpose, we have emphasized the following issues in our work.

(1) Treatment of various emotional expressions

How many and what kinds of emotional expressions to be adopted are both interesting and difficult issues. In our previous study, we investigated four emotional states[1]. Based on our experiences of demonstrating the first version NB to a variety of people and on the belief that an increased number of emotional states would make the interaction between NB and humans richer, this study encompasses the seven emotional states described in Section 8.2.

(2) Speaker-independent and content-independent emotion recognition

Speaker independence is an important aspect of speech/emotion recognition. From a pragmatic viewpoint, a speaker-dependent emotion recognition system requires a tiresome learning stage each time a new speaker wants to use the system; therefore, it is not easy to use. Moreover humans can understand the emotions included in speech, as well as the meaning conveyed by speech, even for arbitrary speakers. Also, content independence is indispensable for emotion recognition. In daily communication, various kinds of emotions are conveyed by the same words or sentences; mastering such nuance is the key to rich and sensitive communications among people. Therefore, by adopting a neural network architecture and by introducing a training stage that uses a large number of training utterances, we have developed a speaker-independent and content-independent emotion recognition system.

8.2 Block diagram of the processing

Fig. 8 is a block diagram of the processing flow. The process mainly consists of three parts: speech processing, emotion recognition and generation of reactions. In the speech processing part, feature parameters of input speech are extracted in real time in the feature extraction stage. Then, by observing the speech power, the period where speech exists is extracted. From the extracted speech, feature parameters are extracted and arranged as an output of the feature
extraction stage. This output is fed into the emotion recognition part, where two-stage emotion recognition is carried out. In the first stage, a combination of plural neural networks each of which is designed and trained to recognize a specific emotion in speech, receives feature parameters and carries out a recognition process. In the second stage the multiple output of the first stage is processed through a specialized logic, and the emotion recognition results are expressed as points on a two-dimensional space on which eight emotions including neutral state are displayed according to our criteria listed in 7.3. The result's position on the emotion plane and its movement determine the reaction of neuro baby, including its facial expressions and actions. These facial expressions and actions were previously created by an intuitive design process developed by one of the authors. These reactions are visualized with computer graphics along with appropriate speech output.

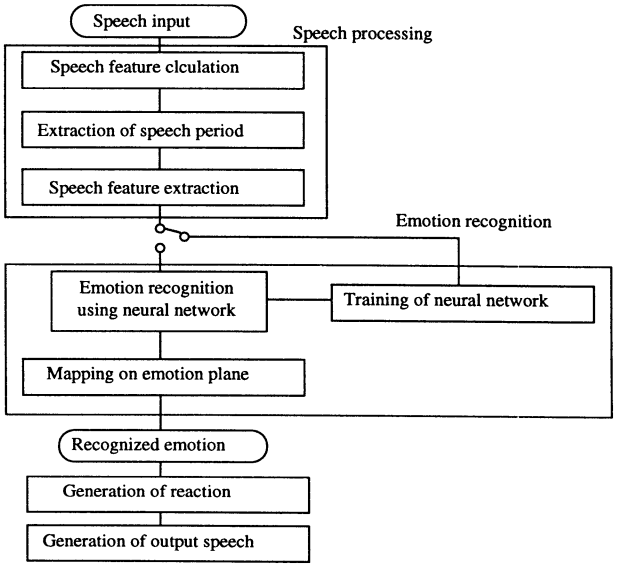


Fig. 8 Blockdiagram of the processing flow

(1) Configuration of neural network

The neural network for emotion recognition is a combination of eight sub-networks (Fig.9). The decision logic stage combines the outputs of theses sub-networks and outputs the final recognition result. Each sub-network is tuned to recognize one of seven emotions (anger, sadness, happiness, fear, surprise, disgust, and teasing) and neutral emotion. Basically, each sub-network has the same network architecture(Fig. 10). It is a three-layered neural network with 150 input nodes corresponding to the dimension of speech features, 20 to 30 intermediate nodes and one output node.

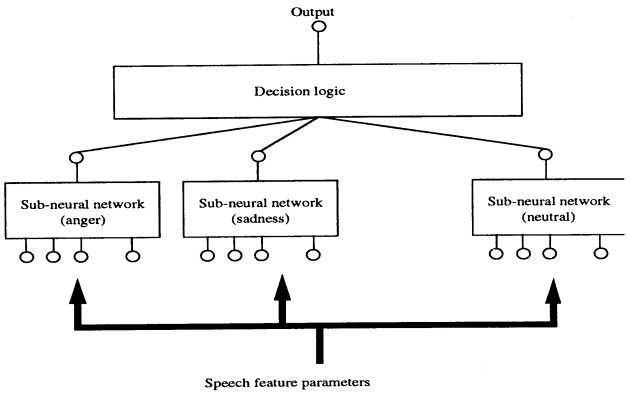


Fig. 9 Configuration of emotion recognition part

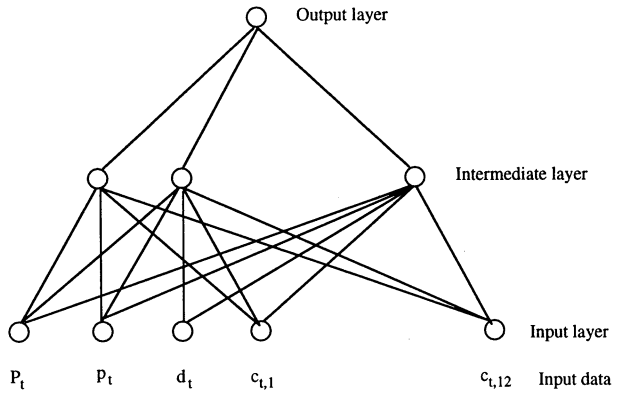


Fig. 10 Configuration of a sub-network

(2) Neural network training

To recognize emotions, it is necessary to train each of the sub-networks. Since our target is speaker-independent and content-independent emotion recognition, the following utterances were prepared for training.

Words: 100 phoneme-balanced words
Speakers: five male speakers and five female speakers
Emotions: neutral, anger, sadness, happiness, fear, surprise, disgust, and teasing
Utterances: Each speaker uttered 100 words eight times. In each of the eight trials, he/she uttered words using different emotional expressions. Thus, a total of 800 utterances for each speaker were obtained as training data.

Using these utterances, we carried out various preliminary training tests. It turned out that preparing two kinds of networks for each emotion, one for male speakers and the other for female speakers, is better than preparing only one network to handle both male and female utterances. In other words, the emotional expressions between males and females are somewhat different and cannot be handled together. The reason for this is not clear and will require further research.

(3) Emotion recognition by a neural network

In the emotion recognition phase, speech feature parameters extracted in speech processing are simultaneously fed into the eight sub-networks and trained as described above. Eight values, V=(v1, v2, ..., v8), are obtained as the result of emotion recognition.

(4) Mapping on an emotion plane

As described above, the output of the emotion recognition network is a vector V=(v1, v2, ..., v8) and the final recognition result should be obtained based on V. In our previous study, we expressed the final emotion state by a point on a two-dimensional plane. Based on the experiences of previous research, in the present study the positions of the eight emotions have been rearranged on emotion plane E (Figs.11).

It is necessary, therefore, to carry out the mapping from V onto E. Let m1 and m2 be the first and second maximum values among v1, v2,...., v8, and also let (xm1, ym1), (xm2, ym2) be the emotion positions corresponding to m1 and m2, respectively. The final emotion position (x, y) is calculated by

$$x = c*xm1 + (1-c)*xm2,\quad y = c*ym1 + (1-c)*ym2$$

(c:constant value).

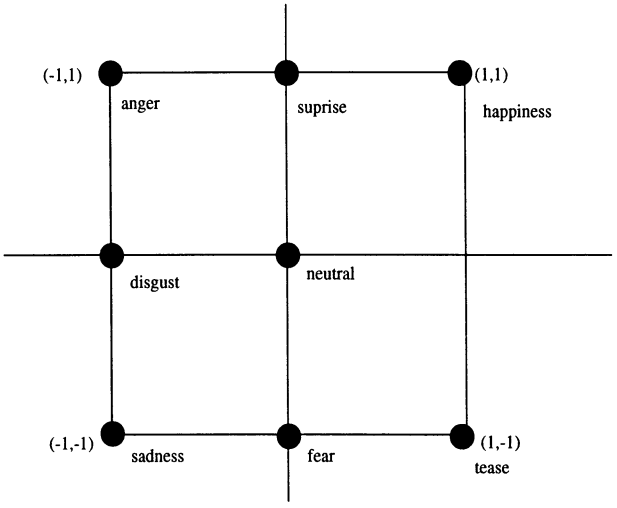


Fig. 11 Emotional plane

8.3 Generation of reaction and selection of output speech

(1) The structure of animation

There are four emotion planes, all of which use the same x,y data (Fig. 11).

a. Plane "a" generates facial animation by choosing the three key frames closest to the (x,y) data point. The computation of a weighted mean frame is done as follows. Let "A" be the area formed by the three key frames, and a1, a2, and a3 the areas shown in Fig. 6. Accordingly, the three weights for each key frame are A/a1, A/a2, and A/a3, respectively. The interpolated frame is then calculated by a weighted average of the three key frames.

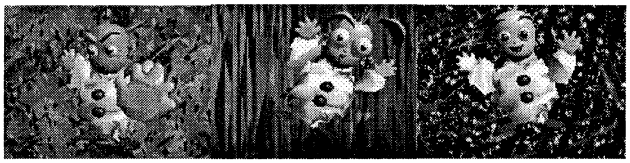
b. Plane "b" generates an animation of the character's body by mapping each (x,y) data point on the plane to a body key frame.

c. Plane "c" is a mapping of each (x,y) data point to camera parameters such as zoom, tilt, and pan.
d. Plane "d" is a mapping of each (x,y) data point to background tiles.
(2) Selection of output speech

From a mapping from the (x,y) data points of the emotion plane to 200 sampled speech utterances, one of the utterances is selected as the output speech. A personal computer is used to play the selected sounds.

8.4 Reaction of the characters.

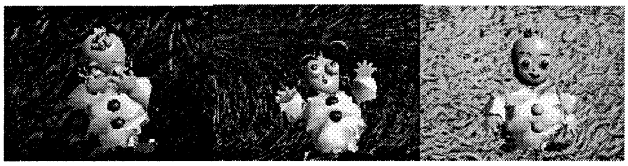
The reactions of MIC could be carefully designed and were visualized with computer graphics. Several examples of emotional expressions by MIC are shown in Fig. 12.



Anger Suprise Joy



Disgust Sleeping Happy



Sadness Fear Teasing

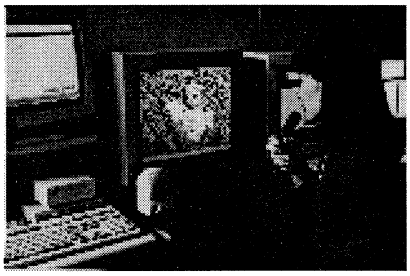


Fig. 12 Example of interaction between Muse and the participant

9. Conclusion

This paper describes two new areas of applied research in artificial life:the "Interactive Poem " created by the interaction between a human and an anthropomorphic computer-generated poet named "MUSE"; and, as pert of next-generation interactive movies, the design of characters that can sense human emotions based on computer graphics. Research in these areas is now expanding into a movie description system consisting of an interaction manager, scene manager, script manager and other functions that enable character scenes and stories to change dynamically. Here, while the properties of anthropomorphic artificial-life characters are often set by internal design, they may also turn "good" or "bad" according to environmental settings and the scheme adopted for communicating with humans. The internal design of characters depends heavily on artificial-life technology, and the ability to communicate requires that an environment be established in which emotions can be introduced naturally. The ultimate objective of combining art with artificial-life research is to achieve works that impact viewers in a new and powerful manner. In this regard, the time is coming when artists and researchers must develop a sharp sense of the best techniques for efficient artistic expression, or in other words, the means of achieving a between technology and creativity.

References

[1] N. Tosa et al., "Neuro-Character," AAAI'94 Workshop, AI and A-Life and Entertainment (1994).
[2] N.Tosa and R. Nakatsu, "Life-like Communication Agent--Emotion Sensing Character 'MIC' and Feeling Session Character 'MUSE'," Proceedings of the International Conference on Multimedia Computing and Systems, pp.12-19(1996).
[3] P. Maes, T. Darrell, B. Blumberg and A. Pentland, "The ALIVE system: Full-body interaction with autonomous agents," Proc. of the Computer Animation'95 Conference (1995).
[4] K. Perlin, "Real-time responsive animation with personality," IEEE Transactions on Visualization and Computer Graphics,Vol.1,No.1 pp.5-15 (1995).
[5] J. Bates, B. Loyall and S. Reilly, "An architecture for action, emotion, and social behavior," Proceedings of the Fourth European Workshop on Modeling Autonomous Agents in a Multi-Agent World (1992).
[6] N. Tosa, et al., "Network Neuro-Baby with robotics hand," Symbiosis of Human and Artifact, Elsevier Science B.V. (1995).

Proc. of Third Int. Symp. on Artificial Life, and Robotics (AROB III' 98),
Oita, Japan, 19-21, January, 1998,

Evolution as artist

T. Ray
ATR Media Integration & Communications Research Laboratories
2-2, Hikaridai, Seika-cho, Soraku-gun, Kyoto, 619-02 Japan
+81-7749-5-1063, E-mail:ray@hip.atr.co.jp

Proc. of Third Int. Symp. on Artificial Life, and Robotics (AROB III' 98),
Oita, Japan, 19-21, January, 1998,

Communications, Artificial Life, and Art

Ryohei Nakatsu
ATR Media Integration & Communications Research Laboratories
2-2, Hikaridai, Seika-cho, Soraku-gun, Kyoto, 619-02 Japan

Abstract

Studies which examine how the computer can support human communications have been the main research issue for artificial intelligence (AI) researchers. However, since human communications has various aspects, it is necessary for researchers to take into account other approaches. This paper considers the basic issues of human communications and points out that the artificial life (AL) approach and artistic approach should be integrated with the conventional AI approach. It also presents examples of research being performed based on this perspective.

1. Introduction

Communication is a basic intellectual human activity. Therefore the research that examines how the computer can support communications between humans and between humans and computers is an important research issue. So far, artificial intelligence (AI) researchers have been studying this research topic by placing emphasis only on the logical aspects of communications. However, in human communications other information, such as non-logical information or non-verbal information, is exchanged. To treat these types of information , AI researchers have to adopt different approaches and integrate them with their traditional approach. Artificial life (AL) research, whose main purpose is to study "life" at its very basic level, will supply many useful viewpoints and research tools. On the other hand, as artists have been dealing with non-logical information for such a long time, it will be fruitful for AI researchers to carry out collaboration with artists.

This paper first examines the basic aspects of human communications and points out that the AL approach and artistic approach should be integrated with the conventional AI approach for communications research. It also presents examples of research being performed at the ATR Media Integration & Communications Research Laboratories.

2. Human Communications and AI[1]

The human communications mechanism can be explained by using a two-layer model (Fig. 1). The first layer, which is on the surface, enables communication based on using languages. Researchers in the field of AI have been concentrating on this area. For example, speech recognition research has only been involved with the logical information involved in speech. However, it is easy to see that this logical information is only a part of the information involved in speech, which contains other, rich forms of information such as that concerning emotions and sensitivity. Information on such things as emotions

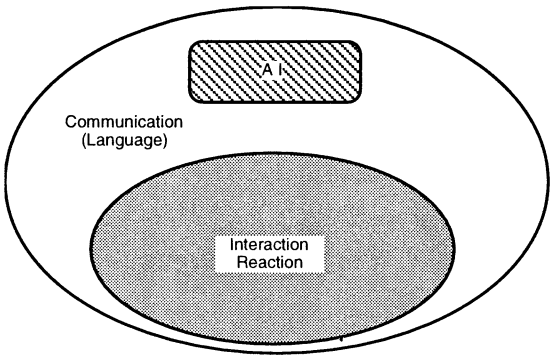


Fig. 1 Communication Model

comes from a deeper layer called the interaction layer, which is the second layer. The interaction layer controls interactive behavior, e.g., the timing for exchanging utterances or turn-taking tactics, in human communications. This layer also controls very basic behaviors like turning our face toward the direction of a sound or closing our eyes upon suddenly sensing a strong light. These functions are considered to be important keys to human-like behavior in daily life.

In the above way, we can say that low-layer functions, which differ from those that deal with logical actions and logical information on a higher layer, play an important role in human communications, and that non-language information, like emotions and sensitivity, is generated and understood by these functions in the lower layers. To therefore achieve comprehensive human communications functions that also include the transmission and reception of non-logical information, the mechanisms of the above interaction and reaction layers must be researched and eventually integrated with the functions of the top communication layer.

3. Aspects of Human Communications

As described above, human communications does not stop at logical information; it includes a wealth of non-logical information that plays a major role in daily communication. We can now pose the question: from what points of view should this kind of information be dealt with? In response, we can say that non-logical information is deeply related to various levels of behavior in human communications, and must therefore be dealt with in terms of the following aspects.

(1) Basic behavior in human communications

Basic actions in human communications, such as the rhythms/timing of conversation and natural gestures, are key research areas.

(2) Group behavior in human communications

While engaged in person-to-person communication, a

human being also communicates as a member of a group. To develop technologies for future communications, therefore, it is necessary to study the basic mechanism of human group behaviors.

(3) High-order behavior in human communications

Humans can engage in communication containing even higher orders of non-logical information. The impressions felt when viewing or listening to a great work of art or music are clearly high-order information, different from the handling of low-order sensory information. When studying human communications, this high-level communications must be considered.

The following sections will describe the way that research should proceed for each of the above aspects, and will introduce studies now being performed at the ATR Media Integration & Communications Research Laboratories as concrete examples of research on the human interface.

4. Basic Behavior in Human Communications

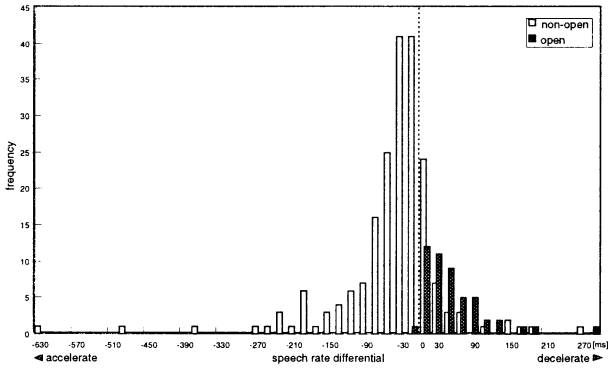
4.1 Approach

The study of basic behaviors in human communications is important because of the following reasons. In addition to human beings, future society will feature virtual entities created by computers. These entities, or "agents," are expected to play a major role in our lives, and as they take on a ubiquitous existence, human beings will have no choice but to coexist with them. The agent side in such a society will therefore have to act in a manner that satisfies the basic and natural nature of communication. For that purpose, it is necessary to observe how people talk to each other and utilize conversation analysis to clarify the basic mechanism and model of human communications and to incorporate it into agents. In this way, agent behavior can be made more human. This approach, which is a sociological and psychological approach rather than an AI approach, will be indispensable for the study of the non-logical aspect of human communications.

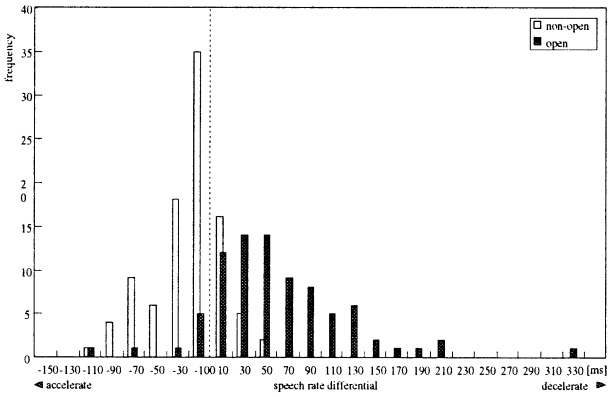
4.2 Research example: rhythm in conversation[2]

Based on the above ideas, we are focusing certain research on the subject of observing and analyzing communication activities among people. Here, we describe the observation of rhythm in a conversation between people as a specific example of this research work.

While it has already been shown that two speakers in a conversation will mutually adjust their response time and speech rate, this research has only been done in a qualitative manner. Here, we will focus on "rhythm" in conversation and observe the way in which rhythm is adjusted between two speakers engaged in a conversation. The target conversation of this analysis is the "Chiba University Map Problem Corpus." This is a task performed over the telephone whereby one speaker informs another speaker of a route on a map. Here, one unit of speaking delimited by an interval of silence is called a sub-utterance unit (SU), and the average mora duration (AMD) within a single SU is taken to be an evaluation standard when measuring rhythm. Two adjacent SUs are called a non-opening pair (NOP) when made up of elements like question/answer and request/consent, and an opening pair (OP) when a new topic of conversation begins. The difference in AMDs between two adjacent SUs is measured:



(a) single speaker



(b) cross speaker

Fig. 2 Speech rate and information openings

a positive result indicates an utterance rhythm that is accelerating, and a negative result an utterance rhythm that is decelerating.

The problem here is to determine how NOPs and OPs accelerate or decelerate for a single speaker and for both speakers in the conversation. The results of the analysis are shown in Fig. 2. It was found that: (1) The rhythm of a conversation accelerates for NOP and decelerates for OP; and (2) This phenomenon is the same when measurements are made for either the same speaker or between two speakers. In other words, each of the two speakers in a conversation adjusts his or her speech to the rhythm (speech rate) of the other party's speech. In addition, rhythm speeds up if the topic of conversation remains unchanged, and the rhythm resets and slows down when the topic changes. In short, the two speakers in a conversation adjust their rhythm just like two dancers, and work closely together when speeding up and slowing down the conversation.

These findings indicate that such a mechanism must be incorporated in agents to make them more human like. It is not sufficient to simply understand the contents of the other party's speech; rather, the rhythm of the other party's speech must be detected and the agent's responding rhythm must be set based on the contents and rhythm of the other party's speech and on the appropriate reply to these. Although much research is being performed on agents having a function for conversing with humans by voice means, there is yet no example of incorporating such a function, and it remains a major research subject.

5. Group Behavior in Human Communica-

tions

5.1 Approach

In the conventional AI approach, communications among group members has been treated as follows. First, the behavior rules of the groups and organizations are described in an explicit way. Then under the consumption that each individual follows these rules, the total behaviors of the groups or organizations are introduced. On the other hand, in daily life, even when we belong to some group or organization our behavior is based on impromptu behavior. The rules of the group or organization act only as a loose restriction or loose limit of our behavior. As a result, the total behavior of humans as a group or an organization becomes vivid and life-like. The conventional AI approach could not explain these phenomena.

On the other hand, the target of AL research is to study the basic mechanisms of life and try to simulate various behaviors of living things. Of course here the high-level behavior of human beings, such as verbal communication, is not the main target. Instead, basic life-like behaviors have been the target of AL research. AL researchers have been focusing on such research areas as developmental models, emergent computation, evolutionary computation, and adaptive behavior. At this point, research into human communications and research into artificial life have various interests and topics in common. Therefore, collaboration between communications researchers and AL researchers will yield fruitful research results, especially in the area of the group behavior of humans.

5.2 Research example: Talking Eye[3]

We propose a communicative agent model with a subsumptive structure which especially aims at the creation of a chatting behavior with humans. The model consists of multiple layers based on a subsumption architecture with competence modules. Each competence module independently performs an interaction with the real world and a behavior is expressed toward the real world as a result of activation/inhibition among competence modules. The higher competence module with an intentional behavior subsumes the lower one with a coordinative behavior. The function of the lower competence module is to maintain basic coordination by invoking conversational behaviors constrained by interactions with the real world. The function of the higher competence modules is to coordinate interactions based on a cooperative mechanism for the achievement of goals which have emerged as a result of the interactions.

Each competence module consists of a set of behavior modules realized as a situated agent. The conversational behavior is performed by activation/inhibition between a set of situated agents and the real world, as well as among the situated agents. Each situated agent is activated using the spreading activation of a dynamic action selection network. Figure 3 illustrates a communicative agent model consisting of three parts: the environmental context, the intentional context and a set of situated agents. The environmental context places constraints on the actions of the situated agents. The set of situated agents for the behaviors from all of the competence modules is represented in Fig. 3 as a single action selection network.

Each situated agent has a condition list, an add list, a delete list and an activation level. The condition list is a

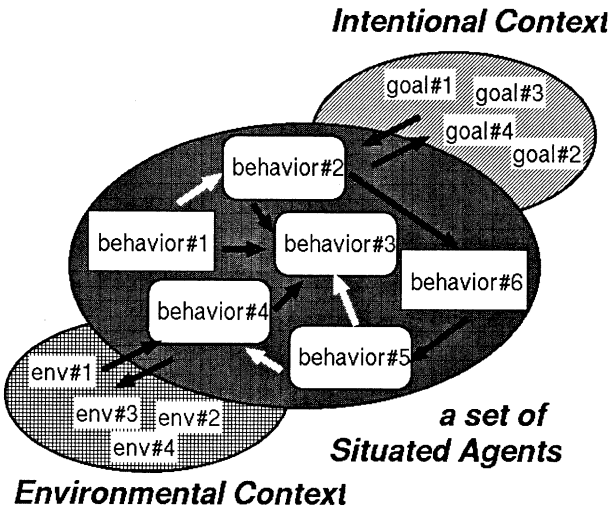


Fig. 3 Architecture of communicative agent model

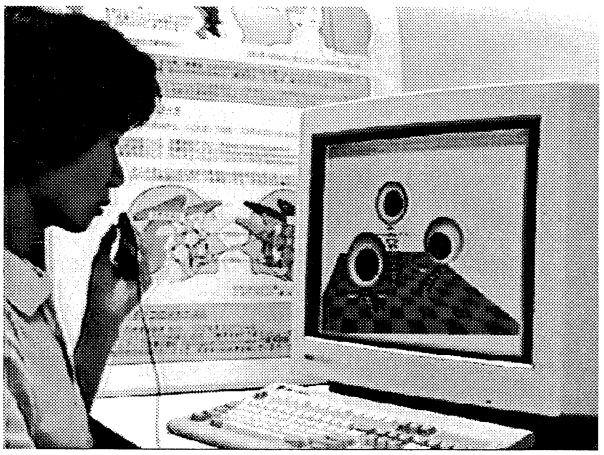


Fig. 4 Appearance of chatting with "Talking Eyes"

list of preconditions which have to be fulfilled before the situated agent can become active. The add list and delete list represent the expected effects of the situated agent's action. In addition, the activation level is the energy value propagated through the network.

In the process of conversation, the two contexts and a set of situated agents are influenced by each other. As a result of such an interaction, one action is released dynamically using activation/inhibition dynamics which make activation energy accumulate.

We have constructed an interactive agent as one test bed of emergent chatting within the communicative agent model as a result of interactions with a human. The interactive agent has the shape of an eyeball generated by 3-D computer graphics and we have called it a "Talking Eye"(Fig. 4). Since a Talking Eye can be represented in such a simple way, we can study the representation of simple modality that the Talking Eye has. At present, it has two modalities, which are utterance generation and motion as actions applied to the real world. It can perceive human conversational behaviors by detecting simple utterance fragments using speech recognition, prosody of speech and simple motion. Furthermore, it can produce about 250 Japanese vocal phrases for chatting by means of speech synthesis. It can also produce about 20 types of eye movements which indicate emotional states, such

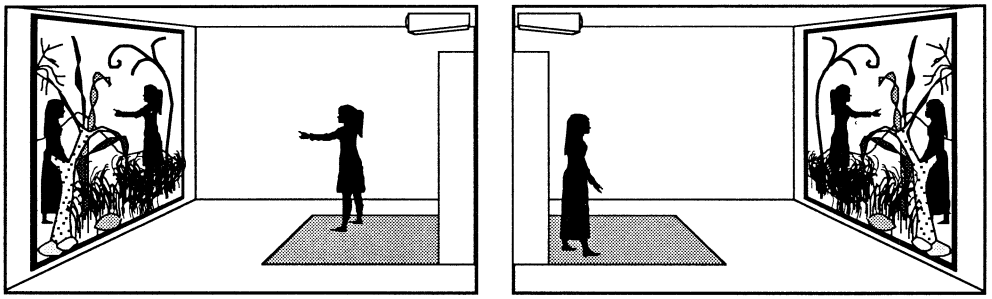


Fig. 5 MIC Exploration Space
(Christa Sommerer & Laurent Mignonneau for ATR MIC Lab, 1995)

as surprise, agreement, disappointment, etc. With its speech recognition capability, the Talking Eye can detect a phrase in real-time (less than one second) and at a high phrase detection rate. Though the recognition rate is a big problem on most conversational interactive systems, it is not a very big problem for the Talking Eye because it interprets its partner's utterance with its own advantage. Therefore, chatting never stops and the Talking Eye can achieve active, non-stop chatting with its communication partner.

6. High-order Behavior in Human Communications

6.1 Approach[1]

As described above, it is now being recognized that behind this external form of communication lies a deeper communication mechanism based on human sensitivity. In particular, high-order sensory information, such as impressions, is very difficult to deal with by using only engineering. On the other hand, artists have long been dealing with issues of sensitivity. Therefore, to deal effectively with high-order sensory information, we can expect research in the coming years to approach the problem from both the engineering and artistic points of view.

At the same time, a field called interactive art is now developing as a new movement in the art world. The new field of interactive art allows the art audience to change the artistic expression of the work by interacting with it. In this process, feedback is first generated from the audience to the work of art, and then from the work to the artist, who examines the modified work. In this way, information flows from the audience to the artist. In short, interactive art enables information to flow in a bi-directional manner thereby achieving a higher level of communication. Unfortunately, interactive art is still in a developing stage and interaction techniques must therefore be enhanced and brought to a higher level of communication by incorporating advanced techniques, especially those associated with image and voice recognition.

In the above way, engineering is seeking the cooperation of the art world to enable high-order sensory information to be handled by computer. At the same time, the art world is searching for new technologies to enhance current interactive art and to raise interaction to a higher level of communication. Since these objectives are mutually agreeable, we can say that the groundwork has been laid for advancing research through cooperation between art and engineering.

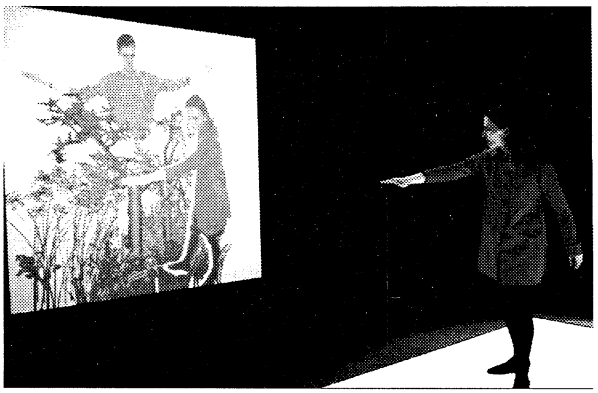


Fig. 6 Interaction in "MIC Exploration Space"

6.2 Research example: interactive communication environment[4]

The environment plays an important role in human communications. In most cases, the environment is fixed and we have to choose a place where communications can be achieved depending on the communication content, such as a meeting room for business, a coffee shop or a restaurant for talk with friends, or a living room for a relaxing time with family members. Now, however, it is possible to create various environments suitable for communications by applying image and speech processing technologies. CG technology is the key among various technologies for creating an environment that changes in real time depending on the content of the communications. We call such a communications environment an "Interactive Communications Environment."

The "MIC Exploration Space" has been produced by Christa Sommerer and Laurent Mignonneau as a concrete example of an interactive communications environment. They are artists in the field of interactive art and have been producing virtual plants and virtual creatures that interact with human beings since the early 1990s. Two representative examples are explained below.

"A-Volve" : The theme of this art work is interaction between virtual creatures and human beings. Virtual lives created according to inputs on a touch screen are projected onto a screen installed under a pool and the audience can interact with the virtual lives by making hand movements in the pool.

"Trans Plant" : The theme here is interaction between virtual plants and human beings. On a screen installed in front of an audience, virtual plants and images of the people

are projected. The virtual plants grow according to the movements of the people. Therefore, the audience can create an environment of their own.

In the MIC Exploration Space, Trans Plant's basic concept of interaction between humans and virtual plants is extended to communications between humans or between humans and the environment. In Fig. 5, the whole image is shown. Suppose that two of the same systems are placed at distant places and they are connected through telecommunication lines. In front of the two screens, two persons are standing. Their images are taken by cameras that are set just above the screens and only the human images are extracted from the background. At the same time, cameras installed above the two persons recognize their standing positions and their simple movements, and CG images of virtual trees, grass and flowers are created according to the recognition results. Overlapped images of the two persons and CG plants are projected onto the screens. Consequently, each person can feel as if he/she is meeting the other person, who is in a remote place, in the virtual space. They can also feel, when their environment changes based on their communications, as if they are able to create their environment based on their communications. In Fig. 6, a situation where this system is used is shown.

7. Conclusion

Human communications has come to be targeted by a wider range of research as the use of computers has continued to spread and the relationship between them and people has taken on new forms. Nevertheless, it still appears that discussions on human communications are for the most part held within the field of AI research. In this paper, we have presented a research area that reconsiders the meaning of the human communications and pointed out that in addition to logical information, non-logical information or non-verbal information is essential in human communications and questions how the computer can support human communications from the aspect of non-verbal or non-logical information. We have also shown that when considering human communications from this point of view, AL and artistic aspects must be taken into account in addition to the AI aspect, and that to study these aspects in future human communications, an interdisciplinary approach including AI, AL, and art will become vitally important. Examples of actual research in this area now being performed at the ATR Media Integration & Communications Research Laboratories have also been presented.

References

[1] Ryohei Nakatsu, "Image/Speech Processing That Adopts an Artistic Approach -Toward Integration of Art and Technology-," Proceedings of ICASSP 97,Vol I/V, pp. 207-210 (1997.4).
[2] Hanae Koiso et al., "Informational Potentials of Dynamic Speech Rate in Dialogue," Proceedings of the 19th Annual Conference of the Cognitive Science Society, pp.394-399 (1997.8).
[3] Noriko Suzuki et al., "Chatting with Interactive Agent," Proceedings of Eurospeech 97, pp. 2243-2246 (1997.9).
[4] Christa Sommerer and Laurent Mignonneau, "MIC Exploration Space," The Bridge: SIGGRAPH'96 Art Show (1996.8).

Proc. of Third Int. Symp. on Artificial Life, and Robotics (AROB III' 98),
Oita, Japan, 19-21, January, 1998,

HMM Analyses of Human Random Number Generators

Mieko Tanaka-Yamawaki, Hiroko Masuda, and Mikiko Kawagoe
Department of Computer Science and Systems Engineering
Faculty of Engineering, Miyazaki University, Miyazaki 889-21 Japan
E-mail: mieko@eagle.cs.miyazaki-u.ac.jp

Abstract

We attempt to extract information on the higher-order functions of brain by means of human random generation tests (HURG). We have analyzed our newly taken data by computing the measures of randomness. Though entropy does not exhibit a visible feature, pair entropy is found to be quite sensitive to the condition as well as the personality difference, which implies that human generated "random" numbers are almost first-order Markovian. This leads us to model the brain by means of hidden Markov models (HMM) which are commonly used in the study of speech recognition. Our result shows that HURG data are not as deterministic as required to fix an HMM model, although we can separate our data into two large categories. We show some other ways to classify our data into two categories.

Key Words : Random Generation Test, HURG, Higher-order function of brain, Originality, Markov process

1 Introduction

Specialty of the human brain lies in its ability to handle abstract notions by means of languages, whose fluency level reflects the condition of a brain. Among various factors to characterize the fluency, abundance of vocabulary and the avoidance of repeated usage of the same word seem to be very important ones. It is therefore natural to conceive a psychological test of random generation, since a person practicing such a test is required a considerable amount of concentration in order to produce a random series continuously. In extreme cases it is known that patients of mental disorder have great difficulty in producing random series. Also there have been attempts to use the randomness in such data as a suitable index to measure the level of originality in thinking by normal persons, based on a hypothesis that the ability of random generation is directly related to the power of human thinking. This line of research was done by a group called 'Human Random Number Generation Society' in 1970's. We performed our preliminary experiment of human random number generation test (we called it HURG) by following their method found in the literature and attempted to extract information on the brain function by means of a statistical modeling[1].

Historically human random generation tests have been practiced in the field of clinical psychology. It is reported that several specific features are seen in the data produced by patients. Applied to normal people, HURG data exhibit much subtler features. A well-trained person in a good condition can generate ten numbers almost evenly in a long span. Still, human-produced random series can be distinguished by the scarcity of immediate repetition of the same numbers. It is quite hard psychologically for anyone to repeat the same number immediately since most people feel uncomfortable to repeat the same number, or word even when the person is well learned that a truly random sequence of digits would produce repetitions with probability one tenth. Other than the scarcity of repetitions it is quite difficult to find a clear signal of human generated random series. Separation of individual is very difficult from the data. However it seems meaningful to classify personalities which produced data into two large categories by using multiple

classifiers. In this paper we employ the Hidden Markov Model (HMM) which are commonly used in the study of speech recognition, various randomness measures, and two-dimensional plot of two adjacent intervals of each number. Our data taken from five people separate two types of personalities.

2 Experiments and Analysis

We took the following version of HURG:

(1) Ask a person(subject) to say 100 single-digit numbers as random as possible, and preferably as quick as possible.

(2) Input the generated data into the computer and make a data file in a prescribed form. This process is to be automated in the near future by using our speech recognition system.

In this way we have collected data from five students (three female:A-C and two male:D,E) in our laboratory. A string of one hundred digits makes one data. Five data were taken from each student. Another set of five data were taken a few months after taking the first data. In total ten data containing one thousand digits per person from five individuals are used in this analysis.

The key issue is to determine what information to extract from the data. We are first interested in the quality of the data. Of course this kind of psychological data cannot be as good as other data from the precise sciences[2]. The first quantity to look at is the randomness of numbers. This can be measured by the entropy H_1 from the probabilities of occurrence P_i of the digits i $(0 \le i \le 9)$. It takes the maximum value 2.30 when all the numbers appear in a sequence evenly, i.e. all the numbers occur in the same probability one tenth.

$$H_1 = -\sum_{i=0}^{9} P_i \log P_i$$

$$H_1^{(\max)} = -\sum_{i=0}^{9} \tilde{P}_i \log \tilde{P}_i = -\sum_{i=0}^{9} \frac{1}{10} \log \frac{1}{10} = 2.3026$$

Although this quantity does not vary strongly, it tends to decrease as the person gets tired after repeated tests as can be seen in Table1 (a)-(d).

Next quantity to examine is the correlation of adjacent numbers. We compute the 2-entropy, H_2 from the probabilities of occurrence P_{ij} of pairs (ij):

$$H_2 = -\sum_{i,j=0}^{9} P_{ij} \log P_{ij}$$

Similarly from P_{ijk} which is the probabilities occurrence of triplets (ijk) we compute H_3. In a string of data, for example, [5 1 3 8 7 9 2 4 1 .....5 1 0 7 3] we count the numbers of pairs by looking at the data as a collection of pairs: [51, 13, 38, 87, 79, 92, 24, 41,.....51, 10, 07, 73] and count triplets by looking at the same data as a collection of triplets: [513, 138, 387, 879, 792, 924, 241, ...510, 107, 073], and so on. The result is shown in Table 1 (a)-(d) for the four persons A, B, C, and D. In Table 1 we used strings of length two hundred by combining two data to compute H_1 and H_2, and used a string of length one thousand to compute H_3.

It seems natural to believe that the random number generation is mostly influenced by the immediate past. This fact suggests us the following two things. One is that, rather than numbers in our raw data, the difference between two adjacent numbers is the most interesting quantity to look at. The other is that that the correlation length in the data do not go beyond 5 or so. Therefore we have converted our raw data strings to a new set of data of differences, and cut them into pieces of length 10. We further contract the information by dividing the differences into three categories: (1) zero (2) 1,-1,2,-2 (3) the others.

and again convert the data strings into a new set of strings made of these three categories: 1, 2, 3 respectively. In other words the data strings are now expressed by the three codes, {1,2,3}. For example, the data [5 1 3 8 7 9 2 4 .....5 1 0 7 3] is first converted to [-4 2 5 -1 2 ....7 -4] and then further converted to [3 2 3 2 2.... 3 3].

3 Hidden Markov Model of HURG

The fact that H_2 is the most sensitive quantity

implies that the sequence of digits in HURG, obtained by requiring to be as random as possible, is actually more like the (first order) Markov Process. This consideration leads us to apply to HURG the Hidden Markov Model [3] which are commonly used in the study of speech recognition.

We assume three states of brain function to generate random numbers, and identify them to

(1) normal state: carefully generating data

(2) innovative state: jumping to a new stage

(3) inactive state: being tired of continuing the experiment

These assumptions fix the sizes of HMM. The transition matrix of states, X, is a 3 by 3 matrix, and the production probability of data symbols at each state is represented by another 3 by 3 matrix, Y. In general, the matrix X is n by n for a model of n hidden states and the matrix Y is n by m if each state can produce m symbols. It is assumed that X and Y are constant matrices, i.e. the transition probabilities between the states and the production probabilities of the symbols are all fixed in a model.

Starting from various initial values, we have attempted to optimize X and Y for five persons by using Baum-Welch method. At present we have not successfully reached a clear-cut result. The contraction of data in three symbols {1,2,3} seems still too rigid to be classified by HMM model. This point calls for a careful study on the basis of HMM. Instead we have examined whether we can classify the global patterns by computing the probabilities of occurrence of each data set by five people A to E in various given HMM models. We have found that all the strings (length 10) A's data and C's data have larger probability of occurrence in all the seven HMM models of "adventurous" type compared to the probabilities of occurrence in the seven HMM models of "even and careful" type, while the corresponding probabilities for most strings taken from D's data and E's data are larger in "even and careful" type HMM models compared to the probabilities of occurrence in "adventurous" type. We can conclude from this that A and C are classified into the same "adventurous" type, while B, D and E into the "even and careful" type in the context of HMM.

4 Intervals of Numbers

Next we examine the intervals of each digit in a sequence. To do this we concatenated ten data of each person to make a long string of length one thousand. The interval of a number 'k' makes a sequence of numbers $(x_1^k, x_2^k, x_3^k, ...)$. This sequence is converted into a set of two dimensional points $(x_i^k \; x_{i+1}^k)$. Typical results are shown in Figure 1 (a)-(d). We can see the similarity between two plots for '0' and '4' by the same person, and a distinguishable difference between plots by two different persons.

5 Conclusion

We have taken HURG data from five students in our laboratory and examined them by computing the measures of randomness, correlation, probabilities of occurrence in various hidden Markov models, and also by plotting the intervals of each digits in two dimension.
It is found that randomness represented in entropy H_1 does not vary much throughout the experiment and the pair entropy H_2 picks up the difference in personalities and the condition. HMM can separate five subjects into two large categories: "even and careful" type and "adventurous" type. Within the limitation of our analyses, the correspondence is consistent, i.e. two people fall into the former type and the other two people fall into the latter type. However the statistics is not good due to the smallness of the total data set. Also, the optimized value of X and Y are extremely sensitive to the initial values, indicating that the parameter space of X and Y have many local minima. Two dimensional plot of intervals express the individual person's feature very well as is shown in Figure 1. Our future task is twofold (1) we need higher statistics with more data. (2) we need study the basis of the Hidden Markov Model more carefully.

References

[1] Yukito Iba and Mieko Tanaka-Yamawaki, "A Statistical Analysis of Human Random Number Generators", in Proceedings of IIZUKA'96, Ed. T.Yamakawa et.al.(World Scientific, 1996) 467-472.

[2] e.g., W.A.Wagenaar, Psychological Bulletin, vol.77(1972)65-72

[3] L.Rabinier, B.-H.Huang, "Fundamentals of Speech Recognition",(Prentice Hall, 1993)

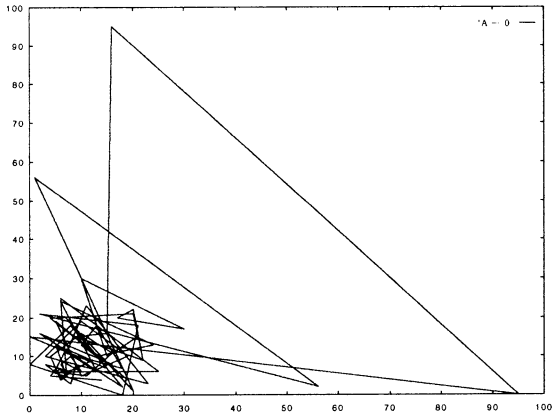


Figure 1(a) ($x_i^k \ x_{i+1}^k$) plot of intervals of '0' for A..

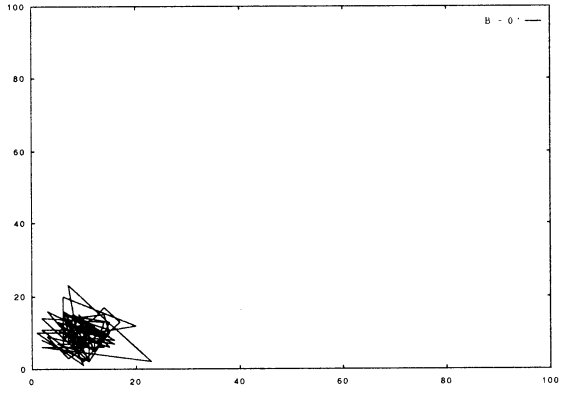


Figure 1(c) ($x_i^k \ x_{i+1}^k$) plot of intervals of '0' for B.

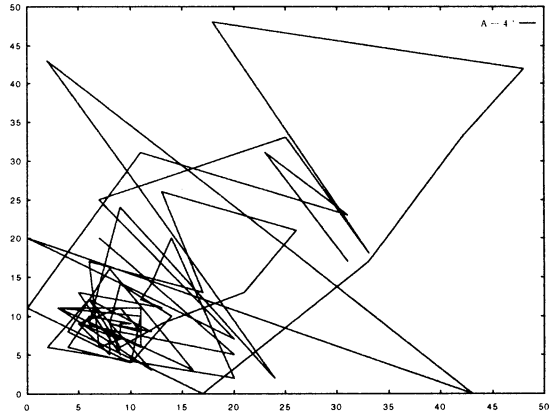


Figure 1(b) ($x_i^k \ x_{i+1}^k$) plot of intervals of '4' for A.

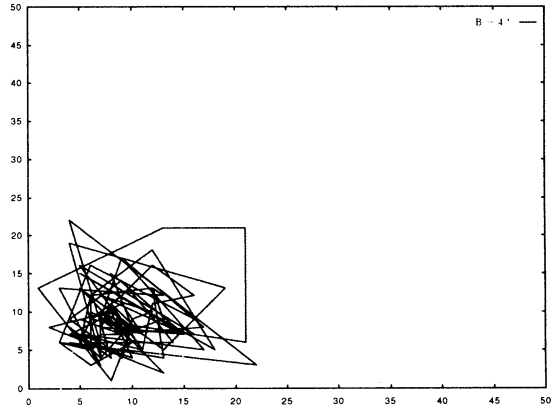


Figure 1(d) ($x_i^k \ x_{i+1}^k$) plot of intervals of '4' for B.

Table 1 (a) female student A

	data12	data34	data56	data78	data910
$H_1/H_1^{(max)}$	0.9905	0.9905	0.9809	0.9658	0.9729
$H_2/H_2^{(max)}$	0.9038	0.9070	0.8997	0.8654	0.9016
$H_3/H_3^{(max)}$	0.8575				

Table 1 (b) female student B

	data12	data34	data56	data78	data910
$H_1/H_1^{(max)}$	0.9984	0.9937	0.9978	0.9967	0.9965
$H_2/H_2^{(max)}$	0.9222	0.9173	0.9073	0.9219	0.9263
$H_3/H_3^{(max)}$	0.8852				

Table 1 (c) female student C.

	data12	data34	data56	data78	data910
$H_1/H_1^{(max)}$	0.9954	0.9955	0.9869	0.9961	0.9962
$H_2/H_2^{(max)}$	0.9093	0.9065	0.9002	0.9218	0.9163
$H_3/H_3^{(max)}$	0.8752				

Table 1 (d) male student D.

	data12	data34	data56	data78	data910
$H_1/H_1^{(max)}$	0.9892	0.9886	0.9815	0.9932	0.9953
$H_2/H_2^{(max)}$	0.9223	0.9188	0.9123	0.9194	0.8950
$H_3/H_3^{(max)}$	0.8815				

Table 1(a)-(d) Ratios of H_1, H_2, H_3 to their maximum values.

Proc. of Third Int. Symp. on Artificial Life, and Robotics (AROB III' 98),
Oita, Japan, 19-21, January, 1998,

Cooperative Task Processing with Adaptive Communication in Baggage Carrying Problem

Makiko KATSURA † Keiji SUZUKI † Azuma OHUCHI †

† Research Group of Complex Systems Engineering,
Graduated School pf Engineering, Hokkaido University,
North-13 West-8, Sapporo 060, Japan
{makiko, suzuki, ohuchi}@complex.eng.hokudai.ac.jp

Abstract

We try to make an adaptive communication mechanism in which the structure of the messages consists of the call part and the action part. The call part represents just the name of agents and the action part represents the behaviors of agents. Under the structure of the messages, the agents should learn the meanings of the lexicons in each part simultaneously. To discussion of the realization methods for the adaptive communication, we introduce the Baggage Carrying Problem (BCP) as the simplified cooperative task processing problem of agents.

1 Introduction

Collective Approaches are expected to perform the flexibility and the adaptability for solving the problems. Several collective approaches are studied in the area of multi-agent systems, evolutionary computations and artificial life[1][2]. The major issue in these approaches is how to construct the cooperative relation between the distributed autonomous agents as the problem solvers. To construct the cooperative relation, the designs of the communication between the agents are important.

Several studies treated the adaptive and evolutional communication in multi-agent systems[3][4]. However, their structures of the messages seem to be quite simple to use in task processing problems. In this paper, we try to make an adaptive communication mechanism in which the structure of the messages consists of the call part and the action part. The call part represents just the name of agents and the action part represents the behaviors of agents. Under the structure of the messages, the agents should learn the meanings of the lexicons in each part simultaneously. Namely, as the adaptive communication of the agents, we expect the agents to realize the abilities that they can distinguish each other with the call part and give the orders to the specific agent with the action part. These abilities seem to be important to apply the agent systems to cooperative task processing systems.

To discussion of the realization methods for the adaptive communication, we introduce the Baggage Carrying Problem (BCP) as the simplified cooperative task processing problem of agents. As the simplification of the communication, we divide the agents into two kinds of them. One is the sender of the messages and another is the receiver of them. That is, the agents in the BCP consist of two distinct agents, the directors and the workers. The directors know the positions of the workers, the baggage and the goals, but they can't carry the baggage. Whereas the workers can carry the baggage but they have only limited sensing abilities. To solve this problem, the cooperative task processing between the directors and the workers are required. Namely, the directors have to send adequate messages to the specific workers who can carry the baggage. The reinforcement learning is introduced to organize the communication adaptively between the directors and the workers.

2 Baggage Carrying Problem

To discussion of the realization methods for the adaptive communication, we introduce the Baggage Carrying Problem (BCP) as the simplified cooperative task processing problem of agents. The environment is a square grid space surrounded by the walls. There are two distinct agents, that is, the directors and the workers, the set of baggage and the goal in the environment. Each of the agents and the set of baggage occupies one of the cells and the position of them doesn't overlap each other. Figure 1 shows sin-

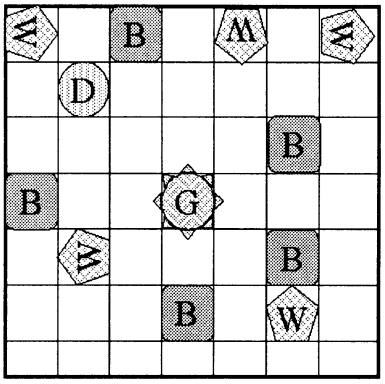


Figure 1: Baggage Carrying Problem

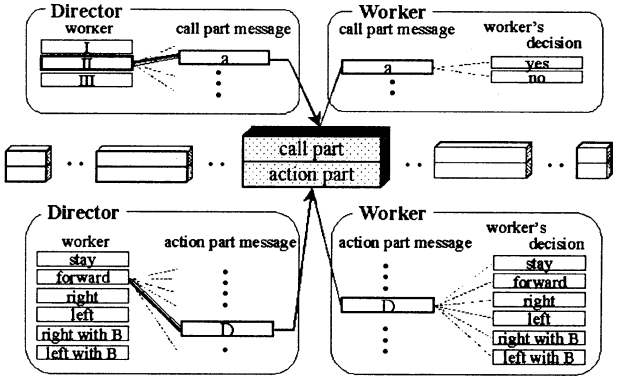


Figure 2: The structure of message

gle director, five workers, five pieces of baggage and single goal. The division of agents in BCP means to simplify the structural communication between them. That is, the director can send the messages and the workers can receive them. The task in this problem is to carry the baggage to the goal. Because the both types of the agents are endowed with the restricted abilities as follows, the communication between them is necessary to complete the task efficiently.

2.1 Directors

The directors can perceive the state of the environment, that is, the position of workers, baggage and goal, the direction of workers correctly within the range of sight. As for the ability of behavior, the directors can move (*stay, up, down, left, right*), send the messages and cannot carry the baggage. Thus, the directors should find a worker and the corresponding piece of baggage, then send the messages intended that the worker carries the piece of the baggage to the goal.

2.2 Workers

The workers have four directions (north, south, west, east) and can carry the baggage. Although the workers cannot perceive the state of the environment basically. Therefore they will not carry the baggage efficiently without the supports of the directors. They select one behavior out of six, that is, *stay, forward, turn left, turn right, turn left with baggage* and *turn right with baggage*. When the piece of the baggage is on the front of the worker, the worker can push the baggage by behaving *forward* until the baggage hits the other obstacles (for example, other agents or a piece of the baggage).

3 Adaptive Communication

To realize the cooperative task processing between the directors and the workers using the communication, we propose the structural message consists of the call part and the action part. The lexicon in the call part represents just the name of a specific worker. The lexicon in the action part represents the action as the given orders from the directors to the worker who is called by the lexicon in the call part. In BCP, the director makes the plan for the actions of the workers to carry the baggage in each step. Then he sends the messages as the plan to the workers. The workers receive the messages and obey the order in the action part of the message if the call part of it indicates themselves. In initial state, the meanings of the lexicons in both parts aren't determined. Thus the agents should learn the meanings of the lexicons in each part simultaneously throughout the task processings. Namely, as the adaptive communication of the agents, we expect the agents to realize the abilities that they can distinguish each other with the call part and behave correctly accordance with the plan presented in the action part. These abilities seem to be important to apply the agent systems to cooperative task processing systems.

As Figure 2 indicates, the number of the lexicons for the call part is five to present the number of the workers. The number of the lexicons for the action part is six that equal to the number of the actions of the workers.

4 Learning of Message

To learn the meanings of lexicons in each part, the reinforcement learning is applied. Both types of agents

have the two reference tables. One of the tables represents the probabilities concerning the pairs of the lexicons and the interpretations as the names of the workers. Another table also represents the probabilities concerning the pairs of the lexicons and the interpretations as the actions of the workers. To reinforce the probabilities in both tables simultaneously, the conditions for receiving the rewards are very restricted. Basically, the reward is given only the case that the worker could succeed to carry the piece of the baggage to the goal. In this case, if the lexicon in the action part is different among the lexicons in the action parts for other workers in the sending messages from the director, the succeeding worker and the director can receive the reward. The reward is used for increase the probabilities of the pairs that are used at final message. In addition, the discounted rewards are propagated to the messages that is used three steps before. The conditions of receiving the rewards seem to be curious. However, without these conditions, we have confirmed that the agents couldn't learn the both lexicons simultaneously.

5 Planning Strategies of Agents

In this section, we present the strategies of the director to be carried the baggage by the workers. To clarify the effectiveness of the proposed structural messages in BCP, we prepare the three types of strategies. The one is optimal planning with that the meanings of the lexicons are fixed correctly. In this strategy, the director calculates the optimal paths for capturing the pieces of the baggage and carrying to the goal for all workers in each step. The strategy, called **TYPE 1**, is prepared as the reference to know the upper-boundary of the solution in BCP. The another strategy, called **TYPE 2**, seems to be sub-optimal planning. In this case, the meanings of the lexicons are also fixed. In this strategy, to be captured the baggage by the workers, the director only allocates the workers to the pieces of the baggage according to the minimal distances between the workers and the baggage. Thus some workers will often cause the conflicts to capture the same piece of the baggage. The director makes the plan to reallocate the worker only when the conflicts are occurred. Therefore, the plan based on the strategy will often causes the deadlock states in the workers and the efficiency of the task processing will be decrease than **TYPE 1**. T hus the strategy will show the sub-optimal boundary of the solution in BCP. From the both strategies, we can know the endowed characteristics of BCP. Our objective is to show the efficiency of the proposed learning mechanism closing to the upper-boundary solution according to the clarifying of the meaning of the lexicons. Then we prepare the planning strategy as **TYPE 3** of which the plan of the worker is same as **TYPE 1**, but the meanings of the lexicons are required the learning. To precisely compare the effects of the learning concerning the structural message, three types of the learning problems are prepared as follows:

TYPE 3(1) Learning of only the call part and the lexicons of the action part being fixed correctly
TYPE 3(2) Learning of only the action part and the lexicons of the call part being fixed correctly
TYPE 3(3) Learning of both parts simultaneously

6 Experiments

To confirm the efficiency of the proposed learning mechanism for the structual message, we executed the experiments based on the above strategies. The learning parameters are set as follows:

grid size	11×11
initial value of each table	1.0
discount factor	0.02
reward	5.0

Table 1: The learning parameters

In Figure 3, these lines show the transition of the success numbers per 10,000 time steps in which each preceding strategy is applied to the agents. Although the lines of **TYPE1** and **TYPE3(1)** are difficult to distinguish because of the overlapping, it means that the performance of agents in **TYPE3(1)** reaches the upper-boundary solution.

Figure 4 shows the probability that the director interprets the call part of message as each worker correspondingly in **TYPE3(1)**. We proved that the workers also interpret the call part of message as the director does. Thus, it is clear that the agents learn the meanings of the call part accurately.

The number of workers who interpret the action part of message as each meaning is indicated in Figure 5 and Figure 6 regarding **TYPE3(2)** and **TYPE3(3)** respectively. We confirmed that the director can send the coherent action part of messages completely in both cases. It is obvious that the workers behave correctly according to the action part in **TYPE3(2)**, but

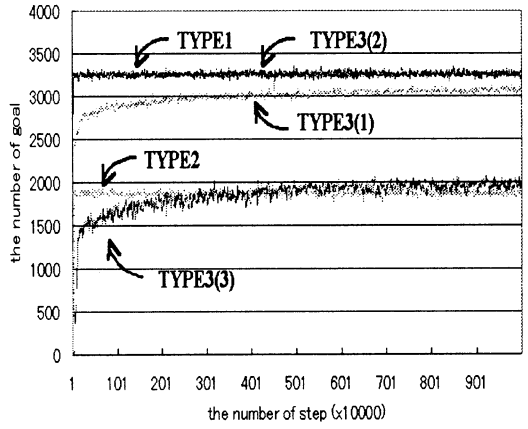


Figure 3: The number of goal

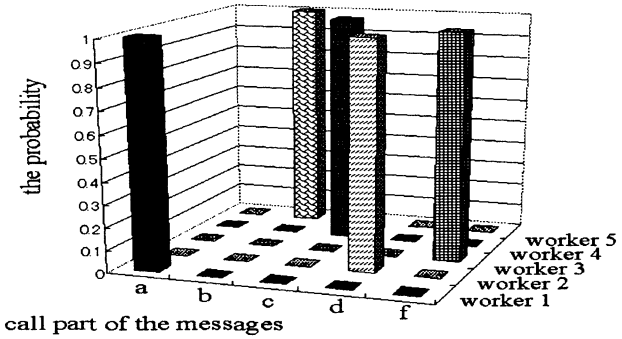


Figure 4: Message of Directors for Workers : TYPE3(1)

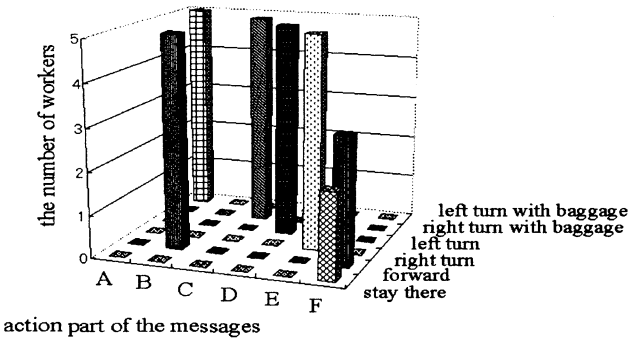


Figure 5: Interpretation of action part about Workers : TYPE3(2)

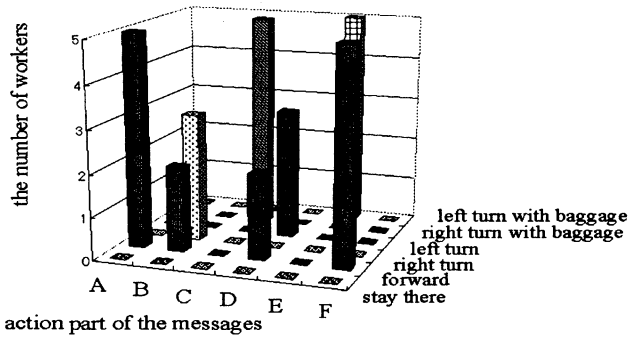


Figure 6: Interpretation of action part about Workers : TYPE3(3)

the workers don't always interpret the action part precisely regarding **TYPE3(3)**. Therefore the difference between **TYPE3(2)** and **TYPE3(3)** in the performance showed in Figure 3 is due to the difference of worker's interpreting ability.

As to **TYPE3(1)** and **TYPE3(2)**, we can see the performance close to the optimal planning solution with realizing the adaptive communication. Although the performance in **TYPE3(3)** also excels the suboptimal planning, it seems to be required more effective mechanism to learn the two parts simultaneously.

7 Conclusion

We have proposed a mechanism to construct the adaptive communication system of which the structure of message consists of the call part and the action part. Moreover we have experimented about the three agents models to examine our mechanism through BCP and confirmed the efficiency of the proposed mechanism in cooperative task processing.

References

[1] Hitoshi Iba, "Emergent Cooperation for Mulitiple Agents Using Genetic Programming," *Parallel Problem Solving from Nature*, pp.32-41, 1982.

[2] Norihiko Ono and Kenji Fukumoto, "Multi-agent Reinforcement Learning: A modular Approach," *Proceedings of Second International Conference on Multi-Agent Systems*, pp.252-258, 1996.

[3] Werner, G.M. and M.G.dyer, "Evolution of Communication in Artificial Organisms," *Artificial Life II*, pp.659-687, 1991.

[4] Luc Steels, "The Spontaneous Self-organization of an Adaptive Language," *Machine Intelligence 15*, 1996.

Proc. of Third Int. Symp. on Artificial Life, and Robotics (AROB III '98),
Oita, Japan, 19-21, January, 1998,

Learning of Pheromone Communication for Adaptive Organizations in Multiple Monkey Banana Problem

Keiji SUZUKI and Azuma OHUCHI
Research Group of Complex Systems Eng.,
Graduate School. of Eng., Hokkaido University,
North-13, West-8, Sapporo 060, JAPAN
e-mail: {suzuki, ohuchi}@complex.eng.hokudai.ac.jp

Abstract

In this paper, we discuss self-reorganization of agents in the multiple monkey banana problem. The problem can be characterized as multiple targets processing problem. In this problem, each target processing requires the cooperative organization that consists of the specified number of agents at least. Because the information of targets is shared insufficiently among the agents, each agent has to decide which target should be processing based on its sensing information, and many organizations occur simultaneously for different targets. Thus, it is easily imagined that some organizations of them will be short-handed for processing the targets. That is, the agents often face the dilemma of whether to give up the current organizing efforts or to wait until the other agents becoming member for filling up the vacancy of the organization. To defeat such dilemma situations, they are required to possess the effective reorganization abilities.

In this paper, we propose an evolutionary acquisition of the pheromone style communication based on the classifier representation. Throughout the experiments, it is shown that the acquired communication rules succeed in the reorganization from the dilemma situations.

1 Introduction

It is easy to watch organized activities in insects; like as bee and ant. For example, they make the organization for building the nests. Also, they construct morphology with themselves; like as bridge for going over gaps. In these activities, it is difficult to image that the insects always keep to cooperative relations explicitly in organizational works. To keep the cooperative relations constantly, they have to infer the plans intelligently for achieving their objectives. Furthermore they have to communicate frequently with each other for working cooperatively. It is hard to believe that the small insects have complex abilities of inference and communication for managing the organizational activities. While, we can regard that the activities of insects are based on simple rules rather than all of the insects are assumed as strategist. Thus, we assume that the organizing abilities in such types of insects emerge from the interactions among the activities based on the simple reactive strategies.

In recent multi agent systems, the agents are embedded with simple reactive strategies inspired by the above assumption. These strategies are designed to use the relations between status of environment and behaviors of agents. Thus, organizations for solving problems are expected to emerge from the interaction among the agents.

When the activities of the agents are independent like as the tag-game and group hunting [1], it will be relatively easy to make the required strategies. However, when the activities of the agents are tightly connected to each other like as making a bridge with themselves, it will be difficult to realize the organizing behaviors. Because, the behavior of each agent depends not only on the status of environment but also on the other agent's behaviors directly. Namely, uncertainty and restrictions are increased in the interaction between agents. As such type of the organizing problems, we introduce the multiple monkey banana problem.

The multiple Monkey Banana Problem is proposed as a test-bed problem for developing the self-organization ability in the multiple target processing environment. In this problem, each target processing requires the cooperative organization that consists of the specified number of agents at least. Because the information of targets is shared insufficiently among the agents, each agent should decide which target should be processing based on its sensing information. Then many organizations occur simultaneously for the different targets. Thus, it is easily imagined that some organizations of them will be short-handed for processing the targets. That is, the agents in this problem often face the dilemma of whether to give up the current organizing efforts or to wait until the other agents becoming a member of the current organization. Therefore, they are required to possess the effective reorganization abilities to defeat such dilemmas.

In this paper, we proposed an evolutionary acquisition of the pheromone style communication based on the classifier representation. Throughout the experiments, it is shown that the acquired communication rules succeed in the reorganization from the dilemma situations.

In next section, we introduce the multiple monkey banana problem.

2 Multiple Monkey Banana Problem

The original monkey banana is a famous planning problem in AI. The introduced problem is extended as an organization problem of multiple agents. There are many bananas hanged from the ceiling and its heights are set random. For taking the above bananas, the agents have to make the organization instead of using the "stand"

and the "pole" in the original problem. This problem is set up as follows:

(i) The agents are located in the grid world (Fig.1). The boundaries of the world are walls. The number of agents is fixed and the initial locations of them are random.
(ii) The agent can sense the status of 1 neighbor sites on the existence of the agents or the targets. Also, the agent can get the distances and the directions of all targets.
(iii) The behavior of the agents is the movements to one of 1 neighbor open sites in one step. The movements include jumping to open space sites and riding on other agents. The wall and other agents are obstacles.
(iv) The agents can ride on supporting area of other agents. The supporting area is upper 3 sites of the agents. The riding agents can't move according to the movements of the supporting agents. Thus, if the riding agents lost the supporting area according to the movements of the supporting agents, the ridding agents fall down to the other supporting areas or floor. (This restriction is important for this problem. Because if this restriction isn't considered, the problem is solved by a very easy algorithm. That is, if all of the agents ride on like as a totem pole and only lowest agent moves left to right, all of the bananas in the height of the totem pole are being taken. To avoid this type of solutions, the restriction can't be removed from the setting of the problem.) In these setting, the agents asynchronously move to make the organization for getting many bananas.
(v) The acquisitions of the bananas are achieved by the agents reaching the sites of the targets.
(vi) The agents can't share the information of the selecting target among them.

Under these specifications, the objective is that the constructing the organizations for getting the bananas based on the autonomous strategy in each agent. Here, each agent can freely select the target banana from them. Thus the agent not only selects the action according to the target of itself but also selects the target itself according to the current situation. Since the selection of the target in each agent is basically free, they can make some organizations simultaneously if it is possible.

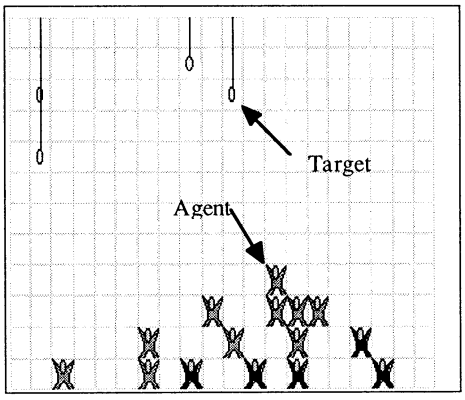


Fig. 1 Multiple Monkey Banana World.

3 Properties of Organization Task

In this section, to reveal the effective strategy of the agents in the introduced problem, the characteristics of the organizations should be discussed.

The processes of constructing the organizations in this problem are different from the tag-game or hunting game [1]. Because, in each step, the actions of the agents are tightly connected with the situations of other agents. For example, the agents in this problem, who want to close the target, require the supporting agents as steps in the direction of the target. However, the action of the agent trying to close the target will fail if the other agents expected to support them leave the site before. Namely, the effects of the actions are frequently changed by others. Therefore, poor strategy of agents for constructing the organization will get only lower bananas. While, superior strategy of them will be able to get very higher bananas relative to the total number of agents. Due to the unexpected moving among each other, in general, the organizing process contains the uncertainty. To decrease the uncertainty, the behavior strategy of the agents will be needed to generate the static environment for succeeding the organization. Therefore, we will take the approach that the behavior strategy is designed to causes the stuck situation. In the next section, the proposed strategy is described.

4 Hill-climbing Moving with Motivation

In this section, the moving strategy with motivation is described. In the game environment, many targets exist. So the agents have to select the target trying to get themselves. After the selection of targets, they should move to close the selected targets according to their moving strategy. In previous section, we discuss the uncertainly of the organizing process in this game. Therefore, the strategy ware required to decrease the uncertainty each other for achieving the successive organizations. Then we employ the hill-climbing strategy related to the selected target for moving of the agent. The employed hill-climbing strategy just make the moving to the site where can be close to the selected target only if the expected site isn't occupied by the other agents and the agent into the place will be expected to be supported by other agents. If the agents have no places satisfying the moving conditions, they remain the same sites until they find the site to be close the targets. These moving conditions are important because all of the agents are basically protected from the unexpected moving by losing the supporting other agents. In addition, to avoid the unexpected moving, we restrict the moving condition of the supporting agents to continue the supporting role till the riding agents leave their supporting areas. Namely, the supporting agents can only select the movements horizontally for continuing to support at least one of the riding agents.

Although the agents with this hill-climbing strategy can avoid the unexpected movements, we can easily image the strategy cause that all of the agents immediately stuck by losing the feasible sites to be close to their targets. That is, all agents will fall into the deadlock situations only by the strategy. Therefore, we have to consider the reorganization of them for escaping the deadlock situations. One way of escaping the situations is that the target is changed. Namely, the agent should abandon to approach to the current target of itself. If the agent losing the feasible sites

change the target, the direction of the hill-climb will change and the agent expects to find the feasible sites to approach the new target. However, all of the agents frequently change the targets, nobody can approach to the targets because the organizations will be frequently broken by the abandonment of the deadlocked agents. Therefore, the agents in the deadlock situations are required not only to abandon the current targets but also to possess the patience to keep them.

To solve the requirement of balancing between the abandonment and the patience concerned with the selecting target, the motivation module is used for selecting the target and keeping of it. The motivation module in the agent works with the hill-climbing module. The motivation module stochastically selects the new target as the motivation among the bananas concerned with the distances between the bananas and the agent. If the motivation module holds the target, the module evaluates the holding target to change or not with the probability determined by the following equation:

$$P(T_g) = \frac{1.0}{1+exp(-1.0 \times G(T_g)/T(t))} \quad (1)$$

where,

$$G(T_g) = \frac{MD - D(T_g)}{MD},$$

Tg: the current target,
MD: maximum distance in the environment,
$D(Tg)$: the distance between the agent and Tg
$T(t)$: temperature.

In above equation, $T(t)$ is affected by the hill-climbing module. If the hill-climbing module succeeds to move to the other site, the module will gradually decrease the temperature in the motivation module as a feedback signal. While if the hill-climbing module loses the feasible sites to move, the module will gradually increase the temperature. Thus, the agents in the deadlock situations become to abandon the current targets in accordance with the holding probabilities, $P(Tg)$, closed to 0. Meanwhile, the agents continuing to approach the targets seldom change the current targets because $P(Tg)$ is closed to 1.

Therefore, the proposed modules interacting each other in accordance with the situations will be expected to decrease the uncertainty and the deadlock situations for achieving the effective organizing processes. The configuration of both modules thought as satisfying the requirements for the organization, however, is sometimes failed to reorganizing the agents. Because the reorganizing property served by the modules still depends on the assignments of the bananas. Namely, even if the agents in the deadlock situations become to change the current targets, it isn't assured that they can find the feasible sites to move. The existence of the feasible sites relies on the directions of new targets. To reduce the dependency of the organizing process to the arrangements of the bananas, we introduce the pheromone style communication methods and the evolutionary learning of it.

5 Evolutionary Learning of Pheromone Style Communication

The pheromone style communication is investigated for improving the organizing ability. In this approach, the pheromones are putted as the marks in the grid with some quantity. According to the time progress, the quantities of the pheromones are decreased. If the marks are remaining in the environment, the agents can observe the pheromone marks. The observed pheromone marks are interpreted as the sub target for the motivation. Namely, the generated pheromone marks can be selected as the targets by the agents like as the bananas. Thus, according to increasing the marks, the chance of the stuck agents will increase to find the feasible sites to move. However, it is remain the question how to determine the mark sites for effectively reorganizing the agents. To acquire the marking rules for the pheromone communication, we introduce the evolutionary learning methods. That is, the generation rules of the pheromone with classifier representation are acquired by Genetic Algorithms.

For the configuration of the generating rules, we assume that the agents make the pheromone in the neighbors of the current targets of themselves. Therefore, the classifier rule consists of the condition of the target's neighbor sites, i.e., space or occupied, the direction of the target from the agent, and the position to generate the pheromone. The rules are represented by the binary code and don't care symbols. All of the agents have same rules and the number of the rules is assumed as four. Genetic Algorithm whose individuals represent the four rules of the classifiers is applied to acquire the appropriate rules. In the next section, we show the experimental results.

6 Experiment

In the experiments, the grid world is set as: the height is 20, and the width is 21. The number of agents is 10. The initial arrangement of the agents is shown in Fig.2. In this arrangement, both groups of agents immediately fall into the stuck situation. To realize the reorganization of them and get the targets, they have to acquire the effective pheromone rules throughout the evolution.

For the evaluation of the rules applied to the situation, the fitness function is set as follows:

$$f(R_i, t) = \frac{MH(t)}{MW(t)} + B(t), \quad (2)$$

where

$MH(t)$: maximum height of the organization at step t,
$MW(t)$: maximum width of the organization at step t,
$B(t)$: reward values related to the number of the obtained bananas.

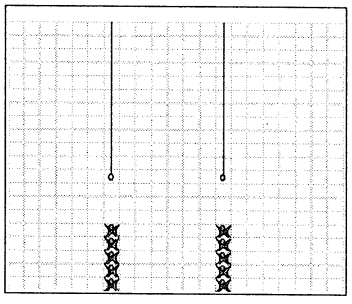


Fig. 2. Initial arrangement of agents.

The fitness value of the rule, *Ri*, is calculated by the average value of *f(Ri, t)* during one trial.

In this experiment, total steps in each trial were increased along to the progress of generation of the genetic algorithms. The results of averaged multiple runs are shown in Fig. 3. In this figure, the progress of the maximum fitness and averaged fitness ware compared with the organization without pheromone in same conditions. Therefore, Since the fitness value is higher than the value of the organization without pheromone, the acquired pheromone communication rules effectively work to take the bananas in this environment. The example of the organizing process is shown in Fig. 4.

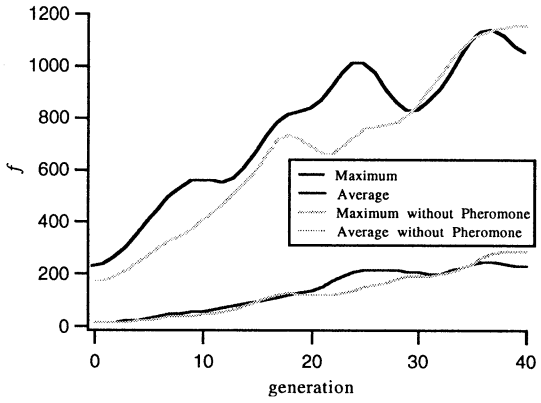


Fig.3 The progress of the fitness according to the evolution.

7 Conclusions

This paper discusses the adaptive pheromone communications for reorganization of the agents in the multiple task processing that required the cooperative organizations. As the organizing problem, we introduce the multiple monkey banana problem and the characteristics of the problem are discussed. Based on this discussion, the simple strategy for the actions of the agents is designed. In this design, we focused on the uncertainty in the organizing behaviors. To decrease the uncertain circumstances, we use a combination of the simple moving strategy and the pheromone style communication. Especially, the communication rules are acquired throughout the evolution. The acquired rules are shown to be effective for reorganizing the agents and to getting the targets.

References

[1]Norihiko Ono, Kenji Fukumoto and Osamu Ikeda: Collective Behavior by Modular Reinforcement-Learning Animats, Proceedings of the Fourth International Conference on Simulation of Adaptive Behavior, Edited by Meyer, J .and Wilson, S.W.,MIT Press, pp.618-624 (1996).

[2] Maes, P.:"A Bottom-upmechanism for Behavior Selection in Artificial Creature", Proceedings of the first international Conference on Simulation of Adaptive Behavior, Meyer J.A. and Wilson S.(eds) MIT Press(1991).

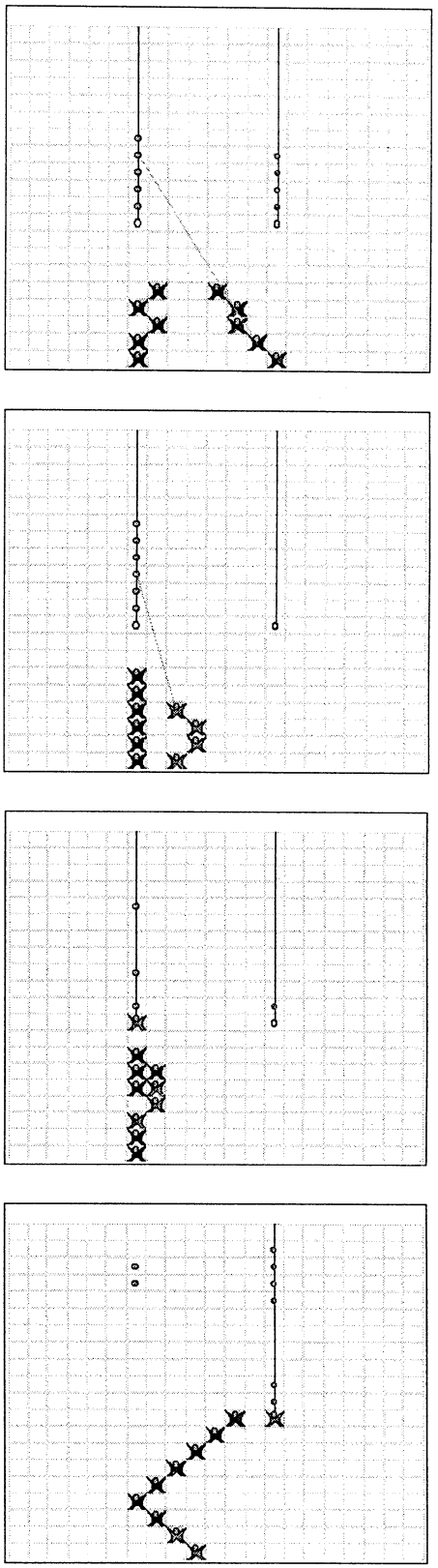


Fig.4 Example of Organization with acquired Pheromone style Communication.

Proc. of Third Int. Symp. on Artificial Life, and Robotics (AROB III' 98),
Oita, Japan, 19-21, January, 1998,

Hovering Control of Model-Helicopter by Vision

Takakazu ISHIMATSU*, KANG Chul Ung*, Taisei FUJITO*, Sumio NAGATA**

*Mechanical Engineering Department of Nagasaki University
Bunkyo-machi,Nagasaki-city,Japan 852
Tel.& Fax. 095-847-3842 , E-mail ishi@net.nagasaki-u.ac.jp

**Technology Center of Nagasaki
Ohmura,Nagasaki,Japan 856
Tel.0957-52-1133 Fax.0957-52-1136

ABSTRACT

An autonomous helicopter system is introduced. A feature of the helicopter system is that autonomous hovering is realized by a vision control system. The vision control system is realized by a camera mounted on the helicopter and the image signal processor on the land. Due to this vision system, the helicopter is able to land and take off without any human assist.

Introduction

In order to realize a low-cost remote-sensing system, a compact model-helicopter and model airplane are often used. However, one problem is that the operation of the helicopter and the airplane require skillful manual operation. Furthermore, the operation is possible only in the range where the operator can recognize the movement of the helicopter and the airplane. Therefore, many advanced technologies are employed to realize autonomous flight without any human assist [1]. For the military purpose, many autonomous flying machines are developed already, neglecting the cost. When we think about the commercial application of the autonomous flying machines, the cost is important factor to be considered. Using the updated computer, electronics devices and also micro-actuators developed in the field of radio-control of model airplane, it is becoming possible to build autonomous flying system with low expenses [2]. In this paper we introduce a low-cost model-helicopter system controlled by a vision system. A feature of the helicopter system is that the system is light and compact, in addition to its low-cost. Another feature of the system is that the hovering, take of and landing is automatically realized by a vision control system. Due to this vision control system, the helicopter system can be operated without any skillful human operations.

The vision system is composed of a TV camera mounted on the bottom of the helicopter, and a specialized land mark on the land which can be readily recognized

from the air. By detecting the land mark, the vision system can obtain the 3-D information about the posture and the position of the helicopter. Based on these 3-D information, the helicopter is controlled by a computer.

System Configuration

In Fig.1, a helicopter system controlled by vision is shown. A feature of this helicopter is that the helicopter has a CCD camera which detects the image of the land mark. The images obtained by the camera is transmitted to a vision control system on the land by the radio signal (12GHz). The vision control system receives the images and extracts the land mark from the images. By analyzing the geometry of the land mark on the images, the three-dimensional posture and the position of the helicopter are obtained. Based on the data obtained, the control signal of the helicopter is determined so that the desired position and posture are realized. The control signal is transmitted to the helicopter by the normal radio-control signal.

Determination of 3-D position and posture by vision

The position and the posture of the helicopter can be obtained by the vision of the land mark. Suppose the shape of the land mark is designed like the letter H. Geometrical relation of the land mark and the image is shown in Fig.2, where the xyz coordinate system is settled at the camera. The film plane corresponds to the plane which is defined as the equation

$$z = f$$

where f is the focal length.

In Fig.2 four ends of the land mark are denoted as Q1,Q2,Q3,Q4. Suppose position vectors of these four points are q1,q2,q3,q4 and position vectors of projected points of Q1,Q2,Q3,Q4 onto the image plane are p1,p2,p3,p4.

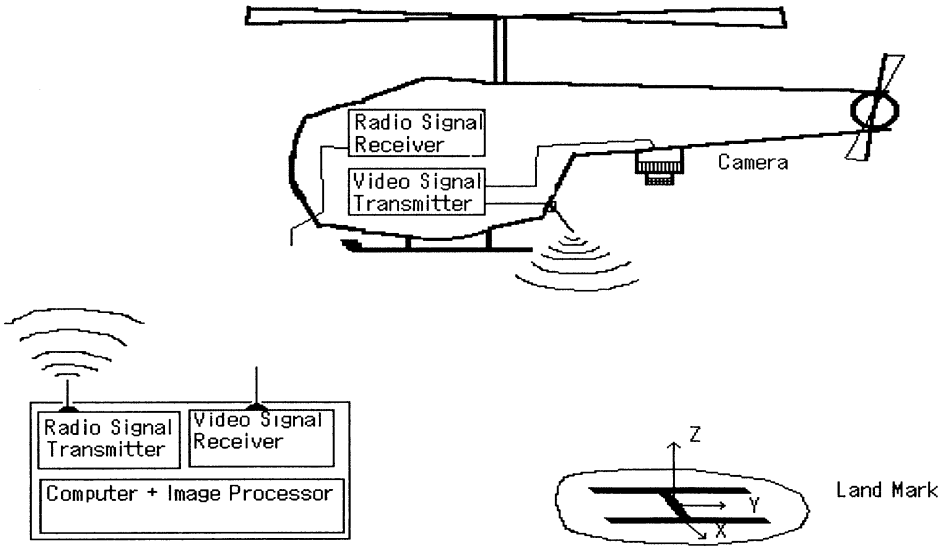


Fig.1 Configuration of Helicopter System

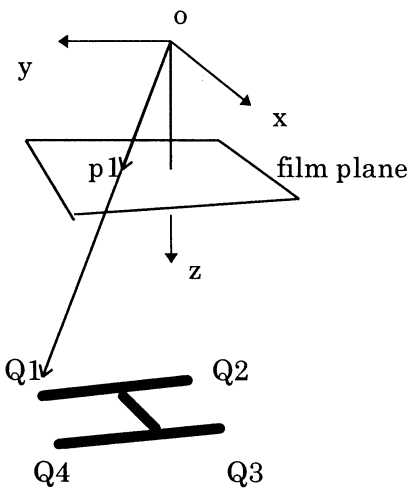


Fig.2 Relation of land mark and its image

This means that elements of the vector $\mathbf{p}_i$ are (xi, yi, f), where (xi, yi) is the raster coordinate of the i-th projected point.

From the above definition, we obtain

$\mathbf{q}_i = k_i\mathbf{p}_i$ where k_i is unknown scalar parameter. Considering the shape of the land mark, the following relation can be readily obtained

$$k_1\mathbf{p}_1 - k_2\mathbf{p}_2 = k_4\mathbf{p}_4 - k_3\mathbf{p}_3$$

By multiplying the $\mathbf{p}_3 \times \mathbf{p}_4$, we obtain

$$k_1\,\mathbf{p}_1 \cdot (\mathbf{p}_3 \times \mathbf{p}_4) = k_2\,\mathbf{p}_2 \cdot (\mathbf{p}_3 \times \mathbf{p}_4)$$

Therefore,

$$k_2 \,/ k_1 = \mathbf{p}_1 \cdot (\mathbf{p}_3 \times \mathbf{p}_4) \,/\, \mathbf{p}_2 \cdot (\mathbf{p}_3 \times \mathbf{p}_4)$$

Similarly we can obtain

$$k_3 \,/ k_1 = \mathbf{p}_1 \cdot (\mathbf{p}_2 \times \mathbf{p}_4) \,/\, \mathbf{p}_3 \cdot (\mathbf{p}_2 \times \mathbf{p}_4)$$

$$k_4 \,/ k_1 = \mathbf{p}_1 \cdot (\mathbf{p}_2 \times \mathbf{p}_3) \,/\, \mathbf{p}_4 \cdot (\mathbf{p}_2 \times \mathbf{p}_3)$$

It is important to note that ratio $k_1{:}k_2{:}k_3{:}k_4$ are determined by the above equations. Parameters $k_1{:}k_2{:}k_3{:}k_4$ can be determined by the fact that the length of edges between Q1 and Q2 and also Q3 and Q4 is known in advance, for example as L. This means parameter k_1 can be determined by equating the following equation,.

$$| k_1\,\mathbf{p}_1 - k_2\,\mathbf{p}_2 | = \mathrm{L}$$

Once all parameters $k_1{:}k_2{:}k_3{:}k_4$ are determined, the position and the posture of the land mark in the camera coordinate system is obtained.

The geometrical relation between the camera coordinate system(xyz) and the world coordinate system(XYZ) can be obtained as follows.

$$\begin{bmatrix} x \\ y \\ z \\ 1 \end{bmatrix} = (\mathbf{w}_1 \quad \mathbf{w}_2 \quad \mathbf{w}_1 \times \mathbf{w}_2 \quad \mathbf{v}) \begin{bmatrix} X \\ Y \\ Z \\ 1 \end{bmatrix}$$

where

$\mathbf{w}_1 = (\mathbf{p}_4 - \mathbf{p}_1) \,/\, |\mathbf{p}_4 - \mathbf{p}_1|$

$\mathbf{w}_2 = (\mathbf{p}_2 - \mathbf{p}_1) \,/\, |\mathbf{p}_2 - \mathbf{p}_1|$

$\mathbf{v} = (\mathbf{p}_1 + \mathbf{p}_2 + \mathbf{p}_3 + \mathbf{p}_4) \,/ 4.$

From the above homogeneous transformation matrix, the position and the posture of the helicopter can be determined.

Experiment

In Fig.4 our test helicopter system is shown. A commercialized compact and light helicopter(payload is 1.0 Kg) is used. The position and the posture data of the helicopter can be obtained 30 times per a second by the image processing.The image processing is executed by a DOS/V machines. The position and posture data are used as feedback signals of PID control of the helicopter.The control signal is calculated 30 times per a second. The control signal calculated is converted to PWM signal by a logic circuit and transmitted to helicopter as a wireless signal.

The size of the land mark was 30cm in height and 30 cm in width. At the beginning the helicopter was settled on the land mark. The command was to move the helicopter from the land to the hovering position, the height of this postion was 2 m. We succeded to levitate the helicopter and keep it at the desired position.Details of the experiment will be mentioned at the presentation.



Fig.4 Test Model Helicopter

Conclusions

A compact and low-cost helicopter system is introduced, whose main body is composed of comercialized low-cost model helicopter. By detecting the position and the posture of the helicopter using the camera on the helicopter, we succeeded to realize auto-hovering of the helicopter without any humn assist. The proposed system employed the video signal communication system. Due to this system, main control system is settled on the land. Therefore, we need not worry about the weight of the computer system of the helicopter system. We are now preparing to install all sensors and computer system on the helicopter, since we already succeeded to fly the model airplane by installing the computer and sensors on the airplanes. Using the advanced RISC computer chips and recent FPGA chips, it is now possible to realize autonomous hovering of the model helicopters.

References

1)T.Yamaguchi er al.,"Intelligent Control of a flying vehicle of using fuzzy associative memory system",Proc.IEEE Int. Cong. on Fuzzy Systems, 1139-1149(1992)

2)S.Mizoguchi et al.,"Modeling and Robust Control of a Saucer-type Helicopter", Proc. Asian Control Conf.,Vol.1, Tokyo, July, 313-316 (1994)

Proc. of Third Int. Symp. on Artificial Life, and Robotics (AROB III' 98),
Oita, Japan, 19-21, January, 1998,

A Morphological Approach to Feature Extraction for Fish Discrimination Robot

Yutaka Nagashima
Dept. of Electrical Eng.
Sasebo National College of Technology
1-1 Okishin, Sasebo, 857-11 JAPAN

Takeshi Nakazono
Dept. of Electrical Eng.
Sasebo National College of Technology
1-1 Okishin, Sasebo, 857-11 JAPAN

Takakazu Ishimatsu
Dept. of Mechanical Systems Eng.
Nagasaki University
1-14 Bunkyo, Nagasaki, 852 JAPAN

Abstract

This paper presents a new method how to extract feature for fish discrimination using morphological filter. Japanese consume great quantities of common fish like Mackerel and Sardine. The fishing industry is very interested in the development of a fish discrimination and sorting system. The conventional method of fish discrimination used parameters which relied upon the physical characteristics of shape and contour. This method was insufficient for practical fish discrimination. There is not a practical application system yet. The mathematical morphology has proven to be the most suitable method to extract the features. We focused on the speckle patterns of the fish as significant identification features. We tried to extract the features of Japanese Horse Mackerel, Pilchard Sardine and Mackerel by implementing newly designed morphological filters. Experimental results show the discrimination performance is superior to conventional methods.

Key words: morphological filter, feature extraction, fish discrimination, speckle patterns

1 Introduction

In this paper, a new morphological approach to extract feature for fish discrimination robot is proposed. The Japanese fishing industry is interested in the development of an effective fish discrimination and sorting system. Because of working condition and laber environment is hard at fish market. The automation of fisheries is desiring earnestly. This technology would enhance the marketing of many fish. In the past, the methods of identifying fish species have relied upon the physical characteristics of shape and contour. Physical parameters were mainly used in regard to body length, depth of body, perimeter, area, and their ratio. To some extent, it was possible to discriminate fish species[1],[2]. Other physical parameters include the colour of the fish. While there are varieties of colouring patterns on fish, it is significant that colouring patterns depend upon the species, and are reliable source of identification.

The identifying characteristics of colour and size of fish often vary in regard to environment and location. Even in the same species of fish, the discrimination by the colour is significantly influenced by the strength and quality of the light source. The observation of fish colour indicates a gradual change of protective colouring along the back and the ventral areas. In this paper, we focused on the fish's speckles (colouring pattern) as significant parameters with which to discriminate fish species. As an efficient tool to extract speckle patterns, we employed newly designed morphological filters. Experimental results show the discrimination performance is superior to conventional methods.

2 Morphological Operation

Mathematical morphology has been of increasing interest in the area of non-linear image processing. Mathematical morphology provides us the theory and the tools to analyze shapes. This benefit has been noticed by many researchers in the shape analysis and several optimal algorithms have been proposed[3]-[5]. The four fundamental kinds of operations are dilation, erosion, opening, and closing. The definition of gray-scale morphological operations are as follows:

Supporse that a set A in the Euclidean N-space (E^N) is given. Let F and K be { x $\in E^{N-1}$ | for some y $\in$ E, (x,y) $\in$ A }, and let the domains of the gray-scale image be f and the gray-scale structuring element be k, respectively. The gray-scale dilation of f by k, which is denoted by $f \oplus k$, defined as

$$(f \oplus k)(x,y) = max\{f(x-m, y-n) + k(m,n)\} \quad (1)$$

for $all(m,n) \in K$ and $(x-m, y-n) \in F$. Dilation causes an expansion of an image and tends to fill in

small background area such as holes or gaps.

The gray-scale erosion of f by k, which is denoted by $f \ominus k$, is defined as

$$(f \ominus k)(x,y) = min\{f(x+m, y+n) - k(m,n)\} \quad (2)$$

for all $(m,n) \in K$ and $(x+m, y+n) \in F$. Erosion causes shrinking of an image and tends to eliminate small structures such as shape peaks of narrow bridges.

When combined in sequence, erosion and dilation give the actions of opening and closing, respectively. The gray-scale opening of f by k, which is denoted $f \circ k$, is defined as

$$f \circ k(x,y) = \{f(x,y) \ominus k(x,y)\} \oplus k(x,y) \quad (3)$$

Opening can reduce noise from image data. The gray-scale closing of f by k, which is denoted $f \bullet k$, is defined as

$$f \bullet k(x,y) = \{f(x,y) \oplus k(x,y)\} \ominus k(x,y) \quad (4)$$

Closing can fill small holes.

3 Extraction Processing

The Japanese Horse Mackerel has about seventy placoid scales along the center line of the lateral body. The Pilchard Sardine has black dots that form a queue along the center of the lateral body. Mackerel has striped patterns on the back of the body. These speckles are constant and remarkable features that serve to distinguish these fish from the others. From this aspect, we propose discrimination algorithms for these fish. A flows of feature extraction are as follows:

3.1 Japanese Horse Mackerel

(1a) Image data was acquired by CCD camera with a size of 512*480 pixels. The feature patterns are extracted from full scale image data in order to reduce the processing time.

(2a) Since the placoid scales are similar to the vertical bar, we tried to eliminate the vertical parts using a opening operation which was made possible by implementing the newly designed horizontal bar filter in Fig.1. The placoid scale is extracted by subtracting the resulting image from original mackeral image data.

1	1	1

Fig.1 Horizontal Bar Filter

(3a)The image is binarized, and the closing operation is processed using the filter as shown in Fig.2. The placoid scales image is eroded by the vertical bar filter in Fig.3.

(4a) To discriminate the Japanese Horse Mackerel, an auto-correlation function was calculated in order to confirm the periodicity of placoid scales.

0	1	0
1	1	1
0	1	0

Fig.2 Binary Disk Filter

1
1
1
1
1

Fig.3 Vertical Bar Filter

3.2 Pilchard Sardine

(1b) The region of black dots is detected utilizing the same method as (1a).

(2b) To eliminate the black dot patterns, the original image is processed by dilation four times, using the newly designed filter in Fig.4. Erosion of the dilation image is implemented four times, using the same filter. We used smaller size filter than the size of black dots in order to decrease the processing time by multi-scale filtering method. The black dot pattern is extracted by the subtraction of the resulting image from original image data.

(3b) The gray-scale image is changed to the binary image data considering threshold level. The closing operation is processed to eliminate noise using binary filter in Fig.2.

(4b) Labeling operation is executed and white clusters in the image are extracted. The number of dots (white clusters) along the center of the lateral body and those area and shapes were examined. The Pilchard Sardine is discriminated from the others.

1	3	1
3	5	3
1	3	1

Fig.4 Gray-scale Disk Filter

3.3 Mackerel

(1c) The region of striped pattern of Mackerel is detected utilizing the same method as (1a).

(2c) The original image of the Mackerel is changed to the binary image data by the calculating threshold

lebel. The striped pattern is dilated to be extracted using a filter in Fig.3.

(3c) The extracted results was widely periodical stripes. To discriminate the Mackerel, the number of same-sized ratio that was calculated as areas divided by perimeters were counted.

4 System Configuration

For the purpose of the features extraction, we configured the parallel image processing system as shown Fig.5. T9 are parallel processing units. The feature extraction and the fish discrimination among fish kinds are processed in parallel. A Parallel Cluster allows for great flexibility of the network topology, utilizing virtual channel processors, and is user-friendly.

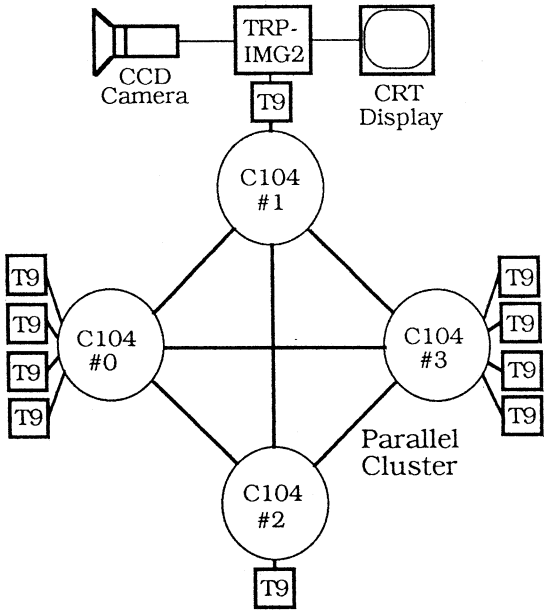


Fig.5 Configuration of Experimental System

5 Experimental Results and Discussions

5.1 Japanese Horse Mackerel

We tested fifty Japanese Horse Mackerels for these experiments. The original Japanese Horse Mackerel image is shown in Fig.6. We obtained good extraction results when the newly designed bar filters were used. The feature extraction result is shown in Fig.7. The feature of Placoid scales are formed by many vertical scales at periodic intervals. An autocorrelation function was calculated to extract the periodicity of pracoid scales. The periodicity of pracoid scales is shown in Fig.8. The percentage of discrimination was about 94%. The results of autocorrelation is indicated from the peaks of two dot to five dot intervals. The periodicity of placoid scales was determined when the number of peaks was more than five. The time of feature extraction was 892ms.

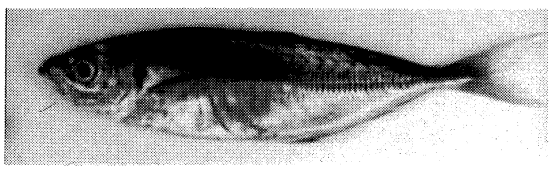


Fig.6 Original Image of Japanese Horse Mackerel

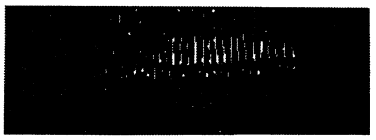


Fig.7 Result of Feature Extraction

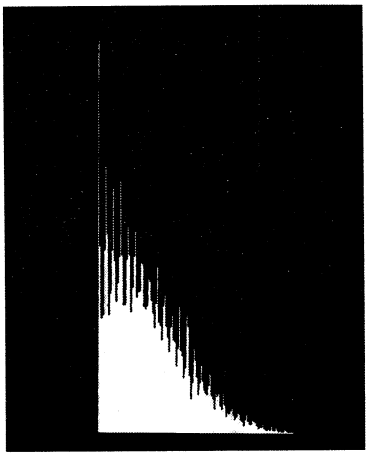


Fig.8 Periodicity of Placoid Scales

5.2 Pilchard Sardine

We tested fifty Pilchard Sardines for these experiments. An example of the original Pilchard Sardine image is shown in Fig.9. A feature extraction result after labeling operation is shown in Fig.10. The discrimination of this Pilchard Sardine is based upon



Fig.9 Original Image of Pilchard Sardine

to the dot queue along the center of the lateral body. The range of dots were within an area of five to fifty. The percentage of discrimination was about 95% using a judgement of more than four dots. The

result were superior to any conventional discrimination methods. The time of feature extraction was 1482ms.

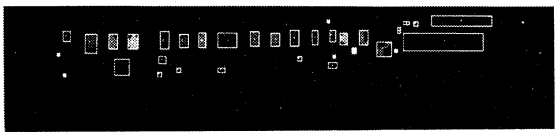


Fig.10 Result of Feature Extraction with Labeling

5.3 Mackerel

The original mackerel image is shown in Fig.11. A feature extraction results is shown in Fig.12. The labeling operation of Mackerel was calculated using the stripes of area and perimeter and its ratio. The range of stripes was decided by the number of a ratio from about three to six. The gravity's interval on each stripe is calculated on a number of fifteen to thirty-five. The percentage of discrimination was about 94%. The time of feature extraction was 610ms.

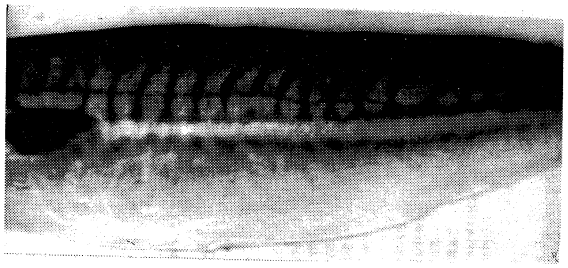


Fig.11 Original Image of Mackerel



Fig.12 Result of Feature Extraction

6 Summary

We studied a new method of feature extraction for fish discrimination using the morphological filter. We focused on the speckle patterns on the fish as significant identification features. We tested to extract the features of Japanese Horse Mackerel, Pilchard Sardine, and Mackerel by implementing the newly designed morphological filters and argorithms. Experimental results show better performance than conventional methods which use the physical characteristics of shape and contour.

This method will be advanced through incorporating the physical characteristics and also parallel argorithms for quicker processing and load balance.

References

[1] T. Hiraoka, K. Yano, and R. Takiyama, "Image Recognition Based on Contour and Texture Information -An Application to Fish Images-", Technical Report of IEICE. PRMU96-148, 1997-1, pp.55-62

[2] F. Kurokawa and H. Matsuo, "Image processing system for Fish Discrimination", The Proceedings of IEICE. Kyusyu Branch annual meeting, 1995-10, pp.688

[3] R. M. Haralick, S. R. Sternberg, and X. Zhuang, "Image Analysis Using Mathematical Morphology", IEEE Transactions on Pattern Analysis and Machine Intelligence, Vol. PAMI-9, No.4, JULY 1987, pp.532-550

[4] Y. Li and H. Kobatake, "Sketch Image Extraction of Face and Its Reconstruction", Technical Report of IEICE. PRMU96-49, 1996-9, pp.1-8

[5] S. Yamamoto, I. Tanaka, M. Senda, Y. Tateno, T. Iinuma, and T. Matsumoto, "Image Processing for Computer-Aided Diagnosis of Lung Cancer by CT(LSCT)", Transaction (D-2) IEICE. Vol.25, 1993-2, pp.250-260

[6] Y. Nagashima, T. Nakazono, and T. Ishimatsu,"Parallel Implementation of features Extraction Using Morphological Filter", The Proceedings of MVA'96 IAPR Workshop on Machine Vision Applications, 1996-11, pp.426-429

Proc. of Third Int. Symp. on Artificial Life, and Robotics (AROB III' 98),
Oita, Japan, 19-21, January, 1998,

Three-dimensional measurement of object surface and moving particles using Circular Bias

Kikuhito Kawasue
Mechanical Engr. Dept.
Sasebo National College of Tech.
1-1 Okishin Sasebo, 857-11 JAPAN

Isamu Iwamoto
Electronics Engr. Detp.
Sasebo National College of Tech
1-1 Okishin Sasebo, 857-11 JAPAN

Takakazu Ishimatsu
Mechanical Eng. Dept.
Nagasaki University
14-1 Bunkyo, 852 JAPAN

Abstract

A new approach to the three-dimensional measurement of the object surface and moving particles is introduced. A single TV camera with an apparatus to add the circular bias to the image enables us to record the three-dimensional information of measuring points as streaks on a single image. Every shape of the streak on the image plane is related to the position of the measuring point. The information is extracted from the image using an image processing technique.

Keywords: Measurement, Image processing, Three-Dimensional, Coupled mirrors, Particle

1. Introduction

The automatic inference of depth information has been one of the primary aims of computer vision system. Stereo vision that calculates the depth by analyzing two or three frames viewed from different angles is used in many cases.[1][2] The results essentially depend on how accurately matching pairs can be found between these frames. There are two problems in implementing the stereo vision. One problem related to the stereo vision is that finding matching pairs between frames causes difficult computer processing since there are, in general, several possibilities for the choice of the matching point. Another problem is a limitation of measurement accuracy in stereo vision system. The measurement accuracy is influenced directly by the resolution of the image capturing apparatus.

In order to cope with the matching problem and improve the measurement accuracy, we developed a new three-dimensional measuring system that uses a single TV camera. By introducing coupled mirrors on the TV camera lens, measuring points that appear on the image plane is displaced according to the depth. Upon rotating the coupled mirrors at high speed (1,800 rpm) during the TV camera exposure, these measuring points are shifted and appeared to be circular streaks on a image plane. The size of the circular streak directly relates to the depth of the measuring point and is inversely proportional to the depth. The depth can be measured easily by processing the circular image, where the cumbersome task to find matching pairs is not necessary. The processing required for the circular streak is to obtain the center point and the diameter. The diameter of each circular streak can be measured more than 100 times at different angles and the final result of the diameter is obtained by taking the average of them. Therefore, the accuracy is not limited by the resolution of the image capturing apparatus and the depth can be measured with sub-pixel accuracy.

One more important feature of our system is the registration of motion information of measuring points. In the case that the measuring point is moving on parallel direction with the retinal plane, the shape of the streak appeared on the retinal plane is changed from circle to spiral. Since the frequency of coupled mirrors is constant, the pitch of the spiral streak is directly proportional to the velocity of measuring point. In the case that the measuring point is moving on vertical direction with the retinal plane, the size of spiral streak is varied according to the depth. Therefore, the spiral streak has all 3-D information such as 3-D position and 3-D motion of measuring point and this information can be estimated using image-processing technique.

2.Measurement system

A simplified setup of our imaging system is shown in Fig. 1. By introducing coupled mirrors on the TV camera lens, the image of the measuring point is displaced with the corresponding displacement related to the distance between the TV camera and the measuring point.

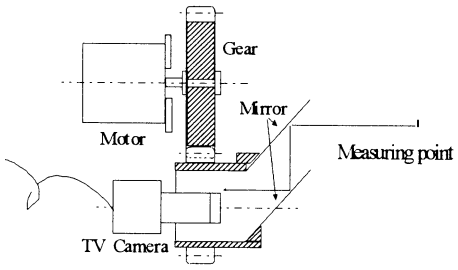


Fig. 1 System set up

That is, the displacement r on the image is inversely proportional to the distance D between the measuring point and the camera as follows.

$$D = \frac{f \cdot d}{r} \tag{1}$$

where f is the focal length of the camera and d is the distance between the coupled mirrors. When the coupled mirrors are rotated physically at high speed during the exposure of the TV camera, circular streaks appear on an

image since the rotational shift is added to the image. Since the size of the streak is inversely proportional to the distance of the measuring point from the camera, the positional information of the measuring point can be obtained by processing the circular streak.

When the measuring point is moving in the exposure of the TV camera, the streak draws spiral streak, If a particle is moving from left to right, it draws spiral streak from left to right and the radius of streak varied depending on the variation of the distance. All spiral streaks have the same rotational direction on the image plane according to the rotational direction of the coupled mirrors. The location and the size of the spiral streak on the image are related to the three-dimensional location of the particle, and the pitch and size variation of the streak are related to the three dimensional velocity of the particle. In Fig.2, the spiral streak of a pendulum movement is shown, where it moved from a far right point to a near left point.

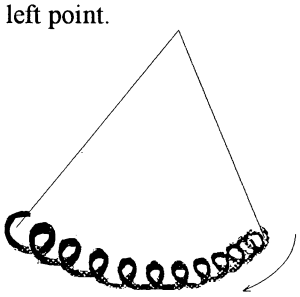


Fig.2 Path-line of a pendulum

3.Image processing

3.1 Extraction of the center point

The following processing is used to find the center point of the circular streak accurately.

By finding the maximum and the minimum position of pixels on circular streaks, the circumscribe rectangle is defined. The example of the rectangle overlapped on the circular streak is shown on Fig.3. The approximate center point Po(Xp,Yp) of the circular streak is calculated easily by finding the center point of this rectangle. The more accurate center point is detected by use of this approximate center point. $r_{x,y}$ is a distance from the line of y=Yp on Fig.3. The top position P1 of the circular streak is calculated accurately by extracting the pixel data on the hatched band by the following equation.

$$Y1 = Y_p + \frac{\sum_{x=x_p-4}^{x_p+4}\sum_{y>y_p} f_{x,y}\cdot r_{x,y}}{\sum_{x=x_p-4}^{x_p+4}\sum_{y>y_p} f_{x,y}} \quad f_{x,y} > \text{threshold level} \quad (2)$$

where $f_{x,y}$ is a pixel intensity on the position (x,y).

The locations of P1, P2 P3 and P4 are calculated by the same way and the center point of the circular streak is recalculated by the following equation.

$$\begin{bmatrix} x_p \\ y_p \end{bmatrix} = \begin{bmatrix} (X1+X2)/2 \\ (Y1+Y2)/2 \end{bmatrix} \quad (3)$$

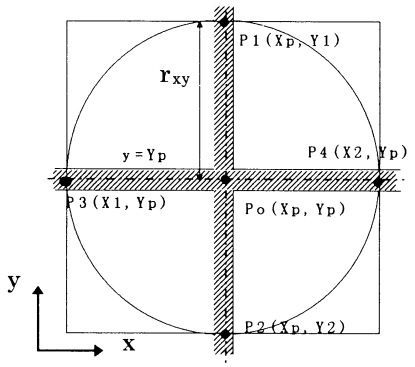


Fig.3 Extraction of the center from circular image

The amount of data to be used for extracting the center point of circular streak is reduced extremely by this technique and it enables the fast processing.

3.2 Extraction of the size of circular streak

The size r_p of the circular streak is inversely proportional to the distance between the TV camera and the measuring point. The depth can be measured by calculating the size of the circular streak. Since the streak is circular, the diameter of this streak can be measured many times at various angles and the final result of the diameter is obtained by taking the average. In order to simplify this procedure, the following technique is used in our system. For the first step, the summation of the pixel intensity where the distance is r from the center point Po is calculated by following equation.

$$F(r) = \sum_{\theta=0}^{2\pi} f(r,\theta) \quad (4)$$

where $f(r, \theta)$ is a pixel intensity. This method is also illustrated in Fig. 4.

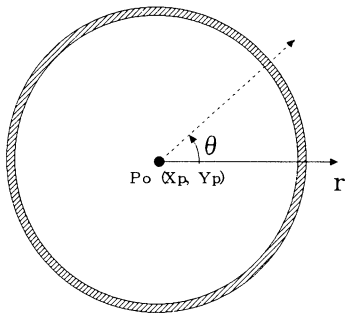


Fig.4 Measuring of the size of circular image

For the second step, Fig.5 is drawn by use of the results of (4).

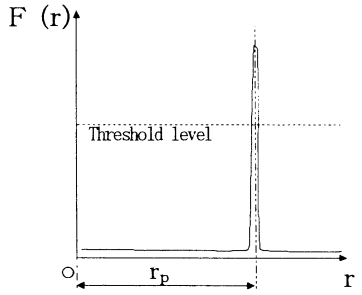


Fig.5 Intensity of pixel on r axis

F(r) over the threshold level is used to find the radius r_p of the circular streak where F(r) peaks within the graph. The r_p is calculated by (5).

$$r_p = \frac{\sum_i r_i \cdot F(r_i)}{\sum_i F(r_i)} \qquad F(r_i) > \text{Threshold level} \qquad (5)$$

3.3. Computation of spiral images

The rotational frequency of the coupled mirrors are synchronized with the frame frequency of the TV camera. It makes the shape of spiral streaks on each frame similar, which simplifies the following image processing. These processes are also robust by searching the similar shape of the streak and considering the connectivity of the spiral streak. In the image processing, one spiral image extracted on the first image is slid on the second image and compared with the second image to estimate the velocity information. Fig.6 shows the one example of extracted spiral image.

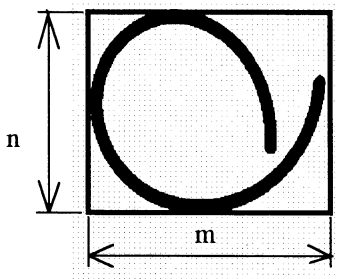


Fig.6 Extracted spiral image

The translational displacement and size variation rate between the two spiral streaks are measured by the use of the pattern matching method. After obtaining the amount of the shift of the spiral image., the coordinate on the image plane is translated to the world coordinate (x_w, y_w, z_w) by the following equation.

$$\begin{bmatrix} x_w \\ y_w \\ z_w \end{bmatrix} = \frac{d}{r_{i0}} \begin{bmatrix} x_{i0} \\ y_{i0} \\ f \end{bmatrix} \quad , \quad \begin{bmatrix} v_{xw} \\ v_{yw} \\ v_{zw} \end{bmatrix} = \frac{d}{\Delta t} \begin{bmatrix} \frac{x_i}{r_i} - \frac{x_{io}}{r_{io}} \\ \frac{y_i}{r_i} - \frac{y_{io}}{r_{io}} \\ \frac{f}{r_i} - \frac{f}{r_{io}} \end{bmatrix} \qquad (6)$$

where f is the focal length of the lens and d is the shift by the mirrors.

4. Experiment

In order to evaluate the feasibility of our system, the following experiment was conducted. The plane board was set on parallel against the image plane of TV camera at the known distance from the TV camera. The measuring point was illuminated on the surface of the board by a laser spot beam. The laser spot drew the circular streak by the rotating coupled mirrors. After the image data of circular streak was stored in the image memory (resolution is 512*512), the data was sent to the personal computer (NEC:PC-9821Xp, DX4-100MHz) and the personal computer calculate the depth of the board from the TV camera. The depth of the board was changed from 300mm to 600mm by every 50mm. The distance between mirrors was set to 40mm and focal length f of the TV camera was 3000[pixel]. The result of this experiment is shown on Fig.7.

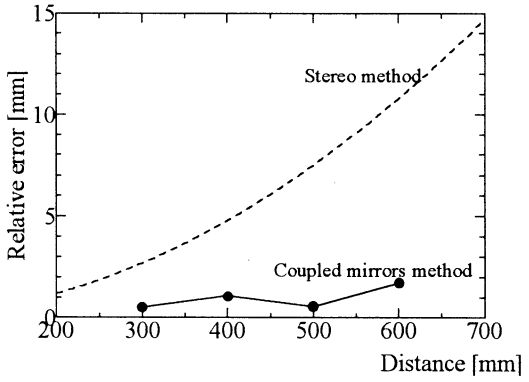


Fig.7 The experimental result of depth measurement

The graph indicates the average error [σ] of depth measurement. The dotted line indicates the theoretical error of stereo method in the case that the distance between TV cameras is same with the distance between mirrors of our system. Therefore these systems are equivalent . The theoretical error of the stereo method can be calculated using the resolution of TV camera. It means the output of the image processing is not sub-pixel accuracy, but pixel accuracy.

Fig.8 is an example of 3-dimensional surface measurement which was measured by scanning a laser spot. The depth from the TV camera was 60[cm] and 40*40 different points were measured on the surface of shells. Photo.1 is an image of measured shells and Fig. 8 is a recovered image from results. The image of Fig.8 was recovered by interpolating from the 40*40 position data.

The next example is a measuring result of moving particle. The experiments are performed on the water flow field through a tank (400x250x250) with offset inlet and outlet ducts. Water is pumped and circulated through a test section. The inlet duct has a cross-section

of a 1.5 cm diameter and is located at the lower-left corner. While the outlet duct has the same cross-section as the inlet at the upper-right furthest corner. The inlet flow velocity is set to 0.3 m/s in the present experiment. Polystyrene particles with 0.5 mm or less in diameter, are introduced in the water as seeding particles. The particles have a specific gravity of 1.03, so that they may be considered neutrally buoyant in water. The entire chamber is made of a clear plexiglas of 10 mm thickness so that light emitted from the projector can pass through the test chamber illuminating the particles in the flow. Fig.9 shows one example of particle streaks in a water flow field. Spiral streaks are recorded on an image. Fig.10 shows the result of the measurement in the chamber. These velocity vectors are calculated on an equidistant grid by the interpolation of the velocity data estimated from the spiral image.

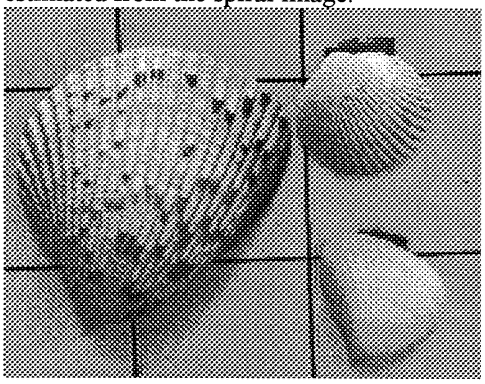


Photo.1 Measured shells

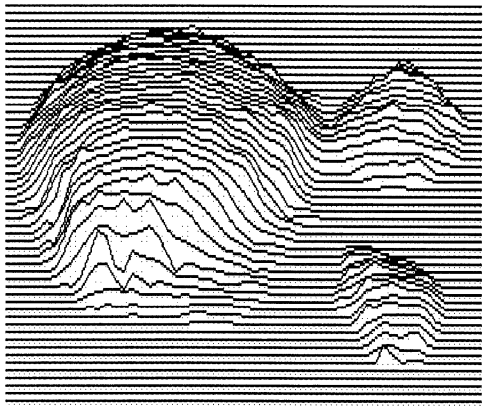


Fig.8 Experimental result

5.Conclusion

The new approach to obtain the depth information is introduced. A single camera and an image rotation apparatus record the three-dimensional information on a single image. The shapes of the circular or spiral streaks recorded on the image plane relate directly to the three dimensional positional information of the individual measuring point. The 3-D information of measuring point is obtained by using an image processing technique. The image processing technique enables an accurate 3-D measurement.

The features of our system is that the system is compact and the set up is simplified since it uses a single camera. To ensure accuracy the object point needs to be illuminated by a spot light or clearly recognized from the background image.

In this paper, the proposed system used a TV camera. A still camera is also available. Therefore, if a more accurate measurement is required, a still camera should be used.

Acknowledgement This work partly supported by the Sasakawa Scientific Research Grant from The Japan Science Society

References

[1]Three-dimensional computer vision, A geometric viewpoint, Olivier Faugeras, 1996

[2]Computer vision: Theory and industrial application, Springer-Verlag, 1992

[3]R. Naavtia, Depth measurement from motion stereo, Comput. Graphics Image Process., 9(1976), pp.203-214.

[4]T.D.Williams: Depth from camera motion in a real world scene, IEEE Trans. Pattern Anal. Machine Intell., PAMI-2(1980), pp.511-516.

[5] G. Sandini and M. Tistarelli, Active tracking strategy for monocular depth inference over multiple frames, IEEE Trans. Pattern Anal. Machine Intell., 12(1990), pp.13-27

[6] M.J. Black and P. Anandan, A model for the detection of motion over time, in third international conference on computer vision(1990), pp.33-37.

[7]A. M. Waxman and S.S. Shinha, Dynamic stereo: Passive ranging to moving objects from relative image flow, IEEE Trans. Pattern Anal. Machine Intell., PAMI-8(1986), pp.406-412.

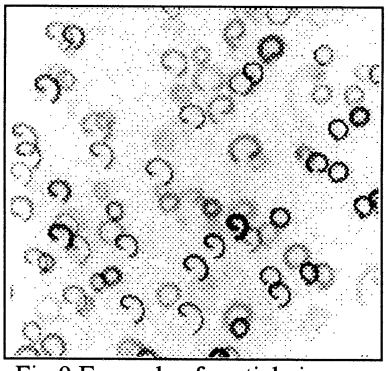


Fig.9 Example of particle images

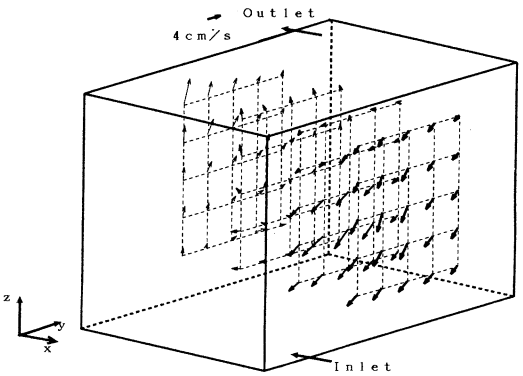


Fig.10 Velocity distribution in a chamber

Proc. of Third Int. Symp. on Artificial Life, and Robotics (AROB III' 98),
Oita, Japan, 19-21, January, 1998,

Computer Input Device for Handicapped Using Vision Sensor

Tsumoru OCHIAI [*] Takakazu ISHIMATSU [**]
Osamu TAKAMI [***] Ryouji MATSUI [*]

* Intelligent System Engineering , Ube National College of Technology , Tokiwadai, Ube 755 , JAPAN
** Department of Mechanical Systems Engineering, Nagasaki University , Bunkyo-machi , Nagasaki 852 , JAPAN
*** Technology Center of Nagasaki Prefecture , Ikeda , Ohmura 856 , JAPAN

abstract

In this paper we propose one computer input device for physically handicapped people, which enables operator to communicate with the computer without typing on the computer keyboard. Input signals of this device are three-dimensional position and posture of head and blinking action of operator. The position and posture of head are detected by image processing. One feature of our device is that the operator is required to wear a special glasses with three LED marks. Due to the special geometry of LED marks, the three-dimensional position and posture of the glasses can be detected. The position and posture of head is used as a positioning signal of the computer cursor on CRT monitor. Blinking action of operator's eye or breathing action is used as a switching signal for selecting items. We applied this input device to operate word-processing system under the environment of Windows95. Experimental results reveal the applicability of our system.

1. Introduction

Nowadays, the increase of the aged people has become one of the notable social problem, and it should be noticed that many of them are handicapped in some meaning. Therefore, development of supporting devices and care equipments for the handicapped people is highly desired. One difficult problem related with the development of such supporting devices is that every handicapped people has various physical abilities. Therefore, supporting devices should be developed considering the remaining ability of every handicapped people. The data input devices which enable the handicapped operator to communicate with the computer are one of the most important keys of the supporting devices. Such input devices have already developed and used practically. Some of them use the breathing action as control signals[1][2]. Some of them use the location of eyeball on the captured image as control signals[3][4].

We have already developed some data input devices for handicapped people. One device is used to operate word-processor machine[5]. This device detects two-dimensional movement of eye location on the captured image. Computer cursor is moved corresponding to the deviation from primary position of eye on the image data. Another device is used to control electric wheel-chair[6]. This device detects three-dimensional position of head by detecting marks attached on the operator's head. The former enables to operate word-processor machine without wearing any equipments. However, the performance to track the location of eye is not enough if the operator moves quickly. The reason is that all of image processing are executed by software. The latter enables to detect three-dimensional position of operator's head accurately. If this device is applied to operate computer cursor on CRT monitor, operator enables to select characters displayed on CRT monitor easily. However, since this device requires to push switch in his mouth by tongue or lips, handicapped people feels that this action is uncomfortable. Therefore we developed a new input device combining the features of above two devices. Namely, the movement of cursor on CRT monitor is controlled by position of LED marks on the operator's head and the selected character is inputted by blinking action or breathing action. As the results of this way, the operator is relieved from the complicated action and ability of tracking is improved extremely. We applied this device to operate word processing software and other computer application softwares under the environment of Windows95.

2. Configuration of input device

This system is composed of a personal computer (PC-9821), CCD camera, image capture board, digital input/output board, pressure sensor which senses operator's breathing action and glasses with three LED marks which is worn on the operator's head as shown in Fig.1. CCD camera is settled on the top of CRT monitor to detect the movement of marks. On the top of glasses three LEDs are mounted to compose a triangle as shown in Fig.2. Three LEDs to emit infrared red. The image board captures the image of operator's head through a CCD camera and LED marks are extracted from this image. The location of eye is estimated considering to these LED marks and the state of eye is detected. Since the geometrical relation of LED marks is known in advance, three-dimensional positions of marks are

calculated easily. As the results of these positions, the position and posture of operator's head is obtained. Each location of eyes on the captured image is detected easily, since the three-dimensional deviation from these marks to eyes is measured in advance. Control signals according to the position and posture of head and the state of eye or breathing action through pressure sensor are sent to the mouse connector of the computer through the digital input/output board.

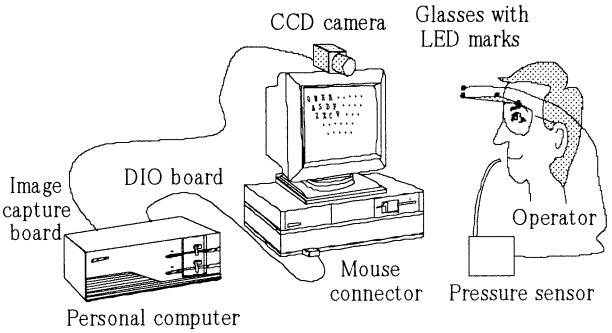


Fig.1 System configuration

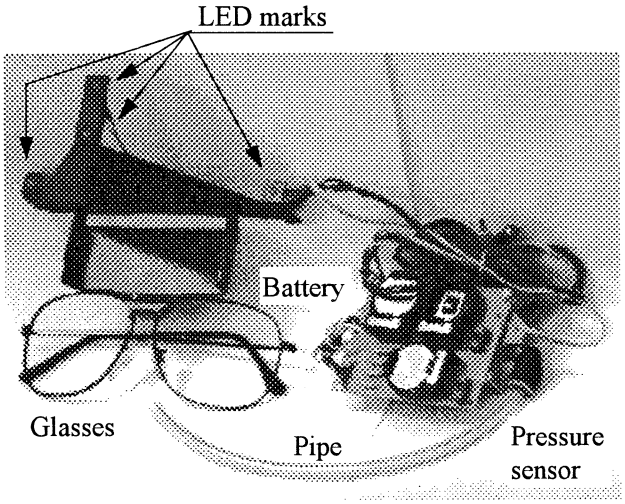


Fig.2 Glasses with three LED marks

3. Measurement of head movement

3.1 Detection of LED marks

Battery

LED marks are extracted easily by applying binary program and labeling program to the captured image. Once the areas of the marks are determined, the center of gravity of the marks are obtained by the following equation in sub-pixel order as shown in Fig.3.

$$x_G = \frac{\sum I(x,y)x}{\sum I(x,y)} \quad , \quad y_G = \frac{\sum I(x,y)y}{\sum I(x,y)} \qquad (1)$$

where, (x_G, y_G) is the center of gravity and $I(x,y)$ is the intensity of the pixel at (x,y).

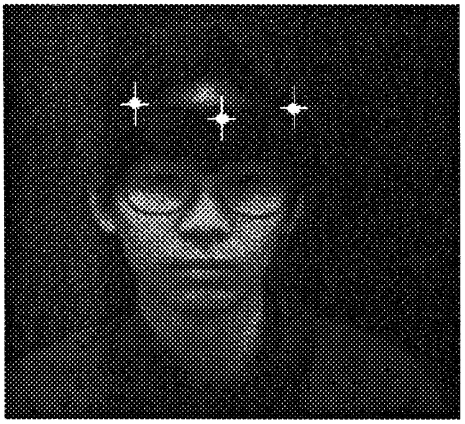


Fig.3 Detection of center of gravity of marks

3.2 Calculation of three-dimensional position of marks

Three LED marks on the camera coordinate is shown in Fig.4. Suppose the position vectors of LED marks are q_1, q_2, q_3 and projected points of these marks are $\mathbf{p}_1, \mathbf{p}_2, \mathbf{p}_3$. The following relation is readily obtained as

$$p_i=(x_{pi}, y_{pi}, f) \qquad (i=1,2,3) \qquad (2)$$

where x_{pi}, y_{pi} are coordinates on the image plane and f is the focal length.

The distance between each LED marks A_{12}, A_{23}, A_{31} are known in advance. The relation among $|q_1|$, $|q_2|$ and $|q_3|$ is expressed as following

$$A_{12}^2 = |\mathbf{q}_1|^2 + |\mathbf{q}_2|^2 - 2|\mathbf{q}_1||\mathbf{q}_2|\cos\theta_{12} \qquad (3)$$

$$A_{23}^2 = |\mathbf{q}_2|^2 + |\mathbf{q}_3|^2 - 2|\mathbf{q}_2||\mathbf{q}_3|\cos\theta_{23} \qquad (4)$$

$$A_{31}^2 = |\mathbf{q}_3|^2 + |\mathbf{q}_1|^2 - 2|\mathbf{q}_3||\mathbf{q}_1|\cos\theta_{31} \qquad (5)$$

where, θ_{ij} is the angle between vector $\mathbf{p}_i$ and $\mathbf{p}_j$, and is calculated by the following equation.

$$\cos\theta_{ij} = \frac{\mathbf{p}_i \bullet \mathbf{p}_j}{|\mathbf{p}_i||\mathbf{p}_j|} \qquad (i,j=1,2,3)$$

Once $|q_1|$, $|q_2|$ and $|q_3|$ are determined by the equations(3),(4) and (5), the position of LED marks is determined as following

$$\mathbf{q}_i = k_i \mathbf{p}_i \qquad (i=1,2,3) \qquad (6)$$

where, k_i is the constant value.

Equations(3),(4) and (5) yields eight solutions[7]. Considering the geometrical relation of marks that the position of mark Q_1 is always located in front of the other two marks Q_2 and Q_3, the desired solution can be determined uniquely as follows.

Firstly, estimate initial value$|q_1|$ as L (L>0). Equation(3) becomes

$$|\mathbf{q}_2| = L\cos\theta_{12} + \sqrt{(L\cos\theta_{12})^2 - (L^2 - A_{12}^2)} \quad (7)$$

From the geometry that $|q_2| > L$ we obtain similarly equation(5) becomes

$$|\mathbf{q}_3| = L\cos\theta_{31} + \sqrt{(L\cos\theta_{31})^2 - (L^2 - A_{31}^2)} \quad (8)$$

Substitution of equations (7),(8) into (4) gives

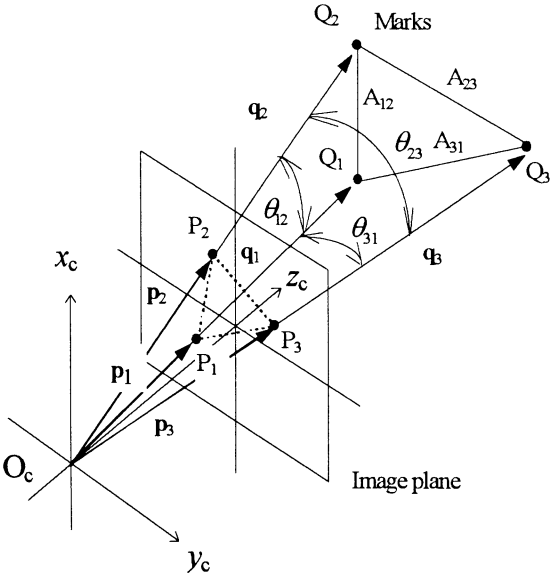
$$|\mathbf{q}_2|^2 + |\mathbf{q}_3|^2 - 2|\mathbf{q}_2||\mathbf{q}_3|\cos\theta_{23} - A_{23}^2 = 0 \quad (9)$$

Estimated value L can be evaluated by the following relation

$$\left| |\mathbf{q}_2|^2 + |\mathbf{q}_3|^2 - 2|\mathbf{q}_2||\mathbf{q}_3|\cos\theta_{23} - A_{23}^2 \right| < \varepsilon \quad (10)$$

where, ε is the positive parameters to determine accuracy of the solution. If the above relation is not satisfied, estimated value L is modified. The above procedures are repeated until the equation(10) is satisfied.

Once the three-dimensional position of three LED marks are determined, the position and posture of operator's head is calculated



Camera coordinates

Fig.4 Three LED marks on the camera coordinates

We had an experiments to test the accuracy of pointing by using our special glasses. The glasses is located 600mm apart from the CCD camera. And azimuth and elevation angle of glasses is specified from -20 degree to 20 degree with 5 degree step. The result is shown in Fig.5. Absolute error was less than 1.0 degree and repeatability is assured with error 0.3 degree.

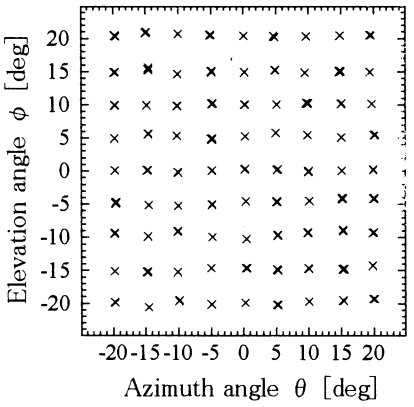


Fig.5 Accuracy of pointing by glasses

To compare the accuracy, other experimental result which is attached LED marks on four corners of glasses is shown in Fig.6 [8]. Accuracy of suggested method in this paper is very high because of including depth information among LED marks from the arrangement of LED marks.

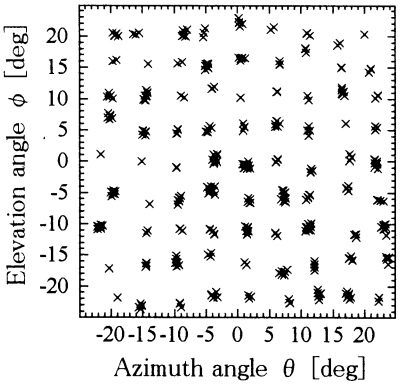


Fig.6 Accuracy of pointing by using four LED marks

4. Input of selected items

We tried two way to input selected items. One is used blinking action and other is used breathing action.

4.1 Case of blinking action

We tried to input selected items by using blinking action of operator's eyes.

4.1.1 Determination of eye location on image

Since the relation between point M and eye is measured in advance as shown in Fig.7, three-dimensional position of eye is determined easily as following equation

$$\mathbf{q}_e = \mathbf{q}_M + \mathbf{l}_{e1} + \mathbf{l}_{e2} + \mathbf{l}_{e3}$$

where, $\mathbf{q}_M=(\mathbf{q}_2+\mathbf{q}_3)/2$ and l_{e1},l_{e2} and l_{e3} which are deviation from the point P_M are given in advance and each unit vectors are calculated from the relation between positions of three marks.

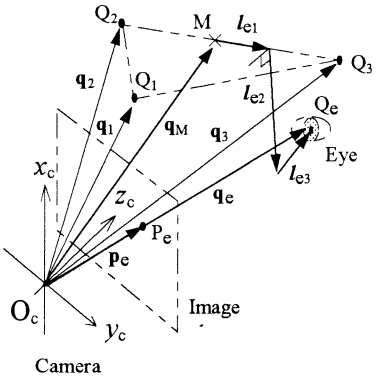
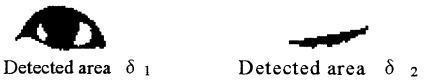


Fig.7 Relation between marks and eye

4.1.2 Determination of blinking

In our system the blinking action of eyes is used as a selection switch of menu items. Therefore, it is necessary to distinguish the intentional blinking from the unconscious blinking. The interval of the eye closed is used for this distinction. Suppose the area of the eye opened is δ_1 in the last image. If the area of the eye detected is smaller than $\delta_1 / 2$ in the current image, then we know the operator is blinking his eyes as shown in Fig.8. Furthermore, if the period of blinking is longer than some designed time, the blinking is recognized as intentional one.



(1) State of eye opened (2) State of eye closed

Fig.8 Detection of the blinking

4.2 Case of breathing action

In other way to input selected items, we tried to use breathing action. According to breathe through pipe connected pressure sensor, the fourth LED mark mounted on the glasses is emitted. Therefore, this action is detected easily by using image processing.

5. Field test

We applied this input device to operate word processing program under the environment of Windows95 as shown in Fig.9.

6. Conclusion

A new input device to use head movement and blinking action or breathing action was developed. While the operator is required to wear the special glasses, detection of three-dimensional head movements is readily realized by the image processing of three LED marks on the glasses. It was possible for physically handicapped people to operate word-processing system under the environment of Windows95. Blinking action is more useful to input selected items than breathing action in this field test because of simple action. However, breathing action is also useful for operator who has thin eye.

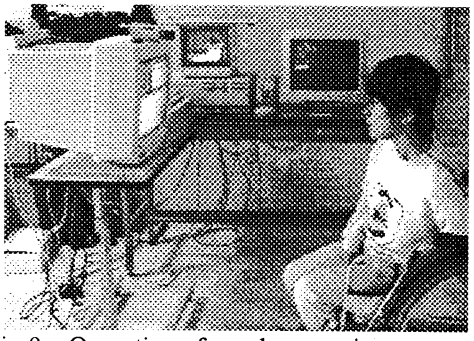


Fig.9 Operation of word processing program

References

[1] H.Kawamura et al., "Experimental Production of Light Mouse using PSD sensor", Proc.of 5th Rehabilitation Engineering (in Japanese), pp.233-236, 1990

[2] Y.Akazawa, J.Aira, "Lip Mouse", Proc. of 8th Rehabilitation Engineering (in Japanese), pp.313-314, 1993

[3] O.Takami, T.Ishimatsu and T.Shimomachi, "Development of the Environmental Control System by Using Eyeball Movements", Proc. of 1st Asian Control Conference, Vol.3, pp.415-418, 1994

[4] O.Takami, T.Shimoyama and T.Ishimatsu, "Development of the Environmental Control System Using Movements of Eyeball, Eyelid and Head", Proc. of 10th JCART (in Japanese), Vol.3, pp.415-418, 1994

[5] T.Ochiai, T.Ishimatsu et al., "Typing Device for Physically Handicapped People Using Eyeball Movements", Proc. of 2nd France-Japan & 1st Europe-Asia Congress on MECHATRONICS, Vol.1, pp.317-321, 1996

[6] T.Ochiai, T.Ishimatsu et al., "3-D Measurement of Head Movement and Its Application", Proc. of 2nd France-Japan & 1st Europe-Asia Congress on MECHATRONICS, Vol.2, pp.816-820, 1996

[7] K.Deguchi, "Image and Space", pp.128-135, Publication of Shoukoudo, 1991

[8] T.Ochiai, T.Ishimatsu, et al., "Computer Input Device for Physically Handicapped People Using Head Movements", Proc. of 5th SICE Chuugoku Branch Annual Conference (in Japanese), pp.52-53, 1996

Proc. of Third Int. Symp. on Artificial Life, and Robotics (AROB III' 98),
Oita, Japan, 19-21, January, 1998,

A Technique of Three-Dimensional Measurement of Huge Object

Kazutaka Fujimoto, Sumio Nagata
Technology Center of Nagasaki Prefecture
2-1303-8, Ikeda, Omura, Nagasaki, 856 Japan

Takakazu Ishimatsu
Nagasaki University
1-14, Bunkyo-machi, Nagasaki, Nagasaki, 852 Japan

Abstract

technique to measure the three-dimensional shape of a huge object under natural lighting condition is proposed. Incorporating the idea of the contour analysis and the bundle technique, the technique is practical. Experiments are executed to measure a plastic bottle and two huge object. The results revealed the applicability of our proposed technique.

1. Introduction

Nowadays three-dimensional information is required in many fields. In order to cope with this requirement, some measuring techniques using vision are proposed. Among them, the slit-ray projection method is one attractive technique, which realizes practical measurement with high accuracy in the case where the target size is less than few meters [1].

In the field of civil engineering, the three-dimensional shape information of huge objects are often required from the stand point of disaster prevention. To such objects, the slit-ray projection method is not applicable any more, since the slit-ray projected on the huge target is often difficult to recognize because of the uncontrollable environment, e.g. sun light, surface condition and the long distance between the camera and the target. A stereo vision might be applicable [2),3)]. However, because of the complex surface of targets, finding matching points is rather difficult. Of course, if we put many marking points on the target surface, finding matching points turns to be much easier [4]. Another practical technique is to analyze images of the target object which are obtained from various positions around the target object [5]. A feature of this technique is that the camera position and posture at every photographing point need not be calibrated in advance. Operators can set the camera freely. Using this technique called Bundle Technique, the three-dimensional positions and postures of the camera at every photographing point can be estimated. One problem of this technique is to extract feature points on the target objects and to find matching points among them. If the target object has prominent feature points, the technique can be readily applicable. However, in case of the natural huge rock considered, finding prominent feature points is almost impossible.

In this paper we propose a three-dimensional measuring technique applicable to a huge object.

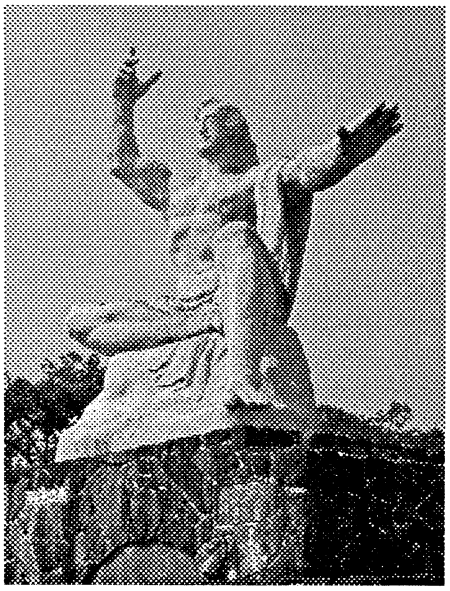


Fig.1 Target Huge Object

A photograph of the target huge object is shown in Fig.1. A feature of this technique is that the three-dimensional shape can be readily recovered by the contour data extracted from the multiple images of the huge object. Authors already proposed another technique based on the contour analysis under the condition that the three-dimensional coordinates of photographing positions and also some marking points on the rock are measured in advance [7]. The task to put marking points whose coordinates are known is undesirable. Therefore, the technique proposed here requires only the condition that some prominent feature points can be recognized. These prominent feature points are used to calibrate the camera setting based on the Bundle Technique.

2 Shape Recovery by Analyzing Multiple Images

By analyzing multiple images obtained at various positions and postures, three-dimensional shape of the target can be estimated [8]. Suppose cameras are settled at position $P_i(i=1,...M)$, and prominent feature position on the target are denoted as $F_j(j=1,...,N)$ as shown in Fig.2. It should be noticed that position P_i and the posture of the cameras are unknown. By the analysis of the image data

at position P_i, we can determine the orientation vectors v_{ij} which runs at position P_i toward the feature positions F_j in the camera coordinate system. It is obvious that the vectors v_{ij}(i=1,...M) should intersect each other at position F_j. Based on this intersecting condition, camera positions P_i(i=1,...,M), feature positions F_j(j=1,...,N) and also the corresponding camera postures can be estimated. Of course, one relative geometrical data between any two positions is required to determine three-dimensional coordinates of every position.

The idea is implemented on a software which is now commercially available named as PhotoModeler. Most important operation requested to the operator is to specify the position of the prominent feature points at every images and specify matching relation among them. When the target object has a simple or special geometry, it is easy to obtain many feature points which are enough to recover three-dimensional shape of the target. However, in case of the huge rock, the number of feature points which can be recognized clearly is limited and is not enough to recover the three-dimensional shape. Therefore, we used the limited number of feature points mainly to calibrate the system setting, like camera position, camera posture.

3 Shape Recovery Based on Contour Analysis

From the multiple images obtained at various positions with various orientations, the three-dimensional shape can be recovered [9),10)]. Suppose the camera is settled at O_i and contour data C_i of the huge object is obtained as shown in Fig.3. It is also assumed that the position and the posture of the camera is known. Under these conditions, consider an imaginary surface IS(z) which is placed at height z. By projecting the contour C_i onto the surface IS(z), curve M_i(z) is obtained. From the geometry, it can be concluded that the cross-section of the target object is confined inner part of this curve. It is understandable that four curves can be projected onto the surface IS(z) as shown in Fig.4, if images are obtained at four positions. As the number of the multiple images increase, the cross-section of the huge object can be estimated more accurately.

But it is required to estimate an accurate cross-section using limited number of images. One technique is to approximate the target cross-section by a polygon defined as shown in Fig.5.

Estimating the cross-section at every height, global three-dimensional shape of the target can be recovered. While the contour analysis is effective to obtain three-dimensional shape, it should be noticed that the concave surface cannot be measured. Therefore, when the target object has concave surface, a stereo vision technique needs to be incorporated.

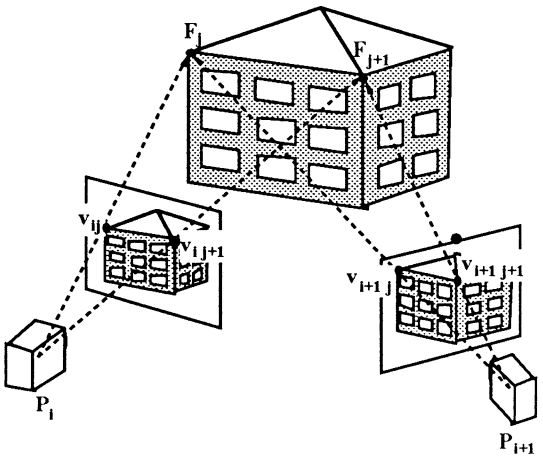


Fig.2 Camera Position and Prominent Feature Position

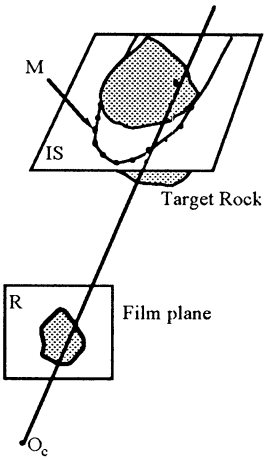


Fig.3 Projected Contour Curves

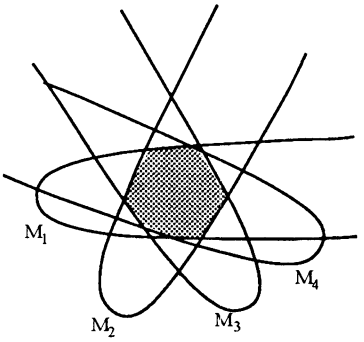


Fig.4 Projected multiple contour curves

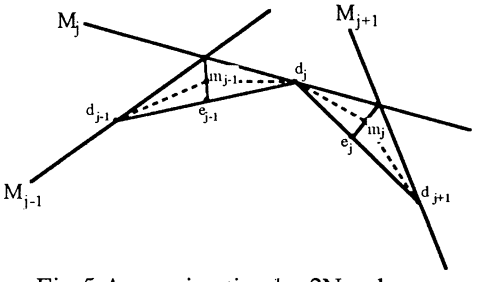


Fig.5 Approximation by 2N polygon

4 Experiments

4.1 Measurement of Bottle

Before we measure the target object, we had an experiment to measure a plastic bottle.

The bottle was settled on the small box as shown in Fig.6. And nine images were obtained at various positions around the bottle by a conventional video camera, and converted into computer data with resolution 640H*480V. More than six points are selected as feature points at every image by the operator using the computer mouse. In addition to these feature points, the contour curve of the bottle was specified. After that, the position and posture of the camera at the instance when the image was obtained were calibrated.

Once the three-dimensional position and the posture of the camera is determined, projection of the contour curves onto the imaginary surface becomes possible. Fig.7 shows results where nine contour curves are projected. The figures reveals that the cross-sections can be estimated by a simple algorithm mentioned above. Data estimated were compared with data measured manually as shown in Table 1, where Cross-section 1 is obtained where the cross-sectional area becomes minimum around the neck of the bottle and Cross-section 2 is obtained where cross-sectional area becomes maximum. In every column, the left data are estimated by proposed method and the right data are obtained by manual measurement. Differences of the data may be caused by the lack of the resolution of the camera and also lack of the pointing accuracy of the computer mouse.

After obtaining cross-sections at various height, the three-dimensional shape of the bottle could be recovered as shown in Fig.8, where the texture of the bottle is mapped onto the recovered model.

Table 1 Experimental Data
(right data is obtained by manual measurement)

	Maximum width	Minimum width
At Cross-section 1	53.0 mm (52.2 mm)	49.8 mm (48.0 mm)
At Cross-section 2	100.6 mm (98.0 mm)	61.8 mm (58.4 mm)



Fig.6 Target plastic bottle

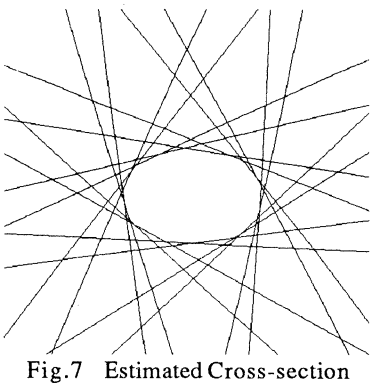


Fig.7 Estimated Cross-section

4.2 Measurement of Huge Object

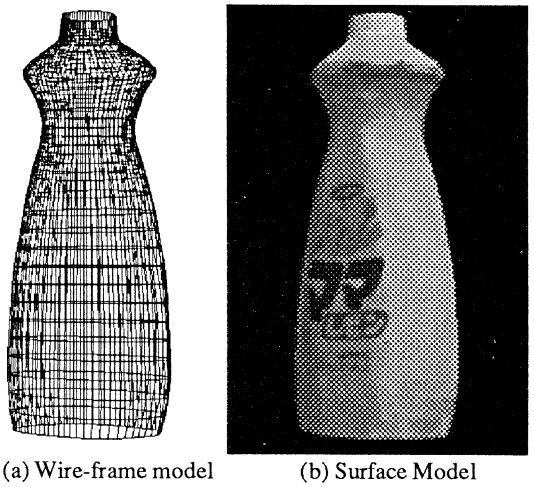
We applied our proposed technique to measure two huge objects. The first one is a huge rock which has a potential risk of falling down. Fig.9 shows the photograph of the rock. Firstly we obtained eight photographs around the rock, and converted into computer data with the resolution of 900H*600V. Feature points and the contour curve of the rock is specified manually by the operator. Using the data of the feature points, the camera position and the posture is calibrated. In Table 2, calibrated position data are shown where data measured by a laser theodolite are shown. It is assumed that the target huge rock stands at the origin of XYZ coordinates. While X and Y coordinates are calibrated accurately, Z coordinate data has bigger calibrating error. This may be caused by the fact that while the horizontal position of the camera varied remarkably, the vertical position of the camera varied slightly. Using these calibrated data, the cross-sections of the huge rock are estimated.

Using these cross-sections, the three-dimensional model of the rock can be recovered as shown in Fig.10 and Fig.11. Comparison with the photographs shown in Fig.9 reveals the shape of the rock is recovered.

The second target of measurement is a statue called "Statue of Peace" in Nagasaki-city.

Fig.1 shows the photograph of the statue. We obtain thirteen images using a digital still camera. And the images were converted into computer data with the resolution 1536H×1024V. Using the data, the three-dimensional model of the statue can be recovered as shown in Fig.12.

Because of the complex shape of the statue, we recovered the shape with each part of the statue. In Fig.12, we show the recovered model of right-arm. Comparison with the photographs shown in Fig.1, the shape of the arm and two fingers are recovered. But, other fingers are not recovered well.

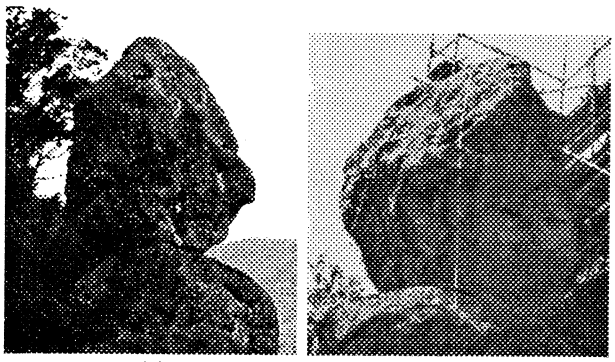


(a) Wire-frame model (b) Surface Model

Fig.8 Recovered Plastic bottle

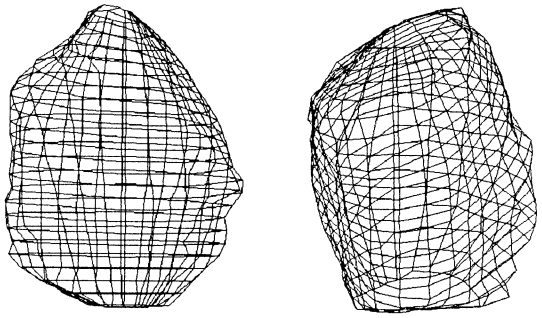
5 Conclusions

Three-dimensional measurement of huge objects under the natural condition is considered. Stereo vision technique is considered to be effective. However, the method has a drawback to apply to measure complex surfaces, since finding matching points among both images is almost impossible except some featuring points. In order to cope with this problem, we already proposed a technique based on the contour analysis. While contour analysis simplified the measuring task remarkably, the technique required marking points whose coordinates are known in advance on the target surface. In this paper we proposed a more practical technique which does not require such condition. The experiments to measure a plastic bottle revealed the applicability of our system.



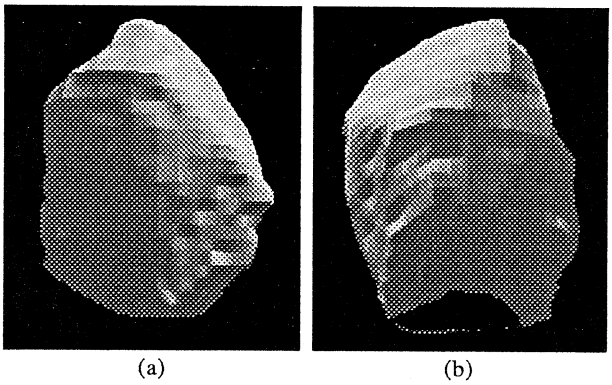
(a) (b)

Fig.9 Target Huge Rock



(a) (b)

Fig.10 Recovered 3-D Wire-frame Model of the Rock



(a) (b)

Fig.11 Recovered 3-D Surface Model of the Rock

Table 2 Calibrated Data of Camera Coordinate
(Left data are obtained by laser theodolite)

Point	X (m)	Y (m)	Z (m)
1	-92.63 (-99.78)	-97.33 (-95.33)	-6.34 (-10.01)
2	-89.27 (-89.78)	-18.56 (-18.31)	-32.50 (-33.32)
3	-89.60 (-89.69)	2.68 (2.54)	-35.98 (-41.79)
4	-113.77 (-114.87)	88.81 (88.29)	-51.35 (-59.81)
5	-47.78 (-48.11)	-71.52 (72.39)	-57.64 (-56.83)
6	59.36 (61.36)	142.25 (140.06)	-54.68 (-58.10)
7	21.85 (21.67)	212.89 (210.65)	-59.23 (-48.94)
8	92.45 (93.95)	260.71 (255.60)	-47.03 (-37.23)

References

[1] T.Ishimatsu et al, (1991) "Fast 3-Dimensional Measuring Technique Using a Look-Up Table", *Trans. Jpn. Soc. Mech. Eng.*, 57,538C, 179-183

[2] H.S.Lim, (1988) "Curved Surface Reconstruction Using Stereo Correspondence", *Proc. Image Understanding Workshop*, 809-819

[3] E.Grosso, (1989) "3D Object Reconstruction Using Stereo and Motion", *IEEE Trans. Syst. Man. Siberne.*, 16(6)

[4] K.Sato, H.Yamamoto and S.Inokuchi, (1986) "3D Shape Measurement of Megalithic Statue-Moai-", *Proc. 8th ICPR*, 675-677

[5] C.J.Poelman and T.Kanade, (1992) "A Paraperspective Factorization Method for Shape and Motion Recovery", Published at Computer Science of CMU

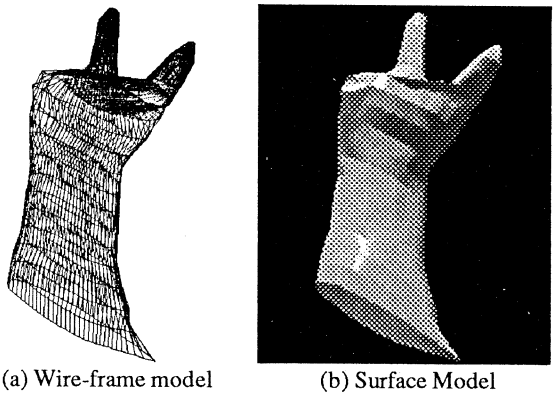
[6] Jan.J.Koenderink, (1984) "What Does the Ocluding Contour Tells Us about Solid Shape", Perception, 17, 75-114

[7] Sun Xiao, T.Ishimatsu, et al, "Reconstruction of Three-Dimensional Shape of Huge Rock Using Visions", *Proc. 15th IASTED*, 1997, 259-262

[8] K.Kanatani, (1990) "Understanding of Images" (in Japanese), Morikita Publisher

[9] Jian Yu Zheng, (1992) "Acquiring 3D Models from Sequences of Contours", *IEEE Trans. on Pattern Analysis and Machine Intelligence*, 14(2), 157-173

[10] T.Miyake and J.Doi, (1984) "Three-Dimensional Shape Approximation System with a Polyhedron" (in Japanese), *Trans. of Japanese Society of Information Processing*, 25(5), 745-754



(a) Wire-frame model (b) Surface Model

Fig.12 Recovered 3-D Model of the Statue (right arm)

Proc. of Third Int. Symp. on Artificial Life, and Robotics (AROB III' 98),
Oita, Japan, 19-21, January, 1998,

Recognition of Both Pattern and Position of Color Objects using a Visual System with Two Cameras

M.Sugisaka, H.Okuzono, K.Yamada

Department of Electrical and Electronic Engineering, Oita university
700 Dannoharu, Oita, 870-11, Japan
E-mail: msugi@cc.oita-u.ac.jp kazuya@cc.oita-u.ac.jp

Abstract

Recently, a method of construction works on telegraph pole using a robot with manipulators has been developed. In order to operate the manipulators, we need to recognize an object and to know three dimensional coordinate of the object. Here we use an artificial neural network constructed in a visual system with twocameras.

In order to recognize some patterns, at first, we calculate moment invariants(*MIs*) for the image data of the object, and make use of the artificial neural network using *MIs*. Secondly, to measure the distance between the visual system and the object, this system makes use of the method of triangulation by measuring two angles between left camera and right camera and the distance between them.

In this paper, we present two methods for both recognition of the object using the artificial neural network and measurement of the distance based on the triangulation.

Keywords: Threshold, Laster Scanning, Moment Invariants, Triangulation

1. Introduction

At present, a method using the robot with manipulators, which are manipulated by worker, is used practically. But there are some problems for the robot to work by itself. For example, it is not clear how the robot can recognize the object and work toward it. The system we have used in our research is produced for the purpose of development of the visual system. The system has two CCD video cameras as a visual part. Both cameras have two stepping motors respectively, so they are able to move freely. Moment invariants of the object is calculated so as to pick up the feature of it, and we recognize the object by means of the neural network using the moment invariants, and we turn two cameras toward the object calculate measure the distance using the triangulation by measuring the moving angle of both cameras. The construction of the visual system is shown in Figure.1.

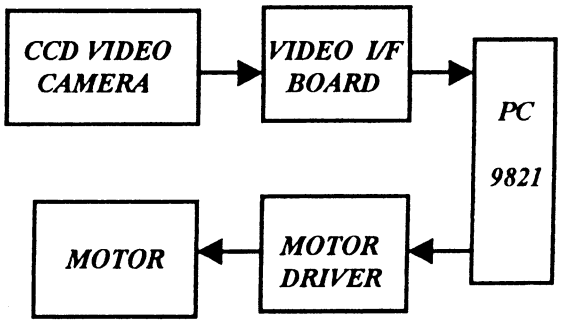


Figure 1. Construction of Visual System

2. Image Processing

2.1 Chromaticity Transformation

Image data obtained from CCD video camera is transformed into digital data. This data is influenced by surrounding condition such as brightness. Thus, the image data of two objects whose color are same, is different according to the surrounding. Although the image data is different, and percentage of RGB of the object does not hardly change. By using this, the image data can be transformed without changing brightness. The transformation equation is as follows:

$$\begin{pmatrix} r \\ g \\ b \end{pmatrix} = \frac{255}{R+G+B} \begin{pmatrix} R \\ G \\ B \end{pmatrix} \qquad (1)$$

where R, G, B are the image data before transformation, and r, g, b are the image data after transformation.

The more the image data is large, the more speed of computer deals with the data is slow. So we decrease the colors of the image using thresh-

old so as to make capacity of the data small. In this way, we classify each *R, G, B* data into "*0*" and "*1*" by the threshold value, and limit the color data to eight kinds of color. This eight color are "*black*", "*blue*", *green*", "*cyan*", "*red*", "*magenta*", "*yellow*", and "*white*". Therefore, the capacity of the color data in the image data is reduced to three bits. We decided the capacity of the image data is eight bits, the capacity of the label data in the image data enter the rest five bits.

2.2 Smoothing

If noise appears randomly in the image, it is difficult to analyze the image. So in order to remove all noise, we use smoothing of the image using filter of 8-neighbors around an image element. At first, for a certain pixel and other eight pixels around it(3×3), we examine color of these nine pixels, and the most color become the color of the central pixel. This operation is done to every pixels by means of laster scanning. So we can obtain the feature of the object without losing if the operation is done too many, we decide to do it three times.

2.3 Labelling

This time we decided color of the object is red, and pick up the pixel whose color is red by means of threshold value. When red region is picked up, the number of region is not usually one but more than two. It is necessary to attach a label(*a series of number*) to the pixels which compose the area. This operation is called *Labelling*, once we make the image attached the label, a specific regions are picked up in the image relying on the label, and features of the region such as area and centroid can be calculated.

3. Recognition of object

3.1 Moment Invariants

The two dimensional $(p+q)th$ order M_{pq} moment of a density distribution function P_{xy} which is equivalently intensity function and is a continuous function can be expressed as follows:

$$M_{pq} = \int_{-\infty}^{\infty}\int_{-\infty}^{\infty} x^p y^q P_{xy} dxdy \qquad (2)$$

where x and y are locations of pixels of the image. Also the central moment μ_{pq} of P_{xy} are defined as

$$\mu_{pq} = \int_{-\infty}^{\infty}\int_{-\infty}^{\infty} (x-\dot{x})^p (y-\dot{y})^q P_{xy} dxdy \qquad (3)$$

For a compressed digital image, with the size 256 pixels(16×16). M_{pq} and μ_{pq} could be approximated by double summations, therefore M_{pq} and μ_{pq} will be expressed by

$$M_{pq} = \sum_{i=1}^{M}\sum_{j=1}^{N} i^p j^q P_{ij} \qquad (4)$$

$$\mu_{pq} = \sum_{i=1}^{M}\sum_{j=1}^{N} (i-\dot{i})^p (j-\dot{j})^q P_{ij} \qquad (5)$$

where P_{ij} is a digital(*1 or 0*) function and i and j have integer values, $\dot{i} = \frac{M_{10}}{M_{00}}$ and $\dot{j} = \frac{M_{01}}{M_{00}}$ are defined by Eq.(4) and called central gravity of object. The summation limits M and N are the dimensions of the intensity matrix P_{ij} in which i and j are the discrete locations of the image pixels.

The *0th* order moment, M_{00} represents the total mass(*areas for binary image*) of the object. The first order moments, M_{10} and M_{01}, together with M_{00} locate the centroid moment of an object in the image. Notice only size is important, not the color of the object. In this case, the intensity function would only have the value *0* or *1*. The central moments may be easily shown invariant under translation and can be also expressed in terms of the moments M defined according to *MIs*. Then, from *MIs*, it is quite easy to express the central moments in terms of the moments. Therefore for first four order, we have

$$\mu_{00} = M_{00} \qquad (6)$$

$$\mu_{01} = M_{01} - \frac{M_{01}}{M_{00}} M_{00} = 0 \qquad (7)$$

$$\mu_{02} = M_{02} - \frac{M_{01}^2}{M_{00}} \qquad (8)$$

$$\mu_{03} = M_{03} - 3\frac{M_{01}}{M_{00}} M_{02} + 2\left(\frac{M_{01}}{M_{00}}\right)^2 M_{01} \qquad (9)$$

$$\mu_{10} = M_{10} - \frac{M_{10}}{M_{00}} M_{00} = 0 \qquad (10)$$

$$\mu_{11} = M_{11} - \frac{M_{01}}{M_{00}} M_{10} \qquad (11)$$

$$\mu_{12} = M_{12} - 2\frac{M_{01}}{M_{00}} M_{11} - \frac{M_{10}}{M_{00}} M_{02} + 2\left(\frac{M_{01}}{M_{00}}\right)^2 M_{10} \qquad (12)$$

$$\mu_{20} = M_{20} - \frac{M_{10}^2}{M_{00}} \qquad (13)$$

$$\mu_{21} = M_{21} - 2\frac{M_{10}}{M_{00}}M_{11} - \frac{M_{01}}{M_{00}}M_{20} + 2\left(\frac{M_{10}}{M_{00}}\right)^2 M_{01} \quad (14)$$

$$\mu_{30} = M_{30} - 3\frac{M_{10}}{M_{00}}M_{20} + 2\left(\frac{M_{10}}{M_{00}}\right)^2 M_{01} \quad (15)$$

By replacing to up to order 3 in μ_{pq}, high speed of computation can be achieved. It derived following functions $\phi_1, \phi_2, ..., \phi_7$ which are invariants under translation and rotation.

$$\phi_1 = \mu_{20} + \mu_{02} \quad (16)$$

$$\phi_2 = (\mu_{20} + \mu_{02})^2 + 4\mu_{11}^2 \quad (17)$$

$$\phi_3 = (\mu_{30} - 3\mu_{12})^2 + (3\mu_{21} - \mu_{03})^2 \quad (18)$$

$$\phi_4 = (\mu_{30} + \mu_{12})^2 + (\mu_{21} + \mu_{03})^2 \quad (19)$$

$$\phi_5 = (\mu_{30} - 3\mu_{12})(\mu_{30} - \mu_{12})[(\mu_{30} + \mu_{12})^2 - 3(\mu_{21} + \mu_{03})^2] + (3\mu_{21} - \mu_{03})(\mu_{21} + \mu_{03})[3(\mu_{30} + \mu_{12})^2 - (\mu_{21} + \mu_{03})^2] \quad (20)$$

$$\phi_6 = (\mu_{20} - \mu_{02})^2[(\mu_{30} + \mu_{12})^2 - (\mu_{21} + \mu_{03})^2] + 4\mu_{11}(\mu_{30} + \mu_{12})(\mu_{21} + \mu_{03}) \quad (21)$$

$$\phi_7 = (3\mu_{21} - \mu_{03})(\mu_{30} + \mu_{12})[(\mu_{30} + \mu_{12})^2 - 3(\mu_{21} + \mu_{03})^2] + (3\mu_{12} - \mu_{30})(\mu_{21} + \mu_{03})[3(\mu_{30} + \mu_{12})^2 - (\mu_{21} + \mu_{03})^2] \quad (22)$$

These equation are transformed as follows:

$$Q_1 = \frac{\sqrt{\phi_2}}{\phi_1} \quad (23) \qquad Q_2 = \frac{\phi_3 M_{00}}{\phi_1 \phi_2} \quad (24) \qquad Q_3 = \frac{\phi_4}{\phi_3} \quad (25)$$

$$Q_4 = \frac{\sqrt{\phi_5}}{\phi_4} \quad (26) \qquad Q_5 = \frac{\phi_6}{\phi_1 \phi_4} \quad (27) \qquad Q_6 = \frac{\phi_7}{\phi_5} \quad (28)$$

Notice that ϕ_7 which is called *orthogonal invariant* is useful in distinguishing mirror images. Actually number of *MIs* used is critical. A smaller number of *MIs* will increase the recognition speed, whereas a larger number would improve recognition rate. The initial experimants were done by using only first two moment invariants Eqs.(16), (17), but the results werenot encouraging. To improve recognition rate, up to seventh *MI* was added. The order *MI* equations were not used, because we had overcome to recognize dynamic patterns without using the rest of *MIs* equations. In this work, we used the value of $\phi_1, \phi_2, ..., \phi_7$ to make dynamic patterns invariance to position and direction.

3.2 Neural Network

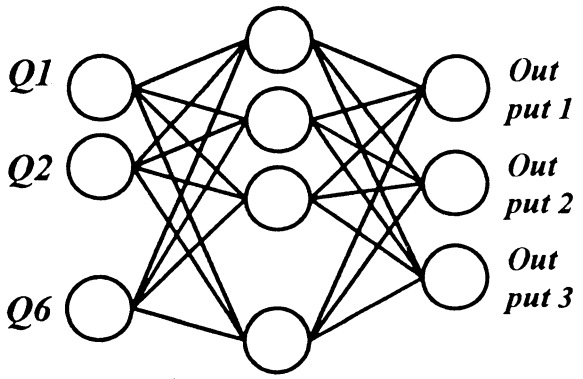


Figure 2. Structure of Neural Network

It is shown Figure.2 that there are three units in output layer which gives decision based on the global state of the processing units. The numbers of input units are six, and these are equivalent to moment invariants. We decided processing units whose numbers are twenty are connected with each other. The state of an unit to excite or suppress is determined by threshold value.

4. Measurement of Distance

We explain a method of triangulation in order to measure distance between visual system and an object. This method is based on the principle of trigonometry, if one side and two angles of triangle are determined, all elements of the triangle are defined. This principle can be written as

$$X = \frac{\sqrt{A^2 + B^2 + 2AB\cos\theta_c}}{2} \quad (29)$$

$$A = \frac{C\sin\theta_a}{\sin\theta_c} \qquad B = \frac{C\sin\theta_b}{\sin\theta_c} \quad (30)$$

where Eq.(30) is the sine theorem.

Two CCD video cameras are moved such as the both center of the object and screen of the camera are same point. To control the cameras, we use deflection between the object and the center of the screen, and calculate angle respectively by counting pulse number of a stepping motor, measure the distance by means of the triangulation.

5. Experimental Results

In our experiment, we decided the color of objects are red to obtain them with ease. The result for recognition of the object is shown in Figure 4. The most highest degree of accuracy object is alphabet 'P'.

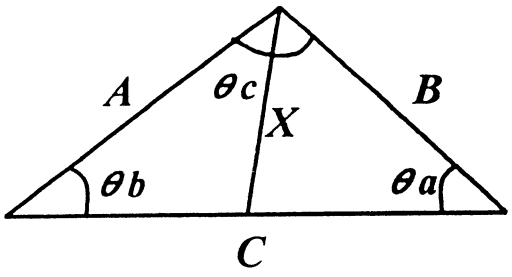


Figure 3. Triangulation Principle

Next, the result for measurement of distance is shown in Figure 5. At position from 80cm to 180cm, each absolute error values are within a few cm.

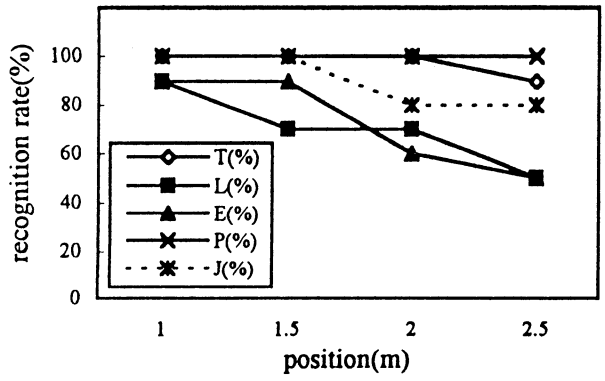


Figure 4. Recognition of Five Objects

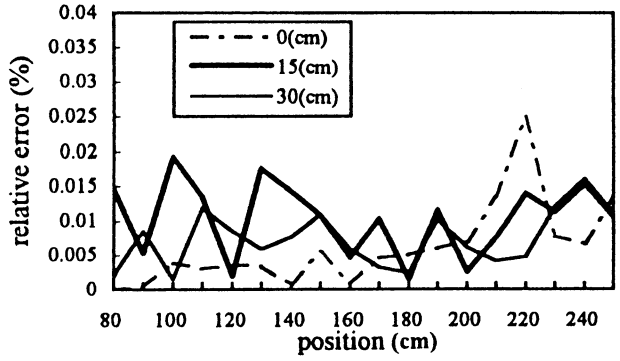


Figure 5. Result for Measurement

6. Conclusion

This paper described a visual system of a robot with manipulators working by itself. The goal of the research is to recognize an electric wire and an insulator which are objects. This time we substitute alphabets for them in its early stages. We were satisfied with the result for recognition of them to some extent. But the system could hardly recognize the object when the object was small or rotating. Actually working outside, so there are various kinds of conditions, we need to develop the visual system to cope with the conditions.

As a result of measurement of the distance, we realized that the system would be used at work. We had tried to measure by another method of fixed two CCD video cameras, the result was a high degree of accuracy. We will try to use both methods, and examine which method is good for working.

References

[1] K.Tezuka, T.Kitabashi, H.Ogawa, "*Digital image processing*", Nikkan Kougyou Sinbunsya, pp.112-118, 1985.

[2] H.Okuzono, "*Object recognition and measurement of distance using visual system has two cameras*", SICE Kyushu branch annual conference, Vol.15, pp.53-54, 1996.

[3] T.Mohammad, "*Dynamic pattern recognition by using moment invariants computation via artificial networks*", A thesis, Oita university, pp.1-91, 1992.

Proc. of Third Int. Symp. on Artificial Life, and Robotics (AROB III' 98),
Oita, Japan, 19-21, January, 1998,

Towards the Theory of Bio-Complexity

Hiroshi Tanaka
Department of Information Medicine
Medical Research Institute
Tokyo Medical and Dental University
Tokyo, Japan 113

Abstract

In this speculative paper we discuss on the question of "What is life?" in two abstract levels: one is about its logical structure and the other is about the physical (thermodynamical) structure of life. In its logical structure we consider life is self-referential system. In its physical structure, we discuss life from the viewpoints of global entropic balance and self organisation theory in nonequilibrium system. Finally the difference beween biotic and abiotic self organisation is investigated as to its informational complexity.

1 Introduction

Despite the remarkable advances in the recent molecular biology, specially in the fields of the molecular genetics, there has been no sufficietly scientific answers as yet to the question of "What is life? or "What is the differences between the non-living and living things"?"

Several theories have been proposed so far as to the essential structure of the life, among which well-known are, (1) Eigen's hypercycle theory of molecular replicators [1], (2) Gánti's autocatlytic chemical reaction cycle(chemoton) [2], (3) Kaufmann's autocatalytic network [3]. We could also cite several other life theories which are not so much mathematically formulated but conceptually much influential on the theories of life, such as Maturana and Varela's autopoiesis theory [4]. Furthermore, other branch of life therories which are primarily based on the thermodynamics, such as global entropic theory of life which is originated by Schrödinger [5]and correctly developed, for example, by Tsuchida [6], or non-equilibrium theory of self-organisation by Prigogine [7]and Haken [8].

We think that these theories grasp the several essential aspects about the structure of life from different viewpoints and different levels. In this, we decompose the question of life in several levels in order that it could be relevently answered. Specially, the question of essential structure of the life is investigated in two aspects: the most abstract level of life and the physical minimal realisation level which make the life possible. We put special interests on the self-structure of the biotic system. Finally, we discuss the life from its complexity level. With the limitation of the space, we cannot fully discuss our theory of life here, so that this study is just a speculative sketch of our life theory. As to detailed investigation and discussion, the reader would refer elsewhere [9].

2 Fundamental Concept of Life

The question of "What is life?" could be answered in various levels. The most abstract level of the answer concerns the logical structure of life. As life is an entity, it would be possible, though it is very hard, to describe the essential characteristics of this entity in logical form. The next level is also abstract but related to the physical structure of life, in other words, physically minimality for the life to exist. As life is considered as a specific collections of the chemical reactions, so that we should clarify what kinds of collection or organisation life is and whether such a collection of chemical reactions is themodynamically possible. The chemoton by Gánti is the example of minimal realisation of life, though we think it lacks in the entropy consideration.

The fundamental concept of life gives us the outline to understand what the life is. As to the most abstract level, we first note that life is an entity described as a certain kind of a dynamical process, so that we would clarify the essential logical structure of the dynamics of life. If we think the life is not just a thing, this thought means life is more than mere existence. Life seeems to "know" what it is. This property, something like psychological "self-consciousness", is denoted by, in more logical word, "self referentiality". Self refer-

ential sysyem is such a system that is being itself as well as being a refer to itself. Self is doubled: it has cognitive relation to self. This self-referentiality has a circulatory or something contradictory aspect. As life is not merely the logical imaginary entity, this circulatory nature composes the gap between two kinds of selves, forming a motive force to drive life in continous change("evolution" in general). Hence we could say as follows:

Proposition 1 (Abstract Definition of Life) *Life is considered to be a self-referential evolutionary system or evolutionary self-reccurent system.*

In more concrete word, life is a cyclic renewing process in itself. A little different but essential same as this fundamental concep could be found elsewhere. For example, in Maturana and Varela's autopoiesis theory, life is thought as a continous reproduction of (productive) network of its componets. As a matter of fact, the componets of life is continously being reproduced by the chmeical metabolic reactions, and this reaction network itself is brought its existence through reaction itself.

3 Thermodynamical Structure of Life

3.1 Life is forced circulation with entropy excretion

We here investigate the next problem of whether life is thermodynamical possible. This has been a problem for many years. It seeems that the life is contradictory to the second law of the thermodynamics. As to this question remarkable change has made when Schrödinger said that life eats negentropy. This is a kind of metaphor, though the exact meaning of this pharase is given in his own revision. As we mentioned, life is a specific organisation of chemical reaction processes. According to Kaufman or Gánti's theories, the elementary process of life is composed of cyclic autocatalytic reactions. The chemical reactions produce the entropy in reaction process. Unless the life dispose of this produced entropy, life becomes full of entropy. From the themodynamical point of view, the life is thought to be a forced circulation process using working substances. Like Carnot cycle, life produces necessary energy by this forced circulative process of the working substance. We can see it through balance of bioentropy as follows. As Prigogine described the entorpy has two kinds: one is entropy production dS_i and entropy flux dS_e. the change of the entropy ds is thus given as

$$dS = dS_i + dS_e$$

So the cyclic integaration gives

$$\oint_C dS = \oint_C dS_i + \oint_C dS_e.$$

The entropy production must be excreted, so that

$$\Delta S_e = \oint_C dS_e \geq -\oint_C dS_i.$$

Then, the balance is given,

$$w = w_0 - f - T\Delta S_e.$$

where w is available bioenergy, w_0 is biological original energy production by cyclic process, f is necessary energy to drive cyclic process, coresponding the themochemical circulation of working substances and, $T\Delta S_e$ is energy necessary to excrete the entropy production within a cycle. So we can say if $w \geq 0$, the life is possible inspite of the second law of thermodynamics. Thus,the following is given:

Proposition 2 (Thermodynamical Possibility of Life) *Life is themodynamically possible in the form of a forced cyclic process in which gained energy spends for excretion of produced entropy.*

This shows the cyclic entropy production must be washed out from life. Entropy disposition mechanism is themodynamically important for the biotic system. Disposition of entropy needs the free energy. So even if it sounds paradoxically, the minimal form of life spend most of energy to wash out the entropy produced by its being alive.

3.2 Self organization in nonequibrium system

Perfectly known self organisation is that in nonequilibrium system. Nonlinear non-equilibrium thermodynamics such as Prigogine's dissipative structure or Haken's Synergetics shows us the mechanism of self-organisation in non-living system. What part of their theories should we learn to incorporate into our theory of life? Both theories, dissipative structure and synergetics, deal with, though abiotic, self-organisation of chemical reaction system. Dissipative structure theory deals with self organisation in non-equilibrium system from excess entropy production δP, which decides the stability of non-equilibrium system. The necessary condition for self-organisation to be possible is

$$\delta P = \frac{d}{dt}\left(\frac{1}{2}\delta S^2\right) = \int \delta \boldsymbol{J} \cdot \delta \boldsymbol{X} dV < 0.$$

where S is the entropy of the nonequilibrium system, $\delta \boldsymbol{J}$ and $\delta \boldsymbol{X}$ are generalized flux and force of perturbed non-equilibrium system. Prigogine found that

in chemical reaction system, the above condition can be satisfied only when chemical reaction system contains autocatalytic reaction. The synergetics specially makes it clear what happens after this start of "phase transition" and the process which leads to self organisation.

According to synergetics,the following steps takes places to form the abiotic self organisation, (1) nonequilibrium force (generalized force) is applied to the equilibrium sysytem. (2) This force brings the system takes far from the equilibrium. (3) The thermodynamical branch (continuation of equilibrium solution in non-equilibrium state) becomes unstable because one mode of the linearized solution around the equilibrium point becomes unstable. (4) The magnitude of this unstable mode of the nonlinear system increases. (5) This unstable mode is nonlinearly fedback to drive the all other stable modes of nonequilibrium system. "Slaving" occurs and the degree of freedom of the system decreases. The amplitude of this unstabel mode becomes "order parameter" in Landau's sense. (6) The saturation of unstable mode occurs and new dynamic state with macroscopic order emerges.
From the above mechanism of abiotic self organisation, we can derive the necessary conditions for autonomous organisation of the unified structure.
(1) *Existence of principal instability*
As shown in the above, The main mechanism for self organisation is instabilization of one of the dynamical modes of nonequilibrium system. This instability constitutes the fundamental motive force (intetionality) of the system. Any self organisation system must have principal instability for the system to evolve,like Marthus instability in biological evolution. Instability of the system is representation of intentionality to future in logical sense. In chemical self organisation, autocatalytic reaction which causes this instability. should be included in the chemical reaction set. Tends to profirate or replicate can also form principal instability.
(2) *Nonlinear mixing and closedness*
Chemical reaction system is nonlinear dynamical system. In the linear system every dynamical modes are independently decomposable. The solution is merely the sum of those components. But in nolinear system, all the componets are fed back to be mixed. This condition is necessary for Haken's "slaving" (reduction of degree of freedom) to occur. This is also necessary condition for system functional closedness. In the chemical system, reaction network must form cyclic structure to form unified charactereistics. By closedness we mean that any perturbation propagates its influence to the every components of the system (reachability). This is only possible when except for the input and out put substances, all substance within the reaction network are reachable each other through the chemical reactions. This fact is also pointed out in several life theories: In autopoietic theory, the functional closedness is one of the most important characters of life.

4 Biotic Self Structure

In the previous section, we derive the two necessary conditions which we come to know crucial for aboitic self organisation. The unified structure which exhibits the above two characteristics as in abiotic self organisation is denoted here as "semi-self structure". Thus,we have
Proposition 3 (Two Conditions of Semi-self) *The necessary conditions for the semi self strucuture to emerge are given as follows:*
(1)Principal intentionality
(2)Reccurent closedness.
In order to discuss the essential characteristics of the biotic self organisation, we first consider the difference between biotic and abiotic self organisation. Fatal conditions are lacking in abiotic self-organisation, which is self-determination of the system boundary. This fact is also considered in the autopoietic theory. The boundary of nonequilibrium system is determined by the enviromental non-equilibrium force, not by itself. On the contrary to abiotic system, biotic system determines the boundary of system by itself. In order for it be possible, system must "know" law of the enviroment. To response rightly to the enviroment, some coupling with the enviroment is necessary. We mentioned that the biotic self structure consists in its self-referentiality. Through self-determination of own boundary, the self-structure has superiority over the enviromental change. There must be information about laws of the enviroment. Information must first be imbedded in active substance on the boundary(membrane).

Hence the difference of the self structure is the information embededness for the right response to the enviromental change. The compelxity of the abiotic system is, though it exhibits seemingly very complicated pattern, restricted, whereas in biotic self structure information of enviroment stored in its self structure. Thus, we distinguish the complexity levels of organisations as follows:
(1) *Spontaneously emergent complexity*
(2) *Information mediated complexity*
Nonequilibrium system with autocatalytic reaction is

considered as the origin of self maintaineous system. We do not think that the biotic self structure continously evolved from the abiotic self organisation. There are large gap of whether it can utilize the information or not.

Origin of information exists in molecular recognition. Hence, origin is quite different from abiotic self organisation. We must think other scenario for the evolution of informational self structure. In the information mediated structure, information substance which exhibits molecular complementarity is mediated in all aspects of the semi-self structure. Hence, in information mediated self structure, principal intentionality is monotonously increasing tendency of information, that is, informational replication which is originated from molecular complementarity. Recurrent closedness is also information substance (ribozyme) mediated, which is enzyme mediated metabolism in present life form. Informational self is based on the molecular complementarity. Hence, autocatalytic cycle of the informational molecules replication is the origin of information storage. There has been controversies on which of the molecular replication or metabolism is more important for the origin of life. If we take present life, we can see both network working in the cell: information molecule reproduction network and metabolic network. Informational molecules not only produce the replication apparatus but also produce the enzyme to promote the metabolism, whereas metabolism produces the elemental substances for information molecules replication. Thus we would conjecture that biotic self structure "phase transition" started when the synbiosis of the information cycle and metabolic cycle occur, or in other words, informtional take over in which metabolic recurrent reaction network is taken over bv informational cycle. On account of this incorporation of information structure into semi-self, the semi-self structure can accumlate the information as to respond the enviroment effectively to form full-self structure.

Proposisiton 4(Biotic Self Structure) *Molecular synbiosis of the informational self structure and abiotic nonequilibrium self-organisation is the start of protoform of current life.*

5 Summary

In this study, we speculate about what life is from various levels and discuss the self structure between aboitic self organisation and protoform of life. We suggest that biological self structure heavily relies on the informational coupling (complimentarity) of molecules.

References

[1] M. Eigen and P. Schuster, The Hypercycle, Springer-Verlag, 1979.

[2] T.Gánti, The Principle of Life, OMIKK, 1987.

[3] S.A. Kaufmann, Origin of Order, Oxford 1993.

[4] H. R. Maturana and F. J. Varela, Autopoiesis and Cognition, D. Reidel Publishing Company, 1980.

[5] E.Schrödinger, What is life?, Cambridge University Press, 1944.

[6] A.Tsuchida, Thermophysics (in Japanese), Asakura, 1992.

[7] G.Nicolis and I.Prigogine, Self Organization in Nonequilibrium Systems?, Joh Wiley, 1977.

[8] H.Haken, Synergetics-An Introduction, Springer, 1978.

[9] H.Tanaka, Computational Theory of Life(in Japanese), Baifukan, 1998.

Proc. of Third Int. Symp. on Artificial Life, and Robotics (AROB III' 98),
Oita, Japan, 19-21, January, 1998,

Evolvability of Machines and Tapes

Takashi Ikegami
Institute of Physics,
The Graduate School of Arts and Sciences
University of Tokyo,
3-8-1 Komaba, Meguro-ku,Tokyo 153

Abstract

A self-reproduction process is described and discussed via a network model of machines and description tapes. Emergence of a core network which dynamically sustains the rewriting processes of machines on tapes are reported. Structures of the core networks are quite generic and includes Eigen's Hyper-cycle as a special case.

In the cell assembly model, where each cell contains machines and tapes, we show that the instability of the core network in some cells is sustained by those cells with stable core networks. The instability of the core network is transfered to its offspring when the cells divide. What is inherited here is not the patterns of tapes, but the way machines read tapes in a core network. [Key words : Mutation, Self-reproduction, Inheritance]

1 Introduction

1.1 Von Neumann's work

The definition of biological self-reproduction is, in the narrowest sense, the protein's copying process of a double helix by synthesizing a complementary chain from one side of the double helix. This is considered universal in the sense that it can copy any double helix independent of its information content. Also, the translation of DNA into a protein structure gives another universality in biology. This process is universal in the same sense that the process systematically translates DNA's pattern. We call it a universal construction-capability.

Universality in von Neumann's theory of self-reproduction is used in the same context. His theory is based on replicating patterns of a 2-dimensional cellular automaton [1], where each cell has 29 different states. A particular spatial configuration is found to work almost in the same way as what copying protein does to a DNA sequence. Von Neumann calls this configuration a universal constructor (UC). There is also a chain configuration (we call it tape) which encodes the universal constructor. When a UC is attached to the tape, it reads the tape and reconstructs the tape and the UC itself, at the specified location, by the tape. This behavior is called "universal" in the sense that any machine can be reconstructed whenever it is described by the tape configuration.

It is remarkable that for this universality to exist in both biology and cellular automaton, the separation of program (i.e., machine) and data (i.e., tape) is prerequisite. The separation should be made in order to prohibit the mutual interference of machines and/or tapes. However, a self-interference is required for self-reproduction. In other words, life has to observe itself in order to replicate itself, but what an individual really observes is the individual who observes himself. Hence, self-observation never stops. Therefore, to achieve a stable self-reproduction we have to obtain a stable *self description*. Von Neumann himself was also annoyed with this problem, but he knew that this fragility of separation meant at the same time of life itself [2]. And as is mentioned, the separation of the tape from the machine is established by preparing 29 states with a peculiar configuration.

1.2 Separation for Evolution

Von Neumann finally constructed a stable description and successfully separated a machine from a tape. But 10 years after von Neumann's work, such separation has proved to be unnecessary in order to have self-reproduction [3]. Also, the concept of universality of self-reproduction was discarded by C. Langton [4] because such universality is not essential to life itself. However, what I want to emphasize here, and what I think von Neumann really was driving at, concerns the problem of evolution. At first glance, self-reproduction in the sense of "making a same object," and evolution

in the sense of "making a different object" sounds very inconsistent. How can we reconcile the two? When we are faced with this problem, the separation of machines and tapes again comes into play. Separation is necessary for self-reproduction in the first place, but at the same time it is necessary for evolution: separation is to evolution as language is to creativity.

By describing an object by language, we can modify the object without modifying the object itself, and we can analyze non-existence objects and paradoxical matters. For example, there is no "false chemical reaction," but there is "false logic." By putting objects into linguistic codes, we can deal with the difference of matters true and false. Or, we can deal with paradoxical sentences. Acquisition of such linguistic codes, therefore, means to have the autonomy of description free from any physical or chemical constraints.

To acquire such linguistic code, it is necessary to separate machines from tapes. In fact, such acquisition has occured in biology. We can say that protein can synthesize new protein by acquiring linguistic codes (e.g., using DNA sequencing). A new protein can be called a "false" protein since it has not existed before acquiring a description. Therefore, the separation of machines from tapes is essential not only for stable self-reproduction; it is also necessary for perpetuating the evolutionary process. But not only mere evolution becomes possible by acquiring separation; evolution of evolvability [5] is obtained at the same time. Evolvability is not just a simple way of adapting to a given environment. It is defined as a meta-adaptability which adapts the method of adaptation itself (i.e., Bateson's deuterolearning [6]).We will discuss the possibility of having evolvability based on our simple computer simulations [8, 9].

2 summary

2.1 A model of machines and tapes

Our system consists of two different objects – tapes and machines. A tape has a bit string of a circular form (7-bit in this simulation). A machine consists of three different parts: a head, a tail, and a transition table. Each head and tail is expressed by a 4-bit string, whose pattern is compared with various tape binary patterns. If a pattern matches, a tape is replicated (with some modification by the machine) on the tape with the transition table. A synthesized tape is translated into the machine which is encoded by the tape pattern.

After introducing an ensemble of tapes and machines, we carry out a machine-tape reaction process. All machines and tapes have a maximum value N. Assuming that there are plenty of materials to make machines and tapes, we let them react in proportion to their numbers in a system. A pair of new machines and tapes are generated, and aged machines and tapes are removed, in order, from the system. Reaction between a pair of machines and tapes is represented, as well as a chemical reaction,

$$\mathbf{M}_i + \mathbf{T}_j \Rightarrow \mathbf{M}_k + \mathbf{T}_l + \mathbf{M}_i + \mathbf{T}_j \qquad (1)$$

where the machine $\mathbf{M}_i$ reads the tape $\mathbf{T}_j$ and the tape $\mathbf{T}_l$ is generated. From this tape, the machine $\mathbf{M}_k$ is translated out.

Here we define two different mutations. The first mutation is caused by external noise, which cannot be controlled by machines or tapes. In this sense, we name it **passive mutation**.This mutation only occurs on the bits which the machine reads. The second mutation is caused by a machine's rewriting process. Some tapes are frequently rewritten, but some are not. Since this rewriting process is completely determined by a machine, we name it **active mutation**. A passive mutation is measured by the frequency of "bit flipping," and an active mutation is measured by the frequency of rewritten bits.

Using this abstract machines and tapes system, the following is noted:

— We initially prepare a random set of machines and tapes in a system. External noise breeds autocatalytic structures, called core networks, in the system. Once the core networks are formed, they are stably replicated as a whole even without external noise. Core networks have general structures, whereas machines as well as tapes are globally replicated in the network. It should be noted that the Eigen's Hypercycle[7], where tapes are replicated only locally, is a special case of the core network.

— Core networks which include a variety of machines emerge for an adequate level of external noise. Too small or too large external noise leads to either a simple autocatalytic core networks, or total extinction. The obtained structure of core networks reflect the property of external noise; namely, a random pathway induced by an external noise is mimicked deterministically in a machine's rewriting processes.

2.2 Evolvability of Core Network

If we have one pool of machines and tapes, a single independent core network emerges in the pool, and

the core network is maintained by the mutually translating process of the machines. What happens if we have interaction between different core networks? In trying to answer this, we introduce a cell assembly of core networks; that is, machines and tapes which are contained in a cell structure. These cells can exchange machines, but not tapes, with other cells.

We assume two different levels of replication. One is replication of machines and tapes within a single cell, and the other is simply replication of cells. If a condition is fulfilled by the cell, it divides to leave a same number of machines and tapes to the daughter cells. Therefore, there emerge two identical cells at division time. The division condition is assumed to be determined by the degree of stability multiplied by the degree of diversity. In practice, we measure the stability by the number of mutually catalyzing machines, and the diversity by the total number of different machines. At the same time, cells which largely fail to satisfy the condition are removed from the pool. A non-responding time is also prepared: once a cell divides, it cannot divide during the non-responding time.

Here we do not initiate any external noise. Instead, machine flows from the other cells play the role of external noise. Machines which are not generated in a core network, perform unknown rewriting events to the core network.

Initially, we prepare several cells and place machines and tapes randomly. These machines and tapes do not constitute the core structure, but emerge from inter-cellular interactions. We set the division condition so that cells with only oscillating core networks can divide. An oscillating core is defined as a core whose network topology is temporally changing, as well as its active mutation rate.

We noticed that there are two different cell lines: one is a stable cell line which leaves an identical core network when it divides, and the other is an unstable cell line which leaves unstable, non-identical core networks. Whether the cells have identical core networks is measured by the average active mutation rates introduced earlier. Similar core networks may have similar values of active mutation rates. In the stable cell lines, both mother and daughter cells have almost identical, regularly oscillating active mutation rates. Conversely, unstable cell lines exhibit irregular and thus non-identical oscillating patterns.

After a given period of time, we turn off the inter-cellular interaction. We then find that the unstable cell assemblies are sustained by the stable cell assemblies. Shortly afterward, we turn off the inter-cellular interaction, and the stable cells increase their population exponentially. On the other hand, unstable cells are soon lost after the turning-off procedure (Fig.1). These unstable cells transition into stable cells without inter-cellular machine exchanges.

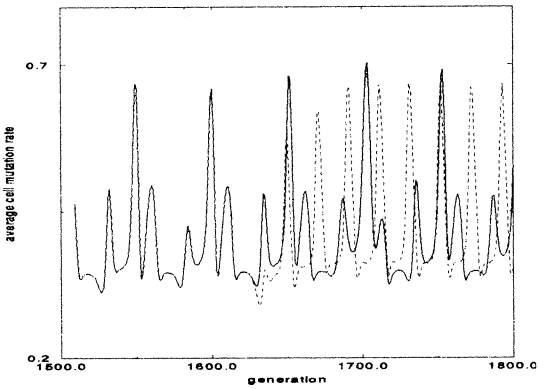


Figure 1: During inhibition of machine inter-cellular exchanges, we see that, after a short period of time, the unstable oscillations of active mutation rates (solid lines) become stable periodic oscillations (broken lines).

Under the inter-cellular machine exchanges, these unstable cells remain. Also, such "instability" of these cells is inherited by the offspring. This inheritance is not strictly deterministic, but the offspring can inherit the seed of this instability. Once it is lost from the mother cell, the instability is difficult to be recovered by the cell lines. In Fig.2 below, we have overlaid the instability quantity on a total cell phylogeny. The figure shows that the instability is indeed transferred to the offspring. However, the environment which sustains this instability transfer is prepared by the stable core networks. In other words, there is a stable environment which can sustain an ensemble of unstable replicators. Finally, it should be noted that what is inherited is not the patterns of tapes, but rather the way machines read tapes. We call this an example of "evolution of evolvability," as it transfers at least a meta-level of description, i.e., how to read tapes.

3 discussions

Fontana's Alchemy [10] shares common features with our system. He uses λ-calculus instead of our machines and tapes. His level 0 system corresponds to our simple fixed-state core, and a level 1 corresponds to stable core structures. Instead of meta-inhibition of

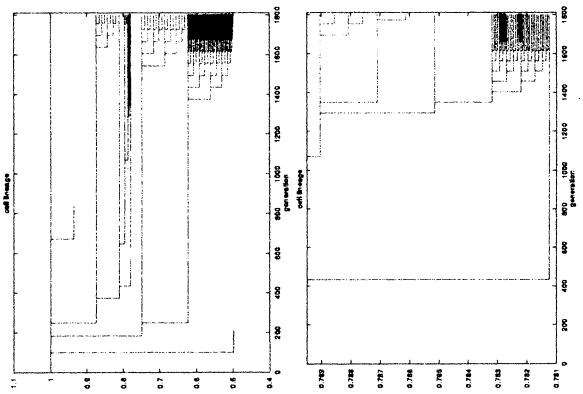


Figure 2: By quantifying the unstable oscillation, we draw the unstable cell line in red. The vertical line corresponds to the cell generation number. The right figure (b) is a scale up of the left figure (a) of the later generations of unstable cell lines.

self-copying in Fontana's model, we have introduced external noise to breed core structures. A level 2 corresponds to the present model, an inter-cellular interacting system. What Fontana calls "glue" corresponds to machine exchanges between different core networks. Inter-cellular interactions produce such glue machines.

Recently, K. Kaneko and his colleagues have shown that cells which contain fixed but complicated chemical networks exhibit a variety of cell differentiation based on cell division and competition dynamics for a common energy source. Their model inspired our construction of cellular division. Since our motivation is to understand the necessity of the machine/tape separation in the context of evolution, we have studied the machine's rewriting process on tapes instead of pure dynamical system modeling. As a result, we have succeeded in studying the evolution of the network as well as its evolvability.

However, the inheritance of different cell types (i.e., different dynamical state with the same core network) is observed in pure dynamical system modeling without being introduced to the separation of machines and tapes. Therefore, in order to show more clearly the necessity of separation, we have to deal with the essentially language-like situation where the difference of a true or false description has an effect; namely, we have to come back to the problem of the interference between data and program. Success of separation opens the way to the general-purpose computer. But complete separation is virtually impossible. Contrary to the prevailing attitude which tries to suppress the impossibility of separation by putting into place numerous syntactical rules [12], we have to analyze the impossibility of separation itself.

Acknowledgments

I wish to thank Dr.Takashi Hashimoto for his collaboration on these works. This work is partially supported by the Grant-in-Aids (No.07243102) for Scientific Research on priority are "System Theory of Function Emergence" from the Japanese Ministry of Education, Science and Culture.

References

[1] J.von Neumann, *Theory of Self-Reproducing Automata* (ed. A.W.Burks, Univ. Illinois Press, 1966)

[2] Von Neumann was referring to Richard's paradox with respect to this thoughts. (ibid. pp.125-126)

[3] R.Laing, *Automaton Models of Reproduction by Self-inspection*j.theor.Biol.66(1977) 437-456.

[4] C. Langton, "Self-Reproduction in Cellular Automata"*Physica* 10D (1984) 134-144.

[5] Rossler discusses evolvability as ultra-plasticity with respect to mutatable mutation rates in, O.E.Rossler, *Recursive Evolution* Biosystems, 11 (1979) pp.193-199.

[6] G.Bateson, *Mind and Nature: A Necessary Unity*(John Brockman Asoc. 1979).

[7] M.Eigen and P.Schuster, *Hypercycle* (Springer-Verlag, 1979).

[8] T.Ikegami and T.Hashimoto, *Active Mutation in Self-reproducing Networks of Machines and Tapes* Artificial Life 2 (1996)305-318.

[9] T.Ikegami and T.Hashimoto, *Replication and Diversity in Machine-Tape Coevolutionary Systems* in Artificial Life V.(eds. C.Langton et al., MIT press, 1997).

[10] W.Fontana and L.W.Buss, Proc.Natl.Acad.Sci. USA 91 (1994) 757-761; W.Fontana and L.W.Buss, Bull. Math. Biol. 56(1994) 1-64.

[11] K.Kaneko and T.Yomo, "Isologous Diversification: A theory of Cell Differentiation", Bull.Math Biol. 59 (1997) pp.139;

[12] B.Meyer, "Introduction to the theory of Programming Languages" (Bertrand Meyer, 1995)

Proc. of Third Int. Symp. on Artificial Life, and Robotics (AROB III' 98),
Oita, Japan, 19-21, January, 1998,

Evolution of Fitness Landscapes

Y. Toquenaga
Institute of Biological Sciences
University of Tsukuba
Tsukuba, Ibaraki 305, Japan

M. J. Wade
Department of Ecology and Evolution
University of Chicago
Chicago, IL 60637, USA

Abstract

We propose a hypothesis that fitness landscapes have been transformed by living things that change genetic operations and redundancy during the course of evolution. At the very beginning of life, the fitness landscape are rugged and mutation is the only clue to surf on irregular landscapes. The aim of evolution is not finding the highest peaks, but to keep living in the given environment. Natural lives then increase genetic redundancy to remain on the tentative peaks in the fitness landscapes. Increasing genetic redundancy is equivalent to increasing the area of basin of a peak. As the basin of a peak increases, its height decreases. Then, recombination (sexual reproduction) takes over powerless mutation for jumping among such fat peaks. Fatter the peaks grow, less powerful mutation and recombination become. For the peaks with broad basin, another external genetic operation, i.e., interdemic selection is required. We constructed GA-based artificial systems that could change genetic redundancy by repairing. The simulation results partially support our hypothesis.

INTRODUCTION

Evolution of complex systems is one of the hottest issues in artificial life (Alife). Conventional evolutionary biology, or population genetics has also dealt with complex biological systems, but its attitude against fitness landscapes is slightly different from that in Alife studies. The fitness landscapes of artificial creatures are often assumed to be rugged and dynamic, whereas evolutionary biology usually assumes flat, smooth, and relatively static landscapes (Fig. 1). We can also see the contrast in the difference in treating mutational effects [7]. In artificial life studies, mutational effects vary case by case, which results in a uniform distribution of the effects. On the contrary, most mutational effects are thought to be neutral in evolutionary biology.

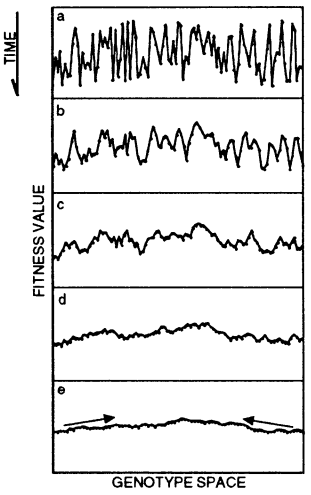


Figure 1: Transition from a rugged to smooth fitness landscapes.

Such discrepancy reflects the difference in evolutionary phases in which each field is interested. Alife researchers who want to create artificial creatures are interested in the origin of lives, and hence, prefer to deal with earlier evolutionary phases of life creation. On the contrary, evolutionary biologists face against real organisms that have well established in nature. Some of them are labeled "primitive," but they have also experienced more than 100 million years of evolution. Thus, evolutionary biologists are tackling with later phases of evolution.

The above contrast in attitude against fitness landscapes raises a simple question, "How has the shape of fitness landscapes changed in the course of evolution of living things?" To answer this question, we propose a hypothesis that fitness landscapes have been transformed by living things that change genetic operations and redundancy. In the following sections, we first describe the three phases in evolution of fitness land-

scapes. Then we show tentative results of computer simulations where genetic repairing is used as the aid of increasing genetic redundancy.

EVOLUTION OF FITNESS LANDSCAPES

Our hypothesis is inspired by the Shifting Balance Theory (SBT) by Sewall Wright [4]. SBT assumes that a species living in nature consists of subdivided populations, and claims three phases operating on them. The first phase is the random drift that creates each subdivided population. The second phase, i.e. mass selection or intrademic selection, trims the genotype/phenotype configuration in each subpopulation. The third phase is the interdemic selection, in which selection is acting at the population level by the differential extinction or propagation of the subpopulations.

A contrasting view against SBT is claimed by Fisher [3]. In Fisherian selection regime, there is no subdivided structure in a species or a population, and the whole population is the target of genetic operations (natural selection, random drift, etc.). Contemporary evolutionary biology is dominated by the Fisherian view [1]. However, SBT is rather preferred to apply in Alife studies [7]. The most unique aspect of SBT is that it provides a way to maintain genotypic configurations which may be destroyed by segregation in the Fisherian regime. Each subpopulation works as a "pocket" of unique genotypic configuration, and resultant variation among the pockets would be used in interdemic selection.

Although SBT assumes nonlinear and dynamic fitness landscapes, it does not mention about the mechanism how the fitness landscapes change their shapes. Our hypothesis addresses on the mechanism. It has also three phases which we will explain in the following subsections. The main issue is connecting genetic redundancy (redundant genetic coding and repairing) and genetic operations (mutation, recombination, and further external genetic operations). For the sake, we dare use a metaphor of mountainous surface for describing fitness landscapes, admitting that a hypercube metaphor is more appropriate for discussing genotypic space [4, 2].

Mutation Era

At the very beginning of life, the fitness landscape are rugged like a collection of frogs (Figs. 1 and 2).

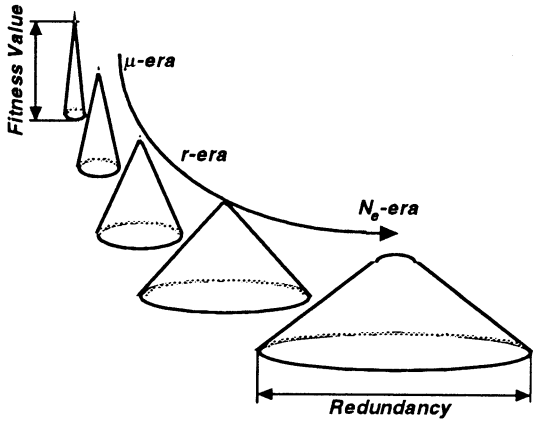


Figure 2: Three eras in evolution of fitness landscapes.

Each phenotype or genotype corresponds to a peak or a valley, and a short distance on the phenotype/genotype space does not guarantee similar fitness values. Mutation is the only clue to surf on such irregular landscapes [2]. However, mutation is a double-edged sword. It enables to find new higher peaks, but at the same time, the new mutational step may result in falling down toward a deep valley of the fitness landscape. In such unpredictable environment, the aim of evolution is not finding the highest peaks, but to keep living in the given environment [5].

Natural lives then increase genetic redundancy to retain the tentative peaks in the fitness landscapes. There are two ways to increase redundancy in genetic systems. One is introducing genetic code redundancy, and the other is adopting genetic repairing. Although the two methods are not completely equivalent, both can achieve many (genotypes) to one (fitness value) relationships. In other words, increasing genetic redundancy is equivalent to increasing the area of basin of a peak on the fitness landscape. As the basin of a peak increases, its height decreases, because there is trade-off between finding new higher peaks and keeping tentative peaks.

Recombination Era

As the basin of a peak increases, it becomes difficult to leave the domain of the peak by a single mutational event. Then, recombination, or sexual reproduction takes over the powerless mutation for jumping among fat peaks (Fig. 2). A single recombination event is equivalent to systematic multiple mutational events, which can step over the boundary of domains of fat

peaks.

Recombination, however, is also a double-edged sword. It may find new and fitter combinations of genotypes, but it can also break the tentative good combination and cause "hybrid breakdown." As in the case with mutation era, living things increase genetic redundancy or ability of repairing to mediate the harm effects of recombination. Then, the basin of each peak becomes larger and larger.

Interdemic Selection Era

Fatter the peaks grow, less powerful mutation and recombination become. For the peaks with broad basin, another external genetic operation, i.e., interdemic selection, or the phase III of SBT is required (Fig. 2). The fat peaks of fitness landscapes correspond to demes in SBT. The interdemic selection is the only clue to jump off the fat peaks. The fat peaks may represent immature species or local populations that still maintain inter-crossing ability. The top of the peaks are flat and neither mutation nor crossing over make a creature leave off from the species domain. The flatness also represent the high variation in phenotype/genotype within species or local populations.

As the three phases of SBT, the above three eras are not mutually exclusive. Some drastic genetic exchange at the higher levels may restart the lower level eras. The key issue is the way of restoring the ability for increasing and decreasing genetic redundancy. In the following section, we show some tentative results of computer simulation that partially support our hypothesis.

MODEL

We construct a model to represent a part (mutation and recombination eras) of our hypothesis using a genetic algorithms (see the definition in [7]). Our tentative goal is to create autonomous genetic systems that increase and decrease genetic redundancy during the course of evolution. Toquenaga et al. [6] proposed the Repairing Genetic Algorithm in his previous work. Thus, we chose genetic repairing for realizing genetic redundancy instead of incorporating a redundant genetic coding.

Each haploid individual in the system consists of a bit-string. There are three equal length parts in the bit-string; genotype bits (G-bits), masking bits (M-bits), and rule bits (R-bits). A mutational event is an external hazard, and the three parts are its targets. However, a locus on the G- and the M-bits is

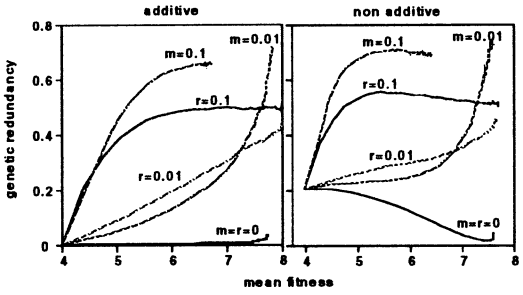


Figure 3: Dynamics of fitness values and genetic redundancy on the additive and non-additive fitness landscapes. 'm' and 'r' represent mutation and recombination rates, respectively.

blocked against mutation if the locus has the same bit on the M- and the R-bits. Thus, the variant genotypes resulted from mutational events are converged to an original genotype by genetic repairing. Note that R-bits are always suffered from the external mutation events, and the blocked loci may be released by futher mutational events. Recombination, or exchanging a part of a bit-string is also applied to each locus in the same way as mutation.

We tested two fitness landscapes. The first one is fixed and external one in which fitness values are determined purely by the number of 1s in P-bits. This is a completely additive fitness landscape, and single mutation always change the fitness value by a single step. We can derive an non-additive fitness landscape from it by shuffling the genotype-fitness relationship. The resultant non-additive fitness landscape retains the same mean and variance of fitness values. A bit-string population can achieve the maximum fitness values if time is long enough and population size is large enough.

The second fitness landscape is variable and internal one in which fitness values are determined by a simple bit-matching rule, or Hamming distance between P-bits of two randomly chosen individuals in a population. Contrary to the fixed external fitness landscapes, a bit-string population cannot achieve the maximum fitness values (= the length a bit-string), and the mean fitness values may fluctuate. We fixed population size, maximum time span, bit-string length, replication size as 256, 250, 8, 25, respectively. Statistics of genetic redundancy is defined by the probability that the fitness value for the original bit-string is the same as that of its variant generated by a single point mutation.

Figure 3 shows the dynamics of mean fitness values

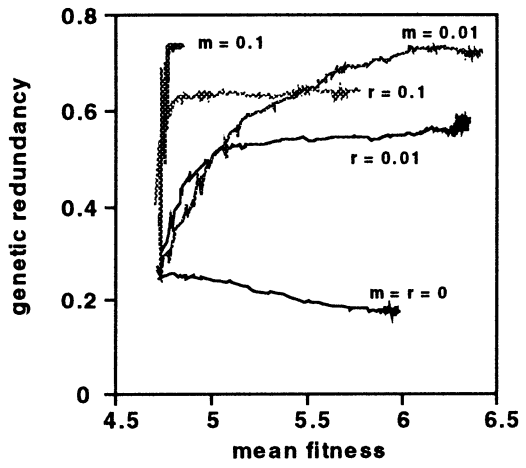


Figure 4: Dynamics of fitness values and genetic redundancy on the bit-matching fitness landscapes. 'm' and 'r' represent mutation and recombination rates, respectively.

and genetic redundancy in the two (linear and non-linear) fixed and external fitness landscapes when only mutation is applied. High mutation rates increased the genetic redundancy sacrificing the increase in fitness values. On the contrary, bit-string population first increased mean fitness values sustaining the genetic redundancy when mutation rate was low. The shape of the curves were similar when recombination was applied.

Figure 4 shows the dynamics of mean fitness and genetic redundancy in the variable and internal fitness landscapes. The genetic redundancy monotonically decreased when there is no mutation and recombination. When the mutation rate is high, genetic redundancy increased without increasing mean fitness values. When mutation rate is low, both genetic redundancy and fitness values increased. Recombination always increased fitness values although the first phase was dominated by increasing genetic redundancy.

DISCUSSION

Simulation results support the classical prediction that variation in fitness values is necessary for natural selection. Non-redundant fitness landscapes are preferred for increasing the fitness value. When mutation and recombination was allowed, bit-string population tried to increase genetic redundancy. Moreover, the fitness values were not always maximized. Note that we did not apply any selection on genetic redundancy per se. The change in genetic redundancy is a side-effect of random drift (because we fixed the total population size) and natural selection. These findings support our hypothesis of evolution of fitness landscapes.

The state of fitness landscape affects the result of evolution of genetic redundancy. When it is fixed and external, mutation and recombination were almost equivalent. On the contrary, when it is variable and internal, high mutation only increased the genetic redundancy. In other words, populations are trapped in a basin of a peak. Recombination can increase both redundancy and fitness values.

Our hypothesis show the full course of evolution in complex systems, which consists of three phases; mutation era, recombination era, and interdemic selection era. It also provides cross-pollination between Alife studies and genetics of evolutionary biology. Further steps are needed to describe interdemic selection eras. We should incorporate a population structure, or a mating structure and create variation of fitness values at higher levels.

References

[1] J. A. Coyne, N. H. Barton, and M. Turelli "A critique of Sewall Wright's Shifting Balance Theory of Evolution," *Evolution*, Vol. 51, pp. 643-671, 1997.

[2] M. Eigen, *Steps towards life*, Oxford UP, 1992.

[3] R. A. Fisher, *The genetical theory of natural selection. 2nd ed.*, Dover, 1958.

[4] W. B. Provine, *Sewall Wright and Evolutionary Biology*, Chicago UP, 1986.

[5] L. B. Slobodkin, A. Rapoport "An optimal strategy of evolution," *Quarterly Review of Biology*, Vol. 49, pp. 181-200, 1974.

[6] Y. Toquenaga, T. Saruwatari, and T. Hoshino "Repairing Genetic Algorithm and diversity in artificial ecosystems," *in C. G. Langton and K. Shimohara (eds.) Artificial Life V, MIT press*, pp. 300-307, 1997.

[7] Y. Toquenaga and M. J. Wade "Sewall Wright meets Artificial Life: The origin and maintenance of evolutionary novelty," *Trends in Ecology and Evolution*, Vol. 11, 478-482, 1996.

Proc. of Third Int. Symp. on Artificial Life, and Robotics (AROB III' 98),
Oita, Japan, 19-21, January, 1998,

A Description of Quasi–Autopoietic Systems based on the Framework of (M,R) Systems

Tatsuya Nomura Katsunori Shimohara
Evolutionary Systems Department
ATR Human Information Processing Research Laboratories
2-2, Hikaridai, Seika-cho, Soraku-gun, Kyoto 619-02 JAPAN

Abstract

In this paper, we discuss a description of autopoietic systems using a mathematical framework of (M,R) systems. Our attempt may be very thoughtless because of the difficulty in interpreting autopoiesis within the framework of the naive set theory. Accordingly, our description does not strictly reflect pure autopoiesis, and can only represent quasi–autopoietic systems. Nevertheless, we believe that this attempt will spur discussions on the formal description of autopoiesis and the relation between autopoiesis, mental systems, and social systems, and so on, which has been a highly controversial point. Based on this belief, we have proposed a rough model of quasi–autopoietic systems[10]. In this paper, we discuss the adequacy of this description, considering view points of relational biology[12] and abstract chemistry by λ–calculus[4, 5].

1 Introduction

Autopoiesis is a neologism, introduced by Maturana and Varela to designate the organization of a minimal living system[8]. An autopoietic system is one that continuously produces the components that specify it, while at the same time realizing itself to be a concrete unity in space and time; this makes the network of production of components possible. An autopoietic system is organized as a network of processes of production of components, where these components:

1. continuously regenerate and realize the network that produces them, and
2. constitute the system as a distinguishable unity in the domain in which they exist.

Later, Luhmann applied autopoiesis to the theory of social systems, developing his own interpretation of it[7]. Recently, this theory has been applied to not only sociology but also psychopathology[2].

Moreover, Kawamoto has continued his own development of autopoiesis. In his book[6], he designated the properties of autopoiesis by comparison with conventional system theories. In addition, he gave the following gist in the concept of autopoietic systems:

1. The set of components of a system is determined by the operation of the system.
2. The operation of the system precedes the initial condition.
3. The operation of the system is executed only to succeed itself and does not aim to produce by–products.
4. In the operation of the system, the things that happen in the system clearly differ from the things that external observers discriminate.

However, there is still no mathematical model that represents autopoiesis itself. A machine learning model inspired by autopoiesis was proposed to do tasks such as pattern recognition[3], but this model does not represent autopoiesis itself. Moreover, although there are some cases where autopoietic systems are represented by simulations using the method of computational chemistry[9], these are specialized for models of living cells and do not represent mathematically integrated formulations of Maturana's original autopoiesis.

2 (M,R) Systems

There are Metabolism–Repair Systems ((M,R) systems), a mathematical system model introduced by Rosen to abstractly formalize the functional activities of a living cell – metabolism, repair, and replication[11]. This system model maintains its metabolic activity through inputs from environments and repair activity.

The simplest (M,R) systems represent the above aspect in the following diagram:

$$A \xrightarrow{f} B \xrightarrow{\phi_f} H(A,B) \xrightarrow{\Phi_f} H(B,H(A,B)) \quad (1)$$

Here, A is a set of inputs from an environment to the system, B is a set of outputs from the system to the environment, f is a component of the system represented as a map from A to B, and ϕ_f is the repair component of f as a map from B to $H(A,B)$ ($H(X,Y)$ is the set of all maps from a set X to a set Y). In biological cells, f corresponds to the metabolism, and ϕ_f to the repair. If $\phi_f(b) = f$ $(b = f(a))$ is satisfied for the input $a \in A$, we can say that the system self–maintains itself. Moreover, the replicator component Φ_f satisfies $\Phi_f(\phi_f(b)) = \Phi_f(f) = \phi_f$ for the above b and f. Figure 1 shows the simplest (M,R) system.

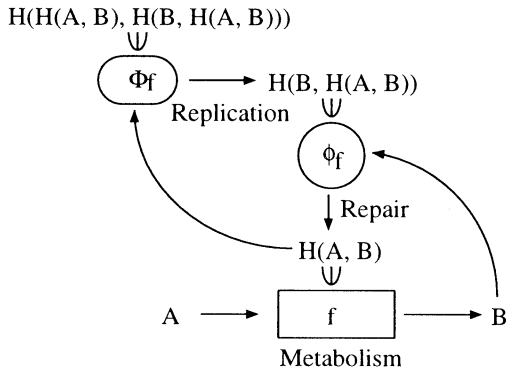


Figure 1: (M,R) Systems

It is important that Φ_f can be constructed within the system in the following way:
For a and b such that $b = f(a)$ and $\phi_f(b) = f$, if $\hat{b} : H(B,H(A,B)) \to H(A,B)$ $(\hat{b}(\phi)(a') = \phi(b)(a')$ $(\phi \in H(B,H(A,B)), a' \in A))$ has the inverse map $\hat{b}^{-1}$, it is easily proved that $\hat{b}^{-1}(f) = \phi_f$. Thus, we can set $\Phi_f = \hat{b}^{-1}$.

Casti developed a theory of (M,R) systems assumed as linear systems, to mathematically analyze the conditions for stability in self–maintenance [1]. Moreover, Zhang and Sugisaka proposed a modified linear (M,R) system to discuss the mechanism of the repair function[13]. We borrow the framework of metabolism and repair in (M,R) systems and apply it to our description of the dynamical aspect of input–output behaviors, and the framework of replication and apply it to our description of the circular operations.

3 Quasi–Autopoietic Systems

Our description of a quasi–autopoietic system is as follows:

$$A \xrightarrow{f} B \xrightarrow{\phi} H(A,B), \quad (2)$$

$$H(B,H(A,B)) \xrightarrow{F} H(B,H(A,B)) \quad (3)$$

Instead of the replication map from $H(A,B)$ to $H(B,H(A,B))$ in (M.R) systems, this system has an iteration map on $H(B,H(A,B))$. This map determines the system's self by defining its self as an invariant set with a kind of ergodicity property for the map; that is, its self QAP is defined as follows:

$$QAP \subset H(B,H(A,B)),\ F(QAP) = QAP, \quad (4)$$

$$^{\forall}\phi, \phi' \in QAP,\ ^{\exists}n \in \boldsymbol{N}\ s.t.\ F^n(\phi') = \phi \quad (5)$$

Figure 2 shows the above aspect.

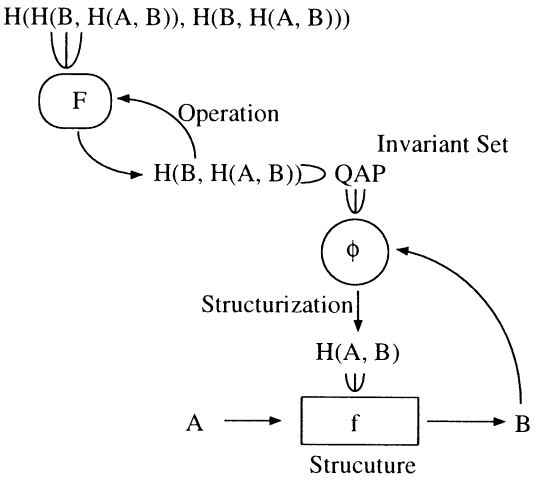


Figure 2: Quasi–Autopoietic Systems

By regarding the map F as the operation and ϕ as the components of the system, we can interpret this system as the one which satisfies the gist of Kawamoto in Section 1 in the following sense:

1. QAP is an invariant set of F. Moreover, whether an element in $H(B,H(A,B))$ belongs to QAP is determined by F, that is, by the reachability from the initial state of the system through F, because of the ergodicity property in (5).

2. In order for the system to exist as a quasi–autopoietic system, the initial state must belong to an invariant set for F.

3. The thing the system executes results in a new state being made within QAP by iterating F, and not in the input–output map f being produced.

4. If external observers watch only the input–output relation in the system and the changes in the relation, the thing that happens in the system, that is, the iteration of F within QAP, differs from the things which these observers discriminate in the system, that is, f.

4 Discussion from View Points of Relational Biology and Abstract Chemistry

Quasi–autopoietic systems we have proposed is the one introduced to represent the aspect of autopoiesis described with natural language within a naive set theory. Thus, it causes some conflicts in comparison with pure autopoiesis.

We introduced an invariant set with the ergodicity property in the set of repair maps in (M,R) systems to represent the self–determination of the system's boundary. However, the space where the system's self exists is determined in advance and then the operator is also determined as the map on it. Moreover, we separated the operator and input–output actions in the system to represent the absence of inputs–outputs in the system. This caused the input–output actions to not affect the self–determination of the system's boundary, and the existence of the operator became groundless.

We discuss these problems considering the view points of relational biology and abstract chemistry.

4.1 Closure under Efficient Cause

Rosen proposed relational analysis, in which systems are grasped as a network that consists of components with functions[12]. Then, he compared machine systems with living systems to clarify the difference between them, based on the relationship among components through entailment. In other words, he focused his attention on where the function of each component results from in the sense of Aristotle's four causal categories, that is, material cause, efficient cause, formal cause, and final cause. Rosen's conclusion is summarized as follows:

1. Machine systems are described with their states. This fact results from considering the category of formal models for the system.

2. If all the components of a machine system must be entailed in the sense of efficient cause, there must be a larger system entailing them. This causes an infinite regress.

3. In a machine system within which all the components are entailed in the sense of efficient cause, an infinite decomposition of the state space happens, thus this also causes an infinite regress.

4. Thus, any machine system is not closed under efficient cause.

Then, Rosen claimed that *a material system is an organism if and only if it is closed to efficient causation.*

(M,R) systems satisfy the above condition "closure under efficient cause" in the sense that the replication map Φ_f is entailed in the system by b, that is , the output of the metabolism f, as mentioned in Section 2. However, our quasi–autopoietic systems do not because just the operation map F is not entailed in the system. If the condition of closure under efficient cause is required for models which represent autopoietic systems, we must find the way in which the operation map is constructed in the system by f and/or ϕ.

4.2 Constructive Dynamical Systems

In relational analysis, the origin of either functions of components or closed relation between them is not considered. This means that the sets where the maps lie are given in advance, in both (M,R) systems and our quasi–autopoietic systems.

As a method to represent the origin of systems, Fontana and Buss proposed constructive dynamical systems by abstract chemistry, in which chemical processes are abstractly represented in terms of λ–calculus.

In this section, we represent their formalization more abstractly. Firstly, a set of symbols $\hat{X}$ is inductively defined by a group of axioms $\{f_i\}$ as follows:

$$
\begin{aligned}
&X_0 : \text{ a primitive set of symbols,}\\
&X : \text{the set of all the sequences}\\
&\quad \text{which consist of elements of } X_0\\
&f_i : D_i \to X \quad (i = 1, \ldots, L)\\
&\left(\begin{array}{ll} {X_0}^{n_i} \subset D_i \subset X^{n_i}, & f_i({X_0}^{n_i})^{n_i} \subset D_i \\ n_i : \text{a natural number} & (i = 1, \ldots, L) \end{array} \right)\\
&X_0 \subset \hat{X} \subset X, \quad \hat{X}^{n_i} \subset D_i \quad (i = 1, \ldots, L) \qquad (6)\\
&{}^{\forall} x \in \hat{X} \; {}^{\exists} i \in \{1, \ldots, L\}, \; (x_1, \ldots, x_{n_i}) \in \hat{X}^{n_i}\\
&\quad s.t., \; f_i(x_1, \ldots, x_{n_i}) = x \qquad (7)
\end{aligned}
$$

Then, given an initial set of sequences $B_0 \subset \hat{X}$ and a translation map entailed by the group of axioms $F_{\{f_i\}} : \hat{X}^N \to \hat{X}$ $(N \geq 2)$, the following dynamics, called constructive dynamical system, is considered:

$$\begin{aligned} B_i &= F_{\{f_i\}}({B_{i-1}}^N) \\ &\equiv \left\{F_{\{f_i\}}(g_1, \ldots, g_N) \; ; \; g_1, \ldots, g_N \in B_{i-1}\right\} \end{aligned} \tag{8}$$

In the λ–calculus approach of Fontana and Buss, $\hat{X}$ is the set of λ–terms and $F_{\{f_i\}}$ is defined by the substitution and reduction to normal forms through transformation. It is reported that there are a variety of self–organized structures such as mutual production and syntactical regularities among objects in the limit set of the above dynamics[4, 5].

It is important that the constructive dynamical system is closed under efficient cause. That is, each element x in the system is not only entailed through $F_{\{f_i\}}$ but also becomes efficient cause in the sense that $F_{\{f_i\}}(x, \cdots)$ entails other elements or x itself. Moreover, the limit in the above dynamics represents a kind of reactant equations in a chemical process. In other words, the state space in the equation is generated through interaction among objects, and autopoietic relation between objects as components and continuation of the translation map as operations is realized in the constructive dynamics.

The source of this autopoietic relation is the fact that the set where the dynamics is defined, is inductively defined, and thus the elements in the set are both components and operations in the system. This direct embedding of elements of the system into the set of the map on it $(\hat{X} \hookrightarrow H(\hat{X}, \hat{X}))$ does not exist in our quasi–autopoietic systems.

5 Conclusion

It was verified that our quasi–autopoietic systems are not sufficient to model autopoiesis from static viewpoints of relational biology and dynamic viewpoints of abstract chemistry. As future problems, we need find models to represent closure under efficient cause and the origin of the organization based on the direct embedding of elements of the system into the set of the map on it by inductively defined sets.

References

[1] Casti, J. L. (1988) The Theory of Metabolism–Repair Systems. *APPLIED MATHEMATICS AND COMPUTATION* 28:113–154.

[2] Ciompi, L. (1994) *Affektlogik* (Japanese Edition). Gakuju Shoin, Publishers, Ltd.

[3] Deffuant, G., Fuhs, T., Monneret, E., Nourgine, P., and Varela, F. (1995) Semi–Algebraic Networks: An Attempt to Design Gemometric Autopoietic Models. *Artificial Life* 2(2):157–177.

[4] Fontana, W., and Buss, L. W. (1994) The Arrival of the Fittest: Toward a Theory of Biological Organization. *Bulletin of Mathematical Biology* 56:1–64.

[5] Fontana, W., and Buss, L. W. (1996) "The barrier of objects": From dynamical systems to bounded organizations. In *Boundaries and Barriers*, J. Casti and A. Karlqvist, Eds. Addison–Wesley, pp. 56–116.

[6] Kawamoto, H. (1995) *Autopoiesis: The Third Generation System* (in Japanese). Seido–sha Publishers.

[7] Kneer, G., and Nassehi, A. (1993) *Niklas Luhmanns Theorie Sozialer Systeme* (Japanese Edition), Shinsensha ed. Wilhelm Fink Verlag.

[8] Maturana, H. R., and Varela, F. J. (1991) *AUTOPOIESIS and COGNITION: THE REALIZATION OF THE LIVING* (Japanese Edition). Kokubun–sha Publishers.

[9] McMullin, B., and Varela, F. (1997) Rediscovering Computational Autopoiesis. In *Proc. Fourth European Conference on Artificial Life (ECAL'97)*, P. Husbands and I. Harvey, Eds., MIT Press, pp. 38–47.

[10] Nomura, T. (1997) An Attempt for Description of Quasi–Autopoietic Systems Using Metabolism–Repair Systems. In *Proc. Fourth European Conference on Artificial Life (ECAL'97)*, P. Husbands and I. Harvey, Eds., MIT Press, pp. 48–56.

[11] Rosen, R. (1972) *FOUNDATIONS OF MATHEMATICAL BIOLOGY*, vol. 2. Academic Press, ch. 4: Some Relational Cell Models: The Metabolism–Repair Systems, pp. 217–253.

[12] Rosen, R. (1991) *LIFE ITSELF*. Columbia University Press.

[13] Zhang, Y. G., and Sugisaka, M. (1997) Some New Look at Metabolism–Repair System. In *Proc. International Symposium on Artificial Life and Robotics (AROB'97)*, S. Fijimura and M. Sugisaka, Eds., pp. 34–37.

Proc. of Third Int. Symp. on Artificial Life, and Robotics (AROB III'98),
Oita, Japan, 19-21, January, 1998,

Development of Meaning Structure by Usage-based Word Relationships

Takashi Hashimoto *
Lab. for Information Synthesis
Brain Science Institute, RIKEN
Hirosawa 2-1, Wako, Saitama, 351-01, JAPAN

Abstract

Development of meaning structure is studied from a usage-based viewpoint by a constructive approach. The meaning structure is represented by relationships between words. A word's relationship to other words, which represents meanings of the word, is derived by analyzing similarity of the word's usage in sentences. Words make clusters according to their similarity. The word clusters are classified into several types and show some remarkable dynamics. The clusters and their dynamics are studied by means of hierarchical cluster analysis and principal coordinate analysis.

Keywords: Usage-based viewpoint; Constructive approach; Evolutionary linguistics; Word similarity; Word clusters

1 introduction

We propose *usage-based viewpoint* as that meanings of words should be discussed in terms of how language is used [1]. Since interrelationships among words are employed as a representation of meanings of words, the point of view means that a word's relation to other words should be derived by analyzing the word's usage in the language.

Constructive approaches are highly advantageous for understanding dynamically complex systems [2]. These approaches are also useful for studying *evolutionary linguistics* which is a new candidate for potentially clarifying the origins and evolution of language [3]. It is important to note that language are typically expressed as such dynamically complex systems as emergence, self-organization, collective behavior, clustering, diversification, hierarchy formation, and so on. It is also important to point out that language systems must have both adaptability and stability. If a language is too rigid, its users will not be able to formulate new expressions to describe diverse experiences, and if it is too unstable, no communication will be possible at all. Such dynamical stability and adaptability is often seen also in complex systems.

We have proposed some models for evolutionary linguistics by constructive approach [4, 5, 6]. In [6], we have tried to catch dynamical aspects of meaning structurization and discuss its relevance with linguistic categorization. In this paper, the model and results of [6] are summarized and hierarchical cluster analysis and principal coordinate analysis for the results are reported.

*E-mail address: takashi@brain.riken.go.jp

2 Word Similarity

In our model, an agents has generative grammar system and word similarity matrix. The agents try to recognize given sentences by means of their own grammar and articulate words from successfully recognized sentences. Word similarity matrix is updated by each recognition of a sentence. The grammar of agents is small at the beginning of simulation and modified according to its usage in the recognition processes. For the detail of the model, refer to [6].

Word similarity matrix is the representation of relationships among words which is calculated by Karov and Edelman's algorithm of words similarity formulae [7] with some revisions. A key concept in this definition is the mutual dependency between words and sentences. That is, similar words are used in similar sentences and similar sentences are composed of similar words.

The similarities between words and between sentences are respectively defined by the following formulae:

$$sim_{n+1}(w_i, w_j) = \begin{cases} \sum_{s \ni w_i} weight(s, w_i) aff_n(s, w_j) & \text{if } i \neq j \ , \\ 1.0 & \text{if } i = j \ , \end{cases} \quad (1)$$

$$sim_{n+1}(s_i, s_j) =$$

$$\begin{cases} \sum_{w \in s_i} weight(w, s_i) aff_n(w, s_j) & \text{if } i \neq j \ , \\ 1.0 & \text{if } i = j \ , \end{cases} \quad (2)$$

$$aff_n(s, w) = \sum_{s' \ni w} weight(s', w) sim_n(s, s') \ , \quad (3)$$

$$aff_n(w, s) = \sum_{w' \in s} weight(w', s) sim_n(w, w') \ , \quad (4)$$

$$weight(s, w) = \frac{factor(s, w)}{\sum_{s' \ni w} factor(s', w)} \ , \quad (5)$$

$$factor(s, w) = \frac{p(s)}{\#(s, w)} \ , \quad (6)$$

$$weight(w, s) = \frac{factor(w, s)}{\sum_{w' \in s} factor(w', s)} \ , \quad (7)$$

and

$$factor(w, s) = \frac{1}{p(w) lg(s)} \ . \quad (8)$$

In the above formulae, a suffix n indicates the times of iterations, $w \in s$ means words included in a sentence s, and $s \ni w$ means sentences including a word w. The functions $weight(s, w)$ and $weight(w, s)$ are normalizing factors that define contribution from the appearance frequency and length of each word and sentence to affinity and similarity. In Eqs. (6) and (8), $p(w)$ and $p(s)$ are the appearance frequencies of a word w and a sentence s, respectively; $lg(s)$ is the length of a sentence s, which is defined by the number of words included in the sentence; and $\#(s, w)$ is the number of appearances of a sentence s including a word w.

At the initial iteration step ($n = 0$), similarity with word itself ($sim_0(w_i, w_i)$) is 1.0, the others are 0.0. Word-sentence affinity (Eq. (4)) at $n = 0$ is calculated from this initial word similarity matrix. Then, these four formulae are iteratively calculated as Eqs. (2) $\rightarrow$ (3) $\rightarrow$ (1) $\rightarrow$ (4) at each successful recognition of a sentence by the agents.

3 Word Cluster

Words are clustered in word similarity space according to having or not having similarity with each other. By using principal coordinate analysis, which is one method of the multi-dimensional scaling [8], the clusters of words are clearly seen in two dimensional space. Fig.1 is an example of scatter diagram constructed from the result of the analysis. The first two axes are used as x and y axes respectively to draw the scatter diagram. We can see three clusters of words in this figure. At top-right and top-left in the diagram there are several words relatively closer relationships, namely similar usage in sentences. Words in the third cluster at bottom-center are solitary words. By this analysis any solitary words are grouped into one cluster (completely same position), since they share the same relation, that is, they have no relationships with any other words.

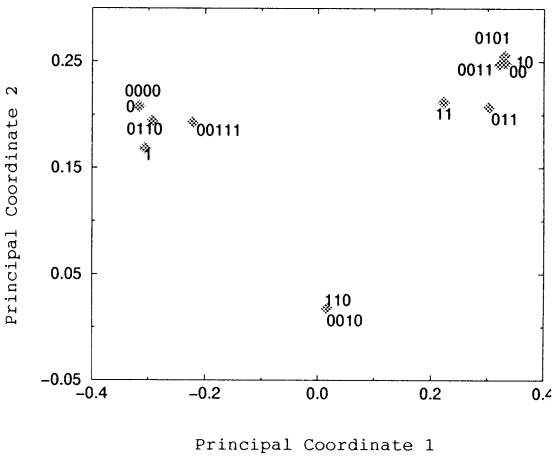


Figure 1: An example of principal coordinate analysis of word similarity matrix $sim(w_i, w_j)$.

Various shapes of cluster structure appear, which depends on the initial grammar of the agents. We have classified the structures in the space of similarity into six types according to their shapes as follows[6]: (a) *solitary word* – a word has no relation to other words; (b) *flat cluster* – words in a cluster have almost identical similarities with each other; (c) *gradual cluster* – similarity between words in a cluster depends on words and gradually changes; (d) *two-peak cluster* – words are in a cluster but there are two peaks of similarity; (e) *sub-clustering* – a cluster has a stepwise structure. (f) Words form plural and unrelated clusters.

We use hierarchical cluster analysis [8] to study the nature of the clusters. The results are shown in Fig.2. Sectioning a dendrogram parallel to the vertical axis at any similarity level yields a partition of words into clusters. Hereafter, sectioning level is denoted by $\widehat{sim}$. For example, sectioning the dendrogram in Fig.2(d) at $\widehat{sim} = 0.65$ yields the clusters (1-5), 6, 7, 8, (9,10). If we decrease the sectioning level, some clusters are combined into one cluster, and vice versa. For instance,

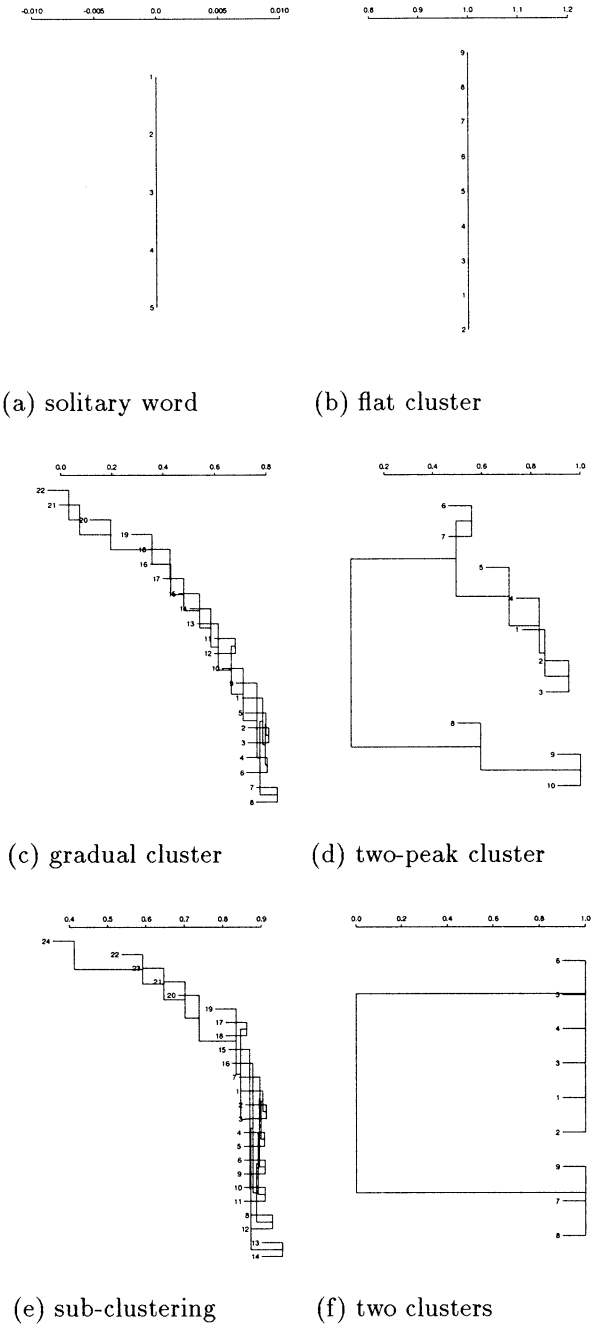
by sectioning the dendrogram in the above example at $\widehat{sim} = 0.58$ clusters 8 and (9,10) are combined into one cluster, and sectioning at $\widehat{sim} = 0.75$ tell word 5 as the different group apart from the cluster (1-4).

The findings from this analysis are summarized as follows: (a) solitary word. Since each word has no similarity with each others, all words are aligned at the line where similarity equals to zero; (b) flat cluster. All words have almost identical similarity with the all other words in the cluster. So, they are aligned at the line where similarity equals to 1.0; (c) gradual cluster. Words are connected to a cluster one after another. In the case of this type, there is no appropriate sectioning point because of the successive connection and the gradual change of similarity; (d) two-peak cluster. Sectioning the dendrogram between $0.05 \leq \widehat{sim} < 0.5$ yields two clusters. Words in each cluster are excluded successively with increasing the sectioning point from $\widehat{sim} = 0.5$. From this analysis, we should say that the two-peak cluster is combined version of two gradual clusters. The two gradual clusters are seen as one cluster when the sectioning point comes below $\widehat{sim} = 0.05$; (e) sub-clustering. The dendrogram shows two parts, dense ($0.8 < sim$) and gradual changing part ($sim \leq 0.76$). The dense part makes almost flat cluster structure and the other part makes the other group. (f) two clusters. We can figure out two independent clusters by sectioning any level between $0.0 < \widehat{sim} < 1.0$;

4 Development of Clusters

A general scenario of the development of structure in the similarity space is the following[6]. At first an agent can recognize only a one-word sentence. It develops the ability to recognize several sentences, but these all are one-word sentences, and therefore there are several solitary words in the similarity space. Then it becomes able to articulate plural words from sentences, which forms relations between words. Eventually words form gradual clusters. In the course of development, some remarkable dynamics of clusters such as boundary expansion, clusters merging, and structural change from gradual to flat cluster are observed. Parallel to this development, syntactic structure also develops from sequential to branch and to loop structures.

In Fig.3, we represent the process of cluster merging by means of principal coordinate analysis [8]. At $n = 10$ there are three clusters in the scatter diagram. Words in the cluster at bottom-center are soli-



(a) solitary word (b) flat cluster

(c) gradual cluster (d) two-peak cluster

(e) sub-clustering (f) two clusters

Figure 2: Examples of structures of word similarity matrices analyzed by hierarchical cluster analysis. The horizontal axis shows similarity between words. Each leaf of branch means each word. Numbers put beside the leaves are indices for words. We have six distinct types of structures. (a) Solitary word. (b) Flat cluster. (c) Gradual cluster. (d) Two-peak cluster. (e) Sub-clustering. (f) Two clusters.

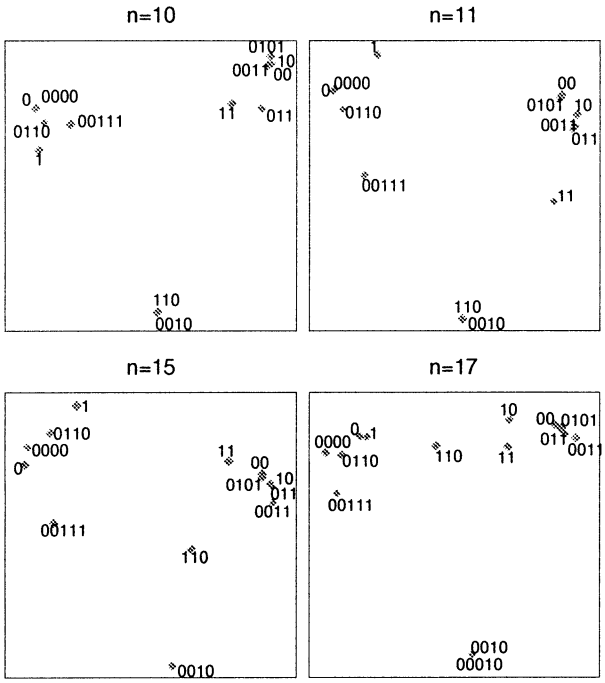


Figure 3: Dynamics of word clusters on merging. These are scatter diagrams from principal coordinate analysis of word-similarity matrix $sim_n(w_i, w_j)$. n is the number of iterations. Since we are interested only in the relative distances among words, value of x and y axis is omitted.

tary words. Two clusters at top-left and top-right are gradual cluster. But from this diagram gradualness of the clusters is not clearly seen. Words in a gradual cluster typically form like a line. At $n = 11$, the two clusters strengthen the gradualness so words in the clusters become to be lined up. At $n = 15$, one of the solitary word, 110, is related with the top-right cluster, then the boundary of the cluster expands. At this time, the two clusters at top of the diagram have small relationships, but from this analysis such feature can not be detected. In the next figure, $n = 17$, these two clusters become one two-peak cluster. We find that word 110 play like a cramp between two cores.

5 Summary

We have proposed an evaluation of meaning representation by relationship among words based on the similarity of language usages from the viewpoint of usage-based meaning. We studied structurization of word cluster in word similarity space by means of an artificial agent with a grammar system. These clusters, classified into six types, are analyzed by hierarchical method of cluster analysis. Each type shows characteristic feature also by this analysis. One of the remarkable dynamics of the structures, cluster merging, is studied by principal coordinate analysis. Development of two clusters from small to gradual ones and mergence to one two-peak cluster can be clearly seen.

Acknowledgments

I am grateful to Mr. Iba for his help on statistical analysis. This work is supported by Special Postdoctoral Researchers Program at Institute of Physical and Chemical Research (RIKEN).

References

[1] Wittgenstein, L., *Philosophische Untersuchungen*, Basil Blackwell, 1953.

[2] Kaneko, K. and Tsuda, I., Constructive complexity and artificial reality: an introduction, *Physica*, **D75**, 1–10, 1994.

[3] Steels, L., Synthesising the origins of language and meaning using co-evolution, self-organisation and level formation, in *Evolution of Human Language*, Hurford, J (ed.), Edinburgh Univ. Press, Edinburgh, 1997.

[4] Hashimoto, T. and Ikegami, T., Evolution of Symbolic Grammar Systems, *Advances in Artificial Life*, F. Morán et al. (eds.), Springer, Belrin, 812–823, 1995.

[5] Hashimoto, T. and Ikegami, T., Emergence of net-grammar in communicating agents, *BioSystems*, **38**,1–14, 1996.

[6] Hashimoto, T., Usage-based Structuralization of Relationships between Words, *Fourth European Conference on Artificial Life* Phil Husbands and Inman Harvey (Eds.), MIT Press, Cambridge, MA pp. 483–492, 1997.

[7] Karov, Y. and Edelman, S., Similarity-based word sense disambiguation, Technical Report of Weizmann Institute, CS-TR 96-06, 1996.

[8] Gordon, A. D., *Classification*, London, Chapman and Hall, 1981.

Proc. of Third Int. Symp. on Artificial Life, and Robotics (AROB III' 98),
Oita, Japan, 19-21, January, 1998,

Nonlinear oscillations on an Abstract Rewriting system on MultiSets

Yasuhiro Suzuki and Hiroshi Tanaka
Medical Research Institute
Tokyo Medical and Dental University
Bunkyo 1-5-45, Tokyo Japan, 113

Abstract

We develop an abstract computational model, called ARMS, to deal with systems of large degree of freedom like liquid and confirm that they can simulate the emergence of the complex behavior of cycles such as if autocatalytic cycles, chemical oscillation which are often found in the emergence of life. In this paper, by use of ARMS, we made experiments on Brusselator model (Brusselator is a model of chemical oscillations which are found on Belousov-Zabotinsky reaction). And we confirm that non-linear oscillation emerges.

1 Introduction

Symbolic computation model which can deal with a system having very large degree of freedom such as liquid has not been proposed so far. However, in the research of complex adaptive systems, specially that about the emergent dynamics of life, the system which we deal with becomes necessarily of large degree of freedom. Thus we create a new computational model, ARMS (Abstract Rewriting System on MutiSets).

ARMS can deal with such systems with large degree of freedom as liquid, gas, and so on, because of our use of multisets in this model, it can also treats the concept of concentration of chemical liquid. So, ARMS can be regarded as an abstraction of chemical system. By using this model, we made experiments on Brusselator model (Brusselator is a model of chemical oscillations which are found on Belousov-Zabotinsky reaction), and we confirm that non-linear oscillation emerges.

2 Abstract Rewriting System

An abstract rewriting system abstracts the algebraic characteristics of calculus, whose example is shown in the above subsection, focusing on rewriting. Introducing this formal structure, several characteristics of rewriting can be discussed in the common framework. Let us first begin with the definition of the abstract rewriting system.

Definition 1 (Abstract Rewriting System) *An abstract rewriting system is defined as a pair (A, R), where A and R denotes a finite alphabet and a finite set of pairs of words over the alphabet A, respectively.* □

Next, the final result of rewriting calculus, called normal form.

Definition 2 (Normal Form) *If there does not exist b such as $a \to b$ and $b \in A$, then $a \in A$ is called normal form.* □

3 ARMS

3.1 Definition of ARMS

Using the concepts of abstract rewriting system, we introduce a new abstract rewriting system on multisets (ARMS for short). ARMS is defined as follows.

Definition 3 *Abstract rewriting system on multisets is defined as a quintuple (A, R, O_R, C, I), where A, R, O_R, C and I denote a set of symbols, a set of rewriting rules, rule order, a multiset of symbols, and a set of input strings, respectively.* □

In this model, a multiset C is used as "a test tube", which contains "symbols" in A, which correspond to chemical compounds. Then, rewriting rules R, corresponding to chemical reactions, act on this multiset, and the symbols matching the right hand side of a rule are transformed into other symbols. Moreover, for simplicity, we assume no character can be removed from the multiset C (except by rewriting).

Normal form can be defined as follows.

Definition 4 (Normal Form in ARMS) *If no rule in R can be applied to C and if no string in I can be input to C, then it is said that C is in normal form.* □

Thus, normal form corresponds to the steady state, or the death of living things.

4 Chemical ARMS

ARMS can be regarded as abstract chemical system, such as Fontana's Algorithmic chemistry [1]. Because, from the chemical point of view, multisets can be regarded as "a test tube", symbols as "chemical compounds", rewriting rules as "chemical reactions/equation". We will call chemical ARMS as CRMS.

In CRMS, we assume that selecting rule has no relation to that the selected rule can act or not. An algorithm for rewriting steps in CRMS is described as shown in Figure 1.

```
procedure CRMS (Rewriting Step)
begin
  count-step ← 0;
  while count-step ≠ n do
    begin
      if term reached Normal Form then
        i:= n;
      else
        if | term | < maximum length of term
        then INPUT;
        Select rule(s);
        if Rewrite term
        then count-step := count-step + 1;
      end if
  end while
end.
```

Figure 1: An Algorithm for CRMS (until n-th step)

4.1 Experimental Results

Reaction rate of chemical reaction is usually in proportion to concentration of reactive substance or multipication of concentration, and it is defined through observation of concentration of reactive substance.

On CRMS, reaction rate corresponds to frequency of rule application. When r_1 has higher reaction rate than r_2 then the CRMS applies rules as following sequence, for example, $\{r_1, r_2, r_1, r_1, r_1, r_1, r_1, r_2, r_1, r_2, r_1 \ldots\}$.

Characteristic Function In order to incorporate frequency of rule application and input, we introduce characteristic function as below.

Definition 5 (Characteristic Function) *Let x be a uniform random number selected from $[0, 1)$. Then a characteristic function $h_\delta(x)$ is defined as:*

$$h_\delta(x) = \begin{cases} 1 & (x < \delta) \\ 0 & (x \geq \delta), \end{cases}$$

where δ denotes a threshold. □

4.2 Brusselator model on CRMS

We made experiment using Brusselator[2] model on CRMS. Brusselator is a model of chemical oscillation as Belousov-Zabotinsky reaction. It consists of differential equation (fig 2).

$$\begin{array}{lcll} \mathrm{A} & \xrightarrow{k_1} & \mathrm{X} & \\ \mathrm{B} + \mathrm{X} & \xrightarrow{k_2} & \mathrm{Y} & + \mathrm{D} \\ 2\mathrm{X} + \mathrm{Y} & \xrightarrow{k_3} & 3\mathrm{X} & \\ \mathrm{X} & \xrightarrow{k_4} & \mathrm{E} & \end{array}$$

Figure 2: Abstract chemical model of Brusselator.

We regard these abstract chemical reaction equation as rewriting rules which is illustrated in Figure 3.

$$\begin{array}{llllllll} & \mathrm{A} & \rightarrow & \mathrm{X} & & & & : r_1 \\ \mathrm{B} & \mathrm{X} & \rightarrow & \mathrm{Y} & \mathrm{D} & & & : r_2 \\ \mathrm{X} & \mathrm{X} & \mathrm{Y} & \rightarrow & \mathrm{X} & \mathrm{X} & \mathrm{X} & : r_3 \\ & & \mathrm{X} & \rightarrow & \mathrm{E} & & & : r_4 \end{array}$$

Figure 3: Rewriting rules for Brusselator.

Initial Condition As to the initial condition, maximum length of term is equal to 5000, initial state of term is set to empty multiset. We assume that "A" and "B" are input continually. So this model is continuously fed stirred tank reactor (CSTR). Threshold for input is 0.05. Thresholds for r_1 and r_4 are fixed to 0.10. Because, we regard these rules as first-order reaction. On the other hand, we treat r_2 and r_3 as higher-order reaction.

Initial State and Final State As mentioned above, the initial state, the term is empty (term $\equiv \{\}$). On the other hand, final state is defined as a normal form defined in the above section. That is, *if no rule in R can be applied to term without the resulting base number exceeding the limit on maximum length of term, then term is in a final state.*

We examine the relationship between frequency of rule application and concentration of "X" and "Y". We regard the number of "X"/"Y" in term as concentration. Then we found that there are three types of behavior pattern about X-Y concentration as follows;

- Stable oscillation,
- Unstable oscillation,
- Divergence and Convergence.

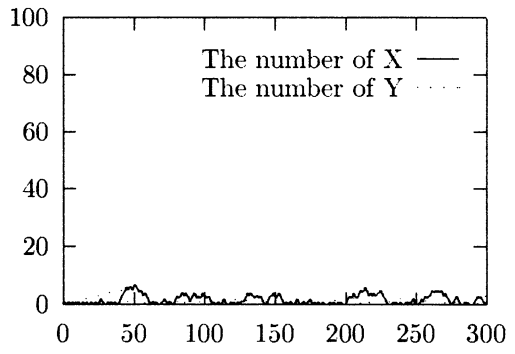


Figure 4: Example of Convergence

Oscillation on the number of between X and Y emerges as follows; at first, the number of X increases and as decreasing the number of X, the number of Y increases. We will call this type of oscillation as **X-Y oscillation**, and oscillations on the number of X or Y itself as **X-oscillation** and **Y-oscillation**, respectively, below.

Stable oscillation

Convergence When the threshold is $r_1 << r_2$, then the system becomes converge; figure 4 shows it. In this case, threshold for r_1, r_2 are 0.1, 0.04 respectively. Only few X-Y oscillations can be found, almost oscillations are X or Y-oscillation.

(quasi) stable oscillation As the threshold for r_2 becomes larger than r_1, the system is apt to generate

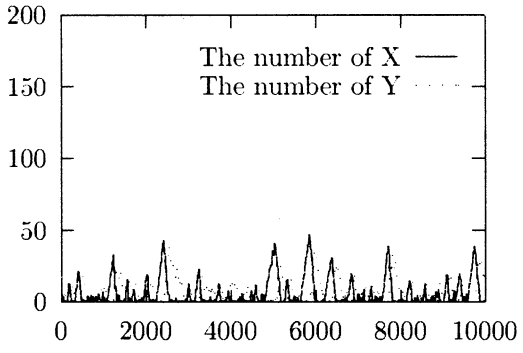


Figure 5: Example of (quasi) Stable oscillation

X-Y oscillation, which resembles limit cycle. Even if perturbation occurred in the system, the system maintains this oscillation. In this case, the number of X or Y-oscillation decreases, on the other hand, the number of X-Y oscillation increases. X-Y oscillations can be classified into following three categories;

(1) The highest peak of the number of X or Y is between 35 and 50,

(2) The highest peak of the number of X or Y is between 15 and 35,

(3) The highest peak of the number of X or Y is between 1 and 15.

Each type of oscillation, (1), (2) and (3), appears irregularly. So in other words, in this case the system generates limit cycle, or rather "strange attractor". Figure 5 shows this case. In this case, threshold for r_1 and r_2 are 0.1 and 0.15, respectively.

Unstable oscillation

As the threshold for r_2 becomes larger than r_1, the system is apt to exhibit unstable oscillation. In this case, there are a few X or Y-oscillation; and almost all the oscillations become X-Y oscillation. A great variety of X-Y oscillation can be found.

So, in this case, in other words, the system becomes chaotic state. This case is not like (quasi) stable case like above; oscillations do not converge on several kind of oscillations such as type (1) to (3). Figure 6 shows unstable oscillations. In this case, the threshold for r_1, r_2 are 0.1, 0.35, respectively.

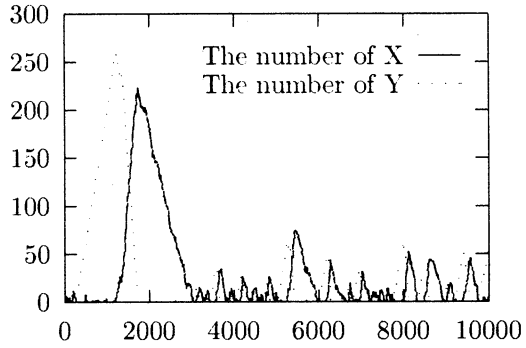


Figure 6: Example of Unstable oscillation

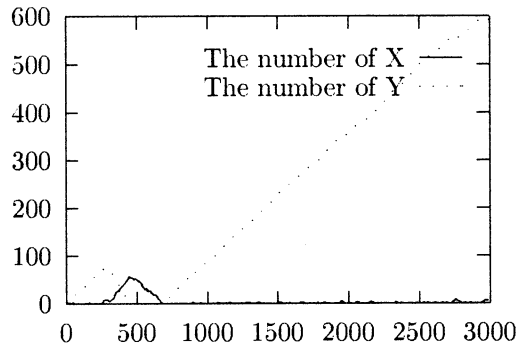


Figure 7: Example of Divergence

Divergence

When the threshold as $r_2 >> r_1$, the system becomes unstable and the system diverges in many cases. In this case, a system generates X-Y oscillations, as shown in Figure 7 (between step 0 and 650). On this regime, the system becomes unstable, and it is apt to diverge by perturbation. It is impossible to predict if the system generates oscillations or diverges. Figure 7 shows this case. The threshold for r_1, r_2 are 0.1, 0.45, respectively.

4.3 On behavior pattern of the system

From experiments, relationship between threshold and system's behavior can be summarized into table 1. As shown in table 1, balance of threshold for r_1 and r_2 controls system's behavior. When $r_1 << r_2$, the system is apt to converge. As the threshold for r_2 becomes larger, the system is likely unstable; then $r_1 << r_2$, the system diverges in many cases.

If a system selects r_1 in the highest frequency, then the system produces many X (by using A $\rightarrow$ X :r_1). And if frequency of selecting r_2 is very low, r_3 hardly

$r_1 >> r_2$	Convergence
$r_1 > r_2$	Stable Oscillation
$r_1 < r_2$	Unstable Oscillation
$r_1 << r_2$	Divergence

Table 1: Relationship between threshold and system's behavior

acts; because r_3 can not act without Y. In this case, X almost will be used by r_4. This relationship, between r_1 and r_4, generates X-oscillation.

From this point of view, one may say that system needs r_2 to generate X-Y oscillation. As threshold for r_2 getting larger, the system is likely to generate Y, by using r_2 (BX $\rightarrow$ YD).

To make X-Y oscillation, system must decrease the number of Y, so it must to use r_3 for this purpose. Because this rule is "autocatalytic reaction" (XXY $\rightarrow$ XXX), it increases X in high rate (1.5 times). Therefore, by using r_3, system is likely to unstable.

5 Conclusion

In this paper, we introduce a new abstract rewriting system on multisets, and model chemical reactions as a symbolic rewriting system which acts on a multiset, which can be viewed as a test tube. Using this model, we made experiments on Brusselator model and we confirm non-linear oscillation emerge.

These results, if properly translated in the terms of chemical reactions, might provide insightful analysis for prebiotic conditions where the proto-from of life emerges as a cycle of reactions.

Acknowledgments

This research is supported by Grants-in-Aid for Scientific Research No.07243203 from the Ministry of Education, Science and Culture in Japan.

References

[1] W. Fontana and L. W. Buss, The Arrival of the fittest: Toward a Theory of biological organization, Bulletin of Mathematical Biology, Vol.56, No.1, 1-64, 1994.

[2] G. Nicolis and I. Prigogine, Exploring Complexity, An Introduction, Freeman and Company, 1989.

Proc. of Third Int. Symp. on Artificial Life, and Robotics (AROB III' 98),
Oita, Japan, 19-21, January, 1998,

A Method of a Mobile Robot Navigation by a Task-Level Feedback Control

Yoshiro HADA Kunikatsu TAKASE

University of Electro-Communications
Graduate School of Information Systems
1-5-1 Chofugaoka, Chofu-shi Tokyo 182, Japan

Abstract

This paper introduces a methodology that will allow robots to execute tasks autonomously and with a high degree of success. Taking as an example the mobility of a robot without collision in a dynamic environment, a task-level feedback control system is proposed. The key idea is to incorporate the real-time recognition and motion planning functions into the task control loop. For real-time recognition of the environment, *mark-based vision* is used. In addition, algorithm to do a global motion planning in the environment where movable obstacles exist is proposed to be implemented. By integrating the real-time recognition and motion planning, we succeed in forming a control loop for the task.

1 Introduction

There is an increasing demand for robots that can be used outside of factory settings, in such locations as offices, hospitals, or homes. But the workspace in such application fields is poorly arranged for robots, and subject to dynamic change. Robots working in such a dynamic environment are basically required to execute tasks autonomously, without human help. In this paper we call this kind of robot an autonomous robot and discuss how to make it.

To date, several control algorithms for an autonomous mobile robot working in a dynamic environment have been proposed. Almost all of these are based on local sensor information, and there is no assurance that they can work successfully throughout the entirety of a large working domain. While some algorithms try to achieve the goal of task globally by introducing a whole domain map[1][2], they can't incorporate environmental changes into the map in real-time. Finally, a behavior-based approach[3] has been shown to hold promise for real-time intelligent control of a rather simple robot, like a insect type one, but we doubt that human-level intelligence can be approximated using such a bottom-up and local model.

In this paper, we propose a task-level feedback control system[4] that will allow an autonomous robot to complete tasks robustly in a dynamic environment. This system extends the concept of motion-level feedback control to a task-level. The actual method consists of iterating the cycle of task-state recognition, motion planning, and task execution in real time, so that the task is achieved robustly, even if there are motion errors or environmental changes.

2 Task-level feedback control

In order to function in a dynamic environment, human beings rely on perpetual reassessment of the state of their tasks. That is, it seems clear that a kind of feedback control exists in human task execution.

In our approach, we introduce a concept of feedback control into the robot task execution to make it possible for the robot to accomplish the task reliably in the dynamic environment. The task-level feedback control can be defined as an iterated control loop wherein the state of a task is repeatedly observed, and the motions repeatedly planned and executed toward the realization of a task. The block diagram of the control is shown in Fig. 1.

The control system is explained in more detail in the following, where a mobile robot is taken as an example. In the control system, the controlled variables are the robot's position and orientation, and the state variables are the position and orientation of a robot and the obstacles in the environment. The error is the path along which a robot moves toward its goal. The manipulated variables are motion parameters to reduce the distance between current position and goal. State feedback is realized by the function of recognition, and the error is obtained by the function

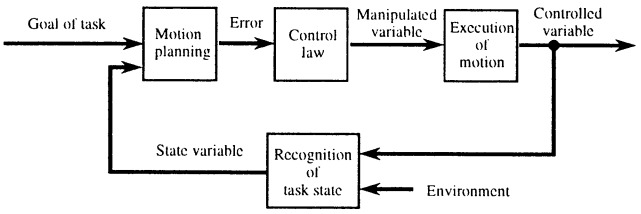


Fig. 1: Block diagram of the feedback control applied to a robotic task.

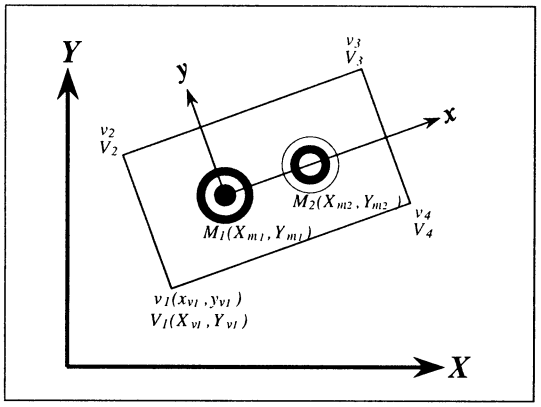


Fig. 2: Parameters for the geometric object model.

of motion planning.

The control procedure is as follows.

1) Identifying a robot and obstacles in the work space and measuring their position and orientation by the function of real-time recognition to be discussed in section 3.

2) Finding a collision-free path between the current robot position and the goal in real-time using the motion planner to be described in section 4.

3) If there is a path, moving the robot by some steps, along the found path. Return to step 1.

4) If there are no paths, stopping the robot. Return to step 1.

This method promises achievement of the task of the robot even if there are some motion errors or changes in environment.

3 Real-time recognition of objects

In this section we describe a method of objects recognition referred to as mark-based vision[4]. The main components of mark-based vision are mark recognition and object model. For the sake of simplicity, it is assumed here that an object is polygonal in shape and does planar motion.

In order to recognize marks in real-time, we use tracking vision [5] and adopt a concentric circular pattern for the mark on an object to simplify the identification and localization of a mark using tracking vision.

An object's generic model can be constructed as follows. A pair of marks is attached on a single object, as shown in Fig. 2. Let $M1$ and $M2$ be the centers of mark1 and mark2, respectively, and X_{m1}, Y_{m1}, and X_{m2}, Y_{m2} be their coordinates with respect to an absolute reference frame (X, Y). And let $M1$ be the origin of the object internal reference frame (x, y) fixed on the object. Making the x axis of the object internal reference frame coincide with $\overline{M_1 M_2}$, the unit vector along the x axis can be given as

$$\boldsymbol{e_x} = \left(\frac{X_{m2} - X_{m1}}{s}, \frac{Y_{m2} - Y_{m1}}{s} \right)^T \tag{1}$$

The unit vector along y axis is given as

$$\boldsymbol{e_y} = \left(-\frac{Y_{m2} - Y_{m1}}{s}, \frac{X_{m2} - X_{m1}}{s} \right)^T \tag{2}$$

where $()^T$ stands for transpose of matrix and s the length between M_1 and M_2.

$$s = \sqrt{(X_{m2} - X_{m1})^2 + (Y_{m2} - Y_{m1})^2} \tag{3}$$

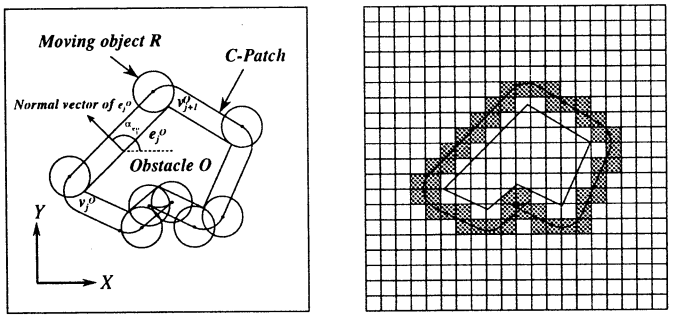
Let the measured coordinate of vertices of a polygon with respect to the absolute reference frame be $V_i(X_{vi}, Y_{vi})$ $(1 \leq i \leq n)$. The vertex coordinate $v_i(x_{vi}, y_{vi})$ with respect to the object's internal reference frame then becomes

$$x_{vi} = (X_{vi} - X_{m1}, Y_{vi} - Y_{m1}) \cdot \boldsymbol{e_x} \tag{4}$$

$$y_{vi} = (X_{vi} - X_{m1}, Y_{vi} - Y_{m1}) \cdot \boldsymbol{e_y} \tag{5}$$

This v_i is a component of the geometric model of the object. The object's geometric model is created according to the following procedure.

1) Give the coordinate of M_1 and M_2 using a cursor on the display.
2) Calculate $\boldsymbol{e_x}$ and $\boldsymbol{e_y}$ by eqs. (1) and (2).
3) Give the coordinate of V_i using the cursor.
4) Calculate v_i by eqs. (4) and (5).



(a) (b)

Fig. 3: Representation of an obstacle in C-space in case a robot is circle.

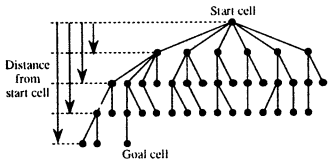


Fig. 4: Tree.

4 Motion planning

We deal with the mobility of a robot without collision in the dynamic environment as a task. In order to find a collision free path, a configuration space (*C-space*)[6] is used. To describe configuration space obstacles (C-obstacles), we use a configuration patch (*C-patch*)[7][4] which is a set of a configuration of a mobile object being in contact with obstacles. The perfect boundary surface of the C-obstacle is composed by the C-patch.

In the case of a robot modeled as a circle, a configuration q of the robot R is defined as $q = (x_c, y_c)$, where x_c and y_c are the coordinates of the center C of R in an absolute reference frame, shown in Fig. 3 (a). We can define two kinds of C-patch of R:

1) a set of configuration of R which is in contact with the edge e_j^O of the obstacle O; and
2) a set of configuration of R which is in contact with the vertex v_j^O of the obstacle O.

In the case of 1, C-patch $q_{e_j^O}$ is the line segment and becomes as,

$$\boldsymbol{q}_{e_j} = \begin{pmatrix} x_j + r\cos\alpha_{e_j^O} + t(x_{j+1} - x_j) \\ y_j + r\sin\alpha_{e_j^O} + t(y_{j+1} - y_j) \end{pmatrix} \quad (6)$$

$$0 \le t \le 1$$

where (x_j, y_j) and (x_{j+1}, y_{j+1}) are the coordinates of the v_j^O and v_{j+1}^O, respectively, r is a radius of R, and $\alpha_{e_j^O}$ is an angle between the normal of e_j^O and the X axis of the absolute reference frame.

In the case of 2, C-path $q_{v_j^O}$ is an arc, and expressed as,

$$\boldsymbol{q}_{v_j} = \begin{pmatrix} x_j + r\cos\alpha \\ y_j + r\sin\alpha \end{pmatrix} \quad (7)$$

$$\alpha_{e_{j-1}} \le \alpha \le \alpha_{e_j}$$

where $\alpha_{e_{j-1}^O}$ is an angle between the normal of e_{j-1}^O and the X axis, and $\alpha_{e_j^O}$ between the normal of e_j^O and the X axis. The union of C-patches of cases 1 and 2 with all j represents the boundary surface of the C-obstacle. As shown in Fig. 3(b), the approximated C-space is constructed by descretizing this plane into cells and each cell is labeled as either START, GOAL, OBSTACLE, or FREE.

We adopt an exhaustive breadth-first search as the method of path finding. The path finding is carried out by examining cell labels to derive a collision-free path. The cell examination begins with the START cell and is repeated until the GOAL cell is reached. The tree shown in Fig. 4 is created as a result of this search. By tracing the branches between the GOAL and root nodes, the shortest path between the START and GOAL cells can be determined. If the GOAL can not be reached by examining all FREE cells in the C-space, a path does not exist.

5 An example of task-level feedback control

In order to verify the effectiveness of the proposed task-level feedback control, we next report an experimental task execution using an omnidirectional mobile robot. The experimental setup is shown in Fig. 5. The control cycle which consists of phases of the recognition, the planning and the execution is synchronized with NTSC signal, as shown in Fig. 6. A single control cycle takes approximately 100[ms]. The control procedure can be stated as follows.

1) A robot and several obstacles (up to 6) are recognized in 1/30[s], using the mark-based vision.
2) Using the geometric model obtained above, the C-space is constructed and the path is generated in 1/30[s].

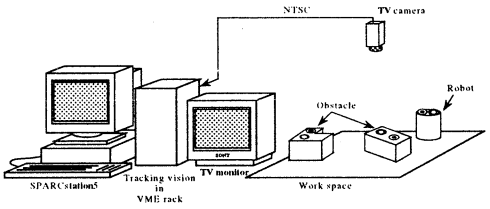


Fig. 5: Experimental equipment.

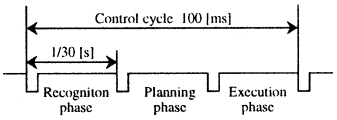


Fig. 6: Control cycle.

3) The move command is sent to the robot. The robot moves along the path obtained above for $0.1[s]$ at the speed of $9.0[cm/s]$. If no paths to the goal are found, the robot stops.

Steps 1 through 3 are iterated until the robot reaches the goal. The control method allows obstacles to move.

The experimental results are shown in Fig. 7. Initially the robot is in the upper right of the picture. White objects are obstacles, and all object have a pair of marks. The goal, indicated with a white circle, is located near the U-shaped object. Fig. 7(a)–(b) show the robot trying to move along a path through the center of the picture. An L-shaped obstacle can be seen blocking the path in Fig. 7(c). Thus the robot detours to avoid the obstacle and reaches the goal without collision (Fig. 7 (d)-(f)).

6 Conclusion

In this paper we propose a task-level feedback control to facilitate the tasks of autonomous robots in dynamic environments. For the recognition of objects in real-time, we propose a system of mark-based vision. And for global motion planning through a dynamic environment, we propose algorithms using C-patch. These two processes, the real-time recognition and motion planning, are then integrated to form a control loop for the task. Finally, we conduct a experiment on a mobile robot moving in a dynamic environment. The results indicate the effectiveness of the proposed method.

References

[1] M.J.Mataric: "Integration of Representation Into Goal-Driven Behavior-Based Robots", IEEE Transaction on Robotics and Automation vol.8, no.3, pp.304–312, 1992.

[2] S.Tachi and K.Komoriya: "Guide Dog Robot", Proc. of 2nd International Symposium of Robotics Research, pp.333–340, 1984

[3] R.A. Brooks: "A Robust Layered Control System for a Mobile Robot", IEEE Journal of Robotics and Automation vol.RA-2-1, pp.12–23, 1986

[4] Y.Hada, K.Takase: "Task-Level Feedback Control of a Robot Based on the Integration of Real-Time Recognition and Motion Planning" Proc. of the 28th International Symposium on Robotics (ISR), pp.13.53-13.63, 1997.

[5] H.Inoue,M.Inaba, T.Mori, T.Tachikawa: "Real-Time Robot Vision System based on Correlation Technology", Proc. of International Symposium on Industrial Robots (ISIR), pp.675–680, 1993.

[6] T. Lozano-Perez: "Spatial Planning: A Configuration Space Approach", IEEE Transaction on Computers, vol.C-32, no.2, pp.108–120, 1983.

[7] Yun-Hui Liu and H.Onda: "Constructing an Approximate Representation of a Configuration Space Without Using an Intersection Check", Proc. of the 1993 IEEE/RSJ International Conference on Intelligent Robots and Systems(IROS'93), pp.644–651, 1993.

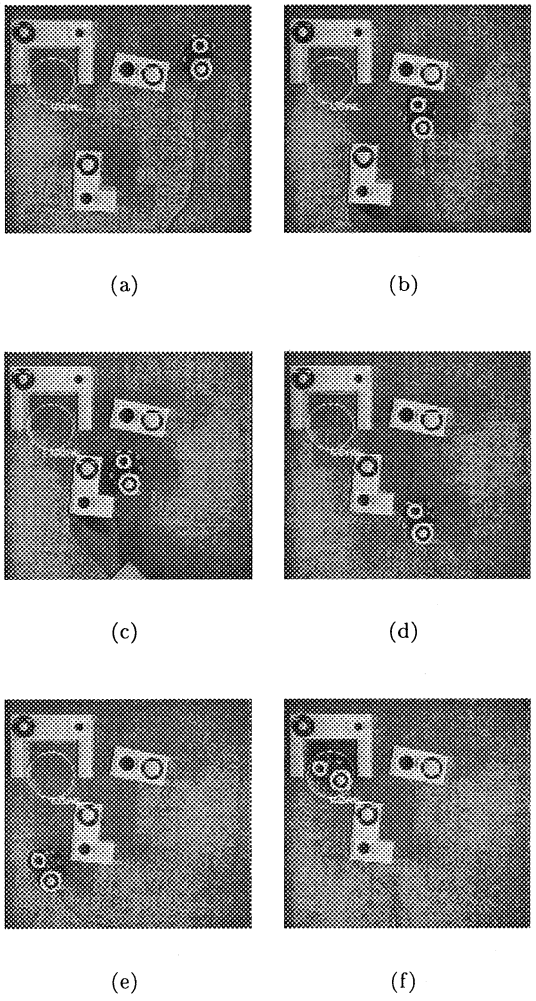


Fig. 7: Result of the experiment

Proc. of Third Int. Symp. on Artificial Life, and Robotics (AROB III' 98),
Oita, Japan, 19-21, January, 1998,

Strategies for Changing Configurations of Autonomous Arms in a Complex Pushing Task

Hongbin Zha, Hiroki Nagahama, Tsutomu Hasegawa

Graduate School of Information Science and Electrical Engineering, Kyushu University
6-10-1 Hakozaki, Higashiku, Fukuoka 812-81 JAPAN
E-mail : zha@is.kyushu-u.ac.jp

Abstract

We have developed a method for pushing an object upward on a slanted plane by cooperating multiple autonomous robot arms. In most cases of the operation, the desired poses (location and orientation) of the object cannot be achieved without changing configurations of arms. In this paper, we propose a new planning algorithm for changing pushing points so that the system consisting of autonomous arms would be more flexible to complicated situations. The validity of the proposed method is investigated by some numerical simulations.

Keywords : autonomous and distributed systems, pushing, cooperation, action planning

1 Introduction

The growing interest has been concentrated on cooperation of multiple robots in order to achieve complex operations that is impossible to be performed by a single robot. Some instances of multiple robots cooperating are found in the domain of object manipulation tasks such as pushing [1] and handling [2].

We have developed a method for pushing an object upward on a slanted plane by multiple autonomous robot arms [4]. This pushing operation is different from general pushing tasks that have been performed on a horizontal plane, because each arm must have take into accounts the influence of the gravity, and the instability of the object as well. This complexity in dynamic environments causes the problem that, usually, the desired poses of the object cannot always be achieved without changing initial pushing configurations of the arms. In this paper, we propose a new planning algorithm for changing pushing points of arms so that the system would have more flexibility to complex situations.

This paper is organized as follows : Section 2 gives a description on our pushing task and the control process for this operation. In Section 3, we propose the strategy for changing pushing points, and Section 4 reports some numerical simulation results. Finally, Section 5 gives some conclusions.

2 Pushing Operation

2.1 Environment

Fig. 1 illustrates the pushing operation considered in our research. This operation requires more than two arms for the stable pushing. In reconfiguration of arms, however, one arm would move to new contacting point while the remaining arms have to support the object. As a result, at least three arms would be essential for reliable and efficient pushing. In our research, we limit the pushing direction to be parallel with the slanted plane, so that the task can be treated in a two dimensional space.

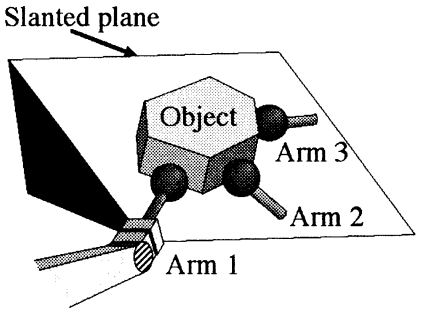


Figure 1: Pushing task on a slanted plane.

In this paper, we make the following assumptions :

1. The object to be pushed is a short prism, and its geometrical shape and mass are known.

2. The object's motions are slow enough that frictional forces dominate inertial forces. This is a quasi-static assumption.

3. Friction coefficients are unknown. Instead, the total force and total moment of support frictions can be calculated.

Assumption 3 means that we can model frictional forces between the object and slanted plane by utilizing the methods proposed in [3].

2.2 Control process for pushing operation

The control algorithm for each arm consists of three main processes: action planning, execution and sensing.

Each arm decide for itself the distance to be pushed for getting to the goal location, and the angle in order to match the object's orientation with the goal orientation. Action planning also includes the planning on reconfiguration of arms discussed in the next section.

If all of the arms have finished the planning, they synchronize with each other. Without synchronizing, one arm may execute pushing while another arm is changing its pushing point. As a result, the object may lose its balance because each arm's behaviors are controlled completely in terms of environments and its own conditions.

After execution, each arm checks the change of the object's pose by using sensors, and makes a decision on whether the given task is completed or not. Each arm performs these processes iteratively.

3 Changing configurations of arms

In this section, we propose a method for planning on the reconfiguration of arms. Fig. 2 shows an outline of this planning. We give detailed explanations on its processes in the following subsections.

3.1 Decision of reconfiguration

At first, each arm makes a judgement on whether it can change its own pushing points or not. It is necessary for arms to remove from the object in order to change pushing points. Therefore, the condition for attempting the reconfiguration is whether the remaining arms can keep the object stable on the slanted plane during the reconfiguration. This is examined by checking whether the equilibrium equations have a solution [5].

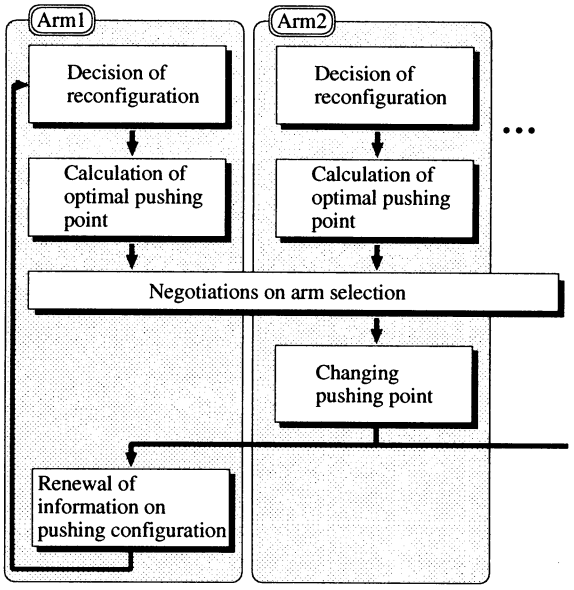


Figure 2: Outline of changing pushing points.

3.2 Calculation of optimal pushing point

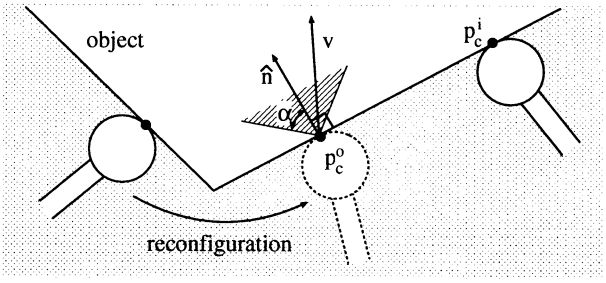


Figure 3: Changing pushing point.

The arms that have to reposition decide their optimal pushing points by maximizing a performance index P defined by

$$P = k_1 p_1 + k_2 \left(\frac{N-1}{\sum_{i \neq k}^{N} \|\boldsymbol{p}_c^o - \boldsymbol{p}_c^i\|^{-2}} + 1 - \frac{N_c}{N-1} \right) + k_3 \varepsilon \quad (1)$$

where

$$p_1 = \begin{cases} 0.2(\pi - \beta)/(\pi - \alpha) & (\beta > \alpha) \\ 1 & (\beta \leq \alpha) \end{cases} \quad (2)$$

$$\beta = \left| \cos^{-1} \frac{\hat{\boldsymbol{n}} \cdot \boldsymbol{v}}{\|\hat{\boldsymbol{n}}\| \|\boldsymbol{v}\|} \right| \quad (3)$$

$$\varepsilon = \begin{cases} 1 & \text{(if the stability of the object can be maintained in next step pushing.)} \\ 0 & \text{(otherwise)} \end{cases}$$

N : total number of arms
$\boldsymbol{p}_c^i$: pushing point of other arm i
$\boldsymbol{p}_c^o$: the next pushing point
N_c : total number of other arms contacting the same surface
α : threshold value with respect to β
$\hat{\boldsymbol{n}}$: unit contact normal vector
$\boldsymbol{v}$: pushing direction
k_i : weighting coefficients

This performance index consists of three sub-indices and the following is a detailed explanation of them.

- The pushing direction should be kept within an certain angle α of $\hat{\boldsymbol{n}}$ (Fig.3) to prevent the contact between the arms and object from slipping. That is why the first sub-index evaluates how close the pushing direction is to the contact normal.
- To have a reasonable load-sharing and to keep the object more stable, in general, the arm needs to change the pushing points to a location as far apart from the others as possible. The second sub-index is hence defined here by evaluation of the following two factors : distances to the other arms, and the number of arms touching on the same surface
- As already mentioned, it is important for the arms to maintain the stability of the object. Then, the last sub-index comes from the expectancy that the next desired pose can be achieved reliably. Note that it is sufficient for each arm to check only static equilibrium during next pushing because of the quasi-static assumption.

In terms of the above definition, it is apparent that the last sub-index is most important, thus k_3 is generally set with a larger value than k_1 and k_2.

3.3 Negotiation among arms

Some arms may reach at the same time the decision of its optimal pushing point by using the method mentioned in 3.2. However, since each arm takes into account the object's balance in the case when only its position is changed, the simultaneous reconfigurations may cause the object to lose its stability. Therefore, the single one arm to execute reconfiguration should be chosen by negotiating among arms. The following two criteria are used in this negotiation.

1. The values of performance index P.
2. The moving distances in the reconfiguration.

One arm maximizing criteria 1 and minimizing criteria 2 is selected here.

4 Simulation Results

We present some results of numerical simulations for the two-dimensional pushing task to examine the validity of the proposed method. Simulation conditions are shown at Table 1, and Fig. 4 shows simulation environments with start pose and goal pose of the object. Note that we put the three robot arms at the center of the object's edge in initial state.

Table 1: Simulation Conditions.

the shape of the object	trapezoid with 1.2[m] upper base, 2.0[m] bottom base, 1.6[m] height
the number of the robots	3
slant angle of the slope	30[deg]
coefficients of friction	uniform(0.5)

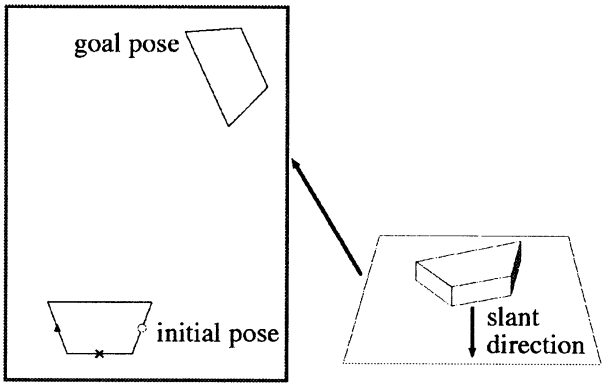
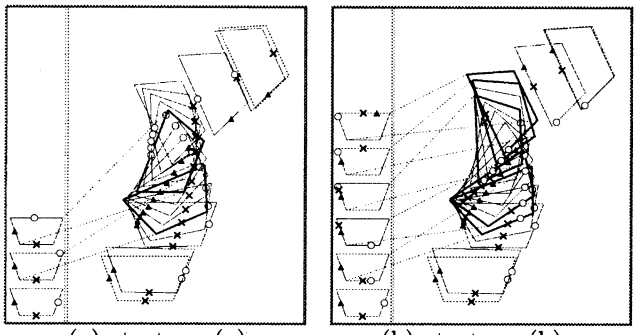


Figure 4: Simulation Environment.

Table 2: Weighting Coefficients of four strategies.

strategy	k_1	k_2	k_3
(a)	0.0	0.2	0.6
(b)	0.2	0.0	0.6
(c)	0.2	0.2	0.0
(d)	0.2	0.2	0.6

We examined the method applied in four cases corresponding, respectively, to different choices of the weighting coefficients in eq. 1 in order to compare the effects of the three kinds of used sub-indices. The chosen values of the coefficients are shown in Table 2. Fig. 5 shows the trajectory of the object and the changes of pushing points during the operation. The pushing points for the three arms are indicated by $\circ$, $\times$ and $\triangle$, respectively, in Fig.5. We also show in Table 3 the total number of reconfigurations and averaged distance between arms during the operation.



(a) strategy-(a) (b) strategy-(b)

(c) strategy-(c) (d) strategy-(d)

Figure 5: Trajectory of the object and the changes of pushing points.

Table 3: Results of four strategies.

strategy	number of reconfigurations	averaged distance between arms[m]
(a)	2	1.76
(b)	5	0.71
(c)	–	–
(d)	2	1.47

Fig. 5(c) shows that the goal pose cannot be achieved without considering the stability of the object. It seems that the Fig. 5(a) is similar to Fig. 5(d). However, one arm is positioned in the opposite side of pushing direction in the final translating push in Fig. 5(a). Therefore, it illustrated that strategy-(a) is less efficient than strategy-(d). We also see from Fig. 5(b) that changing pushing points to regions less occupied by other arms produces in deed the efficient reconfiguration as well as improvement on the object's stability. These simulation results and analysis reveal the effectiveness of the proposed method.

5 Conclusion

We have developed a multi-arm system for pushing an object on a slanted plane in this paper. In particular, strategy for changing pushing points is discussed in detail. We have presented some numerical examples to show the validity of the proposed method.

Improvement of deciding optimal pushing points and the investigation through experiments using real robot arms are needed as further research. Moreover, we will extend this reconfiguration strategy to recover from the unexpected situations such as break-down of arms.

References

[1] D. Rus, B. Donald, J. Jennings, "Moving Furniture with Teams of Autonomous Robots", in *Proc. IEEE/RSJ Int. Conf. on Intelligent Robots and System* , pp.235-242, 1995.

[2] D.J. Stilwell, J.S. Bay, "Toward the Development of a Material Transport System using Swarms of Ant-like Robots", in *Proc. IEEE Int. Conf. on Robotics and Automation*, pp.766-771, 1993.

[3] K.M. Lynch, "Estimating the Friction Parameters of Pushed Objects", in *Proc. IEEE/RSJ Int. Conf. on Intelligent Robots and Systems*, pp.186-193, 1993.

[4] H. Zha, H. Suzuki, T. Nagata, H. Nagahama, "Coordination of Visual and Tactile Sensors for Pushing Operation Using Multiple Arms", in *Proc. IEEE/SICE/RSJ Int. Conf. on Multisensor Fusion and Integration for Intelligent Systems*, pp.581-588, 1996.

[5] H. Zha, H. Nagahama, T. Hasegawa, "On-line Sensing and Action Planning in an Autonomous and Distributed Multi-Arm System", in *Proc. IEEE Int. Conf. on System, Man, and Cybernetics*, pp.3255-3260, 1997.

Proc. of Third Int. Symp. on Artificial Life, and Robotics (AROB III' 98),
Oita, Japan, 19-21, January, 1998,

On Why Should a Robot Recognize Itself ?

L. Berthouze
Humanoid Interaction Lab
Electrotechnical Laboratory
Tsukuba, Ibaraki 305, Japan

S. Itakura
Department of Psychology
Emory University
Atlanta, GA 30322, USA

Abstract

With roboticists' recent endeavours to provide their creatures with cognition, robots are beginning to exhibit some simple form of interactive behaviours, albeit not as complex as those of their animal counterparts. In this paper, we suggest that the robots' lack of body-awareness partially accounts for the above disparity. Lack of body-awareness implies the absence of abilities, such as discrimination between one's body and the environment, understanding of one's physical configuration and mapping of other's behaviours onto one's body, which would otherwise enable social interaction as complex (and beneficial) as imitation. With roboticists increasingly investigating the issue of embodiement and sensory-motor coordination, self-recognition appears as a good first milestone towards body-aware robots. Indeed, a process during which it is shown that human and non-human primates become aware of stable categorical features of self, self-recognition appears as a form of sensory-motor awareness from which robots' interactive behaviours should greatly beneficiate.

Keywords: Robotics, Body awareness, Self-Recognition.

1 Introduction

The observation of animal behaviour provides us with considerable insights about the particular relationship that exists between an animal creature and its self. One may wonder if a cat desperatly trying to catch his tail has any knowledge that this tail belongs to itself. Meanwhile, the same cat could be observed delicately grooming its tail, satisfying an internal discomfort that reveals the existence of this appendix as its own organ. At a higher level, there is evidence that some animals are aware of themselves as physical objects with a certain location in space and also that they exist as actors whose behaviours have a definite impact upon social companions. It has been observed that they use such information to control their behaviour. As far as the authors are aware, there is no robot systems exhibiting such self-awareness and this lack justifies, as explained in Section 3, why robots do not exhibit as complex interactive behaviours as those of their animal counterparts. In order to make robots aware of their self, the mechanisms underlying this discriminative responsiveness to one's self must be understood. A direct engineering of those mechanisms though appear to be all but very delicate and we subsequently suggest to investigate one particular issue of self-awareness, namely mirror self-recognition, in the light of observations made by psychologists on primates and described in next section.

2 Self-Recognition in Primates

According to Elenor Gibson (1995), the first paper about *self-awareness* in infants was the one published in 1948 by Zazzo. Throughout the first three years of his child, he observed his responses to a mirror placed before him and to pictures of himself and concluded: *By the way the child reacts to the image of his body, the mirror therefore reveals the origins of consciousness, the image of the body being essentially the consciousness of the self* (cited from Gibson (1995)). Human children begin to recognize their contingent-independent image in photographs only after mirror self-recognition, with most children at 22 months of age correctly labeling a photograph of themselves among photographs of other infants (Lewis and Brooks-Gunn, 1979, p.12).

Self-recognition in non-human primates is often being equated with mirror self-recognition (Anderson, 1984; Gallup, 1970; Povinelli, 1987). Nevertheless, for humans, *it is the ability to recognize and respond to self independent of contingency which represents the important developmental milestone in self-recognition* (Lewis and Brooks-Gunn, 1979, p.218). Gallup (1970)

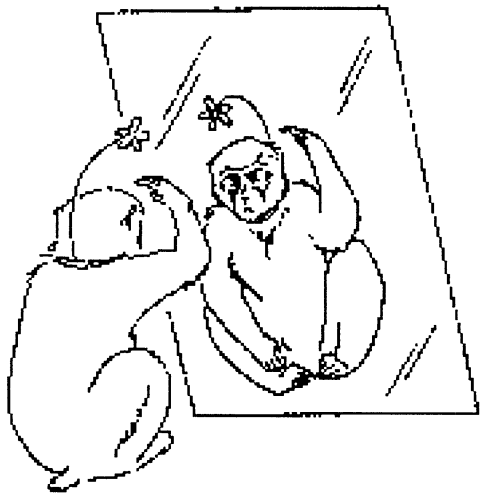


Figure 1: Response of monkey in flower-test.

was the first researcher who found out that chimpanzees were capable of recognizing themselves in a mirror. He exposed chimpanzees to mirror for a period of 10 days. If, at first, chimpanzees responded by engaging in a number of typical social responses, such as threatening, play-behavior, and sexual presentations, after two or three days, they began to show *self-directed behavior* which Gallup labeled. These behavior suggested that the chimpanzees had discovered that the real source of images was themselves. For example, the chimpanzees explored the parts of their bodies and took off something from the teeth while carefully monitoring the mirror images. After 10 days of mirror exposure, the subjects were anesthetized and marked on the upper eyebrow ridge and ear with a bright red dye, which offered little or no olfactory or tactile cues in such a way that chimpanzees couldn't guess its existence once recovered from anethesia. After completely recovery, the chimpanzees were observed for 30-minutes control condition in which the mirror was not presented to the subjects. Any attempt to touch the marked regions was recorded. Next, the mirror was presented to the subjects, and again the number of mark-directed contacts was recorded. The chimpanzees made few if any touches to the dye spot during the control condition, but made a significant number of touches in mirror condition (see Figure 1). Gallup thought that the chimpanzee had discovered the source of the mirror image. Since then, extensive work has been done on other non-human primates, such as macaques, lemurs, capuchins, and orangutans etc. The failure to find self-recognition in members of primates species outside the great ape-human clade has been widely replicated (Benhar, Carlton, and Samuel, 1975; Gallup, 1977, Gallup, Wallnau, and Suarez, 1980; Anderson, 1984). Anderson (1984) and Gallup (1982) concluded that only chimpanzees and orangutans show evidence of self-recognition and therefore a concept of *self*. Again, what could Gallup's chimpanzees do in mirror situation? What does *self-directed behavior* mean ? We may be able to say that chimpanzees could use a mirror to inspect their bodies. During the exposure to the mirror, they learned the association between the movement of the mirror image and their own movement.

Brown et al. (1965) reported that rhesus monkeys are capable of discriminating among objects by observing their mirrored images. They showed that monkeys can be trained to pull a code connected to a blue box containing food rather than a cord attached to an empty red box when these items were seen in the mirror. In this experiment the mirror functioned as a reflector of the discriminative cues. Menzel et al. (1985) call this behavior *mirror-mediated object discrimination* (MMOD) to distinguish it from *mirror-guided behavior* (MGB). They suggest that MMOD is a prerequisite for MGB, behavior in which neither the goal object nor the hand can be viewed directly.

Itakura (1987a, b) trained step-by-step two Japanese macaques to use a mirror to reach an object that could not be seen directly. Given an appropriate training, monkeys could exhibit MGB, i.e. (1) guide their hands (Itakura, 1987a) and also (2) inspect an object attached to their bodies.

Those examples characterize a sensory-motor self-recognition, one among many other levels of self-recognition considered in psychology, similar to the one grounding Gallup (1970)'s demonstration of *self-recognition* and which certainly represents some aspects of *self*.

3 Why is self-recognition crucial for (intelligent) robots ?

In this paper, we will call *intelligent* a robot that can learn, recognize or create new sensory-motor couplings between self, the environment and other agents living in it. Besides the notion of sensory-motor coordination that is more and more discussed within the robotic community, this definition tightly couples in-

telligence with social interaction and is meaningful in regard to observations made by developmental psychology on infants deprived of social/environmental communication. However, uptodate, the robotic community, has mainly ended up in robots either designed and programmed for a specific task in a specific environment or attempting to learn everything from scratch (tabula rasa approach) by themselves through interaction with the environment and by estimating the benefit for itself of his last actions (reinforcement learning). Although in this last case, environment seems involved, it can be shown that the environment simply mediates an interaction with self (for self). In some previous work (Berthouze et al. 1996), we have explained that the solution may lie in an intermediate approach where the robot learns his behaviour by observation of and participation in his environment and other agents living in it.

The main issue here is how to extract/categorize the useful information and how to reinstantiate it ? Our current working hypothesis is that for a robot to establish a meaning (not a labelling) of the observed behaviours, it must be able to map it (in some way) on itself. In such case, the robot can close the loop either by mutual imitation or by feedback from the other, establishing by there a common meaning on the jointly attended act or feature and this without any symbolic representation. The above mapping may take different forms according to whether the mechanical sequence constituting the behaviour is transformed to fit the requirements of a different body structure or whether the goal (if any) of the behaviour is matched to an existing repertoire of behaviours through a mechanism of joint attention. This multiplicity of modalities is another demonstration of the multiplicity of *self*, which, as underlined by Butterworth (1995a) ranges from bodily self or social (personality, role) self to other cognitive characteristics of the individual (emotion, possession, personal pronouns for example). This multiplicity also grounds our suggestion that roboticists at first focus on a single aspect of *self*, namely the sensory-motor categorization.

Whereas this first answer was related to the intelligence of a robot taken as a single individual, self-recognition (and social referencing) cannot be dissociated from group behaviour. A particular instanciation of group is the *society of kin*. As shown by different studies, self-recognition may be seen as a precursor[1] of kin-recognition. Indeed, infants begin at birth to explore their own body moving and acting and it is this early exploration that lays the initial groundwork for the distinction between self and other. And although the self seems to be established later through the interaction with others, it is the knowledge/control infants have of their motion which is the basis of the self/other differentiation. Kin-recognition is a key-factor for the emergence of homogenous society as outlined by (Mataric 1994). By homogenous society, it is understood that agents *are situated in a same environment, are embodied with similar abilities and have same goal structures.* This homogeneity has important implications and mainly (1) the existence in each agent of an innate knowledge about the other ones (which make knowledge about the world implicit), (2) the predictability of one agent's behaviour to another and (3) the interchangeability of one agent by another one which makes bring flexibility to the society. In short, this homogeneity and similarity greatly reduce individual cognitive requirements and therefore simplify the process of both generating and understanding group behaviour.

4 Conclusion

For a robot to develop true complex interactive behaviours, both as an individual interacting with its environment or as a member of a society of kin, it must be able to detect and categorize in its surroundings behavioral, structural as well as sensory-motor similarities with its self in such a way that it can establish a meaning to its perception and control its behaviour accordingly. Such an ability can be observed in mirror self-recognition where indirect (mirrored) perception of one's motion is matched with the actual physical motion, although direct and indirect perceptions are seemingly inconsistent. For roboticists, the key issue raised by this observation is to understand which mechanism makes the primates show such a discriminative responsiveness to their own features. (Eilan et al. 1995) suggested three mechanisms: (1) a specific *body sense* which yields knowledge about the body and nothing else, (2) a special representation that *explain* action and perception and (3) a distinctive phenomenology of the body. Both the existence and the structure of this special representation appears delicate to establish as its interplay with other cognitive mechanisms such as attentional control or rein-

[1] Note that this account can be attacked by observations made on the precedence of recognition of the mother over self-recognition in mirror. However, this sole case of recognition may well rely on the innate abilities of infants to react to the mother's face or any human faces like because it's only later that infants are aware of stable categorical features of self (Butterworth 1995b).

forcement learning is apparent. Additionnally, several important constraints on this map structure can be distinguished such as integrity over time (body development) and over inconsistent perception (direct or through a mirror) of the kinematic and dynamic representation of the mechanical structure or the transition from visually servoed motions, with potential explicit representation to open-loop ballistic motions (such as observed either in explorative mode or after training).

5 References

Anderson, J. R. (1984). *Monkeys with mirrors: Some questions for primates psychology.* International Journal of Primatology, 5, 81-89.

Benhar, E. E., Carlton, P. L., and Samuel, D. (1975). *A search for mirror-image reinforcement and self-recogntion in the baboon.* In S. Kondo, M. Kawai, and S. Ehara (Eds.), *Contemporary primatology*, Proceedings of the 5th International Congress of Primatology, (pp.202-208). New York: Karger.

Berthouze, L., Bakker, P. and Kuniyoshi Y. (1996). *Learning of Oculo-Motor Control: a Prelude to Robotic Imitation.* Proceedings of IEEE/RSJ International Conference on Intelligent Robots and Systems, Osaka, Japan, (pp. 376-381).

Brown, W. L., McDowell, A. A., and Lobinson, E. M. (1965). *Discrimination learning of mirrored cues by rhesus monkeys.* Journal of Genetic Psychology, 106, 123-128.

Butterworth, G. (1995a). *Representations of the Body.* In J.L. Bermudez, A. Marcel and N. Eilan (Eds), *The Body and Self.* Bradford Book: MIT Press.

Butterworth, G. (1995b). *The self as an Object of Consciousness in Infancy.* In P. Rochat (Ed.) *The self in infancy.* Amsterdam: North Holland.

Eilan, N., Marcel, A., and Bermudez, J.L. (1995). *Self-Consciousness and the Body: An Interdisciplinary Introduction.* In J.L. Bermudez, A. Marcel and N. Eilan (Eds), *The Body and Self.* Bradford Book: MIT Press.

Gallup, G. G. Jr. (1970). *Chimpanzees: Self-recognition.* Science, 167, 86-87.

Gallup, G. G. Jr. (1982). *Self-awareness and the emergence of mind in primates.* American Journal of Primatology, 2, 237, 248.

Gallup, G. G. Jr., Wallnau, L. B., and Suarez, S. D. (1980). *Failure to find self-recognition in mother-inafnt and infant-infant rhesus monkeys pairs.* Folia Primatologica, 33, 210-219.

Haug E.J. (1989). *Computer Aided Kinematics and Dynamics of Mechanical Systems.* In Allyn and Bacon Series in Engineering.

Itakura, S. (1987a). *Mirror guided behavior in Japanese monkeys (Macaca fuscata).* Primates, 28, 149-161.

Itakura, S. (1987b). *Use of a mirror to direct their responses in japanese monkeys (Macaca fuscata).* Primates, 28, 343-352.

Lewis, M. and Brooks-Gunn, J. (1979). *Social cognition and the acquisition of self.* New York: Plenum Press.

Mataric, M. J. (1994). In *From Animals to Animats 3*, Proceedings of Third International Conference on Simulation of Adaptive Behaviour.

Menzel, E. W. Jr., Savage-Rumbaugh, E. S., and Lawson, J. (1985). *Chimpanzee (Pan troglodytes) spatial problem solving with the use of mirrors and televised equivalents of mirrors.* Journal of Comparative Psychology, 99, 211-217.

Povinelli, D. J. (1987). *Monkeys, apes, mirrors, and mind: The evolution of self-awareness in primates.* Human Evolution, 2, 493-509.

Proc. of Third Int. Symp. on Artificial Life, and Robotics (AROB III' 98),
Oita, Japan, 19-21, January, 1998,

Interactive 3D Walk-Through System using Dynamic Gestures

DAHLAN NARIMAN, HIROAKI NISHINO AND KOUICHI UTSUMIYA
Department of Computer Science and Intelligent Systems, Oita University, 700 Dannoharu, Oita 870-11, Japan

Abstract

This paper describes the system concept and its implementation technique of an interactive 3D walk-through system using dynamic gestures. Presently, we use mice and keyboards to manipulate 3D virtual worlds. However, there are some problems to control them by using only these devices. Designating the depth and direction information of the world is one of such difficulties. To solve these problems, it is necessary to introduce new interface devices instead. The purpose of the system is to investigate methods of constructing virtual worlds and interacting with their objects in a natural way. This paper also discusses the assessment method of the implemented system compared with those consisting of conventional devices such as mice and keyboards.

Keyword:
Interactive, 3D Virtual World, Walk-through System, Neural Network, Dynamic Gesture

1 Introduction

We are developing a 3D walk-through system to investigate methods of constructing virtual worlds and interacting with their objects. A stereoscopic wide screen projection system or a head mounted display (HMD) is used as an output device in order to give users a feeling as if they are in the virtual worlds. Shutter glasses are available to view the stereo images projected on the screen.

Presently, we use mice and keyboards to manipulate 3D virtual worlds. However, there are some problems to control them by using only these devices. Designating the depth and direction information is one of such difficulties. In addition, the users cannot feel their presense on the interaction with the objects in the worlds because it is not performed by their natural actions. An example is a door opening action. This action is done by clicking the mouse or keyboard button, which is very different from a hand action to open the door in a real world. Another problem occurs in operating the mice or keyboards especially when the users wear the HMD as an output device, because they cannot see the controller devices directly.

To solve these problems, it is necessary to introduce new interface devices which the users can input data with their natural actions [1]. We are enhancing the walk-through system to operate it by using their dynamic gestures. The dynamic gestures in addition to conventional devices such as mice and keyboards are implemented in the system as a multi-modal interface. The mice and keyboards are used to specify a task which is difficult to use gestures.

Figure 1 illustrates the operational environment of the system. Oita university's virtual campus is used as an example of virtual worlds. A user is navigating the world and doing interaction with objects by dynamic gestures.

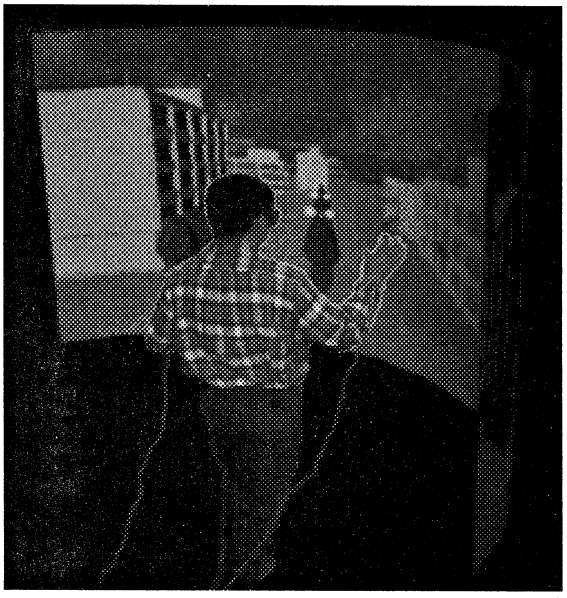


Figure 1: An Interactive 3D Walk-Through System for Navigating Oita University's Virtual Campus

2 System Concept

To solve the problems occured in interacting with the 3D virtual worlds described above, it is necessary to introduce new interfaces using the user's natural actions, which improve the easiness to use and increase the naturalness in interaction with the worlds.

Two sets of a Polhemus Fastrak magnetic sensor and a Virtual Technology's Cyberglove are adopted to detect the user actions. In addition, a magnetic sensor is put on his/her head to detect his/her viewpoint and view direction. The viewpoint and view direction will change according to his/her head movement. The Cyberglove is used to detect the position, direction and shape of each hand in the virtual worlds. The users are allowed to perform some dynamic gestures to control the system. Neural networks are introduced to learn and recognize these dynamic gestures[2]. A neural network is appropriate to deal with intra- and interpersonal variations, improving the gesture recognition performance, and increasing the gesture recognition hit rate.

Table 1 shows the classification of gestures to use in the interactive walk-through system. These gestures with the exception of left- and right-turn are implemented in the system by using neural networks. The turning gestures are implemented by using left- and right-turn movements of the user's head, respectively. The users can interact with the system using specific gestures. The interaction methods with the system can be divided into two parts: the world control action such as forward and backward movements, and the interaction with objects within the world such as grasping or moving them. The world control action can further be divided into two categories: a fly mode in which the users can move in the air at high speed and a walk mode in which they move around in a small virtual world. For example, the walk mode is used to move within a room or from one room to another in a building.

3 Implementation

This section describes our research environment, hardware resources and software design issues to implement the system based on the system concept discussed previously.

Table 1: Gestures for 3D Walk-through System

Control actions		Interaction
Walk Mode	Fly Mode	with object
forward, backward, left-turn, right-turn, stop.	forward, backward left-turn, right-turn up,down, stop.	grasp, release, throw, catch, push,pull, or slide a door, deform an ellastic object, push a button, etc.

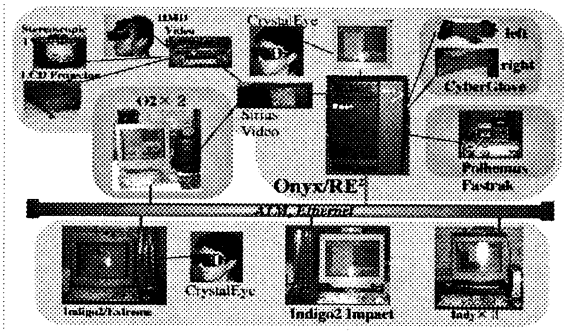


Figure 2: Hardware Environment

3.1 Hardware Environment

Each Cyberglove is connected to a host computer via RS-232C at 9600bps. It has eighteen resistive-strip sensors with a mounted 6DOF Fastrak magnetic sensor. The left-hand glove has a tactile feedback function called the CyberTouch option. The effective data sampling rate from these gloves is approximately 10Hz including the graphics hand drawing operation. There are a total of three Fastrak magnetic sensors available in this system. One of them is put on the user's head to detect his/her viewpoint and view direction. The other two are put on the Cybergloves to detect his/her hand positions and directions in the virtual world.

The output is displayed to the user via an HMD or a stereoscopic wide screen projection system. The shutter glasses(Stereo Graphics CrystalEyes) are available to view the stereo images projected on the screen.

An SGI Onyx is used as a host computer. An SGI Indigo2 workstation is used to provide audio feedback effect. Sun ULTRA workstations are dedicated to train neural networks used in the gesture recognition.

3.2 System Architecture

Figure 3 illustrates the system architecture of the interactive 3D walk-through system using the gestures that we are developing. The data detected from the magnetic sensor on the head are transmitted to the system application program as input data. The viewpoint and view direction will change according to the user's head movements.

The user's hand gestures gatherd by the two-handed Cybergloves are transmitted to the trained neural networks as input data. Then, these networks recognize the current gesture. The recognized gesture, for example, grasping an object, is transmitted to the 3D walk-through system as input data. The system

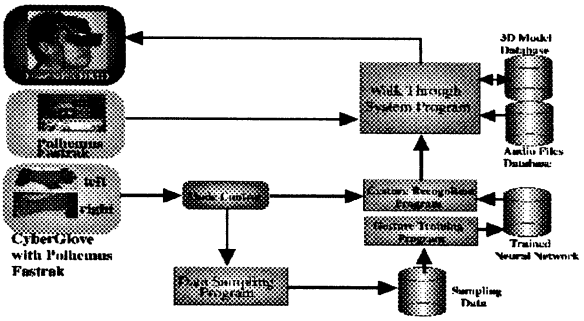


Figure 3: System Architecture

returns its feedback as an updated graphics image to the user based on the current recognized gesture.

The system implements the data sampling function which can also be used to record new gestures or change the trained gestures. Sample data are stored onto the database, and then used as input data for the neural network training. The design and implementation of the dynamic gesture interface is described in the next section.

3.3 Dynamic Gesture Interface

The gestures listed in table 1 are classified in the following two perspectives; one hand vs two hands, and static vs dynamic.Table 2 shows the result of classification they are defined based on the investigation of many users' actions representating their natural and easy to use actions. The majority is the two handed dynamic gestures, while some of other gestures are appropriate to perform with one hand or static. The multi-channel gesture interface is required to realize all of them in the system. Figure 4 illustrates the system architecture of the multi-channel gesture interface.

We adopted a type of recurrent neural network to implement the gesture interface as illustrated in figure.5. This is an Elman-type neural network which is proven to be useful as a pattern classifier for time series data. The units in each layer are fully interconnected to the next layer's unit. The number of input

Table 2: Classification of Gestures

	One-handed	two-handed
Posture (Static gesture)	grasp, release, or catch a small object	grasp, release,or catch a big object, stop
Dynamic gesture	push,pull,slide a door push a button throw a small object	deform an ellastic object, throw a big object, world control actions (Walk Mode and Fly Mode)

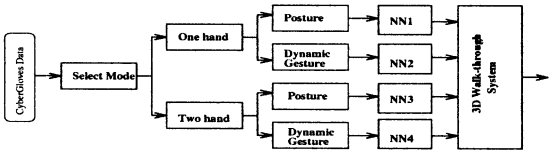


Figure 4: Multi-channel Gesture Interface Architecture

units for two-handed and one-handed gesture recognition are 48 and 24, respectively(eighteen for finger flexion, three for position, and three for orientation of each hand). The default number of output units corresponds to the number of gestures to classify. The number of hidden layer and their units are one and 100, respectively.

One problem in using the neural network is the necessity of off-line training. The neural network receives input data from the database to start the training. The sample data items are normalized to the range from -1.0 to 1.0 by the filter, and then fed into the input layer at every frame. The number of frames for each dynamic gesture is 30, which is approximately 3 seconds of the user's action.

Figure 6 illustrates some example gestures to control the virtual world. Figure 7 illustrates the example gestures for opening doors. Such gestures as pull, push, and slide are needed to open the pulling, pushing, and sliding door, respectively. The shape of a door handle is a very important cue to make the users conscious of which door type they face. Based on the concept of affordances, the different door handles suggest affordances for different actions[3]. Figure 8 illustrates some captured images of user's view; (a) the user's view when approaching the door and desiring to grasp the door handle; (b) a view of opening the door action; And, (c) the situation inside the room after going through the door.

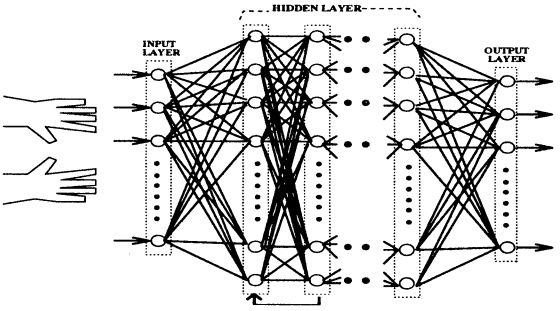


Figure 5: Neural Network for Gesture Recognition

4 System Assessment Method

The system concept and its implementation are described in previous sections. It is necessary to evaluate

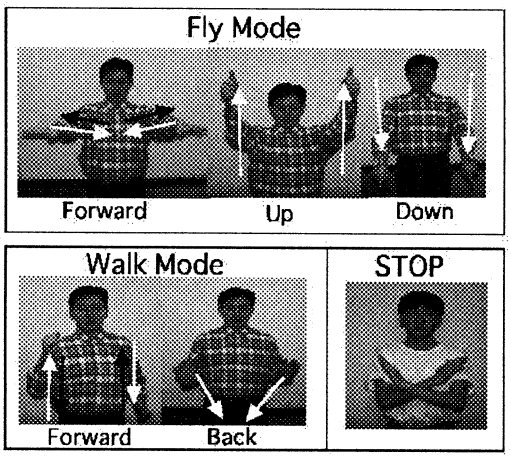


Figure 6: Example gestures to control 3D virtual world

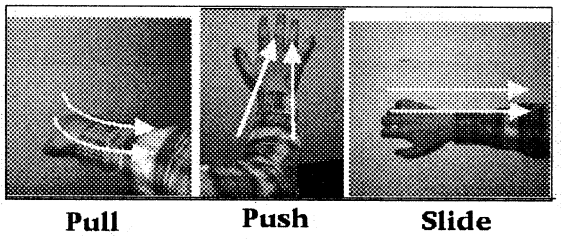


Figure 7: Example gestures to open the door

the implemented system in terms of the effectiveness of the system. Responsiveness, usability, interactivity and presense effect are example items to be evaluated soon after completing of the system implementation [4].

5 Conclusion and future work

The users' natural actions are used to control the system and interact with objects. In addition, the users can feel their presence in the virtual world, because interaction with objects is performed by their natural actions.

For future work, we intend to explore new and more convenient paradigms for navigation and interaction with 3D virtual worlds. We have plans to work on some futher enhancements and development of the system as follows: developing a method of on-line training of the gestures, developing and investigating a method to support multi-user interaction function [5], implementing the object manipulation and deformation function [6], and evaluating the effectiveness of the implemented system.

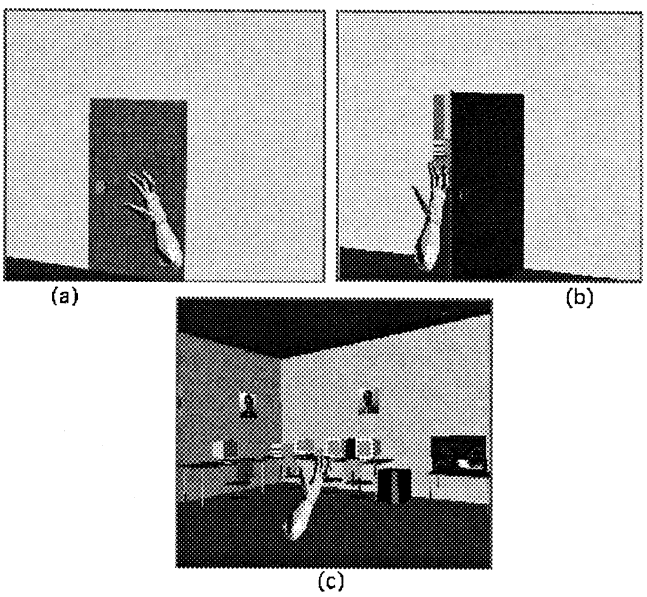


Figure 8: Captured images of user's view: (a), (b) open the door, and then (c) enter the room.

References

[1] Dahlan, Nishino, Utsumiya: 3D Walk-throuh Control Interface (in Japanese), Proc. of the IPSJ'97, 4, pp. 195-196, 1997.

[2] Nishino, Utsumiya, Kuraoka, Yoshioka, Korida: Interactive Two-Handed Gesture Interface in 3D Virtual Environments, Proc. of the ACM VRST'97, pp. 1-8, 1997.

[3] William W. Gaver: Technology affordances, Proc. of CHI'91, pp. 79-84, 1991.

[4] Stuart, R. : The Design of Virtual Environments, McGraw-Hill, 1996.

[5] Olof Hagsand: Interactive Multiuser VEs in the DIVE System, IEEE Multimedia, Vol. 3, Num. 1, pp. 30-39,1996.

[6] Korida, Nishino, Utsumiya: An Interactive 3D Interface for a Virtual Ceramic Art Work Environment , Proc. of VSMM'97, pp. 227-234,1997.

Proc. of Third Int. Symp. on Artificial Life, and Robotics (AROB III' 98),
Oita, Japan, 19-21, January, 1998,

Multi-functional Robot-hand Tactile Sensor for Material Recognition

Katsunori Shida
Faculty of Sci. & Eng., Saga University
1 Honjo-machi, Saga, 840 Japan
E-mail : shida@cc.saga-u.ac.jp

Jun-ichiro Yuji
Faculty of Sci. & Eng., Saga University
1 Honjo-machi, Saga, 840 Japan
E-mail : 96td44@edu.cc.saga-u.ac.jp

Abstract

As a tactile sensing system applying to robot-hands for discrimination of material properties, a new thin plate touch sensor system is proposed here. This sensor system is unique in the point of combination of two different multi-functional sensors each of which is a mono-structure with two compound sensing functions each other. One of them is a mono-material pressure-conductive rubber sensor with temperature sensitivity and the other is a comb shaped mono-structural thin plate touch sensor with capacitive-inductive function. Using this sensor system, four kinds of properties in a material, that is, the hardness, the thermal property of material like the palm of human hand, and in addition, two electrical properties, such as permitivity and permeability of a material, are measured.

1 Introduction

The progress of tactile sensing technology plays an important part in the robotics world. Therefore, many researches and studies concerning the technology have been performed[1][2]. Most of them, however, have been focusing on the detection of existence of material or the recognition of its shape. Under the above-mentioned circumstances, we propose here a new fabricated thin plate touch sensor system which is constructed with two different functional touch sensors, that is, a mono-material pressure-conductive rubber sensor with temperature sensitivity and a comb shaped mono-structural touch sensor with capacitive-inductive function. Each sensor itself is with its characteristics to discriminate some of material properties by placing on the surface of materials.

The mono-material pressure-conductive rubber sensor is actually used as a soft pressure-temperature sensitive sensor which can be discriminate simultaneously differences of hardness and thermal property of material like the palm of human hand. On the other hand, the comb shaped mono-structural touch sensor possess two compound sensing functions for electrical properties, that is, inductive function and capasitive function, while it is a mono-structure formed by a pair of comb shaped wires on a thin insulated plate. Therefore, the measurement of two electrical properties, such as permittivity and permeability, of a material is capable using the comb touch sensor.

The combination of above-mentioned two different multi-functional touch sensors is expected to provide the abundant information for the recognition of material.

2 Mono-material pressure-conductive rubber sensor

Pressure-conductive rubber sheet[3] is a flexible material with a function of pressure p converts into an electrical resistance r. The resistance r of this rubber sheet per unit area in certain constant temperature is expressed as following,

$$r = kp^{-n} \tag{1}$$

where k is constant and n is sensitivity to pressure. Further, this rubber sheet is available to a multi-functional sensing device with pressure and temperature sensing function since the rubber sheet is also sensitive to temperature change.

When a sensor output signal is affected by two kinds of external quantities, the sensor has no capability to indicate two quantities independently at the same time with one sensor output signal alone. Therefore, we made a mono-material pressure-conductive rubber sensor with two different output signals of resistance as shown in **Fig.1**[4]. This rubber sensor consists of a rubber sheet with 0.5 mm thick and 30 mm square heating its substrate kept at constant temperature of 36 ℃ as the human body temperature, and putting three parallel line electrodes of 1 mm wide with two different spaces of 0.5 mm and 16.5 mm on the surface of rubber sheet. This rubber sheet on the substrate is fixed by covering with insulating thin film. When this sensor contacts with a material of which temperature is lower than that of the sensor, two output signals, the resistance R_1 between terminal a and b, and the R_2 between terminal b and c change by both the reaction force given in effective part shown in Fig.1 and the temperature drop of rubber sheet.

Fig.2 shows the temperature characteristics between 20 ℃ and 40 ℃ of R_1 and R_2 in three kinds of

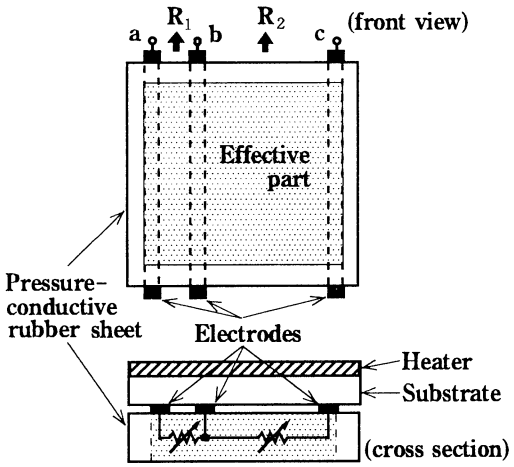


Fig. 1: Structure of a mono-material pressure-conductive rubber sensor with two output signals

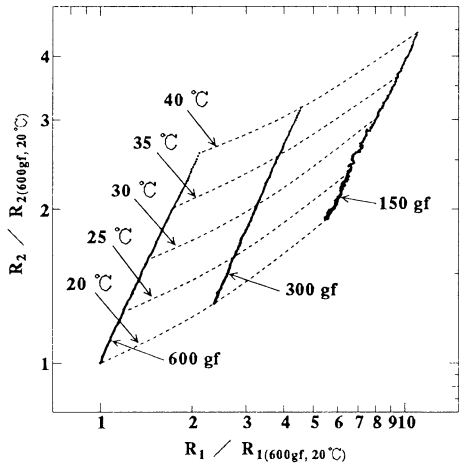


Fig. 2: Temperature characteristics in three kinds of contact forces

contact forces, 600 gf, 300 gf, 150 gf, which are normalized by each resistance value in the condition of 600 gf and 20 ℃. R_1 with a narrow space between both electrodes has a large dependency on contact force more than that of R_2 with wide space of electrodes. On the other hand, R_2 has a large dependency on temperature more than that of R_1. Sensitivity n of (1) was about 1.2 on R_1 and about 0.4 on R_2. It was confirmed that simultaneous sensing of force information and temperature information was possible by changing the space of electrodes in spite of a mono-material sensor.

The hardness and the thermal property of material are separated roughly into four groups, that is, (I).hard and good thermal property, (II).hard and bad thermal property, (III).soft and good thermal property and (IV).soft and bad thermal property.

The soft materials with good thermal property,

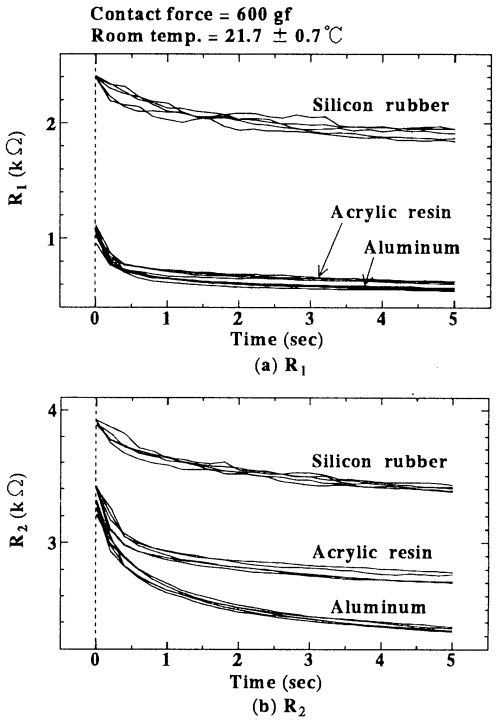


Fig. 3: Time responses of R_1 and R_2 of rubber sensor after contact with materials

however, exist few. Therefore, for the discrimination of the hardness and the thermal property, we prepared three kinds of rectangular typical materials with 10 mm thick, 50 mm square and flat surface. These are the aluminum as a hard material with good thermal property, the acrylic resin as a hard material with bad thermal property and the silicon rubber as soft material like an eraser with bad thermal property.

Fig.3 shows the time responses of rubber sensor of five times after contact with three materials on condition that constant force of 600gf and constant room temperature of 21.7 ± 0.7 ℃. It is indicated that each resistance R_1 and R_2 of the sensor varies in relation to both the hardness and the thermal property.

In order to make clear the discrimination of these test materials, two-dimensional explanation of R_1 and R_2 using the resistance values from three seconds until five seconds in this experiment is shown in **Fig.4**. The discrimination of the hardness and the thermal property in these materials is possible in spite of dispersion in each experiment and creep effect in the rubber sheet itself and temperature drop.

3 Comb shaped mono-structural touch sensor

Fig.5(a) shows the structure of the comb shaped

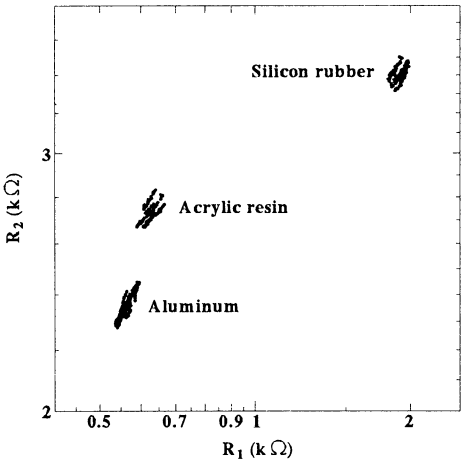


Fig. 4: Two-dimensional explanation of R_1 and R_2 of pressure-conductive rubber sensor

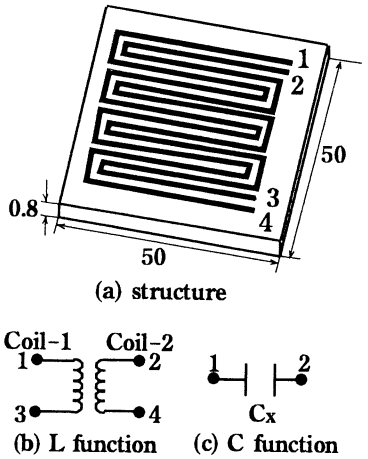


Fig. 5: Structure of the comb shaped mono-structural touch sensor

mono-structural touch sensor. The sensor consists of a pair of thin comb copper wires. Each wire is evaporated on one surface of a thin epoxy resin insulated substrate of 0.8 mm in thickness. The surface of the sensor is covered with insulating film to avoid direct touch with metal samples. The sensor has four terminals, 1, 2, 3, 4 in Fig.5(a), that is, both ends of a pair of comb wires. By selecting one from two kinds of electrical connections with four terminals of sensor, a pair of inductor or capacitor is formed as shown in Fig.5(b) and (c), respectively. When the sensor is in inductive sensing function, one coil is connected to an alternative signal source and another one to a voltmeter to measure the voltage induced between two coils. The output voltage E_0 of sensor can be written as follows[5].

$$E_0 = [j\omega M_1 + (\omega M)^2/(R_x + j\omega L_x)]I_1 \qquad (2)$$

where, I_1 is input current, M_1, M are the mutual inductance between coils, and between a coil and a material. R_x, L_x are the equivalent resistance and the equivalent inductance of material, respectively.

The output of sensor for different materials can be analyzed as follows.

(A) For non-metallic materials, the output voltage E_0 can be approximately expressed as equation (3). In this case, resistance R_x is very high and there exists neither eddy current nor magnetization.

$$E_0 = j\omega M_1 I_1 \qquad (3)$$

Therefore, the equation shows that the output voltage E_0 for non-metallic materials can be simply regarded as only depending on the input frequency.

(B) For non-magnetic metals with large electric conductivity, the output voltage of sensor seems to indicate a small value because of the generation of eddy current.

(C) In the case of magnetic materials, E_0 is much bigger compared with that of non-magnetic materials, because that the magnetization is much stronger than the effect of eddy current.

When each one of a pair of comb wires is connected to a measurement circuit, it is easily found from the structure of surface that the sensor can be used as the capacitive function. The electrical phenomenon of sensor can be explained as the capacitive function in general capacitive structure. If the sensor touches a material, the capacitance C_X of sensor is measured in proportion to the permittivity of the material. Hence, we can estimate one of the output of sensor.

To investigate the ability of the proposed sensor, nine kinds of well-known materials formed as a rectangular plane of 10 cm with 1 cm thick except air were used. **Fig.6** shows experimental results for the input signal with the frequency of 25kHz in both capacitive and inductive sensing functions of the sensor. By indicating the results on x-y plane, it is possible to discriminate the properties of materials using method of pattern recognition.

4 Thin plate touch sensor system with two different multi-functional sensing devices

The mono-material pressure-conductive rubber sensor introduced in chapter 2 can be used to discriminate the difference of hardness and thermal property of material like the palm of human hand.

On the other hand, the comb shaped mono-

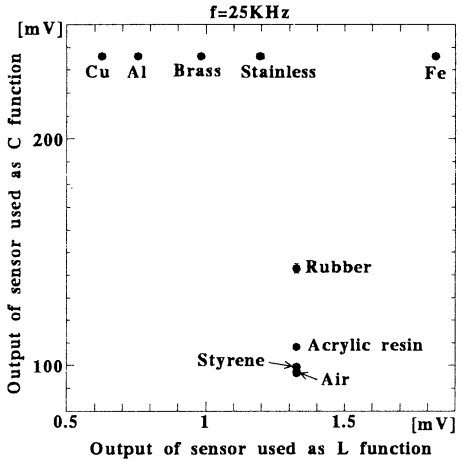


Fig. 6: Experimental results in capacitive and inductive function of comb shaped touch sensor

structural touch sensor written in chapter 3 can be used to measure two electrical properties, such as permittivity and permeability, of a material.

In this chapter, a new fabricated thin plate touch sensor system which is the combination of above-mentioned two different multi-functional touch sensors is proposed to recognize more accurate situation of material. As shown in **Fig.7**, the part of comb shaped mono-structural touch sensing device is fabricated by evaporating a pair of thin comb copper wires on one surface of a very thin insulating sheet of 0.1mm in thickness, and then the other surface of this sheet is pasted on a pressure-conductive rubber sensor with three electrodes in this temperature-controlled opposite side.

This touch sensor system with a mono-block configuration is quite effective in an actual use for acquiring four kinds of properties of material, that is, the hardness and the thermal property of material like the discrimination by the palm, and in addition, two electrical properties, such as permittivity and permeability of material of which recognition are important in industrial fields.

5 Conclusion

In order to discriminate material properties by placing it on the surface of materials, a new thin plate touch sensor system applying robot-hands was proposed as the combination of two kinds of quite different multi-functional sensing device which are both a mono-material pressure-conductive rubber sensor to discriminate differences of hardness and thermal property of material like the palm of human hand, and a comb shaped mono-structural touch sensor to measure two electrical properties of material, such as permittivity and permeability.

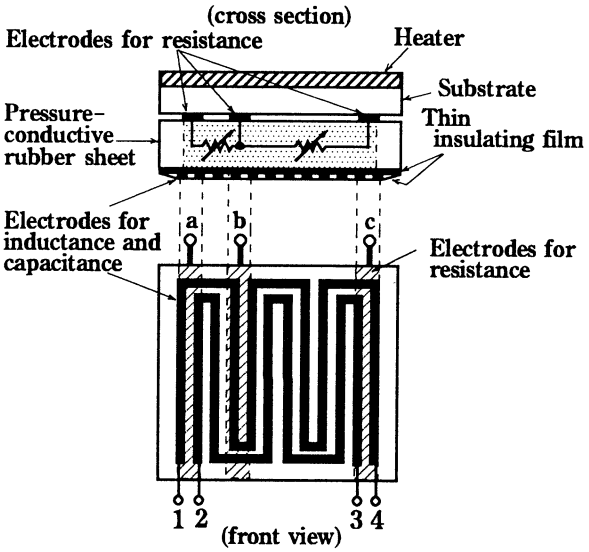


Fig. 7: Compound multi-functional robot-hand tactile sensor

The experimental results in each sensing device for discrimination of material properties were also shown for three kinds of materials, such as aluminum, acrylic resin and silicon rubber and also for eight kinds of well-known materials, such as iron, aluminum, copper, bronze, gum, wood, acrylic resin and styrene foam, respectively.

Using these results as the reference, the possibility of discrimination of an unknown material for the method of pattern recognition and then the realization of an artificial material recognition system as the substitution of tactile sensing function of the human skin are expected in future.

References

[1] P.Dario and D.D.Rossi : "Tactile sensors and the gripping challenge", *IEEE SPECTRUM*, AUGUST, pp.46-52, 1985

[2] D.G.Caldwell and J.O.Gray : " 'Dynamic' Multi-Functional Tactile Sensing", *Lecture notes in control and information sciences*, Vol.187, pp.189-198, 1993

[3] M.Shimojo : "Hysterisis Characteristics of Pressure-Conductive Rubber", *Trans. JSME*, Vol.59, No.564, C, pp.2464-2469, 1993 (in Japanese)

[4] J.Yuji and K.Shida : "Mono-Material Pressure-Conductive Rubber Sensor with Temperature Sensitivity for Artificial Skin Sensing", *Proc. of the 12th KACC*, pp.1314-11317, 1997

[5] D.Li and K.Shida, : "Discrimination of Material Properties by Mono-Structural Touch Sensor with Capacitive-Inductive Function", *J. of Robotics and Mechatronics*, Vol.8, No.2, pp.1314-11317, 1996

Proc. of Third Int. Symp. on Artificial Life, and Robotics (AROB III' 98),
Oita, Japan, 19-21, January, 1998,

Development of a multi-freedoms controller using FPGA

S. Kurono, T. Toyofuku
Dept. of Electrical Engineering
Kyushu Sangyo University
2-3-1,Matsukadai,Higashi-ku,
Fukuoka-shi,813,Japan

S. Aramaki
Dept. of Electronics Engineering
Fukuoka University
8-19-1,Nanakuma,Jonan-ku,
Fukuoka-shi,814-01,Japan

Abstract

We developed a multi-freedoms controller which is able to control a robot having 24 degrees of freedom. Moreover, we developed a small humanoid robot which has 20 degrees of freedom and about 30 cm tall. The controller is composed with a FPGA chip and a Z80 microprocessor board, and the size of it is small (about 60mm*70mm*28mm) enough to be carried on the back of the small humanoid robot. In this study, we have realized some motions such as walking with two legs, turning the walking direction and so on using the multi-freedoms controller.

1 Introduction

It is the human's dream to develop a robot such as Astro-boy,Iron-man No.28 in comics or TV animations. That is capable of performing motions that are as free as or even freer than humans are. We authors are conducting studies on the communication and control system that is required for making robots perform similar motions to humans by developing a robot that has the structure and degrees of freedom(DOF) equivalent to humans. In this study,we developed as the first step,a multijoint robot with 20 DOFs and its controller based on a FPGA chip and a Z80 microprocessor board. This robot uses radio-controlled servo units marketed as joints. This paper points out the two problems that arise when a robot with very large number of DOFs is controlled by radio communication,and discusses its possible solutions. The first problem is that radio-communication-use transmitters/receivers on the market are capable of controlling maximum of only 7 to 8 channels by a single frequency band and are also expensive. Moreover,the communication method called the pulse-position modulation(PPM) which is used in the radio-transmitter/receiver marketed has the second problem that the output torque of the servo motors gradually declines with incleases in the number of channels. The reason why that will be stated later. To solve the above problems,we developed a multi-DOFs controller which is compact enough to be carried on the back of a small robot,and is capable of controlling up to 24 DOFs maximum.

2 Development of a humanoid robot with very large number of DOFs

Fig.1 shows the general view of the control system in this study. The configuration of DOFs was considered prior to constructing the robot. First,the robot should be based on the configuration of human DOFs. The weight of the robot must be reduced by eliminating all useless parts so that the robot will be able to walk. Secondly,the DOF structure of the feet will be such that it permits turnabout during walking. With all these points taken into consideration,a DOF configuration was employed with the total number of DOFs set at 20. The height of the robot is approximately 30cm. The multi-freedoms controller is mounted on the back of the bobot. Eventually,the commands to the robot will be transfered throgh a wirwless commu-

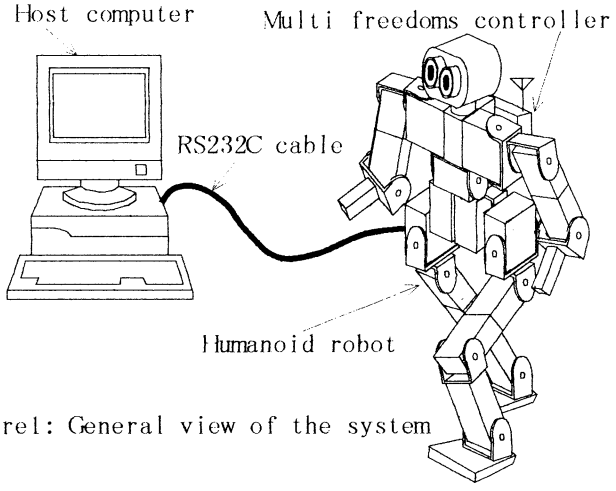


Figure1: General view of the system

nication and the power source will be mounted on the robot itself,but the robot as a first step is connected with a host computer by a RS232C cable and a separate power source is used in this time of study. Fig.2 shows a sketch of the robot.

3 Development of a multi-DOFs controller

3.1 Signal system of the controller

As an example,the manner of control of the four DOFs servos will be briefly explained. Fig.3 shows the output pules from multi-freedoms controller which are supplied into each servo of the robot. The widths of each pulse are proportional to the reference values for each servo and vary from 1.0ms to 2.0ms,neutral at1.5ms. Four pulses are periodically supplied in sequence during each frame time of 20ms(see Fig.3).

3.2 Signal system of a servo mechanism

In the basic configuration of a servo circuit(Fig.4),the width of an input pulse is proportional to the reference value to the servo mechanism,and this signal is simultaniously entered into the pulse width comparison circuit and the monostable mutivibrator. Triggered by an input pulse,the monostablemultivibrator generates another pulse whose width is determined by the resistance of a potentiometer. When the widths of pulse generated by the monostable multivibrator and of the input pulse are the same,the output of the pulse width comparison circuit is zero; hence,the motor does not rotate. When there is a difference between pulse widths,then a positive or negative pulse equivalent to the difference is output.

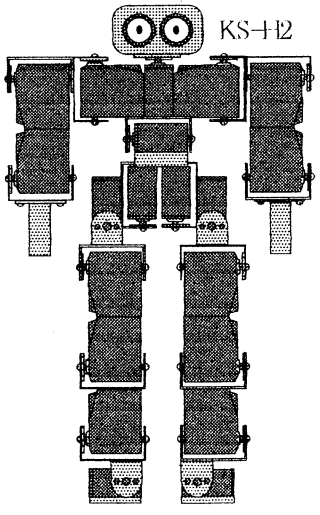


Figure2: A sketch of the robot

The upper circuit is turned on when a positive pulse is output,and the motor rotates clockwise. Likewise,the lower circuit is turned on when a negative pulse is output,and the motor rotates counter-clockwise. The shaft of the motor is engaged with that of the potentiometer via a gearset. Hence,the shafts of the motor and the potentiometer rotate until the output of the pulse width comparison circuit becomes rezo. The widths of the output pulses(deviation pulses) are approximately 0.5-0.6ms at most,and there is only one pulse in 20ms(frame time). Consequently,the current is light,if left as is,and the output torque of servo motor is insufficient. Hence,the deviation pulse is input to switching circuits through a pulse strecher,such as a Schmidt circuit. Diodes serve as protective circuit for preventing the two amplifiers from turning on simultaniously due to signals input.

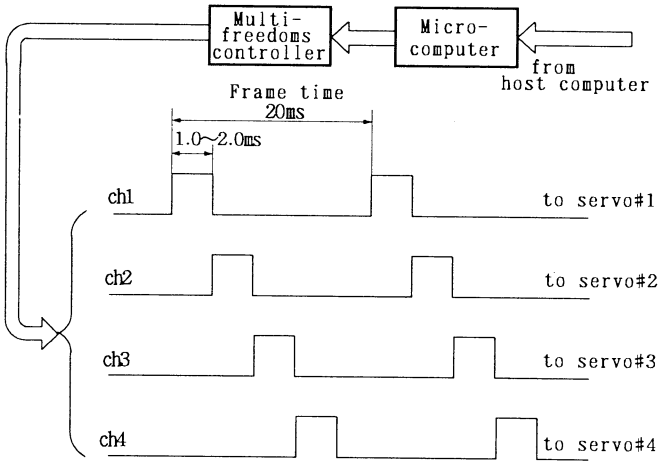


Figure 3: Input pulse to servo-mechanism

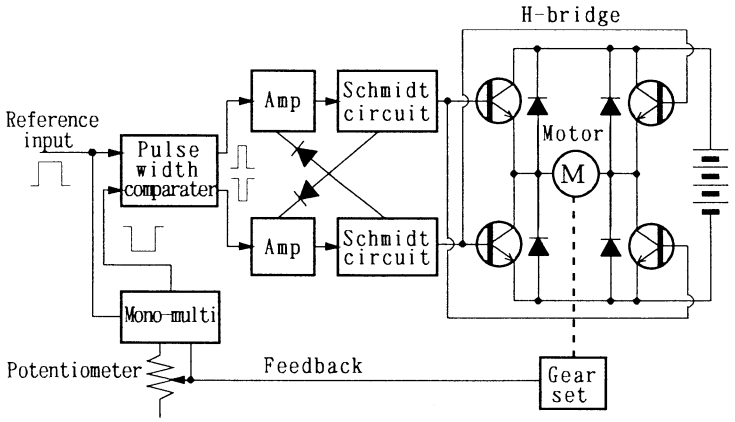


Figure 4: Servo mechanism

3.3 Construction of 24 DOFs controller

In the servo circuit of the above section,the Schmidt circuits stretch,at a constant rate,the pulse width in proportion to the deviation of the feedback pulse from the command pulse,and feeds the pulse to the H-bridge. The pulse width must not exceed 20ms in order to keep a quick response of the servo. If the same manner as shown in Fig.3 is employed to control more than 20 DOFs,a frame time more than 50ms is required,assuming that the maximum pulse width of a single DOF is 2.5ms(including the margin time required for separating pulses corresponding to each DOF). Then,the current supply to servo motors will be halted for 30ms,assuming that the command data is updated once in every frame time(50ms),which causes a significant decline in the output torque of motor. To solve this problem,a multi-freedoms controller was developed using a FPGA. In this study,the circuit to drive four servos illustrated in Fig.3 is modularized as a unit, and 6 units are mounted in a FPGA chip so that it can be used to control up to 24 DOFs maximum. Fig.5 shows a block diagram of the circuits implemented inside a FPGA. As shown in the figure,the control circuit is roughly divided into three blocks. The first is a counter block which measures the lapse of time and generates the frame time. The second is the control unit(enclosed with a rectangular broken line) which receives the reference values for each servo,

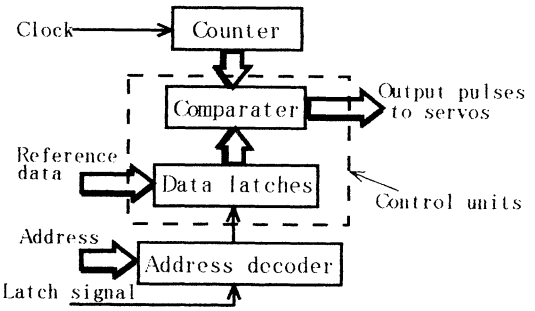


Figure 5: Block diagram of the circuits in FPGA

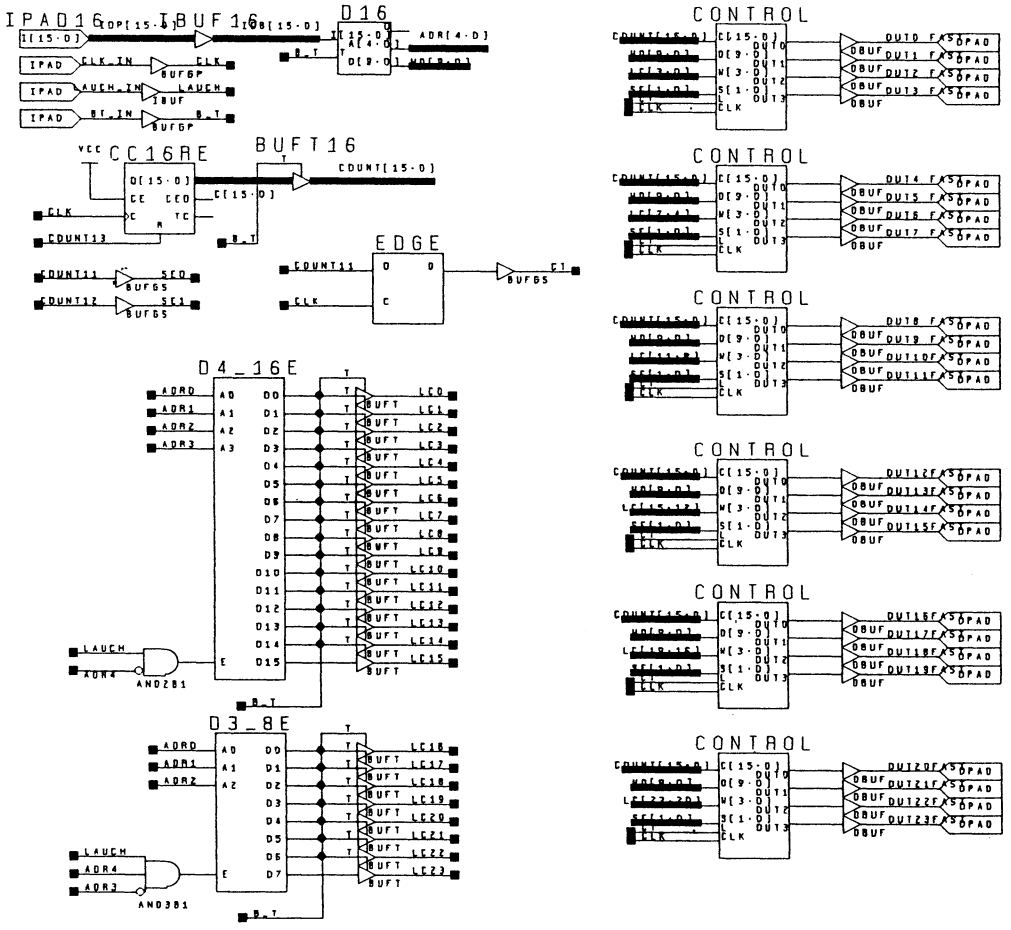


Figure 6: Schematic diagram of FPGA circuits

holds them on the latch circuits, compares the reference values with the output from counter and output the pulses into each servo mechanism. One control unit is capable of handling processes for 4 DOFs of servos. The third is a address decoder which makes 24 signals supplied into corresponding control unit to select one of 24 servos. Fig.6 shows the schematic diagram of whole circuits included in a FPGA chip. The upper-left part of the figure shows the interfaces with a microcomputer and the counter block mentioned above in Fig.5.The lower-left part of the figure corresponds to the address decoder in Fig.5. The right-half of the figure shows 6 control units. Fig.7 shows the detailed circuits inside of the control unit. The left-half of the figure shows 4*16 bits of latches(D-type flip flops) which holds reference values for each of 4 servos and a multiplexer to distribute them to the comparator stated next. The right-half of Fig.7 is composed with 4 elements. The first one from the left is a comparator which compares the reference values for each servo with the output of counter. When the output of counter is less than the reference value,the output of comparator is set to High. The second one is an edge detecter which generates a pulse on the timing of down edge of the comparator output. The pulse resets the RS-flip flop on the next stage. The third one is an RS-flip flop which is set by a pulse whose period is 1/4 of the frame time and reset by the output pulse from the previous stage. The last element is a distributer composed with 4 AND gates which supplies the control pulses into each servo mechanism. Fig.8 shows the timing chart of the signals generated by each element shown in Fig.7.

3.4 Communication processor

In this study,a microcomputer board AKI-80 was used to communicate with the host computer and to control the multi-freedoms controller. This board integrates a Z80 composite CPU chip,Z84C015-12,ROM(32Kbyte) and RAM(32Kbyte). Z84C015 is a 8-bit one chip microcomputer that employs a Z80 CPU as a nucleus and integrates peripheral functions such as CTC(counter timer),PIO(parallel I/O),SIO(serial I/O) and so on. For communication with the host computer,the RS232C serial communication mode was employed. Although the robot is connected with the host computer through a RS232C cable in this experiments, we are planning to use a wireless communication in the next step. Fig.9 shows a photograph of the microcomputer board(left) and the FPGA chip of multi-freedoms controller(right). The microcomputer board and the FPGA chip are piled up each

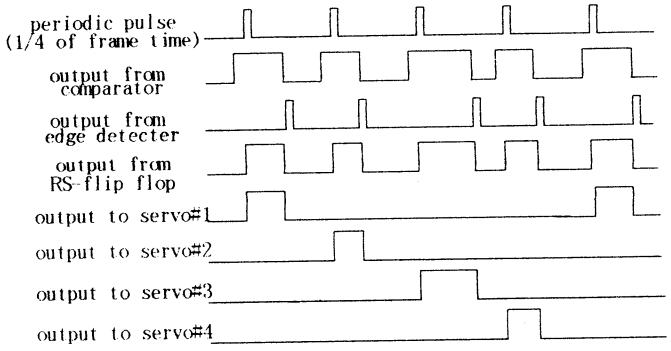


Figure 8: Timing chart of the signals

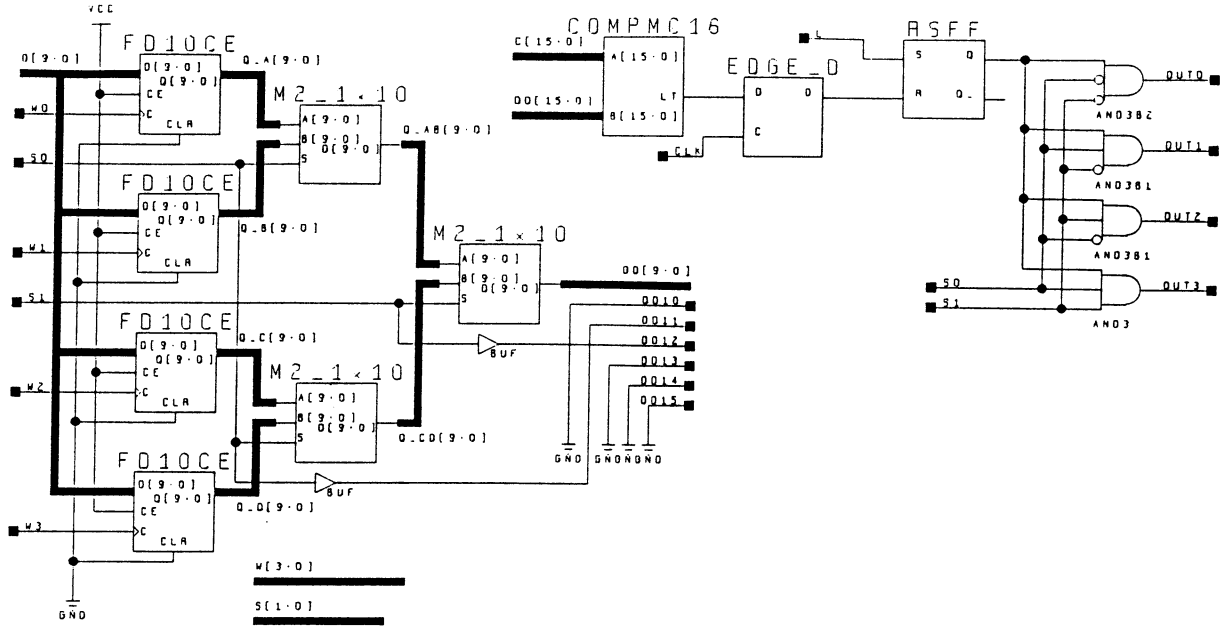


Figure 7: Circuits inside of the control unit

other and mounted on the back of the robot. Eventually,the control characteristics of multi-freedoms controller was greatly improved and the size of it became very small(60mm*70mm*28mm).

4 Motion control of a humanoid robot

Some experiments controlling the humanoid robot with the multi-freedoms controller developed in this study were carried out. The humanoid robot is able to stand up and sit down,turn the direction of walking and walk with two legs. Fig.10 shows a sequence of photographs which demonstrates walking motion of the robot.

5 Conclusions

This study made it possible to greatly inclease the number of DOFs that can be controlled by a small controller. It was verified that the controller is so small that it can be mounted on the back of a small robot which has very large number of DOFs. Although motion speed of the robot is rather slow because of the shortage of motor power, we are considering it is not essential. We are now planning to develop a high power and high speed robot using the multi-freedoms controller developed in this study.

Acknowledgements

We thank Professor Hirochika Inoue and Associate Professor Masayuki Inaba, Faculty of Engineering, Tokyo University for their invaluable advice.

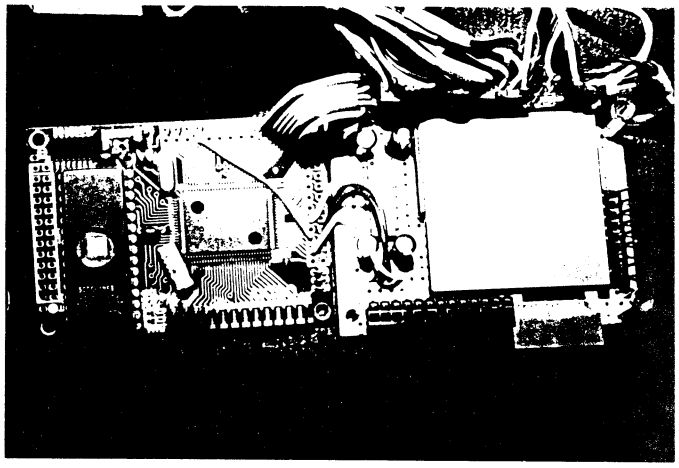


Figure 9: Photograph of the controller

References

[1] Masayuki Inaba,"Remote Brained Robotics: Interfacing AI with Real World Behaviors",*Proceedings of the 6th International Symposium on Robotics Research(ISRR6)*,pp.335-344,(1993).

[2] Masayuki Inaba,"A study on humanoids taking remote brain approach",*Proceedings of the 12th meeting of the Robotics Society of Japan*,pp.305-306,(1994).

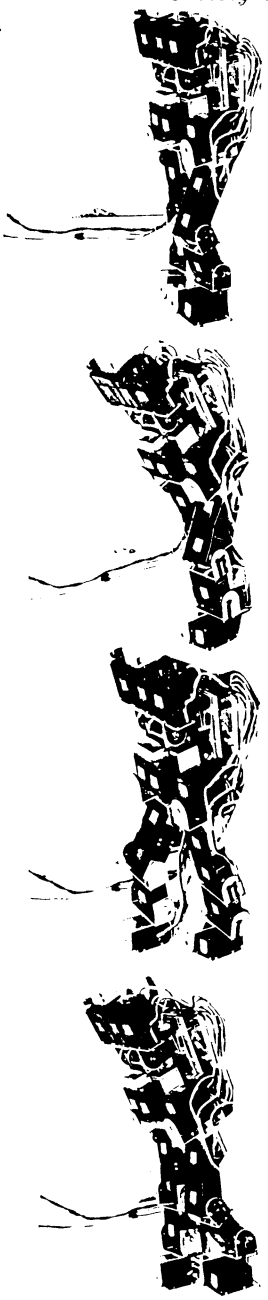


Figure 10: Photographs of walking motion

Proc. of Third Int. Symp. on Artificial Life, and Robotics (AROB III' 98),
Oita, Japan, 19-21, January, 1998,

Analysis of Human Transient Walking by Wavelet Transform

H.Ikeuchi*1, K. Shinkoda*2, R.Katoh*3, M.Sato*4, T.Yamashita*3
1) Department of Human Welfare Engineering, Oita University, Dannoharu Oita 870-11, Japan
Email: hikeucni@cc.oita-u.ac.jp
2) Department of Rehabilitation, University Hospital of Occupational and Environmental Health
3) Department of Control Engineering, Kyushu Institute of Technology
4) Department of Control and Information Engineering, Kitakyushu National College of Technology

Keywords: Measurement, Transient Walking, Floor Reaction Force, Wavelet Analysis

Abstract

This paper reports the dynamic characteristics of human transient walking, there are starting, stopping and changing direction. We obtain the ground reaction force components using two large force plates. And we investigate the characteristics of the ground reaction force components, and then discuss the characteristics and the result of wavelet transform of them. This paper treat the sagittal component of the reaction force, because the similarity in the sagittal component among starting, stopping and changing direction has been obtained in our previous study. The following results are obtained: the time-frequency characteristics in starting, stopping and changing direction are obtained; the difference of frequency characteristics between starting and stopping are obtained; the correlation among starting, stopping and changing direction are discussed.

1. Introduction

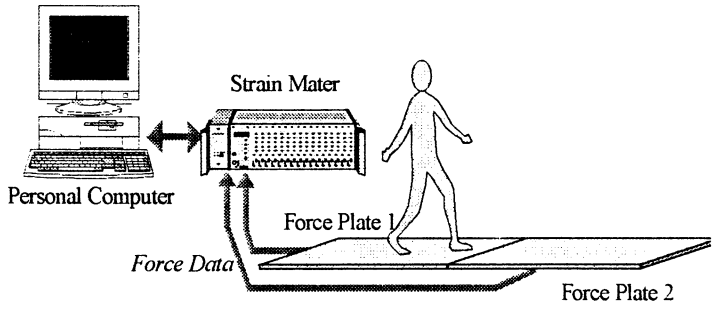
Since the transient walking for example, starting, stopping and changing direction, is one of many human walking modes in our usual activity, it is important to examine the dynamical and kinematic characteristics of the walking for applications such as development of artificial legs, the advice to rehabilitation of handicapped person and synthesis of biped locomotive robots. The dynamical and kinematic experimental data in transient walkings are valuable in these fields. However, they have been rarely studied because of difficulties of experimental measurements. Sato et al. measured the dynamics from start-up to a steady walking using large force plate[1]. McFadyn et al. measured the electromyogram in ascending and descending[2]. Ikeuchi et al. measured the dynamics of stair walking transferring to or from level walking[3]. Katoh et al measured and discussed the kinematic characteristics of stair walking[4].

It is important to obtain frequency characteristics of the system for various applications, for example, designing the artificial legs, detecting abnormal characteristics of handicapped person. Fourier analysis is extremely useful to stationary signal. However, Fourier analysis is not applicable to transient signal, like dynamic characteristics of transient human walking, because time information in the signal is lost in transforming to the frequency domain. Wavelet analysis is useful to transient signals due to an ability to perform local analysis.

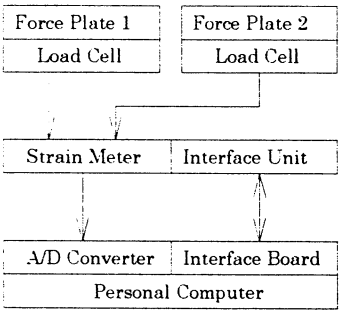
The walking for changing direction is realized by stopping in one direction, then starting in another direction at the same time. Actually, the relations between the cadence and wave peaks in starting, stopping and changing direction were similar[5]. In this paper, we compare the shapes of the result of wavelet transform in each level (frequency band), and discuss these. Additionally, the differences of starting and backward walking are discussed in the same method.

2. Method

Our experiment system is shown in Figure 1; the data acquisition system is composed of two large force plates, dynamic strain meters having amplifiers and low pass filters, and personal computer installed A/D converter board. This system can sense three orthogonal components of the reaction force from floor and their points of application, respectively. Figure 2 shows the method of walking experiments. We used them in parallel as shown in Figure 2(a) in starting and stopping in order to measure independently each leg's reaction force. In changing direction, subject walks as shown in Figure 2(b). We define sagittal component of reaction force as Fx and lateral component of reaction force as Fy. The supporting leg's data is analyzed in each experiment. The orthogonal coordinate system is defined at the center of two plates: x

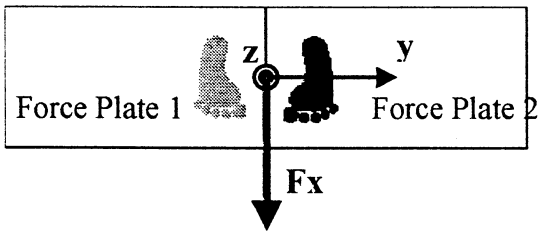


(a) Overview.

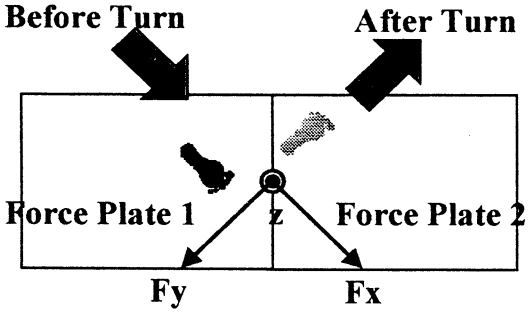


(b) Block diagram.

Figure 1. Experimental system for measuring.



(a) starting and stopping



(b) changing direction

Figure 2. Experimental method: the supporting leg (black) in starting and stoppng, and the first step (black) in changing direction are analysed.

axis is defined as the sagittal direction; y axis as the left direction; z axis as the vertical direction. Subjects are six normal persons (ages of 20 to 50) in starting, stopping and changing direction, and five normal persons in backward starting. Subjects are required to walk at a cadence indicated by computer tone. The cadence is widely changed from 70 step/min to 150 step/min in interval of 20 step/min.

Wavelet analyses are performed using MATLAB. In this paper, we use multi-level decomposition in Discrete Wavelet Transform. Wavelet is Daubechies 5. In multi-level decomposition, an original signal is separated into approximation A1 (low-frequency components) and details D1 (high-frequency components). And this process is iterated as shown in Figure 3. We obtain trend characteristics of each component.

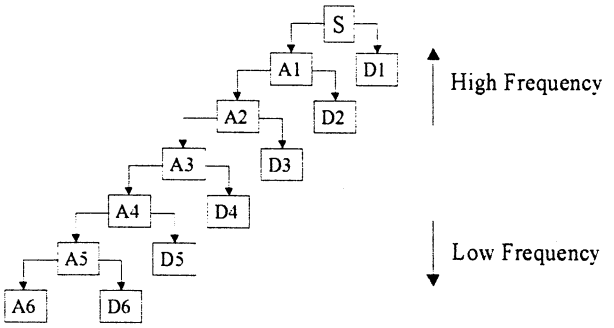


Figure 3. Multi-Level Decomposition

3. Result

Experimental results in 110 step/min, that is average speed in general, are only shown in graphical forms because of page limit. Sampling time of these data is 10 ms. The unit of force (F/Wt) in each figure means dimensionless force (F means each component of reaction force. Wt means subject's weight). 'A' and 'D' indicate approximations and details, respectively. The number after 'A' and 'D' means number of level. Signal in a lower frequency appears at a higher level. The results of all subjects are superimposed in a figure. GI, GS, DC and BA means the shape of the result of wavelet transform in starting,, stopping, changing direction and backward walking, respectively.

3.1 Fx in Starting and Fy in changing direction

Figure 4 shows example of wavelet analysis of the reaction force in Fx in starting and Fy in changing direction. The shapes of reaction force (in top figure) of starting and changing direction look similar, that is, subject does starting movement by Fy component in changing direction.

The GI and DC in level A6 (lowest frequency) are more similar than the reaction forces. In level D6, DC and

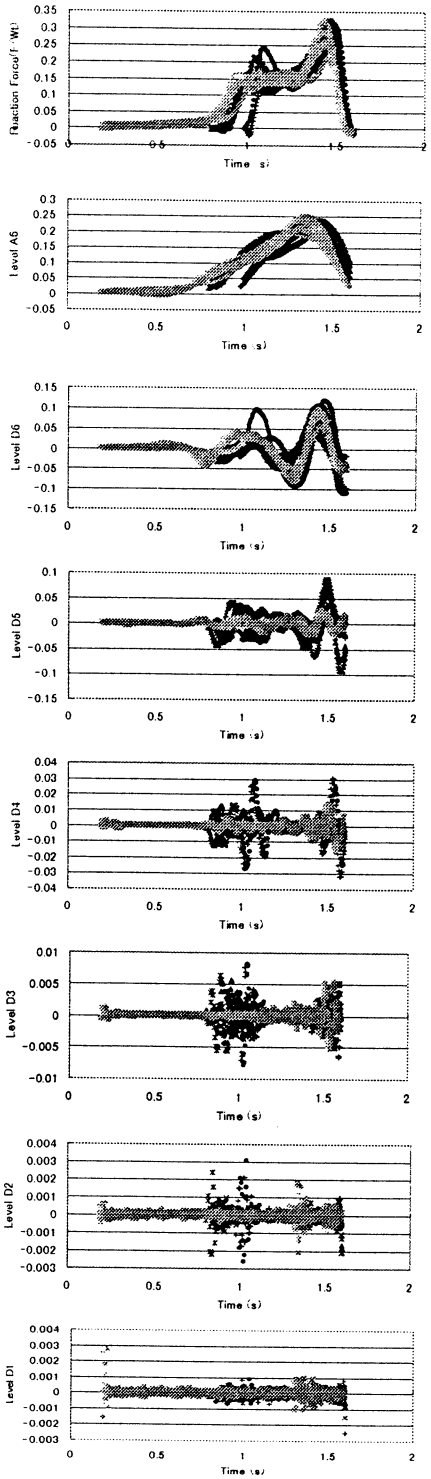


Figure 4. Comparison between Fx in starting and Fy in changing direction. (▩ : Starting, ■ : Changind direction)

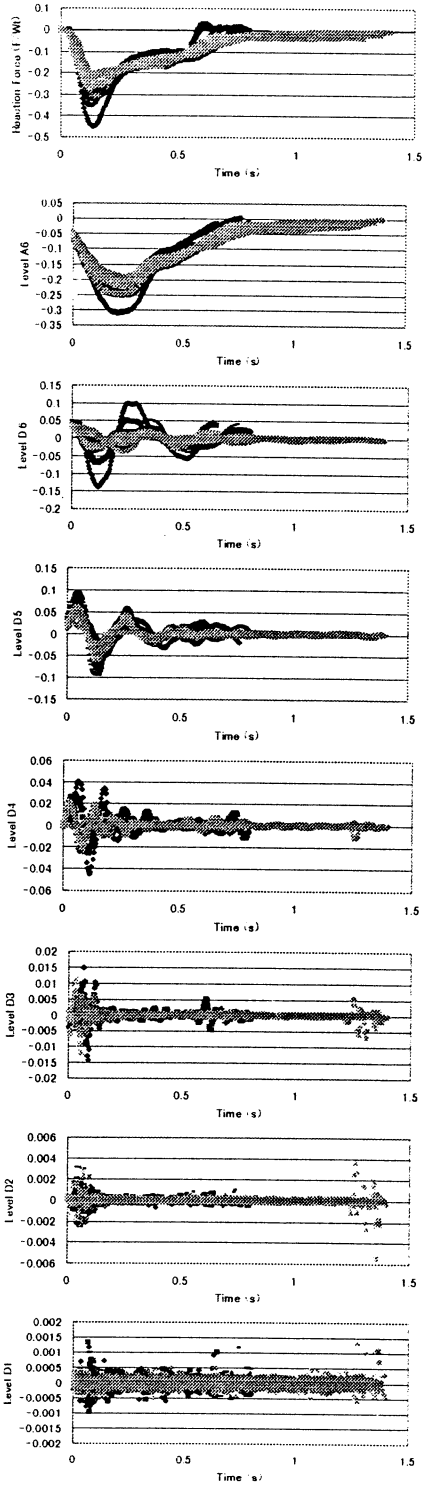


Figure 5. Comparison between Fx in stopping and Fx in changing direction. (▩ : Stopping, ■ : Changind direction)

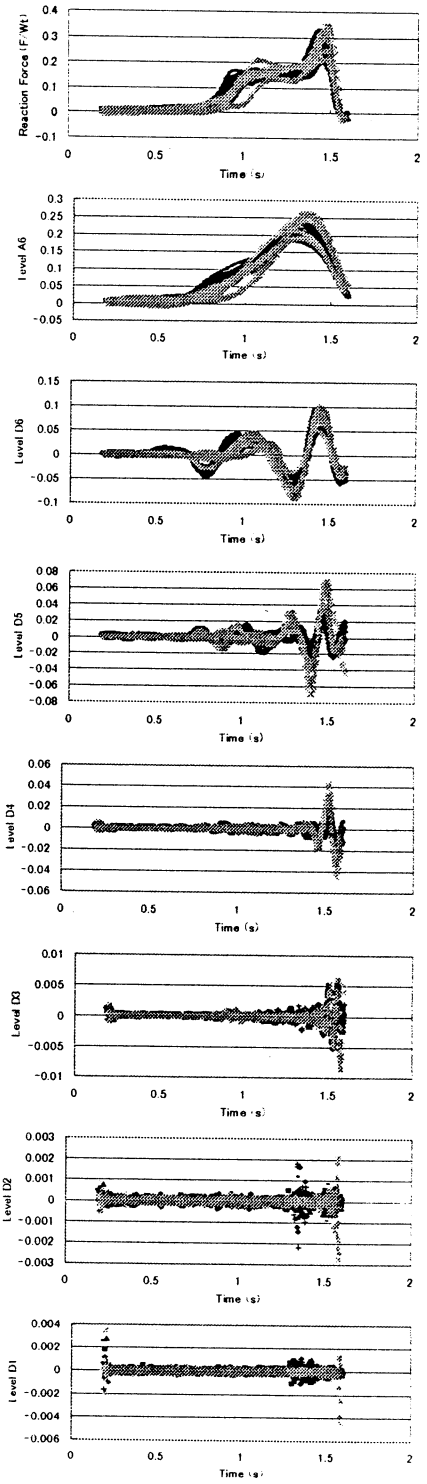


Figure 6. Comparison between Fx in starting and Fx in backward starting.. (▩ : Backward starting, ■ : starting)

GI look similar except one subject. In levels D5 through D2, there are definite periods of larger amplitude in DC than GI. These are at about 1.0 s and 1.5 s. The former period corresponds to the first peak of the reaction force. On the other hand, the wave amplitude of the latter period corresponds to the second peak of the reaction force in levels D3 through D1, having the same size between GI and DC. Large amplitudes at about 1.4 s in D3 to D1 of GI are obtained. These phenomenons aren't obtained in DC.

The characteristics in other cadences are much the same except level A6 in high cadence. In high cadence, the

shapes of level A6 are different between GI and DC. The personal difference is large in DC.

3.2 Fx in stopping and Fx in changing direction

Figure 5 shows example of wavelet analysis of the reaction force in Fx in stopping and Fx in changing direction. The shapes of reaction force (in top figure) of stopping and changing direction are similar, that is, subject does stopping movement by Fx component in changing direction.

The amplitude of the period of the first peak (about 0.4 s) in DC is larger than GS in many levels. The amplitude of D6 in DC is generally larger than GS. In level D4 and D3, there is the period of fluctuation in DC at about 0.6 s.

The difference of amplitude between DC and GS become large as increase of cadence.

3.3 Fx in starting and Fx in backward starting

Figure 6 shows example of wavelet analysis of the reaction force in Fx in starting and Fx in backward starting. The backward starting can be considered starting without using ankle. The characteristics look similar. But there are some differences in small points.

In level D5, the amplitude at about 1.5 s in BA is larger than GI. The period of fluctuations in GI is obtained at about 1.4 s in D2 and D1, but there aren't fluctuations in BA.

The amplitude of D6 and D5 in BA when foot leaves from floor (at 1.5 s in 110 step/min) is small in low cadence. The fluctuations in GI are obtained in all cadences.

4. Discussion

The wave shapes in lowest frequency band (level A6) are very similar in all Figures. This suggests that changing direction is the movement that basically consists of stopping and starting in different direction at the same time.

The reason for that the amplitude in DC is large, stems from the fact that subject is moving at constant speed before and after turn. But both in starting and stopping, there exists a motionless interval in one side of the time axis. These might cause the differences at about 1.0 s in Figure 4 and at about 0.6 s in Figure 5, mainly. These high frequency fluctuations of reaction force cause high frequency fluctuations of joint moment, then the load of bone and joint might be large.

The most interesting point is the fluctuation at about 1.4 s in GI. This fluctuation is obtained in all cadences. But such a fluctuation isn't obtained in Fy direction of DC and BA, that is starting. The difference of these starting is related to the mechanisms of link joint. That is, the kicking by ankle joint is little in Fy direction of DC and BA. The rotation of knee joint is devoid or very little in these movements. The fluctuation in GI might be caused by these mechanical differences of these walking mode.

In levels D5 through D3, it is interesting point that the amplitude of proximate part of toe off in BA is larger than GI. As described above, the kicking of ankle joint in BA isn't large, so this might give the same effect by pushing at toe off.

5. Conclusion

We have obtained the following results:

1. The time-frequency characteristics in starting, stopping, changing direction and backward starting are obtained.
2. The difference of frequency characteristics between starting, stopping and changing direction are obtained. The difference is at the first peak in high frequency, mainly.
3. The difference of frequency characteristics between starting and backward starting; the high frequency fluctuation isn't obtained in backward starting.
4. The relation among starting, stopping and changing direction are discussed

References

[1] Sato, M., Ikeuchi, H., Katoh, R. and Yamashita, T., Analysis of Motion of Body Center in Human Gait Initiation by Force Plate, in: R. Trappl (ed.), *Proc. of 12th European Meeting on Cybernetics and Systems Researc*, Vienna, Austria, 5-8 April 1994, 863-870.

[2] McFadyn, B. J. and Winter, B. A., An Integrated Biomechanical Analysis of Normal Stair Ascent and Descent, *J. Biomechanics*, Vol. 21, No.9, 733-744, 1988.

[3] Ikeuchi, H., Sato, M., Katoh, R. and Yamashita, T., Analysis of Characteristics of Human Stair Walking Transferring to or from Level Walking, *Proc. of Ninth World Congress on the Theory of Machines and Mechanisms*, Milano 29. August - 2. September 1995, 2420-2424.

[4] Katoh, R., Ikeuchi, H., Sato, M. and Yamashita, T., Analysis of Motion of Body Center during Human Stair Gait Using Force Plate, *JSME International Journal Series C*, Vol.39, No.2, 265-271, 1996.

[5] Ikeuchi, H., Sato, M., Katoh, R. and Yamashita, T., Relation between Peak Values of Floor Reaction Forces and Cadence in Human Transient Walking: Starting, Stopping, and Turning (in Japanese), *Trans of the JSME C*, Vol.60, No.577, 195-200, 1994.

Proc. of Third Int. Symp. on Artificial Life, and Robotics (AROB Ⅲ'98),
Oita, Japan, 19-21, January, 1998,

On Fuzzy Stochastic Control Process and Its Application

Toshio Odanaka
Faculty of Business Administration
and Information Science
Hokkaido Information University

Tsutomu Shohdohji
Dept. of Systems Engineering
Faculty of Engineering
Nippon Institute of Technology

Shigeru Kitakubo
Dept. of Systems Engineering
Faculty of Engineering
Nippon Institute of Technology

Abstract

This paper formulates a stochastic dynamic programming functional equation for a multi-stage decision problem whose fuzzy goal is to maximize the membership function that the state variables over all stages do not exceed the fixed levels, starting with an initial state, in a fuzzy environment. We will establish the existence and uniqueness theorem of the functional equation and its application.

It is also expressing about a theory of fuzzy stochastic dynamic programming and a design of the $(\bar{x},S)$ simultaneous control chart by our method.

1. Introduction

In classical dynamic programming as well as in the versions treated so far, the state transition function from stage to stage is assumed to be non-fuzzy and scalar. A logical extension which has real-life applications, particularly with respect to modeling of human decision processes encountered in such as diagnosis, psychotherapy, and even design, is fuzzy state mapping. Decision situation in which the decision constraints, goals, and system dynamics are all fuzzy were treated recently by Baldwin and Pilsworth[1]. Esogbue and Bellman[2] review developments in the field of fuzzy dynamic programming and discuss possible extension. In addition, Odanaka[5-9] extends this treatment to a probabilistic model in which the fuzzy goal is to minimize the membership function that the state variables over all stages exceed the fixed levels, starting with an initial state c.

We present a brief version of this model in the sequel and begin with a few basic definitions. Let $X = \{x\}$ be a collection of object denoted generally by x, then a fuzzy set A in X is a set of ordered pairs, $A = \{x, \mu_A(x)\}$, $x \in X$, where $\mu_A(x)$ is termed the grade of membership of x in A. Let P be a probability measure on R^n. A fuzzy event A in R^n is defined to be a fuzzy subset A of R^n, whose membership function μ_A is measurable. Then, the probability of A is defined by the Lebesgue-Stieltjes integral, $P(A) = \int_{R^n} \mu_A(x) dP$.

Equivalently, $P(A) = E(\mu_A)$, where E denotes the expected value operator. A fuzzy mapping f: X→Y is a fuzzy set on $X \times Y$ with membership function $\mu_f(x,y)$. A fuzzy function $f(x)$ is a fuzzy set on Y with membership function $\mu_{f(x)} = \mu_f(x,y)$. The fuzzy set $f(A)$ on Y is a fuzzy mapping of a fuzzy set defined as

$$\mu_{f(A)}(y) = \max_{x \in X} \{\min(\mu_A(x), \mu_f(x,y)), \forall y \in Y\}.$$

We consider the following fuzzy decision problem. Assume that (1) a fuzzy automation $J=\{U, X, f, F(U), F(X)\}$ with final state $x(T)$, where U, X are spaces for decisions and state sets, respectively, and $f: X \times U \to X$, $F(U)$, $F(X)$ are the sets for the fuzzy decisions and states, respectively; (2) a fuzzy dynamic transition function,

$$\mu_{x_{t+1}}(x(t+1)) = \max_{k \in K} \{\min(\mu_J(k),\ \mu_f(k,\ x(t+1)))\},$$
$$\forall x(t+1) \in X \ \ and \ \ t = (0,1,\cdots,T-1),$$

where $J \equiv X \times U$, $k \in K$ and J is a fuzzy set on K representing fuzzy state $x(t)$ and fuzzy decision $u(t)$ with membership function:

$$\mu_J(x,u) = \min\{\mu_{x(t)}(x), \mu_{u(t)}(u)\}.$$

Previous work has concerned the controlling of a process with a fuzzy goal in the state space, next work is to consider the situation in which the fuzzy decision is assumed to be subjected to fuzzy constraints with a fuzzy goal. In this paper, let us assume that the fuzzy goal is to maximize the membership function that the state variables overall stages do not exceed the final levels, starting with an initial state c, in a fuzzy environment.

2. Mathematical Model

Let us consider problem involving some stochastic processes in a fuzzy environment. Assume that the state at time t+1 in a stochastic system is described by

$$x_{t+1} = x_t + u_t + y_t, \qquad (t = 0,1,\cdots) \qquad (1)$$

where the state x_t, at time t, ranges over a finite set, the input u_t ranges over a finite set and the stochastic variable y_t is assumed to be characterized by a probability density function $\phi_t(\cdot)$. We will use

$\mu_f(x_t, u_t, y_t)$ to denote the membership function for the state transition function (1) when the system is fuzzy. We also assume that at each time t the input u_t is subjected to a fuzzy constraint C^t which is a fuzzy set characterized by a membership function $\mu_{C^t}(u_t)$.

Let us discuss the problem of maximizing some membership function over finite or infinite periods in a fuzzy environment. We define $f_n(c)$ as the membership function that all x_t do not exceed the range (β, α) starting with an initial state c at stage n and ending at stage N, using an optimal policy, subjected to the fuzzy constraint. The objective function f_n can be written as follows,

$$f_n(c) = \max_{u_n, \cdots, u_N} \mu_n(u_n) \otimes \cdots \otimes \mu_N(u_N) \otimes \mu_f(c_n, u_n, y_n) \otimes \cdots \otimes \mu_f(c_N, u_N, y_N) \otimes \Pr\left\{\left(\max_{n \le k \le N} x_k < \alpha\right) \wedge \left(\max_{n \le k \le N} x_k > \beta\right)\right\}. \quad (2)$$

Now we define $A = \{(c, p_1(c))\}$, $B = \{(c, p_2(c))\}$ and $C = \{(c, q(c))\} = \{(c, q_1(c)) \vee (c, q_2(c))\}$, where $p_1(c)$, $p_2(c)$ and $q(c)$ termed the grades of membership of c in $x_1 = [\alpha, +\infty)$, $x_2 = (-\infty, \beta]$ and $x_3 = (\beta, \alpha)$, respectively (see Fig. 1). Then, we have, for n=1, 2, $\cdots$, N,

$$f_n(c) = \begin{cases} p_1(c), & (c \ge \alpha) \\ \max\limits_{u} \min \left[\begin{array}{l} \mu_{C^n}(u) \\ \int_{\alpha - c - u}^{\infty} p_1(c+u+y)\phi_n(y)dy \\ + \int_{-\infty}^{\beta - c - u} p_2(c+u+y)\phi_n(y)dy \\ + \int_{\beta - c - u}^{\alpha - c - u} f_{n+1}(c+u+y)\phi_n(y)dy \\ \int_R \mu_f(c, u, y)\phi_n(y)dy \end{array} \right], & (\beta < c < \alpha), \\ p_2(c), & (c \le \beta) \end{cases} \quad (3)$$

with the following terminal conditions:

$$f_{N+1}(c) = p_1(c) \quad if \ c \ge \alpha,$$
$$q(c) \quad if \ \beta < c < \alpha,$$
$$p_2(c) \quad if \ c \le \beta.$$

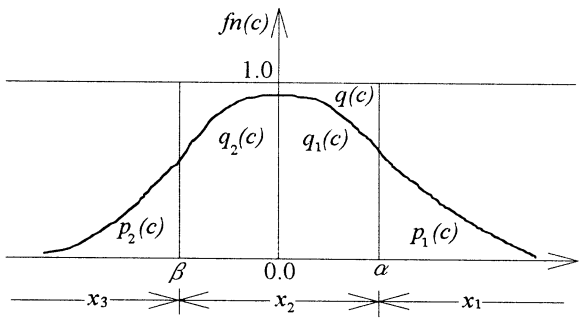


Fig. 1 Membership functions $(x_1 \to A, x_2 \to B, x_3 \to C)$

3. Existence and Uniqueness Theorem

Now we consider the following infinite horizon functional equation,

$$f_n(p) = \max_q \min_i \left[\begin{array}{l} q_n^i(p,q) \\ + \int_R f_{n+1}(p+q+r)\psi_n^i(r)dr \end{array} \right] \quad (4)$$

For this equation, we have the following assumptions.

(A1) For any fixed p, the max-min in the equation (4) is equal to the min-max.

(A2) For all n and i, $\int |\varphi_n^i(r)| dr < a < 1$.

(A3) $\{|g_n^i(p,q)|\}$ is a uniformly bounded sequence of integrable function.

Theorem 1

We consider

$$\begin{cases} W_n^0(p) = W_n(p), \\ W_n^{k+1}(p) = \max\limits_q \min\limits_i \left\{ q_n^i(p,q) + \int W_{n+1}^k(p+q+r)\varphi_n^i(r)dr \right\}. \end{cases} \quad (5)$$

Then we have $W_n^{k+1}(\cdot) \ge W_n^k(\cdot)$, $\forall k$ and $W_n^k(\cdot) \uparrow W_n^*(\cdot)$. Moreover, the limit $W_n^*(p)$ is a unique bounded solution to the equation (4), if we assume (A1), (A2) and (A3).

We will establish existence and uniqueness theorem of equation (3) when the horizon is finite and infinite. Let us impose the following conditions on $\phi_n(y)$, $p_1(y)$, $p_2(y)$ and $q(y)$.

(a) for all n and y, $\phi_n(y) \ge 0$, $\int_{-\infty}^{\infty} \phi_n(y)dy = 1$ and for any w, $\int_{\beta - w}^{\alpha - w} \phi_n(y)dy \le a < 1$,

(b) $0 \le p_1(y) \le 1$, $0 \le p_2(y) \le 1$, $0 \le q(y) \le 1$,

(c) $\mu_C(\cdot)$ and are $\mu_f(\cdot)$ integrable and bounded functions.

Theorem 2

Assume the conditions (a), (b) and (c), then there is a unique solution to finite and infinite horizon functional equation (3).

4. $(\bar{x}, S)$ Control Chart

Let us use the approximating equations:

$$\begin{aligned} \bar{x}_{n+1} &= \bar{x}_n + u_n + w_n, \quad x_k = c_1, \\ S_{n+1} &= S_n + v_n + z_n, \quad S_k = c_2, \\ (n &= k, k+1, \cdots, N-1) \end{aligned} \quad (6)$$

where x_n represents the position of mean in time n, w_n is the random term, and u_n is the forcing term resulting from the control chart is applied. S_n is the standard

deviation in time n and z_n is the random term and v_n the forcing term. The random force are taken to be a stochastic quantity with the probability density function:

$$\Psi(w,z) = \psi_1(w)\psi_2(z).$$

Simply, we define that $S_{n+1} = S_n$ and $\psi_2(z) = \delta(z)$. Let us define, as usual, the function $F_k(c_1,c_2)$ is the probability that the maximum devia-tion of this point in the control system from the origin exceeds a specified bound in the (N - k) stages control processes, starting with the initial state (c_1,c_2) using an optimal policy, subjected to the fuzzy goal, subjected to non fuzzy constraints.

Measuring the derivation from equilibrium by means of the distance $\sqrt{\bar{x}_n^{\,2} + S_n^{\,2}}$, we set

$$F_k(c_1,c_2) = \min_{u_n} \Pr\left\{\max_{k\le n\le N-1} \sqrt{\bar{x}_n^{\,2} + S_n^{\,2}} \ge \alpha\right\}, \qquad (7)$$

subject to $|u_k| \le A$. Then we have from the definition of

$$\begin{aligned} &F_k(c_1,c_2), \\ &F_{N-1}(c_1,c_2) = f(c_1,c_2), \qquad (c_1^{\,2} + c_2^{\,2} \ge \alpha^2) \\ &\qquad\qquad = g(c_1,c_2), \qquad (c_1^{\,2} + c_2^{\,2} < \alpha^2) \end{aligned} \qquad (8)$$

where f and g are membership functions, and

$$F_N(c_1,c_2) = \begin{cases} f(c_1,c_2), & (c_1^{\,2} + c_2^{\,2} \ge \alpha^2), \\ \min_{u_{N-2}} \int_{-\infty}^{\infty} F_{N-1}(c_1 + u + w, c_2)\psi_1(w)dw, & \\ & (c_1^{\,2} + c_2^{\,2} < \alpha^2). \end{cases} \qquad (9)$$

In this section, we present the policy of the case where some assumption concerning the probability density function of random noise is made.

Theorem 3

Let us assume that

a) $\psi_1(y) \ge 0, \quad \int_{-\infty}^{\infty} \psi_1(y)dy = 1,$

b) $0 < \int_{-p-q}^{p-q} \psi_1(y)dy \le a < 1, \quad$ for $p > 0$ and all q,

c) $\psi_1'(y)$ is continuous and unimodal in the interval $(-\infty,\infty)$, (10)

d) $\psi_1'(y) < 0$ in the interval at least $2p$,

e) $f(c_1,c_2)$ and $g(c_1,c_2)$ are continuous and unimodal in $(-\infty,\infty)$,

f) $|u_k| \le A$.

For each k,

$$\begin{aligned} u_k &= A, \qquad (\bar{q}_k \ge c_1 + A) \\ &= \bar{q}_k - c_1, \quad (c_1 - A \le \bar{q}_k < c_1 + A) \\ &= -A, \qquad (\bar{q}_k < c_1 - A) \end{aligned} \qquad (11)$$

where $\bar{q}_k$ is the unique solution of the equation:

$$\int_{-p-q}^{p-q} \{1 - F_{k+1}(c_1 + u + w, c_2)\}\, \psi_1(w)dw = 0. \qquad (12)$$

5. Conclusions

We have many applications of our theory[4].

1) Inventory Control[3]

Luck of sufficient storage capacity in a water supply system led to frequent changes in the load on the filters and hence to poor quality.

In the Philips factories in Eindhoven, H. C. Hamaker carried out experiments to decide how much the storage capacity should be enlarged and how the crude water supply could be controlled in order to obviate these troubles.

We gave the theoretical background for his numerical analysis from the stand point of our theory. We are forced by the following two kinds of risks.

(a) The case that flow over the storage capacity, increasing the inventory.

(b) The case that does not meet the demand, decreasing the inventory. Our problem is to research the supply that minimizes the probability of the two kind of risks.

2) Control Engineering

We wish to discuss the analytical and the numerical consideration for some stochastic control problems connected with the Van der Pol equation:

$$x'' + \lambda(x^2 - 1)x' + x = f(t) + g(t). \qquad (13)$$

We shall suppose that our aim is to prevent the oscillation of this system and to maintain the system in the equilibrium position.

M. Aoki has given computational results when the criterion function of this problem is the expected value of the maximum deviation of system from equilibrium position[4].

We shall choose the control in such a way as to minimize the probability that maximum deviation of the system from equilibrium position exceed a specified bound over the time interval.

3) Miscellany

We applied our theory to engineering problems, but it has applications in many fields, foe example, the price adjustment problem, the resource problem, the pollution problem, and the medical research problem.

References

[1] Baldwin J.F. and B.W. Pilsworth(1982), Dynamic Programming for Fuzzy Systems with Fuzzy Environment, *Journal of Mathematical Analysis and Applications*, Vol. 85, pp. 1-23.

[2] Esogbue, A. O. and R. E. Bellman(1984), Fuzzy Dynamic Programming and its Extensions, in J. F. Baldwin, H. J. Zimmermann and L. A. Zadeh, Eds., Fuzzy Sets and Decision Analysis, *TIMS Studies in Management Science*, Vol. 20, pp. 147-167.

[3] Odanaka, T(1968), Inventory Control Problem of Hamaker, H. C. (in Japanese) , *Keieikagaku*, Vol. 11, No. 3/4, pp. 180-187.

[4] Odanaka, T(1986), Stochastic Control Processes and Management Science, *Journal of Mathematical Analysis and Applications*, Vol. 104, No. 1, pp. 104-109.

[5] Odanaka, T(1986), *Optimal Inventory Process*, Katakura Libri, Inc., Tokyo.

[6] Odanaka, T(1990), *Dynamic Management Decision and Stochastic Control Processes*, World Scientific Publishing Co. Pte. Ltd.

[7] Odanaka, T(1991), Control Chart and Stochastic Control Processes, *Journal of Computers and Mathematics with Applications*, Vol. 21, No. 11/12, pp. 65-78.

[8] Odanaka, T(1996), *Fuzzy Dynamic Programming* (in Japanese), Maki Shoten.

[9] Odanaka, T., T. Shohdohji, and S. Kitakubo(1997), Some Membership Functions and the Generalized Control Chart, in *Proceedings of The 14th International Conference on Production Research*, Vol.1, Osaka Japan, August 4-8, 1997, pp.202-205.

Proc. of Third Int. Symp. on Artificial Life, and Robotics (AROB III' 98),
Oita, Japan, 19-21, January, 1998,

Holonic Control System using Fuzzy Criterion

Naohiro Kusumi,Kotaro Hirasawa,Masanao Ohbayashi and Jinglu Hu
Department of Electrical and Electronic Systems Engineering
Graduate School of Information Science and Electrical Engineering
Kyushu University
6-10-1 Hakozaki Higashi-ku Fukuoka,812-81,JAPAN
E-mail:kusumi@scel.ees.kyushu-u.ac.jp

Abstract

Holonic concept was originated from Arthur Koestler in 1905. Holonic-type control system using its concept has been presented. The aim of holonic control design is to harmonize with the partial and the whole system which have a hierarchical structure. Holonic control system is based on Universal Learning Network(ULN) Theory. The purpose of this paper is to show that the holonic control system using fuzzy criterion is effective.

Keywords: Holon concept,harmony,fuzzy criterion

1 Introduction

Recently, as the research on Artificial Life has been studied, making use of life phenomena to many engineering fields has increased. For this reason it is natural to apply the life phenomena to large-scale complicated control systems. Generally speaking, the design of large-scale complicated control systems requires compromising a lot of specifications in order to realize their objects. However, it is difficult for the system to satisfy a large number of specifications at once. For example, if we take every specifications seriously, it is difficult for us to find the optimal solution, because each specification is different in nature, and it takes too much time to calculate the best solution.

To overcome these circumstances, holonic concept was proposed by Arthur Koestler in 1905. This concept is based on the relation between the whole and part, where a harmonized solution between the self-assertion of the part and unity of the whole is tried to find. That is to say, holonic concept is based on an idea that exaggerates harmony rather than optimization, in other words, solution in view of the specific criterion function may not be the best solution but each subsystem can function considerably well in a general point of view.

We have presented a control method of the large-scale complicated systems using the above-mentioned holonic concept and proved that holonic control methodology is very powerful to find the solution in a harmonized manner[2]. The purpose of this paper is to extend the holonic control system to the system using fuzzy criterion.

Holonic control system is based on Universal Learning Network (ULN) theory. The basic idea of ULN is that most of the large-scale complicated systems can be modeled by the network which consists of nonlinearly operated nodes and branches that may have arbitrary time delays including zero or minus ones. Therefore, ULN can be applied to many kinds of systems which are difficult to be expressed by ordinary first order difference equations with one sampling time delay.

In simulations, the extended holonic control system is applied to a nonlinear tank network system and comparisons between the holonic control system using fuzzy criterion and the conventional holonic control system are carried out.

The results of our experiments clearly show that we can obtain a better harmonized solution by making use of this new methodology than the conventional method.

2 Holonic Control System

The structure of holonic subsystem is shown in **Fig.1**. The holonic system is made up of the holonic subsystems HS_g, and the holonic subsystem HS_g is also made up of the physical subsystems PS_f and its controllers SC_f.

The holonic subsystems are connected with each other by the interface values which can be used to harmonize the holonic subsystems.

The optimization of the holonic subsystem is exe-

cuted subsystem by subsystem using ULN, given the interface values which were calculated by other subsystems.

Physical System:PS

$$PS = \{PS_f, SC_f | f \in F\} \quad (1)$$

PS_f : fth physical subsystem
SC_f : controller of fth physical subsystem PS_f
F : set of numbers of physical subsystems

Holonic System:HS

$$HS = \{HS_g | g \in G\} \quad (2)$$
$$HS_g = \{PS_f, SC_f | f \in F(g)\} \quad (3)$$

HS_g : gth holonic subsystem
G : set of numbers of holonic subsystems
$F(g)$: set of numbers of physical subsystems which are included in the holonic subsystem HS_g

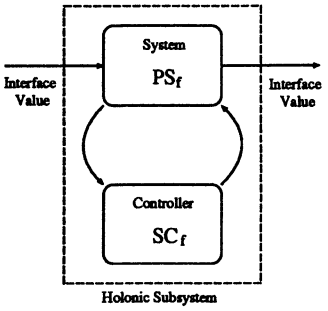


Fig.1 Structure of holonic subsystem

3 Nonlinear Tank Network System

The concept of holonic control can be applied to a tank network system in **Fig.2**. The tank network can be made up of three groups which are connected with each other by the water pipes that have time delays. Each tank in the same group is also connected with each other. The structure of each tank which is a nonlinear one is depicted in **Fig.3**.

Here, the group means the holonic subsystem and each tank corresponds to the physical subsystem mentioned above.

Inflow of the tank T_1^1, T_1^2, T_1^3 and the valves between the tanks in the same or different groups are controlled by the feed forward neural networks.

For example, valves between T_1^1 and T_2^3, T_3^1 and T_2^2, T_1^1 and T_2^1, T_2^1 and T_3^1 and T_1^1 and T_3^1 are controlled by the 1st tank group neural network controller.

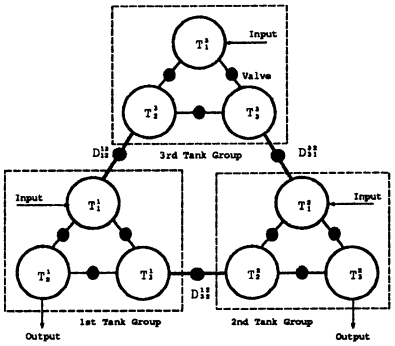


Fig.2 Tank network system

where

T_j^g : j th tank of holonic subsystem g
$D_{jj'}^{gg'}$: time delay from T_j^g to $T_{j'}^{g'}$ $(= D_{j'j}^{g'g})$

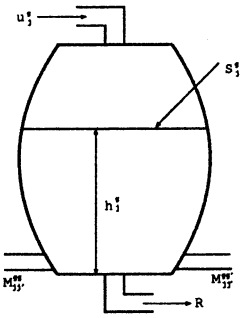


Fig.3 Structure of tank

where

u_j^g : inflow of T_j^g
h_j^g : water level of T_j^g
$S_j^g(h_j^g)$: cross section area of T_j^g at h_j^g
$M_{jj'}^{gg'}$: coefficient of valve between T_j^g and $T_{j'}^{g'}$ (between holonic subsystem)
$M_{jj'}^{gg}$: coefficient of valve between T_j^g and $T_{j'}^{g}$ (inside holonic subsystem)
r_j^g : outflow of T_j^g

Equation of the dynamics of the tank network is expressed as follows.

$$\begin{aligned} & S_j^g(h_j^g)dh_j^g(t) \\ &= u_j^g(t)dt \\ &- \sum_{(g'j')\in\widetilde{G_j^g}} M_{jj'}^{gg'}\sqrt{2g(h_j^g(t) - h_{j'}^{g'}(t - D_{jj'}^{gg'}))}dt \\ &- \sum_{j'\in G_j^g} M_{jj'}^{gg}\sqrt{2g(h_j^g(t) - h_{j'}^{g}(t))}dt \\ &- r_j^g(t)dt \end{aligned} \quad (4)$$

where

$\widetilde{G_j^g}$: set of products of holonic subsystem numbers and tank numbers of the different holonic subsystem from T_j^g

G_j^g : set of tank numbers of the same holonic subsystem as T_j^g

Then, Eq.(4) can be expressed in the following discrete form.

$$\begin{aligned} & h_j^g(t+1) \\ &= h_j^g(t) + \frac{T_s}{S_j^g(h_j^g(t))}\Big(u_j^g(t) \\ &- \sum_{(g'j')\in\widetilde{G_j^g}} M_{jj'}^{gg'}\sqrt{2g(h_j^g(t) - h_{j'}^{g'}(t - D_{jj'}^{gg'}))} \\ &- \sum_{j'\in G_j^g} M_{jj'}^{gg}\sqrt{2g(h_j^g(t) - h_{j'}^g(t))} - r_j^g(t)\Big) \end{aligned} \quad (5)$$

where

T_s : sampling time

Outflows of the Tank T_2^1 and T_2^2 were shown in **Fig.4**.

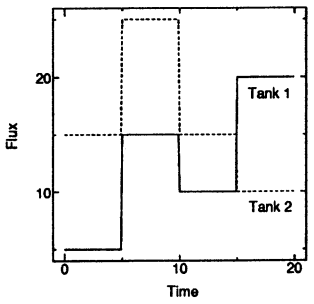


Fig.4 Outflows of the 1st & 2nd holonic subsystem

4 Holonic algorithm with fuzzy criterion

A proposed holonic control system with fuzzy criterion function in this paper has a slightly different type of criterion function from that of the previous paper[2].

The criterion function EHS_g of holonic subsystem HS_g is changed to a fuzzy criterion function such as $FEHS_g$ with membership function $\mu_{EHS_g}(EHS_g)$ expressed by Eq.(6).

Therefore, harmonized solutions by the holonic methodology can be obtained considering the fuzzy criterion $FEHS_g$.

We set the fuzzy criterion function as follows.

$$FEHS_g = \{1 - \mu_{EHS_g}(EHS_g)\}EHS_g \quad (6)$$

where

$$\mu_{EHS_g}(EHS_g) = \frac{1}{1 + \left|\frac{EHS_g}{W_g}\right|^{2B_g}} \quad (7)$$

B_g is a gradient of membership function and W_g is a degree of satisfaction. For example, if W_g has a large value, a degree of satisfaction becomes not severe.

An original criterion function of each holonic subsystem is represented as follows,

$$\begin{aligned} EHS_1 &= \frac{1}{2}\sum_t[\sum_f^{|F(1)|} Q_f^1(h_{f\ ref}^1 - h_f^1(t))^2 \\ &+ K_1u_1(t)^2 + H_{13}(M_{21}^{31}(t) - M'^{31}_{21}(t))^2 \\ &+ H_{12}(M_{23}^{21}(t) - M'^{21}_{23}(t))^2] \\ EHS_2 &= \frac{1}{2}\sum_t[\sum_f^{|F(2)|} Q_f^2(h_{f\ ref}^2 - h_f^2(t))^2 \\ &+ K_2u_2(t)^2 + H_{21}(M_{32}^{12}(t) - M'^{12}_{32}(t))^2 \\ &+ H_{23}(M_{31}^{32}(t) - M'^{32}_{31}(t))^2] \\ EHS_3 &= \frac{1}{2}\sum_t[\sum_f^{|F(3)|} Q_f^3(h_{f\ ref}^3 - h_f^3(t))^2 \\ &+ K_3u_3(t)^2 + H_{31}(M_{12}^{13}(t) - M'^{13}_{12}(t))^2 \\ &+ H_{32}(M_{13}^{23}(t) - M'^{23}_{13}(t))^2] \end{aligned}$$

Q_f^g : coefficient of weight of tank T_f^g

K_g : coefficient of weight of gth holonic subsystem input

$h_{f\ ref}^g$: desired water level of tank T_f^g

H_{mn} : holonic coefficient (from mth holonic subsystem to nth holonic subsystem)

$M(t)$: coefficient of valve which should be calculated

$M'(t)$: coefficient of valve which was obtained by other holonic subsystems

From the foregoing, the learning is to search for the parameters, which minimize the fuzzy criterion function $FEHS_g$ by the ULN. For more information concerning ULN and its applications, see Ref.[1],[3] and [4].

5 Simulations

Simulation conditions are shown in **Table.1**.

Table.1 Conditions of simulation

height of tank	10.0[m]
radius of bottom	5.0[m]
radius of center	7.5[m]
Q_1^1, Q_2^1, Q_3^1	10.0, 100.0, 10.0
Q_1^2, Q_2^2, Q_3^2	10.0, 10.0, 100.0
Q_1^3, Q_2^3, Q_3^3	100.0, 10.0, 10.0
K_1, K_2, K_3	10.0, 10.0, 10.0
H_{13}, H_{12}	1.0, 1.0
H_{21}, H_{23}	1.0, 1.0
H_{31}, H_{32}	1.0, 1.0
B_1, B_2, B_3	1.0, 1.0, 1.0
W_1, W_2, W_3	100.0, 1.0, 100.0
number of learning	60000

First, a result of conventional holonic control system is shown in **Fig.5**. We see from this figure that a harmonized solution is not obtained. If the *Holonic Coefficient* H_{31}, H_{32} is set to a large value, we may get a harmonized solution. But we should point out that the method of finding optimal quantitative values for *Holonic Coefficients* is not easy.

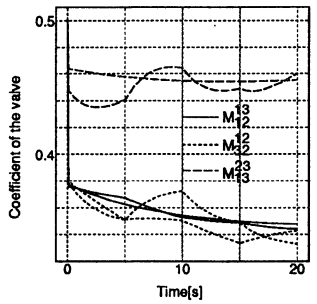


Fig.5 Result of conventional holonic control system

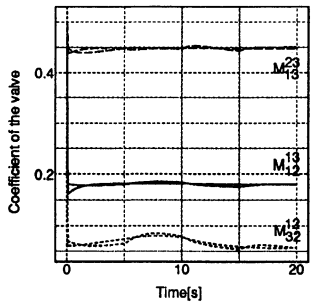


Fig.6 Result of extended holonic control system

Thus, to overcome the above-mentioned problem, we applied the extended holonic control to the same problem. A result of this case is shown in **Fig.6**.

A glance at **Fig.6** will reveal that the harmonized solution is obtained in the case with fuzzy criterion. It is clear that the fuzzy criterion is useful for getting harmonization in the large-scale complicated systems.

6 Conclusions

So far we have presented the extended holonic control system. The results of our simulations clearly show that we can obtain a better harmonized solution rather than the one by the conventional manner.

The future work we should do is to study the stability problem of the holonic control system by using the stability analysis method of ULN[5]. And improvement of the structure of the controller is one of the problems which remain to be solved.

References

[1] K.Hirasawa,M.Ohbayashi and J.Murata, "Universal Learning Network and Computation of its Higher Order Derivatives," *Proc. of IEEE International Conference on Neural Networks*, **Vol.3**,pp.1273-1277,1995.

[2] N.Kusumi,K.Hirasawa and M.Ohbayashi, "Holonic Control System for Large-scale Systems," *Proc. of 2nd Asian Control Conference*,**Vol.III**,pp.659-662,1997.

[3] M.Koga,K.Hirasawa,J.Murata and M.Ohbatashi, "Chaos Control on Multi-Branch Universal Learning Network," *Proc. of International Symposium on Artificial Life and Robotics (AROB 1st)*, pp.112-117,1996.

[4] M.Ohbayashi,K.Hirasawa and J.Murata, "Evaluation of Robust Control by Universal Learning Network," *Proc. of International Symposium on Artificial Life and Robotics (AROB 1st)*, pp.107-111,1996.

[5] K.Hirasawa,M.Ohbayashi,M.Koga and N.Kusumi, "Stability Theory of Universal Learning Network," *Proc. of IEEE International Conference on System, Man and Cybernetics*, **Vol.2**,pp.1352-1357,1996.

Proc. of Third Int. Symp. on Artificial Life, and Robotics (AROB III' 98),
Oita, Japan, 19-21, January, 1998,

AUTONOMOUS NAVIGATION FOR MOBILE ROBOT USING HIERARCHICAL FUZZY INFERENCE AND GENETIC ALGORITHM

D.Y. JU, M. NEMOTO, T. IWATA
Department of Mechanical Engineering
Saitama Institute of Technology
Fusaiji 1690, Okabe 369-02, Japan

K. TOYOTA
Department of Mechanical Engineering
Ebara Corporation
Hata Asahi 11-1, Oda-ku, Tokyo, Japan

Abstract

An important problem in the development of autonomous mobile robot is how to develop an intelligent controller. In this paper, a new self-creating and organizing fuzzy inference based on a genetic algorithm is proposed. The genetic algorithm are used to optimize the membership function of output in hierarchical fuzzy controller, so it can deal with a more complex uncertain workspace. Using this method, the mobile robot can find a path from a specified starting robot configuration to a specified goal configuration that avoids collisions with the obstacles. From the results of our research work, we know that the method can effectively present the performance of a path planning for the autonomous navigation of the mobile robot.

1 Introduction

The ability to guarantee the feasibility of a mobile robot during autonomous navigation in uncertain workspace with some objects is important to the integration of an intelligent controller or algorithm[1]. Thus, incompatibility between plans prepared using the intelligent system and the actual execution of these plans based on recognition of paths using multi-sensor of a mobile robot can be avoided. For instance, when a path planning is completed to follow the local recognition of a workspace for a task of autonomous navigation, the position of the mobile robot has to be satisfied , while the orientation can be arbitrary. On the other hand, with an autonomous navigation and path planning of the mobile robot, it is important exactly to recognize a neighboring environment of its own position for the robot. However, irrespective to make a performance of the sensors has to be improved, it is an inevitability thing due to there are many mistakes to come from some error of sensors and movement of the actuators as well as other hardware during the actual execution of the mobile robot. In order to settle these problems, an intelligence control system is hoped for a human being and living thing, so it is flexibility dealing with workspace recognition depending on some sensors. As an intelligent controller, the fuzzy logic method always is applied into the autonomous path planning of the mobile robot by many researchers[2]-[3], recently. In the autonomous navigation for multi-goal, in order to adapt oneself to every goal, a multi-layer or hierarchical fuzzy control and autonomous regulation of membership functions in which combined with each rule of the fuzzy controller for deference goals have to be considered. However, it is often very difficult to determine the optimal membership function of a unknown workspace which only employ the fuzzy logic method. On the other hand, genetic algorithm (GA) have are applied into many research filed including robot controller [4]-[7] as a new intelligent method, recently.

In order solve the problem, in this paper, we propose a new architecture of a self-creating and organizing fuzzy inference based on a genetic algorithm that guarantees the feasibility of a planned path during autonomous navigation of the mobile robot. The genetic algorithm is employed to realize autonomous organization of membership functions in a hierarchical fuzzy controller. Using this method, the mobile robot can find a path from a specified starting robot configuration to a specified goal configuration that avoids collisions with the obstacles. From the some simulation, we know that the method can be effectively presented to the complex performance during the autonomous navigation of the mobile robot.

2 Fuzzy Inference for Robotic Navigation

As an autonomous mobile robot, it must have abilities for determining correct distance and direc-

tion of its walking or moving through recognizing to workspace based on some sensor, generally. Because the mobile robot need to regulate the walking distance and moving direction in the robot navigation, we define that the moving direction is looked on the first stage of fuzzy inference and that the moving distance is looked on of the second stage of fuzzy inference. In this research work, we use a mobile robot with a rotating ultrasonic sensor for estimating distances from obstacles to itself. The obtained distances based on he ultrasonic sensor is used to calculate area of workspace around the robot.

2.1 Rule base

In the first stage of fuzzy controller, a ruler base consists of four rules for determining the moving direction of the robot can be defined as follows,

$$R_i^1: \quad IF\ \bar{A}\ is\ F_i\ THEN\ \theta_i\ is\ \bar{\Theta}\ .\ (i=1,2,...,4) \tag{1}$$

Here, $\bar{A} \in [-1,1]$ is defined by

$$\bar{A} = 2\frac{A^r}{A^r + A^l}\ , \tag{2}$$

with

$$A^r = \Sigma_{k=1}^{N/2-1} \Delta\phi_k^r D_k^r\ ; A^l = \Sigma_{k=1}^{N/2-1} \Delta\phi_k^l D_k^l\ ,$$

where D_k^r and D_k^l are the smallest distances on right and left of from the robot to obstacles. $\Delta\phi_k$ is an angle between two distance which be measured by an ultrasonic sensor. The subscript k denotes the distance on kth direction. i shows ith fuzzy rule. Also, F_i, Θ_i are fuzzy subsets corresponding to the parameter $\bar{A}$ (deviation of area) and turning angle θ_i of the robot, respectively.

In the second stage of fuzzy controller, a ruler base consists of four rules utilized results of the first stage is used to determine the moving distance of the robot as follows,

$$R_i^2: \ IF\ \bar{D}\ is\ M_i\ and\ \theta_i\ is\ \bar{\Theta}_i\ THEN\ p_f\ is\ P_i\ .$$

$$(i=1,2,...,4) \tag{3}$$

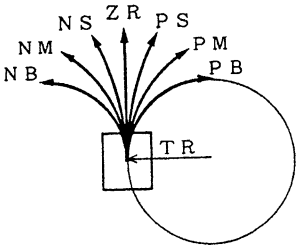
Here, $\bar{D} \in [-1,1]$ is defined by

$$\bar{D} = 2\frac{D_k^r}{D_k^r + D_k^l} - 1; (k=1,2,...,N/2)\ , \tag{4}$$

where M_i, $\bar{\Theta}$ are fuzzy subsets corresponding to the parameter $\bar{D}$ (deviation of distances from robot to obstacles) and turning angle θ_i of the robot. The four rules are shown in Table 1. Figure 1 shows a local workspace in the robot navigation.

Table 1 Rules

θ \ DD	NB	NS	ZR	PS	PB
NB	PB	PB	PM	ZR	ZR
NS	PB	PM	PS	ZR	ZR
ZR	PM	PS	ZR	NS	NM
PS	ZR	ZR	NS	NM	NB
PB	ZR	ZR	NM	NB	NB



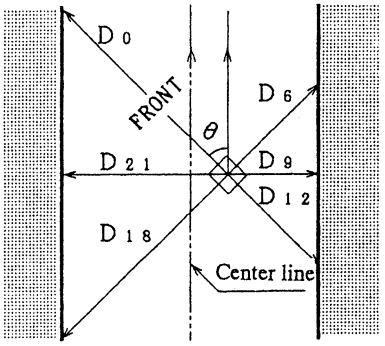


Fig. 1 A local workspace in the robot navigation.

2.2 Fuzzy inference

Let $\mu(\bar{k}_i)$ be the membership function for a subset of the output which is the results of the ith rule. Each linguistic label F_i or M_i is associated with the membership function, $\mu(\bar{k}_i)$ which specifies the degree to which a given input value satisfies the quantifier F_i or M_i. The membership function is convex and normally distributed. Actually, a wide variety of functions have been suggested for use as membership functions, such as triangular and trapezoidal-shaped functions. Here, we employ a bell-shaped membership function, such as

$$\mu(x) = \frac{1}{1 + [(\frac{x-c_i}{a_i}]^{b_i}}\ , \tag{5}$$

where a_i, b_i and c_i are denoted as width, steepness and mean of membership function, respectively.

For each rule base, we use Min-Max operation to perform fuzzy inference. Then, it can be obtained by

$$\mu(\bar{k}_i) = Min(\mu_1, \mu_2, ...\mu_n)\ . \tag{6}$$

From the results of the four rules, the final membership function $\mu(\bar{k}_f)$ can be obtained by using Max operator:

$$\mu(\bar{k}_f) = Max(\mu_1, \mu_2, ...\mu_n)\ . \tag{7}$$

Given a consequent function f_i of input values, the kth output component y_k of the fuzzy system is inferred as follows[2]:

$$y_k = \frac{\Sigma_{j=1}^{N} \mu_j f_j}{\Sigma_{j=1}^{N} \mu_j} \quad . \quad k = 1, ..., p \tag{8}$$

Finally, the center-average method is employed to obtain the final output components, as described in Equation (8).

3 Genetic Operatoration

3.1 Combined method of fuzzy-genetic algorithm

In fuzzy inference, it is important to determine range of the membership function as each rule. However, in many problems, we can not predict the range due to variation of the range. Such as the robot navigation, workspace round the robot often is changed, so that we should also change range of the membership functions. In order to realize the operation, in this paper, a combined method based on genetic algorithm is proposed. Figure 2 shows the combined operation between fuzzy inference and genetic algorithm. Here, four points which separated range of membership function on a output player are defined as the genetic individual. A flow of fuzzy-genetic programming is shown in Fig.3. In the robot navigation, a exploitation based on uniform crossover is used in this paper. After of the crossover operation, all genetic individual are arranged according to them fitness.

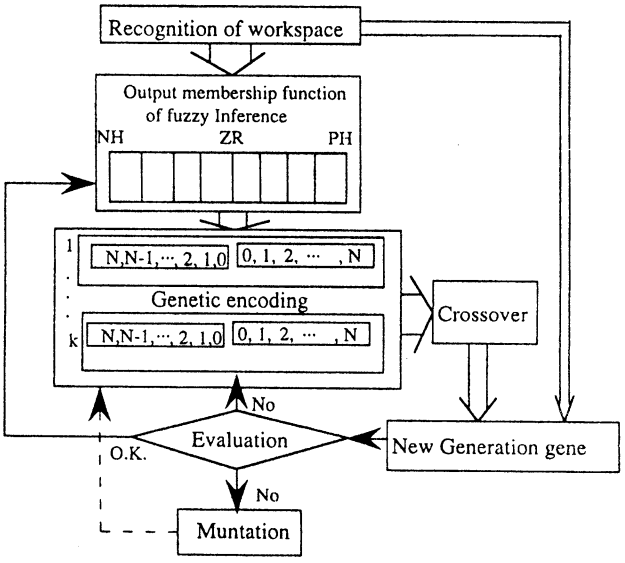


Fig.2 Combined operation of fuzzy-genetic algorithm.

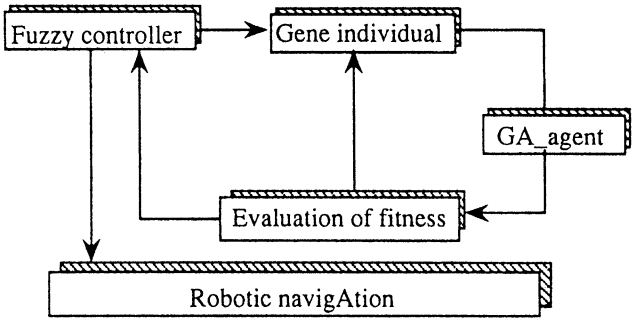


Fig.3 Flow chart of genetic algorithm.

3.2 Evaluation in the robot navigation

In navigation of an autonomous mobile robot, real size of the robot should be considered. In order to determine the fitness of membership function during the robot navigation, a dangerous area round the robot is shown in Fig.4. Here, two pass coefficients of the robot on the right side and left side are defined as follows

$$\gamma^r = \frac{min(D_k^r)}{D_0} \quad and \quad \gamma^l = \frac{min(D_k^l)}{D_0} \quad . \tag{9}$$

When an uniform value γ^r or γ^l of membership function on the right side or left side is shown as follows

$$\bar{\mu}^r = (\Sigma_{i=1}^{N/2-1} \mu_i^r)/(N/2-1) \; ;$$
$$\bar{\mu}^l = (\Sigma_{i=1}^{N/2-1} \mu_i^l)/(N/2-1) \; . \tag{10}$$

Thus the fitness in the robot navigation can be defined as

$$\lambda^r = \frac{1}{\mid \gamma^r - \bar{\mu}^r \mid} \quad and \quad \lambda^l = \frac{1}{\mid \gamma^l - \bar{\mu}^l \mid} \quad . \tag{11}$$

When the fitness is a large value than a evaluated criterion, the local optimization and evaluation should be completed and be turn to the next step of the robot navigation.

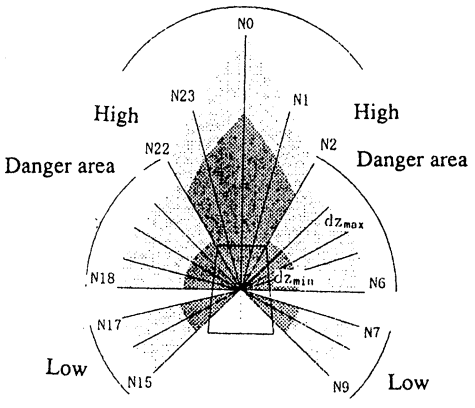


Fig.4 Dangerous area round the robot.

4 Results of Simulation

Our primary objective is to come up with optimal fuzzy membership function. In order to verify the intelligent algorithm, we carry out a sample of simulation for the robot navigation. Two navigation courses with complex workspace map will now be discussed. Both models employ the same genetic parameters: population size=100, evaluted criterion of the fitness = 99. For the model1, the trajectories of autonomous navigation under the crossover operation N=100 and N=300 are shown in Fig.5(a)-(b). Figure 5(c)-(d) shows distribution of the fitness on the increase of generation. Trajectories on the another model of simulation with same conditions to the model 1. are shown in Figure 6(a)-(d).

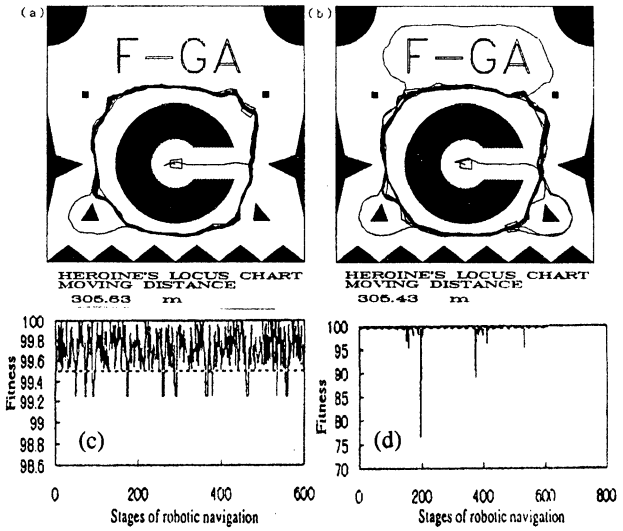


Fig.5 Results of moder 1.

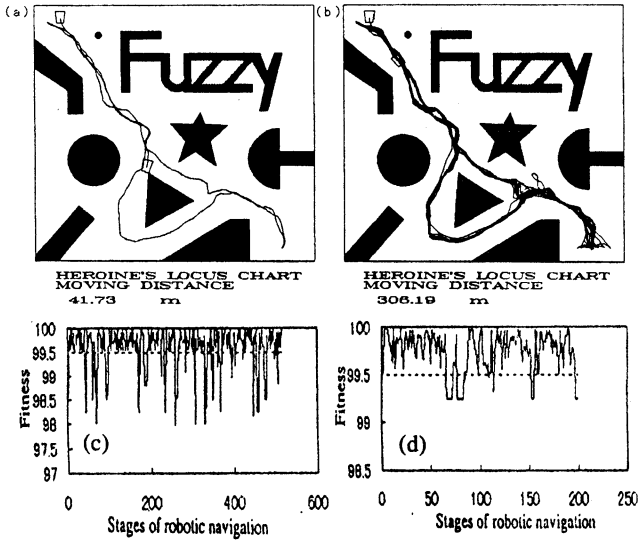


Fig.6 Results of model 2.

From these results, we can know that the robotic navigation with the intelligent algorithm can adapt the change of workspace and the crossover operations also can give out very large effect to the robotic navigation.

5 Summary

We have presented a system of autonomous mobile robot in which imitates intelligent learning. As control tasks of robot become ever more demanding, more intelligent controller are needed. A optimizer method, which combined with fuzzy logic and genetic algorithm, offers a promising technology that supports optimization of the parameters of membership function of fuzzy logic. Our research work developed a new technique for fuzzy inference and GA including a local learning method in robotic navigation. Based on some successful performances of simulation, we know the method can applied to navigation of autonomous mobile robot.

Reference

1. Rodney A. Brooks, "A Robust Layered Control System for a Mobile Robot", IEEE Journal of Robotics and Automation, Vol. RA-2, No. 1, pp.14-23, 1986.

2. T. Takagi and M. Sugeno,"Derivation of fuzzy control rules from human operator's control actions", in Proc. *IFAC Symp.* Fuzzy Information, knowledge Representation and Decision Analysis, July 1983, pp.55-60.

3. Y.F. Li and C.C. Lau, "Application of Fuzzy Control for Servo System, Proc. of IEEE R&A, Vol.3, pp.1511-1519,1988.

4. H.J. Zimmermann, "Fuzzy Set Theory and Its Application, Second, Revised Edition", Kluwer Academic Publisher, 1991.

5. S. Mahadevan and J. Connell, "Automatic Programming of Behavior-based Robots using Reinforcement Learning", Aritifial Intelligence, Vol. 55, pp.311-365, 1991.

6. John H. Holland, Genetic Algorithms, Scientific American, 1992.

7. A. Varsek, T. Urbancic and B. Filipic, "Genetic Algorithms in Controller Design and Tuning", IEEE Transaction on Systems, Man, and Cybernetics, Vol. 23, No.5, pp.1330-1339, 1993.

Proc. of Third Int. Symp. on Artificial Life, and Robotics (AROB III' 98),
Oita, Japan, 19-21, January, 1998,

Kinetic Characteristics of Human Binocular Vision for Wide View Head Mounted Display in Virtual Reality

Jing-Long WU, Lei WANG and Katsutoshi KURIBAYASHI

Department of Mechanical Engineering, Yamaguchi University
Tokiwadai 2557, Ube, Yamaguchi 755, Japan
Email: wu@mechgw.mech.yamaguchi-u.ac.jp

Abstract

In order to design a new type head mounted display (HMD) with wide view, using hardware only is difficult because double images are perceived if a large binocular disparities are set in the peripheral field of the wide view. Hence, the human kinetic characteristic is very important. In this study, an experimental system is produced to measure the kinetic characteristics of binocular stereoacuity, and basing on the experimental results, a method to design a new HMD with wide view is proposed.

1. Introduction

Virtual reality technology has been widely applied in building design, telerobotics, medicine and so on. For example, instead of human body, a virtual body can be used in order to training medical students. The virtual reality operating system is specially effective as a training system of operation because operating by inexpertness is risk. In order to realize a high reality environment, the head mounted display (HMD) is very important to present 3D images for user.

In HMD, the depth information of 3D images is obtained from the binocular disparity as shown in Fig. 1. We can see a stereo view through HMD when a proper disparity between the left-eye and the right-eye images is set (Fig. 1(a)). However, the present HMD systems have a problem that the field of view is too small. In order to design a new type HMD with wide view, if uniform binocular disparity is set (a constant disparity is set in whole view field), double images would be perceived in the peripheral view field even through the stereo images can be perceived in the central view field. This problem of present HMD can be demonstrated by Fig. 1(b). In order to develop a wide view HMD with natural 3D images, we need to investigate the characteristic of human binocular stereoacuity (i.e., the acuity of that the human perceive the binocular depth).

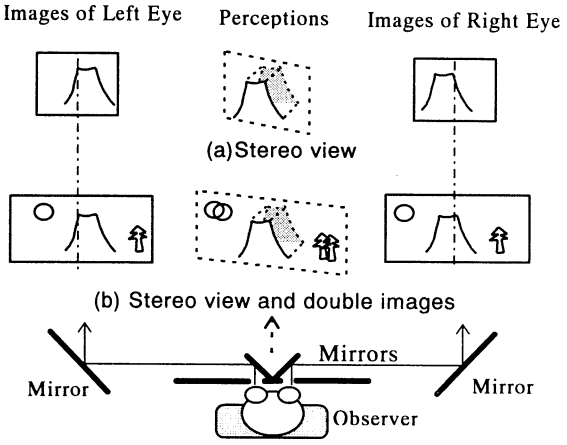


Fig. 1 An example shows that a stereo view based on binocular disparity in HMD. (a), A stereo view is perceived for small field of HMD. (b), A stereo view in the central area and double images in the peripheral area are perceived in wide view HMD.

2. A Wide View HMD

In our previous studies, the static characteristics of binocular stereoacuity were measured [1, 2]. The results are shown in Fig. 2. It means that the human have high stereoacuity in the center of the wide view field, and have low stereoacuity in the peripheral area. That is to say, the human is difficult to perceived the depth information in the peripheral area of the wide view field. Based on this characteristics of the binocular vision, a wide view HMD is designed. The concept of the designed wide view HMD can be explained as shown in Fig. 3.

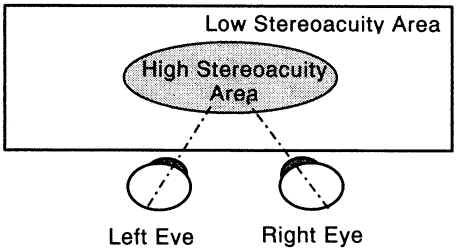


Fig. 2 Static characteristics of binocular stereoacuity

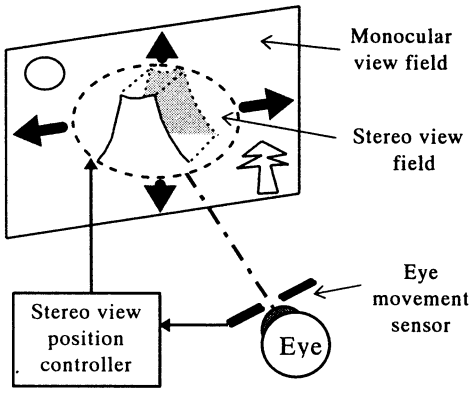


Fig. 3 The concept of wide view HMD

In the center of wide view filed, a narrow stereo images are presented. While in the peripheral view filed, a wide view monocular images are presented. Because human can not perceived the depth information in the peripheral view field. The stereo images of center view can be moved by the stereo view position controller if the observer's eye moved. Therefore, can see a natural wide view images usually. The images in the center view field is a 3D stereo view, in the peripheral view field is a monocular view. As shown in Fig. 3, how to design the size of the stereo view field is a very important problem in order to realize the wide view HMD. In general, both the static images and the dynamic images are usually used in HMD. Therefore, we need to investigate the kinetic characteristics of binocular vision in order to decided the size of the stereo view field. In this paper, a wide view measurement system is developed to measure the kinetic characteristics of binocular vision, and basing on the experimental results, a method to design the size of stereo view field in the wide view HMD system is proposed.

3. Measurement system

In the present paper, a wide view measurement system was produced in order to measure the kinetic characteristics of binocular stereoacuity. As shown in Fig. 4, the measurement system was consisted by a hemi-globe screen, a movable stand, and a control unit.

The hemi-globe screen was used as an uniform background stimulus was of white flooring 750mm in radius. It subtended 190 degrees from the observer's position at the center of the screen arc and was uniformly illuminated by multi-light (halogen lamps) at the all field of the screen, the illuminance of the background was kept at 1200 lx uniformly.

In order to obtain exact results, the eye movement of the observers was monitored by a CCD camera. Therefore, the data only from proper eye-position was utilized. A chain rest and a head fixer was used to stabilize the observer's head, and all observers were able to maintain satisfactory fixation during targets presentation. The observer's response panel consisted of 2 buttons, one of which was used to initiate the targets presentation sequence; the other one was used for observers making their response to the targets.

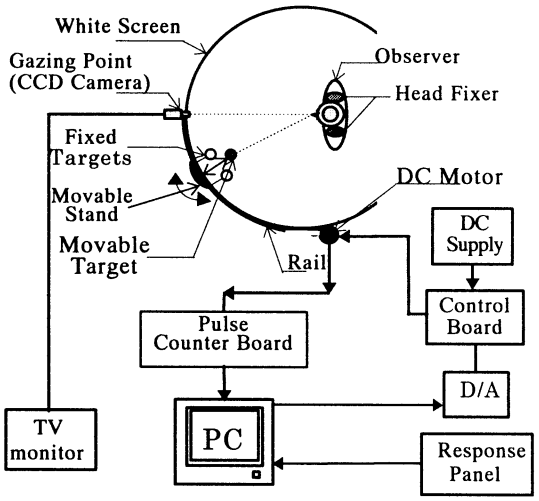


Fig. 4 Schematic diagram of the experimental system to measure the kinetic characteristics of human binocular vision

As shown in Fig. 5, three sphere targets were used to present depth information. They were 6mm in radius, and were painted by mat black. Two outside targets were fixed, and the distance between two outside targets was 60 mm. The depth between the center target and the fixed targets in depth direction could be adjusted from 0 mm to 80 mm by changing the center target. Three targets were fixed on the movable stand. The movable stand motion was controlled by a personal computer (PC) through a servo motor wire unit. Variation of targets angular velocity was obtained using PC through a D/A converter to change the voltage applied to the servo motor. Targets velocity was measured by an encoder of the DC motor through a counter board.

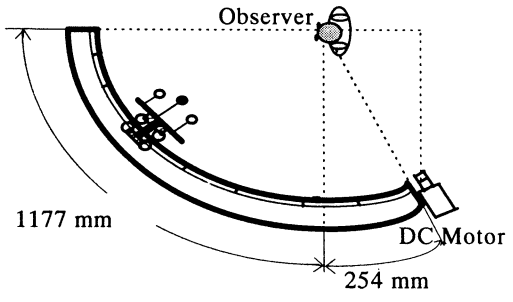


Fig. 5 mechanism of the movable targets

4. Measurement Procedure

The experimental condition is that the observer usually gaze the gazing point(CCD camera), and perceive the movement targets stimulus with peripheral vision(i.e., the targets image is reflected at the periphery of the retain). When the targets are moved along the horizontal meridian from the periphery to the center with variant velocities, if the observer has incompatible sensation between the movable target and the fixed targets, then he/she answers "Yes" using response panel. In this moment, the position (eccentricity angle) of the movement targets is memorized by PC. We define this eccentricity angle as a kinetic binocular stereoacuity. The velocities of the targets are 7 kinds i.e. 1, 2, 3, 5, 10, 15 and 25 deg/sec. The depths of targets is set at 80 mm in depth direction. In one session, 7 kinds (for one observer is 6 kinds) of velocities were presented in a random order. This entire procedure was repeated three times for each observer. Two graduate students were served as observers in this experiment. The measurement procedure is summarized as follows:

(1) ***Set-up procedure***: The observer was seated at the center of the screen arc with his head in a headrest as shown in Fig. 4. The observer was instructed to fixate a gazing point (CCD camera) straight ahead of him and was specifically instructed that no eye movements were to be made during the targets exposure. All observers were able to maintain satisfactory fixation during targets presentation by using the chin rest and the head fixer.

(2) ***Light Adaptation***: The observers adapt to the illuminance condition for five minutes .

(3) ***Measurement***: Targets angular velocity and depth were set in a random order by PC to prevent the observers from anticipating the next depth. The observers paced the experiment, initiating targets presentation and making his response when they detect any difference between the movable target and the fixed targets.

5. Measurement Results

The results of two observers are shown in Figs. 6 and 7, respectively. The Figs. (a) and (b) show the results of that the targets are moved from the left side to center and from the right side to center, respectively. Each datum point is the average of nine measurements for one observer. The vertical bars indicate one standard error. The ordinate shows the kinetic binocular stereoacuity in eccentricity angle. The abscissa shows the angular velocity of the movement targets. As shown in Figs. 6 and 7, there is a large kinetic binocular stereoacuity when the targets are moved with that the velocity is about 3 degree/sec. It means that the depths of the targets can be perceived easily if the targets with velocity about 3 degree/sec. As the angular velocity of the targets increases from 3 to 25 degree/sec or decreases from 3 to 1 degree/sec, the kinetic binocular stereoacuity radically decreases. Therefore, perception of the depth of movable targets is difficult if the velocity of the targets is higher than about 3 degree/sec or slower than it.

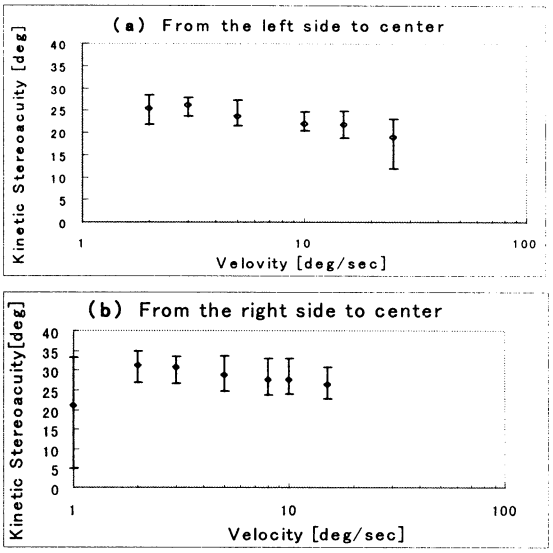


Fig. 6 The kinetic binocular stereoacuity as a function of the angular velocity of the movement targets for observer MW

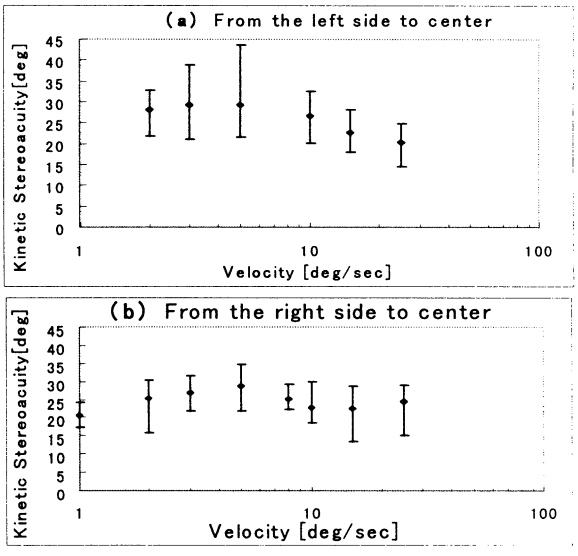


Fig. 7 The kinetic binocular stereoacuity as a function of the angular velocity of the movement targets for observer MZ

6. Discussion

The experimental average results of two observers are shown in Fig. 8. As shown in Fig. 8(b), the kinetic stereoacuity has a maximum value 30 degrees at that the velocity of the movement targets is about 2 degree/sec. This results are similar to the results of previous study on the kinetic monocular acuity[3]. In the left side, the kinetic stereoacuity can not measured at that the velocity is 1 degree/sec. Considering the psychological knowledge, the kinetic stereoacuity will be changed in continuous manner. The results between 1 and 2 degree/sec can be expected by a dashed line as shown in Fig. 8(a).

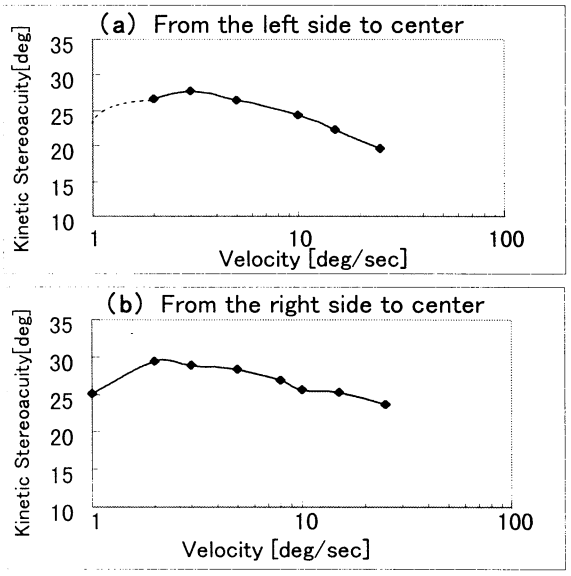


Fig. 8 Experimental results of average of two observers. It is replotted from Figs. 6 and 7.

In order to investigate the detail, the experimental results of Fig. 8 can be explained by Fig. 9. The horizontal axis shows the kinetic stereoacuity in eccentricity angle, the positive and negative signs show the right side and the left side of the view field, respectively. The vertical axis shows the velocity of the movement targets. The origin of coordinates is defined as the central position of the view field (this position is reflected to the fovea of the retain). From the results of Fig. 9, it can be seen that the human perceive movement stereo targets easily with a suitable velocity. In the right(left) side of the view field, if the velocity of the movement target is about 2(3) degree/sec, the human has maximum kinetic stereoacuity 30(28) degrees. The unsymmetrized characteristic of the kinetic stereoacuity at the left side and the right side is similar to the static stereoacuity[2]. The experimental results suggest that in the wide view HMD the size of the stereo view field is not need to set larger than about 30 degrees. Because if the peripheral angle is larger than 30 degrees, human can not perceive the stereo images clearly.

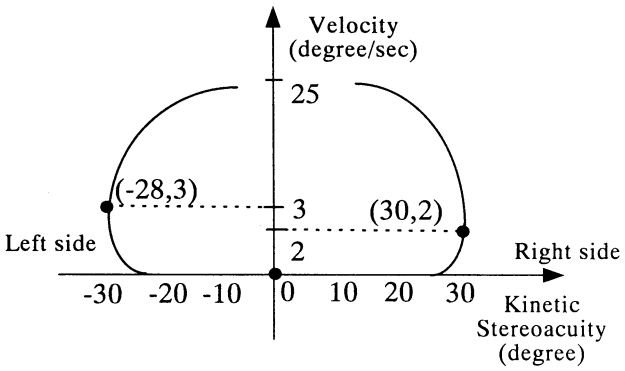


Fig. 9 Kinetic binocular stereoacuity as a function of the velocity of movement stimulus

7. Conclusion

In order to design the size of the stereo view field in a wide view HMD, the human kinetic characteristics are need to measure. In this study, we have developed an experimental system to measure the kinetic binocular stereoacuity. By using this system, the kinetic binocular stereoacuity has been measured. The measurement results suggested that the human kinetic binocular stereoacuity has a maximum value. It is about 30 degree. That is to say, if the present position of the movement stereo images is larger than 30 degrees of the eccentricity angle or smaller than it, we can not perceive the stereo images clearly. Based on the experimental results, we can concluded that the size of the stereo view field in the wide view HMD is not need to set larger than 30 degrees.

References

[1] Jing-Long Wu, Masaomi Nakahata, Sadao Kawamura: "A New Head Mounted Display System with Adjustable Disparity for High Depth-Performance." Proc. of *IEEE International Conference on Systems, Man and Cybernetics.* **Vol. 1**, pp. 298/303 (1995)

[2] Jing-Long Wu, M. Nakahata, S. Kawamura, I.Nishikawa and H. Tokumaru, "Measurement of Binocular Stereoacuity for Design of Head Mounted Display System with Wide View." *IEEE International Conference of Systems, Man and Cybernetics.* **Vol. 2**, pp. 929-934 (1996)

[3] Brian Brown, "Resolution Thresholds for Moving Targets at Fovea and in the Peripheral Retina", *Vision Res.* **Vol. 12**, pp. 293/304(1972)

Proc. of Third Int. Symp. on Artificial Life, and Robotics (AROB III' 98),
Oita, Japan, 19-21, January, 1998,

Measurement of Human Visual and Auditory Characteristics for A Virtual Driving System

Jing-Long Wu, Hiroaki Mizuhara and Yoshikazu Nishikawa*

Department of Mechanical Engineering, Yamaguchi University
Tokiwadai 2557, Ube, Yamaguchi 755, Japan
Email: wu@mechgw.mech.yamaguchi-u.ac.jp
*Faculty of Information Sciences, Osaka Institute of Technology
Kitayama 1-79-1, Hirakata 473, Japan

Abstract

Recently, the cause of many car accidents is to use car-phone while driving. In order to investigate the cause, human visual and auditory characteristics are measured. The measurement results suggest that if the visual and the auditory stimuli are presented concurrently, the visual reaction time is longer than that the case of the visual stimulus is presented only. Namely, the human visual perception is affected by the auditory information. Based on the experimental results, a virtual driving system is designed. Using it, we can experience the danger of the automobile traffic accidents to promote safe driving.

1. Introduction

How to reduce the automobile traffic accidents is a very important social problem. Recently, the cause of many car accidents is to use the car-phone while driving[1]. Therefore, we need a virtual driving system to experience the danger of the automobile traffic accidents for safe driving. In general, it is difficult to develop a virtual driving system to promote safe driving. On the other hand, in our previous studies, the human information processing has interactive characteristics between the visual and the tactile perception[2]. If we assume that the visual information processing is affected by the auditory information. The cause of the accidents is that if the driver concentrates his attention on the car-phone, the visual information is misperceived. So the driver will meet with the traffic accident.

In order to evidence the hypothesis, there is need to measure the interactive characteristics between the human visual and the auditory perception. Considering the condition of to use car-phone while driving, the tasks of the visual search and the speech perception are focused on the visual and the auditory experiments, respectively, and the visual or/and the auditory characteristics are measured. The experimental results suggest that the visual perception is affected by the auditory information. Based on the experimental results, a virtual driving system is designed.

2. Experiment of Visual Characteristic

2.1 Experimental System

A proposed experimental system is shown in Fig. 1. The visual stimuli were generated by an image maker (IM-9800M), and were presented by the image maker and an image animator (AD-981) for the left and the right eyes of the subjects through two RGB monitors (SONY-PVM1440), respectively. The stimuli of the left and the right eyes could controlled by a personal computer (NEC PC-9821) independently. The subject could see a stereo view by using a mirror stereoscope.

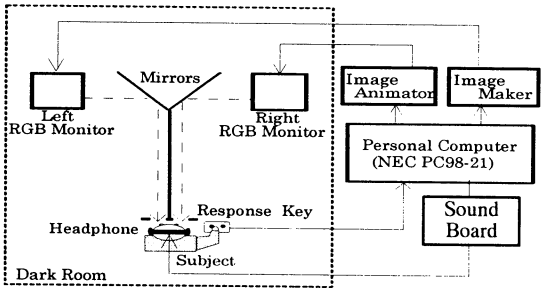


Fig. 1 Schematic diagram of experimental system

2.2 Experimental Method

The visual experimental stimuli were shown in Fig. 2. The left and the right stimuli were independently presented for the left and the right eyes of the subjects, respectively. Then, the stimuli could be perceived as fusion images. The frame size of the stimuli was 4.5°×10°. Dark markers of cross (0.4°×0.4°) were used as gazing points to aid fusion. The kinds of the stimulus were set at 1 target (presented at center in frame), 9 targets (3 rows), 15 targets (5 rows) or 21 targets (7 rows). The size of the targets was set at 0.5°×0.5°. The spacing of the targets was set at 1°×1°.

The visual experimental task was to search only one difference of the characteristic in any targets[3]. The time of searching was measured. This time was defined as the visual reaction time. The time chart of the measurement was shown in Fig. 3. The subject was required to find a target that was distinguished by an unique feature, and as soon as finding the target, to press the response key to indicate whether the target was to be or not. In the visual experiments, two kinds of the targets were used to measure the reaction time. In Experiment 1, the targets had same form (square), but they were deferent color with red (indicated by black square) or blue (indicated by gray square) as shown in Fig. 2(a). Experiment 1 was called "color" experiment. In Experiment 2, the targets had same form (arrow) and same color(blue), but they were set at

deferent directions (up versus down) as shown in Fig. 2(b). Experiment 2 was called "motion" experiment.

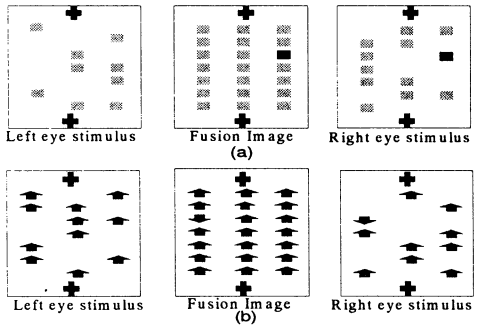


Fig. 2 The visual stimuli: (a) for color experiment; (b) for motion experiment.



Fig.3 The time chart of the visual measurement

Three senior students were served as subjects for all experiment. The conditions of three subjects were shown in Table 1.

Table 1 Subjects Conditions

Subject	Age	Sex	Visual Acuity	Dominant Eye
H.M	22	male	R:1.2, L:1.2	Right
K.K	22	male	R:1.0, L:1.0	Right
T.M	23	male	R:1.2, L:0.5	Right

2.3 Results and Discussion

The experimental results of the color and the motion are shown in Fig. 4. The horizontal and the vertical axes show the visual numbers of the targets and the visual reaction time, respectively. Each datum point is the average of sixty measurements for one subject, and the vertical bars indicate the standard deviations. From Fig. 4, it can be seen that the reaction times of the motion

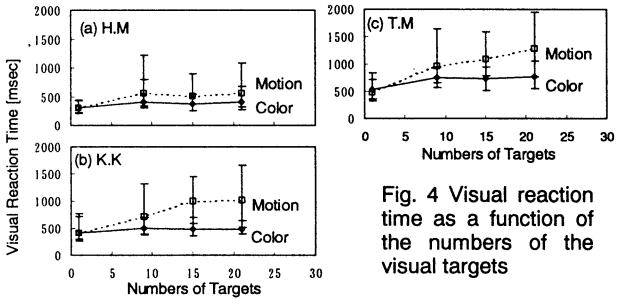


Fig. 4 Visual reaction time as a function of the numbers of the visual targets

experiment increase as the numbers of the visual targets increase from small to large. In the color experiment, the reaction time is 21 ~ 45 msec in all subjects, there are not remarkable changes. These result coincided with 'pop out' which is defined as no rise of reaction time with increased the numbers of targets in case of the only feature differed from any targets[4]. In the motion experiment, an alteration of reaction time is 48 ~ 316 msec in all subjects. These alteration is higher than the color experiment. The experimental results mean that human found the motion task to be more difficult than the color task.

3. Experiment of Auditory Characteristic

The auditory experimental system was similar to the visual experiment as shown in Fig. 1. The auditory stimuli were generated by the personal computer with a sound board (Sound Blaster Edutainment 16), and were presented to subjects through a headphone (VICTOR HP-S35). The subjects used response key to reply for these stimuli. All of these experiments were done in the quiet dark room as shown in Fig. 1.

3.1 Experimental Method

The auditory experimental task was to answer the mental arithmetic problems of addition. For example, when a speech *"one plus one equal three"*(in Japanese) was presented to subject through the headphone, the subject was required to judge this problem is right or no with using the response key to indicate his/her answer "Yes" or "No". The time of answering was measured. This time was defined as the auditory reaction time. As auditory stimuli, the kinds of the mental arithmetic problems could be expressed by the following equations:

$$A + B =, > or < C \quad (1)$$

$$A = a_2 10^2 + a_1 10^1 + a_0 10^0 \quad (2)$$

$$B = b_2 10^2 + b_1 10^1 + b_0 10^0 \quad (3)$$

Namely, the auditory stimuli were presented by the speech "*A* plus *B* equal *C* ". Variables $a_2 \sim a_0$ and $b_2 \sim b_0$ were set at 0 ~ 9. However, the speeches of that three figures plus three figures and three figures plus two figures could not presented in this paper. Because they were too difficult for mental arithmetic. *C* was a random numeral, but it was smaller than three figures. The time chart of the measurement was shown in Fig. 5.

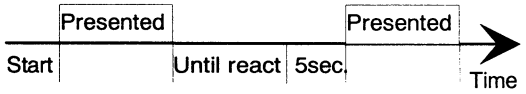


Fig. 5 The time chart of the auditory measurement

3.2 Results and Discussion

The experimental results of three subjects are shown in Fig. 6. The horizontal and the vertical axes show the difficulty of auditory stimuli (DAS) and the auditory reaction time, respectively. We define $DAS\ (n_2, n_1, n_0, l, m)$ as following equation:

$$DAS\ (n_{a2}, n_{a1}, n_{a0}, n_{b2}, n_{b1}, n_{b0}, l, m) = \{(\alpha n_{2a} + \beta n_{1a} + \gamma n_{0a}) + (\alpha n_{2b} + \beta n_{1b} + \gamma n_{0b})\}(\xi m + 1) + \zeta l \quad (4)$$

Where, variables $n_{a2} \sim n_{a0}$ and $n_{b2} \sim n_{b0}$ are either 1 or 0, if $a_2 \sim a_0$ and $b_2 \sim b_0$ (in equation(1)) are set at not zero or zero, respectively. l is a parameter of advance concerned with the double figures. If it is to be, l is substituted 1.

Conversely, l is 0. m is similar to l, it indicates an advance of the single figures.

Coefficients α, β, γ, ξ and ζ are chosen so as to minimize the difference between the experimental results and the calculating results. They are decided as α =5.32, β =4.46, γ =2.63, ξ =-0.14 and ζ =1.10, respectively.

In Fig. 6, each datum point is the average of thirty measurements for one subject, and the vertical bars indicate the standard deviations. The solid lines show the approximate calculating results. From Fig. 6, it can be seen that the auditory reaction times increase as the DAS increase.

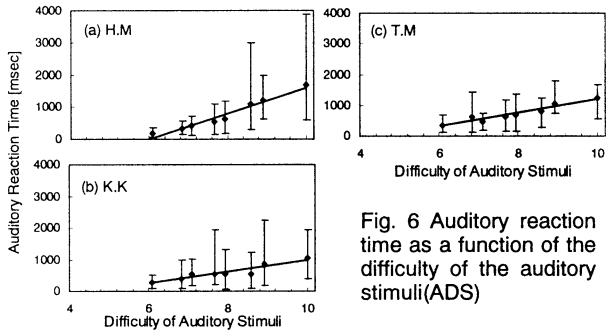


Fig. 6 Auditory reaction time as a function of the difficulty of the auditory stimuli(ADS)

4. Experiment of visual and auditory characteristics

4.1 Experimental Method

In the experiment of the visual and the auditory, the visual stimuli(Fig. 2) and the auditory stimuli(explained in Section 3.1) were presented to the subjects concurrently. The tasks of the visual and the auditory were same to their independent experiments. The time chart of the measurement was shown in Fig. 7. The visual stimulus was presented at the moment of the presentation of the auditory speech was finished. The subjects were required to judge both the visual and the auditory stimuli using two response buttons with his/her left and right hands, respectively. The experimental kinds were summarized in Table 2.

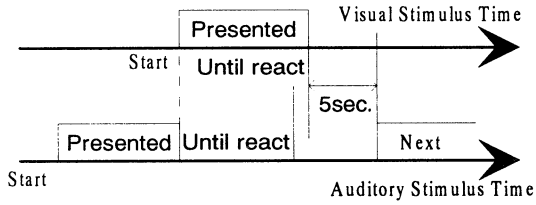


Fig. 7 Time chart of the visual and auditory measurement

Table 2 Experimental kinds

Experimental Kind	Visual stimulus	Auditory Stimulus (DAS)
(1)	Color	6
(2)	Color	8.92
(3)	Color	10
(4)	Motion	6
(5)	Motion	8.92
(6)	Motion	10

4.2 Results and Discussion

Six kinds experimental results of subject H.M are shown in Figs. 8(1) ~ (6). The horizontal and the vertical axes show the numbers of the visual targets and the reaction time, respectively. From Fig. 8, it can be seen that the visual reaction time(solid lines) is longer than the auditory reaction time(dashed lines) in all experiments. The experimental results of the subject K.K and T.M are similar to Fig. 8.

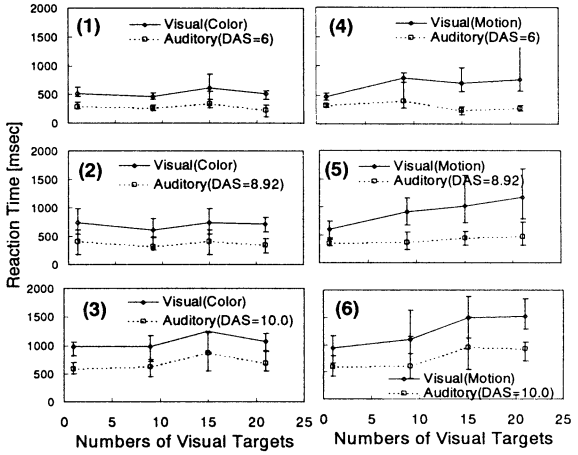


Fig. 8 Reaction time as a function of the numbers of visual targets and the DAS for subject H.M

The difference between the visual reaction time and the auditory reaction time can be plotted in Fig. 9 for three subjects. The horizontal and the vertical axes show DAS and the reaction time, respectively. Figs. 9(a) and (b) show the results of that the visual stimuli are color and motion, respectively. The results of three subjects show that the visual reaction time are longer than the auditory reaction time about 250 ~ 530 msec.

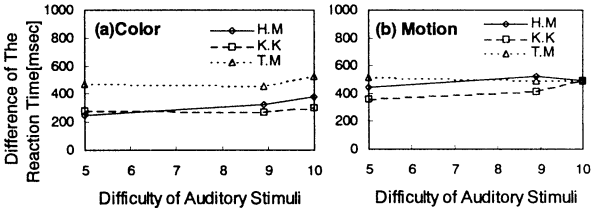


Fig. 9 Difference of the reaction time between the visual and the auditory tasks

5. General Discussion

In order to investigate the cause of car accidents of that the driver to use the car-phone while driving, the difference of the reaction tiem between the visual separate experiment and the visual and the auditory concurrent experiment is a key point. Figure 10 shows the visual reaction time of the visual separate experiment and the visual and the auditory concurrent experiment for subject H.M, it is replotted from Fig. 4(a) and Figs. 8(1)~(3). The horizontal and the vertical axes show the numbers of the visual targets and the visual reaction time, respectively. The solid circle symbols(●) show the results

of the visual separate experiment. The symbols □, △ and ×show the results of the visual and the auditory concurrent experiment, and DAS of the auditory stimuli are 6, 8.92 and 10, respectively. From Fig. 10, it can be seen that the visual reaction time is increased as the DAS increase. That is to say, if the visual and the auditory stimuli are presented concurrently, the time of that the human perceived the visual stimuli is longer than that the case of the visual stimuli are presented only.

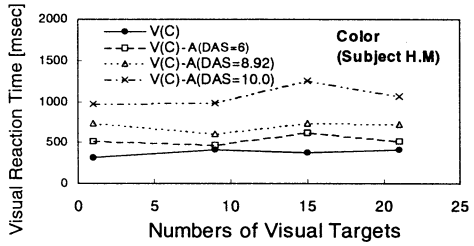


Fig. 10 The comparison of the reaction time of the visual separate experiment and the visual and auditory concurrent experiment for subject H.M.

In order to investigate the detail of that the auditory information is how to affect the visual perception, the ratios of the visual reaction time of the Visual and the Auditory concurrent experiment to the visual reaction time of the Visual only experiment(VA/V) are calculated in Fig. 11 for three subjects. The horizontal and the vertical axes show DAS and RV/A in percentage, respectively. From Fig. 11, it can be seen that the visual reaction time is increased about 50%~180% for subject H.M when the visual and the auditory stimuli are presented concurrently. The increases of subjects K.K and T.T are about 25%~70% and 40%~50% as DAS increase from 6 to 10, respectively. This results suggested that the human visual perception is affected by the speeches. Therefore, to use car-phone while driving is danger, especially the driver talks about difficult speeches with some one.

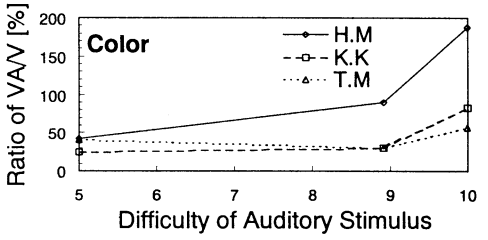


Fig. 11 The ratio of the visual reaction time of the Visual and the Auditory concurrent experiment to the visual reaction time of the Visual only experiment(VA/V)

6. Design a Virtual Driving System

Based on above experimental results, a virtual driving system is designed. The concept of the designed virtual driving system is illustrated in Fig. 12. 3D images of the virtual world are presented to a driver through a head mounted display (HMD). At the same time, the auditory information is presented by a virtual speaker. In the designed virtual driving system, HMD system is proposed by our previous study[5], the auditory information can be generated by a personal computer through a sound board.

Using the virtual driving system, the driver driving a car and talking with a virtual speaker concurrently. The difficulties of the visual images and the speches can be changed by the personal computer based on obtained human experimental results. If the virtual speaker talking about difficult speeches with the driver, he/she may has misperception of the visual information. So the driver will meet with the traffic accident in the virtual world. Therefore, we can experience the danger of the automobile traffic accidents to promote safe driving.

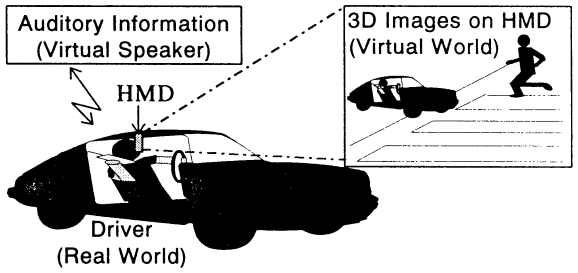


Fig. 12 The concept of a virtual driving system

7. Conclusion

In order to investigate the cause of car accidents of that the driver using a car-phone while driving, we have been measured the human visual and the auditory characteristics. The experimental results suggested that the visual reaction time of that the visual and the auditory stimuli are concurrent presented, is longer than that the case of the visual stimuli are presented only. Namely, the human visual perception is affected by the speeches. Based on the experimental results, a virtual driving system has been designed. Using it, we can experience the danger of the automobile traffic accidents to promote safe driving.

Acknowledgments

We would like to express our gratitude to President Yuji Hayashi of Oriental Electronics, Inc. for his useful help in developing the experimental system. The authors are also grateful to Mr. Masayuki Kitazawa for his help in the programming of the experiments.

References

[1] D. Redelmeier and J. Tibshirani, "Association between Cellular-Telephone Calls and Motor Vehicle Collisions", *The New England Journal of Medicine*, **Vol.336**, No.7, pp.453-458(1997)

[2] Jing-Long Wu, S .morita and S. Kawamura, "Human Sensory Fusion on Visual and Tactile Sensing for Virtual Reality", *IEEE International Conference on Robotics and Automation*, **Vol.2**, pp.2365-2370(1996)

[3] A. Treisman, "Features and Objectsin Visual Processing", *Scientific America*, Vol.254, No.11, pp.114-124(1986)

[4] K. Yokosawa and T. Kumada, "Visual Search-Phenomena and Processes(in Japanese)", *Cognitive Science*, **Vol.3**, No.4, pp.119-138(1996)

[5] Jing-Long Wu, M. Nakahata and S. Kawamura, "A New Head Mounted Display System with Adjustable Disparity for High Depth-Performance", *IEEE International Conference on Systems, Man and Cybernetics*, **Vol. 1**, pp.298-303,(1995)

Proc. of Third Int. Symp. on Artificial Life, and Robotics (AROB Ⅲ' 98),
Oita, Japan, 19-21, January, 1998,

Human Visual and Haptic Characteristics on Distance Perception for Virtual Teleoperation Systems

Jing-Long WU and Toshio MIYAKE

Department of Mechanical Engineering, Yamaguchi University
Tokiwadai 2557, Ube, Yamaguchi 755, Japan
Email: wu@mechgw.mech.yamaguchi-u.ac.jp

Abstract

In order to realize a virtual operation system with high reality-performance, the haptic information is very important. Unfortunately, it is very difficult to realize a device to display the haptic information. Because the spatial scale of the virtual world is different from the real world in the teleoperation system. On the other hand, human have illusory characteristics on the visual and the haptic perception. If we make good use the human characteristics, a haptic device may be simplified. From such motivation, human visual and haptic characteristics on distance perception are measured. From the measurement results, some important points are suggested to design a haptic device for virtual operation systems.

Key words: *Human visual and haptic perception, Teleoperation system, Virtual reality.*

1. Introduction

Up to now, virtual reality has been mainly developed for visual applications[1~3]. However, in many cases the haptic information is important as well as the visual information. As shown in Fig. 1, in the virtual world, the haptic information is very important in order to operate a teleoperator. Unfortunately, it is very difficult to realize a device to display the haptic information. Because the spatial scale of the real world is different from the virtual world.

On the other hand, in the psychological studies, human perceptions have illusory characteristics[3]. Namely, human perceptive quantity on distance perception is different from the actual quantity. Therefore, we can recognize distance through visual and haptic sensation, even if exact distance information is not presented. Hence, by utilizing human characteristics, to realize a haptic device can be simplified.

From such motivation, a measurement system is developed, and the human visual and haptic characteristics on distance perception are measured. The results of experiments suggest how we should to design a haptic device for virtual teleoperation systems.

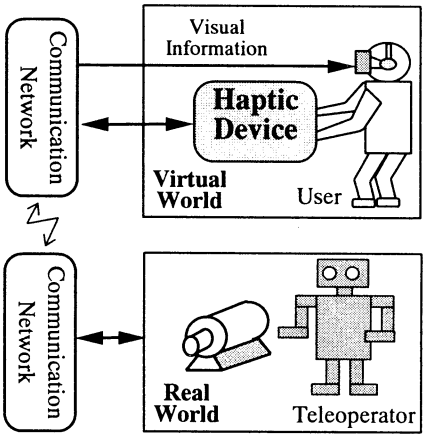


Fig. 1 An example of virtual teleoperation system

2. Visual and Haptic Characteristics

2.1 Experimental Apparatus

In order to measure the characteristics of the visual and the haptic spatial distance perception, an experimental system was developed as shown in Fig. 2. The tactile information were presented by two movable touch targets for the left and the right hands, respectively, they could be moved in depth direction by a personal computer though control drivers and DC motors. The actual distances between the subject and the movable touch targets are measured by a distance sensor, and they could be measured by an arm angles sensors.

Two arms (left and right) angles sensors were proposed. The concept of the arm angles sensor was explained as shown in Fig. 3. X was defined as the actual distance between the center line of the subject and the tips of the fingers. A, B and C shown the lengths from the shoulder joint to the elbow joint, from the elbow joint to the wrist joint and from the wrist joint to the tips of the fingers, respectively. They were made of three aluminum frames, their length could be changed in order to suit several subject. The angles α, β and γ were defined as shown in Fig. 3. They were measured by three general angle sensors. In the experiments, two proposed arm angles sensors were worn on the left and the right arms of the

subject, respectively (Fig. 4). Then, the distance X was calculated as follow equation:

$$X = A\sin(\alpha) + B\sin(\beta - \alpha) - C\sin(-\alpha + \beta + \gamma) \quad (1)$$

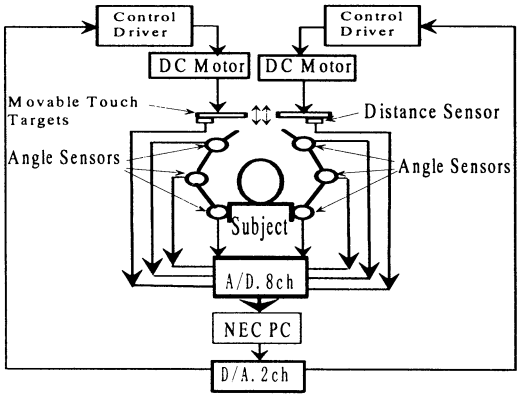


Fig. 2 Geometric diagram of experimental system to measure the human visual and haptic characteristics

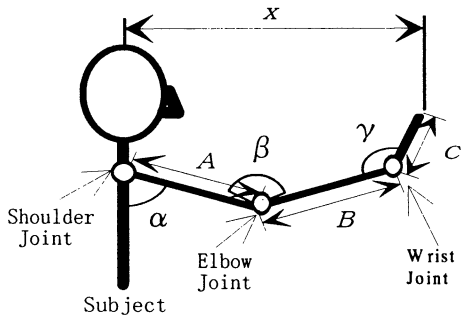


Fig. 3 The concept of the arm angles sensor

2.2 Method of Experiments

In four experiments, the subject was required to stretch his/her two arms to present (or perceive) a distance. The subject's two arms were concurrently stretched in the horizontal plane and with a right angle of the frontal plane. The actual distance and the human perceptive distance were measured concurrently. The experimental kinds were summarized in Table 1.

Table 1 Experimental kinds

Experiment No.	Using Touch	Using Vision
1	No	No
2	No	Yes
3	Yes	No
4	Yes	Yes

In Experiment 1, the subject was required to stretch his/her arm in order to present some distance without the visual and the tactile information. The experimental condition was shown in Fig. 4. Two arm angles sensors were worn on the left and the right arms of the subject, and his eyes were hidden by a black band. The subject was required to present the distance 10, 20, 30, 40 or 50cm in a random order. For example, if "*please present 30 cm*" was required the subject stretched his/her arms of the left and the right to present this distance. In this case, the haptic perceptive distance X was measured by the arm angles sensors (calculated by equation 1), the actual distance was the required 30 cm.

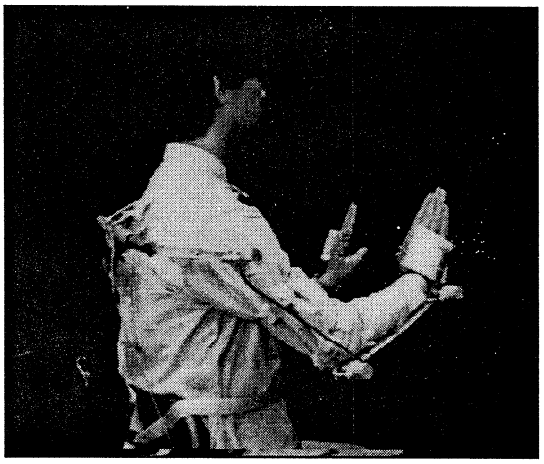


Fig. 4 Overview of the experiments to measure the human visual and haptic characteristics

Experiment 2 was similar to Experiment 1, but in order to present a required distance, the subject could use vision.

In Experiment 3, when a distance (10, 20, 30, 40 or 50cm) was set by a tactile target (black plywood) in a random order, the subject was required to answer his/her perceptive distance with touch but without vision. Namely, the subject stretched his/her two arms to touch the set tactile target with his/her finger tips, and answered his/her perceptive distance between himself and the tactile target.

Experiment 4 was similar to Experiment 3, but in order to answer a set distance, the subject used the touch and the vision concurrently.

2.3 Subjects

Four senior students were served as subjects for all experiments. The conditions of four subjects were summarized in Table 2.

Table 2 Subjects Conditions

Sub.	Arm	*A*	*B*	*C*	DA	Visual Acuity		DE
HM	Right	26.5	27.1	17.7	Right	Left	Right	Right
	Left	26	27	18		0.6	0.7	
HS	Right	27	27.3	17.7	Right	0.7	0.7	Left
	Left	26.8	27.4	18				
YS	Right	27.6	26.1	17.8	Right	1.5	1.2	Right
	Left	27.7	26.3	17.4				
HK	Right	26.9	26.9	17.8	Right	0.7	0.7	Left
	Left	27	26.7	16.6				

Sub.: Subject, ***A***, ***B*** and ***C*** were shown in equation (1), all units were the centimeter, **DA**: Dominant Arm, **DE**: Dominant Eye.

2.4 Results and Discussion

2.4.1 Experiments 1 and 2

The results of Experiments 1 and 2 of subject YS are shown in Fig. 5(a). The horizontal and the vertical axes show the actual distance and the perceptive distance, respectively. Each datum point is the average of fifteen measurements for one subject, and the vertical bars indicate the standard deviations. The symbols ▲ and △ show the perceptive distance of the left and the right arms in Experiment 1 (without visual and tactile information), respectively. The symbols ● and ○ show the perceptive distance of the left and the right arms in Experiment 2 (without tactile information but using vision), respectively.

The differences between the perceptive and the actual distances of the Experiments 1 and 2 are plotted as shown in Fig. 5(b). It can be seen that the perceptive distances are smaller than the actual distance (indicated by negative sign). The difference increases as the actual distance increases. As shown in Fig. 5(b), the absolute differences of the right arm (△ and ○) are smaller than the left arm's results(▲ and ●). However, there is not remarkable differences between Experiments 1 and 2. Such characteristics of the results of subjects HM, HS and HK are similar to Fig. 5.

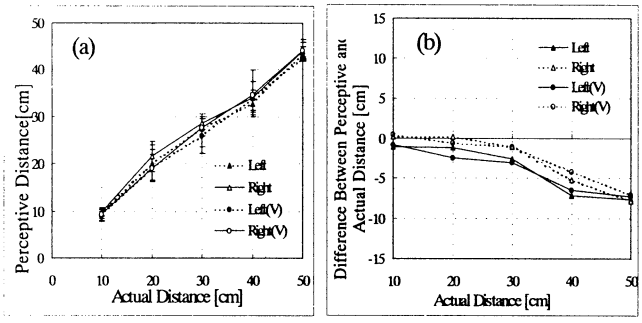


Fig. 5 (a) The results of Experiments 1 and 2 of the distance perception for subject YS; (b) The differences between the perceptive distance and the actual distance as a function of the actual distance are replotted from (a).

2.4.2 Experiments 3 and 4

The results of Experiments 3 and 4 of subject YS are shown in Fig. 6(a). The horizontal and the vertical axes show the actual distance and the perceptive distance, respectively. Each datum point is the average of fifteen measurements for one subject, and the vertical bars indicate the standard deviations. The symbols ◆ and □ show the perceptive distances of Experiment 3 (with touch but without vision) and Experiment 4 (with touch and vision), respectively.

The differences between the perceptive and the actual distance of the Experiments 3 and 4 are plotted as shown in Fig. 6(b). It can be seen that the perceptive distances are larger than the actual distance (indicated by positive sign). The difference increases as the actual distance increases. As shown in Fig. 6(b), the absolute differences of the Experiment 4 (□) are smaller than the results of Experiment 3 (◆). Such characteristics of the results of subjects HM, HS and HK are similar to Fig. 6 .

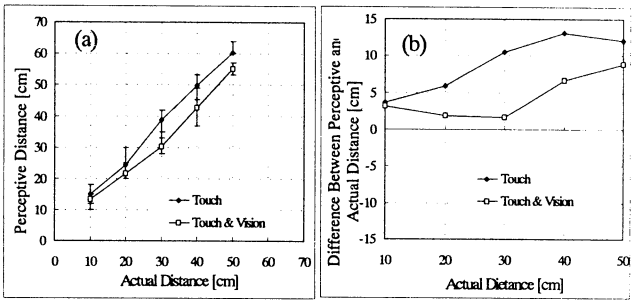


Fig. 6 (a) The results of Experiments 3 and 4 of the distance perception for subject YS; (b) The differences between the perceptive distance and the actual distance as a function of the actual distance are replotted from (a).

3. General Discussion

In order to investigate the detail of the human distance perceptive characteristics, the differences between the perceptive and the actual distances of Experiments 1(△ and ▲) and 3(◆), and Experiments 2(○ and ●) and 4 (□) are shown in Figs. 7(a) and (b), respectively. In all experiments, the difference increases as the actual distance increases, and it can be seen that the perceptive distances are smaller(larger) than the actual distance of Experiments 1 and 2 (Experiments 3 and 4). Furthermore, the Ratios of the differences between the Perceptive distances to the Actual distance(*RPA*) are calculated as shown in Table 3. Each datum is the average of five measurement points (10, 20, 30, 40 and 50 cm) for one subject, and the average of four subjects are calculated as shown at the last line in Table 3. The ratios are shown in percentage, the positive (negative) signs show that the perceptive distance is larger (smaller) than the actual distance.

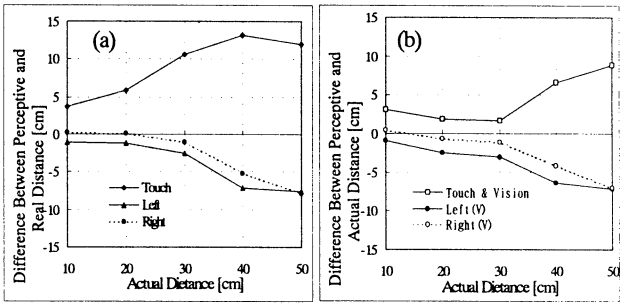


Fig. 7 The differences between the perceptive distance and the actual distance as a function of the actual distance are replotted from Figs. 5(a) and 6(a).

Based on the experimental results and above discussions, the human visual and tactile distance perceptive characteristics are summarized as following:

(1) *Human perceptive distances are overestimated or underestimated when with using touch or touch is not used, respectively.*

As shown in Fig. 6 and Table 3 (Exps. 3 and 4), with using touch (Experiments 3 and 4) the perceptive distance is larger than the actual distance (*RPA* > *0*). While, the distance is underestimated (*RPA* < *0*) if touch is not used as shown in Fig. 5 and Table 3 (Exps. 1 and 2).

(2) ***Right arm has high distance perceptive sensitivity.***

As shown in Table 3 (Exps. 1 and 2), the difference ratios (*RPA*) of the right arm are smaller than the left arm for all subjects. The results may can be explained by that the dominant arm has high sensitivity. Because the dominant arms of four subjects are the right arms as shown in Table 1.

(3) ***The distance perceptive sensitivity is advanced by using vision if touch is used, however there is not remarkable effects in the cases of without touch.***

As shown in Fig. 6 and Table 3, with using the vision and the touch, the differences of the perceptive and the actual distances (Exp. 4, *RPA*=8.2%) are smaller than the cases of without vision (Exp. 3, *RPA*= 18.9%). However, *RPA* have not remarkable difference between the Experiments 1 (without vision) and 2 (with vision) as shown in Table 3.

Table 3 The Ratio of the differences between the Perceptive and the actual distance to the Actual distance (*RPA*) in percentage [%]

RPA Exp. / Sub.	Exp. 1		Exp. 2		Exp. 3	Exp. 4
	Right	Left	Right	Left		
HM	-14.5	-31.2	-18.2	-24.7	11.4	9.8
HS	-11.7	-18.2	-6.3	-22.2	20.6	3.3
YS	-6.9	-13.5	-6.3	-14.1	23.9	13.4
HK	-21.5	-28.8	-17.0	-22.6	19.7	6.6
Average	-13.6	-22.9	-12.0	-20.9	18.9	8.2

Sub.: Subject, **Exp.** : Experiment. All units of *RPA* are the percentage.

4. Design A Haptic Device

In the virtual reality systems, to design a high performance display based on the human characteristics is an effective approach [3][4]. As analyzed in Section 3, the human have high distance perceptive sensitivity if the tactile and the visual information are presented concurrently. Namely, if the tactile and the visual information are concurrently presented, the virtual operation system can obtain a high distance performance. Therefore, we design a haptic device with vision to presented the distance information for a user as shown in Fig. 8. The designed haptic device is constructed from a tactile display and a head mounted display (HMD). 3D images of the real world are presented by HMD, at the same time, the tactile information is presented by a tactile display for the user. In the designed haptic device, HMD system is proposed by our previous study[2]. The haptic display can presented the tactile curved surface (touch information) and the tactile distance information. In order to present touch information, a tactile curved surface display is designed by our previous study[4]. In the tactile display, the tactile distance can be presented by movement of the tactile curved surface. To realize this haptic device is our future work.

Using the tactile device, in the virtual world the user can operate a teleoperator of the real world with high reality-performance.

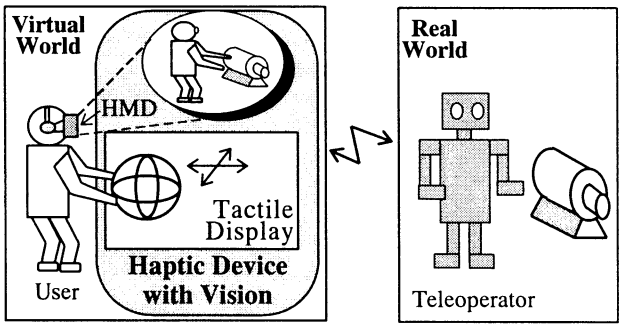


Fig. 8 The concept of a haptic device with vision for virtual operation system

5. Conclusion

In this study, a measurement system has bee developed. By using the experimental system, the human visual and haptic characteristics on distance perception were measured. The results of experiments suggested that the human visual and haptic perception have following main characteristics:

(1) Human have illusory characteristics on distance perception. Namely, the perceptive distances are different from the actual distances,

(2) If the visual and the tactile information are presented concurrently, human have high distance perceptive sensitivity.

Based on the experimental results, a haptic device has been designed in the virtual teleoperation system. Using the designed tactile device, the user could operate a teleoperator with high reality-performance in the virtual world.

Acknowledgments

We would like to express our gratitude to Dr. Sadao Kawamura and Mr. Masayuki Kitazawa for their useful help in developing the experimental system and the measurement programming.

References

[1] S.S. Fisher, M. McGreevy, J. Humphries and W. Robinett: "Virtual Environment Display System", *ACM Workshop on Interaction 3D Graphics*, pp.23/24(1986)

[2] Jing-Long Wu, M. Nakahata and S. Kawamura: "A New Head Mounted Display System with Adjustable Disparity for High Depth-Performance". *IEEE International Conference on Systems, Man and Cybernetics.* **Vol. 1**, pp. 298/303 (1995)

[3] Jing-Long Wu, M. Nakahata, S. Kawamura, I. Nishikawa and H. Tokumaru, "Measurement of Binocular Stereoacuity for Design of Head Mounted Display System with Wide View", *IEEE International Conference of Systems, Man and Cybernetics.* **Vol. 2**, pp. 929-934 (1996)

[4] Jing-Long Wu, S. Morita, S. Kawamura, "Human Sensory Fusion on Visual and Tactile Sensing for Virtual Reality", *IEEE International Conference on Robotics and Automation,* **Vol. 2**, pp. 2365-2370 (1996)

Proc. of Third Int. Symp. on Artificial Life, and Robotics (AROB III' 98),
Oita, Japan, 19-21, January, 1998,

Competitive Associative Networks for Control of Linear and Nonlinear Plants

S.Ren
Department of Control Engineering
Kyushu Institute of Technology
Kitakyushu, 804 Japan

S.Kurogi
Department of Control Engineering
Kyushu Institute of Technology
Kitakyushu, 804 Japan

Abstract

Two competitive associative neural networks (CAN1 and CAN2) are presented and applied to control of plants. The CAN1 learns and stores the input and output data of the function to be approximated and interpolates the function value via a temporal associative memory. The CAN2 learns and stores the vectors for partitioning the input space into Voronoi regions and the associative memories corresponding to the regions. The inverse controller with CAN1 and CAN2 controlled linear and nonlinear plants with inverse-dynamics. The predictive controller with not CAN1 but CAN2 controlled all plants with and without inverse-dynamics.

1 Introduction

The associative memory using the generalized inverse of a matrix provides least-square approximation of a function [1]. For more accurate approximation of nonlinear functions, two neural networks to achieve piecewise linear regression have been presented [3].

2 Competitive Associative Networks and Function Approximation

We briefly show the networks [3] and several properties in function approximation.

2.1 Recursive Associative Memory

Here, we consider n-dimensional vectors $\boldsymbol{x}_i = (x_{i1}, x_{i2}, \cdots, x_{in})^T$ and its function values $y_i = f(\boldsymbol{x}_i)$ for $i = 1, 2, \cdots$, where x_{ij} and y_i are in $\mathbb{R}$ and $\boldsymbol{x}^T$ is the transpose of $\boldsymbol{x}$. The associative memory M which minimize $\sum_{i=1}^{k}(y_i - M\boldsymbol{x}_i)^2$ is given by $M_k = Y_k X_k^+$ where and X_k^+ is the generalized inverse of $X_k = [\boldsymbol{x}_1, \boldsymbol{x}_2, \cdots, \boldsymbol{x}_k]$, and $Y_k = [y_1, y_2, \cdots, y_k]$. To obtain M_k, we use the adaptive algorithm given in [1]:

$$M_k = M_{k-1} + (y_k - M_{k-1}\boldsymbol{x}_k)\boldsymbol{p}_k^T, \tag{1}$$

where $M_0 = O$ (null matrix), and $\boldsymbol{p}_k$ is given by

$$\boldsymbol{p}_k = \begin{cases} \dfrac{\Phi_{k-1}\boldsymbol{x}_k}{\boldsymbol{x}_k^T \Phi_{k-1}^T \Phi_{k-1} \boldsymbol{x}_k}, & \text{if } ||\Phi_{k-1}\boldsymbol{x}_k|| \le \theta_0, \\ \dfrac{\Psi_{k-1}\boldsymbol{x}_k}{1 + \boldsymbol{x}_k^T \Psi_{k-1}^T \boldsymbol{x}_k}, & \text{otherwise,} \end{cases} \tag{2}$$

where

$$\Phi_k = \begin{cases} \Phi_{k-1} - \Phi_{k-1}\boldsymbol{x}_k \boldsymbol{p}_k^T, & \text{if } ||\Phi_{k-1}\boldsymbol{x}_k|| \le \theta_0, \\ \Phi_{k-1}, & \text{otherwise,} \end{cases} \tag{3}$$

$$\Psi_k = \begin{cases} \Psi_{k-1} + (1 + \boldsymbol{x}_k^T \Psi_{k-1} \boldsymbol{x}_k)\boldsymbol{p}_k \boldsymbol{p}_k^T \\ \quad - \Psi_{k-1}\boldsymbol{x}_k \boldsymbol{p}_k^T - \boldsymbol{p}_k \boldsymbol{x}_k^T \Psi_{k-1}^T, \\ \qquad \text{if } ||\Phi_{k-1}\boldsymbol{x}_k|| \le \theta_0, \\ \Phi_{k-1} - \Psi_{k-1}\boldsymbol{x}_k \boldsymbol{p}_k^T, \text{ otherwise,} \end{cases} \tag{4}$$

where θ_0 is a small constant, and $\Phi_0 = I$ (unit matrix) and $\Psi_0 = O$.

2.2 CAN1

A Competitive Associative Network (CAN1) consists of cells C_i, each of which stores the vector $\boldsymbol{x}_i$, the function value y_i and the data value v_i for $i = 1, 2, \cdots, M$, where $v_i = 0$ initially. Note that the data value v_i, or the firing number as a statistical value, is introduced to eliminate under-utilized cells for learning vector quantization nets [2, 4]. To calculate $\hat{y}$, an approximation of $y = f(\boldsymbol{x})$, the net searches m cells whose $\boldsymbol{x}_i$ are closer to $\boldsymbol{x}$ than others, and then calculates $\hat{y} = M_m\boldsymbol{x} = Y_m X_m^+ \boldsymbol{x}$, where we suppose $X_m = [\boldsymbol{x}_1, \boldsymbol{x}_2, \cdots, \boldsymbol{x}_m]$ and $||\boldsymbol{x}_i - \boldsymbol{x}|| \le ||\boldsymbol{x}_{i+1} - \boldsymbol{x}||$ for $i = 1, 2, \cdots, M$. Since the above $\boldsymbol{x}$ and the closest m vectors $\boldsymbol{x}_i$ are to be in a linear region, the vectors close to the boundary of the linear region are important so that the net learns input data $\boldsymbol{x}$ and y as follows. When $||y - M_m\boldsymbol{x}|| \le \theta_e$ for a small constant θ_e and there is a boundary of linear region

or the index b which satisfies $||y_b - M_m x_b|| \leq \theta_e$ and $||y_{b+1} - M_m x_{b+1}|| > \theta_e$, the data of m cells closer to the boundary are changed as follows: $x_i = \alpha_i x_i + (1-\alpha_i)x_b$, $y_i = \alpha_i y_i + (1-\alpha_i)y_b$ and $v_i = v_i + 1$ where $\alpha_i = 1/(1 + 1/v_i)$. When $||y - M_m x|| > \theta_e$, search the cell C_l with the minimum data value and replace its data x_l and y_l by the input data, and v_l by the data value of the cell C_c whose x_c is closest to x.

2.3 CAN2

Another Competitive Associative Network (CAN2) has cells C_i, each of which stores a vector x_i, an associative matrix M_i and its data value v_i, where Φ_i and Ψ_i should also be stored in order to calculate M_i with Eqs.(1)-(4). To approximate the function value of x, the net searches a cell C_c whose x_c are closest to x, with which the net calculates $\hat{y} = M_c x$. When the cell C_c has the data value v_c less than a threshold θ_v, its data are changed as $x_c = \alpha_c x_c + (1-\alpha_c)x$, $v_c = v_c + 1$, and M_c is changed by Eqs.(1)-(4). Otherwise, the following is performed. When $||y - M_c x|| \leq \theta_e$, search several cells whose x_i are closer to x than others, and find the cell $C_{c'}$, among them, whose error $||y - M_{c'} x||$ is the minimum. Then when x is in a window between $x_{c'}$ and x_c (Cf. Kohonen LVQ2), the data is modified as $v_{c'} = \alpha_{c'} x_{c'} + (1 - \alpha_{c'})x$, $v_{c'} = v_{c'} + 1$, and $M_{c'}$ is renewed by Eqs.(1)-(4). When $||y - M_c x|| > \theta_e$, the cell C_l with minimum data value replaces x_l by x_l, v_l by that of the cell closest to x and renew M_l.

2.4 Properties

The above networks and MLP (multi-layer perceptron; three layer feed-forward net with the sigmoidal output function and the error back-propagation learning) have already been applied to the approximation of several functions [3]. Both CAN1 and CAN2 provided small mean absolute errors but several irregular errors were generated via CAN1, which is considered to be owing to numerical unstability of the generalized inverse matrix and the net architecture. The conventional MLP tended to learn global variations of the functions and resulted in bigger mean absolute errors than CAN1 and CAN2.

3 CONTROL OF PLANTS

3.1 Plants

We examined mathematical plants given by

$$\begin{aligned} y(t+1) &= p_i(u(t))\,|_{\boldsymbol{y}[t;t-1],u(t-1)} \\ &= 1.9y(t) - 0.92y(t-1) + 0.00097g_i(u(t)) + \\ &\quad 0.00095g_i(u(t-1)), \end{aligned} \tag{5}$$

where $g_i(u) = u$, $a\tanh(u)$, $\sinh(u)$, $\mathrm{atanh}(u)$, $\mathrm{asinh}(u)$ for $i = 1, 2, \cdots, 5$, respectively, $\boldsymbol{y}[t; t-k] = (y(t), y(t-1), \cdots, y(t-k))$, and a is a constant. We also use the following plant:

$$\begin{aligned} y(t+1) &= p_6(u(t))\,|_{\boldsymbol{y}[t;t-2],u(t-1)} \\ &= \frac{y(t)y(t-1)(y(t)+0.5)+0.5u(t-1)}{1+y(t)^2+y(t-1)^2} + \\ &\quad \frac{0.2y(t-1)u(t)}{1+y(t)y(t-2)}. \end{aligned} \tag{6}$$

The plant $p_i (i \leq 5)$ has the inverse-dynamics:

$$\begin{aligned} u(t) &= p_i^{-1}(y(t+1))\,|_{\boldsymbol{y}[t;t-1],u(t-1)} \\ &= g^{-1}(y(t+1) - 1.9y(t) + 0.92y(t-1) - \\ &\quad 0.00095g_i(u(t-1))), \end{aligned} \tag{7}$$

but p_6 has no inverse-dynamics because

$$u(t) = \begin{cases} \dfrac{1+y(t)y(t-2)}{0.2y(t-1)}(y(t+1) - \\ \qquad \dfrac{y(t)y(t-1)(y(t)+0.5)+0.5u(t-1)}{1+y(t)^2+y(t-1)^2}), \\ \qquad \text{if } y(t-1) \neq 0, \\ any, \quad \text{otherwise}, \end{cases} \tag{8}$$

i.e., $u(t)$ is not determined by $y(t+1)$ when $y(t-1) = 0$.

3.2 Control Architectures

We applied two usual neuro-control architectures which do not need any parameterization of plants. The first one is the inverse control consisting of learning the inverse-dynamics $u(t) = p_i^{-1}(y(t+1))\,|_{\boldsymbol{y}[t;t-k_i],u(t-1)}$ and controlling with $u(t) = y_N(t)$ where $y_N(t) = F_i(y_d(t+1), \boldsymbol{y}[t; t-k_i], u(t-1))$, is the output of the neural net, $y_d(t)$ is the desired output, and $k_i = 1$ for $i \leq 5$ and $k_6 = 2$.

The other architecture is the predictive control [5] consisting of learning the dynamics and controlling with $u(t) = u_P$ minimizing

$$J_{u_P} = \lambda[u_P - u(t-1)]^2 + \sum_{j=1}^{N_p}[y_d(t+j) - y_N(t+j)]^2 \tag{9}$$

where λ is a constant and $y_N(t) = F_i(\boldsymbol{y}[t-1;t-1-k_i], \boldsymbol{u}[t-1;t-2])$ is the output of the neural net. The value u_P minimizing J_u was obtained with the simplex method [5].

3.3 Advantages and Problems

An advantage of neuro-controllers is the applicability to both linear and nonlinear plants where any parameterization of the plants is not necessary. Further, since the feedback of the above controllers is not the output error of the plant but the output of the plant itself, the control delay is expected to be smaller than the conventional "error" feedback controllers, such as PID controller, adaptive controller, H_∞ controller, etc..

The problems are whether or not the control system is controllable, stable, robust, etc.. It is clear that the above controllers can control the plant when the inverse-dynamics and the dynamics are learned to be reproduced with no errors. Further, since the controllers calculate the input to the plant every step of time with the current state (the output sequence) of the plant, the controllers are expected to control the plant if the nets approximate without errors for almost all states. Thus, from the properties of CAN1, CAN2 and MLP (see Sect.2.4), the controllers with CAN1 and CAN2 are expected to control the plants, but the controllers with MLP are not, because it approximates global variations of the functions. However, the simplex method used by the predictive control architecture assumes that the function J_{u_P} is smooth and searches many possible inputs u_P, thus the predictive controller may be affected by the several irregular errors much more than the inverse dynamics controller.

3.4 Results and Concluding Remarks

The inverse controller with CAN1 and CAN2 could control all the plants except p_6 (Fig.1 and 2). The predictive controller with CAN2 could all the plants (Fig.3) but only p_1 with CAN1. We used 50 and 10 cells for CAN1 and CAN2, respectively. Before applying the controller, the nets were trained with the input and output data of the plants, where the inputs were generated randomly. The number of the data for the inverse controller could be less than those for the predictive controller; a set of 600 successive input and output data of the plants were used for the former, and ten set of 600 successive data were used for the latter. After the training, the plants were controlled while the nets continued learning (online learning). After five iterations of 600 steps of control to track an objective trajectory, the output trajectories in Fig.1-3 were obtained, where the plant p_6 needed the predictive steps $N_p = 2$, and the other plants were controlled with $N_P = 1$. The plant inputs were truncated by $\pm u_{\max}$ during the training and the control phases, and the value $u_{\max}$ should have been selected carefully much more for the predictive controller than for the inverse controller (see Fig.4 as a result).

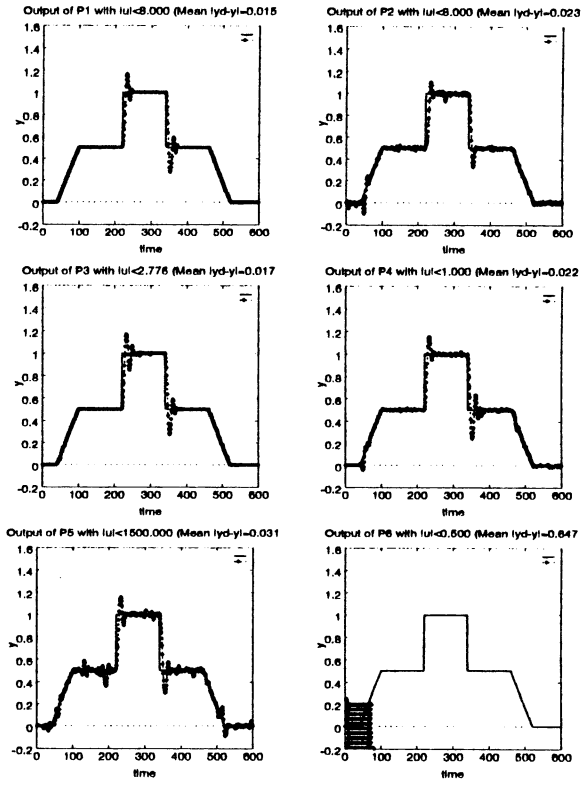


Figure 1: The output of the plants $p_1, p_2, \cdots, p_6$ controlled via the inverse controller with CAN1.

The results via PID controllers are shown in Fig.5, where the delays at the slope of the objective trajectory are clearly larger than via the above nets. Note that the PID parameters should be selected via try and error method because the step and the frequency responses depend on the input values for the nonlinear plants, thus, traditional methods, such as Ziegler-Nichols', could not be applied. The MLP nets have not provided good performance even if it achieved small mean absolute errors. One of the reason is that the net tended to learn global variations (see Sect.2.4) and could hardly reproduce the data around the stationary point, i.e, $0 = p_i(0) \mid_{\boldsymbol{y}[t;t-k_i]=\boldsymbol{0}, u(t-1)=0}$.

When the noises are involved in the observed plant outputs, CAN2 will eliminate the noise by the least

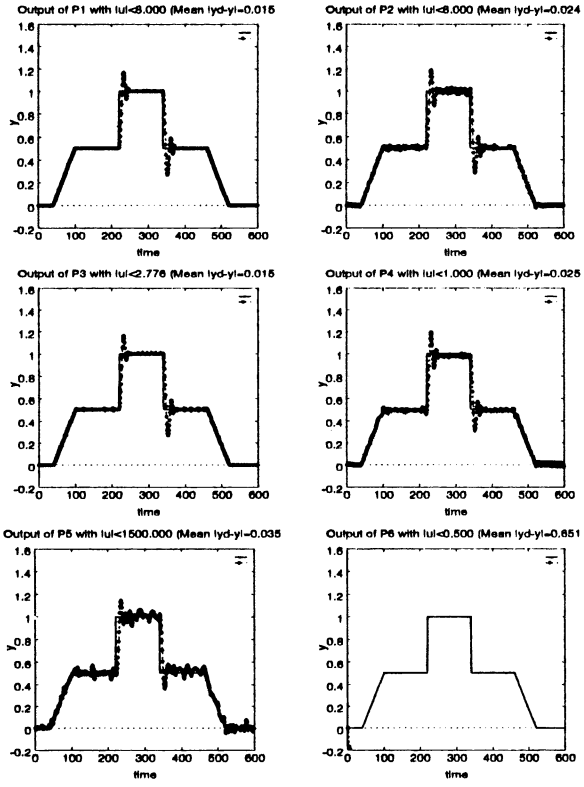


Figure 2: The output of the plants $p_1, p_2, \cdots, p_6$ controlled via the inverse controller with CAN2.

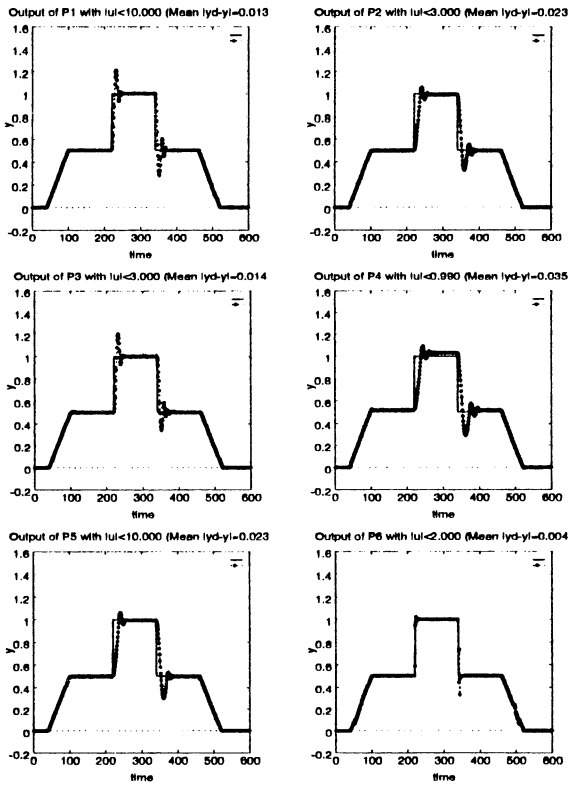


Figure 3: The output of the plants $p_1, p_2, \cdots, p_6$ controlled via the predictive controller with CAN2.

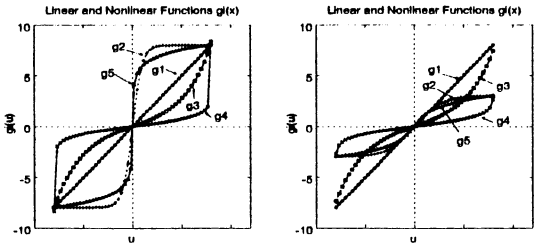


Figure 4: The ranges of the function values $g_i(u)$ for the inverse (left) and the predictive (right) controller where x is normalized.

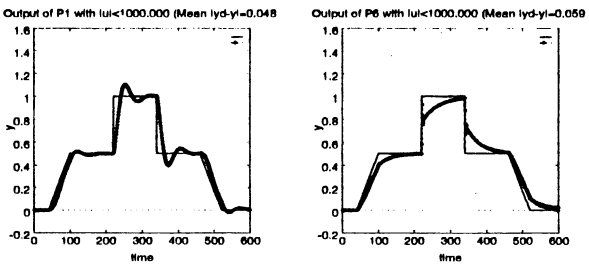


Figure 5: The output of the plants controlled via the PID controller with KP=4.5, KI=0.1, KP=10 for p_1, and KP=2, KI=0.1, KP=0.1 for p_6.

square approximation in the Voronoi regions, which we will examine in the future research.

References

[1] T.Kohonen, "Associative memory," Springer-Verlag, 1977.

[2] S.Kurogi, M.Hachimaru, & S.Ren, "Two Layered LVQ Net Evaluating Memorized Vectors for Tracking Control," Proc. of Int. Conf. EANN96, 175-178, 1996.

[3] S.Kurogi, & S.Ren, "Competitive Associative Networks for Function Approximation and Control of Plants,"Proc. of NOLTA'97, 1997

[4] S.Ren, & S.Kurogi, "Learning algorithms using firing numbers of weight vectors for WTA networks in rotation invariant pattern classification," IEICE Trans. on FECCS (accepted on Sep., 29, 1997)

[5] Y.Takahashi, "Adaptive predictive control of nonlinear time-varying systems using neural network," Kagaku-Gijutsusha, Japan, 1992

Proc. of Third Int. Symp. on Artificial Life, and Robotics (AROB III' 98),
Oita, Japan, 19-21, January, 1998,

A General Class of Neural Nets for Principal and Minor Component Analysis

Kiyotoshi MATSUOKA
Department of Control Engineering, Kyushu Institute of Technology
Tobata, Kitakyushu, 804 Japan

Abstract - This paper describes a unified theory of a class of learning neural nets for principal component analysis (PCA) and minor component analysis (MCA). First, some fundamental properties are addressed which all neural nets in the class share in common. Second, it is clarified what kind of asymmetric structure is required in the learning algorithm to obtain the individual eigenvectors of the correlation matrix of data sequence. Third, focusing on the single-neuron model, a systematic way for deriving both PCA and MCA learning algorithms is shown.

Key words - principal component analysis, minor component analysis, neural nets, unsupervised learning

1. Introduction

Principal component analysis (PCA) is an essential technique for data compression and feature extraction. Given a (vector) data sequence $\mathbf{x}(t) = [x_1(t), ..., x_N(t)]^T$ by a stationary random process, the principal components are defined as follows. Let the eigenvalues and the corresponding unit eigenvectors of the correlation matrix $\mathbf{R} = E[\mathbf{x}(t)\mathbf{x}(t)^T]$ be λ_i ($\lambda_1 > \lambda_2 > ... > \lambda_N > 0$) and $\mathbf{u}^{(i)}$ (i = 1, ..., N), respectively. Then, $\mathbf{u}^{(i)T}\mathbf{x}(t)$ (i = 1, ..., M) are called M dominant principal components.

It is well known that certain learning neural nets are able to extract the principal components of the input vector. Let $\mathbf{x}(t)$ and $\mathbf{y}(t) = [y_1(t), ..., y_M(t)]^T$ be an input vector and an output vector of a single-layer neural net, respectively. The output $y_j(t)$ of neuron j is given by a linear combination of $x_1(t), ..., x_N(t)$:

$$\mathbf{y}(t) = \mathbf{W}(t)^T\mathbf{x}(t) \tag{1}$$

where $\mathbf{W}(t) = [w_{ij}(t)]$ is an $N \times M$ matrix ($M \le N$). If $\mathbf{W}(t) = [\mathbf{u}^{(1)}, ..., \mathbf{u}^{(M)}]$, then the outputs $y_i(t)$ (i = 1, ..., M) provide M dominant principal components of $\mathbf{x}(t)$. The purpose of a neural principal component analyzer is to acquire such a function in an unsupervised manner.

The most well known neural algorithm for PCA might be the one proposed by Oja (1989) (the Subspace Learning):

$$\Delta\mathbf{W}(t) = \alpha(t)\left\{\mathbf{x}(t)\mathbf{y}(t)^T - \mathbf{W}(t)\mathbf{y}(t)\mathbf{y}(t)^T\right\} \tag{2}$$

where $\alpha(t)$ is a positive learning coefficient. The first term in the righthand side implies that this algorithm is a kind of Hebb-type learning algorithm. The second term works to normalize the weight matrix. After learning, the columns of $\mathbf{W}(t)$ will become an orthonormal basis in the dominant eigenspace of $\mathbf{R}$, i.e., the subspace spanned by the M dominant eigenvectors.

For $M > 1$, as known well, the Subspace Learning does not find the individual eignvectors, $[\mathbf{u}^{(1)}, ..., \mathbf{u}^{(M)}]$; it is only capable of finding their rotated basis. An approach to this issue is to incorporate some asymmetric sturucture into eqn (2). For instance, Sanger (1989) and Oja (1992) propose the following algorithms (the Generalized Hebbian Learning and the Stochastic Gradient Learning):

$$\Delta\mathbf{W}(t) = \alpha(t)[\mathbf{x}(t)\mathbf{y}(t)^T - \mathbf{W}(t)\left\{diag(\mathbf{y}(t)\mathbf{y}(t)^T) + lower(\mathbf{y}(t)\mathbf{y}(t)^T)\right\}] \tag{3}$$

$$\Delta\mathbf{W}(t) = \alpha(t)[\mathbf{x}(t)\mathbf{y}(t)^T - \mathbf{W}(t)\left\{diag(\mathbf{y}(t)\mathbf{y}(t)^T) + 2\,lower(\mathbf{y}(t)\mathbf{y}(t)^T)\right\}] \tag{4}$$

where $diag(\cdot)$ sets all nondiagonal elements of its matrix argument to zeros and $lower(\cdot)$ sets all elements on and above the diagonal to zeros. Oja, Ogawa and Wangviwattana (1992) describe (the Weighted Subspace Learning)

$$\Delta\mathbf{W}(t) = \alpha(t)\left\{\mathbf{x}(t)\mathbf{y}(t)^T - \mathbf{W}(t)\mathbf{D}\mathbf{y}(t)\mathbf{y}(t)^T\mathbf{D}^{-1}\right\} \tag{5}$$

where $\mathbf{D}$ is a diagonal matrix with positive diagonal elements different from each other. With these algorithms the columns of $\mathbf{W}(t)$ become M dominant eigenvectors, i.e., $\mathbf{W}(\infty) = [\mathbf{u}^{(1)}, ..., \mathbf{u}^{(M)}]$. In section 3, eqns (3)-(5) will be extended to a more general form and it will be clarified what kind of asymmetry should be incorporated in general to obtain the individual eigenvectors.

Recently, minor component analysis (MCA) has also received an attention from a viewpoint of signal processing. The purpose of the neural minor component analyzer is to find the least dominant eigenvector $\mathbf{u}^{(N)}$ in an unsupervised manner. It should be noted that the simple reversal of the sign in a PCA learning algorithms does not give a stable algorithm.

Xu et al. (1992) propose the following algorithm:

$$\Delta\mathbf{w}(t) = -\alpha(t)\left\{\mathbf{x}(t)y(t) - \mathbf{w}(t)\|\mathbf{w}(t)\|^{-2}y(t)^2\right\} \tag{6}$$

The negative coefficient, $-\alpha(t)$, implies that this is an anti-Hebbian learning. It is, so to say, a semi-stable model, that is, the magnitude $\|\mathbf{w}(\infty)\|$ of the weight vector is totally determined by the initial value $\|\mathbf{w}(0)\|$. A strictly stable model is given by Oja (1992), which normalizes the weight vector as $\|\mathbf{w}(\infty)\| = 1$:

$$\Delta\mathbf{w}(t) = -\alpha(t)\left[\mathbf{x}(t)y(t) - \mathbf{w}(t)\left\{y(t)^2 + \gamma\left(1 - \|\mathbf{w}\|^2\right)\right\}\right] \tag{7}$$

Gao et al. (1994) describes another form of anti-Hebbian learning (the Constraint Anti-Hebbian Learning), where the normalization is made in a different fashion from the usual models:

$$\Delta\mathbf{w}(t) = -\alpha(t)\left\{\mathbf{x}(t)y(t) - \mathbf{w}(t)x_N(t)y(t)\right\} \tag{8}$$

with $w_N(t) \equiv 1$. In the above equation the update of the N-th elements in $\mathbf{w}(t)$ is immaterial; it is fixed at unity.

Although these learning algorithms for MCA (6)-(8) look different from each other, they can be derived in a systematic way, as shown in section 4.

All the above algorithms for PCA and MCA can be categorized into a general class. In the next section we shall give a couple of fundamental properties that all the networks belonging to the class have universally.

2. Fundamental Properties of a Class of Neural Principal and Minor Component Analyzers

All the learning algorithms we want to investigate in this paper take the form

$$\Delta\mathbf{W}(t) = \pm\alpha(t)\left\{\mathbf{x}(t)\mathbf{y}(t)^T - \mathbf{W}(t)\bar{\mathbf{F}}(\mathbf{x}(t),\mathbf{y}(t),\mathbf{W}(t))\right\} \quad (9)$$
$$= \pm\alpha(t)\left\{\mathbf{x}(t)\mathbf{x}(t)^T\mathbf{W}(t) - \mathbf{W}(t)\bar{\mathbf{F}}(\mathbf{x}(t),\mathbf{W}(t)^T\mathbf{x}(t),\mathbf{W}(t))\right\}$$

where $\bar{\mathbf{F}}(\cdot,\cdot,\cdot)$ is an $M\times M$ matrix function. Every learning algorithm described in Introduction can be categorized into this type. The first term with signs, + and –, represents Hebbian and anti-Hebbian learnings, leading to principal and minor component analyzers, respectively. The second term aims at a normalization of the final value of $\mathbf{W}(t)$, but in this section $\bar{\mathbf{F}}(\cdot,\cdot,\cdot)$ is basically arbitrary.

Define function $\mathbf{F}(\mathbf{W}) = E\left[\bar{\mathbf{F}}(\mathbf{x}(t),\mathbf{W}^T\mathbf{x}(t),\mathbf{W})\right]$, in which the statistical expectation is made with respect to $\mathbf{x}(t)$. If the learning coefficient $\alpha(t)$ is appropriately decreased with time, then $\mathbf{x}(t)\mathbf{x}(t)^T$ and $\bar{\mathbf{F}}(\mathbf{x}(t),\mathbf{W}(t)\mathbf{x}(t),\mathbf{W}(t))$ in eqn (9) can be replaced with $\mathbf{R}$ and $\mathbf{F}(\mathbf{W}(t))$ respectively, and the dynamics of the difference equation (9) can be approximated by the following differential equation:

$$\frac{d\mathbf{W}(t)}{dt} = \pm\left\{\mathbf{R}\mathbf{W}(t) - \mathbf{W}(t)\mathbf{F}(\mathbf{W}(t))\right\} \quad (10)$$

This is the continuous learning equation we want to investigate below in detail.

First we want to show a universal property that eqn (10) has independently of the form of $\mathbf{F}(\cdot)$. To avoid complicated and uninteresting discussion we assume that the initial value of $\mathbf{W}(t)$ and the function $\mathbf{F}(\cdot)$ are chosen such that the following conditions be satisfied: (A1) given the initial value $\mathbf{W}(0)$, eqn (10) has a solution for $0 \le t < \infty$ and it is unique; (A2) matrix $\mathbf{W}(t)$ is column full-rank for $0 \le t < \infty$.

Let $\Pi_{\mathbf{W}}(t)$ be the M-dimensional subspace spanned by the columns $\mathbf{w}^{(i)}(t)$ (i = 1, ..., M) of $\mathbf{W}(t)$ in the N-dimensional Euclidean space. Under the above assumptions we can prove:

Theorem 1 The motion of the subspace $\Pi_{\mathbf{W}}(t)$ is independent of function $\mathbf{F}(\cdot)$.

In the special case of $\mathbf{F}(\mathbf{W}) \equiv \mathbf{0}$, eqn (9) reduces to M independent equations with respect to $\mathbf{w}^{(i)}(t)$, among which no interaction exists. From that we find that every $\mathbf{w}^{(i)}(t)$ grows (+) or shrinks (–) to a large or small vector *closely* in the direction of $\mathbf{u}^{(1)}$ or $\mathbf{u}^{(N)}$. However, $\mathbf{w}^{(i)}(t)$ (i = 1, ..., M) will continue spanning an M-dimensional (moving) subspace unless initially they happen to be put on a lower dimensional subspace than M.

It can easily be proved that, for almost every initial value of $\mathbf{W}(t)$, the subspace $\Pi_{\mathbf{W}}(t)$ stably converges to the subspace spanned by $\mathbf{u}^{(1)}$, ..., $\mathbf{u}^{(M)}$ or $\mathbf{u}^{(N-M+1)}$, ..., $\mathbf{u}^{(N)}$. According to Theorem 1, this argument holds for any learning equation in the present class . Thus we have

Theorem 2 For almost every initial value of $\mathbf{W}(t)$, the subspace $\Pi_{\mathbf{W}}(t)$ stably converges to the dominant or least dominant eigenspace.

Moreover, the motion of $\Pi_{\mathbf{W}}(t)$ is monotone in a sense. Let O_M be the manifold made of all the orthogonal projection matrices of rank M defined in the N-dimensional Euclidean space; the orthogonal projection matrix is given by $\mathbf{Z}(t) \triangleq \mathbf{W}(t)(\mathbf{W}(t)^T\mathbf{W}(t))^{-1}\mathbf{W}(t)^T$. We define the following scalar function on O_M and refer to it as the energy function: $\phi(\mathbf{Z}) = tr\{\mathbf{RZ}\}$, where $tr\{\cdot\}$ stands for trace and $\mathbf{Z}$ is a point on O_M. The energy function $\phi(\mathbf{Z})$ ($\mathbf{Z}\in O_M$) takes the only local (hence global) minimum and the only local (hence global) minimum at

$$\mathbf{Z}_{\max} \triangleq \mathbf{U}\begin{bmatrix}\mathbf{I}_M & \mathbf{0}\\ \mathbf{0} & \mathbf{0}\end{bmatrix}\mathbf{U}^T, \qquad \mathbf{Z}_{\min} \triangleq \mathbf{U}\begin{bmatrix}\mathbf{0} & \mathbf{0}\\ \mathbf{0} & \mathbf{I}_M\end{bmatrix}\mathbf{U}^T$$

where $\mathbf{U} = [\mathbf{u}^{(1)}, ..., \mathbf{u}^{(N)}]$ and $\mathbf{I}_M$ is the identity matrix of size M. We can prove:

Theorem 3 The energy function $\phi(\mathbf{Z}(t))$ monotonically increases (+) or decreases (-) with time.

3. The Generalized Asymmetric Learning

Let us begin with the Subspace Learning algorithm for PCA. Eqn (2) leads to

$$\frac{d\mathbf{W}(t)}{dt} = \mathbf{R}\mathbf{W}(t) - \mathbf{W}(t)\mathbf{W}(t)^T\mathbf{R}\mathbf{W}(t) \quad (11)$$

The corresponding learning equation for MCA is

$$\frac{d\mathbf{W}(t)}{dt} = -\mathbf{R}\mathbf{W}(t) \quad (12)$$
$$+ \mathbf{W}(t)(\mathbf{W}(t)^T\mathbf{W}(t))^{-1}\mathbf{W}(t)^T\mathbf{R}\mathbf{W}(t)(\mathbf{W}(t)^T\mathbf{W}(t))^{-1}$$

It can be shown that $\mathbf{W}(t)^T\mathbf{W}(t)$ converges to the identity matrix $\mathbf{I}_M$, implying that the set of column vectors $\mathbf{w}^{(i)}(t)$ (i = 1, ..., M) tends to an orthonormal system on the dominant or least dominant eigenspace of $\mathbf{R}$. In the particular case of $M = N$, this result states no more than that $\mathbf{W}(\infty)$ becomes an orthogonal matrix. So, the algorithm is not so interesting in the case of $M > 1$. A remedy for the drawback of the algorithm is to introduce some asymmetric structure in the learning algorithm, as shown below.

Define function $\mathbf{F}_{\mathbf{A}}(\mathbf{X}) = [a_{ij}x_{ij}]$, where $\mathbf{A} = [a_{ij}]$ and $\mathbf{X} = [x_{ij}]$ are both $M\times M$ matrices. Using this we introduce a generalized model:

$$(+)\ \frac{d\mathbf{W}(t)}{dt} = \mathbf{R}\mathbf{W}(t) - \mathbf{W}(t)\mathbf{F}_{\mathbf{A}}\left(\mathbf{W}(t)^T\mathbf{R}\mathbf{W}(t)\right) \quad (13)$$

$$(-)\ \frac{d\mathbf{W}(t)}{dt} = -\mathbf{R}\mathbf{W}(t) \quad (14)$$
$$+ \mathbf{W}(t)\mathbf{F}_{\mathbf{A}}\left(\left(\mathbf{W}(t)^T\mathbf{W}(t)\right)^{-1}\mathbf{W}(t)^T\mathbf{R}\mathbf{W}(t)\left(\mathbf{W}(t)^T\mathbf{W}(t)\right)^{-1}\right)$$

Obviously, the choice of $\mathbf{A} = \mathbf{I}_M$ gives eqns (11) and (12). In the sequel we investigate eqn (13) only; for eqn (14) a similar result can also be obtained in the same way. Moreover, for simplicity of description we investigate the special case $M = N$, though the following results hold for

the general case $1 \le M \le N$.

Defining new matrix variable $\mathbf{V}(t) = \mathbf{U}^T\mathbf{W}(t)$, eqn (13) reads

$$\frac{d\mathbf{V}(t)}{dt} = \Lambda\mathbf{V}(t) - \mathbf{V}(t)\mathbf{F}_{\mathbf{A}}\left(\mathbf{V}(t)^T\Lambda\mathbf{V}(t)\right) \tag{15}$$

Here we impose the following requirement to matrix **A**: '**W** = **U** (or **V** = **I**)is a (locally) asymptotically stable equilibrium of eqn (13) (or (15)) for any values of λ_1, ..., λ_N ($\lambda_1 > \ldots > \lambda_N > 0$).' This simple constraint determines the basic structure of matrix **A**. Namely, we find that every pair of a_{ij} and a_{ji} ($i > j$) must satisfy either of the following conditions: (i) $1 < a_{ji} \le a_{ij}$; (ii) $1 = a_{ji} < a_{ij}$; (iii) $-1 \le a_{ji} < 1 \le a_{ij}$; (iv) $1 < -a_{ji} \le a_{ij}$. We refer to eqn (22) with these conditions as the Generalized Asymmetric Learning though it includes a symmetric learning as a special case.

We take up two special cases here:

(B1) $a_{ii} = 1$ ($i = 1, \ldots, N$), $\quad -1 \le a_{ji} < 1 \le a_{ij}$ $\quad (i > j)$

(B2) $a_{ii} = 1$ ($i = 1, \ldots, N$), $\quad 1 < a_{ji} = a_{ij} = a$ $\quad (i \ne j)$

Obviously, the Generalized Hebbian Learning, the Stochastic Gradient Learning, and the Weighted Subspace Learning described in Introduction are just examples of (B1). Interestingly, the individual eigenvectors can also be obtained by a symmetric Hebbian learning (B2).

Any matrix of the following form easily proves to be an equilibrium of eqn (15):

$$\mathbf{V} = \mathbf{P}\Gamma \tag{16}$$

where **P** is a permutation matrix, $\Gamma = diag\{\gamma_1, \ldots, \gamma_N\}$, and γ_i is 0 or ± 1. We can prove the following theorem.

Theorem 4 Assume that matrix **A** is given as (B1). Then, among the equilibria given by eqn (16), only $\mathbf{V} = \mathbf{I}_N$ is locally stable (more specifically, with arbitrary sign reversal of the diagonal elemens).

In the case of (B2) eqn (15) reads

$$\frac{d\mathbf{V}(t)}{dt} = \Lambda\mathbf{V}(t) - \mathbf{V}(t)\left\{a\mathbf{V}(t)^T\Lambda\mathbf{V}(t) - (a-1)diag\left(\mathbf{V}(t)^T\Lambda\mathbf{V}(t)\right)\right\} \tag{17}$$

Although eqn (27) also gives some equilbria, this equation has other equilibria, due to its symmetric structure. A general form is

$$\mathbf{V} = \mathbf{P}_1\begin{bmatrix}\mathbf{Q}_1 & \mathbf{0} & \cdots & \mathbf{0}\\ \mathbf{0} & \mathbf{Q}_2 & \ddots & \vdots\\ \vdots & \ddots & \ddots & \mathbf{0}\\ \mathbf{0} & \cdots & \mathbf{0} & \mathbf{Q}_r\end{bmatrix}\mathbf{P}_2 \tag{18}$$

where $\mathbf{P}_1$ and $\mathbf{P}_2$ are arbitrary permutation matrices, and $\mathbf{Q}_k$ ($k = 1, \ldots, r$) is a square matrix of size n_k, taking the form

$$\mathbf{Q}_k = \begin{bmatrix}q_k & q_k & \cdots & q_k\\ 0 & 0 & \cdots & 0\\ \vdots & & & \vdots\\ 0 & 0 & \cdots & 0\end{bmatrix},$$

$$q_k = 0 \text{ or } \pm\{a(n_k - 1) + 1\}^{-1/2}$$

As for the equilibria given by this we have

Theorem 5 Assume that matrix **A** is given as (B2). Then, among the above equilibria (18), only $\mathbf{V} = \mathbf{P}$ is locally stable, where **P** is an arbitrary permutation matrix.

4. A Systematic Derivation of Various Neural Algorithms for PCA and MCA

We here concentrate on the single-neuron model ($M = 1$), for which we write

$$\frac{d\mathbf{w}(t)}{dt} = \pm\{\mathbf{R}\mathbf{w}(t) - \mathbf{w}(t)f(\mathbf{w}(t))\}. \tag{19}$$

The aim of this section is to derive a systematic method for obtaining the principal and minor component analyzers in which the weight vector will be normalized as $g(\mathbf{w}(\infty)) = 1$. We assume that $g(\cdot)$ is a continuously differentiable function that satisfies

$$g(c\mathbf{w}) = c^{\beta}g(\mathbf{w}) \text{ for every } c > 0 \quad (\beta > 0) \tag{20}$$

The particular choice of $g(\cdot)$ considerably simplifies the algorithm. Eqn (20) implies

$$\bar{\mathbf{g}}(\mathbf{w}(t))^T\mathbf{w}(t) = \beta g(\mathbf{w})$$

where $\bar{\mathbf{g}}(\cdot)$ stands for the gradient of $g(\cdot)$.

We want to determine function $f(\cdot)$ so that $g(\mathbf{w}(t))$ obeys a dynamics of the following form:

$$\frac{dg(\mathbf{w}(t))}{dt} = h(\mathbf{w}(t))\{1 - g(\mathbf{w}(t))\} \tag{21}$$

If $h(\mathbf{w}(t)) \ge 0$ for every t, then $g(\mathbf{w}(t))$ will converge to 1. Or at least, if $g(\mathbf{w}(0)) = 1$, then $g(\mathbf{w}(t))$ keep the initial value 1. From eqn (19) we have

$$\frac{dg(\mathbf{w}(t))}{dt} = \pm\bar{\mathbf{g}}(\mathbf{w}(t))^T\{\mathbf{R}\mathbf{w}(t) - \mathbf{w}(t)f(\mathbf{w}(t))\}$$

By equating the righthand side of this equation with that of eqn (21), we find that $f(\cdot)$ should take the form

$$f(\mathbf{w}) = \frac{\bar{\mathbf{g}}(\mathbf{w})^T\mathbf{R}\mathbf{w} \pm h(\mathbf{w})(g(\mathbf{w}) - 1)}{\bar{\mathbf{g}}(\mathbf{w})^T\mathbf{w}} = \frac{\bar{\mathbf{g}}(\mathbf{w})^T\mathbf{R}\mathbf{w} \pm h(\mathbf{w})(g(\mathbf{w}) - 1)}{\beta g(\mathbf{w})} \tag{22}$$

If we are solely interested in obtaining just a stable model, we have only to choose $h(\cdot)$ as $h(\mathbf{w}) \equiv 1$ for example. However, this does not provide a simple learning algorithm in two respects: (i) $f(\mathbf{w})$ is of a fractional form; (ii) the nominator contains three terms. Though these complexities cannot be removed simultaneously, either one can be resolved by choosing $h(\cdot)$ appropriately.

As for (i) we may choose

$$h(\mathbf{w}) = 2\gamma g(\mathbf{w}) \pm \bar{\mathbf{g}}(\mathbf{w})^T\mathbf{R}\mathbf{w} \quad (\gamma > 0) \tag{23}$$

leading to

$$f(\mathbf{w}) = \frac{1}{\beta}\bar{\mathbf{g}}(\mathbf{w})^T\mathbf{R}\mathbf{w} \pm \frac{2\gamma}{\beta}\mathbf{w}(g(\mathbf{w}) - 1) \tag{24}$$

or

$$\frac{d\mathbf{w}(t)}{dt} = \pm\left\{\mathbf{R}\mathbf{w}(t) - \frac{1}{\beta}\mathbf{w}(t)\bar{\mathbf{g}}(\mathbf{w})^T\mathbf{R}\mathbf{w}\right\} + \frac{2\gamma}{\beta}\mathbf{w}(t)(1 - g(\mathbf{w}(t))) \tag{25}$$

If $h(\mathbf{w})$ (eqn (23)) is a positive definite function we have a globally stable algorithm.

Example 1 $\quad g(\mathbf{w}) = \|\mathbf{w}\|^2 = \mathbf{w}^T\mathbf{w}$

$$\frac{d\mathbf{w}(t)}{dt} = \pm\left\{\mathbf{R}\mathbf{w}(t) - \mathbf{w}(t)\mathbf{w}(t)^T\mathbf{R}\mathbf{w}(t)\right\} + \gamma\mathbf{w}(t)\left(1 - \|\mathbf{w}(t)\|^2\right)$$

In the case of negative sign, this is no more than the minor component analyzer proposed by Oja et al (1992).

As for (ii) two alternatives are conceivable:

(±)

$$h(\mathbf{w}) = \begin{cases} h^{+}(\mathbf{w}) \overset{\Delta}{=} \bar{\mathbf{g}}(\mathbf{w})^{T}\mathbf{R}\mathbf{w} & \text{for the Hebbian} \\ h^{-}(\mathbf{w}) \overset{\Delta}{=} \dfrac{\bar{\mathbf{g}}(\mathbf{w})^{T}\mathbf{R}\mathbf{w}}{g(\mathbf{w})} & \text{for the anti - Hebbian} \end{cases}$$

(0) $h(\mathbf{w}) = h^{0}(\mathbf{w}) \overset{\Delta}{=} 0$ for both the Hebbian and anti-Hebbian learnings

The above choices for $h(\mathbf{w})$ provide $f(\mathbf{w})$ with simple forms:

$$(\pm)\quad f(\mathbf{w}) = \begin{cases} f^{+}(\mathbf{w}) \overset{\Delta}{=} \dfrac{1}{\beta}\bar{\mathbf{g}}(\mathbf{w})^{T}\mathbf{R}\mathbf{w} \\ f^{-}(\mathbf{w}) \overset{\Delta}{=} \dfrac{\bar{\mathbf{g}}(\mathbf{w})^{T}\mathbf{R}\mathbf{w}}{\beta g(\mathbf{w})^{2}} \end{cases}$$

$$(0)\quad f(\mathbf{w}) = f^{0}(\mathbf{w}) \overset{\Delta}{=} \frac{\bar{\mathbf{g}}(\mathbf{w})^{T}\mathbf{R}\mathbf{w}}{\beta g(\mathbf{w})}$$

Among these there is a symmetric relation as

$$g(\mathbf{w})^{-1} f^{+}(\mathbf{w}) = f^{0}(\mathbf{w}) = g(\mathbf{w}) f^{-}(\mathbf{w}) \qquad (26)$$

Example 2 $g(\mathbf{w}) = \|\mathbf{w}\|^{2} = \mathbf{w}^{T}\mathbf{w}$

$$(\pm)\frac{d\mathbf{w}(t)}{dt} = \mathbf{R}\mathbf{w}(t) - \mathbf{w}(t)\mathbf{w}(t)^{T}\mathbf{R}\mathbf{w}(t)$$

$$\frac{d\mathbf{w}(t)}{dt} = -\mathbf{R}\mathbf{w}(t) + \mathbf{w}(t)\frac{\mathbf{w}(t)^{T}\mathbf{R}\mathbf{w}(t)}{\|\mathbf{w}(t)\|^{4}}$$

$$(0)\frac{d\mathbf{w}(t)}{dt} = \pm\left\{\mathbf{R}\mathbf{w}(t) - \mathbf{w}(t)\frac{\mathbf{w}(t)^{T}\mathbf{R}\mathbf{w}(t)}{\|\mathbf{w}(t)\|^{2}}\right\}$$

In this case $h^{\pm}(\mathbf{w})$ become positive definite functions unconditionally. The first one is the well-known Oja's Constraint Hebbian Learning for PCA. The second is the corresponding one for MCA. The third algorithm (0) with sign (-) is the MCA algorithm given by Xu et al. (1992).

In case that function $h^{0}(\mathbf{w}) \equiv 0$ is chosen, the learning algorithm becomes in general

$$\frac{d\mathbf{w}(t)}{dt} = \pm\left\{\mathbf{R}\mathbf{w}(t) - \mathbf{w}(t)\frac{\bar{\mathbf{g}}(\mathbf{w}(t))^{T}\mathbf{R}\mathbf{w}(t)}{\beta g(\mathbf{w}(t))}\right\} \qquad (27)$$

According to eqn (21), $dg(\mathbf{w}(t))/dt \equiv 0$. So, if $\mathbf{w}(0)$ is chosen such that $g(\mathbf{w}(0)) = 1$, $g(\mathbf{w}(t))$ continues being unity. If we constrain the position of $\mathbf{w}(t)$ on the surface $g(\mathbf{w}) = 1$ by reducing the dimension of the weight vector to $N - 1$, we obtain a strictly stable model. Assume that the equation $g(\mathbf{w}) = 1$ can be solved with respect to a variable, say w_N, as $w_N = g'(\mathbf{w}')$, where $\mathbf{w}' = [w_1, ..., w_{N-1}]^{T}$. Then, from eqn (27) we obtain the following algorithm:

$$\frac{d\mathbf{w}'(t)}{dt} = \pm\left\{\mathbf{R}'\mathbf{w}(t) - \frac{1}{\beta}\mathbf{w}'(t)\bar{\mathbf{g}}(\mathbf{w}(t))^{T}\mathbf{R}\mathbf{w}(t)\right\} \qquad (28)$$

$$w_N(t) = g'(\mathbf{w}'(t)), \quad \mathbf{w}(t) = [\mathbf{w}'(t)^{T}, w_N(t)]^{T}$$

where $\mathbf{R}' = \mathrm{E}[\mathbf{x}'(t)\mathbf{x}(t)^{T}]$ and $\mathbf{x}'(t) = [x_1(t), ..., x_{N-1}(t)]^{T}$.

Example 3 $g(\mathbf{w}) = \mathbf{a}^{T}\mathbf{w}$, where $\mathbf{a}$ is a column vector ($a_N \neq 0$). Substituting this into eqn (28), we have

$$\frac{d\mathbf{w}'(t)}{dt} = \pm\left\{\mathbf{R}'\mathbf{w}(t) - \mathbf{w}'(t)\mathbf{a}^{T}\mathbf{R}\mathbf{w}(t)\right\}$$

In the case of $\mathbf{a} = [1, 1, ..., 1]^{T}$ for example, the above equation leads to

$$\frac{dw_i(t)}{dt} = \pm\left\{x_i(t)y(t) - w_i(t)\sum_{j=1}^{N}x_j(t)y(t)\right\}$$

$$(i = 1, ..., N-1)$$

$$w_N(t) = 1 - \sum_{j=1}^{N-1}w_j(t)$$

The sum (not squared sum) of the elements $w_i(\infty)$ (i = 1, ..., N) will become unity. As another example, consider $\mathbf{a} = [0, .., 0, 1]^{T}$, and we obtain

$$\frac{dw_i(t)}{dt} = \pm\{x_i(t)y(t) - w_i(t)x_N(t)y(t)\} \quad (i = 1, ..., N-1)$$

with $w_N(t) = 1$. This algorithm with negative sign is given by Gao et al. (1994).

5. Conclusion

First we have introduced a general class of neural nets for PCA and MCA. Next, we have investigated a subclass called the Generalized Asymmetric Learning, which includes some well-known algorithm for PCM. As a byproduct a symmetric learning algorithm is derived. In the last section we showed a unified derivation of neural PCA and MCA algorithms, focusing on the single-neuron model.

Acknowledgment This research is supported by the Grand-in-aid for the Scientific Research of the Ministry of Education, Science and Culture of Japan: No. 09268227.

References

1. K. Gao, M. O. Ahmad, and M. N. S. Swamy, A constrained anti-Hebbian learning algorithm for total least-square estimation with applications to adaptive FIR and IIR filtering, IEEE Trans. Circuit and Systems-II, Vol. 41, 718-729, 1994
2. E. Oja, Neural networks, principal components, and subspaces, International Journal of Neural Systems, Vol. 1, No. 1, 61- 68, 1989.
3. E. Oja, Principal components, minor components, and linear neural networks, Neural Networks, Vol. 5, 927-935, 1992.
4. E. Oja, H. Ogawa, and J. Wangviwattana, Principal component analysis by homogeneous neural networks, Part II, IEICE Trans. Inf. & Syst., Vol E75-D, 376-382 (1992)
5. T. D. Sanger, Optimal unsupervised learning in a single-layer linear feedforward neural network, Neural Networks, Vol. 2, 459-472, 1989.
6. L. Xu, E. Oja, and C. Y. Suen, Modified Hebbian learning for curve and surface fitting, Neural networks, Vol. 5, 441-457, 1992.
7. W.-Y. Yan, U. Helmke, and J. B. Moore, Global analysis of Oja's flow for neural networks, IEEE Trans. Neural Networks, Vol. 5, 674-683, 1994.

Proc. of Third Int. Symp. on Artificial Life, and Robotics (AROB III' 98),
Oita, Japan, 19-21, January, 1998,

Blind Signal Separation of Convolved Non-stationary Signals

Mitsuru KAWAMOTO[1], Kiyotoshi MATSUOKA[2], and Noboru OHNISHI[1,3]

1. Bio-Mimetic Control Research Center, RIKEN

2271-130 Anagahora, Shimoshidami, Moriyama-ku, Nagoya, 463

2. Department of Control Engineering, Kyushu Institute of Technology,

3. Graduate School of Engineering, Nagoya University

Abstract

This paper deals with *Blind signal separation* which separates non-stationary signals from their convolutive mixtures. An adaptive network acquires the function of blind signal separation by modifying the network's parameters so that a cost function takes the minimum at every time. We apply the proposed method to an experiment that uses the mixed signals observed in an anechoic room.

Key words: Blind signal separation, Non-stationary signal, Convolutive mixture, Second-order moment

1. Introduction

This paper presents a network for *Blind signal separation* of non-stationary signals. Blind signal separation is a signal processing technique that extracts the original signals (source signals) from their mixtures (observed signals) observed by the same number of sensors. An attractive feature of blind signal separation is that the source signals can be recovered without any assumption about the source signals or the mixing process, i.e., the transfer function between signal sources and sensors. The only a priori knowledge is, basically, that the source signals are statistically mutually independent. Therefore, this technique can be applied to various fields, e.g., speech recognition, image processing, medical measurement, etc.

1. 1 Blind Signal Separation Problem

Various methods for blind signal separation have been proposed. According to those methods, as a model of the transfer function between signal sources and sensors, there exit two types: instantaneous mixture and convolutive mixture. Instantaneous mixture is a mixing model which does not take into account any delays. Writing source signals as $\mathbf{s}(t)=[s_1(t),\ldots,s_N(t)]^T$ and observed signals as $\mathbf{x}(t)=[x_1(t),\ldots,x_N(t)]^T$, instantaneous mixture is expressed as the following model:

$$\mathbf{x}(t) = \mathbf{A}\mathbf{s}(t) \tag{1}$$

where $\mathbf{A}=[a_{ij}]$ is a square matrix and is assumed to be unknown matrix. Convolutive mixture involves some delays in the mixing process. The mixing process is expressed as

$$\mathbf{x}(t) = \overline{\mathbf{A}}\,(z^{-1})\mathbf{s}(t) \tag{2}$$

where $\overline{\mathbf{A}}\,(z^{-1})=[\,\overline{a}_{ij}(z^{-1})]$ is a transfer function which takes into account some delays. $\overline{\mathbf{A}}\,(z^{-1})$ is assumed to be unknown transfer function. From eqn (2), the observed signals $x_i(t)$ $(i = 1,\ldots,N)$ are given by the following equation:

$$x_i(t) = \sum_{j=1}^{N} \overline{a}_{ij}(z^{-1})s_j(t) \qquad (i = 1,\ldots,N) \tag{3}$$

where $\overline{a}_{ij}(z^{-1}) = \sum_{k=-\infty}^{\infty} a_{ij}(k)z^{-k}$ is the transfer function from the *j*-th input (source signal) to the *i*-th output (observed signal), and z^{-k} is a delay operator, i.e., $s_i(t)z^{-k} = s_i(t-k)$. This paper deals with a convolutive mixture in the mixing process. That is, we consider the problem of

how the source signals can be separated from their convolutive mixtures.

1. 2 Blind Signal Separation Method

If the transfer function between signal sources and sensors are estimated, then the source signals can be extracted by applying the inverse dynamics of the transfer function to the observed signals. Therefore, the problem can be reduced to that of how to identify the transfer function by only using the observed signals. To estimate the transfer function, the conventional methods [1,4,6,7] assume that the source signals are non-Gaussian, and utilize information about whether the source signals are super-Gaussian or sub-Gaussian. However, it is difficult to investigate from the observed signals whether the source signals are super- or sub-Gaussian signals.

In this paper, we assume that the source signals are non-stationary (e.g., speech signals), and use this information to separate the signals. The proposed method does not require any additional information about whether the source signals are super- or sub-Gaussian. We only make use of the second-order moments of the observed signals. The transfer function between signal sources and sensors is estimated by modifying the parameters of an adaptive network. The learning rule of the network's parameter is derived from the steepest descent minimization of a cost function.

In order to confirm the validity of the proposed method, we apply the method to an experiment that extracts source signals from their mixtures observed in an anechoic room

2. Source Signals

Suppose that source signals $s_i(t)$ (i = 1,...,N; t = ..., -1,0,1,...) are generated by N mutually independent sources. Source signals are assumed to be mutually independent non-stationary signals with zero mean. From this assumption, the auto-correlation matrix $\mathbf{R}(t,\tau_1,\tau_2)$ of $\mathbf{s}(t)$ becomes a diagonal matrix:

$$\begin{aligned}\mathbf{R}(t,\tau_1,\tau_2) &= E[\mathbf{s}(t-\tau_1)\,\mathbf{s}(t-\tau_2)^T] \\ &= \mathrm{diag}\{E[s_1(t-\tau_1)s_1(t-\tau_2)],\ldots,E[s_N(t-\tau_1)s_N(t-\tau_2)]\} \\ &\equiv \mathrm{diag}\{r_1(t,\tau_1,\tau_2),\ldots,r_N(t,\tau_1,\tau_2)\} \qquad (4)\end{aligned}$$

where diag{...} represents a diagonal matrix with the diagonal element {...}, and E[x] is the ensemble average of x. We treat the signals satisfying the following assumption as non-stationary signals.

Assumption 1 For every τ_1,τ_2, each $r_i(t,\tau_1,\tau_2)$ changes independently with time t.

Namely, we deal with non-stationary signals whose auto-correlations change with time. Observed signals $\mathbf{x}(t)$ (or $x_i(t)$) are given by the process of eqn (2) (or eqn (3)). As for $\overline{\mathbf{A}}(z^{-1})$, we assume:

Assumption 2 $\overline{\mathbf{A}}(z^{-1})^{-1}$ does not have poles on the unit circle $|z| = 1$

3. Separation Network

To separate the source signals from the observed signals, we use an adaptive feedforward network shown in Figure 1. The input signals of the network are the observed signals $x_i(t)$ (i = 1,...,N). The network's outputs are given by the following equation:

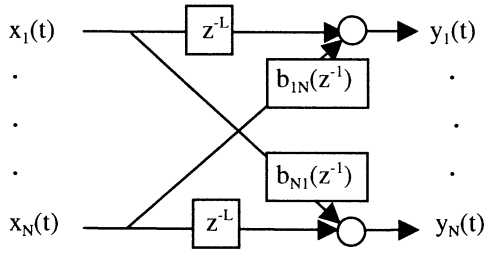


Fig. 1 Signal Separation Network

$$y_i(t) = x_i(t-L) + \sum_{\substack{j=1 \\ j\neq i}}^{N} \sum_{k=0}^{M} b_{ij}(k)x_j(t-k)$$

$$(i = 1,\ldots,N;\ 0 \leq L < M) \qquad (5)$$

$$= \sum_{j=1}^{N} \bar{b}_{ij}(z^{-1})x_j(t) \qquad (6)$$

where $\bar{b}_{ij}(z^{-1}) = \sum_{k=0}^{M} b_{ij}(k)z^{-k}$ $(i, j = 1, \ldots,N;\ i \neq j)$ represents the transfer function between j-th input (observed signal) and i-th output (output signal). $\bar{b}_{ii}(z^{-1}) = z^{-L}$ $(i = 1,\ldots,N;\ 0 \leq L < M)$. Eqn (6) can be expressed in vector notation as

$$\mathbf{y}(t) = \bar{\mathbf{B}}(z^{-1})\mathbf{x}(t) \qquad (7)$$

where $\mathbf{y}(t) = [y_1(t),\ldots,y_N(t)]^T$, $\bar{\mathbf{B}}(z^{-1}) = [\bar{b}_{ij}(z^{-1})] = \sum_{k=0}^{M} \mathbf{B}(k)\, z^{-k}$, $\mathbf{B}(k) = [b_{ij}(k)]$. Substituting eqn (2) into eqn (7), we have

$$\mathbf{y}(t) = \bar{\mathbf{B}}(z^{-1})\bar{\mathbf{A}}(z^{-1})\mathbf{s}(t) \qquad (8)$$

If $\mathbf{C}(z^{-1}) \equiv \bar{\mathbf{B}}(z^{-1})\bar{\mathbf{A}}(z^{-1}) = \mathbf{D}(z^{-1})\mathbf{P}$, the outputs of the network become a filtered and permuted source signals $\bar{\mathbf{s}}(t)=[\bar{s}_1(t),\ldots,\bar{s}_N(t)]^T = \mathbf{D}(z^{-1})\mathbf{P}\mathbf{s}(t)$. Here, $\mathbf{P}$ is an arbitrary permutation matrix, and $\mathbf{D}(z^{-1})$ is a diagonal matrix expressed as

$$\mathbf{D}(z^{-1}) = \mathrm{diag}\{\sum_{k=-\infty}^{\infty} d_1(k)z^{-k},\ldots,\sum_{k=-\infty}^{\infty} d_N(k)z^{-k}\}$$

$\bar{s}_i(t)$ $(i = 1,\ldots,N)$ may also be regarded as source signals, because $\bar{s}_i(t)$ $(i = 1,\ldots,N)$ are mutually independent signals. Therefore, our goal is now to find the matrix $\bar{\mathbf{B}}(z^{-1})$ satisfying $\mathbf{C}(z^{-1}) = \mathbf{D}(z^{-1})\mathbf{P}$.

4. The Proposed Method for Blind Signal Separation

When the mixing process is assumed to be an instantaneous mixture, that is, $\mathbf{x}(t) = \mathbf{A}\mathbf{s}(t)$ (eqn (1)), and $\mathbf{s}(t)$ is non-stationary signal, Matsuoka, Oya, and Kawamoto showed that blind signal separation can be achieved by implementing $E[y_i(t)y_j(t)] = 0$ $(i, j = 1,\ldots,N;\ i \neq j)$ for every time t [5]. [On the output signal $y_i(t)$ $(i = 1,\ldots,N)$ in their method, see [5].]

In this paper, we apply their idea to the case of convolutive mixture. To this end, we consider the following function:

$$Q(t, \bar{b}_{ij}(z^{-1})) = \frac{1}{2}\sum_{\substack{i,j=1 \\ j>i}}^{N} E[y_i(t)y_j(t)]^2 \qquad (9)$$

The function $Q(t, \bar{b}_{ij}(z^{-1}))$ takes the minimum only when $E[y_i(t)y_j(t)]$ $(i, j = 1,\ldots,N;\ i \neq j)$ are equal to zero. Matrix $\bar{\mathbf{B}}(z^{-1})$ satisfying $\mathbf{C}(z^{-1}) = \mathbf{D}(z^{-1})\mathbf{P}$ is found by minimizing the function $Q(t, \bar{b}_{ij}(z^{-1}))$. In order to implement this we consider the following steepest descent search:

$$\Delta b_{ij}(k) = -\alpha \frac{\partial Q(t, \bar{b}_{ij}(z^{-1}))}{\partial b_{ij}(k)}$$

$$(i, j = 1,\ldots,N;\ i \neq j;\ k = 0,\ldots,M) \qquad (10)$$

where α is a small constant. Calculating the right side of eqn (10), we have

$$\Delta b_{ij}(k) = -\alpha \sum_{\substack{m=1 \\ m\neq i}}^{N} E[y_i(t)y_m(t)]E[y_m(t)x_j(t-k)] \qquad (11)$$

To actually implement eqn (11), we replace $E[y_i(t)y_m(t)]$ by its instantaneous value $y_i(t)y_m(t)$:

$$\Delta b_{ij}(k) = -\alpha \sum_{\substack{m=1 \\ m\neq i}}^{N} y_i(t)y_m(t)E[y_m(t)x_j(t-k)] \qquad (12)$$

For the estimation of $E[y_m(t)x_j(t-k)]$, we use the following moving average:

$$\phi_{mj}(t,k) = \beta\phi_{mj}(t-1,k) + (1-\beta)\, y_m(t)x_j(t-k) \qquad (13)$$

$$(0 < \beta < 1)$$

Then, eqn (12) becomes

$$\Delta b_{ij}(k) = -\alpha \sum_{\substack{m=1 \\ m\neq i}}^{N} y_i(t)y_m(t)\,\phi_{mj}(t,k)$$

$$(i, j = 1,\ldots,N;\ i \neq j;\ k = 0,\ldots,M) \qquad (14)$$

Eqn (14) together with eqn (13) is the algorithm to update $b_{ij}(k)$ $(i, j = 1,\ldots,N;\ i \neq j;\ k = 0,\ldots,M)$ we propose for blind

signal separation of convolved non-stationary signals.

5. Simulation Result

We show an example to check the validity of the proposed method. The number of sources is assumed to be two, that is, N = 2. For this case, eqn (14) becomes

$$\begin{bmatrix}\Delta b_{12}(k)\\ \Delta b_{21}(k)\end{bmatrix} = -\alpha y_1(t)y_2(t)\begin{bmatrix}\phi_{21}(t,k)\\ \phi_{12}(t,k)\end{bmatrix} \quad (15)$$

In this simulation, we rewrite eqn (15) as

$$\begin{bmatrix}\Delta b_{12}(k)\\ \Delta b_{21}(k)\end{bmatrix} = -\alpha y_1(t)y_2(t)\mathbf{W}(t)\begin{bmatrix}\phi_{21}(t,k)\\ \phi_{12}(t,k)\end{bmatrix} \quad (16)$$

If $\mathbf{W}(t)$ is a positive definite matrix, eqn (16) surely converge to the minimum of eqn (9). The matrix $\mathbf{W}(t)$ is introduced to improve convergence speed. We adopt the following $\mathbf{W}(t)$:

$$\mathbf{W}(t) = \begin{bmatrix}1/E[y_1(t)^2] & 0\\ 0 & 1/E[y_2(t)^2]\end{bmatrix}$$

For the estimation of $E[y_i(t)^2]$ (i = 1,2), we use the following moving average:

$$\psi_i(t) = \gamma\psi_i(t-1) + (1-\gamma)\, y_i(t)^2 \quad (i = 1,2;\ 0 < \gamma < 1) \quad (17)$$

Example:

This example deals with signals which were obtained in an *anechoic room*. Source signals $s_1(t)$ and $s_2(t)$ were a female and a male voice, respectively. The signals $x_i(t)$ (i = 1, 2) were observed by two microphones. The configuration of two signal sources and two microphones is shown in Fig. 2. Parameters M and L of eqn (5) were set to 9 and 0, respectively. The parameters of the learning algorithm were chosen as $\alpha = 0.00002$, $\beta = 0.9$, $\gamma = 0.9$, and the initial values of $b_{12}(k)$, $b_{21}(k)$ (k = 0,...,9), $\phi_{12}(t)$, $\phi_{21}(t)$, and $\psi_i(t)$ were set to 0, 0, 1, 1, and 1, respectively.

Figure 3 shows the plots of $s_i(t)$, $x_i(t)$, and $y_i(t)$ (i = 1,2). It can be seen that the output signals $y_1(t)$ and $y_2(t)$ are nearly close to the original speech signals $s_1(t)$ and $s_2(t)$, respectively.

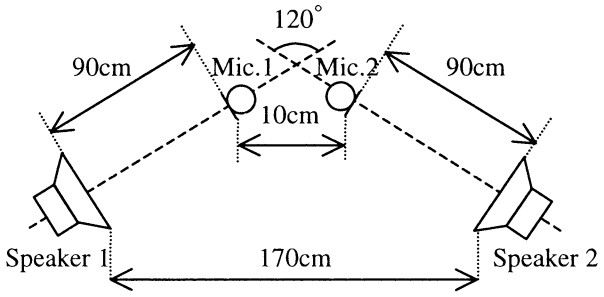
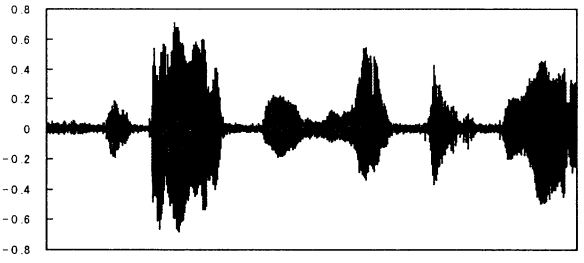
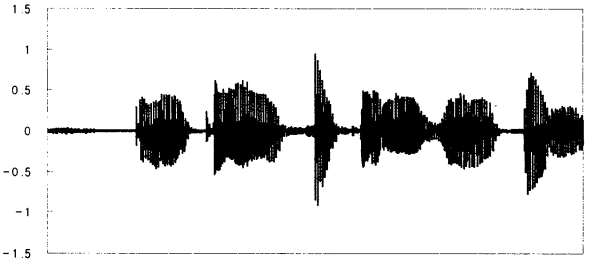


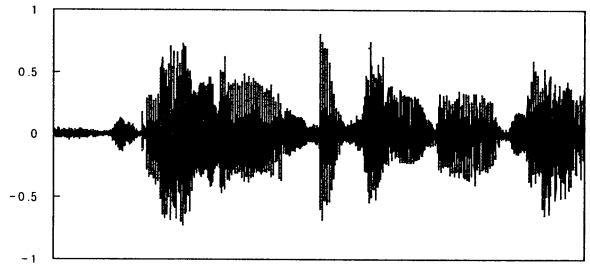
Fig. 2 The configuration of two signal sources and two microphones



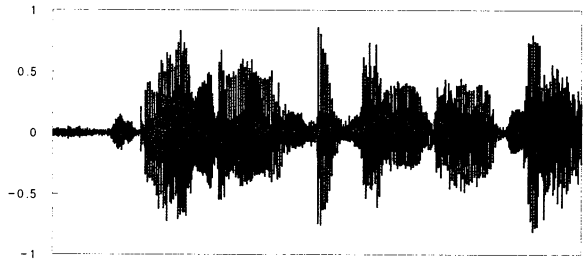
(a) Source signal $s_1(t)$



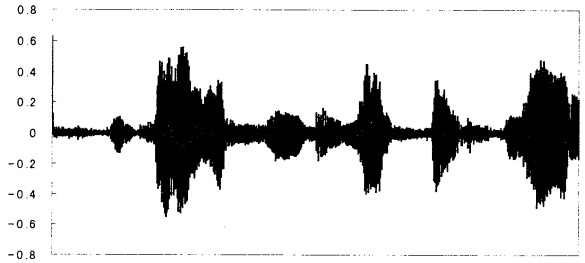
(b) Source signal $s_2(t)$



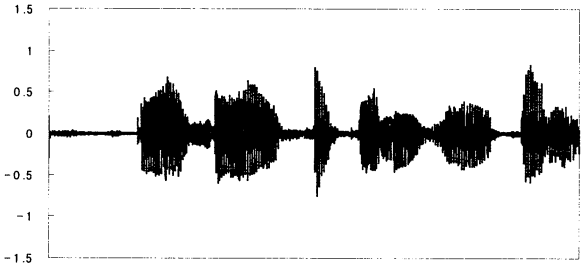
(c) Observed signal $x_1(t)$



(d) Observed signal $x_2(t)$



(e) Output signal $y_1(t)$



(f) Output signal $y_2(t)$

Fig. 3 The plots of $s_i(t)$, $x_i(t)$, and $y_i(t)$ (i = 1,2)

6. Conclusion

We have proposed a method for blind signal separation of convolved non-stationary signals. The method implements blind signal separation by minimizing the cost function that takes zero only when the network outputs are uncorrelated with each other.

We have shown that the proposed learning rule can separate the original signals from their mixtures observed in an anechoic room.

References

[1] A. Cichoki, S. Amari, and J. Cao, "Blind separation of delayed and convolutive signals with self-adaptive learning rate," Proceedings of 1996 International Symposium on Nonlinear Theory and its Applications, pp. 229-232, 1996.

[2] C. Jutten and J. Herault, "Blind separation of sources, part I: an adaptive algorithm based on neuromimetic architecture," Signal Processing, Vol. 24, No. 1, pp. 1-10, 1991.

[3] M. Kawamoto, K. Matsuoka, and M. Oya, "Blind separation of sources using temporal correlation of the observed signals," IEICE Trans. Fundamentals, Vol. E80-A, No. 4, April 1997.

[4] T. W. Lee, A. J. Bell, and R. H. Lambert, "Blind separation of delayed and convolved sources," Advances in Neural Information Processing Systems, 1996 (to appear).

[5] K. Matsuoka, M. Oya, and M. Kawamoto, "A Neural Net for Blind separation of Nonstationary Signals," Neural Networks, Vol. 8, No. 3, pp. 411-419, 1995.

[6] K. Torkkola, "Blind separation of convolutive sources based on information maximization, Neural Networks for Signal Processing VI, pp. 423-432, 1996.

[7] J. Xi and J. P. Reilly, "Blind separation of signals in a convolutive environment," Proc. ICASSP, pp. 1327-1331, 1997.

Proc. of Third Int. Symp. on Artificial Life, and Robotics (AROB III' 98),
Oita, Japan, 19-21, January, 1998,

Negatively Correlated Neural Networks for Classification

Yong Liu and Xin Yao
Computational Intelligence Group, School of Computer Science
University College, The University of New South Wales
Australian Defence Force Academy, Canberra, ACT, Australia 2600
Email: {liuy,xin}@cs.adfa.oz.au

Abstract

A new approach to designing neural network ensembles has been proposed recently [1]. Experimental studies on some regression tasks have shown that the new approach performs significantly better than previous ones [1]. However, the regression tasks considered did not include any noise. This paper presents a new algorithm for designing neural network ensembles for classification problems with noise. This new algorithm is different from that used for regression tasks although the idea is similar. The idea behind this new algorithm is to encourage different individual networks in an ensemble to learn different parts or aspects of the training data so that the whole ensemble can learn the whole training data better. Negatively correlated networks are trained with a novel correlation penalty term in the error function to encourage such specialisation. In our algorithm, individual networks are trained simultaneously rather than sequentially. This provides an opportunity for different networks to interact with other and to specialise. Experiments on a real-world problem demonstrate that the new algorithm can produce neural network ensembles with good generalisation ability.

1 Introduction

Neural network ensembles [2, 3] have been used increasingly often in recent years to improve classifier's generalisation. There are several methods of designing neural network ensembles. Most of them follow the two-stage design process [2]; first generating individual networks, and then combining them. Usually, the individual networks are trained independent of each other. One of the disadvantages of such an approach is the loss of interactions among individual networks during learning. There is no feedback from the combination stage to the individual network design stage either. It is possible that some of the independently designed individuals do not make much contribution to the whole ensemble.

This paper proposes a new algorithm for designing neural network ensembles. The idea behind the new algorithm is to encourage different individual networks to learn different parts or aspects of the training data so that the whole ensemble can learn the training data better. Unlike previous work on neural network ensemble design where individual networks were trained sequentially, all individual networks are trained simultaneously in our algorithm. Simultaneous training provides an opportunity for individual networks to interact and specialise.

In order to encourage different individual networks to learn different things, negatively correlated neural networks are trained using a novel correlation penalty term in the error function. It has been shown that an ensemble of negatively correlated neural networks can perform significantly better than previous systems for regression tasks without any noise [1]. For classification problems with noise, the correlation penalty term used in the regression tasks does not work very well because it tends to overfit the training data. A new correlation penalty term is studied in this paper and is shown to be quite effective for problems with noise.

The rest of this paper is organised as follows: Section 2 presents the algorithm for training an ensemble of negatively correlated neural networks simultaneously. Section 3 describes the experimental result of applying this algorithm to solve a real-world problem. Finally, Section 4 concludes the paper.

2 Simultaneous Learning of Negatively Correlated Neural Networks

Suppose that we have a training set

$$D = \{(\mathbf{x}(1), d(1)), \cdots, (\mathbf{x}(N), d(N))\}$$

where $\mathbf{x} \in R^p$ and d is a scalar. The assumption that the output d is a scalar has been made merely to simplify exposition of ideas without loss of generality.

The functional relationship between $\mathbf{x}$ and d can be expressed as

$$d = g(\mathbf{x}) + \epsilon \tag{1}$$

where $g(\mathbf{x})$ is some function of vector $\mathbf{x}$, and ϵ is a random expectational error that reflects the fact that simultaneous specification of a set of input vectors, $\{\mathbf{x}(1), \cdots, \mathbf{x}(N)\}$, does not uniquely specify an output value (unless ϵ is a constant). Function $g(\mathbf{x})$ is often defined by [4]

$$g(\mathbf{x}) = E[d|\mathbf{x}] \tag{2}$$

where E is the statistical expectation operator.

The exact functional relationship between $\mathbf{x}$ and d is usually unknown. The purpose of neural network learning is to use $\mathbf{x}$ to explain or predict d. It does so by encoding the empirical knowledge represented by the training set D into a set of synaptic weights, $\mathbf{w}$. One criterion for optimising weights is the minimisation of the mean-square error

$$J(\mathbf{w}) = E\left[(d - F(\mathbf{x}, \mathbf{w}))^2\right] \tag{3}$$

where $F(\mathbf{x}, \mathbf{w})$ is the actual response of the network.

The error function $J(\mathbf{w})$ may be expressed as the sum of two terms

$$J(\mathbf{w}) = E\left[(d - g(\mathbf{x}))^2\right] + E\left[(g(\mathbf{x}) - F(\mathbf{x}, \mathbf{w}))^2\right] \tag{4}$$

where the first term is independent of $\mathbf{w}$. It is sufficient to minimise the second term. To be explicit about dependence on the training set D, the approximating function may be rewritten as $F(\mathbf{x}, D)$. Consider then the mean-squared error of the function $F(\mathbf{x}, D)$ as an estimator of $g(\mathbf{x}) = E[d|\mathbf{x}]$, which is defined by

$$E_D\left[(E[d|\mathbf{x}] - F(\mathbf{x}, D))^2\right]$$

where the expectation operator E_D represents the average over all the patterns in the training set D.

In this section we consider estimating $g(\mathbf{x}) = E[d|\mathbf{x}]$ by forming a simple average of a set of $F_i(\mathbf{x}, D)$ which are trained using the same training data set D

$$F(\mathbf{x}, D) = \frac{1}{M}\Sigma_{i=1}^{M} F_i(\mathbf{x}, D) \tag{5}$$

where M is the number of individual neural networks.

A correlation penalty term is introduced into the error function of each individual network so that the individual network can be trained simultaneously to specialise. The error function E_i for individual i is defined by

$$\begin{aligned} E_i &= \frac{1}{N}\Sigma_{n=1}^{N} E_i(n) \\ &= \frac{1}{N}\Sigma_{n=1}^{N}\left[\frac{1}{2}(d(n) - F_i(n))^2 + \lambda p_i(n)\right] \end{aligned} \tag{6}$$

where N is the number of training patterns, $E_i(n)$ is the value of the error of network i at presentation of the nth training pattern, $F_i(n)$ is the output of individual network i on the nth training pattern, and p_i is the correlation penalty function. The purpose of minimising p_i is to de-correlate each individual's error with errors for the rest of the ensemble. The parameter $\lambda > 0$ is inserted so that the strength of the penalty can be adjusted. The function p_i can be chosen as

$$p_i(n) = (F_i(n) - 0.5)\,\Sigma_{j \neq i}\,(F_j(n) - 0.5) \tag{7}$$

for classification problems with noise.

The partial derivative of E_i with respect to the output of individual i on nth training pattern is

$$\frac{\partial E_i(n)}{\partial F_i(n)} = F_i(n) - d(n) + \lambda\Sigma_{j \neq i}(F_{j,n} - 0.5) \tag{8}$$

The standard back-propagation (BP) algorithm with pattern-by-pattern updating [5] has been used for weight adjustments in our ensembles. Weight updating of all the individual networks is performed simultaneously using Eq.(8) after the presentation of each training case. One complete presentation of the entire training set during the learning process is called an *epoch*.

From Eqs.(6) and (8), the following observations can be made:

1. During the training process, all the individual networks interact each other through their penalty functions, i.e., Eq.(7).

2. For $\lambda = 0.0$, there is no correlation penalty term in the the error functions of the individual networks, and the individual networks are trained independently using BP. That is, independent learning using BP for the individual networks is a special case of our algorithm.

By adjusting the value of the strength parameter λ, we can control the bias, variance, and covariance of the ensemble to achieve better performance.

3 Experimental Studies

Experimental studies have been carried out to test our new algorithm for neural network ensemble learning.

The Australian credit card assessment problem [6, 7] was used as an example. The problem is to assess applications for credit cards based on a number of attributes. There are 690 cases in total. The output has two classes. The 14 attributes include 6 numeric values and 8 discrete ones, the latter having from 2 to 14 possible values. This data set was obtained from the UCI machine learning repository. The input attributes used for neural networks are rescaled to between 0.0 and 0.1 by a linear function. The whole data set is randomly partitioned into a training (518 cases) and a testing set (172 cases). In order to reduce the influence of random partition on the evaluation, the ratio of class 1 to class 2 in the training and testing set was roughly the same.The testing set was not seen by any neural network during the training phase. It is only used for testing the generalisation of the neural network ensemble after it is trained.

The ensemble used in our experiment consisted of five strictly-layered feedforward neural networks. All individual networks had the same architecture. They had three layers and 5 hidden nodes in the hidden layer. The learning-rate η in BP is 0.1, and λ is 0.375. These parameters were chosen after limited preliminary experiments. They are not meant to be optimal.

Table 1 summarises the results of 25 independent runs of our algorithm at epoch 500 and 1000 for the Australian credit card assessment problem. Figure 1 shows the average result over the 25 runs. The result shows that there was a dramatic reduction in both training and testing error rates in the first 50 epochs. Table 2 shows the size of the correct response sets of individual networks on the testing set and their intersections. The correct response set Ω_i of individual network i on the testing set consists of all the cases in the testing set which are classified correctly by the individual network i. It appears that different individual networks were able to specialise to different parts or aspects of the testing data set. Since the data set was automatically decomposed into smaller and more specialised tasks, the individual networks were able to learn them quickly. After that, the testing error rate improved slowly as the training time increased.

It is interesting in Figure 1 that the testing error rate was smaller than or similar to the training error rate for nearly 300 epochs in the beginning. This illustrates the good generalisation of learned ensembles. As the training time increases, the training error rate decreases as expected. However, the testing error rate remains roughly the same for a very long period without displaying signs for overfitting. This implies that our algorithm is quite resistant to overfitting. It can produce neural network ensembles with good generalisation abil-

	Training set		Test set	
# epochs	500	1000	500	1000
Mean	0.1093	0.0846	0.1177	0.1163
SD	0.0092	0.0088	0.0182	0.0159
Min	0.0927	0.0676	0.0698	0.0756
Max	0.1255	0.1004	0.1628	0.1454

Table 1: Error rates of CELS for the Australian credit card assessment problem.

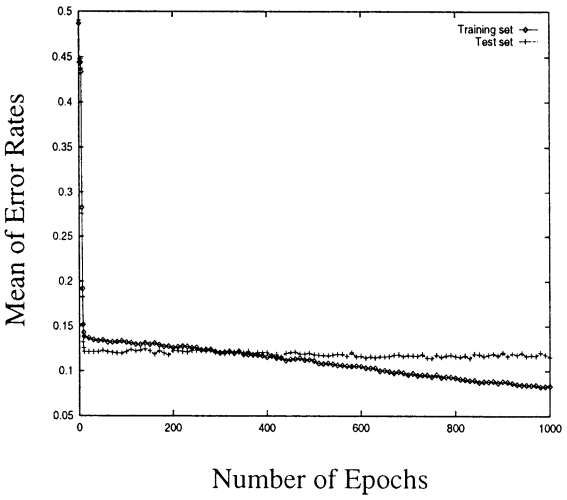


Figure 1: The average result over 25 runs of our ensemble learning algorithm for the Australian credit card assessment problem. The horizontal axis indicates the number of training epochs. The vertical axis indicates the error rate.

$\Omega_1 = 146$	$\Omega_2 = 148$	$\Omega_3 = 149$
$\Omega_4 = 151$	$\Omega_5 = 150$	$\Omega_{12} = 137$
$\Omega_{13} = 137$	$\Omega_{14} = 141$	$\Omega_{15} = 139$
$\Omega_{23} = 140$	$\Omega_{24} = 141$	$\Omega_{25} = 146$
$\Omega_{34} = 139$	$\Omega_{35} = 140$	$\Omega_{45} = 142$
$\Omega_{123} = 132$	$\Omega_{124} = 133$	$\Omega_{125} = 136$
$\Omega_{134} = 133$	$\Omega_{135} = 133$	$\Omega_{145} = 135$
$\Omega_{234} = 134$	$\Omega_{235} = 138$	$\Omega_{245} = 139$
$\Omega_{345} = 134$	$\Omega_{1234} = 128$	$\Omega_{1235} = 131$
$\Omega_{1245} = 132$	$\Omega_{1345} = 129$	$\Omega_{2345} = 132$
$\Omega_{12345} = 127$		

Table 2: The sizes of the correct response sets of individual networks on the testing set and their intersections for the Australian credit card assessment problem.

ity without using techniques such as cross-validation.

The results given in Table 1 is comparable to those obtained using evolutionary approaches [8, 9], but better than others [6]. Table 3 compares the average testing error rates among different algorithms.

Algorithm	TER	Algorithm	TER
NCNN	0.116	Logdisc	0.141
EPNet	0.115	CART	0.145
Evo-En-RLS	0.131	RBF	0.145
Cal5	0.137	CASTLE	0.148
ITrule	0.141	NaiveBay	0.151
DIPOL92	0.141	IndCART	0.152
Discrim	0.141	BP	0.154

Table 3: Comparison among our ensemble learning algorithm (NCNN), EPNet [8], an evolutionary ensemble learning algorithm (Evo-En-RLS) [9], and others [6] in terms of the average testing error rate. TER stands for Testing Error Rate in the table.

4 Conclusions

This paper describes a new approach to designing neural network ensembles for classification problems with noise. The new approach can be regarded as one way of decomposing a large problem into smaller and specialised ones, so that each subproblem can be dealt with by an individual neural network relatively easily. A correlation penalty term in the error function was proposed to encourage the formation of specialists in the ensemble. A real-world problem, i.e., the Australian credit card assessment problem, was used as an example to demonstrate the effectiveness of this new approach.

There are, however, some issues that need resolving. First, all individual neural networks have the same architecture in our current algorithm. This may not be optimal. An automatic way to generate or construct different individual networks would be ideal. Second, the size of ensembles is fixed at the moment. It would be desirable to develop a learning algorithm which can vary the ensemble size dynamically. Third, more empirical studies on other benchmark problems should be carried out in order to evaluate our algorithm further.

ACKNOWLEDGEMENT — This work is partially supported by the Australian Research Council through its small grant scheme.

References

[1] Y. Liu and X. Yao, "A cooperative ensemble learning system," in *1998 IEEE International Conference on Neural Networks, Anchorage, USA*, IEEE Press, New York, NY, 5-9 May 1998.

[2] A. Sharkey, "On combining artificial neural nets," *Connection Science*, vol. 8, pp. 299–313, 1996.

[3] X. Yao and Y. Liu, "Ensemble structure of evolutionary artificial neural networks," in *Proc. of the 1996 IEEE Int'l Conf. on Evolutionary Computation (ICEC'96), Nagoya, Japan*, pp. 659–664, IEEE Press, New York, NY 10017-2394, 1996.

[4] H. White, "Learning in artificial neural networks: A statistical perspective," *Neural Computation*, vol. 1, pp. 425–464, 1989.

[5] S. Haykin, *Neural Networks: A Comprehensive Foundation.*
New York, NY 10022: Macmillan College Publishing Company, Inc., 1994.

[6] D. Michie, D. J. Spiegelhalter, and C. C. Taylor, *Machine Learning, Neural and Statistical Classification.*
London: Ellis Horwood Limited, 1994.

[7] J. R. Quinlan, *C4.5: Programs for Machine Learning.*
San Mateo, CA: Morgan Kaufmann, 1993.

[8] X. Yao and Y. Liu, "A new evolutionary system for evolving artificial neural networks," *IEEE Transactions on Neural Networks*, vol. 8, no. 3, May 1997.

[9] X. Yao and Y. Liu, "Making use of population information in evolutionary artificial neural networks," *IEEE Transactions on Systems, Man, and Cybernetics*, vol. 28B, no. 2, April 1998.

Proc. of Third Int. Symp. on Artificial Life, and Robotics (AROB III' 98),
Oita, Japan, 19-21, January, 1998,

On-Line Evolutionary Learning of NN-MLP

Tomoyuki Suzuki and Qiangfu Zhao

The University of Aizu
Aizu-Wakamatsu, Fukushima 965-80, Japan
Email: {m5011114, qf-zhao}@u-aizu.ac.jp

Abstract

To design the nearest neighbor based multilayer perceptron (NN-MLP) efficiently, we have proposed a non-genetic evolutionary algorithm called the R^4-rule. For off-line learning, the R^4-rule can produce the smallest or nearly smallest networks with high generalization ability by iteratively performing four basic operations: *recognition, remembrance, reduction* and *review*. For on-line learning, we have introduced two parameters: the *review limitation* β and the *reduction rate* γ. These two parameters are very useful for stabilizing the algorithm, provided that their values are chosen properly. In this paper, we propose a method for finding good parameters based on a simple genetic algorithm (SGA). The efficiency of combining the genetic algorithm with the non-genetic R^4-rule is illustrated using experimental results.

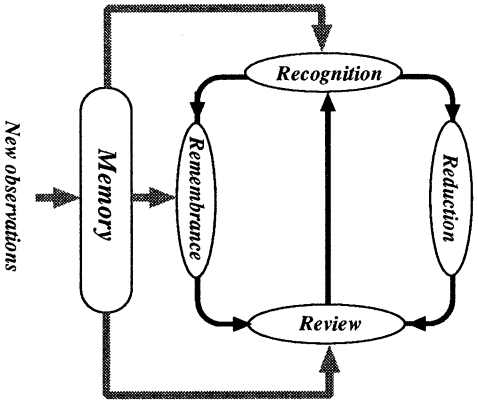


Figure 1: R^4-rule for evolutionary learning

1 Introduction

The nearest neighbor based multilayer perceptron (NN-MLP) is a neural network realization of the nearest neighbor classifier (NNC). It is a single-hidden-layer network with each hidden neuron corresponding to a *prototype* and each output neuron corresponding to a *pattern class*. The NN-MLP is very simple but very useful for pattern recognition. Actually, it can be used for any complex decision making provided that the number of hidden neurons (prototypes) is sufficiently large [1]. In addition, since patterns are represented *locally*, NN-MLP is very suitable for *on-line learning* and *evolutionary learning*. It is for these reasons that NN-MLP has been studied extensively by many researchers in different forms [2]-[13].

To realize the NN-MLP more efficiently, and to increase its generalization ability, it is necessary to use as less hidden neurons as possible in the network. For this purpose, many methods have been proposed in the literature. The most efficient one, to the authors knowledge, is the R^4-rule given in [2]-[4]. This algorithm can produce the smallest or nearly smallest NN-MLP with high generalization ability. There are four basic operations in the R^4-rule: *recognition*, *remembrance*, *reduction* and *review*. One evolutionary cycle is defined as $recognition \wedge (remembrance \vee reduction) \wedge review$, where $\wedge$ and $\vee$ are logical AND and OR, respectively. The learning can be performed cycle after cycle until some criterion is satisfied. Experimental results have shown that, for off-line learning, the performance of the network will become better and better, and will finally be good enough to classify all training samples using a small number of hidden neurons.

To apply the R^4-rule to on-line learning, we introduced two parameters in [4]: the *review limitation* β and the *reduction rate* γ. These two parameters are very useful to stabilize the R^4-rule if their values are chosen properly. In this paper, we propose a method for finding good parameters based on a simple genetic algorithm (SGA). The efficiency of combining the genetic algorithm with the non-genetic R^4-rule will be illustrated using experimental results.

2 A Brief Review of the R^4-Rule

The relations between the four operations of the R^4-rule are shown in see Fig. 2. Each operation is performed by a process or a subroutine. Briefly speaking, *recognition* is a process to test the ability of the recent network and the fitness of each hidden neuron. After *recognition*, we can know how the present network performs and how important each hidden neuron is. If there are too many recognition errors, some of the hidden neurons should be added in the process *remembrance*. On the other hand, if the recognition rate is very high, some of the hidden neurons with very low fitness can be removed by *reduction* to make the network more efficient. The process *review* is necessary when some hidden neurons are removed or added. In *review*, network parameters are readjusted so that the network can achieve better performance using recent hidden neurons.

In the process *recognition*, the ability of the network can be tested as usual by using the nearest neighbor rule. The key point here is to test the fitness of the hidden neurons. In [2] and [3], the fitness or goodness of a hidden neuron was tested through intra-class competition, and in [5], the fitness was tested by the classification ability of the neuron. For *remembrance*, a direct method is to add a hidden neuron whenever a sample is mis-classified, but this is not so efficient because the network may soon become too large. In our study, only one hidden neuron is added for each mis-classified class in the operation *remembrance*, and this is done only when the recognition rate is smaller than a desired value r_0. The strategy for *reduction* is also a key point. We can remove a hidden neuron if its fitness is smaller than a threshold. However, to make the learning process more stable, only one hidden neuron with very small fitness is removed, and this neuron is selected *at random*. For *review*, any supervised competitive learning method can be used, as long as it is simple and efficient. In the off-line version of the R^4-rule, the DSM (decision surface mapping) algorithm given in [12] is adopted.

The two operations *review* and *reduction* play a very important role in stabilization of the R^4-rule. In the on-line version of the R^4-rule, the algorithm for *review* is given as follows:

- Step 1: $\forall x$ in the current training set Ω, test if x can be recognized. If yes, no change; otherwise, update the weights as follows:

$$\begin{aligned} p_0 &= p_0 + \alpha(x - p_0) \\ p_1 &= p_1 - \alpha(x - p_1) \end{aligned} \quad if\ \|x - p_0\| < \beta \quad (1)$$

where α is the *convergent rate*, and β is the *review limitation*.

- Step 2: Terminate if the number of iterations reaches to a given value, or all samples have been correctly recognized; otherwise, return to Step 1.

Actually, this algorithm is a combination of the DSM algorithm and the ART algorithm.

For *reduction*, it is necessary to define the fitness of the hidden neurons properly. This is given as follows. For any $x \in \Omega$, suppose that there are q hidden neurons $p_1, p_2, ..., p_q$ with the same label as x, and they fire simultaneously. If p_w and p_l satisfy

$$\begin{aligned} \rho(p_w) &= \max\ \rho(p_i) \\ \rho(p_l) &= \min\ \rho(p_i) \end{aligned} \qquad i = 1, 2, ..., q \quad (2)$$

where $\rho(p)$ is the fitness of p, we say p_w is the winner, and p_l is the loser. The fitness of a hidden neuron is defined by

$$\rho(p) = \frac{\nu(p)}{\mu(p)} \quad (3)$$

where $\nu(p)$ is the total number of samples represented by p, and $\mu(p)$ is the *age* of p. The age of a hidden neuron is initially 1, and is increased by one after each learning cycle. The parameter $\nu(p)$ is initially zero, and is increased by one for each sample in Ω if p is a winner, or decreased by one if p is a loser.

In each learning cycle, one of the hidden neurons with ρ smaller than $\gamma \times \xi$ was selected at random, and was removed from the network. Here, ξ is the possible number of samples per class in Ω, and is given by

$$\xi = \frac{size\ of\ \Omega}{number\ of\ class}, \quad (4)$$

and γ is the *reduction rate*, which is the percentage of samples in the same class represented by a hidden neuron.

3 The Simple Genetic Algorithm

There are many parameters used in the on-line version of the R^4-rule. They are

1. N_t: the number of training samples available in each learning cycle,
2. N_o: the number of newly observed samples in each learning cycle,
3. r_0: the desired recognition rate,

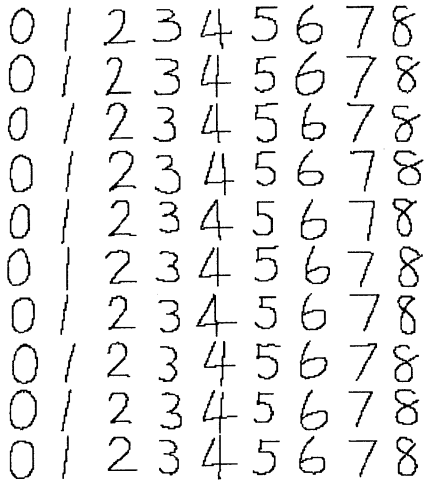


Figure 2: Part of samples used in the experiments

4. N_l: the number of learning cycles,
5. N_r. the number of epochs for *review*,
6. α: the convergent rate,
7. β: the review limitation,
8. γ: the reduction rate.

The first 4 parameters can be *given* according to some physical conditions. The fifth parameter is fixed to 10 in all of our experiments because the review algorithm usual converges in about epochs [3]. The most important thing here is to determine the last three parameters.

Now let us find the proper values of α, β and γ using SGA. In the SGA, an individual is a binary bit string with three equal length segments. Each segment is the binary representation of one of the parameters. The available values of α, β and γ are

$$\alpha \in (0,1), \quad \beta \in (0,2), \quad \gamma \in (0,\frac{1}{2}). \qquad (5)$$

In each generation, all individuals in the populations are first sorted according to their fitness, and r_s% of the individuals with lower fitness are replaced by offsprings of other individuals, where r_s is the selection rate. One-point cross-over and mutation are used for reproduction. The fitness of an individual is defined as the recognition rate of the NN-MLP obtained by the R^4-rule. The recognition rate is defined using the *testing samples*. Therefore, precisely speaking, the learning is still *semi-on-line* because the test set is not available for real on-line learning. Results for real on-line evolutionary learning will be given in the future.

Table 1: Experimental results for first run (seed =0)

N_g	α	β	γ	f_{max}	N_u	f_{ave}
1	0.15	1.94	0.43	0.941	9	0.872
6	0.25	1.45	0.03	0.944	17	0.908
13	0.25	1.45	0.03	0.950	20	0.922
17	0.34	0.94	0.02	0.956	25	0.923
40	0.19	1.04	0.03	0.958	18	0.931
73	0.26	1.14	0.02	0.967	26	0.935
103	0.31	1.15	0.03	0.975	18	0.937

4 Experimental Results

To demonstrate the performance of the SGA for finding good parameters used by the R^4–rule, we have conducted several experiments with a handwritten digit recognition problem. In this problem, 80 samples were written by the one of the authors in an ordinary manner for each class. The first 40 samples of each class are used for training, and the remaining samples are used for testing. In the experiment, every digit was written using mouse in a 256×256 frame. No normalization of any kind was performed. Part of the samples are shown in Fig. 3. The digit 9 is not considered because features used in the experiment are rotationally invariant. Specifically, the features are the crossing numbers on some concentric circles, with the center of the concentric circles being the center of gravity of the image.

In the experiment, the population size is 50, the selection rate is 40%, the cross-over rate is 100%, and the mutation rate is 1%. The binary representation of each parameter is of 16-bits. The parameters for the R^4-rule are: the number of training samples per learning cycle $N_t = 45$, the number of newly observed samples $N_o = 1$, the desired recognition rate $r_0 = 99\%$, the number of learning cycles $N_l = 360$, and the number of epochs for *review* $N_r = 10$. In each learning cycle, one new training sample is randomly chosen and is put into the current training set.

The experimental results are given in Table 1, where f_{max} is the maximum fitness, f_{ave} is the average fitness, and N_u is the number of neurons used by the best network. Compared with the results given in [4], we can see that good parameters can be generated automatically by the SGA, and the recognition rate is

much more better than that obtained by using *hand-chosen* parameters.

5 Concluding Remarks

In this paper, we have proposed to use the simple genetic algorithm for finding the parameters used by the R^4-rule. Experimental results have shown the efficiency of combining the genetic algorithm and the non-genetic R^4-rule. Of course, the experiments conducted here are still too simple to show the efficiency of the algorithm for solving practical problems. We are expecting more results of more runs. We are also trying to apply the algorithm to some well-known data base (say, the ETL data base). All these results will be presented at the conference. Currently, we are trying to apply the SGA to real on-line learning, so that good R^4-rules with good parameters can be created automatically without knowing a complete *test set*.

References

[1] T. M. Cover and P. E. Hart, "Nearest neighbor pattern classification," IEEE Trans. on Information Theory, Vol. IT-13, No. 1, pp. 21-27, Jan. 1967.

[2] Q. F. Zhao and T. Higuchi, "Supervised organization of nearest neighbor MLP," Proc. International Conference on Neural Information Processing, pp. 1398-1403, Seoul, Korea, Oct. 1994.

[3] Q. F. Zhao and T. Higuchi, "Evolutionary learning of nearest neighbor MLP," IEEE Trans. on Neural Networks, Vol.7, No. 3, pp. 762-767, 1996.

[4] Q. F. Zhao, "Stable on-line evolutionary learning of NN-MLP," to be published in IEEE Trans. on Neural Networks, Vol.8, No. 6, 1997.

[5] Q. F. Zhao and T. Higuchi, "On-line minimization of nearest neighbor based MLP," Proc. World Congress on Neural Networks, pp. I636-I641, Washington, D.C., July 1995.

[6] O. J. Murphy, "Nearest neighbor pattern classification perceptrons," Proc. IEEE, Vol. 78, No. 10, pp. 1595-1598, Oct. 1990.

[7] N. K. Bose and A. K. Garga, "Neural network design using Voronoi diagrams," IEEE Trans. on Neural Networks, Vol. 4, No. 5, pp. 778-787, Sept. 1993.

[8] T. Kohonen, "Self-organized formation of topologically correct feature maps," Biolog. Cybern.,Vol. 43, pp. 59-69, 1982.

[9] T. Kohonen, "The self-organizing map," Proc. IEEE, Vol. 78, No. 9, pp. 1464-1480, Sept. 1990.

[10] G. A. Carpenter and S. Grossberg, "ART 2: self-organization of stable category recognition codes for analog input patterns," Applied Optics, Vol. 26, No. 23, pp. 4919-4930, Dec. 1987.

[11] G. A. Carpenter and S. Grossberg, "The ART of adaptive pattern recognition by a self-organizing neural network," IEEE Computer, Vol. 21, No. 3, pp. 77-88, Mar. 1988.

[12] S. Geva and J. Sitte, "Adaptive nearest neighbor pattern classification," IEEE Trans. on Neural Networks, Vol. 2, No.2, pp. 318-322, Mar. 1991.

[13] D. L. Reilly, L. N. Cooper and C. Elbaum, "A neural model for category learning," Biol. Cybern. 45, pp. 35-41, 1982.

[14] P. E. Hart, "The condensed nearest neighbor rule, " IEEE Trans. on Information Theory, Vol. 14, No. 5, pp. 515-516, May 1968.

[15] G. W. Gates, "The reduced nearest neighbor rule, " IEEE Trans. on Information Theory, Vol. 18, No. 5, pp. 431-433, May 1972.

[16] E. I. Chang, and R.P. Lippmann, "Using genetic algorithms to improve pattern classification performance," *Advances in Neural Information Processing Systems*, pp. 797-803, 1991.

[17] Y. Linde, A. Buzo and R. M. Gray, "An algorithm for vector quantizer design," IEEE Trans. on Communication, Vol. COM-28, No. 1, pp. 84-95, Jan. 1980.

[18] T. Poggio and F. Girosi, "Networks for approximation and learning," Proc. IEEE, Vol. 78, No. 9, pp. 1481-1497, 1990.

Proc. of Third Int. Symp. on Artificial Life, and Robotics (AROB III' 98),
Oita, Japan, 19-21, January, 1998,

Autonomous mobile robot rendezvous

P. Pawicz, P. Kalata, and M. Kam
Repartment of Electrical and Computer Engineering
Drexel University
Philadelphia, Pennsylvania 19104 USA

The manuscript of this talk will be distributed at the symposium.

Author Index

A

Abe, K. 145, 358
Adachi, M. 332
Agah, A. 258
Aihara, K. ... 328, 332, 342, 350
Akimoto, K. 110
Akisato, Y. 372
An, K. 47
Ando, H. 190
Aramaki, S. 690
Arthur, W. B. I-34
Asada, H. 190
Ascott, R. 594

B

Bae, J.-I. 572
Barrett, C. L. I-28
Berthouze, L. 678
Bubnicki, Z. 490
Burnham, K. J. 541

C

Casti, J. L. I-12
Chatterjee, R. 380
Cho, J. 564
Cho, S.-B. 271
Christaller, T. 495

D

Dautenhahn, K. 435
Doyle, J. I-40

E

Egashira, N. 568

F

Franco, M. G. 448
Fraser, S. M. 161
Froyland, G. 346
Fujii, A. 119
Fujii, K. 314, 324
Fujii, M. 532
Fujito, T. 622
Fujimoto, K. 638
Fujita, Y. I-47
Fujiwara, S. 406
Fujiyama, H. 7
Fukuda, T. I-41
Fukushima, S. 7
Funahashi, Y. 55, 59, 63
Furuhashi, T. 141, 532

G

Garis, H. D. 186, 258, 263
Gen, M. 27, 31, 35, 39
43, 47
Gers, F. 258, 263
Goto, S. 568
Goto, T. 414
Guo, Q. 388

H

Hada, Y. 670
Hajiri, K. 392, 397
Han, M. 224
Han, S.-H. 572
Hanagata, M. 336
Haneda, H. 289
Hara, S. 306
Harashima, F. 578
Harris, C. J. 384
Hase, K. 174
Hasegawa, T. 674
Hashem,M.M.A. 514
Hashimoto, H. 578
Hashimoto, M. 73, 224
Hashimoto, T. 662
He, W. 200, 427
Hemmi, H. 186, 196, 267
Henrich, D. 590
Hiji, M. 39
Hikage, T. 196, 267
Hikawa, H. 586
Hiraishi, H. 149
Hirakawa, M. 228
Hirasawa, K. 224, 703
Hitaka, Y. 51
Holland, J. H. I-34
Hong, Y.-J. 166
Honma, N. 358
Horio, Y. 336
Hu, J. 224, 703
Hyun, W. K. 564

I

Ichikawa, M. · · · · · · · · 205, 207
Ichinose, N. · · · · · · · · · · 328
Ida, K. · · · · · · · · · 31, 43
Iida, M. · · · · · · · · · · 242
Ikeda, Y. · · · · · · · · · · 510
Ikegami, T. · · · · · · · · · · 650
Ikeguchi, T. · · · · · · · · · · 342
Ikeuchi, H. · · · · · · · · · · 695
Imou, K. · · · · · · · · · · 238
Inoue, K. · · · · · · · · · 234, 289
Ishida, M. · · · · · · · · · · 238
Ishiguro, A. · · · · · · · · · · 119
Ishimatsu, T. · · · · 622, 626, 630, 634
638
Itakura, S. · · · · · · · · · · 678
Ito, A. · · · · · · · · · 474, 478
Ito, M. · · · · · · I-1, 101, 114
Ito, S. · · · · · · · · · · 101
Itokawa, N. · · · · · · · · · · 238
Itou, M. · · · · · · · · · · 414
Iwaki, H. · · · · · · · · · · 119
Iwamoto, H. · · · · · · · · · · 289
Iwamoto, I. · · · · · · · · · · 630
Iwasaki, M. · · · · · · · · · · 254
Iwata, T. · · · · · · · · · · 707
Izumi, K. · · · · 510, 514, 518, 524
Izumi, T. · · · · · · · · · · 51

J

James, D. J.G. · · · · · · · · · · 541
Johnson, J. · · · · · · · · · · 503
Ju, D.-Y. · · · · · · · · · · 707
Jun, H. B. · · · · · · · · · · 454

K

Kabashima, Y. · · · · · · · · · · 310
Kage, H. · · · · · · · · · · 182
Kakuda, Y. · · · · · · · · · · 77
Kalata, P. · · · · · · · · · · 744
Kam, M. · · · · · · · · · · 744
Kamano, T. · · · · · · · · · · 537
Kanasugi, A. · · · · · · · · · · 293
Kaneko, M. · · · · · · · · · · 67
Kang, L. · · · · · · 200, 279, 427
Katai, O. · · · · · · · · · · 1
Kataoka, Y. · · · · · · · · · · 537
Katoh, R. · · · · · · · · · · 695
Katsuki, T. · · · · · · · · · · 228
Katsura, M. · · · · · · · · · · 614
Kauffman, S. A. · · · · · · · · · · I-48
Kawagoe, M. · · · · · · · · · · 610
Kawaguchi, S. · · · · · · · · · · 289
Kawai, T. · · · · · · · · · · 190
Kawaji, S. · · · · · · · · · · 125
Kawamoto, M. · · · · · · · · · · 731
Kawano, H. · · · · · · · · · · 11
Kawasue, K. · · · · · · · · · · 630
Kim, D.-H. · · · · · · · · · · 550
Kim, D.-J. · · · · · · · · · · 454
Kim, J. · · · · · · · · · · 47
Kim, J.-H. · · · · · · · · · · 550
Kim, J.-R . · · · · · · · · · · 43
Kim, Y.-J. · · · · · · · · · · 550
Kim. K.-C. · · · · · · · · · · 550
Kimura, H. · · · · · · · · · · 301
Kinoshita, N. · · · · · · · · · · 228
Kitahashi, M. · · · · · · · · · · 170
Kitakubo, S. · · · · · · · · · · 699
Kitamura, S. · · · · · · · · · 77, 85
Kitano, H. · · · · · · · · · · 509
Kitazoe, T. · · · · · · · · · 318, 366
Kobayashi, S. · · · · · · · · · · 81
Koerner, E. · · · · · · · · · 214, 220
Koerner, U. · · · · · · · · · · 214
Komeya, H. · · · · · · · · · · 448
Kondo, H. · · · · · · · · · · 220
Kondo, K. · · · · · · · · · · 293
Korkin, M. · · · · · · · · · 258, 263
Kozima, H. · · · · · · · · · 474, 478
Kubo, M. · · · · · · · · · · 204
Kubota, N · · · · · · I-41, 314, 324
Kubota, S. · · · · · · · · · · 242
Kumabe, K. · · · · · · · · · · 537
Kuribayashi, K. · · · · · · · · · 448, 711
Kurogi, S. · · · · · · · · · · 723
Kurono, S. · · · · · · · · · · 690
Kuroyama, K. · · · · · · · · · · 89
Kusumi, N. · · · · · · · · · · 703
Kyuma, K. · · · · · · · · · · 182
Kyura, N. · · · · · · · · · · 568

L

LeBaron, B. · · · · · · · · · · I-34
Lee, D.-W. · · · · · · · · · · 462
Lee, B. · · · · · · · · · · 470
Lee, M. · · · · · · · · · · 470
Lee, J. · · · · · · · · · · 43
Lee, J.-H. · · · · · · · · · · 271
Lee, J.-J. · · · · · I-49, 178, 582

Lee, M.-H. 572
Lee, S.-H. 462
Lee, S.-I. 271
Li, T. 376
Li, Y.-Z. 31
Liu, W. 376
Liu, Y. 736
Liu, Z.-J. 444
Lu, J. L. 388
Luo, Z.-W. 101

M

Ma, L. 354
Masuda, H. 610
Matsui, R. 634
Matsumoto, G. I-24, 205, 207
Matsumoto, S. 448
Matsunaga, N. 125
Matsuno, F. 380
Matsuo, T. 406
Matsuoka, K. 727, 731
Messom, C. H. 422
Migita, M. 402
Mikami, S. 204
Mimura, N. 55, 59, 63
Mine, K. 314, 324
Misao, Y. 246
Mistiri, F. S. 556
Miyajima, H. 354
Miyakawa, N. 207
Miyake, T. 719
Miyake, Y. 182
Miyano, T. 350
Miyazaki, T. 228, 514
Mizoguchi, F. 149
Mizuhara, H. 715
Moon, C. 47
Morikawa, D. 7
Morimoto, F. 314
Morioka, S. 73
Moriyama, T. 466
Mouri, T. 59
Murakami, K. 448
Murakami, N. 234
Murao, H. 85
Murata, T. 418
Murata, J. 224
Murata, M. 362

N

Nagahama, H. 674
Nagami, A. 350
Nagasaka, Y. 250, 410
Nagashima, Y. 626
Nagata, S. 622, 638
Nakamine, H. 17
Nakamura, M. 362, 568
Nakamura, Y. 89
Nakasuka, S. 392, 397
Nakatsu, R. 605
Nakatsukasa, K. 578
Nakaya, N. 293
Nakazono, T. 626
Namikawa, K. 254
Nariman, D. 682
Nawa, N. E. 258
Nehaniv, C. 435
Nemoto, M. 707
Nian, W. 440
Nishii, J. 106
Nishikawa, Y. 715
Nishino, H. 682
Nomura, T. 392, 397, 658
Nonaka, S. 324

O

Ochiai, T. 634
Odanaka, T. 699
Odashima, T. 114
Ogawa, K. 106
Ohbayashi, M. 224, 703
Ohnishi, N. 731
Ohuchi, A. 297,372,418,486
614,618
Okado, A. 238
Okamoto, M. 228
Okazaki, K. 440
Okita, T. 431
Okubo, S. 376
Okuzono, H. 642
Omatu, S. 137, 528
Onaga, K. 362
Ono, I. 81
Ono, T. 362
Otani, R. 250, 410
Otuka, K. 234

P

Palmer, R. G. I-34
Park, C. S. 564
Park, K.-B. 582
Park, T. K. 564
Pawicz, P. 744

Q

Qi, Y. 279

R

Ray, T. 604
Reidys, C. M. I-28, 161
Ren, S. 723
Richardson, M. J. 541
Rietman, E. A. 186

S

Saha, S. K. 55
Sakamoto, T. 448
Sakurayama, T. 55
Sannomiya, N. 17
Sato, K. 586
Sato, M. 695
Satoh, T. 431
Sawada, T. 297
Sawaragi, T. 1
Schilhabel, T. E. 384
Schuster, P. I-18
Selvarajan, M. 546
Sengoku, H. 283
Shida, K. 686
Shigematsu, Y. 210
Shigeta, K. 250, 410
Shimada, T. 190
Shimoda, H. 7
Shimohara, K. 186,196,267,392 397,658
Shin, S. 129
Shinkonda, K. 695
Shinozawa, K. 267
Shohdohji, T. 699
Shono, K. 486
Sim K. B. 454, 462
Slous, R. 186
Song, G.-B. 271
Suemitsu, H. 406
Sugawara, K. 145
Sugimoto, M. 234
Sugisaka, M. I-2, 23, 178, 275 444, 499, 642
Sugiura, H. 190
Suzuki, K. 297, 372, 418, 486 614,618
Suzuki, R. 106
Suzuki, T. 537, 740
Suzuki, Y. 63, 666
Svinin, M. M. 89

T

Tabuse, M. 482
Tagawa, K. 289
Takadama, K. 392, 397
Takami, O. 634
Takano, Y. 414
Takase, K. 670
Takayama, M. 27
Takeda, H. 254, 358
Takenaga, H. 238
Tamaki, H. 77
Tamura, H. 510
Tamura, S. 440
Tanaka, M. 482, 610
Tanaka, H. 646, 666
Tanaka, K. 133
Tanaka, Y. 67
Tang, J. 448, 458
Taniwaki, K. 250, 410
Tatebe, Y. 318
Tatsuzawa, Y. 81
Tokuda, I. 350
Toquenaga, Y. 654
Tomiyama, J. 318, 366
Tosa, N. 598
Toyoda, K. 707
Toyofuku, T. 690
Tsuchiya, K. 11
Tsuji, T. 67, 582
Tsujimura, Y. 39
Tsujino, H. 220
Tsujita, K. 11

U

Uchikawa,Y. 119
Ueda, K. 89, 93, 402
Ueno, S. 556
Umeda, M. 242, 254
Ung, K. C. 622
Utsumiya, K. 682

V

Vaario, J. · · · · · · · · · · · 93
Vadakkepat, P. · · · · · · · · · · 550

W

Wada, M. · · · · · · · · · · · 204
Wade, M. J. · · · · · · · · · · 654
Wang, A. P. · · · · · · · · · · 556
Wang, B. · · · · · 200, 279, 427
Wang, L. · · · · · · · · · · · 711
Wang, Q. · · · · · · · · · · · 157
Wang, X. S. · · · · · · · · · · 178
Wang, X. · · · · · · · · · · · 275
Watanabe, K. · · · 510, 514, 518, 524
Watanabe, S. · · · · · · · · · · 110
Wells, W. R. · · · · · · · · · · 546
Williams, R. A. · · · · · · · · · · 541
Worn, H. · · · · · · · · · · · 590
Wu, J.-L. · · · · · · 711, 715, 719
Wu, X. · · · · · · · · · · · 23
Wu, Y. · · · · · · · · · · · 388
Wurll, C. · · · · · · · · · · · 590

X

Xu, B. · · · · · · · · · · · 354
Xu, C. M. · · · · · · · · · · · 499

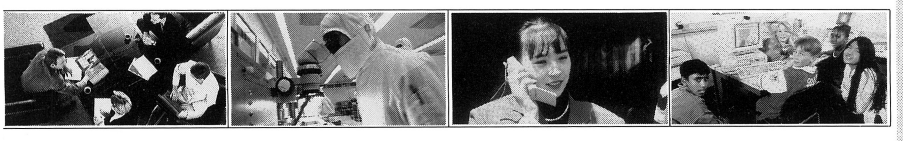
Y

Yachida, M. · · · · · · · · · · · 170
Yamada, H. · · · · · · · · · · · 205
Yamada, K. · · · · · · · · · · · 642
Yamada, T. · · · · · · · 55, 59, 63
Yamaguchi, S. · · · · · · · · · 314,324
Yamaguchi, T. · · · · · · · · · · 170
Yamamoto, R. · · · · · · · · · · 73
Yamashita, T. · · · · · · · · · · 695
Yamazaki, N. · · · · · · · · · · 174
Yanagihara, D. · · · · · · · · · 97, 101
Yano, M. · · · · · · · · · · · 110
Yao, X. · · · · · · · · · · · 736
Yasubayashi, M. · · · · · · · · · · 114
Yasuda, H. · · · · · · · · · · · 336
Yasuno, T. · · · · · · · · · · · 537
Yim, W. · · · · · · · · · · · 546
Yoon, K.-S. · · · · · · · · · · · 572
Yoshihara, I. · · · · · · · · · 145, 283
Yoshikawa, H. · · · · · · · · · · · 7
Yoshitomi, Y. · · · · · · · · · 318, 366
Yoshitomi, T. · · · · · · · · · · · 153
Yuasa, H. · · · · · · · · · 101, 114
Yuji, J. · · · · · · · · · · · 686

Z

Zha, H. · · · · · · · · · · · 674
Zhang, Y. G. · · · · · · · 23, 458, 499
Zhang, B.-T. · · · · · · · · · · · 166
Zhao, Q. · · · · · · · · · · · 740
Zheng, D. · · · · · · · · · · · 35
Zhou, G. · · · · · · · · · · · 27
Zhou, H. · · · · · · · · · · · 51
Zhou, T. · · · · · · · · · · · 306

NEC Multimedia at Work



As one of the world's leading manufacturers in each of the three key multimedia technologies of telecommunications, computers and semiconductors, NEC provides the products and services that are helping to build tomorrow's Global Information Society. Just imagine what you can achieve by putting NEC Multimedia to work.

just imagine

NEC MULTIMEDIA

NEC

http://www.nec-global.com/just_imagine